



Title	Supramolecular Complexes of Lithium Ion-Encapsulated Fullerene for Photoinduced Charge Separation and Light-Energy Conversion
Author(s)	川島, 雄樹
Citation	大阪大学, 2015, 博士論文
Version Type	VoR
URL	<a href="https://doi.org/10.18910/52154">https://doi.org/10.18910/52154</a>
rights	
Note	

*The University of Osaka Institutional Knowledge Archive : OUKA*

<https://ir.library.osaka-u.ac.jp/>

The University of Osaka

Doctoral Dissertation

**Supramolecular Complexes of  
Lithium Ion-Encapsulated Fullerene for Photoinduced  
Charge Separation and Light-Energy Conversion**

Yuki Kawashima

January 2015

*Graduate School of Engineering  
Osaka University*

---

## Contents

<b>General Introduction</b>		1
<b>Chapter 1</b>	Ion-Controlled On-Off Switch of Electron Transfer from Tetrathiafulvalene Calix[4]pyrroles to $\text{Li}^+@\text{C}_{60}$	14
<b>Chapter 2</b>	Enhanced Photoinduced Electron-Transfer Reduction of $\text{Li}^+@\text{C}_{60}$ in Comparison with $\text{C}_{60}$	33
<b>Chapter 3</b>	Small Reorganization Energies of Photoinduced Electron Transfer between Spherical Fullerenes	51
<b>Chapter 4</b>	Strong Supramolecular Binding of $\text{Li}^+@\text{C}_{60}$ with Sulfonated <i>meso</i> -Tetraphenylporphyrins and Long-Lived Photoinduced Charge Separation	69
<b>Chapter 5</b>	Supramolecular Formation of $\text{Li}^+@\text{PCBM}$ Fullerene with Sulfonated Porphyrins and Long-Lived Charge Separation	81
<b>Chapter 6</b>	Electron Transfer in a Supramolecular Complex of Zinc Chlorin Carboxylate Anion with $\text{Li}^+@\text{C}_{60}$ Affording the Long-Lived Charge-Separated State	109
<b>Chapter 7</b>	Robust Inclusion Complexes of Crown Ether Fused Tetrathiafulvalenes with $\text{Li}^+@\text{C}_{60}$ to Afford Efficient Photodriven Charge Separation	135
<b>Chapter 8</b>	Long-Lived Charge Separation in a Rigid Pentiptycene Bis(Crown Ether)- $\text{Li}^+@\text{C}_{60}$ Host-Guest Complex	157

---

<b>Chapter 9</b>	Long-Lived Charge-Separated States Produced in Supramolecular Complexes between Anionic and Cationic Porphyrins	170
<b>Chapter 10</b>	Photoinduced Electron Transfer from a Tetrathiafulvalene-Calix[4]pyrrole to a Porphyrin Carboxylate within a Supramolecular Ensemble	196
<b>Chapter 11</b>	Photoinduced Electron Transfer in a Dynamic Supramolecular System with Curved $\pi$ -Structures	223
<b>Chapter 12</b>	Near-Infrared Photoelectrochemical Conversion via Photoinduced Charge Separation in Supramolecules of Anionic Phthalocyanines with $\text{Li}^+@\text{C}_{60}$	235
<b>Chapter 13</b>	Photoelectrochemical Properties of Supramolecular Composites of an Anionic Zinc Chlorin and $\text{Li}^+@\text{C}_{60}$ on $\text{SnO}_2$	270
<b>Chapter 14</b>	Enhanced Photoelectrochemical Performance of Composite Photovoltaic Cells of $\text{Li}^+@\text{C}_{60}$ -Sulfonated Porphyrin Supramolecular Nanoclusters	286
<b>Concluding Remarks</b>		296
<b>List of Publication</b>		301
<b>Acknowledgments</b>		306

---



## General Introduction

The development of sustainable sources of energy is the most important issue of this century. Fossil fuel emits carbon dioxide (CO<sub>2</sub>) during burning, which has caused the greenhouse effect.<sup>1-4</sup> In addition, current energy resources will run out in the near future.<sup>5,6</sup> Thus, it is extremely important to utilize solar energy by using solar cells to resolve these energy problems. Emerging photovoltaic cells such as perovskite cells<sup>7</sup>, organic dye-sensitized solar cells<sup>8-13</sup> and organic thin film solar cells<sup>14-18</sup> have gained increased attention among various solar cells, because their production and energy costs are lower than those of inorganic solar cells. In the case of perovskite solar cells, the energy conversion efficiencies are approaching *ca.* 20%,<sup>7</sup> which is close to those of inorganic solar cells such as multicrystalline silicon type solar cells.<sup>19</sup> However, perovskite solar cells contain heavy metals such as lead, which are toxic. In contrast to perovskite solar cells, organic solar cells such as organic dye-sensitized solar cells<sup>8-13</sup> and organic thin film solar cells<sup>14-18</sup> do not contain heavy metals. Dye-sensitized solar cells have the advantage of production cost as compared with organic thin film solar cells because fabrication of dye-sensitized solar cells requires only a small amount of material. The energy conversion efficiencies of organic solar cells are around 10%, which are still lower than those of inorganic solar cells.<sup>19</sup> Photovoltaic cells convert the energy from sunlight into electricity, and this process is divided into three processes. In the case of thin film solar cells, first, an electron donor is excited by photoirradiation to produce the excited state of the electron donor, which diffuses into the donor-acceptor interface. Electron transfer from the excited state of the donor to the acceptor occurs to produce electrons and holes [charge-separated (CS) state], which move to the corresponding electrodes. In the case of dye-sensitized solar cells, electrons move to an electrode from the photoinduced CS state of donor-acceptor systems or the excited state of photosensitizers.<sup>8-13</sup> The resulting oxidized species can receive electrons from a cathode via an electron mediator. The long-lived excited state of photosensitizers or CS state of donor-acceptor systems afford a high energy conversion efficiency because which can supply electrons to an electrode. Ru complexes, which are well-known photosensitizer, show a short-lived excited state (~ 100 ns) and contain a minor metal. Thus, it is suitable to use donor-acceptor systems, which have the long-lived CS state.

In the nature, the photosynthetic reaction center achieves of a long lifetime (*ca.* 1 s) of the final CS state via photoinduced multistep electron transfer from the excited chlorophyll dimer

---

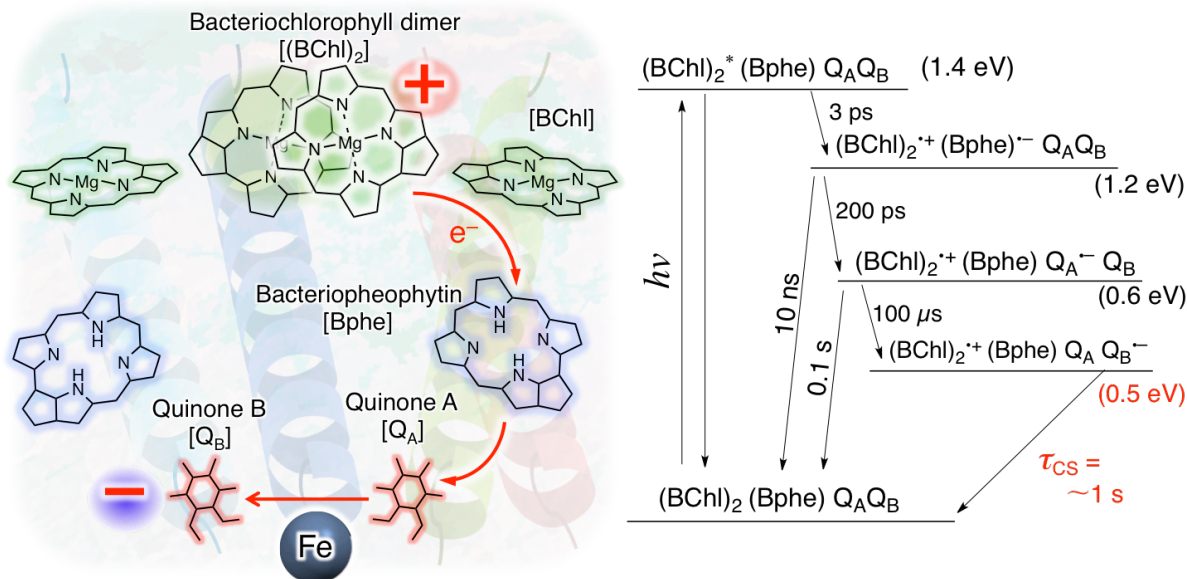


**Figure 1.** Illustration of the photosynthetic reaction center of purple bacteria and energy diagram of charge-separation processes.

(special pair) to the quinone derivative by spatially separating generated electrons and holes to prepare high-energy compounds such as ATP (adenosine triphosphate) and NADPH (dihydronicotinamide adenine dinucleotide phosphate), as shown in Figure 1.<sup>20,21</sup> In the field of artificial photosynthesis, the mimicry of the natural photosynthesis has prompted design of synthetic donor-acceptor linked ensembles including triads, tetrads and pentads.<sup>22-38</sup> Instead of the quinone in the photosynthetic reaction center, fullerenes, which have similar one-electron reduction potential with the quinone,<sup>35</sup> have been widely used as electron acceptors. Fullerenes have the three-dimensional curved surface together with the rigid and confined structure of aromatic  $\pi$ -sphere and show the small reorganization energy ( $\lambda$ ) because the extremely small structural and solvation change occurs in the electron-transfer reduction on the highly delocalized fullerene cage.<sup>39-42</sup> The small reorganization energy is suitable for the electron acceptors of donor-acceptor linked systems to achieve the long-lived and high energy CS states ( $\tau_{CS}$ ), which is explained by the Marcus equation for non-adiabatic electron transfer reactions (eq 1),<sup>43</sup>

$$k_{ET} = \left( \frac{4\pi^3}{h^2 \lambda k_B T} \right)^{1/2} V^2 \exp\left[ -\frac{(\Delta G_{ET} + \lambda)^2}{4\lambda k_B T} \right] \quad (1)$$

where  $k_{ET}$  is the rate constant of intramolecular electron transfer,  $\lambda$  is the reorganization energy of electron transfer,  $V$  is the electronic coupling term,  $-\Delta G_{ET}$  is the driving force for electron transfer (Figure 2a) and  $k_B$  is the Boltzmann constant.<sup>43</sup> The rate constant of electron transfer

increases with the driving force ( $-\Delta G_{ET}$ ) in the Marcus normal region ( $-\Delta G_{ET} < \lambda$ ), and reaches a maximum value, which is controlled by the electronic coupling term in case of non-adiabatic electron transfer, when the  $-\Delta G_{ET}$  becomes the same as the reorganization energy ( $-\Delta G_{ET} = \lambda$ ). When  $-\Delta G_{ET}$  becomes larger than the reorganization energy ( $-\Delta G_{ET} > \lambda$ ), the rate constant of electron transfer decreases with increasing  $-\Delta G_{ET}$  due to the poor vibrational overlap of function waves between the initial and final states of electron transfer.<sup>44</sup> This region ( $-\Delta G_{ET} > \lambda$ ) is called the Marcus inverted region. Thus, the reorganization energy is the key parameter to control the rate of forward and backward electron transfer. For instance, a decrease in the reorganization energy of back electron transfer from 1.0 to 0.4 eV results in an increase in the rate constant of forward electron transfer of a donor–acceptor system with the driving force of 0.4 eV, whereas the back electron transfer process with the driving force of 1.4 eV is remarkably retarded, as shown as the blue line in Figure 2b. Such an expansion of the difference in the rate constants of forward electron transfer (blue dots in Figure 2b) and back electron transfer (blue circles in Figure 2b) affords the long-lived CS state. In addition, the electronic coupling term ( $V$ ) between the electron acceptor and donor affects also on the lifetime of the CS state. Zinc porphyrin–fullerene linked dyad (ZnP–C<sub>60</sub>) has the short CS lifetime of 0.77  $\mu$ s and the  $V$  value of 3.9 cm<sup>-1</sup>.<sup>36,37</sup> In contrast to the dyad, a covalently linked ferrocene–zinc porphyrin–free base porphyrin–fullerene tetrad (Fc–ZnP–H<sub>2</sub>P–C<sub>60</sub>) affords the long CS lifetime (0.38 s), which is comparable to the CS lifetime of the photosynthetic reaction center, even though the tetrad has larger  $\lambda$  value (1.32 eV) than that of the dyad (0.66 eV) due to the increase in the molecular

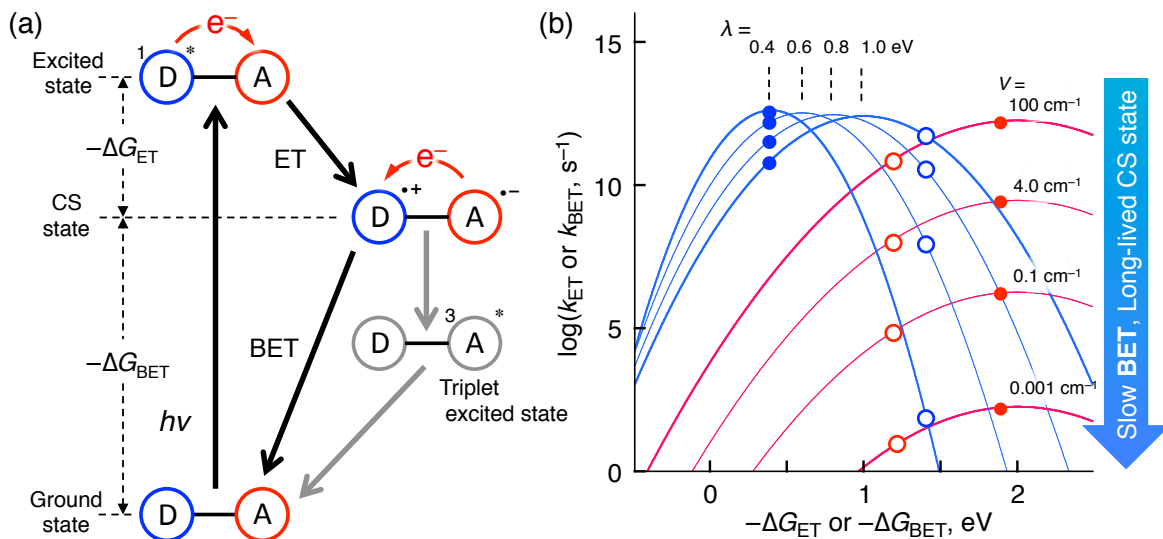


**Figure 2.** (a) Energy diagram of donor-acceptor system. (b) Driving force dependence of  $\log k_{ET}$  of ET (dot) and BET (circle) with various  $\lambda$  and  $V$  values ( $\lambda = 1.0, 0.8, 0.6$  and  $0.4$  eV and  $V = 100$  cm<sup>-1</sup> for blue lines;  $\lambda = 2.0$  eV and  $V = 100, 4.0, 0.1$  and  $0.001$  cm<sup>-1</sup> for red lines).

size.<sup>36,37</sup> This result is explained by the extremely small  $V$  value of tetrad ( $1.7 \times 10^{-4} \text{ cm}^{-1}$ ) due to the spatially separated ferrocenium ion and  $\text{C}_{60}$  radical anion of the CS state ( $\text{Fc}^+ - \text{ZnP} - \text{H}_2\text{P} - \text{C}_{60}^{\cdot-}$ ) by a long edge-to-edge distance (48.9 Å).<sup>36,37</sup> The donor-acceptor system which has small electronic coupling term afford a long-lived CS state even if the donor-acceptor system has a large  $\lambda$  value, and a smaller  $-\Delta G_{\text{BET}}$  value than the  $\lambda$  value, as shown in Figure 2b. For instance, a decrease in the  $V$  value from  $100 \text{ cm}^{-1}$  to  $0.001 \text{ cm}^{-1}$  results in deceleration of back electron transfer (red circles in Figure 2b) to afford a long-lived CS state (Figure 2b). However the synthesis of multi-component donor-acceptor liked molecules such as  $\text{Fc} - \text{ZnP} - \text{H}_2\text{P} - \text{C}_{60}$  is difficult and time-consuming.

In contrast to covalently linked donor-acceptor systems, supramolecular systems have attracted much attention because they can be easily prepared without complicated and time-consuming synthesis.<sup>45-58</sup> As with covalently linked donor-acceptor systems, a combination of porphyrinoid and fullerene, which are an efficiently light-harvesting electron donor and a superior electron acceptor, have been widely studied using non-covalent interactions such as hydrogen bonds and coordination bonds to form the long-lived CS states.<sup>52-59</sup> It has been known that the stronger supramolecular binding occurs in nonpolar solvent such as toluene.<sup>59,60</sup> However, photoinduced electron transfer is energetically disfavored in nonpolar solvents. The energies of the CS states are often higher than those of the excited states of fullerenes and porphyrinoids.<sup>38</sup> In such a case, back electron transfer in the CS state results in formation of the triplet excited chromophores or fullerenes rather than the ground states, as shown in Figure 2a. In contrast to nonpolar solvents, polar solvents such as benzonitrile (PhCN) can stabilize the CS state by strong solvation, which facilitates photoinduced electron transfer but destabilizes hydrogen bonds and coordination bonds between electron donors and acceptors.<sup>55,56</sup> Non-covalent interactions, which are favored in polar solvents, are electrostatic interactions. Thus, it is highly desired to design electron donor-acceptor supramolecular complexes with strong electrostatic interaction.

Among fullerenes used as electron acceptors, [60]PCBM (phenyl- $\text{C}_{61}$ -butyric-acid-methyl ester) is one of the most sophisticated functionalized-fullerene in terms of solubility and utility. [60]PCBM has been utilized to fabricate organic solar cells as the electron acceptor that exhibits high light-energy conversion efficiencies.<sup>61</sup> However, the one-electron reduction potential of [60]PCBM is *ca.* 0.1 V more negative than that of pristine  $\text{C}_{60}$ . An electron-withdrawing fluorine substituted fullerene,  $\text{C}_{60}\text{F}_{36}$ ,<sup>62</sup> exhibits a 0.8 V higher reduction potential than that of pristine  $\text{C}_{60}$ , however,  $\text{C}_{60}\text{F}_{36}$  lost a nature as fullerene due to the damaged spherical  $\pi$  system. It is difficult to

---

obtain a suitable electron acceptor for the supramolecular donor-acceptor systems by introduction of substituents. Endohedral fullerenes as an electron acceptor may be the best choice to maintain the spherical fullerene  $\pi$  cage and be changeable redox properties by encapsulated metal ion or cluster.

Endohedral fullerenes can capture some atoms or clusters inside the cage. Noble gases (He, Ne, Ar, Kr, and Xe) encapsulated fullerenes are prepared by exposing fullerene and corresponding noble gas under the high pressure.<sup>63</sup> Simple and neutral molecules such as H<sub>2</sub>O is also encapsulated inside fullerene cages.<sup>64</sup> In the case of the neutral molecule endohedral fullerenes, there are no interaction between the endohedral molecules and the fullerene cages, whereas an electron affinity of fullerenes can be controlled by the encapsulation of metal atoms in fullerenes.<sup>65-69</sup> A pioneering study in endohedral metallofullerenes is the preparation of La@C<sub>82</sub>,<sup>66</sup> in which three electrons are transferred from the endohedral lanthanum to the C<sub>82</sub> cage with an electronic structure defined as La<sup>3+</sup>@C<sub>82</sub><sup>3-</sup>, as shown in Figure 3. Since then, numerous endohedral metallofullerenes composed of different metals and cage sizes were successfully synthesized, isolated, and characterized. Metal nitride clusters such as Sc<sub>3</sub>N, Y<sub>3</sub>N, Er<sub>3</sub>N, and Gd<sub>3</sub>N were also encapsulated in the C<sub>80</sub> cage. Metal carbides (Sc<sub>2</sub>C<sub>2</sub>@C<sub>84</sub>),<sup>67</sup> hydrogenated metal carbides (Sc<sub>3</sub>CH@C<sub>80</sub>),<sup>68</sup> metal nitrogen carbides (Sc<sub>3</sub>NC@C<sub>80</sub>),<sup>69</sup> metal oxides (Sc<sub>4</sub>O<sub>2</sub>@C<sub>80</sub>),<sup>70</sup> and metal sulfides (Sc<sub>2</sub>S@C<sub>82</sub>)<sup>71,72</sup> have also been identified and characterized. Endohedral metal and metal cluster afford not only the strong electron affinity but also unique properties. An unstable  $I_h$ -symmetric C<sub>80</sub> cage is stabilized by endohedral Sc<sub>3</sub>N cluster because Sc<sub>3</sub>N donates six electrons to C<sub>80</sub> cage and fill the open shell C<sub>80</sub> cage.<sup>73</sup> A higher

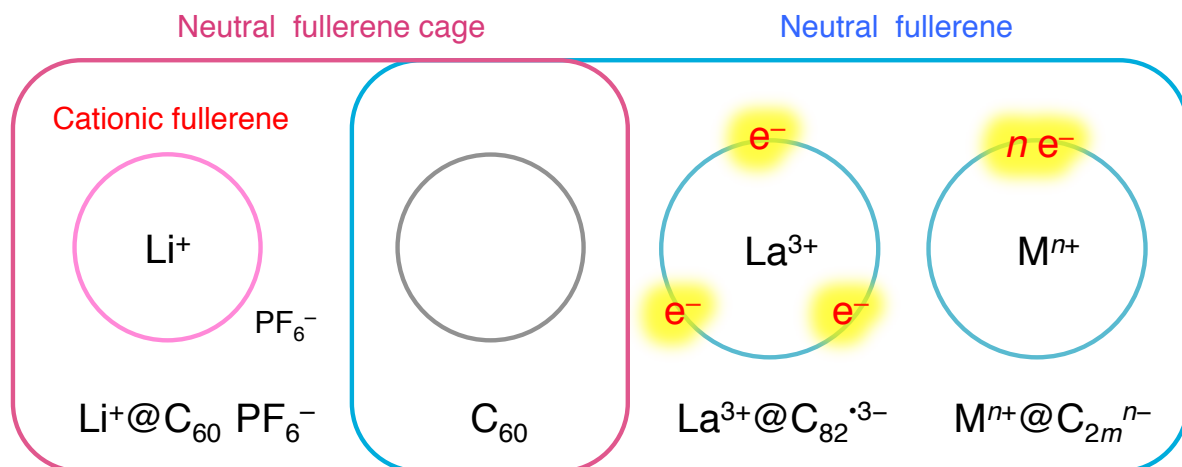


**Figure 3.** Electronic structures of Li<sup>+</sup>@C<sub>60</sub>, pristine C<sub>60</sub>, La@C<sub>82</sub>, and metal endohedral fullerenes.

fullerene cage of  $\text{Sc}_2@\text{C}_{2v}(4348)\text{-C}_{84}$  violates the isolated pentagon rule (IPR).<sup>74</sup> The IPR states that fullerenes with isolated pentagon rings are kinetically stable than their fused pentagon counterparts, which was proposed by Kroto.<sup>75</sup> The encaged metals cover from Groups I to IV on periodical table, with lanthanide being the most popular. However the total charges of endohedral metallofullerenes are neutral when fullerene cages are reduced accompanied by oxidation of metals to metal ions as the case of  $\text{La}^{3+}@\text{C}_{82}^{3-}$ ,<sup>76</sup> indicating that they can not bind with electron donors to form supramolecular complexes with strong binding in polar solvent.

In contrast to these endohedral metallofullerenes, a lithium ion-encapsulated  $\text{C}_{60}$  ( $\text{Li}^+@\text{C}_{60}$  salt) has the neutral  $\text{C}_{60}$  cage with a lithium cation.<sup>77-79</sup> The one-electron reduction potential of  $\text{Li}^+@\text{C}_{60}$  (0.14 V vs SCE) is by 0.57 V higher than that of  $\text{C}_{60}$  (-0.43 V vs SCE) in benzonitrile (PhCN). The absorption spectrum of  $[\text{Li}^+@\text{C}_{60}]\text{SbCl}_6^-$  exhibits the similar dipole-allowed transition ( $t_{1u} \leftarrow g_g + h_g$ ) and dipole-forbidden transition ( $t_{1u} \leftarrow h_u$ ) between HOMO and LUMO with that of pristine  $\text{C}_{60}$ , indicating the relative energy level of  $\text{C}_{60}$  cage is unchanged by encapsulated  $\text{Li}^+$ .<sup>77</sup> These results indicate that enhanced electron affinity of  $\text{Li}^+@\text{C}_{60}$  arise from the stabilized energy levels of HOMO and LUMO of  $\text{Li}^+@\text{C}_{60}$  by Coulomb interaction between  $\text{C}_{60}$  cage and encapsulated  $\text{Li}^+$ .<sup>77</sup>

Cationic  $\text{Li}^+@\text{C}_{60}$  is expected to construct supramolecular complexes with electron donors by using electrostatic interactions. The author finds four merits to use  $\text{Li}^+@\text{C}_{60}$  in the supramolecular systems with electron donors. Firstly, strong supramolecular complexes are formed between electron donors and  $\text{Li}^+@\text{C}_{60}$  by electrostatic interaction in a polar solvent in contrast to the case of neutral  $\text{C}_{60}$ . Secondly, the structure of such supramolecular complexes of  $\text{Li}^+@\text{C}_{60}$  can be easily controlled by the positions of minus charges of electron donors. When the symmetrical anionic porphyrinoid is employed, it is expected that  $\text{Li}^+@\text{C}_{60}$  is placed on the

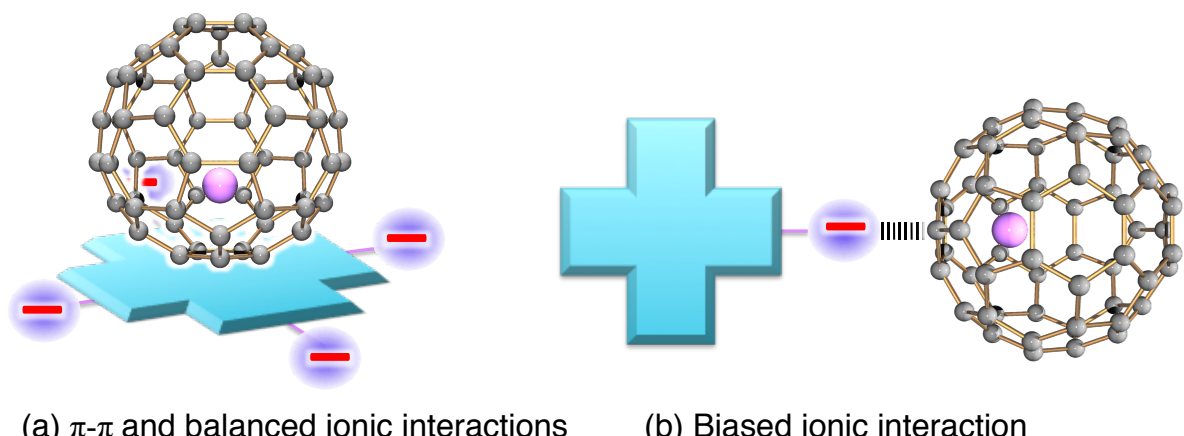


**Figure 4.** Supramolecular complexes of  $\text{Li}^+@\text{C}_{60}$  with (a) symmetrical anionic porphyrinoid and (b) porphyrinoid which has an anionic substituent.

surface of porphyrinoid due to the  $\pi$ - $\pi$  and balanced ionic interactions at the center of surface of porphyrinoid, as shown in Figure 4. On the other hand, when the porphyrinoid, which has an anionic substituent, is employed,  $\text{Li}^+@\text{C}_{60}$  binds to an anionic substituent because of biased interaction towards an anionic substituent to pull the donor and acceptor apart. Specially separated donor and acceptor molecules decrease the electronic coupling terms, affording the long-lived CS state. Thirdly, the CS state is stabilized by the encapsulation of  $\text{Li}^+$  in  $\text{C}_{60}$  to afford the long-lived CS state, because of higher one-electron reduction potential of  $\text{Li}^+@\text{C}_{60}$  than that of pristine  $\text{C}_{60}$ . Fourthly, light absorption is reinforced due to the formation of new absorption bands by charge-transfer interactions, which enhances the power conversion efficiency of organic solar cells.

$\text{Li}^+@\text{C}_{60}$  was produced by Campbell and her colleagues successfully by exposing monolayers of  $\text{C}_{60}$  to an intense beam of  $\text{Li}^+$  at energy, which is large enough for  $\text{Li}^+$  to penetrate the carbon cage but small enough not to destroy the cage.<sup>77</sup> However, they could not obtain enough quantities of  $\text{Li}^+@\text{C}_{60}$  to carry out a sufficient characterization. A bulk synthesis of  $\text{Li}^+@\text{C}_{60}$  was prevented by a low encapsulating rate of  $\text{Li}^+$  into  $\text{C}_{60}$  cage, and a difficulty of purification due to charge-transfer interaction between produced  $\text{Li}^+@\text{C}_{60}$  and unreacted  $\text{C}_{60}$ . The bulk synthesis and crystal structure of  $[\text{Li}^+@\text{C}_{60}]\text{SbCl}_6^-$  was reported in 2010 by Aoyagi et al. to show that the lithium cation is located at off-center positions inside the neutral  $\text{C}_{60}$  cage.<sup>77,78</sup> Although the bulk synthesis of  $\text{Li}^+@\text{C}_{60}$ , which have attracted attention due to the possibility as an electron acceptor and a material for photovoltaics, was established, the electron-transfer properties and facile supramolecular formation of charge-separation systems composed  $\text{Li}^+@\text{C}_{60}$  have yet to be examined.

In this thesis, the author studied firstly the thermal electron-transfer between  $\text{Li}^+@\text{C}_{60}$  and electron donors in Chapter 1 to gain a better understanding of the electron transfer properties of  $\text{Li}^+@\text{C}_{60}$ . Secondly, photoinduced electron-transfer reduction of  $\text{Li}^+@\text{C}_{60}$  via intermolecular electron transfer was investigated in Chapters 2 and 3. Thirdly, the formation of supramolecular complexes between  $\text{Li}^+@\text{C}_{60}$  (and functionalized  $\text{Li}^+@\text{C}_{60}$ ) and various electron donors with strong binding and long-lived CS states was studied in Chapters 4–8. The author examined the formation of supramolecular complexes, which do not contain  $\text{Li}^+@\text{C}_{60}$  (Chapters 9–11) as well to gain a better understanding of supramolecular formation in polar solvent. Finally, the photoelectrochemical performance of dye-sensitized solar cells composed of supramolecular complexes was studied in detail (Chapters 12–14). The brief explanations of each Chapter are described below.

In Chapter 1, the author described the formation of supramolecular complexes between  $\text{Li}^+@\text{C}_{60}$  and two tetrathiafulvalene calix[4]pyrrole (TTF-C4P) donors and showed that the judicious addition of an anion or a cation allows to control the direction of the resulting thermal electron transfer process.

In Chapter 2, the author revealed the change in the electron acceptability of  $\text{Li}^+@\text{C}_{60}$  as compared with pristine  $\text{C}_{60}$  on photoinduced electron transfer between aromatic compounds and  $\text{Li}^+@\text{C}_{60}$ , due to the encapsulated lithium-cation. In Chapter 3, the author investigated the driving force dependence of the rate constants of electron transfer between  $I_h$ -symmetric fullerenes, which are ideal molecules to verify the Marcus theory of electron transfer.

The supramolecular formation between  $\text{Li}^+@\text{C}_{60}$  and various electron donors, and the formation of CS states are discussed in Chapters 4 to 8. In Chapters 4 and 5, the author showed the formation of supramolecular complexes of anionic phthalocyanine with  $\text{Li}^+@\text{C}_{60}$  and lithium ion-encapsulated [6,6]-phenyl- $\text{C}_{61}$ -butyric acid methyl ester fullerene ( $\text{Li}^+@\text{PCBM}$ ), which stabilized the CS state. The electron-transfer pathways of these supramolecular complexes were also investigated. Zinc chlorin calboxylate ( $\text{ZnCh}^-$ ) was employed as an electron donor of supramolecular complex with  $\text{Li}^+@\text{C}_{60}$ , which has the small electronic coupling term due to the spatially separated electron donor and acceptor (Chapter 6). In Chapters 7 and 8, the author showed supramolecular complexes of  $\text{Li}^+@\text{C}_{60}$  with crown-ether-fused tetrathiafulvalenes (Chapter 7) and a pentiptycene bis(crown ether) (Chapter 8).

Additionally, the author mentioned the charge separation in supramolecular complexes of anionic porphyrin/cationic porphyrin (Chapter 9), anionic porphyrin/TTF-C4P (Chapter 10), and finite single-wall CNT $\supset\text{C}_{60}$  (Chapter 11) to gain a better understanding of supramolecular formation in polar solvent.

The photoelectrochemical performances of dye-sensitized solar cells composed of supramolecular nanocluster are described in Chapters 12–14. The dye-sensitized solar cells of  $\text{ZnCh}^-/\text{Li}^+@\text{C}_{60}$  supramolecular nanoclusters (Chapter 12) and anionic phthalocyanine/ $\text{Li}^+@\text{C}_{60}$  supramolecular nanoclusters (Chapter 13) were evaluated. These two porphyrinoids have intense absorption bands in near infrared region. The dye-sensitized solar cells of anionic porphyrin/ $\text{Li}^+@\text{C}_{60}$  supramolecular nanoclusters were also developed (Chapter 14). This porphyrin has an intense absorption band in visible region.

Thus, this thesis provides promising strategies for efficient energy conversion by fully utilizing unique properties of  $\text{Li}^+@\text{C}_{60}$ .

---

## References

- (1) Raval, A.; Ramanathan, V. *Nature* **1989**, *342*, 758–761.
- (2) Loriois, C.; Jouzel, J.; Raynaud, D.; Hansen, J.; Treut, H. L. *Nature* **1990**, *347*, 139–145.
- (3) Hansen, J. E.; Lacis, A. A. *Nature* **1990**, *346*, 713–719.
- (4) Slovic, P.; Flynn, J. H.; Layman, M. *Science* **1991**, *254*, 1603–1607.
- (5) Armaroli, N.; Balzani, V. *Angew. Chem., Int. Ed.* **2007**, *46*, 52–66.
- (6) Nyambuu, U.; Semmler, W. *Econ. Model.* **2014**, *37*, 271–279.
- (7) Green, M. A.; Ho-Baillie, A.; Snaith, H. J. *Nature Photonics* **2014**, *8*, 506–514.
- (8) Hagfeldt, A.; Grätzel, M. *Chem. Rev.* **1995**, *95*, 49–68.
- (9) Grätzel, M. *Nature* **2001**, *414*, 338–344.
- (10) Hasobe, T. *Phys. Chem. Chem. Phys.* **2012**, *14*, 15975–15987.
- (11) Hasobe, T.; Sakai, H. *ECS J. Solid State Sci. Technol.* **2013**, *2*, M3015–M3022.
- (12) (a) Martín-Gomis, L.; Fernández-Lázaro, F.; Sastre-Santos, Á. *J. Mater. Chem. A* **2014**, *2*, 15672–15682. (b) Wang, Z.-S.; Kawauchi, H.; Kashima, T.; Arakawa, H. *Coord. Chem. Rev.* **2004**, *248*, 1381–1389.
- (13) Sauvage, J. P.; Collin, J. P.; Chambron, J. C.; Guillerez, S.; Coudret, C.; Balzani, V.; Barigelletti, F.; De Cola, L.; Flamigni, L. *Chem. Rev.* **1994**, *94*, 993–1019.
- (14) Tang, C. W. *Appl. Phys. Lett.* **1986**, *48*, 183–185.
- (15) Sariciftci, N. S.; Smilowitz, L.; Heeger, A. J.; Wudl, F. *Science* **1992**, *258*, 1474–1746.
- (16) Lee, M. M.; Teuscher, J.; Miyasaka, T.; Murakami, T. N.; Snaith, H. J. *Science* **2012**, *338*, 643–647.
- (17) Rossel, R. B.; Cardona, C. M.; Guldin, D. M.; Sankaranarayanan, S. G.; Reese, M. O.; Kopidakis, N.; Peet, J.; Walker, B.; Bazan, G. C.; Van Keuren, E.; Holloway, B. C.; Drees, M. *Nature Chem.* **2009**, *8*, 208–212.
- (18) Matsuo, Y.; Sato, Y.; Niinomi, T.; Soga, I.; Tanaka, H.; Nakamura, E. *J. Am. Chem. Soc.* **2009**, *131*, 16048–16050.
- (19) Green, M. A.; Emery, K.; Hishikawa, Y.; Warta, W.; Dunlop, E. D. *Prog. Photovolt: Res. Appl.* **2014**, *22*, 701–710.
- (20) *The Photosynthetic Reaction Center*, Deisenhofer, J., Norris, J. R., Eds.; Academic Press: San Diego, 1993.
- (21) *Molecular Level Artificial Photosynthetic Materials*, Meyer, G. J., Ed.; Wiley: New York, 1997.

(22) Connolly, J. S.; Bolton, J. R. In *Photoinduced Electron Transfer*; Fox, M. A., Chanon, M., Eds.; Elsevier: Amsterdam, 1988; Part D, pp 303–393.

(23) Wasielewski, M. R. In *Photoinduced Electron Transfer*; Fox, M. A., Chanon, M., Eds.; Elsevier: Amsterdam, 1988; Part A, pp 161–206.

(24) Frey, J.; Kodis, G.; Straight, S. D.; Moore, T. A.; Moore, A. L.; Gust, D. *J. Phys. Chem. A* **2013**, *117*, 607–615.

(25) Kurreck, H.; Huber, M. *Angew. Chem., Int. Ed.* **1995**, *34*, 849–866.

(26) Gust, D.; Moore, T. A. In *The Porphyrin Handbook*; Kadish, K. M., Smith, K. M., Guilard, R., Eds.; Academic Press: San Diego, CA, 2000; Vol. 8, pp 153–190.

(27) Elliott, K. J.; Harriman, A.; Le Pleux, L.; Pellegrin, Y.; Blart, E.; Mayer, C. R.; Odobel, F. *Phys. Chem. Chem. Phys.* **2009**, *11*, 8767–8773.

(28) Benniston, A. C.; Harriman, A. *Mater. Today* **2008**, *11*, 26–34.

(29) Odobel, F.; Séverac, M.; Pellegrin, Y.; Blart, E.; Fosse, C.; Cannizzo, C.; Mayer, C. R.; Elliott, K. J.; Harriman, A. *Chem.–Eur. J.* **2009**, *15*, 3130–3138.

(30) Fukuzumi, S.; Saito, K.; Ohkubo, K.; Troiani, V.; Qiu, H.; Gadde, S.; D’Souza, F.; Solladié, N. *Phys. Chem. Chem. Phys.* **2011**, *13*, 17019–1702.

(31) Verhoeven, J. W. In *Electron Transfer-From Isolated Molecules to Biomolecules*; Jortner, J., Bixon, M., Eds.; John Wiley & Sons: New York, 1999; Part 1, pp 603–644.

(32) Tokuji, S.; Yorimitsu, H.; Osuka, A. *Angew. Chem., Int. Ed.* **2012**, *51*, 12357–12361.

(33) Yoon, M.-C.; Lee, S.; Tokuji, S.; Yorimitsu, H.; Osuka, A.; Kim, D. *Chem. Sci.* **2013**, *4*, 1756–1746.

(34) (a) Kim, K. S.; Lim, J. M.; Osuka, A.; Kim, D. *J. Photochem. Photobiol. C* **2008**, *9*, 13–28.  
(b) Sun, L.; Hammarström, L.; Åkermark, B.; Styring, S. *Chem. Soc. Rev.* **2001**, *30*, 36–49.

(35) (a) Hiroshi, I.; Kiyoshi, H.; Tsuyoshi, A.; Masanori, A.; Seiji, T.; Tadashi, O.; Masahiro, S.; Yoshiteru, S. *Chem. Phys. Lett.* **1996**, *263*, 545–550. (b) Guldi, D. M. *Chem. Soc. Rev.* **2002**, *31*, 22–36.

(36) Imahori, H.; Sekiguchi, Y.; Kashiwagi, Y.; Sato, T.; Araki, Y.; Ito, O.; Yamada, H.; Fukuzumi, S. *Chem.–Eur. J.* **2004**, *10*, 3184–3196.

(37) Imahori, H.; Guldi, D. M.; Tamaki, K.; Yoshida, Y.; Luo, C.; Sakata, Y.; Fukuzumi, S. *J. Am. Chem. Soc.* **2001**, *123*, 6617–6628.

(38) Imahori, H.; El-Khouly, M. E.; Fujitsuka, M.; Ito, O.; Sakata, Y.; Fukuzumi, S. *J. Phys. Chem. A* **2001**, *105*, 325–332.

(39) Echegoyen, L.; Diederich, F.; Echegoyen, L. E. In *Fullerenes, Chemistry, Physics, and*

---

Technology; Kadish, K. M., Ruoff, R. S., Eds.; Wiley-Interscience: New York, 2000, pp 1–51.

(40) Guldi, D. M.; Fukuzumi, S. In *Fullerenes: From Synthesis to Optoelectronic Properties*, Guldi, D. M., Martin, N., Eds.; Kluwer: Dordrecht, 2003, pp 237–265.

(41) Sgobba, V.; Rahman, G. M. A.; Guldi, D. M. In *Carbon Nanotubes in Electron Donor–Acceptor Nanocomposites, Chemistry of Carbon Nanotubes*; Basiuk, V. A., Ed.; American Scientific Publishers: CA, 2006.

(42) Fukuzumi, S.; Guldi, D. M. In *Electron Transfer in Chemistry* Balzani, V., Ed.; Wiley-VCH: Weinheim, 2001; Vol. 2, pp 270–337.

(43) (a) Marcus, R. A. *Annu. Rev. Phys. Chem.* **1964**, *15*, 155–196. (b) Marcus, R. A. *Angew. Chem., Int. Ed.* **1993**, *32*, 1111–1121.

(44) Miller, J. R.; Calcaterra, L. T.; Closs, G. L. *J. Am. Chem. Soc.* **1984**, *106*, 3047–3049.

(45) Fukuzumi, S. *Org. Biomol. Chem.* **2003**, *1*, 609–620.

(46) Wielopolski, M.; Molina-Ontoria, A.; Schubert, C.; Margraf, J. T.; Krokos, E.; Kirschner, J.; Goulioumis, A.; Clark, T.; Guldi, D. M.; Martín, N. *J. Am. Chem. Soc.* **2013**, *135*, 10372–10381.

(47) Garg, V.; Kodis, G.; Chachisvilis, M.; Hambourger, M.; Moore, A. L.; Moore, T. A.; Gust, D. *J. Am. Chem. Soc.* **2011**, *133*, 2944–2954.

(48) Balzani, V. *Coord. Chem. Rev.* **2001**, *219-221*, 545–572.

(49) Imahori, H.; Tamaki, K.; Guldi, D. M.; Luo, C.; Fujitsuka, M.; Ito, O.; Sakata, Y.; Fukuzumi, S. *J. Am. Chem. Soc.* **2001**, *123*, 2607–2617.

(50) Gould, I. R.; Young, R. H.; Mueller, L. J.; Albrecht, A. C.; Farid, S. *J. Am. Chem. Soc.* **1994**, *116*, 3147–3148.

(51) Faiz, J. A.; Heitz, V.; Sauvage, J.-P. *Chem. Soc. Rev.* **2009**, *38*, 422–442.

(52) El-Khouly, M. E.; Fukuzumi, S.; D’Souza, F. *ChemPhysChem* **2014**, *15*, 30–47.

(53) Kirner, S.; Sekita, M.; Guldi, D. M. *Adv. Mater.* **2014**, *26*, 1482–1493.

(54) Fukuzumi, S.; Ohkubo, K. *J. Mater. Chem.* **2012**, *22*, 4575–4587.

(55) Murakami, M.; Ohkubo, K.; Hasobe, T.; Sgobba, V.; Guldi, D. M.; Wessendorf, F.; Hirsch, A.; Fukuzumi, S. *J. Mater. Chem.* **2010**, *20*, 1457–1466.

(56) Yan, Q.; Luo, Z.; Cai, K.; Ma, Y.; Zhao, D. *Chem. Soc. Rev.* **2014**, *43*, 4199–4221.

(57) Nobukuni, H.; Tani, F.; Shimazaki, Y.; Naruta, Y.; Ohkubo, K.; Nakanishi, T.; Kojima, T.; Fukuzumi, S.; Seki, S. *J. Phys. Chem. C* **2009**, *113*, 19694–19699.

(58) Hosseini, A.; Taylor, S.; Accorsi, G.; Armaroli, N.; Reed, C. A.; Boyd, P. D. W. *J. Am.*

*Chem. Soc.* **2006**, *128*, 15903–15913.

(59) Chitta, R.; D’Souza, F. *J. Mater. Chem.* **2008**, *18*, 1440–1471.

(60) Haino, T.; Yanase, M.; Fukunaga, C.; Fukazawa, Y. *Tetrahedron* **2006**, *62*, 2025–2035.

(61) Yu, G.; Gao, J.; Hummelen, J. C.; Wudl, F.; Heeger, A. J. *Science* **1995**, *270*, 1789–1791.

(62) (a) Boltalina, O. V.; Borschhevskii, A. Y.; Sidorov, L. N.; Street, J. M.; Taylor, R. *Chem. Commun.* **1996**, 529–530. (b) Liu, N.; Morio, Y.; Okino, F.; Touhara, H.; Boltalina, O. V.; Pavlovich, V. K. *Synth. Met.* **1997**, *86*, 2289–2290.

(63) Saunders, M.; Jimenez-Vázquez, H. A.; Cross, R. J.; Mroczkowski, S.; Gross, M. L.; Giblin, D. E.; Poreda, R. J. *J. Am. Chem. Soc.* **1994**, *116*, 2193–2194.

(64) Kurotobi, K.; Murata, Y. *Science* **2011**, *333*, 613–616.

(65) Lu, X. Akasaka, T. Nagase, S. *Acc. Chem. Res.* **2013**, *46*, 1627–1635.

(66) Conga, H. Yua, B. Akasaka, T. Lu, X. *Coord. Chem. Rev.* **2013**, *257*, 2880–2898.

(67) Wang, C.-R. Kai, T. Tomiyama, T. Yoshida, T. Kobayashi, Y. Nishibori, E. Takata, M. Sakata, M. Shinohara, H. *Angew. Chem., Int. Ed.* **2001**, *40*, 397–399.

(68) Krause, M. Ziegs, F. Popov, A. A. Dunsch, L. *ChemPhysChem* **2007**, *8*, 537–540.

(69) Wang, T.-S. Feng, L. Wu, J.-Y. Xu, W. Xiang, J.-F. Tan, K. Ma, Y.-H. Zheng, J.-P. Jiang, L. Lu, X. Shu, C.-Y. Wang, C.-R. *J. Am. Chem. Soc.* **2010**, *132*, 16362–16364.

(70) Stevenson, S.; Mackey, M. A.; Stuart, M. A.; Phillips, J. P.; Easterling, M. L.; Chancellor, C. J.; Olmstead, M. M.; Balch, A. L. *J. Am. Chem. Soc.* **2008**, *130*, 11844–11845.

(71) Dunsch, L.; Yang, S.; Zhang, L.; Svitova, A.; Oswald, S.; Popov, A. A. *J. Am. Chem. Soc.* **2010**, *132*, 5413–5421.

(72) Chen, N.; Chaur, M. N.; Moore, C.; Pinzón, J. R.; Valencia, R.; Rodríguez-Fortea, A.; Poblet, J. M.; Echegoyen, L. *Chem. Commun.* **2010**, *46*, 4818–4820.

(73) Zhang, J.; Stevenson, S.; Dorn, H. C. *Acc. Chem. Res.* **2013**, *46*, 1548–1557.

(74) Wang, C. R.; Kai, T.; Tomiyama, T.; Yoshida, T.; Kobayashi, Y.; Nishibori, E.; Takata, M.; Sakata, M.; Shinohara, H. *Nature* **2000**, *408*, 426–427.

(75) Kroto, H. W. *Nature* **1987**, *329*, 529–531.

(76) Akasaka, T.; Kato, T.; Kobayashi, K.; Nagase, S.; Yamamoto, K.; Funasaka, H.; Takahashi, T. *Nature* **1995**, *374*, 600–601.

(77) Aoyagi, S.; Nishibori, E.; Sawa, H.; Sugimoto, K.; Takata, M.; Miyata, Y.; Kitaura, R.; Shinohara, H.; Okada, H.; Sakai, T.; Ono, Y.; Kawachi, K.; Yokoo, K.; Ono, S.; Omote, K.; Kasama, Y.; Ishikawa, S.; Komuro, T.; Tobita, H. *Nature Chem.* **2010**, *2*, 678–683.

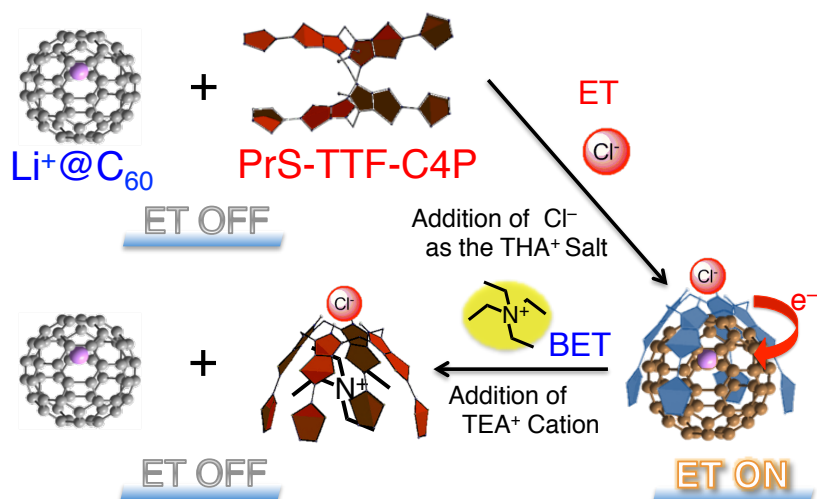
(78) Aoyagi, S.; Sado, Y.; Nishibori, E.; Sawa, H.; Okada, H.; Tobita, H.; Kasama, Y.; Kitaura,

R.; Shinohara, H. *Angew. Chem., Int. Ed.* **2012**, *51*, 3377–3381.

(79) Tellgmann, R.; Krawez, N.; Lin, S.-H.; Hertel, I. V.; Campbell, E. E. B. *Nature* **1996**, *382*, 407–408.

## Chapter 1

**Ion-Controlled On-Off Switch of Electron Transfer from  
Tetrathiafulvalene Calix[4]pyrroles to  $\text{Li}^+@\text{C}_{60}$**



**Abstract:** Upon mixing  $\text{Li}^+@\text{C}_{60}$  and tetrathiafulvalene calix[4]pyrrole (PrS-TTF-C4P) in mixed solvent (benzonitrile:chloroform (v/v) = 1:1), no evidence of ET is observed because of one-electron oxidation potential of this TTF-C4P is higher than the one-electron reduction potential of  $\text{Li}^+@\text{C}_{60}$ . On the other hand, the addition of tetra-*n*-hexylammonium chloride to this solution of PrS-TTF-C4P and  $\text{Li}^+@\text{C}_{60}$  induces electron transfer from the PrS-TTF-C4P to the  $\text{Li}^+@\text{C}_{60}$  by binding of  $\text{Cl}^-$  to the calix[4]pyrrole moiety. As a definitive evidence of ET, the structure of ET product was obtained by X-ray crystal analysis. When tetraethylammonium chloride was added to the ET products produced from PrS-TTF-C4P and  $\text{Li}^+@\text{C}_{60}$  in the presence of THACl in this solution, the absorbance due to  $\text{Li}^+@\text{C}_{60}^-$  was seen to decrease as a function of increasing TEACl concentration. The  $\text{TEA}^+$  is known to bind effectively to the PrS-TTF-C4P cavity, thereby repelling  $\text{Li}^+@\text{C}_{60}^-$  from the cavity. This expulsion results in back electron transfer from  $\text{Li}^+@\text{C}_{60}^-$  to PrS-TTF-C4P $^{+}$  to produce the original  $\text{Li}^+@\text{C}_{60}$  and the  $\text{TEA}^+$ -encapsulated form of PrS-TTF-C4P.

## Introduction

Supramolecular complexes of  $C_{60}$  with electron donor hosts have attracted significant attention because of the their ability to promote efficient photoinduced electron transfer and thus advance potential applications involving energy conversion, including organic solar cells.<sup>1-8</sup> One of the current challenges involves extending this chemistry into the realm of thermal, or non-photoinduced electron transfer reactions. For these latter studies to be most informative, a combination of solution phase electron transfer studies and solid state structural analyses is likely to be required. There are many examples of X-ray crystal structures of supramolecular complexes of  $C_{60}$ .<sup>9-11</sup> In most cases, however, complete electron transfer (ET) from electron rich hosts (acting as donors) to the bound  $C_{60}$  (acting as an acceptor) is only made possible by photoirradiation.<sup>1-8</sup> The lack of complete ET conversion in the absence of a photoinduced process reflects the fact that in the ground state  $C_{60}$  is not a sufficiently strong electron acceptor to support a thermal electron transfer reaction unless very strong electron donors are employed.<sup>12,13</sup> Recently  $Li^+@C_{60}$  has been reported to act as a more effective electron acceptor than pristine  $C_{60}$ .<sup>14</sup> However, to my knowledge, there have been no reports of supramolecular complexes of  $Li^+@C_{60}$ .

I report here the formation of supramolecular complexes of  $Li^+@C_{60}$  with two tetrathiafulvalene calix[4]pyrrole (TTF-C4P) donors<sup>15</sup> and show that the judicious addition of anions or cations allows to control the direction of the resulting ground state (thermal) electron transfer process.<sup>16</sup> The single crystal X-ray structure of one radical ion pair complex,  $Li^+@C_{60}^-/PrS-TTF-C4P^+/Cl^-$  derived from PrS-TTF-C4P (Figure 1), has been determined. It reveals a 1:1 binding stoichiometry in the solid state. This stands in contrast to what was inferred in previous studies of  $C_{60}$  and PrS-TTF-C4P.<sup>17</sup>

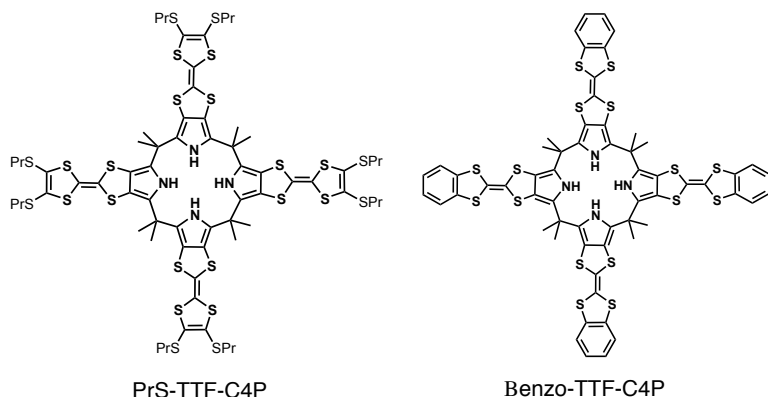


**Figure 1.** Structures of TTF-C4P derivatives (PrS-TTF-C4P and Benzo-TTF-C4P).

## Experimental Section

**Materials and General Methods.**  $\text{Li}^+@\text{C}_{60} \text{ PF}_6^-$  (98% purity) was obtained from Daiichi Jitsugyo Co., Ltd. All of the other reagents used in the syntheses were obtained from Aldrich Chemicals and Tokyo Chemical Industry Co., Ltd. These reagents were of the best available purity and used without further purification. Benzonitrile (PhCN) was purified according to literature procedures<sup>18</sup> and distilled over  $\text{P}_2\text{O}_5$  under Ar prior to use. Vis–NIR spectra were recorded using a SHIMADZU UV-3100PC spectrophotometer with a quartz cuvette (path length = 10 mm) at 298 K.

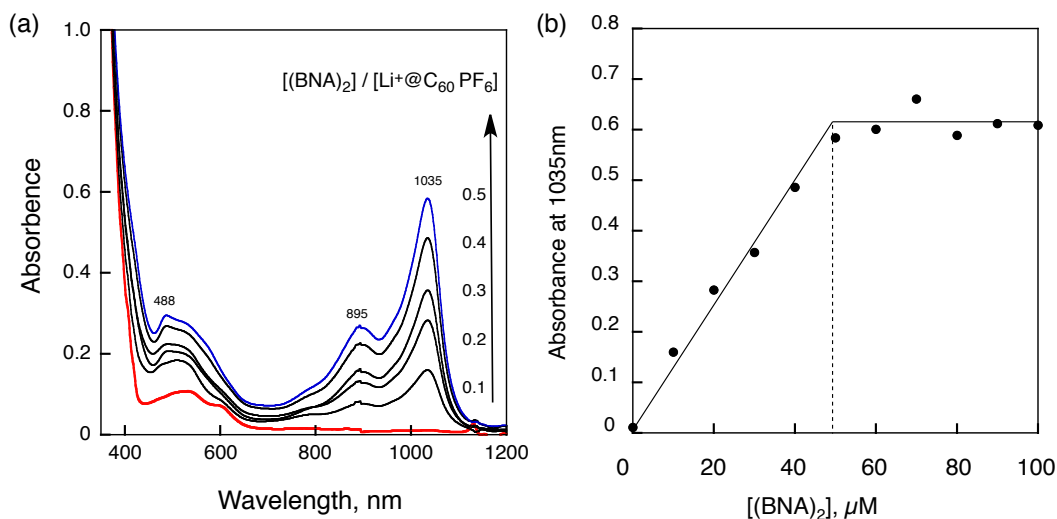
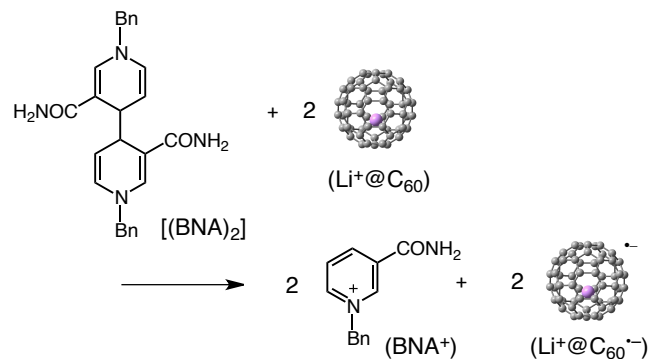
**Electrochemical Measurements.** Electrochemical measurements were performed on an ALS630B electrochemical analyzer in deaerated solvent containing 0.1 M  $\text{Bu}_4\text{NPF}_6$  as the supporting electrolyte at 298 K. A conventional three-electrode cell was used with a platinum or gold working electrode (surface area of 0.3 mm<sup>2</sup>) and a platinum wire as a counter electrode. The platinum working electrodes (BAS) were routinely polished with BAS polishing alumina suspension and rinsed with acetone and acetonitrile before use. The measured potentials were recorded with respect to an  $\text{Ag}/\text{AgNO}_3$  (0.01 M) reference electrode. All potentials (vs  $\text{Ag}/\text{Ag}^+$ ) were converted to values vs SCE by adding 0.29 V.<sup>19</sup> All electrochemical measurements were carried out under an Ar atmosphere.

**EPR Measurements.** The EPR spectra were taken on a JEOL X-band spectrometer (JES-RE1XE) under non-saturating microwave power conditions (1.0 mW) operating at 9.2 GHz. The magnitude of the modulation was chosen to optimize the resolution and the signal to noise ratio (S/N) of the observed spectrum (modulation width, 20 G; modulation frequency, 100 kHz). The *g* values were calibrated using an  $\text{Mn}^{2+}$  marker.

## Results and discussion

It is known that thermal electron transfer from 1-benzyl-1,4-dihydronicotinamide dimer  $[(\text{BNA})_2]$ , which can act as a two-electron donor,<sup>20</sup> to pristine  $\text{C}_{60}$  does not take place in benzonitrile (PhCN). However, photoinduced electron transfer occurs to produce  $\text{BNA}^+$  and two equiv of  $\text{C}_{60}^{\bullet-}$ .<sup>21</sup> In contrast, in the case of  $\text{Li}^+@\text{C}_{60} \text{ PF}_6^-$ , thermal electron transfer occurs efficiently in PhCN to produce  $\text{BNA}^+$  and two equiv of  $\text{Li}^+@\text{C}_{60}^{\bullet-}$  (Scheme 1). The absorption spectrum of  $\text{Li}^+@\text{C}_{60}^{\bullet-}$  produced as the result of this ET process is shown in Figure 2a. The absorption maximum ( $\lambda_{\text{max}} = 1035$  nm) is blue-shifted relative to that of anionic  $\text{C}_{60}^{\bullet-}$  ( $\lambda_{\text{max}} = 1080$  nm).<sup>19</sup> A spectral titration (Figure 2b) provided support for the stoichiometry proposed in

---

**Scheme 1**

**Figure 2.** (a) Vis–NIR spectra of  $Li^+@C_{60}^-$  produced via electron transfer from  $(BNA)_2$  to  $Li^+@C_{60} PF_6^- (1.0 \times 10^{-4} M)$  in PhCN. (b) Plot of absorbance at 1035 nm due to  $Li^+@C_{60}^-$  vs concentration of  $(BNA)_2$  corresponding to electron transfer from  $(BNA)_2$  to  $Li^+@C_{60} PF_6^- (1.0 \times 10^{-4} M)$  in PhCN at 298 K.

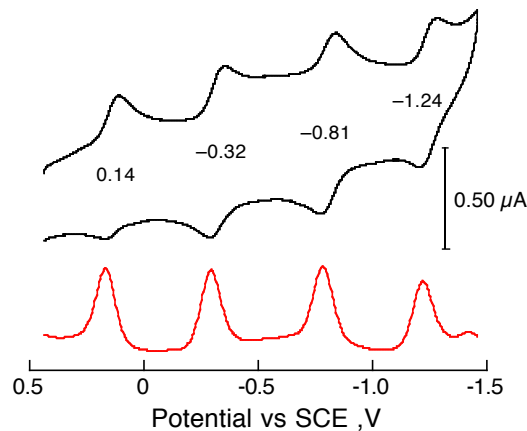
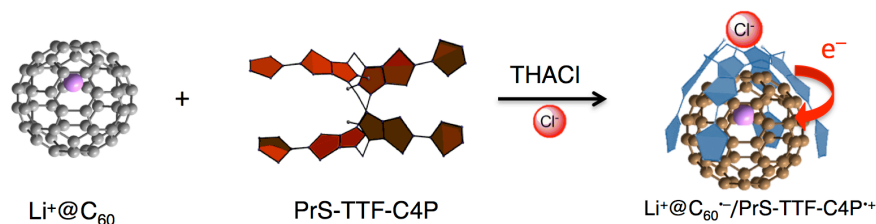


**Figure 3.** Cyclic voltammogram (CV, black) and differential pulse voltammogram (DPV, red) of  $Li^+@C_{60} PF_6^- (1.0 \times 10^{-4} M)$  recorded in PhCN containing 0.10 M tetra-*n*-butylammonium hexafluorophosphate (TBAPF<sub>6</sub>).

Scheme 1. The stronger electron-accepting ability of  $\text{Li}^+@\text{C}_{60}$  was confirmed by cyclic voltammogram (CV) and differential pulse voltammogram (DPV) experiments, as shown in Figure 3. The first one-electron reduction potential of  $\text{Li}^+@\text{C}_{60} \text{PF}_6^-$  was determined to be 0.14 V (vs SCE), which is positively shifted by +0.57 V compared to  $\text{C}_{60}$ .<sup>21,22</sup>

When PrS-TTF-C4P and  $\text{Li}^+@\text{C}_{60} \text{PF}_6^-$  were mixed in mixed solvent (benzonitrile:chloroform (v/v) = 1:1), no evidence of electron transfer is observed, a finding ascribed to the fact that the one-electron oxidation potential of this TTF-C4P ( $E_{\text{ox}} = 0.51$  V vs SCE) is higher than the one-electron reduction potential of  $\text{Li}^+@\text{C}_{60}$  (0.14 V vs SCE; *cf.* Figure 3). On the other hand, the addition of tetra-*n*-hexylammonium chloride (THACl) to solution of PrS-TTF-C4P and  $\text{Li}^+@\text{C}_{60}$  induces electron transfer from the PrS-TTF-C4P donor to the  $\text{Li}^+@\text{C}_{60}$  acceptor, as inferred from the appearance of an absorption band at 1035 nm ascribable to the reduced, neutral  $\text{Li}^+@\text{C}_{60}^{\cdot-}$  species (see Figure 4a). The absorbance at 1035 nm increases with increasing THACl concentration to reach a constant value at the point where electron transfer is deemed complete (*ca.* 10 equiv). It is known that  $\text{Cl}^-$  binds to PrS-TTF-C4P to induce a conformation change from the so-called 1,3-alternate (Scheme 2, left) to the cone conformation (Scheme 2, right) due to concerted NH-anion hydrogen bonding interactions.<sup>16</sup> Such a conformation change makes it possible to stabilize the radical ion pair involving the PrS-TTF-C4P<sup>+</sup> host and the bound  $\text{Li}^+@\text{C}_{60}^{\cdot-}$  guest. On the basis of a spectral titration that could be fit to a 1:1 binding profile, the binding constant corresponding to the interaction of  $\text{Cl}^-$  to PrS-TTF-C4P in mixed solvent was determined to be *ca.*  $1.9 \times 10^4 \text{ M}^{-1}$  (Figure 4b).

**Scheme 2**



It is noteworthy that the proposed ET event did not give rise to a broad NIR absorption band. Such a band would be expected if the oxidized donor, PrS-TTF-C4P<sup>+</sup>, were produced as a free radical cation due to the internal formation of a  $\pi$ -dimer radical cation involving an oxidized TTF<sup>+</sup> moiety and a neutral TTF subunit likewise present in PrS-TTF-C4P<sup>+</sup>.<sup>10</sup> The absence of a broad NIR feature thus suggests that the oxidized host, PrS-TTF-C4P<sup>+</sup>, interacts strongly with the reduced  $\text{Li}^+@\text{C}_{60}^{\cdot-}$  guest to produce an overall neutral complex,  $\text{Li}^+@\text{C}_{60}^{\cdot-}/\text{PrS-TTF-C4P}^+/\text{Cl}^-$ .

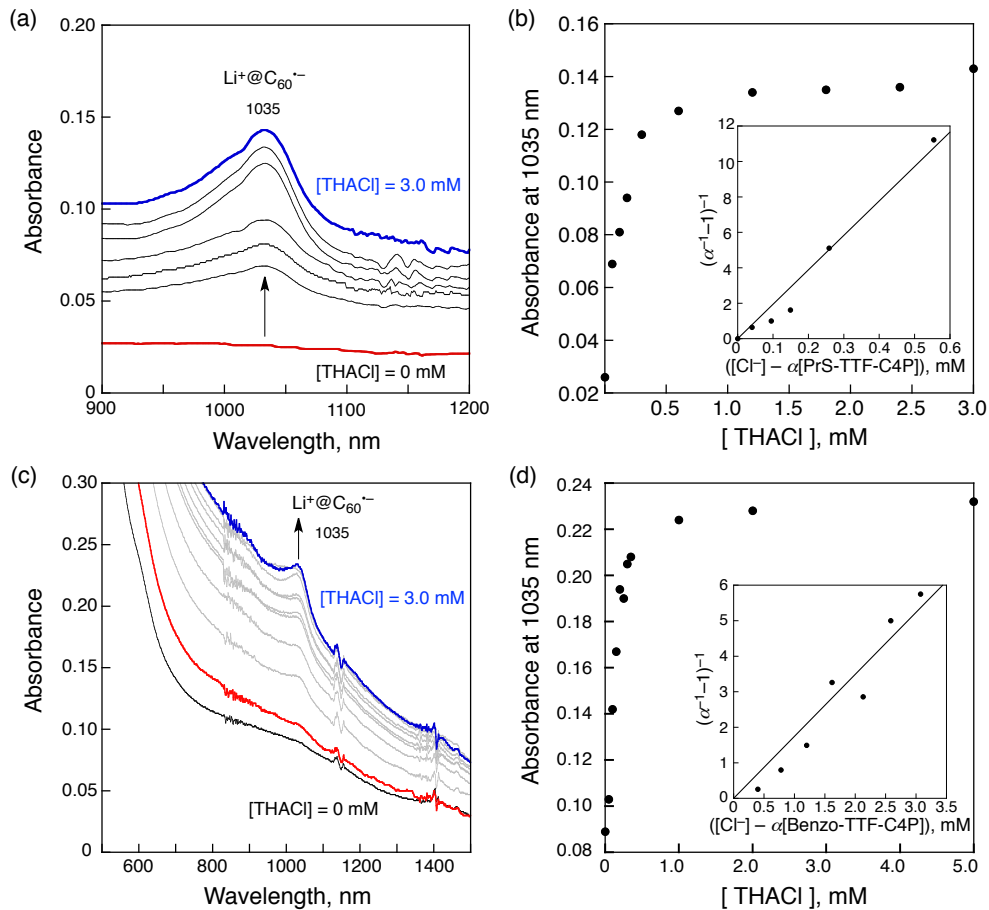


**Figure 4.** NIR absorption spectral change in  $\text{Cl}^-$ -promoted electron transfer from (a) PrS-TTF-C4P, (c) Benzo-TTF-C4P ( $5.0 \times 10^{-5}$  M) to  $\text{Li}^+@\text{C}_60$  ( $5.0 \times 10^{-5}$  M) in the presence of increasing concentrations of THACl in mixed solvent. Plot of absorbance at 1035 nm vs concentration of  $\text{Cl}^-$ . Inset: Plot used to determine the approximate binding constant for the interaction of  $\text{Cl}^-$  with (b) PrS-TTF-C4P, (d) Benzo-TTF-C4P in mixed solvent at 298 K;  $\alpha = (A - A_0)/(A_\infty - A_0)$ .

The EPR spectrum recorded after the proposed electron transfer from PrS-TTF-C4P to  $\text{Li}^+@\text{C}_60$  in the presence of  $\text{Cl}^-$  is shown in Figure 5a. Here, the four-line signal is ascribed to the  $\text{PrS-TTF-C4P}^{+}$  radical cation in which electron spin is localized at only one TTF moiety ( $a_N = 0.91$  G;  $a_H = 1.10$  G determined by computer simulation, values that are consistent with those predicted by DFT calculations: see Figure 6), rather than delocalized within a  $\pi$ -dimer radical cation complex (formed by reaction with another TTF moiety). The localized nature of this spin density is thus consistent with the suggested inclusion of the reduced  $\text{Li}^+@\text{C}_60^-$  guest within the cavity present in the cone conformation of  $\text{PrS-TTF-C4P}^{+}$ , since such a binding mode would preclude the  $\pi$ - $\pi$  interaction between oxidized and neutral TTF moieties required to stabilize a  $\pi$ -dimer radical cation. Unfortunately, an EPR signal ascribable to  $\text{Li}^+@\text{C}_60^-$  could not be

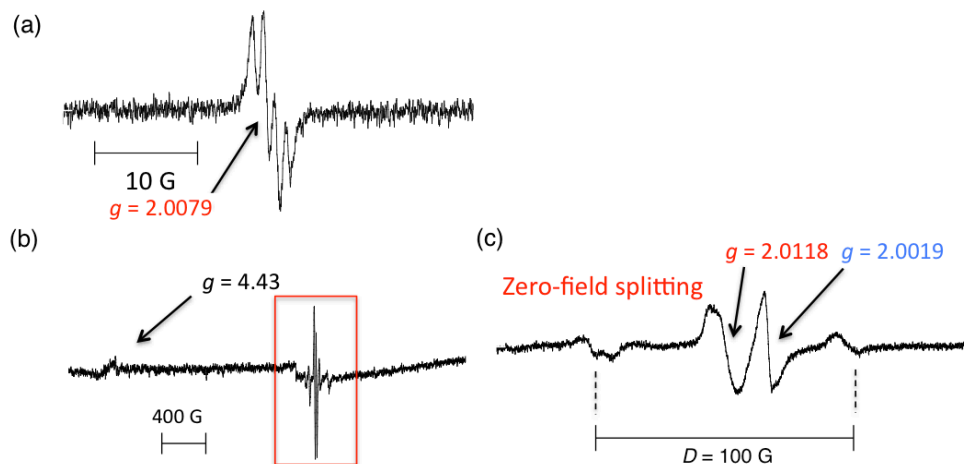


**Figure 5.** (a) EPR spectrum of the products of electron transfer from PrS-TTF-C4P ( $5.0 \times 10^{-5}$  M) to  $\text{Li}^+@\text{C}_{60}$  ( $5.0 \times 10^{-5}$  M) in the presence of TEACl ( $3.0 \times 10^{-4}$  M) in mixed solvent at 298 K. (b) EPR spectrum of the radical ion pair (PrS-TTF-C4P $^+$ /Li $^+@\text{C}_{60}^-$ ) at 77 K. (c) Expanded view of the magnetic field region highlighted by the red rectangular frame in (b).

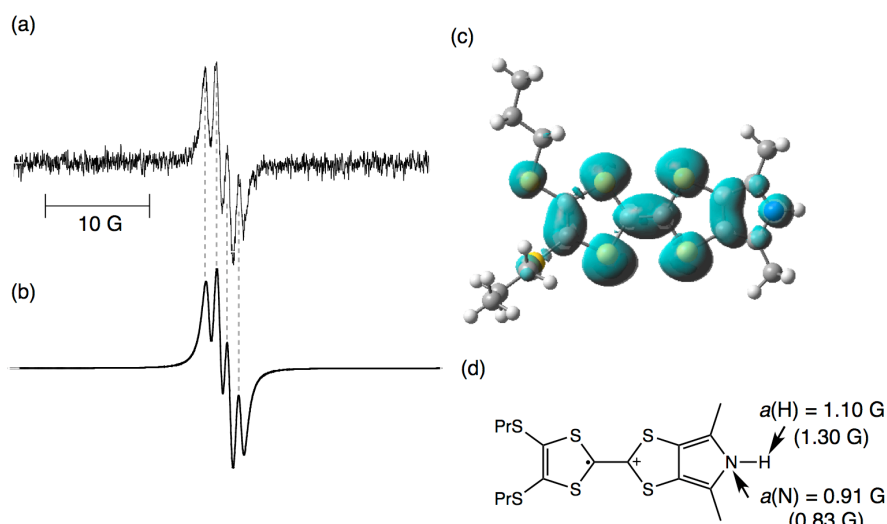


**Figure 6.** (a) EPR spectrum of the products of electron transfer from PrS-TTF-C4P ( $5.0 \times 10^{-5}$  M) to  $\text{Li}^+@\text{C}_{60}$  ( $5.0 \times 10^{-5}$  M) in the presence of TEACl ( $3.0 \times 10^{-4}$  M) in mixed solvent at 298 K. (b) Computer simulated spectrum with  $a(\text{H}) = 1.10$  G,  $a(\text{N}) = 0.91$  and  $H_{\text{msl}} = 0.60$  G. (c) Spin distribution of a TTF monomer radical cation calculated by DFT with the UB3LYP/6-31+G(d,p) basis set. (d) Hyperfine coupling constants determined from the computer simulation. The values in parenthesis are determined from DFT with the UB3LYP/6-31+G(d,p) basis set.

observed; presumably, this reflects a short relaxation time for this latter species in solution at 298 K. When the EPR spectrum was taken at 77 K, however, the triplet signal at  $g = 4.43$  is clearly observed in Figure 5b together with the fine structure in Figure 5c. From the zero-field splitting value ( $D = 100$  G), the distance ( $r$ ) between two electron spins was estimated to be 6.5 Å using

the relation,  $D = 27800/r^3$ .<sup>16</sup> This  $r$  value is consistent with the distance between  $\text{PrS-TTF-C4P}^+$  and  $\text{Li}^+@\text{C}_{60}^{\bullet-}$  expected to pertain in the intra-complex radical ion pair (Scheme 2).

In the case of Benzo-TTF-C4P, the addition of  $\text{Cl}^-$  (as the  $\text{THA}^+$  salt) to the solution of this host and  $\text{Li}^+@\text{C}_{60}$  again produced a radical ion pair created from the oxidized host (Benzo-TTF-C4P $^+$ ) and the reduced guest ( $\text{Li}^+@\text{C}_{60}^{\bullet-}$ ). The binding constant corresponding to the interaction of  $\text{Cl}^-$  with Benzo-TTF-C4P was found to be essentially the same as that for  $\text{PrS-TTF-C4P}$  ( $1.7 \times 10^4 \text{ M}^{-1}$  vs  $1.9 \times 10^4 \text{ M}^{-1}$ ; Figure 4d).

The formation of the radical ion pair between Benzo-TTF-C4P $^+$  and  $\text{Li}^+@\text{C}_{60}^{\bullet-}$  affects the one-electron redox potential of each component as shown in Figure 7. The one-electron reduction potential of  $\text{Li}^+@\text{C}_{60}$  ( $E_{\text{red}} = 0.12 \text{ V}$  vs SCE) in the absence of  $\text{Cl}^-$  is shifted to  $0.26 \text{ V}$  vs SCE in the presence of  $\text{Cl}^-$  ( $0.10 \text{ M}$ ), when the radical ion pair is formed. The one-electron oxidation potential of Benzo-TTF-C4P ( $E_{\text{ox}} = 0.55 \text{ V}$  vs SCE) was also shifted to  $0.68 \text{ V}$  vs SCE. Such shifts in the  $E_{\text{red}}$  value for  $\text{Li}^+@\text{C}_{60}$  and the  $E_{\text{ox}}$  of Benzo-TTF-C4P are thought to reflect a strong interaction between the cobound Benzo-TTF-C4P $^+$  and  $\text{Li}^+@\text{C}_{60}^{\bullet-}$ .

Definitive evidence for the formation of a supramolecular complex between the chloride anion-bound form of  $\text{PrS-TTF-C4P}^+$  and  $\text{Li}^+@\text{C}_{60}^{\bullet-}$  in the solid state was obtained from a single-crystal X-ray diffraction analysis of a mixture consisting of  $\text{PrS-TTF-C4P}$ , tetra-*n*-butylammonium chloride (TBACl), and  $[\text{Li}^+@\text{C}_{60}]^+\text{PF}_6^-$  dissolved in  $\text{CH}_2\text{Cl}_2$  and subjected

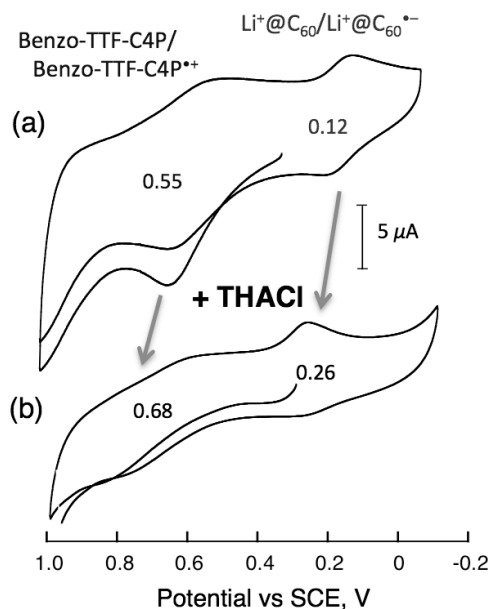


**Figure 7.** Cyclic voltammograms of Benzo-TTF-C4P and  $\text{Li}^+@\text{C}_{60}$  recorded (a) without THACl in the presence of  $0.10 \text{ M}$  TBAPF $_6$  and (b) with THACl ( $0.10 \text{ M}$ ) in mixed solvent; working electrode: Au, counter electrode: Pt; sweep rate:  $100 \text{ mV s}^{-1}$ .

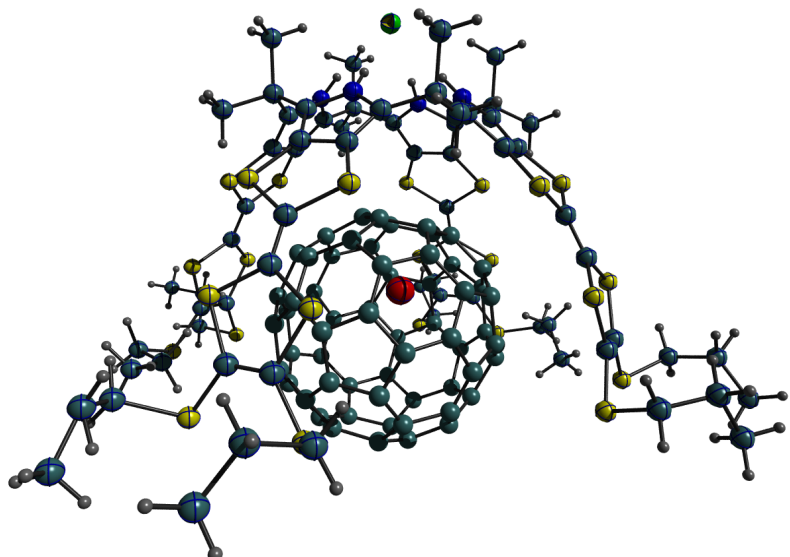


**Figure 8.** Single crystal X-ray structure of the product of electron transfer from PrS-TTF-C4P to  $\text{Li}^+@\text{C}_{60}$  in the presence of THACl in mixed solvent. Note that the  $\text{Li}^+$  cation is disordered over two positions but is seen in the difference map. Disordered solvent molecules have been removed for clarity. However, no other charged species are seen in the crystal lattice. Alternate views and other data are shown in Supporting Information.

to slow diffusion with hexanes. The resulting structure (Figure 8) reveals the expected cone conformation for the  $\text{Cl}^-$ -bound TTF-C4P moiety, a bowl-like species that tightly encapsulates a  $\text{Li}^+@\text{C}_{60}^{\bullet-}$  guest to form an overall neutral 1:1 complex, as inferred from the absence of any additional charged species within the crystalline lattice (*e.g.*,  $\text{TBA}^+$  or  $\text{PF}_6^-$ ). On the basis of the structural parameters, the complex in question is a tightly coupled 1:1 radical ion pair consisting of  $\text{PrS-TTF-C4P}^{\bullet+}$  and  $\text{Li}^+@\text{C}_{60}^{\bullet-}$ .

The 1:1 stoichiometry observed in the case of  $\text{Li}^+@\text{C}_{60}^{\bullet-}/\text{PrS-TTF-C4P}^{\bullet+}/\text{Cl}^-$  stands in sharp contrast to the 2:1 ET complex formed between  $\text{PrS-TTF-C4P}^{\bullet+}$  and the one-electron-reduced species generated by chloride-induced thermal electron transfer to a dicationic bisimidazolium quinone ( $\text{BIQ}^{\bullet+}$ ) acceptor.<sup>16</sup> Presumably, this stoichiometric difference reflects the fact that the  $\text{BIQ}^{\bullet+}$ , a species considerably larger than  $\text{Li}^+@\text{C}_{60}^{\bullet-}$ , is better encapsulated by two TTF-C4P moieties (one oxidized and one reduced) acting in concert. The present 1:1 stoichiometry also calls into question the original suggestion that PrS-TTF-C4P forms a 2:1 (receptor-fullerene) complex with  $\text{C}_{60}$ .<sup>17</sup>

When tetraethylammonium chloride (TEACl) was added to the ET products produced from PrS-TTF-C4P and  $\text{Li}^+@\text{C}_{60}$  in the presence of THACl in mixed solvent, the absorbance at 1035 nm due to  $\text{Li}^+@\text{C}_{60}^{\bullet-}$  was seen to decrease as a function of increasing TEACl concentration. The  $\text{TEA}^+$  cation is known to bind effectively to the PrS-TTF-C4P cavity,<sup>16</sup> thereby repelling

$\text{Li}^+@\text{C}_{60}^{\bullet-}$  from the cavity. This expulsion results in back-ET from  $\text{Li}^+@\text{C}_{60}^{\bullet-}$  to  $\text{PrS-TTF-C4P}^{\bullet+}$  to produce the original  $\text{Li}^+@\text{C}_{60}$  cation and the  $\text{TEA}^+$ -encapsulated form of  $\text{PrS-TTF-C4P}$  as shown in Scheme 3. The effective binding constant of  $\text{TEA}^+$  to  $\text{PrS-TTF-C4P}$ , corresponding to

**Scheme 3**

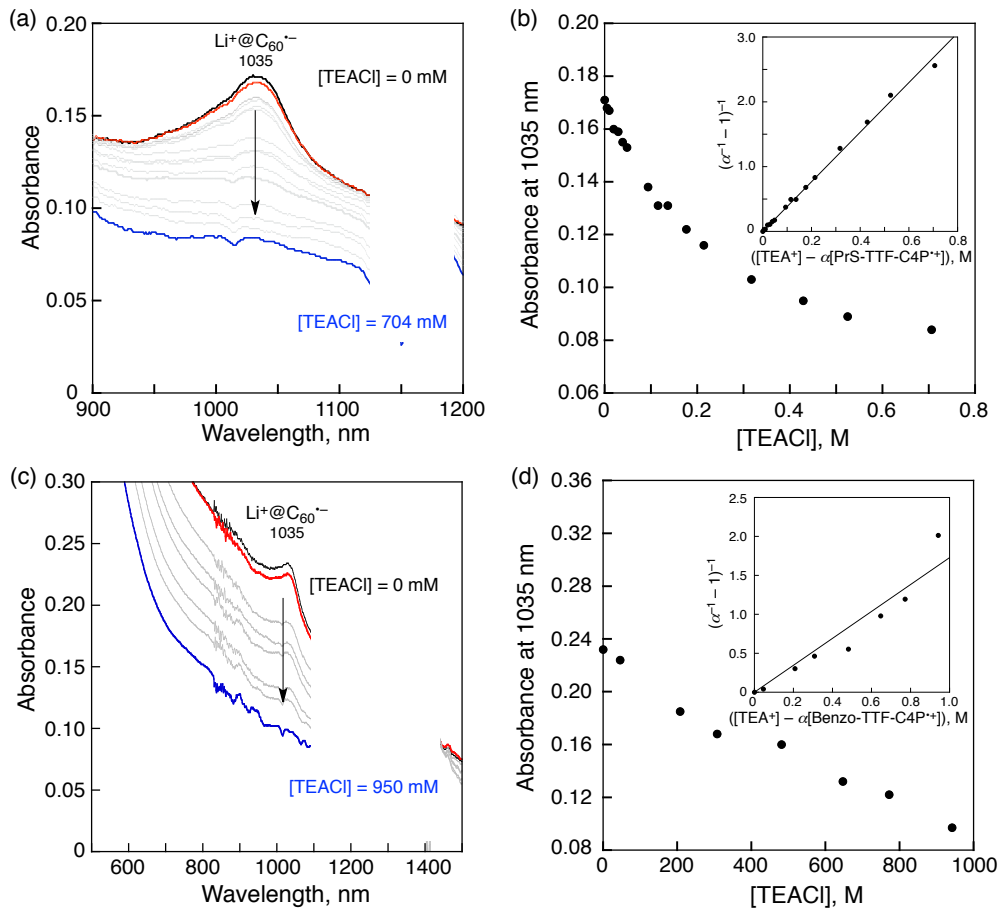
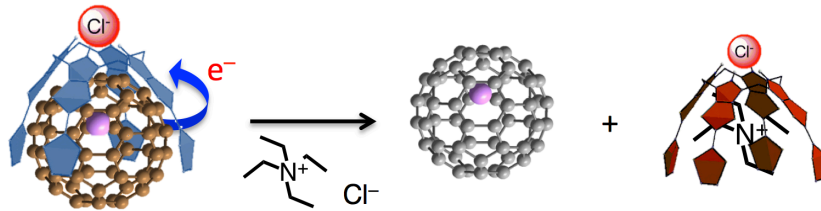


**Figure 9.** NIR spectral changes corresponding to the  $\text{TEA}^+$ -promoted back electron transfer from  $\text{Li}^+@\text{C}_{60}^{\bullet-}$  to (a)  $\text{PrS-TTF-C4P}^{\bullet+}$ , (c)  $\text{Benzo-TTF-C4P}^{\bullet+}$  within the originally formed radical ion pair ( $5.0 \times 10^{-5}$  M) in the presence of various concentrations of TEACl in mixed solvent. Change in absorbance at 1035 nm seen upon the addition of increasing concentrations of TEACl to a preformed mixture of (b)  $\text{PrS-TTF-C4P}^{\bullet+}$ , (d)  $\text{Benzo-TTF-C4P}^{\bullet+}$ ,  $\text{Li}^+@\text{C}_{60}$  and THACl in mixed solvent. Inset: Plot for determination of the binding constant for the interaction of TEACl with TTF-C4P;  $\alpha = (A - A_0)/(A_\infty - A_0)$ .

the displacement of  $\text{Li}^+@\text{C}_{60}^{\bullet-}$  by  $\text{TEA}^+$  under these conditions was found to be *ca.*  $3.8 \text{ M}^{-1}$ , as determined from the decrease in absorbance at 1035 nm as a function of [TEACl] (Figure 9c and 9d). Similar results were found in the case of the analogous Benzo-TTF-C4P/ $\text{Li}^+@\text{C}_{60}$ /THACl ET system. However, the effective binding constant for TEACl,  $1.7 \text{ M}^{-1}$ , was found to be smaller than in the case of PrS-TTF-C4P (*cf.* Figure 9a and 9b).

## Conclusion

Electron transfer from TTF-C4P to  $\text{Li}^+@\text{C}_{60}$  is switched on by the addition of  $\text{Cl}^-$  to produce the 1:1 radical ion pair between  $\text{TTF-C4P}^+$  and  $\text{Li}^+@\text{C}_{60}^{\bullet-}$ , whereas it is switched off by the addition of  $\text{TEA}^+$ . This ability to control thermal electron transfer via the appropriate choice of receptor, substrate, and adjuvant (TTF-C4P,  $\text{Li}^+@\text{C}_{60}$ , and  $\text{Cl}^-$  or  $\text{TEA}^+$  in the present instance) has important implications for the design of new charge storage devices, including perhaps the development of new organic batteries.

## References

- (1) (a) Guldi, D. *Phys. Chem. Chem. Phys.* **2007**, *9*, 1400–1420. (b) Guldi, D. M. *Chem. Soc. Rev.* **2002**, *31*, 22–36.
- (2) (a) D’Souza, F.; Ito, O. *Chem. Commun.* **2009**, 4913–4928. (b) F. D’Souza, F.; Ito, O. *Coord. Chem. Rev.* **2005**, *249*, 1410–1422.
- (3) (a) Hasobe, T.; Imahori, H.; Kamat, P. V.; Ahn, T. K.; Kim, S. K.; Kim, D.; Fujimoto, A.; Hirakawa, T.; Fukuzumi, S. *J. Am. Chem. Soc.* **2005**, *127*, 1216–1228. (b) Hasobe, T.; Saito, K.; Kamat, P. V.; Troiani, V.; Qiu, H.; Solladie, N.; Kim, K. S.; Park, J. K.; Kim, D.; D’Souza, F.; Fukuzumi, S. *J. Mater. Chem.* **2007**, *17*, 4160–4170.
- (4) Gust, D.; Moore, T. A.; Moore, A. L. *Acc. Chem. Res.* **2001**, *34*, 40–48.
- (5) (a) Fukuzumi, S.; Honda, T.; Ohkubo, K.; Kojima, T. *Dalton Trans.* **2009**, 3880–3890. (b) Fukuzumi, S. *Phys. Chem. Chem. Phys.* **2008**, *10*, 2283–2297. (b) Fukuzumi, S.; Kojima, T. *J. Mater. Chem.* **2008**, *18*, 1427–1439.
- (6) Babu, S. S.; Möhwald, H.; Nakanishi, T. *Chem. Soc. Rev.* **2010**, *39*, 4021–4035.
- (7) (a) Sánchez, L.; Otero, R.; Gallego, J. M.; Miranda, R.; Martíín, N. *Chem. Rev.* **2009**, *109*, 2081–2091. (b) Bonifazi, D.; Engerc, O.; Diederich, F. *Chem. Soc. Rev.* **2007**, *36*, 390–414.
- (8) (a) Matsuo, Y.; Nakamura, E. *Chem. Rev.* **2008**, *108*, 3016–3028. (b) Matsuo, Y.; Sato, Y.;

Niinomi, T.; Soga, I.; Tanaka, H.; Nakamura, E. *J. Am. Chem. Soc.* **2009**, *131*, 16048–16050.

(9) (a) Tashiro, K.; Aida, T. *Chem. Soc. Rev.* **2007**, *36*, 189–197. (b) Zheng, J. -Y.; Tashiro, K.; Hirabayashi, Y.; Kinbara, K.; Saigo, K.; Aida, T.; Sakamoto, S.; Yamaguchi, K. *Angew. Chem., Int. Ed.* **2001**, *40*, 1857–1861. (c) Yamaguchi, T.; Ishii, N.; Tashiro, K.; Aida, T. *J. Am. Chem. Soc.* **2003**, *125*, 13934–13935.

(10) Boyd, P. D. W.; Reed, C. A. *Acc. Chem. Res.* **2005**, *38*, 235–242.

(11) (a) Nobukuni, H.; Tani, F.; Shimazaki, Y.; Naruta, Y.; Ohkubo, K.; Nakanishi, T.; Kojima, T.; Fukuzumi, S.; Seki, S. *J. Phys. Chem. C* **2009**, *113*, 19694–19699. (b) Nobukuni, H.; Shimazaki, Y.; Uno, H.; Naruta, Y.; Ohkubo, Kei; Kojima, T.; Fukuzumi, S.; Seki, S.; Sakai, H.; Hasobe, T.; Tani, F. *Chem.–Eur. J.* **2010**, *16*, 11611–11623.

(12) Konarev, D. V.; Khasanov, S. S.; Otsuka, A.; Maesato, M.; Saito, G.; Lyubovskaya, R. N. *Angew. Chem., Int. Ed.* **2010**, *49*, 4829–4832.

(13) Konarev, D. V.; Kuzmin, A. V.; Simonov, S. V.; Khasanov, S. S.; Evgeniya I. Yudanova, E. I.; Rimma N. Lyubovskaya, R. N. *Dalton Trans.* **2011**, *40*, 4453–4458.

(14) Aoyagi, S.; Nishibori, E.; Sawa, H.; Sugimoto, K.; Takata, M.; Miyata, Y.; Kitaura, R.; Shinohara, H.; Okada, H.; Sakai, T.; Ono, Y.; Kawachi, K.; Yokoo, K.; Ono, S.; Omote, K.; Kasama, Y.; Ishikawa, S.; Komuro, T.; Tobita, H. *Nature Chem.* **2010**, *2*, 678–683.

(15) (a) Nielsen, K. A.; Cho, W.-S.; Jeppesen, J. O.; Lynch, V. M.; Becher, J.; Sessler, J. L. *J. Am. Chem. Soc.* **2004**, *126*, 16296–16297. (b) Park, J. S.; Le Derf, F. Lynch, V. M.; Bejger, C. M.; Sessler, J. L.; Nielsen, K. A.; Johnsen, C.; Jeppesen, J. O. *Chem. –Eur. J.* **2010**, *16*, 848–854.

(16) Park, J. S.; Karnas, E.; Ohkubo, K.; Chen, P.; Kadish, K. M.; Fukuzumi, S.; Bielawski, C. W.; Hudnall, T. W.; Lynch, V. M.; Sessler, J. L. *Science* **2010**, *329*, 1324–1327.

(17) (a) Nielsen, K. A.; Cho, W.-S.; Sarova, G.; Petersen, B. M.; Bond, A. D.; Becher, J.; Jensen, F.; Guldi, D. M.; Sessler, J. L.; Jeppesen, J. O. *Angew. Chem., Int. Ed.* **2006**, *45*, 6848–6853. (b) Nielsen, K. A.; Martín-Gomis, L.; Sarova, G. H.; Sanguinet, L.; Gross, D. E.; Fernández-Lázaro, F.; Stein, P. C; Levillain, E.; Sessler, J. L.; Guldi, D. M.; Sastre-Santos, Á. Jeppesen, J. O. *Tetrahedron* **2008**, *64*, 8449–8463.

(18) *Purification of Laboratory Chemicals*; Armarego, W. L. F.; Perrin, D. D., Eds.; Pergamon Press: Oxford, 1997.

(19) Mann, C. K.; Barnes, K. K. *Electrochemical Reactions in Non-aqueous Systems*; Mercel Dekker: New York, 1970.

- (20) Fukuzumi, S.; Patz, M.; Suenobu, T.; Kuwahara, Y.; Itoh, S. *J. Am. Chem. Soc.* **1999**, *121*, 1605–1606.
- (21) Fukuzumi, S.; Suenobu, T.; Patz, M.; Hirasaka T.; Itoh, S.; Fujitsuka, M.; Ito, O. *J. Am. Chem. Soc.* **1998**, *120*, 8060–8068.
- (22) Echegoyen, L.; Echegoyen, L. E. *Acc. Chem. Res.* **1998**, *31*, 593–601.

## Supporting Information for Chapter 1

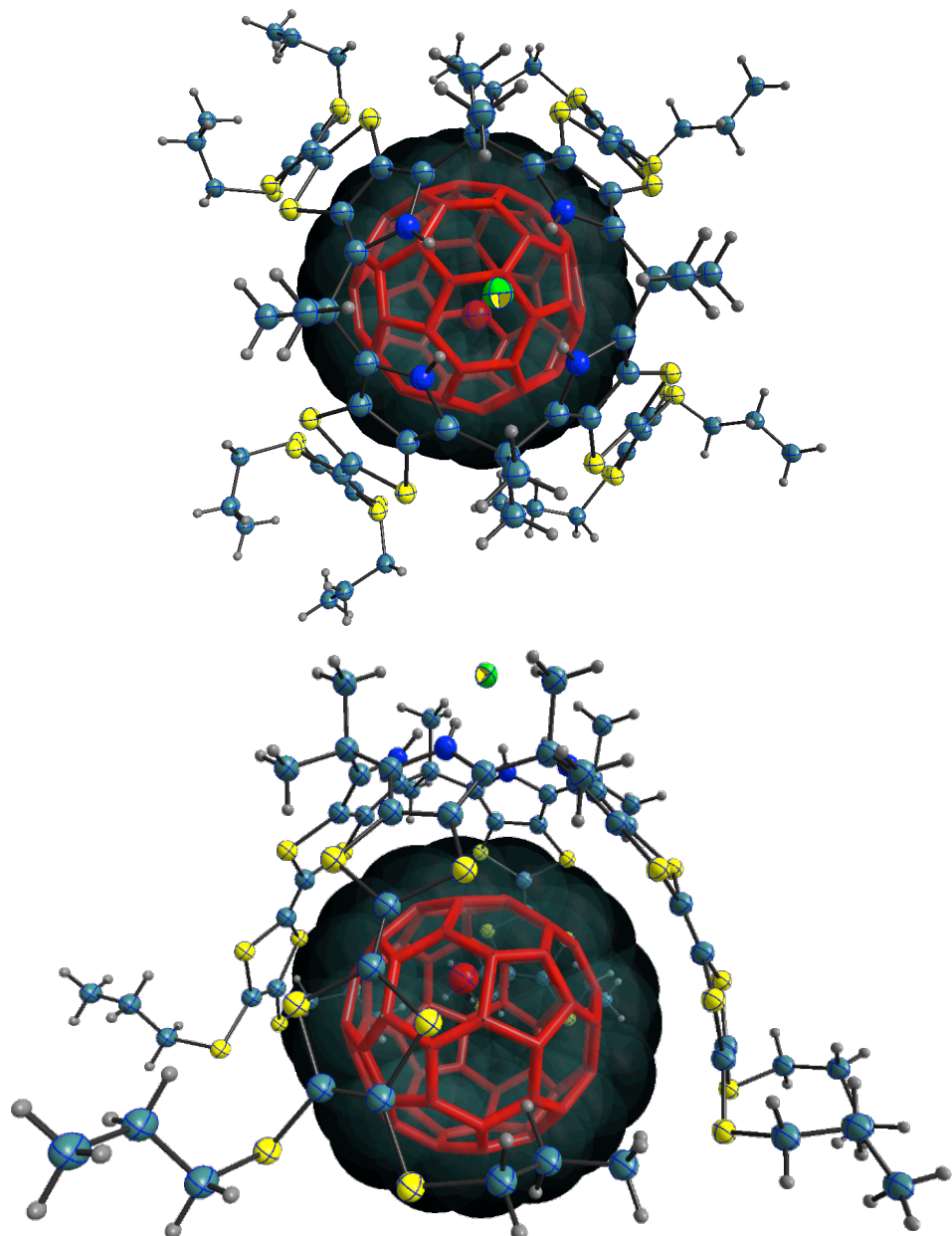


**Figure S1.** Alternate views of the single crystal X-ray structure of the product of electron transfer from PrS-TTF-C4P to  $\text{Li}^+@\text{C}_{60}$  in the presence of THACl in PhCN.

**X-ray Experimental for (C<sub>68</sub>H<sub>84</sub>N<sub>4</sub>S<sub>24</sub>) C<sub>60</sub> Li<sup>+</sup> Cl<sup>-</sup> - 2 CH<sub>2</sub>Cl<sub>2</sub>.** Crystals grew as black plates by slow evaporation from dichloromethane and hexanes. The data crystal was cut from a larger crystal and had approximate dimensions; 0.32 × 0.22 × 0.11 mm. The data were collected on a Rigaku SCX Mini diffractometer with a Mercury CCD using a graphite monochromator with MoK $\alpha$  radiation ( $\lambda = 0.71075 \text{ \AA}$ ). A total of 966 frames of data were collected using  $\omega$ -scans with a scan range of 0.5° and a counting time of 34 seconds per frame. The data were collected at 153 K using a Rigaku XStream low temperature device. Details of crystal data, data collection and structure refinement are listed in Table 1. Data reduction were performed using the Rigaku Americas Corporation's Crystal Clear version 1.40.<sup>1</sup> The structure was solved by direct methods using SIR97<sup>2</sup> and refined by full-matrix least-squares on  $F^2$  with anisotropic displacement parameters for the non-H atoms using SHELXL-97.<sup>3</sup> Structure analysis was aided by use of the programs PLATON98<sup>4</sup> and WinGX.<sup>5</sup> The hydrogen atoms were calculated in ideal positions with isotropic displacement parameters set to 1.2xUeq of the attached atom (1.5xUeq for methyl hydrogen atoms).

The C<sub>60</sub> molecule was disordered around the crystallographic mirror plane of symmetry at  $y = 1/4$ . The C<sub>60</sub> molecule has two different C-C bonds. One kind of bond is that fuses adjacent six membered rings. The second type involves fusion of five membered rings to six membered rings. The C<sub>60</sub> molecule was refined so that the bonds involving fusion of six membered rings were restrained to be equivalent and those involving fusion involving five membered rings to six membered rings were restrained to be equivalent. These geometric restraints were retained throughout the refinement procedure. In addition, the carbon atoms were refined with anisotropic displacement parameters restrained to be approximately isotropic.

One molecule of dichloromethane was disordered in the vicinity of the crystallographic mirror plane of symmetry at  $y = 1/4$ . One Cl atom resides on the mirror, Cl1a, while the carbon atom, C1aa, and the second Cl atom, Cl2a were slightly offset from the mirror. The geometry of the two orientations was restrained to be equal throughout the refinement. The site occupancy was fixed at 1/2 due to the mirror symmetry.

Additionally, two of the propyl side chains were also disordered as is common in these molecules. The disorder was modeled by assigning the variable x to the site occupancy for one orientation of the disordered atoms and (1-x) to the site occupancy factors for the alternate orientation. The geometry of this group was restrained to have equivalent C-Cl bonds.

A molecule of what appeared to be dichloromethane was found to be badly disordered. Attempts to model the disorder were unsatisfactory. The contributions to the scattering factors

due to this solvent molecule were removed by use of the utility SQUEEZE<sup>6</sup> in PLATON98.<sup>6</sup> PLATON98 was used as incorporated in WinGX.<sup>5</sup>

The function,  $\Sigma w(|F_o|^2 - |F_c|^2)^2$ , was minimized, where  $w = 1/[(\sigma(F_o))^2 + (0.0967*P)^2]$  and  $P = (|F_o|^2 + 2|F_c|^2)/3$ .  $R_w(F^2)$  refined to 0.192, with  $R(F)$  equal to 0.0710 and a goodness of fit,  $S$ , = 1.28. Definitions used for calculating  $R(F)$ ,  $R_w(F^2)$  and the goodness of fit,  $S$ , are given below.<sup>6</sup> The data were checked for secondary extinction effects but no correction was necessary. Neutral atom scattering factors and values used to calculate the linear absorption coefficient are from the International Tables for X-ray Crystallography (1992).<sup>7</sup> All figures were generated using SHELXTL/PC.<sup>8</sup> Tables of positional and thermal parameters, bond lengths and angles, torsion angles and supplementary X-ray figures showing partial atom labeling (Figure S2) and the thermal ellipsoids scaled to the 30% probability level (Figure S3) are given below.

## References for X-ray Structure Determination

- (1) Otwinowski, Z.; Minor, W. Processing of X-ray Diffraction Data Collected in Oscillation Mode. *Methods in Enzymology*; Carter, C. W., Jr., Sweet, R. M., Eds.; Academic Press: New York, 1997; Vol. 276, Macromolecular Crystallography, Part A, pp 307–326.
- (2) Altomare, A.; Burla, M. C.; Camalli, M.; Cascarano, G. L.; Giacovazzo, C.; Guagliardi, A.; Moliterni, A. G. G.; Polidori, G.; Spagna, R. *J. Appl. Crystallogr.* **1999**, *32*, 115-119.
- (3) Sheldrick, G. M. *SHELXL-97 Program for the Refinement of Crystal Structures*; University of Göttingen: Göttingen, Germany, 1997.
- (4) Spek, A. L. *PLATON, A Multipurpose Crystallographic Tool*; Utrecht University: The Netherlands, 1998.
- (5) (a) Farrugia, L. J. *WinGX an Integrated System of Windows Programs for the Solution, Refinement and Analysis of Single Crystal X-Ray Diffraction Data, version 1.64*; University of Glasgow: Glasgow, U.K., 1999–2003. (b) Farrugia, L. J. *J. Appl. Crystallogr.* **1999**, *32*, 837-838.
- (6) Sluis, P. v. d.; Spek, A. L. *Acta Cryst.* **1990**, *A46*, 194-201.
- (7)  $R_w(F^2) = \{\Sigma w(|F_o|^2 - |F_c|^2)^2 / \Sigma w(|F_o|)^4\}^{1/2}$  where  $w$  is the weight given each reflection.  
 $R(F) = \Sigma(|F_o| - |F_c|) / \Sigma |F_o|$  for reflections with  $F_o > 4(\sigma(F_o))$ .  
 $S = [\Sigma w(|F_o|^2 - |F_c|^2)^2 / (n - p)]^{1/2}$ , where  $n$  is the number of reflections and  $p$  is the number of refined parameters.
- (8) *International Tables for X-ray Crystallography*; Wilson, A. J. C., Ed.; Kluwer Academic Press: Boston, 1992; Vol. C, Tables 4.2.6.8 and 6.1.1.4.

---

(9) Sheldrick, G. M. *SHELXTL/PC (Version 5.03)*; Siemens Analytical X-ray Instruments, Inc.: Madison; WI, 1994.

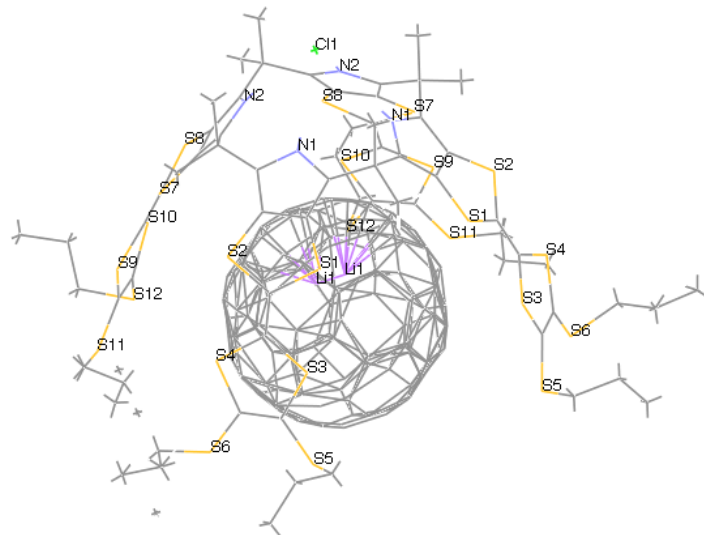


**Figure S2.** View of  $(C_{68}H_{84}N_4S_{24})C_{60} Li^+ Cl^- - 2 CH_2Cl_2$  showing a partial atom labeling scheme. The solvent has been omitted for clarity.

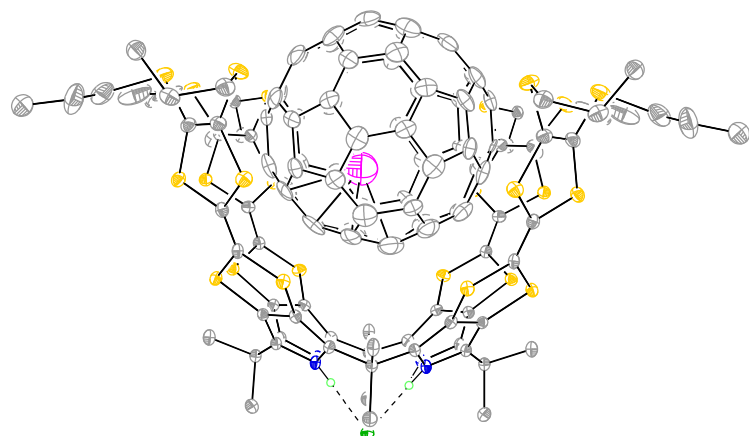


**Figure S3.** View of  $(C_{68}H_{84}N_4S_{24})C_{60} Li^+ Cl^- - 2 CH_2Cl_2$  showing the displacement ellipsoids scaled to the 30% probability level. The solvent has been omitted for clarity.

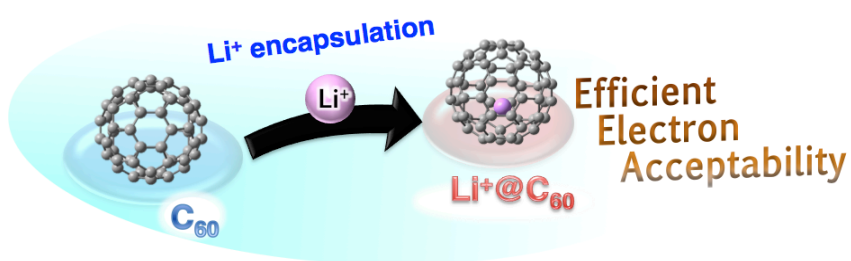
**Table S1.** Crystal Data and Structure Refinement for the Radical Ion Pair (PrS-TTF-C4P<sup>•+</sup>/Li<sup>+</sup>@C<sub>60</sub><sup>•-</sup>)

Empirical formula	C130 H88 N4 Cl5 S24 Li		
Formula weight	2659.68		
Temperature	100(2) K		
Wavelength (MoK $\alpha$ )	0.71075 Å		
Crystal system	Monoclinic		
Space group	<i>P</i> 2 <sub>1</sub> / <i>m</i>		
Unit cell dimensions	<i>a</i> = 14.8753(12) Å	$\alpha$ = 90°.	
	<i>b</i> = 26.441(2) Å	$\beta$ = 107.903(3)°.	
	<i>c</i> = 15.4218(15) Å	$\gamma$ = 90°.	
Volume	5772.0(9) Å <sup>3</sup>		
<i>Z</i>	2		
Density (calculated)	1.530 g cm <sup>-3</sup>		
Absorption coefficient	0.616 mm <sup>-1</sup>		
<i>F</i> (000)	2736		
Crystal size	0.32 × 0.22 × 0.11 mm		
Theta range for data collection	3.08 to 27.49°.		
Index ranges	-19 $\leftarrow$ <i>h</i> $\leftarrow$ 18, 0 $\leftarrow$ <i>k</i> $\leftarrow$ 34, 0 $\leftarrow$ <i>l</i> $\leftarrow$ 20		
Reflections collected	13510		
Independent reflections	13510 [ <i>R</i> (int) = 0.0000]		
Completeness to theta = 27.49°	99.8%		
Absorption correction	Semi-empirical from equivalents		
Max. and min. transmission	1.00 and 0.725		
Refinement method	Full-matrix least-squares on <i>F</i> <sup>2</sup>		
Data / restraints / parameters	13510 / 3352 / 1054		
Goodness-of-fit on <i>F</i> <sup>2</sup>	1.282		
Final <i>R</i> indices [ <i>I</i> >2σ( <i>I</i> )]	<i>R</i> <sub>1</sub> = 0.0710, <i>wR</i> <sub>2</sub> = 0.1919		
<i>R</i> indices (all data)	<i>R</i> <sub>1</sub> = 0.1064, <i>wR</i> <sub>2</sub> = 0.2056		
Largest diff. peak and hole	0.823 and -1.108 e.Å <sup>-3</sup>		

CCDC 860359.

## Chapter 2

### Enhanced Photoinduced Electron-Transfer Reduction of $\text{Li}^+@\text{C}_{60}$ in Comparison with $\text{C}_{60}$



**Abstract:** Kinetics of photoinduced electron transfer from a series of electron donors to the triplet excited state of lithium ion-encapsulated  $\text{C}_{60}$  ( $\text{Li}^+@\text{C}_{60}$ ) was investigated in comparison with the corresponding kinetics of the photoinduced electron transfer to the triplet excited state of pristine  $\text{C}_{60}$ . Femtosecond laser flash photolysis measurements of  $\text{Li}^+@\text{C}_{60}$  revealed that singlet excited state of  $\text{Li}^+@\text{C}_{60}$  ( $\lambda_{\text{max}} = 960 \text{ nm}$ ) underwent intersystem crossing to the triplet excited state [ ${}^3(\text{Li}^+@\text{C}_{60})^*$ :  $\lambda_{\text{max}} = 750 \text{ nm}$ ] with a rate constant of  $8.9 \times 10^8 \text{ s}^{-1}$  in deaerated benzonitrile (PhCN). The lifetime of  ${}^3(\text{Li}^+@\text{C}_{60})^*$  was determined by nanosecond laser flash photolysis measurements to be  $48 \mu\text{s}$ , which is comparable to that of  $\text{C}_{60}$ . Efficient photoinduced electron transfer from a series of electron donors to  ${}^3(\text{Li}^+@\text{C}_{60})^*$  occurred to produce the radical cations and  $\text{Li}^+@\text{C}_{60}^{\cdot+}$ . The rate constants of photoinduced electron transfer of  $\text{Li}^+@\text{C}_{60}^{\cdot+}$  are significantly larger than those of  $\text{C}_{60}$  when the rate constants are less than the diffusion-limited value in PhCN. The enhanced reactivity of  ${}^3(\text{Li}^+@\text{C}_{60})^*$  as compared with  ${}^3\text{C}_{60}^*$  results from the much higher one-electron reduction potential of  $\text{Li}^+@\text{C}_{60}$  (0.14 V vs SCE) than that of  $\text{C}_{60}$  (-0.43 V vs SCE). The rate constants of photoinduced electron transfer reactions of  $\text{Li}^+@\text{C}_{60}$  and  $\text{C}_{60}$  were evaluated in light of the Marcus theory of electron transfer to determine the reorganization energies of electron transfer. The reorganization energy of electron transfer of  $\text{Li}^+@\text{C}_{60}$  was determined from the driving force dependence of electron transfer rate to be 1.01 eV, which is by 0.28 eV larger than that of  $\text{C}_{60}$  (0.73 eV), probably because of the change in electrostatic interaction of encapsulated  $\text{Li}^+$  upon electron transfer in PhCN.

## Introduction

Fullerenes have attracted considerable interest for a wide range of practical applications because of the unique electrical and chemical properties, in particular the excellent electron-transfer properties at the ground and photoexcited states.<sup>1-20</sup> Because fullerenes have spacious inner cavities, some metals can be encapsulated inside the fullerene cages to form endohedral metallofullerenes.<sup>21-28</sup> The metal(s) are normally encapsulated in fullerenes having higher cages (so called higher fullerenes such as C<sub>72</sub>, C<sub>80</sub> and C<sub>82</sub>), in which the fullerene cage is reduced by encapsulated metals.<sup>21-27</sup> As a typical metallofullerene, La@C<sub>82</sub> has a La<sup>3+</sup> in a three-electron reduced C<sub>82</sub> trianion radical cage.<sup>21-23</sup> On the other hand, lithium ion-encapsulated C<sub>60</sub> (Li<sup>+</sup>@C<sub>60</sub>) was recently isolated and the X-ray crystal structure was determined.<sup>28,29</sup> In the case of Li<sup>+</sup>@C<sub>60</sub>, the C<sub>60</sub> cage remains to be neutral.<sup>28</sup> The electron acceptor ability of Li<sup>+</sup>@C<sub>60</sub> was significantly enhanced as compared to pristine C<sub>60</sub>.<sup>28-30</sup> The enhanced electron acceptor ability of Li<sup>+</sup>@C<sub>60</sub> has made it possible to form supramolecular electron-transfer complex between a tetrathiafulvalene calix[4]pyrrole (TTF-C4P) and Li<sup>+</sup>@C<sub>60</sub> with chloride anion.<sup>29</sup> Although photoinduced electron-transfer reactions of C<sub>60</sub> have extensively been studied, the photoexcited state and the electron transfer reactivity of Li<sup>+</sup>@C<sub>60</sub> have yet to be examined.

I report herein photodynamics of Li<sup>+</sup>@C<sub>60</sub> and photoinduced electron-transfer reactions of Li<sup>+</sup>@C<sub>60</sub>, which were examined using femtosecond and nanosecond laser flash photolysis. Rate constants of photoinduced electron transfer from a series of electors donors to the triplet excited state of Li<sup>+</sup>@C<sub>60</sub> were determined in comparison with those of C<sub>60</sub>. The results were analyzed in light of the Marcus theory of electron transfer,<sup>31</sup> to determine the reorganization energy of electron transfer of Li<sup>+</sup>@C<sub>60</sub>. Li<sup>+</sup>@C<sub>60</sub> is one of the abundantly and commercially available endohedral metallofullerenes. The knowledge of electron-transfer properties of Li<sup>+</sup>@C<sub>60</sub> provides valuable information to expand the metallofullerene chemistry.

## Experimental Section

**Materials.** Chemicals were purchased from commercial sources and used without further purification, unless otherwise noted. Lithium ion-encapsulated C<sub>60</sub> (Li<sup>+</sup>@C<sub>60</sub>: 96%) was obtained from Daiichi Jitsugyo Co. Ltd, Japan. C<sub>60</sub>, 1,2,4,5-tetramethylbenzene, pentamethylbenzene, hexamethylbenzene, 1,4-dimethoxybenzene, ferrocene (Fc) and Fe(bpy)<sub>3</sub>(PF<sub>6</sub>)<sub>2</sub> (bpy = 2,2'-bipyridine) were also purchased from commercial sources and used without further purification. 1-Benzyl-1,4-dihydronicotinamide (BNAH) was obtained from Tokyo Chemical

---

Industry, Japan and purified by recrystallization from methanol. 10-Methyl-9,10-dihydroacridine ( $\text{AcrH}_2$ ) was synthesized by literature method and purified by recrystallization from ethanol.<sup>32</sup> Benzonitrile (PhCN) used as a solvent was distilled over phosphorus pentoxide.<sup>33</sup>

**Emission Spectral Measurements.** Phosphorescence was measured on a Horiba FluoroMax-4 spectrofluorophotometer. A 2-methyltetrahydrofuran solution of  $\text{Li}^+@\text{C}_{60}$  in a quartz tube (3 mm in diameter) was degassed by nitrogen bubbling for 10 min prior to the measurements. The sample tube was put in a quartz liquid nitrogen dewar. The measurements were carried out by excitation at 300 nm.

**Laser Flash Photolysis Measurements.** Femtosecond transient absorption spectroscopy experiments were conducted using an ultrafast source: Integra-C (Quantronix Corp.), an optical parametric amplifier: TOPAS (Light Conversion Ltd.) and a commercially available optical detection system: Helios provided by Ultrafast Systems LLC. The source for the pump and probe pulses were derived from the fundamental output of Integra-C ( $\lambda = 786$  nm, 2 mJ/pulse and  $\text{fwhm} = 130$  fs) at a repetition rate of 1 kHz. 75% of the fundamental output of the laser was introduced into a second harmonic generation (SHG) unit: Apollo (Ultrafast Systems) for excitation light generation at  $\lambda = 393$  nm, while the rest of the output was used for white light generation. The laser pulse was focused on a sapphire plate of 3 mm thickness and then white light continuum covering the visible region from  $\lambda = 410$  nm to 800 nm was generated via self-phase modulation. A variable neutral density filter, an optical aperture, and a pair of polarizer were inserted in the path in order to generate stable white light continuum. Prior to generating the probe continuum, the laser pulse was fed to a delay line that provides an experimental time window of 3.2 ns with a maximum step resolution of 7 fs. In my experiments, a wavelength at  $\lambda = 393$  nm of SHG output was irradiated at the sample cell with a spot size of 1 mm diameter where it was merged with the white probe pulse in a close angle ( $< 10^\circ$ ). The probe beam after passing through the 2 mm sample cell was focused on a fiber optic cable that was connected to a CMOS spectrograph for recording the time-resolved spectra ( $\lambda = 410 - 800$  nm). Typically, 1500 excitation pulses were averaged for 3 seconds to obtain the transient spectrum at a set delay time. Kinetic traces at appropriate wavelengths were assembled from the time-resolved spectral data. All measurements were conducted at room temperature, 295 K.

Nanosecond transient absorption spectral measurements were made according to the following procedure. A deaerated PhCN solution containing  $\text{Li}^+@\text{C}_{60}$  or  $\text{C}_{60}$  with an electron donor was excited by a Panther OPO pumped Nd:YAG laser (Continuum, SLII-10, 4-6 ns  $\text{fwhm}$ ) at 355 nm for 1,2,4,5-tetramethylbenzene, pentamethylbenzene, hexamethylbenzene,

---

1,4-dimethoxybenzene, AcrH<sub>2</sub>, BNAH, Fc and Fe(bpy)<sub>3</sub>(PF<sub>6</sub>)<sub>2</sub>. The resulting time-resolved transient absorption spectra were measured by using a continuous Xe-lamp (150 W) and a photodiode (Hamamatsu 2949) as the probe light and detector, respectively. The output from the photodiode and the photomultiplier tube was recorded using a digitizing oscilloscope (Tektronix, TDS3032, 300 MHz). The solutions were deoxygenated by N<sub>2</sub> purging for 10 min prior to measurements. Rates of photoinduced electron-transfer reactions were monitored by the decay of the absorption band due to the triplet excited state of Li<sup>+</sup>@C<sub>60</sub> with various concentrations of electron donors. The observed rate constants were determined by a least-squares curve fit. All experiments were performed at 298 K.

**Electrochemical Measurements.** Cyclic voltammetry (CV) measurements of Li<sup>+</sup>@C<sub>60</sub> were performed with an ALS630B electrochemical analyzer in deaerated PhCN containing 0.1 M Bu<sub>4</sub>N<sup>+</sup>ClO<sub>4</sub><sup>-</sup> (TBAP) as a supporting electrolyte at 298 K. The platinum working electrode (BAS, surface i.d. 1.6 mm) was polished with BAS polishing alumina suspension and rinsed with acetone before use. The counter electrode was a platinum wire (0.5 mm dia.). The measured potentials were recorded with respect to an Ag/AgNO<sub>3</sub> (0.01 M) reference electrode. The values of redox potentials (vs Ag/AgNO<sub>3</sub>) are converted into those vs SCE by addition of 0.29 V.<sup>34</sup>

**Theoretical Calculations.** Density functional theory (DFT) calculations were performed on an 8CPU workstation (PQS, Quantum Cube QS8-2400C-064). Geometry optimizations were carried out using the RB3LYP/6-31G(d) basis set for Li<sup>+</sup>@C<sub>60</sub> and C<sub>60</sub> and UB3LYP/6-31G(d) basis set for Li<sup>+</sup>@C<sub>60</sub><sup>•-</sup> and C<sub>60</sub><sup>•-</sup> as implemented in the Gaussian 09 program Revision A.02.<sup>35,36</sup>

## Results and Discussion

**Characterizations of Excited State of Li<sup>+</sup>@C<sub>60</sub>.** No emission of Li<sup>+</sup>@C<sub>60</sub> was observed by photoirradiation of a deaerated benzonitrile (PhCN) solution at room temperature. The emission spectrum of Li<sup>+</sup>@C<sub>60</sub> could be detected in a deaerated 2-methyltetrahydrofuran glass at 77 K (see the Experimental Section). The emission bands were clearly observed at 678 and 809 nm (Figure 1). The triplet excitation energy was, thus, determined as 1.53 eV, which is similar to the triplet energy of C<sub>60</sub> ( $E(T) = 1.57$  eV).<sup>37,38</sup> The emission band at 678 nm may be the fluorescence from the singlet excited state ( $E(S) = 1.94$  eV).<sup>39</sup> No fluorescence was observed at room temperature because fluorescence quantum yield is too small to be detected.

Ultrafast photodynamics for the intersystem crossing (ISC) from the singlet to the triplet excited state of Li<sup>+</sup>@C<sub>60</sub> was observed by femtosecond laser flash photolysis. The transient absorption band at 960 nm taken at 10 ps is assigned to the singlet excited state of Li<sup>+</sup>@C<sub>60</sub>

---

$[{}^1(\text{Li}^+@\text{C}_{60})^*]$  (Figure 2a). The decay of absorbance of  $[{}^1(\text{Li}^+@\text{C}_{60})^*]$  coincides with appearance of the new absorption band at 750 nm due to the triplet excited state of  $\text{Li}^+@\text{C}_{60}$   $[{}^3(\text{Li}^+@\text{C}_{60})^*]$  with an isosbestic point at 800 nm, which is formed by the intersystem crossing. The transient absorption band of  $[{}^3(\text{Li}^+@\text{C}_{60})^*]$  is similar to that of the triplet pristine  $\text{C}_{60}$  ( $\lambda_{\text{max}} = 740$  nm in PhCN).<sup>37</sup> The absorption changes of the rise at 750 nm and decay at 960 nm were analyzed by first-order kinetics (Figure 2b). The rate constant of intersystem crossing ( $k_{\text{ISC}}$ ) was determined to be  $8.9 \times 10^8 \text{ s}^{-1}$  which is larger than that of pristine  $\text{C}_{60}$  ( $4.1 \times 10^8 \text{ s}^{-1}$ ) in PhCN.<sup>38</sup>

The triplet-triplet (T-T) absorption spectrum of  $[{}^3(\text{Li}^+@\text{C}_{60})^*]$  in deaerated PhCN was also detected by nanosecond laser flash photolysis as shown in Figure 3a, which was observed at 1.0

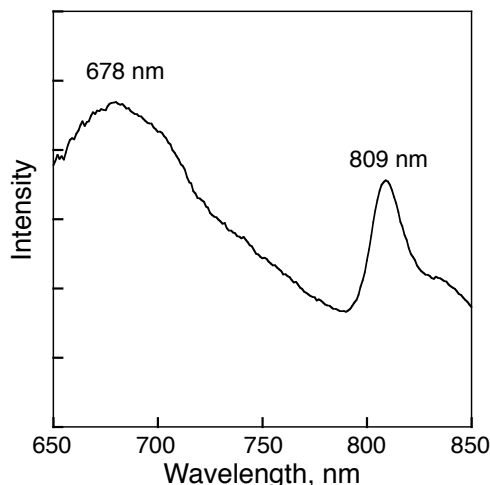


**Figure 1.** Emission spectrum of  $\text{Li}^+@\text{C}_{60}$  ( $150 \mu\text{M}$ ) in a deaerated 2-methyltetrahydrofuran glass. Excitation wavelength: 300 nm;  $T = 77 \text{ K}$ .

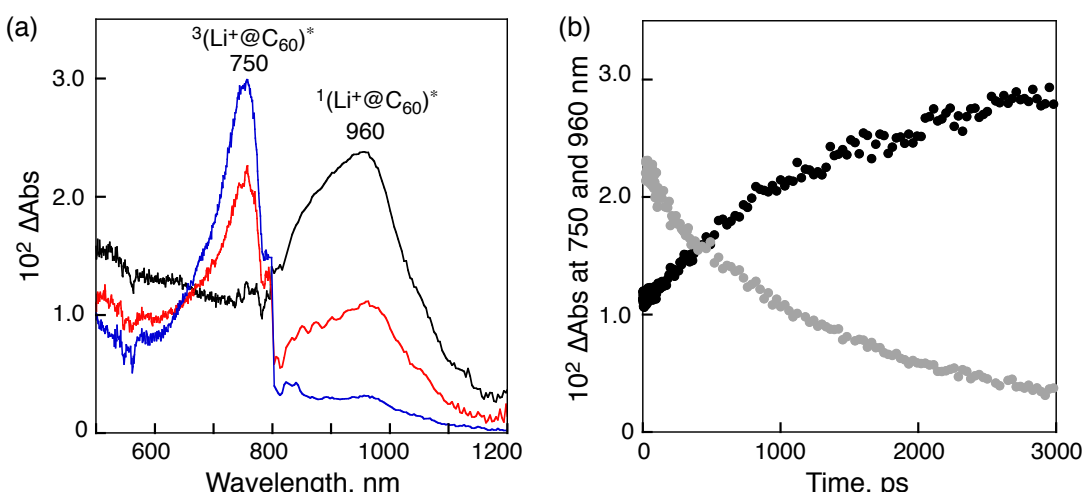


**Figure 2.** (a) Transient absorption spectra of  $\text{Li}^+@\text{C}_{60}$  in PhCN observed at 10 (black line), 1000 (red line) and 3000 ps (blue line) after laser excitation at 410 nm. (b) Rise and decay time profile at 750 (black circle) and 960 nm (gray circle).

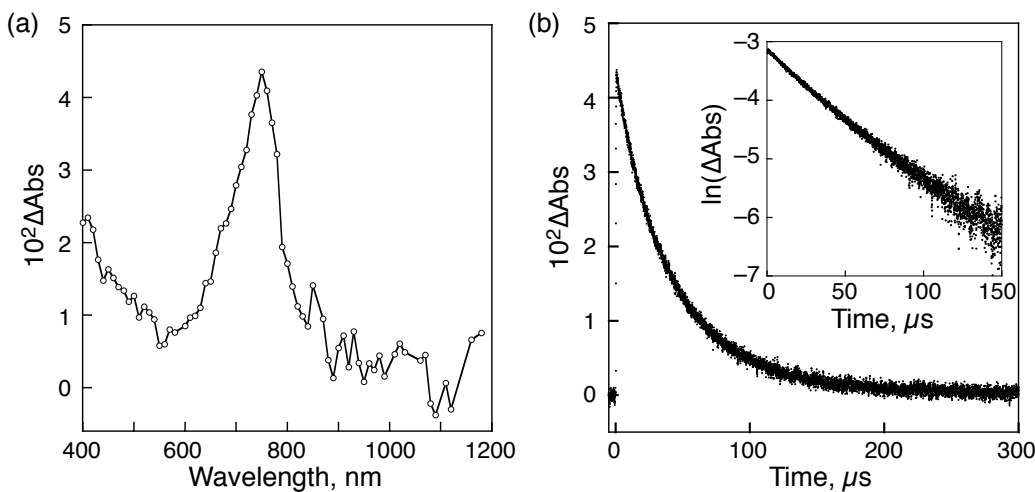
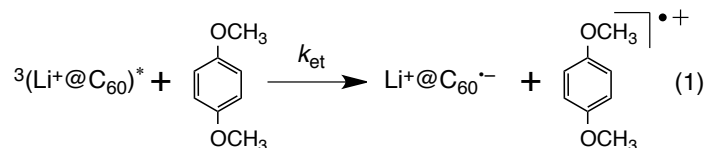


**Figure 3.** (a) Transient absorption spectrum of  $\text{Li}^+@\text{C}_{60}$  (25  $\mu\text{M}$ ) in PhCN measured at 1.0  $\mu\text{s}$  (○) after laser excitation at 355 nm. (b) Time profile at 750 nm. Inset: First-order plot.

$\mu\text{s}$  after laser excitation. The decay of the absorbance at 750 nm due to  ${}^3(\text{Li}^+@\text{C}_{60})^*$  obeys first-order kinetics (Figure 3b). The decay rate constant ( $k_{\text{T}}$ ) is determined from the linear first-order plot to be  $2.1 \times 10^4 \text{ s}^{-1}$  at 298 K (Inset of Figure 3b). There is no significant contribution of T-T annihilation under the present laser excitation conditions. The triplet lifetime determined is 48  $\mu\text{s}$ , which is comparable to that of  $\text{C}_{60}$  (49  $\mu\text{s}$ ).<sup>37,40</sup>

**Photoinduced Electron-Transfer Reduction of  $\text{Li}^+@\text{C}_{60}$ .** The triplet excited state of  $\text{Li}^+@\text{C}_{60}$  is relatively stable to be able to use as an electron acceptor in the photoinduced electron-transfer reactions. The one-electron reduction potential of  ${}^3(\text{Li}^+@\text{C}_{60})^*$  is determined to be 1.67 V vs SCE from the one-electron reduction potential of  $\text{Li}^+@\text{C}_{60}$  (0.14 V vs SCE in PhCN)<sup>30</sup> and the triplet excited energy (1.53 eV). Thus,  ${}^3(\text{Li}^+@\text{C}_{60})^*$  has a strong oxidizing ability to oxidize the substrate such as aromatic compounds. Time-resolved transient absorption spectral measurements of  $\text{Li}^+@\text{C}_{60}$  with aromatic electron donors were examined to observe the dynamics of electron-transfer reduction  ${}^3(\text{Li}^+@\text{C}_{60})^*$ . The one-electron oxidation potential of 1,4-dimethoxybenzene as an electron donor is 1.21 V vs SCE in PhCN,<sup>41</sup> which is smaller than the reduction potential of  ${}^3(\text{Li}^+@\text{C}_{60})^*$ , when the driving force of electron transfer from 1,4-dimethoxybenzene to  ${}^3(\text{Li}^+@\text{C}_{60})^*$  is highly positive ( $-\Delta G_{\text{et}} = 0.46 \text{ eV}$ ). This suggests that electron transfer from 1,4-dimethoxybenzene to  ${}^3(\text{Li}^+@\text{C}_{60})^*$  is energetically favorable (eq 1).



Nanosecond laser excitation of a deaerated PhCN solution containing  $\text{Li}^+@\text{C}_{60}$  and 1,4-dimethoxybenzene results in electron transfer from 1,4-dimethoxybenzene to  ${}^3(\text{Li}^+@\text{C}_{60})^*$  to produce 1,4-dimethoxybenzene radical cation ( $\lambda_{\text{max}} = 430 \text{ nm}$ )<sup>42</sup> and  $\text{Li}^+@\text{C}_{60}^{\cdot-}$  ( $\lambda_{\text{max}} = 1035 \text{ nm}$ )<sup>29,30</sup> as shown in Figure 4a. The triplet-triplet (T-T) absorption spectrum due to  ${}^3(\text{Li}^+@\text{C}_{60})^*$  observed at 1  $\mu\text{s}$  after the laser excitation (●) is changed to the transient absorption spectra at 2 (○) and 10  $\mu\text{s}$  (■) in Figure 4a. The time profile of the decay of absorbance at 750 nm due to  ${}^3(\text{Li}^+@\text{C}_{60})^*$  coincides with the rise in the absorbance at 430 and 1035 nm due to 1,4-dimethoxybenzene radical cation and  $\text{Li}^+@\text{C}_{60}^{\cdot-}$ , respectively, as shown in Figure 4b.

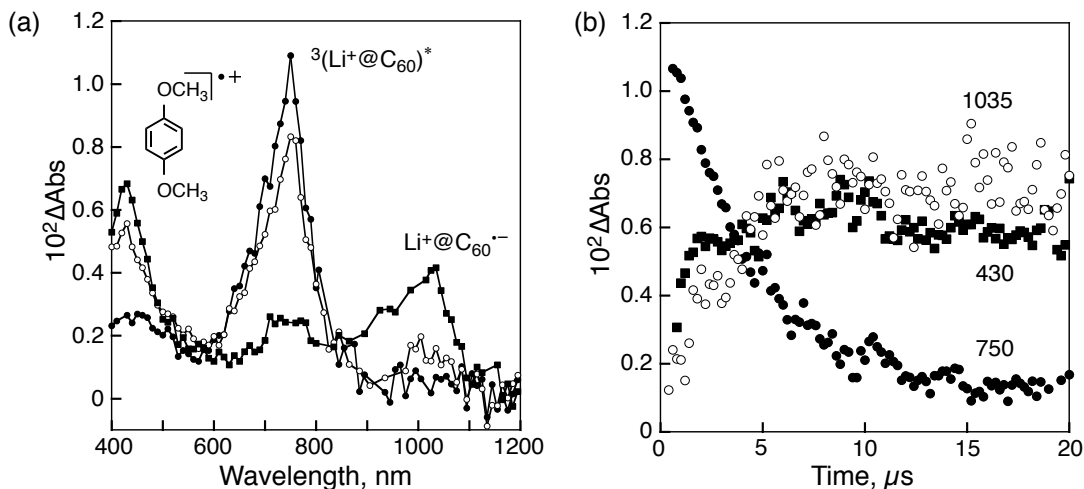


**Figure 4.** (a) Transient absorption spectra of  $\text{Li}^+@\text{C}_{60}$  (25  $\mu\text{M}$ ) in the presence of 1,4-dimethoxybenzene (50  $\mu\text{M}$ ) in deaerated PhCN at 298 K taken at 1 (●), 2 (○) and 10  $\mu\text{s}$  (■) after nanosecond laser excitation at 355 nm. (b) Absorption time profiles (■: 430 nm, ●: 750 nm, ○: 1035 nm).

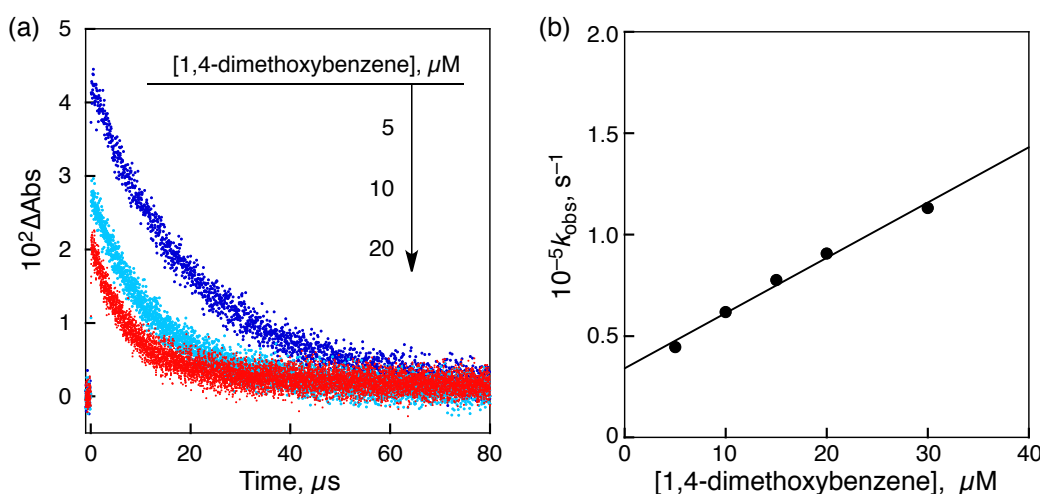


**Figure 5.** (a) Time profiles at 750 nm of  $\text{Li}^+@\text{C}_{60}$  (25  $\mu\text{M}$ ) in the presence of various concentrations of 1,4-dimethoxybenzene in PhCN. (b) Plot of the pseudo-first-order rate constant ( $k_{\text{obs}}$ ) vs the concentration of 1,4-dimethoxybenzene.

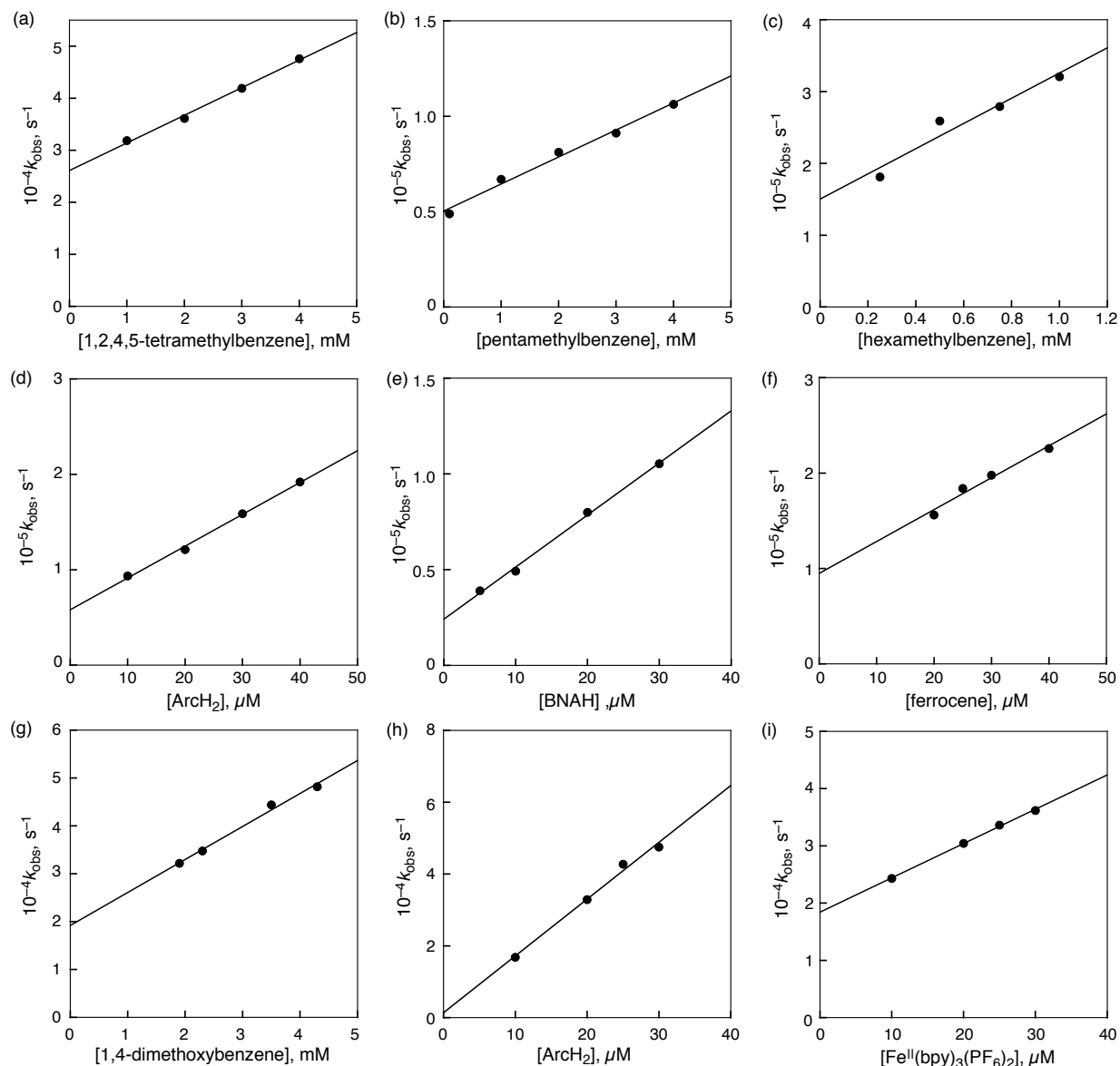


**Figure 6.** Plots of the pseudo-first-order rate constant ( $k_{\text{obs}}$ ) vs concentration of aromatic electron donors for photoinduced electron transfer from (a) 1,2,4,5-tetramethylbenzene, (b) pentamethylbenzene, (c) hexamethylbenzene, (d) AcrH<sub>2</sub>, (e) BNAH, (f) ferrocene to Li<sup>+</sup>@C<sub>60</sub> (25 μM) in deaerated PhCN at 298 K. Plot of the pseudo-first-order rate constant ( $k_{\text{obs}}$ ) vs concentration of electron donors for photoinduced electron transfer from (g) 1,4-dimethoxybenzene, (h) ArcH<sub>2</sub>, (i) Fe<sup>II</sup>(bpy)<sub>3</sub>(PF<sub>6</sub>)<sub>2</sub> to C<sub>60</sub> (25 μM) in deaerated PhCN at 298 K.

The decay rate of the T-T absorption ( $\lambda_{\text{max}} = 750$  nm) increases with increasing the concentration of 1,4-dimethoxybenzene as shown in Figure 5a. From the slope of the linear plot depicted in Figure 5b, the second-order rate constant for the bimolecular electron transfer ( $k_{\text{et}}$ ) from 1,4-dimethoxybenzene to  ${}^3(\text{Li}^+@\text{C}_{60})^*$  is determined to be  $2.7 \times 10^9 \text{ M}^{-1} \text{ s}^{-1}$ , which is close to the diffusion limited value in PhCN ( $5.6 \times 10^9 \text{ M}^{-1} \text{ s}^{-1}$ ).<sup>49</sup> Similarly, the  $k_{\text{et}}$  values for

photoinduced electron-transfer reactions of  $\text{Li}^+@\text{C}_{60}$  and  $\text{C}_{60}$  with various electron donors were determined by the T-T quenching experiments. The data obtained are shown in Figure 6 and summarized in Table 1 and 2. The absorption band at 1035 nm due to  $\text{Li}^+@\text{C}_{60}^{\bullet-}$  of the radical ion pair decays obeying second-order bimolecular kinetics as shown in Figure 7. In the case of  $\text{Li}^+@\text{C}_{60}^{\bullet-}$ /1,2,4,5-tetra-methylbenzene radical cation, the second-order plot for the decay of  $\text{Li}^+@\text{C}_{60}^{\bullet-}$  obtained from the absorbance change at 1035 nm and the  $\epsilon$  value ( $7300 \text{ M}^{-1} \text{ cm}^{-1}$ )<sup>29</sup> gives a linear plot (see inset of Figure 7a). The second-order rate constant for the back electron transfer from  $\text{Li}^+@\text{C}_{60}^{\bullet-}$  to 1,2,4,5-tetramethylbenzene radical cation is determined from the slope to be  $4.4 \times 10^9 \text{ M}^{-1} \text{ s}^{-1}$ , which is close to the diffusion-limited value in PhCN.<sup>49</sup> When 1,2,4,5-tetramethylbenzene was replaced by pentamethylbenzene, the  $k_{\text{bet}}$  value was determined to be  $5.2 \times 10^9 \text{ M}^{-1} \text{ s}^{-1}$  (Figure 7b, entry 8 in Table 1).

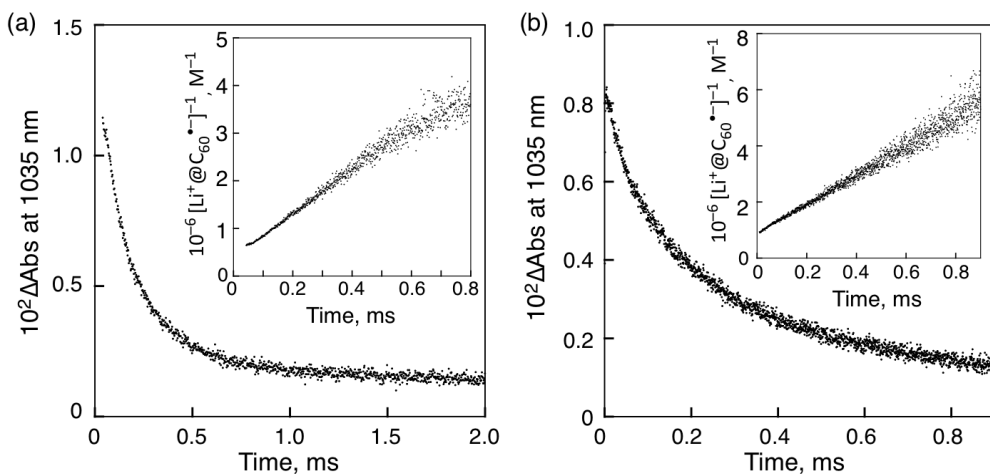


**Figure 7.** Decay time profile at 1035 nm for back electron transfer from  $\text{Li}^+@\text{C}_{60}^{\bullet-}$  to (a) 1,2,4,5-tetramethylbenzene radical cation, (b) pentamethylbenzene radical cation obtained by nanosecond laser excitation of  $\text{Li}^+@\text{C}_{60}$  ( $25 \mu\text{M}$ ) with aromatic electron donors ( $5.0 \text{ mM}$ ) in PhCN. Inset: The second-order plot of the decay of  $\text{Li}^+@\text{C}_{60}^{\bullet-}$  obtained from the absorbance at 1035 nm using the  $\epsilon$  value ( $7300 \text{ M}^{-1} \text{ cm}^{-1}$ ).

**Photoinduced Electron-Transfer Reduction of  $\text{Li}^+@\text{C}_{60}$  in Comparison with  $\text{C}_{60}$ .** The  $k_{\text{et}}$  values for electron transfer from electron donors to the triplet excited state of pristine  $\text{C}_{60}$  ( ${}^3\text{C}_{60}^*$ ) were determined by using 1,4-dimethoxybenzene,  $\text{Fe}(\text{bpy})_3^{2+}$  (bpy = 2,2'-bipyridine) and 10-methyl-9,10-dihydroacridine ( $\text{AcrH}_2$ ), which are summarized in Table 2. The rate constants of photoinduced electron transfer of  $\text{Li}^+@\text{C}_{60}$  are significantly larger than those of  $\text{C}_{60}$  when the rate constants less than the diffusion-limited value are compared at the same  $E_{\text{ox}}$  values of electron donors. For example, the  $k_{\text{et}}$  value of electron transfer from 1,4-dimethoxybenzene ( $E_{\text{ox}} = 1.21 \text{ V}$  vs SCE) to  ${}^3(\text{Li}^+@\text{C}_{60})^*$  is 390 times faster than that to  ${}^3\text{C}_{60}^*$  ( $6.9 \times 10^6 \text{ M}^{-1} \text{ s}^{-1}$ ). When

the stronger electron donors with the lower  $E_{\text{ox}}$  value than 1,4-dimethoxybenzene such as  $\text{AcrH}_2$  ( $E_{\text{ox}} = 0.81$  V) were employed, the deference in the  $k_{\text{et}}$  values (2 times) is smaller than that of 1,4-dimethoxybenzene. Such a difference in the  $k_{\text{et}}$  values between  $\text{Li}^+@\text{C}_{60}$  and  $\text{C}_{60}$  results from the higher one-electron reduction potential of  $\text{Li}^+@\text{C}_{60}$  ( $E_{\text{red}} = 0.14$  V vs SCE) than that of  $\text{C}_{60}$  ( $E_{\text{red}} = -0.43$  V vs SCE).<sup>37</sup> Plots of  $\log k_{\text{et}}$  vs  $E_{\text{ox}}$  for  ${}^3(\text{Li}^+@\text{C}_{60})^*$  and  ${}^3\text{C}_{60}^*$  are shown in Figure 8. In each case, the  $k_{\text{et}}$  value increases with decreasing the  $E_{\text{ox}}$  value to reach a diffusion-limited value.

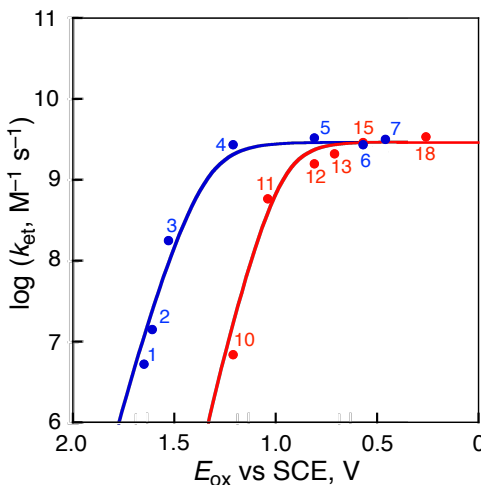


**Figure 8.** Plots of  $\log k_{\text{et}}$  vs the one-electron oxidation potentials of electron donors ( $E_{\text{ox}}$ ) for electron transfer from various electron donors to  ${}^3(\text{Li}^+@\text{C}_{60})^*$  (blue) and  ${}^3\text{C}_{60}^*$  (red) in PhCN. Numbers refer to electron donors in Tables 1 and 2.

The driving force of electron transfer from electron donors to electron acceptors ( $\text{Li}^+@\text{C}_{60}$  or fullerenes), can be obtained by using eq 2:

$$\Delta G_{\text{et}} = e[E_{\text{ox(donor)}} - E_{\text{red(acceptor)}}] \quad (2)$$

The dependence of  $k_{\text{et}}$  on the driving force of electron transfer ( $-\Delta G_{\text{et}}$ ) is shown in Figure 9 and Table 1 and 2. The  $\log k_{\text{et}}$  value increases with increasing the driving force to reach a diffusion-limited value and then decreases with further increase in the driving force. The plateau in Figure 9 corresponds to the diffusion-limited region in which the rate of electron transfer is faster than the rate of diffusion. According to the Marcus theory of electron transfer, the observed rate constant of an intermolecular electron transfer is given as eq 3,<sup>31</sup>

$$\frac{1}{k_{\text{et}}} = \frac{1}{k_{\text{diff}}} + \frac{1}{Z \exp\left[-(\lambda/4)(1 + \Delta G_{\text{et}}/\lambda)^2/k_{\text{B}}T\right]} \quad (3)$$

where  $k_{\text{diff}}$  is the diffusion rate constant,  $Z$  is the collision frequency, which is taken as  $1 \times 10^{11} \text{ M}^{-1} \text{ s}^{-1}$ ,  $\lambda$  is the reorganization energy of electron transfer, and  $k_{\text{B}}$  is the Boltzmann constant. By

fitting the data based on the Marcus equation for intermolecular electron transfer, the reorganization energy of the electron-transfer reduction ( $\lambda$ ) of  $\text{Li}^+@\text{C}_{60}$  was determined to be 1.01 eV, which is larger than the  $\lambda$  value of  $\text{C}_{60}$  (0.73 eV). The Marcus inverted region for bimolecular electron-transfer reactions was not observed because of the larger reorganization energy for electron-transfer reactions of  $\text{Li}^+@\text{C}_{60}$  than  $\text{C}_{60}$ . The reorganization energy consists of

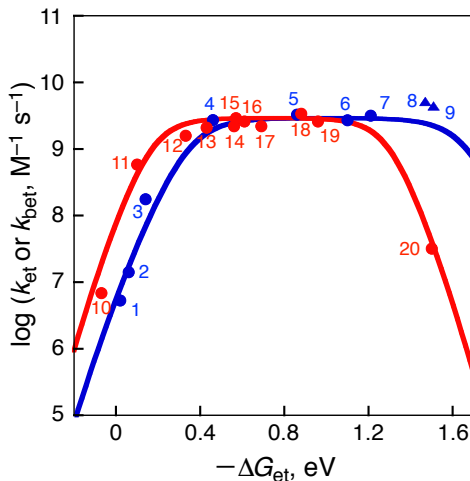


**Figure 9.** Driving force dependences of  $\log k_{\text{et}}$  for electron transfer from electron donors to  $\text{Li}^+@\text{C}_{60}$  (blue circle) or  $\text{C}_{60}$  (red circle) in PhCN at 298 K, electron transfer from  $\text{Li}^+@\text{C}_{60}^-$  (blue triangle) to radical cations in PhCN at 298 K and the fit of the curve based on the Marcus theory of electron transfer (eq 3) is shown by the blue line ( $\text{Li}^+@\text{C}_{60}$ ) and red line ( $\text{C}_{60}$ ). Numbers refer in Tables 1 and 2.

**Table 1.** One-Electron Redox Potentials and Rate Constants of Electron Transfer and Back Electron Transfer from Electron Donors to  ${}^3(\text{Li}^+@\text{C}_{60})^*$  in PhCN at 298 K

entry	acceptor	$E_{\text{red}}$	donor	$E_{\text{ox}}$	$-\Delta G_{\text{et}}$ eV	$k_{\text{et}}$ $\text{M}^{-1} \text{s}^{-1}$
1	${}^3(\text{Li}^+@\text{C}_{60})^*$	1.67	1,2,4,5-tetramethylbenzene	1.65 <sup>b</sup>	0.02	$5.3 \times 10^6$
2	${}^3(\text{Li}^+@\text{C}_{60})^*$	1.67	pentamethylbenzene	1.61	0.06	$1.4 \times 10^7$
3	${}^3(\text{Li}^+@\text{C}_{60})^*$	1.67	hexamethylbenzene	1.53 <sup>b</sup>	0.14	$1.8 \times 10^8$
4	${}^3(\text{Li}^+@\text{C}_{60})^*$	1.67	1,4-dimethoxybenzene	1.21 <sup>b</sup>	0.46	$2.7 \times 10^9$
5	${}^3(\text{Li}^+@\text{C}_{60})^*$	1.67	$\text{AcrH}_2$	0.81 <sup>c</sup>	0.86	$3.3 \times 10^9$
6	${}^3(\text{Li}^+@\text{C}_{60})^*$	1.67	BNAH	0.57 <sup>d</sup>	1.10	$2.7 \times 10^9$
7	${}^3(\text{Li}^+@\text{C}_{60})^*$	1.67	ferrocene	0.46	1.21	$3.3 \times 10^9$
8	pentamethylbenzene <sup>++</sup>	1.61	$\text{Li}^+@\text{C}_{60}^-$	0.14	1.47	$5.2 \times 10^9$
9	1,2,4,5-tetramethylbenzene <sup>++</sup>	1.53	$\text{Li}^+@\text{C}_{60}^-$	0.14	1.39	$4.4 \times 10^9$

<sup>a</sup> V vs SCE. <sup>b</sup> ref 41. <sup>c</sup> ref 44. <sup>d</sup> ref 45.

**Table 2.** One-Electron Oxidation Potentials ( $E_{\text{ox}}$ ) of Electron Donors and Rate Constants of Electron Transfer ( $k_{\text{et}}$ ) from Electron Donors to  $\text{C}_{60}$  in PhCN

entry	acceptor	donor	$E_{\text{ox}}$ vs SCE V	$-\Delta G_{\text{et}}$ eV	$k_{\text{et}}$ $\text{M}^{-1} \text{s}^{-1}$	ref
10	${}^3\text{C}_{60}^*$	1,4-dimethoxybenzene	1.21 <sup>a</sup>	-0.07	$6.9 \times 10^6$	this study
11	${}^3\text{C}_{60}^*$	$\text{Fe}(\text{bpy})_3^{2+}$	1.04 <sup>b</sup>	0.10	$6.0 \times 10^8$	this study
12	${}^3\text{C}_{60}^*$	$\text{AcrH}_2$	0.81 <sup>c</sup>	0.33	$1.6 \times 10^9$	this study
13	${}^3\text{C}_{60}^*$	<i>tert</i> -BuBNAH	0.73	0.43	$2.1 \times 10^9$	<sup>d</sup>
14	$\text{C}_{60}$	$\text{GeTPP}^{\bullet-}$	-0.99	0.56	$2.2 \times 10^9$	<sup>e</sup>
15	${}^3\text{C}_{60}^*$	BNAH	0.57	0.57	$2.9 \times 10^9$	<sup>d</sup>
16	$\text{C}_{60}$	$\text{InTPP}^{\bullet-}$	-1.04	0.61	$2.6 \times 10^9$	<sup>e</sup>
17	$\text{C}_{60}$	$\text{GaTPP}^{\bullet-}$	-1.12	0.69	$2.2 \times 10^9$	<sup>e</sup>
18	${}^3\text{C}_{60}^*$	$(\text{BNA})_2$	0.26	0.88	$3.4 \times 10^9$	<sup>d</sup>
19	$\text{C}_{60}$	$\text{ZnTPP}^{\bullet-}$	-1.39	0.96	$2.6 \times 10^9$	<sup>e</sup>
20	$\text{C}_{60}$	anthracene $^{\bullet-}$	-1.93	1.50	$3.2 \times 10^7$	<sup>f</sup>

<sup>a</sup> ref 41. <sup>b</sup> ref 46. <sup>c</sup> ref 44. <sup>d</sup> ref 37. <sup>e</sup> ref 47. <sup>f</sup> ref 48

the solvent reorganization energy ( $\lambda_s$ ) and intermolecular reorganization energy ( $\lambda_i$ ), that is,  $\lambda = \lambda_s + \lambda_i$ . In the case of fullerenes,  $\lambda$  values are mainly composed of  $\lambda_s$ . The larger  $\lambda$  value for electron-transfer reduction of  $\text{C}_{60}$  in PhCN than the  $\lambda$  value for electron transfer oxidation of fullerenes in  $\text{CH}_2\text{Cl}_2$  (0.36 eV) results from the larger solvent reorganization in the more polar solvent (PhCN) than  $\text{CH}_2\text{Cl}_2$ .

The reorganization energies for the one-electron reduction of  $\text{Li}^+@\text{C}_{60}$  and  $\text{C}_{60}$  were evaluated theoretically by using the density functional theory (DFT) calculations at the B3LYP/6-31G(d) level of theory (see Experimental Section).<sup>50,51</sup> The difference between the energy of  $\text{Li}^+@\text{C}_{60}^{\bullet-}$  with the same structure as  $\text{Li}^+@\text{C}_{60}$  and the energy with the optimized structure of  $\text{Li}^+@\text{C}_{60}^{\bullet-}$  can be regarded as the reorganization energy of the inner coordination spheres ( $\lambda_i$ ) associated with the structural change upon the electron-transfer reduction of  $\text{Li}^+@\text{C}_{60}$  in the gas phase. The  $\lambda_i$  value thus obtained is 0.14 eV (3.43 kcal mol<sup>-1</sup>). The corresponding  $\lambda_i$  value for the one-electron reduction of  $\text{C}_{60}$  is calculated as 0.15 eV (3.16 kcal mol<sup>-1</sup>). This value is slightly smaller than that of  $\text{Li}^+@\text{C}_{60}$ . Thus, the small  $\lambda_i$  values as compared with the observed  $\lambda$  values which include the solvent reorganization energy indicate that solvent reorganization plays a major role in determining the intrinsic barrier of the electron-transfer reduction of  $\text{Li}^+@\text{C}_{60}$  and  $\text{C}_{60}$ . Such a large  $\lambda$  value of  $\text{Li}^+@\text{C}_{60}$  may result from the localized LUMO of  $\text{Li}^+@\text{C}_{60}$  by the changing the electrostatic interaction of encapsulated  $\text{Li}^+$  upon electron transfer, as shown in Figure 10.

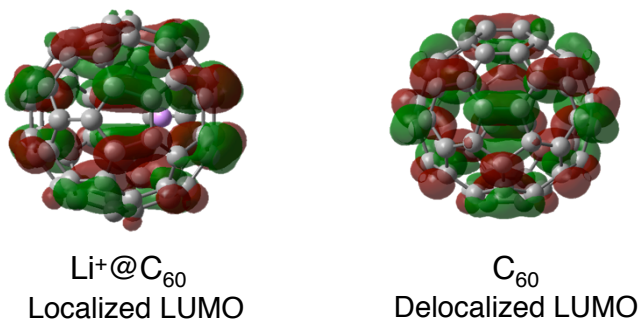


**Figure 10.** LUMOs of  $\text{Li}^+@\text{C}_{60}$  and  $\text{C}_{60}$  obtained by calculation at B3LYP/6-31G(d).

## Conclusion

In summary, I have characterized the photoexcited  $\text{Li}^+@\text{C}_{60}$  by femto- and nanosecond laser flash photolysis. The reactivity of the electron-transfer reduction of  ${}^3(\text{Li}^+@\text{C}_{60})^*$  is much higher than that of the pristine  ${}^3\text{C}_{60}^*$ . I have successfully shown the driving force dependence of the rate constant of electron-transfer reduction of fullerenes with small reorganization energies. The reorganization energy of electron transfer reduction of  $\text{Li}^+@\text{C}_{60}$  is slightly larger than the value of  $\text{C}_{60}$ , which comes from the larger solvent reorganization energy due to the change in solvation of  $\text{Li}^+@\text{C}_{60}$  upon the electron transfer. This study provides valuable information for further utilization of  $\text{Li}^+@\text{C}_{60}$  as an efficient electron acceptor.

## References

- (1) (a) Konarev, D. V.; Khasanov, S. S.; Otsuka, A.; Maesato, M.; Saito, G.; Lyubovskaya, R. N. *Angew. Chem., Int. Ed.* **2010**, *49*, 4829–4832. (b) Konarev, D. V.; Kuzmin, A. V.; Simonov, S. V.; Khasanov, S. S.; Yudanova, E. I.; Lyubovskaya, R. N. *Dalton Trans.* **2011**, *40*, 4453–4458.
- (2) Krokos, E.; Spänig, F.; Ruppert, M.; Hirsch, A.; Guldi, D. M. *Chem.–Eur. J.* **2012**, *18*, 1328–1341.
- (3) Li, C. Z.; Matsuo, Y.; Nakamura, E. *Tetrahedron* **2011**, *67*, 9944–9949.
- (4) Taylor, R.; Walton, D. R. M. *Nature* **1993**, *363*, 685–693.
- (5) Echegoyen, L.; Diederich, F.; Echegoyen, L. E. In *Fullerenes: Chemistry, Physics, and Technology*, Kadish, K. M., Ruoff, R. S., Eds.; Wiley-Interscience: New York, 2000; pp 1–51.
- (6) (a) Guldi, D. M.; Fukuzumi, S. In *Fullerenes: From Synthesis to Optoelectronic Properties*; Guldi, D. M., Martin, N., Eds.; Kluwer: Dordrecht, 2003; pp 237–265. (b)

Sgobba, V.; Rahman, G. M. A.; Guldi, D. M. In *Carbon Nanotubes in Electron Donor–Acceptor Nanocomposites, Chemistry of Carbon Nanotubes*; Basiuk, V. A., Ed.; American Scientific Publishers: California, 2006.

(7) Fukuzumi, S.; Guldi, D. M. In *Electron Transfer in Chemistry*, Vol. 2, Balzani, V., Ed.; Wiley-VCH: Weinheim, 2001; pp 270–337.

(8) (a) Fukuzumi, S.; Ohkubo, K. *J. Mater. Chem.* **2012**, *22*, 4575–4587. (b) Ohkubo, K.; Fukuzumi, S. *J. Porphyrins Phthalocyanines* **2008**, *12*, 993–1004. (c) Fukuzumi, S. *Phys. Chem. Chem. Phys.* **2008**, *10*, 2283–2297. (d) Fukuzumi, S. *Bull. Chem. Soc. Jpn.* **2006**, *79*, 177–195. (e) Ohkubo, K.; Fukuzumi, S. *Bull. Chem. Soc. Jpn.* **2009**, *82*, 303–315.

(9) (a) Imahori, H.; Tamaki, K.; Guldi, D. M.; Luo, C.; Fujitsuka, M.; Ito, O.; Sakata, Y.; Fukuzumi, S. *J. Am. Chem. Soc.* **2001**, *123*, 2607–2617. (b) Imahori, H.; Guldi, D. M.; Tamaki, K.; Yoshida, Y.; Luo, C.; Sakata, Y.; Fukuzumi, S. *J. Am. Chem. Soc.* **2001**, *123*, 6617–6628. (c) Imahori, H.; Tamaki, K.; Araki, Y.; Sekiguchi, Y.; Ito, O.; Sakata, Y.; Fukuzumi, S. *J. Am. Chem. Soc.* **2002**, *124*, 5165–5174. (d) Imahori, H.; Sekiguchi, Y.; Kashiwagi, Y.; Sato, T.; Araki, Y.; Ito, O.; Yamada, H.; Fukuzumi, S. *Chem.-Eur. J.* **2004**, *10*, 3184–3196. (e) Guldi, D. M.; Imahori, H.; Tamaki, K.; Kashiwagi, Y.; Yamada, H.; Sakata, Y.; Fukuzumi, S. *J. Phys. Chem. A* **2004**, *108*, 541–548.

(10) (a) Hasobe, T.; Imahori, H.; Kamat, P. V.; Ahn, T. K.; Kim, S. K.; Kim, D.; Fujimoto, A.; Hirakawa, T.; Fukuzumi, S. *J. Am. Chem. Soc.* **2005**, *127*, 1216–1228. (b) Hasobe, T.; Saito, K.; Kamat, P. V.; Troiani, V.; Qiu, H.; Solladié, N.; Kim, K. S.; Park, J. K.; Kim, D.; D’Souza, F.; Fukuzumi, S. *J. Mater. Chem.* **2007**, *17*, 4160–4170.

(11) (a) Fukuzumi, S.; Ohkubo, K.; Imahori, H.; Shao, J.; Ou, Z.; Zheng, G.; Chen, Y.; Pandey, R. K.; Fujitsuka, M.; Ito, O.; Kadish, K. M. *J. Am. Chem. Soc.* **2001**, *123*, 10676–10683. (b) Ohkubo, K.; Imahori, H.; Shao, J.; Ou, Z.; Kadish, K. M.; Chen, Y.; Pandey, R. K.; Fujitsuka, M.; Ito, O.; Fukuzumi, S. *J. Phys. Chem. A* **2002**, *106*, 10991–10998. (c) Ohkubo, K.; Shao, J.; Ou, Z.; Kadish, K. M.; Li, G.; Pandey, R. K.; Fujitsuka, M.; Ito, O.; Imahori, H.; Fukuzumi, S. *Angew. Chem., Int. Ed.* **2004**, *43*, 853–856.

(12) (a) Kashiwagi, Y.; Ohkubo, K.; McDonald, J. A.; Blake, I. M.; Crossley, M. J.; Araki, Y.; Ito, O.; Imahori, H.; Fukuzumi, S. *Org. Lett.* **2003**, *5*, 2719–2721. (b) Curiel, D.; Ohkubo, K.; Reimers, J. R.; Fukuzumi, S.; Crossley, M. J. *Phys. Chem. Chem. Phys.* **2007**, *9*, 5260–5266. (c) Lee, S.-H.; Larsen, A. G.; Ohkubo, K.; Cai, Z.-L.; Reimers, J. R.; Fukuzumi, S.; Crossley, M. J. *Chem. Sci.* **2012**, *3*, 257–269.

(13) D’Souza, F.; Chitta, R.; Ohkubo, K.; Tasior, M.; Subbaiyan, N. K.; Zandler, M. E.;

---

Rogacki, M. K.; Gryko, D. T.; Fukuzumi, S. *J. Am. Chem. Soc.* **2008**, *130*, 14263–14272.

(14) Spänig, F.; Kovacs, C.; Hauke, F.; Ohkubo, K.; Fukuzumi, S.; Guldi, D. M.; Hirsch, A. *J. Am. Chem. Soc.* **2009**, *131*, 8180–8195.

(15) (a) Martín-Gomis, L.; Ohkubo, K.; Fernández-Lázaro, F.; Fukuzumi, S.; Sastre-Santos, Á. *Chem. Commun.* **2010**, *46*, 3944–3946. (b) Sastre-Santos, Á.; Parejo, C.; Martín-Gomis, L.; Ohkubo, K.; Fernández-Lázaro, F.; Fukuzumi, S. *J. Mater. Chem.* **2011**, *21*, 1509–1515. (c) Ohkubo, K.; Ortiz, J.; Martín-Gomis, L.; Fernández-Lázaro, F.; Sastre-Santos, Á.; Fukuzumi, S. *Chem. Commun.* **2007**, 589–591. (d) Céspedes-Guirao, F. J.; Ohkubo, K.; Fukuzumi, S.; Sastre-Santos, Á.; Fernández-Lázaro, F. *J. Org. Chem.* **2009**, *74*, 5871–5880. (e) Fukuzumi, S.; Ohkubo, K.; Ortiz, J.; Gutiérrez, A. M.; Fernández-Lázaro, F.; Sastre-Santos, Á. *Chem. Commun.* **2005**, 3814–3815. (f) Blas-Ferrando, V. M.; Ortiz, J.; Bouissane, L.; Ohkubo, K.; Fukuzumi, S.; Fernández-Lázaro, F.; Sastre-Santos, Á. *Chem. Commun.* **2012**, *48*, 6241–6243.

(16) (a) D'Souza, F.; Maligaspe, E.; Ohkubo, K.; Zandler, M. E.; Subbaiyan, N. K.; Fukuzumi, S. *J. Am. Chem. Soc.* **2009**, *131*, 8787–8797. (b) Wijesinghe, C. A.; El-Khouly, M. E.; Subbaiyan, N. K.; Supur, M.; Zandler, M. E.; Ohkubo, K.; Fukuzumi, S.; D'Souza, F. *Chem.–Eur. J.* **2011**, *17*, 3147–3156. (c) Murakami, M.; Ohkubo, K.; Hasobe, T.; Sgobba, V.; Guldi, D. M.; Wessendorf, F.; Hirsh, A.; Fukuzumi, S. *J. Mater. Chem.* **2010**, *20*, 1457–1466. (d) D'Souza, F.; Maligaspe, E.; Karr, P. A.; Schumacher, A. L.; Ojaimi, M. E.; Gros, C. P.; Barbe, J.-M.; Ohkubo, K.; Fukuzumi, S. *Chem.–Eur. J.* **2008**, *14*, 674–681. (e) D'Souza, F.; Maligaspe, E.; Zandler, M. E.; Subbaiyan, N. K.; Ohkubo, K.; Fukuzumi, S. *J. Am. Chem. Soc.* **2008**, *130*, 16959–16967.

(17) (a) Fukuzumi, S.; Saito, K.; Ohkubo, K.; Khoury, T.; Kashiwagi, Y.; Absalom, M. A.; Gadde, S.; D'Souza, F.; Araki, Y.; Ito, O. Crossley, M. J. *Chem. Commun.* **2011**, *47*, 7980–7982. (b) Fukuzumi, S.; Ohkubo, K.; Saito, K.; Kashiwagi, Y.; Khoury, T.; Crossley, M. J. *J. Porphyrins Phthalocyanines* **2011**, *15*, 1292–1298.

(18) Choi, J. H.; Son, K.-I.; Kim, T.; Kim, K.; Ohkubo, K.; Fukuzumi, S. *J. Mater. Chem.* **2010**, *20*, 475–482.

(19) (a) Yu, G.; Gao, J.; Hummelen, J. C.; Wudl, F.; Heeger, A. J. *Science* **1995**, *270*, 1789–1791. (b) Gunes, S.; Neugebauer, H.; Sariciftci, N. S. *Chem. Rev.* **2007**, *107*, 1324–1338. (c) Thompson, B. C.; Fréchet, J. M. J. *Angew. Chem., Int. Ed.* **2008**, *47*, 58–77. (d) Brabec, C. J.; Sariciftci, N. S.; Hummenlen, J. C. *Adv. Funct. Mater.* **2001**, *11*, 15–26.

(20) (a) Nobukuni, H.; Shimazaki, Y.; Uno, H.; Naruta, Y.; Ohkubo, K.; Kojima, T.;

Fukuzumi, S.; Seki, S.; Sakai, H.; Hasobe, T.; Tani, F. *Chem.–Eur. J.* **2010**, *16*, 11611–11623. (b) Hasobe, T.; Hattori, S.; Kotani, H.; Ohkubo, K.; Hosomizu, K.; Imahori, H.; Kamat, P. V.; Fukuzumi, S. *Org. Lett.* **2004**, *6*, 3103–3106.

(21) Lu, X.; Akasaka, T.; Nagase, S. *Chem. Commun.* **2011**, *47*, 5942–5957.

(22) Maeda, Y.; Lu, J.; Akasaka, T.; Nagase, S. In *Chemistry of Nanocarbons*, Akasaka, T., Wuldi, F., Nagase, S., Eds.; Wiley-VCH, Verlag GmbH & Co. KGaA: Weinheim, 2010; pp 491–523.

(23) Akasaka, T.; Kato, T.; Kobayashi, K.; Nagase, S.; Yamamoto, K.; Funasaka, H.; Takahashi, T. *Nature* **1995**, *374*, 600–601.

(24) Xu, J. X.; Lu, X.; Zhou, X. H.; He, X. R.; Shi, Z. J.; Gu, Z. N. *Chem. Mater.* **2004**, *16*, 2959–2964.

(25) Shinohara, H. *Rep. Prog. Phys.* **2000**, *63*, 843–892.

(26) Li, F.-F.; Pinzón, J. R.; Mercado, B. Q.; Olmstead, M. M.; Balch, A. L.; Echegoyen, L. *J. Am. Chem. Soc.* **2011**, *133*, 1563–1571.

(27) Huang, H. J.; Yang, S. H. *J. Phys. Chem. B* **1998**, *102*, 10196–10200.

(28) (a) Aoyagi, S.; Nishibori, E.; Sawa, H.; Sugimoto, K.; Takata, M.; Miyata, Y.; Kitaura, R.; Shinohara, H.; Okada, H.; Sakai, T.; Ono, Y.; Kawachi, K.; Yokoo, K.; Ono, S.; Omote, K.; Kasama, Y.; Ishikawa, S.; Komuro, T.; Tobita, H. *Nature Chem.* **2010**, *2*, 678–683. (b) Aoyagi, S.; Nishibori, E.; Sawa, H.; Okada, H.; Tobita, H.; Kasama, Y.; Kitaura, R.; Shinohara, H. *Angew. Chem., Int. Ed.* **2012**, *51*, 3377–3381.

(29) Fukuzumi, S.; Ohkubo, K.; Kawashima, Y.; Kim, D. S.; Park, J. S.; Jana, A.; Lynch, V. M.; Kim, D.; Sessler, J. L. *J. Am. Chem. Soc.* **2011**, *133*, 15938–15941.

(30) Ohkubo, K.; Kawashima, Y.; Fukuzumi, S. *Chem. Commun.* **2012**, *48*, 4314–4316.

(31) (a) Marcus, R. A. *Annu. Rev. Phys. Chem.* **1964**, *15*, 155–196. (b) Marcus, R. A. *Angew. Chem., Int. Ed. Engl.* **1993**, *32*, 1111–1121.

(32) Fukuzumi, S.; Tokuda, Y.; Kitano, T.; Okamoto, T.; Otera, J. *J. Am. Chem. Soc.* **1993**, *115*, 8960–8968.

(33) Armarego, W. L. F.; Chai, C. L. L. *Purification of Laboratory Chemicals*, 6<sup>th</sup> ed; Pergamon Press: Oxford, 2009.

(34) Mann, C. K.; Barnes, K. K. In *Electrochemical Reactions in Non-aqueous Systems*; Marcel Dekker: New York, 1970.

(35) Frisch, M. J.; Trucks, G. W.; Schlegel, H. B.; Scuseria, G. E.; Robb, M. A.; Cheeseman, J. R.; Scalmani, G.; Barone, V.; Mennucci, B.; Petersson, G. A.; Nakatsuji, H.; Caricato,

---

M.; Li, X.; Hratchian, H. P.; Izmaylov, A. F.; Bloino, J.; Zheng, G.; Sonnenberg, J. L.; Hada, M.; Ehara, M.; Toyota, K.; Fukuda, R.; Hasegawa, J.; Ishida, M.; Nakajima, T.; Honda, Y.; Kitao, O.; Nakai, H.; Vreven, T.; Montgomery, J. A., Jr.; Peralta, J. E.; Ogliaro, F.; Bearpark, M.; Heyd, J. J.; Brothers, E.; Kudin, K. N.; Staroverov, V. N.; Kobayashi, R.; Normand, J.; Raghavachari, K.; Rendell, A.; Burant, J. C.; Iyengar, S. S.; Tomasi, J.; Cossi, M.; Rega, N.; Millam, J. M.; Klene, M.; Knox, J. E.; Cross, J. B.; Bakken, V.; Adamo, C.; Jaramillo, J.; Gomperts, R.; Stratmann, R. E.; Yazyev, O.; Austin, A. J.; Cammi, R.; Pomelli, C.; Ochterski, J. W.; Martin, R. L.; Morokuma, K.; Zakrzewski, V. G.; Voth, G. A.; Salvador, P.; Dannenberg, J. J.; Dapprich, S.; Daniels, A. D.; Farkas, O.; Foresman, J. B.; Ortiz, J. V.; Cioslowski, J.; Fox, D. J. *Gaussian 09, revision A.02*; Gaussian, Inc.: Wallingford, CT, 2009.

(36) (a) Becke, A. D. *J. Chem. Phys.* **1993**, *98*, 5648–5652. (b) Lee, C.; Yang, W.; Parr, R. G. *Phys. Rev. B* **1988**, *37*, 785–789.

(37) Fukuzumi, S.; Suenobu, T.; Patz, M.; Hirasaka, T.; Itoh, S.; Fujitsuka, M.; Ito, O. *J. Am. Chem. Soc.* **1998**, *120*, 8060–8068.

(38) Guldi, D. M.; Hungerbuehler, H.; Carmichael, I.; Asmus, K.-D.; Maggini, M. *J. Phys. Chem. A* **2000**, *104*, 8601–8608.

(39) The singlet excited energy was determined from the average value of absorption and fluorescence maxima.

(40) (a) Arbogast, J. W.; Darmanyan, A. P.; Foote, C. S.; Rubin, Y.; Diederich, F. N.; Alvarez, M. M.; Anz, S. J.; Whetten, R. L. *J. Phys. Chem.* **1991**, *95*, 11–12. (b) Arbogast, J. W.; Foote, C. S. *J. Am. Chem. Soc.* **1991**, *113*, 8886–8889. (c) Kajii, Y.; Nakagawa, T.; Suzuki, S.; Achiba, Y.; Obi, K.; Shibuya, K. *Chem. Phys. Lett.* **1991**, *181*, 100–104. (d) Ebbesen, T. W.; Tanigaki, K.; Kuroshima, S. *Chem. Phys. Lett.* **1991**, *181*, 501–504.

(41) Murakami, M.; Ohkubo, K.; Fukuzumi, S. *Chem.–Eur. J.* **2010**, *16*, 7820–7832.

(42) Márquez, M. C.; Márquez, O. P.; Márquez, J.; Hahn, F.; Beden, B.; Crouigneau, P.; Rakotondrainibe, A.; Lamy, C. *Synth. Met.* **1997**, *88*, 187–196.

(43) Sunahara, H.; Urano, Y.; Kojima, H.; Nagano, T. *J. Am. Chem. Soc.* **2007**, *129*, 5597–5604.

(44) (a) Fukuzumi, S.; Ohkubo, K.; Tokuda, Y.; Suenobu, T. *J. Am. Chem. Soc.* **2000**, *122*, 4286–4294. (b) Fukuzumi, S.; Yuasa, J.; Satoh, N.; Suenobu, T. *J. Am. Chem. Soc.* **2004**, *126*, 7585–7594.

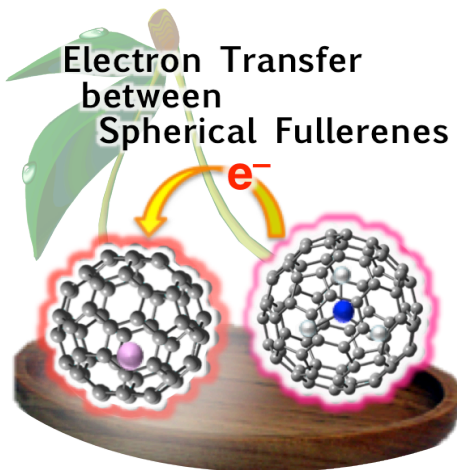
(45) Fukuzumi, S.; Koumitsu, S.; Hironaka, K.; Tanaka, T. *J. Am. Chem. Soc.* **1987**, *109*,

305–316.

- (46) Ohkubo, K.; Fukuzumi, S. *J. Phys. Chem. A* **2005**, *109*, 1105–1113.
- (47) Guldi, D. M.; Neta, P.; Asmus, K.-D. *J. Phys. Chem.* **1994**, *98*, 4617–4621.
- (48) Fukuzumi, S.; Ohkubo, K.; Imahori, H.; Guldi, D. M. *Chem.–Eur. J.* **2003**, *9*, 1585–1593.
- (49) Arbogast, J. W.; Foote, C. S.; Kao, M. *J. Am. Chem. Soc.* **1992**, *114*, 2277–2279.
- (50) Sakanoue, K.; Motoda, M.; Sugimoto, M.; Sakai, S. *J. Phys. Chem. A* **1999**, *103*, 5551–5556.
- (51) Fukuzumi, S.; Nakanishi, I.; Suenobu, T.; Kadish, K. M. *J. Am. Chem. Soc.* **1999**, *121*, 3468–3474.

## Chapter 3

### Small Reorganization Energies of Photoinduced Electron Transfer between Spherical Fullerenes



**Abstract:** Rate constants of photoinduced electron transfer between spherical fullerenes were determined using triscandium nitride encapsulated C<sub>80</sub> fullerene (Sc<sub>3</sub>N@C<sub>80</sub>) as an electron donor and the triplet excited state of lithium ion-encapsulated C<sub>60</sub> fullerene (Li<sup>+</sup>@C<sub>60</sub>) as an electron acceptor in polar and less polar solvents by laser flash photolysis measurements. Upon nanosecond laser excitation at 355 nm of a benzonitrile (PhCN) solution of Li<sup>+</sup>@C<sub>60</sub> and Sc<sub>3</sub>N@C<sub>80</sub>, electron transfer from Sc<sub>3</sub>N@C<sub>80</sub> to the triplet excited state [<sup>3</sup>(Li<sup>+</sup>@C<sub>60</sub>)<sup>\*</sup>] occurred to produce Sc<sub>3</sub>N@C<sub>80</sub><sup>+</sup> and Li<sup>+</sup>@C<sub>60</sub><sup>−</sup> ( $\lambda_{\text{max}} = 1035 \text{ nm}$ ). The rates of the photoinduced electron transfer were monitored by the decay of absorption at  $\lambda_{\text{max}} = 750 \text{ nm}$  due to <sup>3</sup>(Li<sup>+</sup>@C<sub>60</sub>)<sup>\*</sup>. The second-order rate constant of electron transfer from Sc<sub>3</sub>N@C<sub>80</sub> to <sup>3</sup>(Li<sup>+</sup>@C<sub>60</sub>)<sup>\*</sup> was determined to be  $k_{\text{et}} = 1.5 \times 10^9 \text{ M}^{-1} \text{ s}^{-1}$  from dependence of decay rate constant of <sup>3</sup>(Li<sup>+</sup>@C<sub>60</sub>)<sup>\*</sup> on the Sc<sub>3</sub>N@C<sub>80</sub> concentration. The rate constant of back electron transfer from Li<sup>+</sup>@C<sub>60</sub><sup>−</sup> to Sc<sub>3</sub>N@C<sub>80</sub><sup>+</sup> was also determined to be  $k_{\text{bet}} = 1.9 \times 10^9 \text{ M}^{-1} \text{ s}^{-1}$ , which is close to be the diffusion limited value in PhCN. Similarly, the rate constants of photoinduced electron transfer from C<sub>60</sub> to <sup>3</sup>(Li<sup>+</sup>@C<sub>60</sub>)<sup>\*</sup> and from Sc<sub>3</sub>N@C<sub>80</sub> to <sup>3</sup>C<sub>60</sub><sup>\*</sup> were determined together with the back electron-transfer reactions. The driving force dependence of log  $k_{\text{et}}$  and log  $k_{\text{bet}}$  was well fitted by using the Marcus theory of outer-sphere electron transfer, in which the internal (bond)

reorganization energy ( $\lambda_i$ ) was estimated by DFT calculations and the solvent reorganization energy ( $\lambda_s$ ) was calculated by the Marcus equation. When PhCN was replaced by *o*-dichlorobenzene (*o*-DCB), the  $\lambda$  value was decreased because of the smaller solvation changes of highly spherical fullerenes upon electron transfer in a less polar solvent.

## Introduction

Fullerenes, which have a highly delocalized three-dimensional  $\pi$ -system, are suitable for efficient electron acceptor because the uptake or release of electrons results in minimal structural and solvation changes upon electron transfer. Thus, fullerene has been frequently employed as an efficient electron acceptor for the donor-acceptor charge-separation systems.<sup>1–17</sup> On the Marcus theory of intermolecular electron transfer, the solvent reorganization energy was calculated by assuming that the electron donor and acceptor molecules are spheres.<sup>18,19</sup> Because C<sub>60</sub> is virtually spherical, it is an ideal molecule to examine the electron-transfer reactions involving C<sub>60</sub> in light of the Marcus theory of electron transfer. Because fullerenes have spacious inner cavities, some metals can be encapsulated inside of the fullerene cages to form endohedral metallofullerenes.<sup>20–25</sup> Such endohedral fullerenes have recently gained increasing attention with regard to the potential applicability due to the specific reactivities, being spherical molecules ( $I_h$ -symmetry) like C<sub>60</sub>. For instance, lithium ion-encapsulated C<sub>60</sub> fullerene (Li<sup>+</sup>@C<sub>60</sub>) has an  $I_h$ -symmetric C<sub>60</sub> cage. It shows enhanced electron acceptability as compared to pristine C<sub>60</sub>.<sup>26–35</sup> Trimetal nitride C<sub>80</sub> fullerene, M<sub>3</sub>N@ $I_h$ -C<sub>80</sub>, also has an  $I_h$ -symmetric C<sub>80</sub> fullerene cage, which is stabilized by encapsulating M<sub>3</sub>N cluster to donate six electrons to C<sub>80</sub> cage. In contrast to Li<sup>+</sup>@C<sub>60</sub>, M<sub>3</sub>N@C<sub>80</sub> shows a lower oxidation potential than pristine C<sub>60</sub>.<sup>36–39</sup> Among various M<sub>3</sub>N@C<sub>80</sub>, Sc<sub>3</sub>N@C<sub>80</sub> was best characterized in terms of structure and reactivity.<sup>40–42</sup> Although such ideal molecules to test the validity of the Marcus theory of electron transfer with regard to solvent reorganization energies have been known, the electron-transfer reactions between  $I_h$ -symmetric fullerenes have yet to be examined.

I report herein the photoinduced electron-transfer reactions from Sc<sub>3</sub>N@ $I_h$ -C<sub>80</sub> to Li<sup>+</sup>@C<sub>60</sub> (or C<sub>60</sub>) and also from C<sub>60</sub> to Li<sup>+</sup>@C<sub>60</sub> together with the back electron-transfer reactions in benzonitrile (PhCN) and *o*-dichlorobenzene (*o*-DCB), which were examined by using nanosecond laser flash photolysis measurements. The Marcus theory of outer-sphere electron transfer provides a quantitative basis to predict the deriving force dependence of the rate constants of photoinduced electron transfer and the back electron-transfer reactions in PhCN and

---

*o*-DCB using the internal (bond) reorganization energy ( $\lambda_i$ ) estimated by DFT calculations and the solvent reorganization energy ( $\lambda_s$ ) calculated by the Marcus equation.<sup>18,19</sup>

## Experimental Section

**Materials.** Chemicals were purchased from commercial sources and used without further purification, unless otherwise noted. Lithium ion-encapsulated C<sub>60</sub> fullerene hexafluorophosphate salt (Li<sup>+</sup>@C<sub>60</sub> PF<sub>6</sub><sup>-</sup>: 96%, Idea International Corp.) was obtained from Diichi Jitsugyo Co., Ltd., Japan. Triscandium nitride encapsulated C<sub>80</sub> fullerene (Sc<sub>3</sub>N@C<sub>80</sub>: 97%) was obtained from SES research company, USA. C<sub>60</sub> was also purchased from commercial sources and used without further purification. PhCN used as a solvent was distilled over phosphorus pentoxide.<sup>43</sup> *o*-DCB was purchased from Sigma-Aldrich Inc. and used as received. [Ru<sup>III</sup>(bpy)<sub>3</sub>](PF<sub>6</sub>)<sub>3</sub> was prepared as reported previously.<sup>44</sup> 1-Benzyl-1,4-dihydronicotinamide dimer [(BNA)<sub>2</sub>] was also prepared according to published procedures.<sup>45</sup>

**UV–Vis Absorption Spectral Measurements.** Absorption spectra were recorded on a JASCO V-670 UV–Vis–NIR spectrophotometer at room temperature.

**Laser Flash Photolysis Measurements.** Nanosecond transient absorption spectral measurements were performed according to the following procedure. A deaerated PhCN solution containing fullerenes (C<sub>60</sub>, Li<sup>+</sup>@C<sub>60</sub> and Sc<sub>3</sub>N@C<sub>80</sub>) was excited by a Panther OPO pumped Nd:YAG laser (Continuum, SLII-10, 4–6 ns fwhm) at 355 or 420 nm. The resulting time-resolved transient absorption spectra were measured by using a continuous Xe-lamp (150 W) and a photodiode (Hamamatsu 2949) as the probe light and detector, respectively. The output from the photodiode and the photomultiplier tube was recorded using a digitizing oscilloscope (Tektronix, TDS3032, 300 MHz). The solutions were deoxygenated by N<sub>2</sub> purging for 10 min prior to measurements. Rates of photoinduced electron-transfer reactions were monitored by the decay of the absorption band due to the triplet excited state of Li<sup>+</sup>@C<sub>60</sub> (or C<sub>60</sub>) with various concentrations of electron donors. The observed rate constants were determined by a least-squares curve fit. All experiments were performed at 298 K.

**Electrochemical Measurements.** Cyclic voltammetry (CV) measurements were performed with an ALS630B electrochemical analyzer in deaerated PhCN containing 0.1 M Bu<sub>4</sub>N<sup>+</sup>PF<sub>6</sub><sup>-</sup> (TBAPF<sub>6</sub>) as a supporting electrolyte at 298 K. The platinum working electrode (BAS, surface i.d. 1.6 mm) was polished with BAS polishing alumina suspension and rinsed with acetone before use. The counter electrode was a platinum wire (0.5 mm diam.). The measured potentials

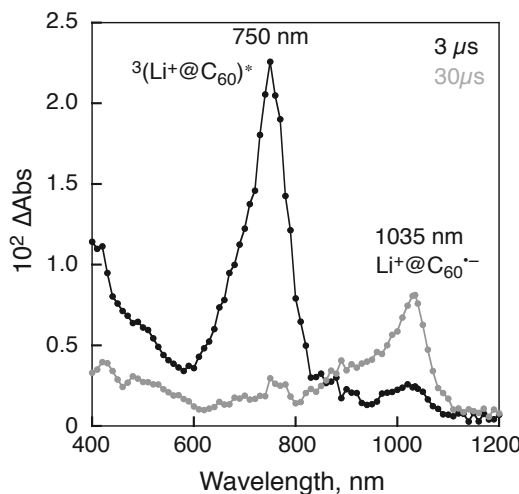
were recorded with respect to an Ag/AgNO<sub>3</sub> (0.01 M) reference electrode. The values of redox potentials (vs Ag/AgNO<sub>3</sub>) are converted into those vs SCE by addition of 0.29 V.<sup>46</sup>

**Theoretical Calculations.** Density functional theory (DFT) calculations were performed on a 32CPU workstation (PQS, Quantum Cube QS8-2400C-064). Geometry optimizations were carried out using the B3LYP/6-311G(d) basis set for Li<sup>+</sup>@C<sub>60</sub>, Li<sup>+</sup>@C<sub>60</sub><sup>•-</sup>, C<sub>60</sub>, C<sub>60</sub><sup>•-</sup>, C<sub>60</sub><sup>•+</sup>, Sc<sub>3</sub>N@C<sub>80</sub> and Sc<sub>3</sub>N@C<sub>80</sub><sup>•+</sup> as implemented in the Gaussian 09 program, revision A.02.<sup>47-49</sup>

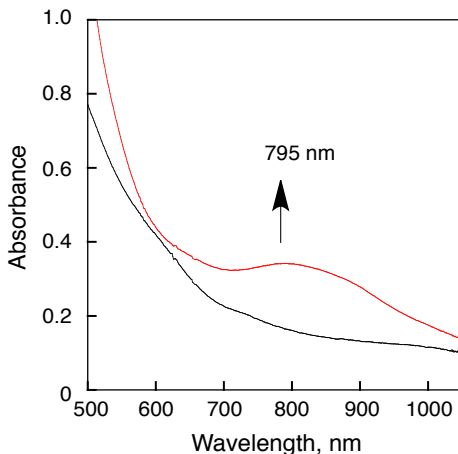
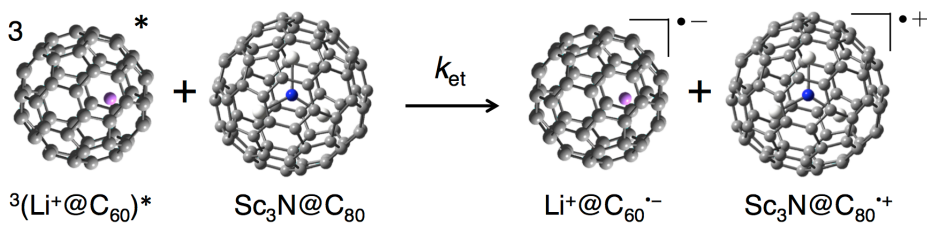
## Results and Discussion

**Photoinduced Electron Transfer between Spherical Fullerenes.** Nanosecond laser excitation of a deaerated PhCN solution containing Li<sup>+</sup>@C<sub>60</sub> and Sc<sub>3</sub>N@C<sub>80</sub> results in observation of triplet-triplet (T-T) absorption due to <sup>3</sup>(Li<sup>+</sup>@C<sub>60</sub>)<sup>\*</sup> (\* indicated the excited state) at 3  $\mu$ s (black line) after the laser excitation.<sup>31</sup> This absorption spectrum was changed to the transient absorption at 30  $\mu$ s (blue line), which shows the absorption band at 1035 nm due to Li<sup>+</sup>@C<sub>60</sub> radical anion (Li<sup>+</sup>@C<sub>60</sub><sup>•-</sup>) as shown in Figure 1.<sup>32-34</sup> These results indicate that photoinduced electron transfer from Sc<sub>3</sub>N@C<sub>80</sub> to <sup>3</sup>(Li<sup>+</sup>@C<sub>60</sub>)<sup>\*</sup> occurs to produce Sc<sub>3</sub>N@C<sub>80</sub> radical cation (Sc<sub>3</sub>N@C<sub>80</sub><sup>•+</sup>) and Li<sup>+</sup>@C<sub>60</sub><sup>•-</sup> as shown in Scheme 1.

Unfortunately, Sc<sub>3</sub>N@C<sub>80</sub><sup>•+</sup> was not observed as a typical absorption band because the absorption was too small and broad at 795 nm ( $\epsilon_{\text{max}} = 1700 \text{ M}^{-1} \text{ cm}^{-1}$ ). The assignment of the absorption spectrum due to Sc<sub>3</sub>N@C<sub>80</sub><sup>•+</sup> was carried out by the steady-state Vis–NIR spectral measurement of Sc<sub>3</sub>N@C<sub>80</sub><sup>•+</sup> generated by the oxidation of Sc<sub>3</sub>N@C<sub>80</sub> with Ru(bpy)<sub>3</sub>(PF<sub>6</sub>)<sub>3</sub>



**Figure 1.** Transient absorption spectra of Li<sup>+</sup>@C<sub>60</sub> ( $5.0 \times 10^{-5}$  M) in the presence of Sc<sub>3</sub>N@C<sub>80</sub> ( $5.0 \times 10^{-5}$  M) in deaerated PhCN at 298 K taken at 3 (black line) and 30  $\mu$ s (gray line) after nanosecond laser excitation at 355 nm.

**Scheme 1**

**Figure 2.** Vis–NIR absorption spectra of  $\text{Sc}_3\text{N}@\text{C}_{80}$  (black) and  $\text{Sc}_3\text{N}@\text{C}_{80}^{\bullet+}$  (red) produced via electron transfer from  $\text{Sc}_3\text{N}@\text{C}_{80}$  ( $2.0 \times 10^{-4}$  M) to  $\text{Ru}(\text{bpy})_3(\text{PF}_6)_3$  ( $2.0 \times 10^{-4}$  M) in PhCN.

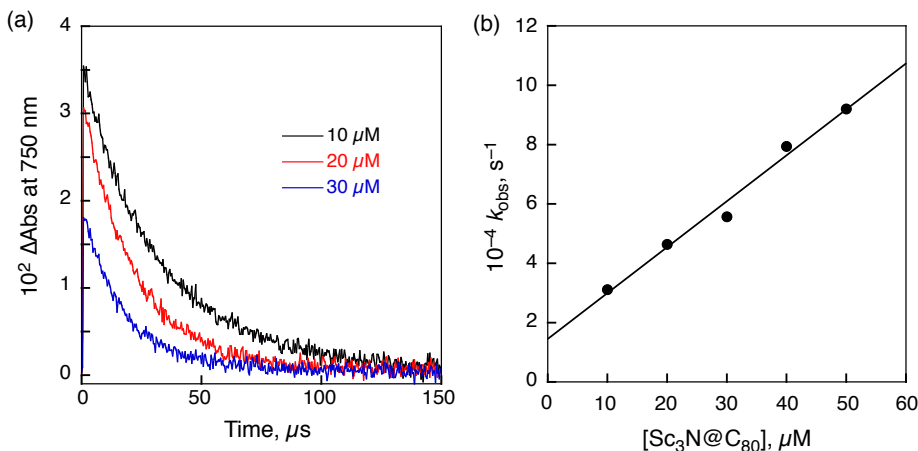


**Figure 3.** (a) Decay profiles at 750 nm of  ${}^3(\text{Li}^+@\text{C}_{60})^*$  in the presence of various concentrations of  $\text{Sc}_3\text{N}@\text{C}_{80}$  in PhCN. (b) Plot of the decay rate constant ( $k_{\text{obs}}$ ) versus the concentration of  $\text{Sc}_3\text{N}@\text{C}_{80}$ .

( $E_{\text{ox}} = 1.24$  V vs SCE)<sup>50</sup> in PhCN as shown in Figure 2. The second-order rate constant ( $k_{\text{et}}$ ) of bimolecular electron transfer from  $\text{Sc}_3\text{N}@\text{C}_{80}$  to  ${}^3(\text{Li}^+@\text{C}_{60})^*$  was determined from the dependence of the decay rate constant ( $k_{\text{obs}}$ ) of the T-T absorption due to  ${}^3(\text{Li}^+@\text{C}_{60})^*$  ( $\lambda_{\text{max}} = 750$  nm) on the concentration of  $\text{Sc}_3\text{N}@\text{C}_{80}$ . The  $k_{\text{obs}}$  value increased with increasing the

concentration of  $\text{Sc}_3\text{N}@\text{C}_{80}$  as shown in Figure 3a. From the slope of the linear plot depicted in Figure 3b, the  $k_{\text{et}}$  value was determined to be  $1.5 \times 10^9 \text{ M}^{-1} \text{ s}^{-1}$ , which is close to the diffusion limited value in PhCN ( $\sim 5.6 \times 10^9 \text{ M}^{-1} \text{ s}^{-1}$ ).<sup>51</sup>

The absorption band at 1035 nm due to  $\text{Li}^+@\text{C}_{60}^{\cdot-}$  decayed obeying second-order kinetics as shown in Figure 4. In the case of  $\text{Li}^+@\text{C}_{60}^{\cdot-}/\text{Sc}_3\text{N}@\text{C}_{80}^{\cdot+}$ , the second-order plot for the decay of  $\text{Li}^+@\text{C}_{60}^{\cdot-}$  obtained from the absorbance change at 1035 nm and the  $\varepsilon$  value ( $7300 \text{ M}^{-1} \text{ cm}^{-1}$ )<sup>30</sup> gives a linear plot (see inset of Figure 4). The second-order rate constant ( $k_{\text{bet}}$ ) of the back electron transfer from  $\text{Li}^+@\text{C}_{60}^{\cdot-}$  to  $\text{Sc}_3\text{N}@\text{C}_{80}^{\cdot+}$  was determined from the slope of the linear plot to be  $1.9 \times 10^9 \text{ M}^{-1} \text{ s}^{-1}$ . The driving force ( $-\Delta G_{\text{et}}$ ) of electron transfer from an electron donor to an electron acceptor is determined from the one-electron redox potentials by using eq 1:

$$-\Delta G_{\text{et}} = e[E_{\text{red}(\text{acceptor})} - E_{\text{ox}(\text{donor})}] \quad (1)$$

To evaluate the electron-transfer driving force, electrochemical measurements (cyclic voltammetry and differential pulse voltammetry) were performed as shown in Figure 5. The driving force of electron transfer from  $\text{Sc}_3\text{N}@\text{C}_{80}$  to  ${}^3(\text{Li}^+@\text{C}_{60})^*$  was determined to be  $-\Delta G_{\text{et}} = 0.58 \text{ eV}$  from the potential difference between one-electron oxidation of  $\text{Sc}_3\text{N}@\text{C}_{80}$  (1.09 V vs SCE) and one-electron reduction of  ${}^3(\text{Li}^+@\text{C}_{60})^*$  (1.67 V).<sup>31</sup> The driving force of back electron transfer ( $-\Delta G_{\text{bet}}$ ) from  $\text{Li}^+@\text{C}_{60}^{\cdot-}$  to  $\text{Sc}_3\text{N}@\text{C}_{80}^{\cdot+}$  in PhCN was determined to be 0.95 eV from the potential difference between one-electron oxidation potential of  $\text{Sc}_3\text{N}@\text{C}_{80}$  (1.09 V) and one-electron reduction potential of  $\text{Li}^+@\text{C}_{60}$  (0.14 V).<sup>30</sup> Therefore, both electron-transfer reactions are energetically favorable in PhCN.

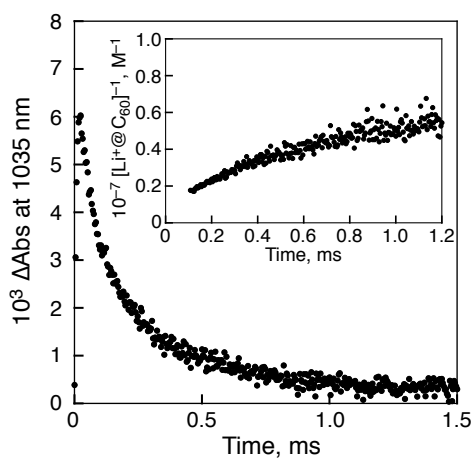


**Figure 4.** Decay time profile at 1035 nm for back electron transfer from  $\text{Li}^+@\text{C}_{60}^{\cdot-}$  to  $\text{Sc}_3\text{N}@\text{C}_{80}^{\cdot+}$  obtained by nanosecond laser excitation of  $\text{Li}^+@\text{C}_{60}$  ( $5.0 \times 10^{-5} \text{ M}$ ) with  $\text{Sc}_3\text{N}@\text{C}_{80}$  ( $5.0 \times 10^{-5} \text{ M}$ ) in PhCN. Inset: The second-order plot.

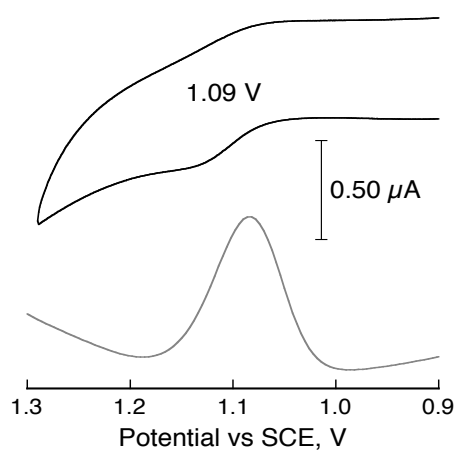


**Figure 5.** Cyclic voltammogram (CV, black) and difference pulse voltammogram (DPV, gray) of  $\text{Sc}_3\text{N}@\text{C}_{80}$  ( $2.0 \times 10^{-4}$  M) in deaerated PhCN containing  $\text{TBAPF}_6$  (0.10 M) as an electrolyte. Scan rate: 100  $\text{mV s}^{-1}$  for CV and 4  $\text{mV s}^{-1}$  for DPV.

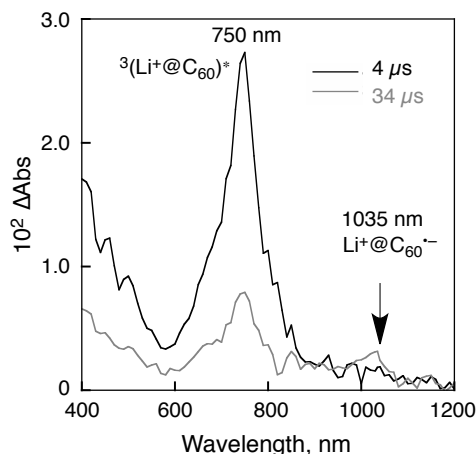


**Figure 6.** Transient absorption spectra of  $\text{Li}^+@\text{C}_{60}$  ( $5.0 \times 10^{-5}$  M) in the presence of  $\text{C}_{60}$  ( $5.0 \times 10^{-5}$  M) in deaerated PhCN at 298 K taken at 4 (black line) and 34  $\mu\text{s}$  (gray line) after nanosecond laser excitation at 355 nm.

When  $\text{Sc}_3\text{N}@\text{C}_{80}$  was replaced by  $\text{C}_{60}$ , electron transfer from  $\text{C}_{60}$  to  ${}^3(\text{Li}^+@\text{C}_{60})^*$  also occurred to produce  $\text{Li}^+@\text{C}_{60}^{\bullet-}$  and  $\text{C}_{60}^{\bullet+}$  as shown in Figure 6, where the absorption band at 1035 nm due to  $\text{Li}^+@\text{C}_{60}^{\bullet-}$  is overlapped with that at 980 nm due to  $\text{C}_{60}^{\bullet+}$ .<sup>52</sup> Although the driving force of this reaction is slightly negative ( $-\Delta G_{\text{et}} = 0.09$  eV), the expected yield of  $\text{Li}^+@\text{C}_{60}^{\bullet-}$  (50%) under the present experimental conditions is large enough to be detected using large excess  $\text{C}_{60}$  as compared to  ${}^3(\text{Li}^+@\text{C}_{60})^*$ . The  $k_{\text{et}}$  value was determined from the slope of the linear plot of the observed first-order decay rate constant of  ${}^3(\text{Li}^+@\text{C}_{60})^*$  versus concentration of  $\text{C}_{60}$  in Figure 7a to be  $2.6 \times 10^7 \text{ M}^{-1} \text{ s}^{-1}$  in PhCN at 298 K. The larger intercept value in Figure 7a as compared to that in Figure 3b results from the back electron transfer from  $\text{Li}^+@\text{C}_{60}^{\bullet-}$  to  $\text{C}_{60}^{\bullet+}$  to reproduce  ${}^3(\text{Li}^+@\text{C}_{60})^*$ . The back electron transfer from  $\text{Li}^+@\text{C}_{60}^{\bullet-}$  to  $\text{C}_{60}^{\bullet+}$  produces not only  ${}^3(\text{Li}^+@\text{C}_{60})^*$

but also  ${}^3\text{C}_{60}^*$  rather than the ground state of  $\text{Li}^+@\text{C}_{60}$  and  $\text{C}_{60}$ . This is because the rate of back electron transfer to the ground state is much slower due to the much larger driving force [ $-\Delta G_{\text{bet}}$  (ground state) = 1.62 eV] than the  $\lambda$  values of  $\text{C}_{60}$  and  $\text{Li}^+@\text{C}_{60}$  in the Marcus inverted region.<sup>31</sup> The driving force of back electron transfer to the triplet excited state [ $-\Delta G_{\text{bet (triplet)}}$ ] is estimated to be 0.09 eV. The  $k_{\text{bet}}$  value was determined from the second-order decay of  $\text{Li}^+@\text{C}_{60}^{\cdot-}$  (Figure 7b) to be  $1.4 \times 10^9 \text{ M}^{-1} \text{ s}^{-1}$ .

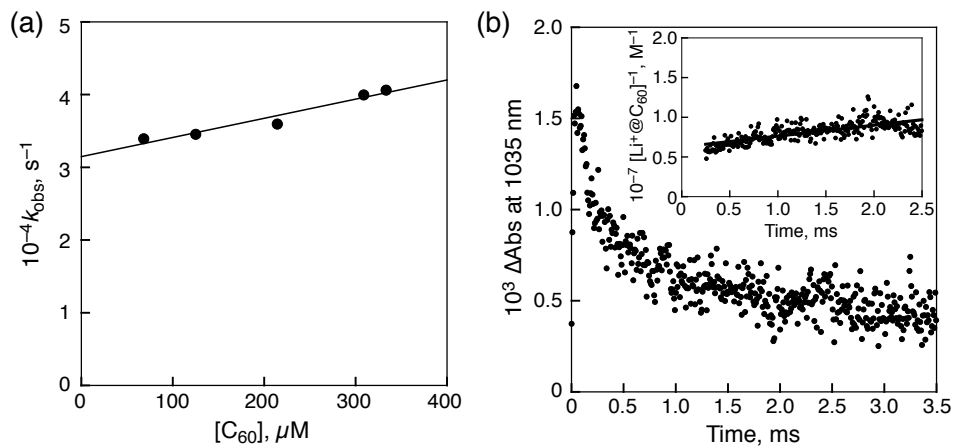


**Figure 7.** (a) Plot of the pseudo-first-order rate constant ( $k_{\text{obs}}$ ) versus concentration of  $\text{C}_{60}$  for photoinduced electron transfer from  $\text{C}_{60}$  to  $\text{Li}^+@\text{C}_{60}$  ( $5.0 \times 10^{-5} \text{ M}$ ) in deaerated PhCN at 298 K. (b) Time profile of absorbance at 1035 nm due to  $\text{Li}^+@\text{C}_{60}^{\cdot-}$  upon nanosecond laser excitation of a deaerated PhCN solution of  $\text{Li}^+@\text{C}_{60}$  ( $5.0 \times 10^{-5} \text{ M}$ ) and  $\text{C}_{60}$  ( $5.0 \times 10^{-5} \text{ M}$ ). Insert: The second-order plot of the decay of  $\text{Li}^+@\text{C}_{60}^{\cdot-}$  obtained from the absorbance at 1035 nm and the  $\varepsilon$  value ( $7300 \text{ M}^{-1} \text{ cm}^{-1}$ ).

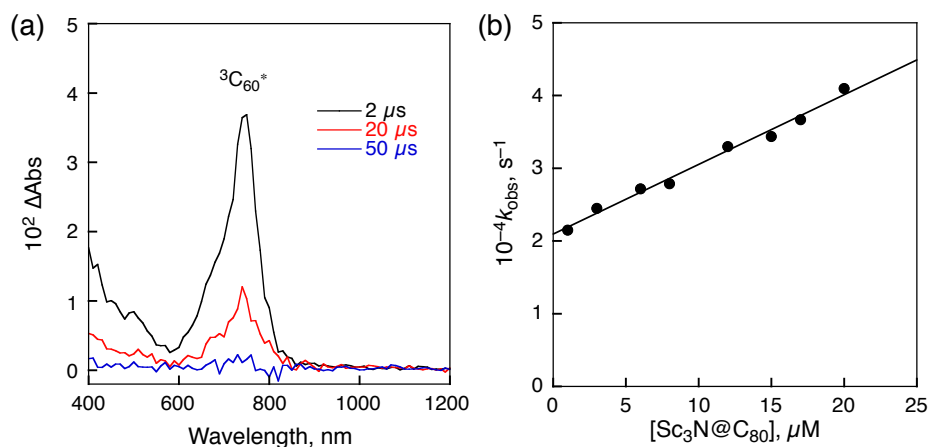


**Figure 8.** (a) Transient absorption spectra of  $\text{C}_{60}$  ( $5.0 \times 10^{-5} \text{ M}$ ) in the presence of  $\text{Sc}_3\text{N}@\text{C}_{80}$  ( $5.0 \times 10^{-5} \text{ M}$ ) in deaerated PhCN at 298 K taken at 2 (black line), 20  $\mu\text{s}$  (red line) and 50  $\mu\text{s}$  (blue line) after nanosecond laser excitation at 355 nm. (b) Plot of the pseudo-first-order rate constant ( $k_{\text{obs}}$ ) versus concentration of  $\text{Sc}_3\text{N}@\text{C}_{80}$  for photoinduced electron transfer from  $\text{Sc}_3\text{N}@\text{C}_{80}$  to  $\text{C}_{60}$  ( $5.0 \times 10^{-5} \text{ M}$ ) in deaerated PhCN at 298 K.

In the case of photoinduced electron transfer from  $\text{Sc}_3\text{N}@\text{C}_{80}$  to  ${}^3\text{C}_{60}^*$  in PhCN, the electron-transfer products ( $\text{C}_{60}^{\cdot-}$  and  $\text{Sc}_3\text{N}@\text{C}_{80}^{\cdot+}$ ) were not observed as shown in Figure 8a, because the back electron transfer is faster than the photoinduced electron transfer. The  $k_{\text{et}}$  value was determined from the decay rate of  ${}^3\text{C}_{60}^*$ , which increased with increasing the concentration of  $\text{Sc}_3\text{N}@\text{C}_{80}$  to be  $9.6 \times 10^8 \text{ M}^{-1} \text{ s}^{-1}$  at 298 K (Figure 8b). The back electron transfer from  $\text{C}_{60}^{\cdot-}$  to  $\text{Sc}_3\text{N}@\text{C}_{80}^{\cdot+}$  may produce  ${}^3\text{Sc}_3\text{N}@\text{C}_{80}^*$  (1.20 eV)<sup>42</sup> rather than the ground state of  $\text{C}_{60}$  and  $\text{Sc}_3\text{N}@\text{C}_{80}$ , because the rate of back electron transfer to ground state is much slower due to the much larger driving force [ $-\Delta G_{\text{bet}}(\text{ground state}) = 1.52 \text{ eV}$ ] than the  $\lambda$  values of  $\text{C}_{60}$  and  $\text{Li}^+@\text{C}_{60}$  in the Marcus inverted region. These data are summarized in Table 1.

The  $k_{\text{et}}$  values of photoinduced electron-transfer reactions of  $\text{Li}^+@\text{C}_{60}$ ,  $\text{C}_{60}$  and  $\text{Sc}_3\text{N}@\text{C}_{80}$  were also determined in *o*-DCB, which is less polar than PhCN (Figures 9 and 10). To determine the  $k_{\text{bet}}$  values in *o*-DCB, the extinction coefficient of the absorption band at 1035 nm due to  $\text{Li}^+@\text{C}_{60}^{\cdot-}$  was determined in *o*-DCB.  $\text{Li}^+@\text{C}_{60}^{\cdot-}$  was generated by photoinduced electron-transfer reduction of  $\text{Li}^+@\text{C}_{60}$  by using 1-benzyl-1,4-dihydronicotineamid dimer  $[(\text{BNA})_2]$ , which is known to act as a two-electron donor.<sup>53</sup> The absorption coefficient of

**Table 1.** One-Electron Redox Potentials and Rate Constants of Electron Transfer in PhCN or *o*-DCB at 298 K

entry	donor	$E_{\text{ox}}$ vs SCE, V	acceptor	$E_{\text{red}}$ vs SCE, V	solvent	$-\Delta G_{\text{et}}$ , eV	$k_{\text{et}}$ , $\text{M}^{-1} \text{ s}^{-1}$
1	$\text{Sc}_3\text{N}@\text{C}_{80}$	1.09	${}^3(\text{Li}^+@\text{C}_{60})^*$	1.67	PhCN	0.58	$1.5 \times 10^9$
2	$\text{Li}^+@\text{C}_{60}^{\cdot-}$	0.14	$\text{Sc}_3\text{N}@\text{C}_{80}^{\cdot+}$	1.09	PhCN	0.95	$1.9 \times 10^9$
3	$\text{C}_{60}$	1.76	${}^3(\text{Li}^+@\text{C}_{60})^*$	1.67	PhCN	-0.09	$2.6 \times 10^7$
4	$\text{Li}^+@\text{C}_{60}^{\cdot-}$	0.14	$\text{C}_{60}^{\cdot+}$	1.76	PhCN	$1.62$ (0.09) <sup>b</sup>	$1.4 \times 10^9$
5	$\text{Sc}_3\text{N}@\text{C}_{80}$	1.09	${}^3\text{C}_{60}^*$	1.14	PhCN	0.05	$9.6 \times 10^8$
6	$\text{C}_{60}^{\cdot-}$	-0.43	$\text{Sc}_3\text{N}@\text{C}_{80}^{\cdot+}$	1.09	PhCN	$1.52$ (0.32) <sup>b</sup>	-
7	$\text{Sc}_3\text{N}@\text{C}_{80}$	1.15	${}^3(\text{Li}^+@\text{C}_{60})^*$	1.70	<i>o</i> -DCB	0.55	$3.8 \times 10^9$
8	$\text{Li}^+@\text{C}_{60}^{\cdot-}$	0.17	$\text{Sc}_3\text{N}@\text{C}_{80}^{\cdot+}$	1.15	<i>o</i> -DCB	0.98	$3.7 \times 10^9$
9	$\text{C}_{60}$	1.80	${}^3(\text{Li}^+@\text{C}_{60})^*$	1.70	<i>o</i> -DCB	-0.10	$2.1 \times 10^8$
10	$\text{Li}^+@\text{C}_{60}^{\cdot-}$	0.17	$\text{C}_{60}^{\cdot+}$	1.80	<i>o</i> -DCB	$1.63$ (0.10) <sup>b</sup>	$4.3 \times 10^9$
11	$\text{Sc}_3\text{N}@\text{C}_{80}$	1.15	${}^3\text{C}_{60}^*$	1.05	<i>o</i> -DCB	-0.10	-
12	$\text{C}_{60}^{\cdot-}$	-0.52	$\text{Sc}_3\text{N}@\text{C}_{80}^{\cdot+}$	1.15	<i>o</i> -DCB	1.67	-

<sup>a</sup> CV and DPV of  $\text{Li}^+@\text{C}_{60}$ ,  $\text{C}_{60}$ , and  $\text{Sc}_3\text{N}@\text{C}_{80}$  in *o*-DCB are shown in Figure 11. <sup>b</sup> Driving force of back electron transfer to produce  ${}^3(\text{Li}^+@\text{C}_{60})^*$  and  ${}^3(\text{Li}^+@\text{C}_{60})^*$ .

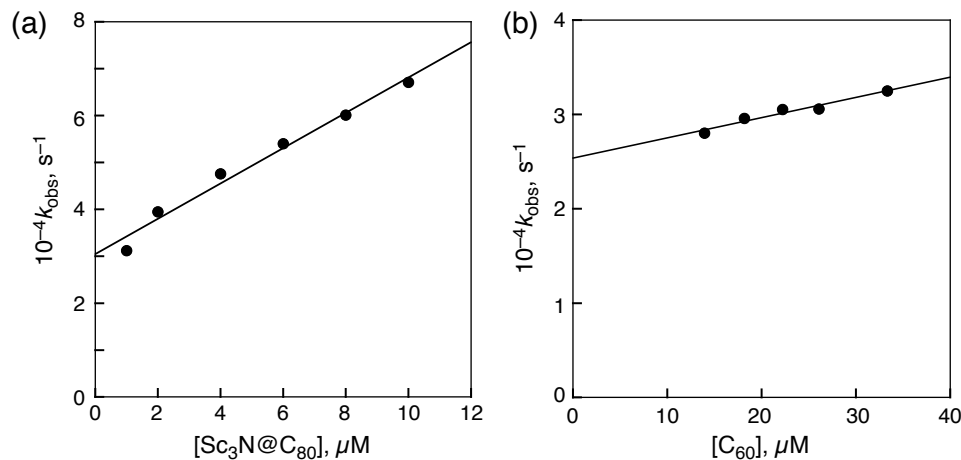


**Figure 9.** Plots of the pseudo-first-order rate constant ( $k_{\text{obs}}$ ) vs concentration of (a)  $\text{Sc}_3\text{N}@\text{C}_{80}$  for photoinduced electron transfer from  $\text{Sc}_3\text{N}@\text{C}_{80}$  to  $\text{Li}^+@\text{C}_{60}$  ( $5.0 \times 10^{-5}$  M) and (b)  $\text{C}_{60}$  for photoinduced electron transfer from  $\text{C}_{60}$  to  $\text{Li}^+@\text{C}_{60}$  ( $5.0 \times 10^{-5}$  M) in deaerated *o*-DCB at 298 K.

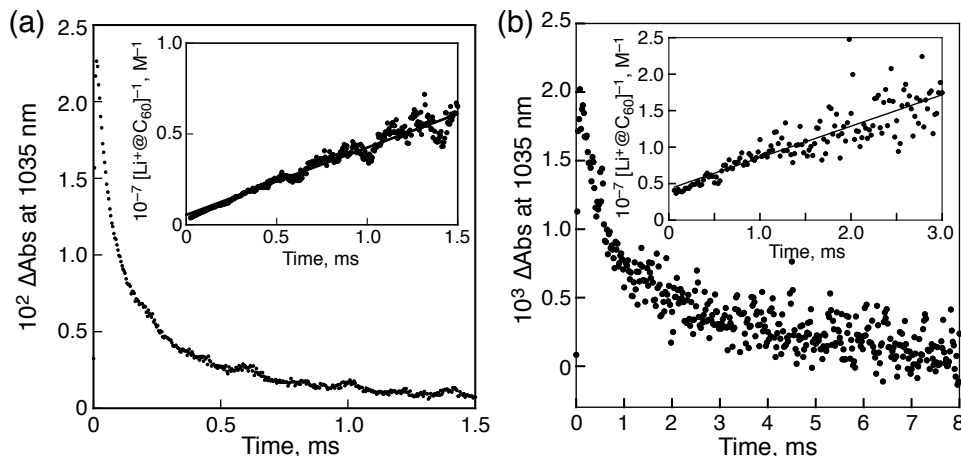


**Figure 10.** Time profile of absorbance at 1035 nm due to  $\text{Li}^+@\text{C}_{60}^-$  upon nanosecond laser excitation of a deaerated *o*-DCB solution of  $\text{Li}^+@\text{C}_{60}$  ( $5.0 \times 10^{-5}$  M) and (a)  $\text{Sc}_3\text{N}@\text{C}_{80}$  ( $5.0 \times 10^{-5}$  M) and (b)  $\text{C}_{60}$ . Insert: The second-order plot of the decay of  $\text{Li}^+@\text{C}_{60}^-$  obtained from the absorbance at 1035 nm and the  $\epsilon$  value ( $8000 \text{ M}^{-1} \text{ cm}^{-1}$ ).

$\text{Li}^+@\text{C}_{60}^-$  was determined to be  $8000 \text{ M}^{-1} \text{ cm}^{-1}$  in *o*-DCB (Figure 12). The  $k_{\text{et}}$  values and the driving forces of electron transfer in *o*-DCB are also summarized in Table 1.

The  $k_{\text{et}}$  values of photoinduced electron-transfer reactions of  $\text{Li}^+@\text{C}_{60}$ ,  $\text{C}_{60}$  and  $\text{Sc}_3\text{N}@\text{C}_{80}$  were also determined in *o*-DCB, which is less polar than PhCN (Figures 9 and 10). To determine the  $k_{\text{bet}}$  values in *o*-DCB, the extinction coefficient of the absorption band at 1035 nm due to  $\text{Li}^+@\text{C}_{60}^-$  was determined in *o*-DCB.  $\text{Li}^+@\text{C}_{60}^-$  was generated by photoinduced electron-transfer reduction of  $\text{Li}^+@\text{C}_{60}$  by using 1-benzyl-1,4-dihydronicotineamid dimer  $[(\text{BNA})_2]$ , which is known to act as a two-electron donor.<sup>53</sup> The absorption coefficient of

$\text{Li}^+@\text{C}_{60}^{\bullet-}$  was determined to be  $8000 \text{ M}^{-1} \text{ cm}^{-1}$  in *o*-DCB (Figure 12). The  $k_{\text{et}}$  values and the driving forces of electron transfer in *o*-DCB are also summarized in Table 1.

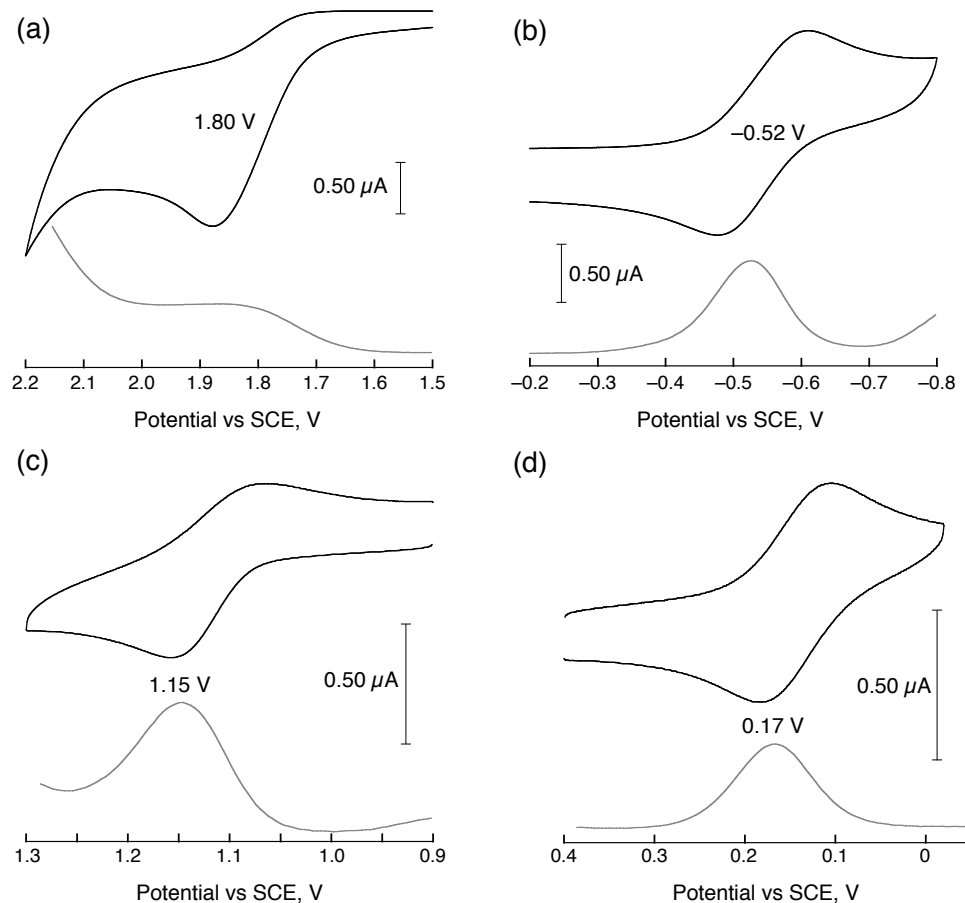


**Figure 11.** Cyclic voltammograms (CVs, black) and difference pulse voltammograms (DPVs, gray) of (a) (b)  $\text{C}_{60}$  ( $4.0 \times 10^{-4}$  M) (c)  $\text{Sc}_3\text{N}@\text{C}_{80}$  ( $2.0 \times 10^{-4}$  M) (d)  $\text{Li}^+@\text{C}_{60}$  ( $2.0 \times 10^{-4}$  M) in deaerated *o*-DCB containing TBAPF<sub>6</sub> (0.10 M) as an electrolyte. Scan rate: 100 mV s<sup>-1</sup> for CV and 4 mV s<sup>-1</sup> for DPV.

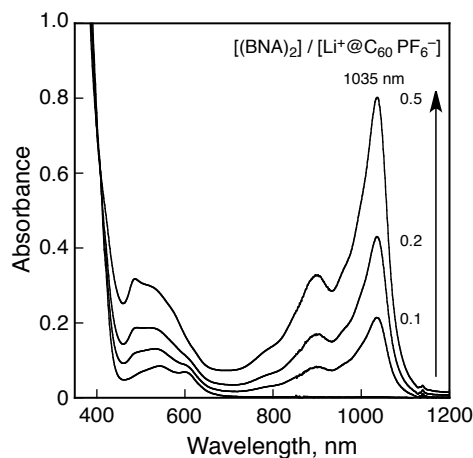


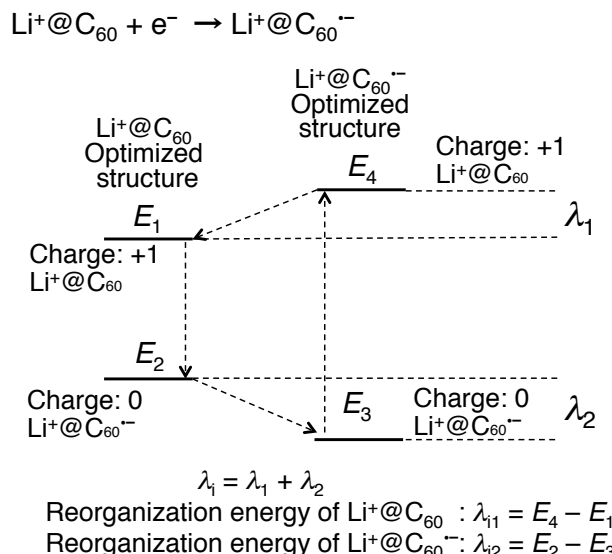
**Figure 12.** UV-Vis-NIR spectra of  $\text{Li}^+@\text{C}_{60}^{\bullet-}$  produced via electron transfer from (BNA)<sub>2</sub> to  $[\text{Li}^+@\text{C}_{60}]^{\bullet-}\text{PF}_6^-$  (1.0  $\times 10^{-4}$  M) in *o*-DCB.

**Driving Force Dependence of Rate Constants of Photoinduced Electron Transfer and Back Electron Transfer.** According to the Marcus theory of intermolecular outer-sphere electron transfer, the observed second-order rate constant of electron transfer is given by eq 2,<sup>18,19</sup>

$$\frac{1}{k_{\text{et}}} = \frac{1}{k_{\text{diff}}} + \frac{1}{Z \exp\left[-(\lambda/4)(1 + \Delta G_{\text{et}}/\lambda)^2/k_{\text{B}}T\right]} \quad (3)$$

where  $k_{\text{diff}}$  is the diffusion limited rate constant,  $Z$  is the collision frequency,  $\lambda$  is the reorganization energy of electron transfer, and  $k_{\text{B}}$  is the Boltzmann constant. The reorganization energy of electron transfer ( $\lambda$ ) consists of internal (bond) reorganization energy ( $\lambda_i$ ) and the solvent reorganization energy ( $\lambda_s$ ), that is,  $\lambda = \lambda_i + \lambda_s$ . The  $\lambda_i$  values of  $\text{Li}^+@\text{C}_{60}/\text{Li}^+@\text{C}_{60}^{\cdot-}$ ,  $\text{C}_{60}/\text{C}_{60}^{\cdot-}$ ,  $\text{C}_{60}^{\cdot+}/\text{C}_{60}$  and  $\text{Sc}_3\text{N}@\text{C}_{80}^{\cdot+}/\text{Sc}_3\text{N}@\text{C}_{80}$  were evaluated theoretically by using the density functional theory (DFT) calculations at the B3LYP/6-311G(d) level of theory.<sup>31,54,55</sup> In the case of reduction of  $\text{Li}^+@\text{C}_{60}$ , the reorganization energy ( $\lambda_i = \lambda_{i1} + \lambda_{i2}$ ) can be estimated as a sum of the difference between the energy of  $\text{Li}^+@\text{C}_{60}$  (charge +1) with the optimized structure of  $\text{Li}^+@\text{C}_{60}^{\cdot-}$  ( $E_4$ ) and that with optimized structure of  $\text{Li}^+@\text{C}_{60}$  and the difference between the energy of  $\text{Li}^+@\text{C}_{60}^{\cdot-}$  (charge 0) with the optimized structure of  $\text{Li}^+@\text{C}_{60}$  ( $E_2$ ) and that with the optimized

### Scheme 2



structure  $\text{Li}^+@\text{C}_{60}^{\cdot-}$  ( $E_3$ ), as shown in Scheme 2. The  $\lambda_i$  value for one-electron reduction of  $\text{Li}^+@\text{C}_{60}$  and  $\text{C}_{60}$  were estimated to be 0.144 and 0.135 eV, respectively. The corresponding  $\lambda_i$  value for the one-electron oxidation of  $\text{C}_{60}$  and  $\text{Sc}_3\text{N}@\text{C}_{80}$  were also calculated to be 0.173 and

0.088 eV, respectively. In the case of  $\text{Li}^+@\text{C}_{60}/\text{C}_{60}$  system, the  $\lambda_i$  value of electron transfer between  $\text{Li}^+@\text{C}_{60}$  and  $\text{C}_{60}$  is calculated to be 0.159 eV from the mean of the  $\lambda_i$  value for  $\text{Li}^+@\text{C}_{60}$  and  $\text{C}_{60}$ .

According to the Marcus theory of electron transfer, the  $\lambda_s$  value is given by eq 3,<sup>18,19</sup>

$$\lambda_s = \frac{(\Delta e)^2}{4\pi\epsilon_0} \left( \frac{1}{2r_D} + \frac{1}{2r_A} - \frac{1}{d} \right) \left( \frac{1}{\epsilon_{op}} - \frac{1}{\epsilon_s} \right) \quad (3)$$

where  $\Delta e$  is the amount of transferred charge ( $\Delta e = e$ ),  $\epsilon_0$  is the dielectric constant in a vacuum,  $r_A$  and  $r_D$  are the van der Waals radii of electron donor and acceptor,  $d$  is the contact distance,  $\epsilon_{op}$  is optical dielectric constant ( $\epsilon_{op} = n^2$ , where  $n$  is refractive index.  $n = 1.5252$  for PhCN, 1.5515 for *o*-DCB),<sup>56,57</sup> and  $\epsilon_s$  is the dielectric constant ( $\epsilon_s = 25.2$  for PhCN, 9.93 for *o*-DCB)<sup>58,59</sup> of the solvent. The van der Waals radii are 5.02 Å for  $\text{C}_{60}$  and  $\text{Li}^+@\text{C}_{60}$ ,<sup>60</sup> and 5.80 Å for  $\text{Sc}_3\text{N}@\text{C}_{80}$ , which are determined from the sum of the van der Waals radii of carbon atom<sup>61</sup> and the distance between center and surface of  $\text{Sc}_3\text{N}@\text{C}_{80}$ .<sup>40</sup> The  $\lambda_s$  values were calculated to be 0.560 eV for  $\text{Li}^+@\text{C}_{60}/\text{C}_{60}$  and 0.525 eV for  $\text{Li}^+@\text{C}_{60}$  (or  $\text{C}_{60}/\text{Sc}_3\text{N}@\text{C}_{80}$ ). These values are summarized in Table 2.

**Table 2.** Experimental and Calculated Values of Reorganization Energy

entry	donor/acceptor	solvent	calculated value, eV			
			$\lambda_{\text{Average}}$	$\lambda$	$\lambda_i$	$\lambda_s$
1	$\text{Li}^+@\text{C}_{60}/\text{Sc}_3\text{N}@\text{C}_{80}$			0.641	0.116	0.525
2	$\text{Li}^+@\text{C}_{60}/\text{C}_{60}$	PhCN	0.67	0.718	0.159	0.560
3	$\text{Sc}_3\text{N}@\text{C}_{80}/\text{C}_{60}$			0.636	0.112	0.525
4	$\text{Li}^+@\text{C}_{60}/\text{Sc}_3\text{N}@\text{C}_{80}$			0.539	0.116	0.423
5	$\text{Li}^+@\text{C}_{60}/\text{C}_{60}$	<i>o</i> -DCB	0.56	0.610	0.159	0.451
6	$\text{Sc}_3\text{N}@\text{C}_{80}/\text{C}_{60}$			0.535	0.112	0.423

The averaged calculated  $\lambda$  values (0.67 and 0.56 eV in PhCN and *o*-DCB, respectively) were used to fit the data based on the Marcus equation for outer-sphere electron transfer (eq 3) as shown in Figure 13, where the diffusion limited rate constants were taken as  $1.9 \times 10^9$  and  $5.2 \times 10^9 \text{ M}^{-1} \text{ s}^{-1}$  in PhCN and *o*-DCB, respectively<sup>62</sup> (the largest value in each solvent in Table 1). The  $Z$  value is given by eq 4,

$$Z = k_B T k_{\text{diff}}/h k_{\text{-diff}} = k_B T K/ h \quad (K = k_{\text{diff}}/k_{\text{-diff}}) \quad (4)$$

where  $h$  is the Planck's constant,  $k_{\text{-diff}}$  is the dissociation constant of the encounter complex,  $K$  is the equilibrium constant of formation of the encounter complex. The fitting curves largely agree with the observed  $k_{\text{et}}$  values using the  $Z$  value of  $1.0 \times 10^{11} \text{ M}^{-1} \text{ s}^{-1}$ , which is normally used for outer-sphere electron transfer reactions.<sup>18,19</sup> The smaller  $\lambda$  value in *o*-DCB than in PhCN results from a decrease in the solvent reorganization energy of electron transfer because the bond reorganization energy must be the same irrespective of solvent polarity.

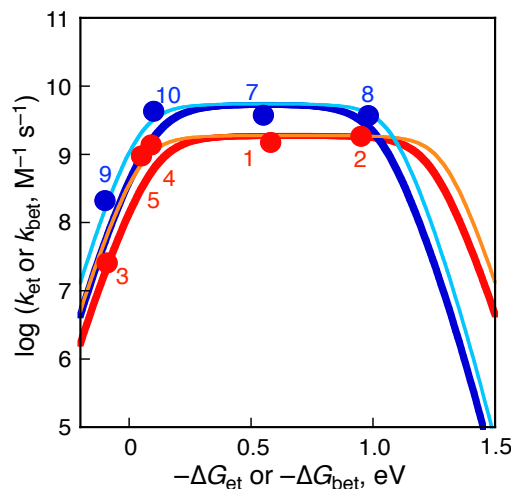


**Figure 13.** Driving force dependences of  $\log k_{\text{et}}$  and  $\log k_{\text{bet}}$  for electron transfer between fullerenes in PhCN (red ●) and *o*-DCB (blue ●) at 298 K. Numbers refer to reactions in Tables 1. The lines are drawn by using eq 3, where the  $\lambda$ ,  $k_{\text{diff}}$  and  $Z$  values are  $\lambda = 0.67 \text{ eV}$ ,  $k_{\text{diff}} = 1.9 \times 10^9 \text{ M}^{-1} \text{ s}^{-1}$ ,  $Z = 1.0 \times 10^{11} \text{ M}^{-1} \text{ s}^{-1}$  (red line),  $Z = 3.0 \times 10^{11} \text{ M}^{-1} \text{ s}^{-1}$  (orange line) in PhCN;  $\lambda = 0.56 \text{ eV}$ ,  $k_{\text{diff}} = 5.6 \times 10^9 \text{ M}^{-1} \text{ s}^{-1}$ , and  $Z = 1.0 \times 10^{11} \text{ M}^{-1} \text{ s}^{-1}$  (dark blue line),  $Z = 3.0 \times 10^{11} \text{ M}^{-1} \text{ s}^{-1}$  (light blue line) in *o*-DCB.

The small deviation of the observed  $k_{\text{et}}$  values for the fitting curves in the region of driving force close to zero may result from the difference in the  $K$  values of the encounter complex, which was reported to be dependent on the driving force of electron transfer.<sup>63</sup> Because the interaction in the encounter complex is mainly due to charge transfer between electron donors and acceptors, the  $K$  value is the largest when the driving force of electron transfer is zero.<sup>63</sup> When the  $Z$  value of  $3.0 \times 10^{11} \text{ M}^{-1} \text{ s}^{-1}$  ( $K = 0.050 \text{ M}^{-1}$ ), which is larger than the  $Z$  value of  $1.0 \times 10^{11} \text{ M}^{-1} \text{ s}^{-1}$  ( $K = 0.016 \text{ M}^{-1}$ ), is used in eq 3, the better fitting was observed in the region of driving force close to zero in Figure 13.

## Conclusion

In summary, I have determined the driving force dependence of the rate constants of photoinduced electron transfer between  $I_h$ -symmetric fullerenes and the back electron-transfer reactions by nanosecond laser flash photolysis. The predicted driving force dependence of the rate constants of electron transfer between spherical fullerenes in both PhCN and *o*-DCB using the Marcus theory of outer-sphere electron transfer with the calculated  $\lambda$  values fits well with the observed rate constants of electron transfer.

## References

- (1) Echegoyen, L.; Diederich, F; Echegoyen, L. E. In *Fullerenes, Chemistry, Physics, and Technology*; Kadish, K. M., Ruoff, R. S., Eds.; Wiley-Interscience: New York, 2000; pp 1–51.
- (2) Guldi, D. M.; Fukuzumi, S. In *Fullerenes: From Synthesis to Optoelectronic Properties*; Guldi, D. M., Martin, N., Eds.; Kluwer: Dordrecht, 2003, pp 237–265.
- (3) Sgobba, V.; Rahman, G. M. A.; Guldi, D. M. In *Carbon Nanotubes in Electron Donor-Acceptor Nanocomposites, Chemistry of Carbon Nanotubes*; Basiuk, V. A., Ed.; American Scientific Publishers: CA, 2006.
- (4) Fukuzumi, S.; Guldi, D. M. In *Electron Transfer in Chemistry* Balzani, V., Ed.; Wiley-VCH: Weinheim, 2001; Vol. 2, pp 270–337.
- (5) Connolly, J. S.; Bolton, J. R. In *Photoinduced Electron Transfer*; Fox, M. A., Chanon, M., Eds.; Elsevier: Amsterdam, 1988; Part D, pp 303–393.
- (6) Wasielewski, M. R. In *Photoinduced Electron Transfer*; Fox, M. A., Chanon, M., Eds.; Elsevier: Amsterdam, 1988; Part A, pp 161–206.
- (7) D’Souza, F.; Deviprasad, G. R.; Zandler, M. E.; Hoang, V. T.; Klykov, A.; VanStipdonk, M.; Perera, A.; El-Khouly, M. E.; Fujitsuka, M.; Ito, O. *J. Phys. Chem. A* **2002**, *106*, 3243–3252.
- (8) El-Khouly, M. E.; Rogers, L. M.; Zandler, M. E.; Suresh, G.; Fujitsuka, M.; Ito, O.; D’Souza, F. *ChemPhysChem* **2003**, *4*, 474–481.
- (9) Xiao, S.; El-Khouly, M. E.; Li, Y.; Gan, Z.; Liu, H.; Jiang, L.; Araki, Y.; Ito, O.; Zhu, D. *J. Phys. Chem. B* **2005**, *109*, 3658–3667.
- (10) Grimm, B.; Schornbaum, J.; Cardona, C. M.; van Paauwe, J. D.; Boyd, P. D. W.; Guldi, D. M. *Chem. Sci.* **2011**, 1530–1537.
- (11) Fukuzumi, S. *Phys. Chem. Chem. Phys.* **2008**, *10*, 2283–2297.

(12) Ohkubo, K.; Fukuzumi, S. *J. Porphyrins Phthalocyanines* **2008**, *12*, 993–1004.

(13) Ohkubo, K.; Fukuzumi, S. *Bull. Chem. Soc. Jpn.* **2009**, *82*, 303–315.

(14) Imahori, H.; Tamaki, K.; Araki, Y.; Sekiguchi, Y.; Ito, O.; Sakata, Y.; Fukuzumi, S. *J. Am. Chem. Soc.* **2002**, *124*, 5165–5174.

(15) Imahori, H.; Sekiguchi, Y.; Kashiwagi, Y.; Sato, T.; Araki, Y.; Ito, O.; Yamada, H.; Fukuzumi, S. *Chem.–Eur. J.* **2004**, *10*, 3184–3196.

(16) Imahori, H.; Guldi, D. M.; Tamaki, K.; Yoshida, Y.; Luo, C.; Sakata, Y.; Fukuzumi, S. *J. Am. Chem. Soc.* **2001**, *123*, 6617–6628.

(17) Guldi, D. M.; Imahori, H.; Tamaki, K.; Kashiwagi, Y.; Yamada, H.; Sakata, Y.; Fukuzumi, S. *J. Phys. Chem. A* **2004**, *108*, 541–548.

(18) Marcus, R. A. *Annu. Rev. Phys. Chem.* **1964**, *15*, 155–196.

(19) Marcus, R. A. *Angew. Chem., Int. Ed. Engl.* **1993**, *32*, 1111–1121.

(20) Maeda, Y.; Lu, J.; Akasaka, T.; Nagase, S. In *Chemistry of Nanocarbons*; Akasaka, T., Wuldi, F., Nagase, S., Ed.; Wiley-VCH, Verlag GmbH & Co. KGaA: Weinheim, 2010; pp 491–523.

(21) Akasaka, T.; Kato, T.; Kobayashi, K.; Nagase, S.; Yamamoto, K.; Funasaka H.; Takahashi, T. *Nature* **1995**, *374*, 600–601.

(22) Xu, J. X.; Lu, X.; Zhou, X. H.; He, X. R.; Shi, Z. J.; Gu, Z. N. *Chem. Mater.* **2004**, *16*, 2959–2964.

(23) Shinohara, H. *Rep. Prog. Phys.* **2000**, *63*, 843–892.

(24) Li, F.-F.; Pinzón, J. R.; Mercado, B. Q.; Olmstead, M. M.; Balch, A. L.; Echegoyen, L. *J. Am. Chem. Soc.* **2011**, *133*, 1563–1571.

(25) Huang, H.; Yang, S. *J. Phys. Chem. B* **1998**, *102*, 10196–10200.

(26) Aoyagi, S.; Nishibori, E.; Sawa, H.; Sugimoto, K.; Takata, M.; Miyata, Y.; Kitaura, R.; Shinohara, H.; Okada, H.; Sakai, T.; Ono, Y.; Kawachi, K.; Yokoo, K.; Ono, S.; Omote, K.; Kasama, Y.; Ishikawa, S.; Komuro, T.; Tobita, H. *Nature Chem.* **2010**, *2*, 678–683.

(27) Aoyagi, S.; Nishibori, E.; Sawa, H.; Okada, H.; Tobita, H.; Kasama, Y.; Kitaura, R.; Shinohara, H. *Angew. Chem., Int. Ed.* **2012**, *51*, 3377–3381.

(28) Matsuo, Y.; Okada, H.; Maruyama, M.; Sato, H.; Tobita, H.; Ono, Y.; Omote, K.; Kawachi, K.; Kasama, Y. *Org. Lett.* **2012**, *14*, 3784–3787.

(29) Ueno, H.; Nakamura, Y.; Ikuma, N.; Kokubo, K.; Oshima, T. *Nano Res.* **2012**, *5*, 558–564.

(30) Fukuzumi, S.; Ohkubo, K.; Kawashima, Y.; Kim, D. S.; Park, J. S.; Jana, A.; Lynch, V. M.; Kim, D.; Sessler, J. L. *J. Am. Chem. Soc.* **2011**, *133*, 15938–15941.

---

(31) Kawashima, Y.; Ohkubo, K.; Fukuzumi, S. *J. Phys. Chem. A* **2012**, *116*, 8942–8948.

(32) Ohkubo, K.; Kawashima, Y.; Fukuzumi, S. *Chem. Commun.* **2012**, *48*, 4314–4316.

(33) Kamimura, T.; Ohkubo, K.; Kawashima, Y.; Nobukuni, H.; Naruta, Y.; Tani, F.; Fukuzumi, S. *Chem. Sci.* **2013**, *4*, 1451–1461.

(34) Ohkubo, K.; Kawashima, Y.; Sakai, H.; Hasobe, T.; Fukuzumi, S. *Chem. Commun.* **2013**, *49*, 4474–4476.

(35) Bill N. L.; Ishida, M.; Bähring, S.; Lim, J. M.; Lee, S.; Davis, C. M.; Lynch, V. M.; Nielsen, K. A.; Jeppesen, J. O.; Ohkubo, K.; Fukuzumi, S.; Kim, D.; Sessler, J. L. *J. Am. Chem. Soc.* **2013**, *135*, 10852–10862.

(36) Zhang, J.; Stevenson, S.; Dorn, H. C. *Acc. Chem. Res.* **2013**, *46*, 1548–1557.

(37) Rudolf, M.; Wolfrum, S.; Guldi, D. M.; Feng, L.; Tsuchiya, T.; Akasaka, T.; Echegoyen, L. *Chem.–Eur. J.* **2012**, *18*, 5136–5148.

(38) Lu, X.; Akasaka, T.; Nagase, S. Chemistry of Endohedral Metallofullerenes: the Role of Metals. *Chem. Commun.* **2011**, *47*, 5942–5957.

(39) Popov, A. A.; Yang, S.; Dunsch, L. *Chem. Rev.* **2013**, *133*, 5989–6113.

(40) Wang, T.-S.; Feng, L.; Wu, J.-Y.; Xu, W.; Xiang, J.-F.; Tan, K.; Ma, Y.-H.; Zheng, J.-P.; Jiang, L.; Lu, X.; Shu, C.-Y.; Wang, C.-R. *J. Am. Chem. Soc.* **2010**, *132*, 16362–16364.

(41) Iiduka, Y.; Ikenaga, O.; Sakuraba, A.; Wakahara, T.; Tsuchiya, T.; Maeda, Y.; Nakahodo, T.; Akasaka, T.; Kako, M.; Mizorogi, N.; Nagase, S. *J. Am. Chem. Soc.* **2005**, *127*, 9956–9957.

(42) Feng, L.; Radhakrishnan, S. G.; Mizorogi, N.; Slanina, Z.; Nikawa, H.; Tsuchiya, T.; Akasaka, T.; Nagase, S.; Martín, N.; Guldi, D. M. *J. Am. Chem. Soc.* **2011**, *133*, 7608–7618.

(43) Armarego, W. L. F.; Chai, C. L. L. *Purification of Laboratory Chemicals*, 6 th ed; Pergamon Press: Oxford, 2009.

(44) Duan, L.; Xu, Y.; Zhang, P.; Wang, M.; Sun, L. *Inorg. Chem.* **2010**, *49*, 209–215.

(45) Fukuzumi, S.; Suenobu, T.; Patz, M.; Hirasaka, T.; Itoh, S.; Fujitsuka, M.; Ito, O. *J. Am. Chem. Soc.* **1998**, *120*, 8060–8068.

(46) Mann, C. K.; Barnes, K. K. In *Electrochemical Reactions in Non-aqueous Systems*; Mercel Dekker: New York, 1970.

(47) Frisch, M. J.; Trucks, G. W.; Schlegel, H. B.; Scuseria, G. E.; Robb, M. A.; Cheeseman, J. R.; Scalmani, G.; Barone, V.; Mennucci, B.; Petersson, G. A.; Nakatsuji, H.; Caricato, M.; Li, X.; Hratchian, H. P.; Izmaylov, A. F.; Bloino, J.; Zheng, G.; Sonnenberg, J. L.; Hada,

M.; Ehara, M.; Toyota, K.; Fukuda, R.; Hasegawa, J.; Ishida, M.; Nakajima, T.; Honda, Y.; Kitao, O.; Nakai, H.; Vreven, T.; Montgomery, J. A., Jr.; Peralta, J. E.; Ogliaro, F.; Bearpark, M.; Heyd, J. J.; Brothers, E.; Kudin, K. N.; Staroverov, V. N.; Kobayashi, R.; Normand, J.; Raghavachari, K.; Rendell, A.; Burant, J. C.; Iyengar, S. S.; Tomasi, J.; Cossi, M.; Rega, N.; Millam, J. M.; Klene, M.; Knox, J. E.; Cross, J. B.; Bakken, V.; Adamo, C.; Jaramillo, J.; Gomperts, R.; Stratmann, R. E.; Yazyev, O.; Austin, A. J.; Cammi, R.; Pomelli, C.; Ochterski, J. W.; Martin, R. L.; Morokuma, K.; Zakrzewski, V. G.; Voth, G. A.; Salvador, P.; Dannenberg, J. J.; Dapprich, S.; Daniels, A. D.; Farkas, O.; Foresman, J. B.; Ortiz, J. V.; Cioslowski, J.; Fox, D. J. *Gaussian 09, revision A.02*; Gaussian, Inc.: Wallingford, CT, 2009.

(48) Becke, A. D. *J. Chem. Phys.* **1993**, *98*, 5648–5652.

(49) Lee, C.; Yang, W.; Parr, R. G. *Phys. Rev. B* **1988**, *37*, 785–789.

(50) Park, J.; Morimoto, Y.; Lee, Y.-M.; You, Y.; Nam, W.; Fukuzumi, S. *Inorg. Chem.* **2011**, *50*, 11612–11622.

(51) Arbogast, J. W.; Foote, C. S.; Kao, M. *J. Am. Chem. Soc.* **1992**, *114*, 2277–2279.

(52) Nonell, S.; Arbogast, J. W.; Foote, C. S. *P J. Phys. Chem.* **1992**, *96*, 4169–4170.

(53) Fukuzumi, S.; Patz, M.; Suenobu, T.; Kuwahara, Y.; Itoh, S. *J. Am. Chem. Soc.* **1999**, *121*, 1605–1606.

(54) Fukuzumi, S.; Nakanishi, I.; Suenobu, T.; Kadish, K. M. *J. Am. Chem. Soc.* **1999**, *121*, 3468–3474.

(55) Sakanoue, K.; Motoda, M.; Sugimoto, M.; Sakai, S. *J. Phys. Chem. A* **1999**, *103*, 5551–5556.

(56) Letcher, T. M.; Naicker, P. K. *J. Chem. Eng. Data* **2001**, *46*, 1436–1441.

(57) Domańska, U. J.; Letcher, T. M. *J. Chem. Thermodyn.* **2000**, *32*, 1635–1645.

(58) Ho, P. C.; Ramsey, J. B. *J. Chem. Eng. Data* **1986**, *31*, 430–434.

(59) Curry, H. L.; Gilkerson, W. R. *J. Am. Chem. Soc.* **1957**, *79*, 4021–4023.

(60) Kikuchi, K.; Suzuki, S.; Saito, K.; Shiromaru, H.; Ikemoto, I.; Achiba, Y.; Zakhidov, A. A.; Ugawa, A.; Imaeda, K.; Inokuchi, H.; Yakushi, K. *Physica C* **1991**, *185-189*, 415–416.

(61) Batsanov, S. S. *Inorg. Mater.* **2001**, *37*, 871–885.

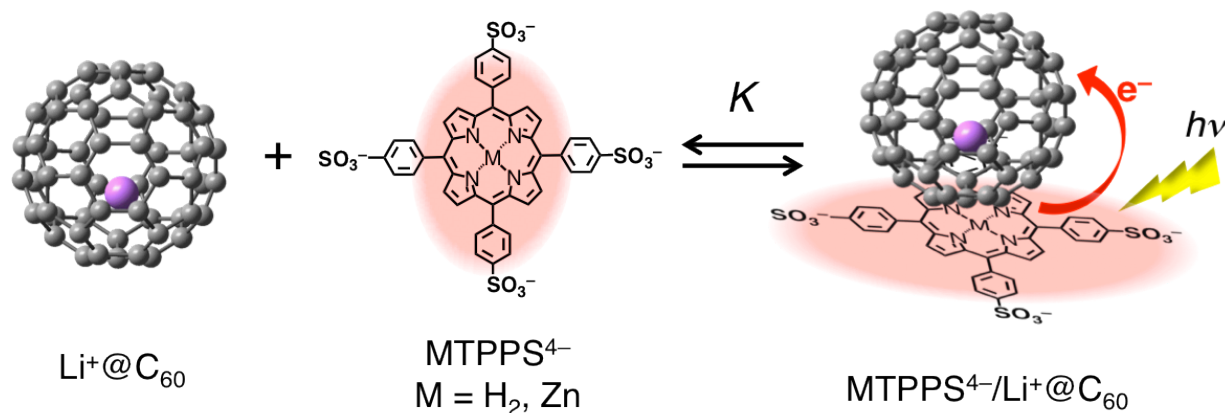
(62) The diffusion control of *o*-DCB was determined to be  $k_{\text{diff}} = 5.2 \times 10^9 \text{ M}^{-1} \text{ s}^{-1}$  by using the equation  $k_{\text{diff}} = 6.61 \times 10^9 / \eta$  and viscosity ( $\eta = 1.277 \text{ mPa}$ ). See: Okamoto, M.; Teranishi, H. *J. Phys. Chem.* **1984**, *88*, 5644–5646. Curry, H.; Gilkerson, W. *J. Am. Chem. Soc.* **1957**, *79*, 4021–4023.

(63) Hubig, S. M.; Rathore, R.; Kochi, J. K. *J. Am. Chem. Soc.* **1999**, *121*, 617–626.

---

## Chapter 4

Strong Supramolecular Binding of  $\text{Li}^+@\text{C}_{60}$  with Anionic Porphyrin and Long-Lived Photoinduced Charge Separation



**Abstract:** I report herein construction of supramolecular donor-acceptor systems composed of anionic sulfonated porphyrins ( $\text{H}_2\text{TPPS}^{4-}$  and  $\text{ZnTPPS}^{4-}$ ) as electron donors and a cationic lithium ion-encapsulated [60]fullerene, ( $\text{Li}^+@\text{C}_{60}$ ) as an electron acceptor in polar coordinating solvent, which are combined by using ionic and  $\pi$ - $\pi$  interaction. A strong supramolecular formation and long CS lifetime were observed in benzonitrile (PhCN) solution. The formation constant of supramolecule was determined from the absorption change to be  $3.0 \times 10^5 \text{ M}^{-1}$  in PhCN. The transient absorption spectra taken by nanosecond laser flash photolysis shows the superposition of the absorption bands of  $\text{H}_2\text{TPPS}^{4-}$  radical cation and that of  $\text{Li}^+@\text{C}_{60}$  radical anion. The lifetime of CS state is  $310 \mu\text{s}$ .

## Introduction

Fullerenes have been widely used as a three-dimensional electron-acceptor, due to their small reorganization energy associated with electron-transfer reactions, which results from the  $\pi$ -electron system being highly delocalized over the three-dimensional curved surface together with the rigid and confined structure of the aromatic  $\pi$ -sphere.<sup>1-4</sup> Porphyrins are known to have very intense absorption bands in the visible region and rich electron-donating properties.<sup>4,5</sup> There have been many reports on donor-acceptor linked molecules as well as supramolecular systems composed of fullerenes and porphyrins as the excellent building blocks.<sup>1-11</sup>

A numbers of fullerene/porphyrin supramolecular systems as artificial photosynthetic model have been extensively developed to mimic the energy- and electron-transfer processes in natural photosynthesis. When a nonpolar solvent is used to form a supramolecular complex with strong binding, the donor-acceptor ensembles afford efficiently charge-separated (CS) states by photoinduced electron transfer, but there are normally extremely short-lived.<sup>8-11</sup> The CS states usually decay to give the triplet excited states because the energy of radical ion pair is higher than the excited energy of the chromophores. The limit of CS energy is *ca.* 1.5 eV, which is the triplet excited energies of fullerene and porphyrin.<sup>11</sup> In contrast, the CS state could be long-lived in a polar solvent such as benzonitrile (PhCN), but the supramolecular binding between the donor and acceptor moieties is normally weak due to the solvent polarization.

I report herein construction of supramolecular donor-acceptor systems composed of anionic sulfonated porphyrins ( $\text{H}_2\text{TPPS}^{4-}$  and  $\text{ZnTPPS}^{4-}$ ) as electron donors and a cationic lithium ion-encapsulated fullerene, ( $\text{Li}^+@\text{C}_{60}$ ) as an electron acceptor,<sup>12</sup> which are connected by using ionic and  $\pi$ - $\pi$  interaction in a polar solvent.

## Experimental Method

**Materials.** Chemicals were purchased from commercial sources and used without further purification, unless otherwise noted. Lithium ion-encapsulated fullerene hexafluorophosphate salt ( $\text{Li}^+@\text{C}_{60}$   $\text{PF}_6^-$ : 96%) was obtained from Daiichi Jitsugyo Co. Ltd, Japan.  $(\text{Bu}_4\text{N}^+)_4\text{MTPPS}^{4-}$  ( $\text{M} = \text{H}_2, \text{Zn}$ ) were synthesized by the neutralization of tetrasulphonated porphyrin (Tokyo Chemical Industry Co. Ltd.) with 4 equiv. of tetrabutylammonium hydroxide in MeOH. Benzonitrile (PhCN) used as a solvent was distilled over phosphorus

---

pentoxide. Acetonitrile (MeCN) was purchased from WAKO pure chemical and used as received.

**UV–Vis Measurements.** Ultraviolet–visible (UV–Vis) absorption spectra were recorded on Hewlett Packard 8453 diode array spectrophotometer.

**Emission Spectral Measurements.** Fluorescence spectra were measured on a Horiba FluoroMax-4 spectrofluorophotometer with a quartz cuvette (path length = 10 mm) at 298 K. Phosphorescence spectra were measured on a Horiba FluoroMax-4 spectrofluorophotometer with a quartz tube (i.d. = 4 mm) at 77 K.

**Laser Flash Photolysis Measurements.** Femtosecond transient absorption spectroscopy experiments were conducted using an ultrafast source: Integra-C (Quantronix Corp.), an optical parametric amplifier: TOPAS (Light Conversion Ltd.) and a commercially available optical detection system: Helios provided by Ultrafast Systems LLC. The source for the pump and probe pulses were derived from the fundamental output of Integra-C ( $\lambda$  = 786 nm, 2 mJ/pulse and fwhm = 130 fs) at a repetition rate of 1 kHz. 75% of the fundamental output of the laser was introduced into a second harmonic generation (SHG) unit: Apollo (Ultrafast Systems) for excitation light generation at  $\lambda$  = 393 nm, while the rest of the output was used for white light generation. The laser pulse was focused on a sapphire plate of 3 mm thickness and then white light continuum covering the visible region from  $\lambda$  = 410 nm to 800 nm was generated via self-phase modulation. A variable neutral density filter, an optical aperture, and a pair of polarizer were inserted in the path in order to generate stable white light continuum. Prior to generating the probe continuum, the laser pulse was fed to a delay line that provides an experimental time window of 3.2 ns with a maximum step resolution of 7 fs. In our experiments, a wavelength at  $\lambda$  = 393 nm of SHG output was irradiated at the sample cell with a spot size of 1 mm diameter where it was merged with the white probe pulse in a close angle ( $< 10^\circ$ ). The probe beam after passing through the 2 mm sample cell was focused on a fiber optic cable that was connected to a CMOS spectrograph for recording the time-resolved spectra ( $\lambda$  = 410 - 800 nm). Typically, 1500 excitation pulses were averaged for 3 seconds to obtain the transient spectrum at a set delay time. Kinetic traces at appropriate wavelengths were assembled from the time-resolved spectral data. All measurements were conducted at room temperature, 295 K.

Nanosecond time-resolved transient absorption measurements were carried out using the laser system provided by UNISOKU Co., Ltd. Measurements of nanosecond transient absorption spectrum were performed according to the following procedure. A deaerated

---

solution containing supramolecule was excited by a Panther OPO pumped by a Nd:YAG laser (Continuum SLII-10, 4-6 ns fwhm). The photodynamics was monitored by continuous exposure to a Xenon lamp (150 W) as a probe light and a photomultiplier tube (Hamamatsu 2949) as a detector. The solution was oxygenated by nitrogen purging for 15 min prior to measurements.

**Electrochemical Measurements.** Electrochemical measurements were performed on an ALS630B electrochemical analyzer in deaerated PhCN and the mix solvent containing 0.1 M  $\text{Bu}_4\text{NPF}_6$  as the supporting electrolyte at 298 K. A conventional three-electrode cell was used with a platinum working electrode (surface area of  $0.3 \text{ mm}^2$ ) and a platinum wire as a counter electrode. The platinum working electrodes (BAS) were routinely polished with BAS polishing alumina suspension and rinsed with acetone and acetonitrile before use. The measured potentials were recorded with respect to an  $\text{Ag}/\text{AgNO}_3$  (0.01 M) reference electrode. All potentials (vs  $\text{Ag}/\text{Ag}^+$ ) were converted to values vs SCE by adding 0.29 V. All electrochemical measurements were carried out under an Ar atmosphere.

## Results and Discussion

A strong supramolecular binding and a long CS lifetime were attained in PhCN at 298 K. UV-Vis spectra of free base tetraphenylporphyrin tetrasulfonate  $[(\text{Bu}_4\text{N}^+)_4\text{H}_2\text{TPPS}^{4-}]$  in PhCN at 298 K are changed upon addition of  $\text{Li}^+@\text{C}_{60} \text{PF}_6^-$ , where the Soret band is red-shifted to 427 nm with an isosbestic point at 430 nm (Figure 1a). The absorbance change exhibits a saturation behavior with increasing  $\text{Li}^+@\text{C}_{60}$  concentration. According to eq 1, the absorbance change is given by eqs 2 and 3, which predict a linear correlation between  $(\alpha^{-1} - 1)^{-1}$  and  $([\text{Li}^+@\text{C}_{60}] - \alpha[\text{H}_2\text{TPPS}^{4-}]_0)$ , where  $A_0$  and  $A$  are the absorbance of  $\text{H}_2\text{TPPS}^{4-}$  at 424 nm in the absence and presence of  $\text{Li}^+@\text{C}_{60}$ , and  $[\text{H}_2\text{TPPS}^{4-}]_0$  is the initial concentration of  $\text{H}_2\text{TPPS}^{4-}$ . From a linear plot in the inset of Figure 1b, the formation constant ( $K$ ) of the  $\text{H}_2\text{TPPS}^{4-}/\text{Li}^+@\text{C}_{60}$  complex was determined to be  $3.0 \times 10^5 \text{ M}^{-1}$  in PhCN (Figure 1b). When  $\text{H}_2\text{TPPS}^{4-}$  is replaced by  $\text{ZnTPPS}^{4-}$ , the  $K$  value was determined to be  $1.6 \times 10^5 \text{ M}^{-1}$ , which is slightly smaller than that of  $\text{H}_2\text{TPPS}^{4-}$  (Figure 1d). The Job's plots confirmed that  $\text{Li}^+@\text{C}_{60}$  formed 1:1 complexes with  $\text{H}_2\text{TPPS}^{4-}$  and  $\text{ZnTPPS}^{4-}$  (Figure 2).

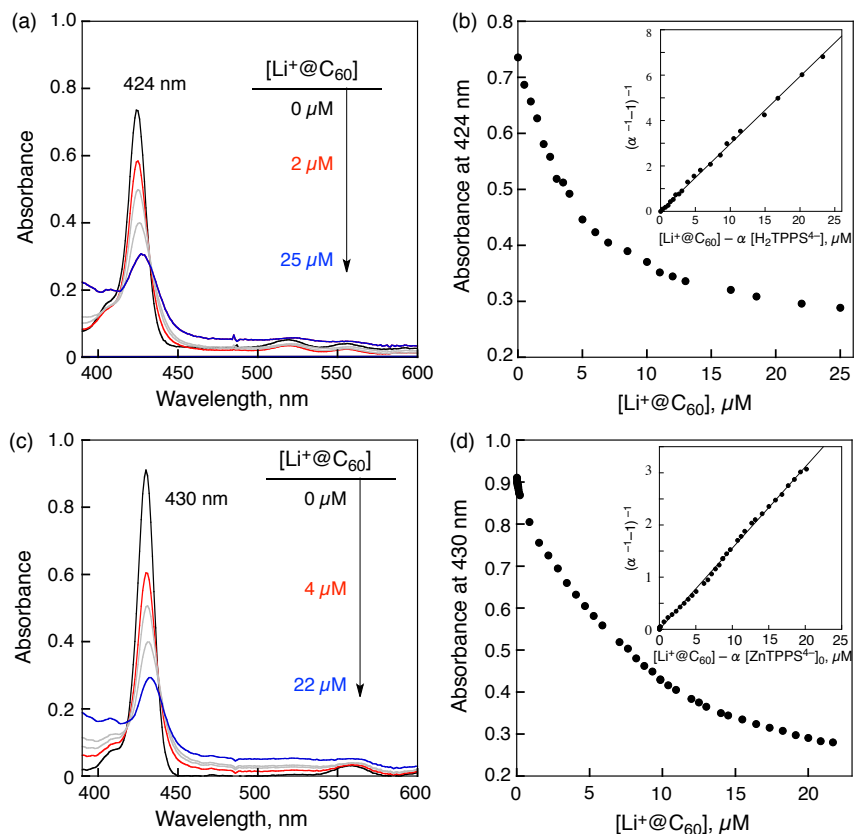
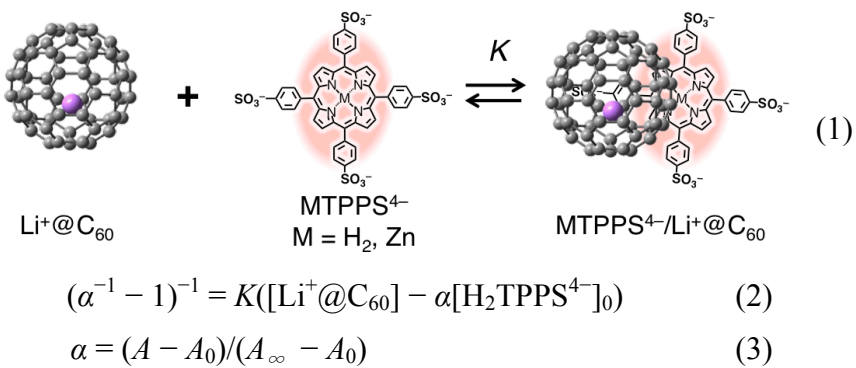


**Figure 1.** UV-Vis absorption spectra of (a)  $H_2TPPS^{4-}$  ( $2.0 \times 10^{-6}$  M), (c)  $ZnTPPS^{4-}$  ( $2.0 \times 10^{-6}$  M) in the presence of various concentrations of  $Li^+@C_{60}$  in PhCN; Absorption profile at (b) 424 nm and (d) 430 nm. Inset: Plot of  $(\alpha^{-1} - 1)^{-1}$  vs  $[Li^+@C_{60}] - \alpha[H_2TPPS^{4-}]$ .

Photoexcitation of the Soret band of  $H_2TPPS^{4-}$  at 430 nm in PhCN results in fluorescence at  $\lambda_{max} = 654$  and 722 nm. Addition of  $Li^+@C_{60}$  to a PhCN solution of  $H_2TPPS^{4-}$  resulted in a significant decrease in the fluorescence intensity of  $H_2TPPS^{4-}$  (Figure 3a). The fluorescence intensity decreases to reach a constant value with increasing  $Li^+@C_{60}$  concentration as the  $H_2TPPS^{4-}/Li^+@C_{60}$  complex is formed (Figure 3b). Virtually the same  $K$  value ( $3.4 \times 10^5 M^{-1}$ ) was obtained from the change in the fluorescence spectrum of  $H_2TPPS^{4-}$  in the presence of

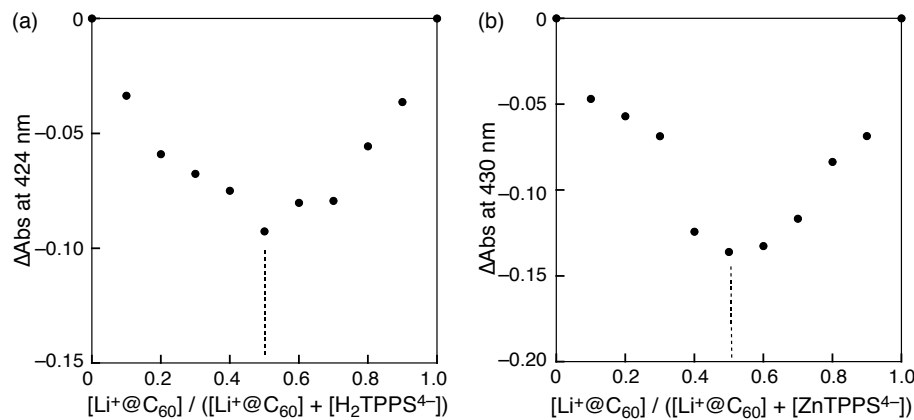


**Figure 2.** Job's plots for the formation of supramolecule between (a)  $\text{H}_2\text{TPPS}^{4-}$  (b)  $\text{ZnTPPS}^{4-}$  and  $\text{Li}^+@\text{C}_{60}$  in PhCN.

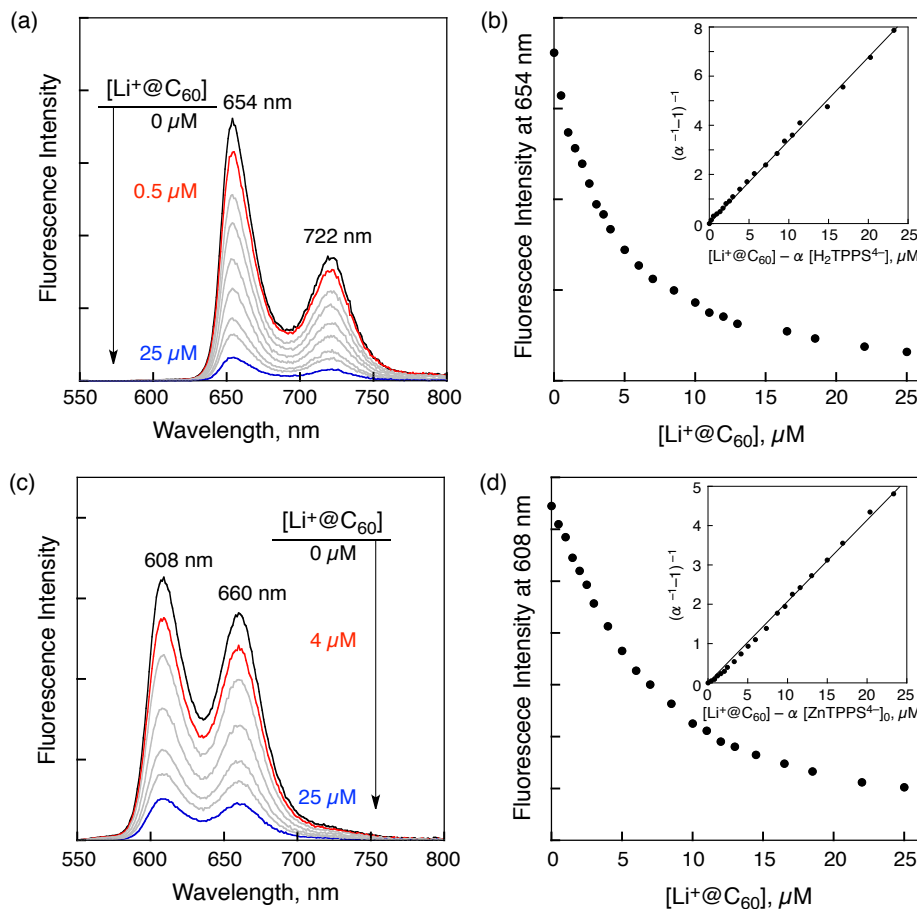


**Figure 3.** Fluorescence spectra of (a)  $\text{H}_2\text{TPPS}^{4-}$  ( $2.0 \times 10^{-6}$  M) and (c)  $\text{ZnTPPS}^{4-}$  ( $2.0 \times 10^{-6}$  M) in the presence of various concentrations of  $\text{Li}^+@\text{C}_{60}$  (0 to  $2.5 \times 10^{-5}$  M) in deaerated PhCN. The arrow indicates the direction of change. Changes in the fluorescence intensity of (b)  $\text{H}_2\text{TPPS}^{4-}$  and (d)  $\text{ZnTPPS}^{4-}$ . Inset: Plot of  $(\alpha^{-1} - 1)^{-1}$  vs  $[\text{Li}^+@\text{C}_{60}] - \alpha[\text{MTPPS}^{4-}]_0$ ;  $\alpha = (I - I_0)/(I_\infty - I_0)$ .

$\text{Li}^+@\text{C}_{60}$  (Figure 3b) as the value obtained from the absorption spectral change (*vide supra*). When  $\text{H}_2\text{TPPS}^{4-}$  was replaced by  $\text{ZnTPPS}^{4-}$ , the  $K$  value was determined to be  $2.1 \times 10^5 \text{ M}^{-1}$ , which is slightly smaller than that of  $\text{H}_2\text{TPPS}^{4-}$  (Figure 3d). The photophysical data are summarized in Table 1.

In order to determine the driving force of photoinduced electron transfer ( $-\Delta G_{\text{ET}}$ ), the redox potentials of  $\text{H}_2\text{TPPS}^{4-}$ ,  $\text{H}_2\text{TPPS}^{4-}/\text{Li}^+@\text{C}_{60}$  complex,  $\text{ZnTPPS}^{4-}$ ,  $\text{ZnTPPS}^{4-}/\text{Li}^+@\text{C}_{60}$  complex and  $\text{Li}^+@\text{C}_{60}$  were determined by the cyclic and differential pulse voltammetry measurements in PhCN (Figure 4). The  $-\Delta G_{\text{ET}}$  values of electron transfer from  $\text{H}_2\text{TPPS}^{4-}$  to  ${}^1[\text{Li}^+@\text{C}_{60}]^*$  and  ${}^3[\text{Li}^+@\text{C}_{60}]^*$  were determined from the one-electron oxidation potential of  $\text{H}_2\text{TPPS}^{4-}$  (1.00 V vs SCE), reduction potential of  $\text{Li}^+@\text{C}_{60}$  (+0.14 V vs SCE) and the excitation energies of  ${}^1[\text{Li}^+@\text{C}_{60}]^*$  ( $S_1 = 1.94 \text{ eV}$ ) and  ${}^3[\text{Li}^+@\text{C}_{60}]^*$  ( $T_1 = 1.53 \text{ eV}$ ) to be 1.08 and 0.67 eV, respectively.<sup>13</sup> Thus, the photoinduced electron transfer from  $\text{H}_2\text{TPPS}^{4-}$  to both the singlet and triplet excited states of  $\text{Li}^+@\text{C}_{60}$  in PhCN are exergonic.

**Table 1.** Formation Constants of Supramolecules and CS Lifetimes and Quantum Yields of  $\text{MTPPS}^{4-}/\text{Li}^+@\text{C}_{60}$  in PhCN

	$K, {}^a \text{ M}^{-1}$	$K, {}^b \text{ M}^{-1}$	$k_{\text{EN}}, \text{ s}^{-1}$	$\tau_{\text{CS}}, \mu\text{s}$	$\Phi_{\text{CS}}$
$\text{H}_2\text{TPPS}^{4-}$	$3.0 \times 10^5$	$3.4 \times 10^5$	$9.7 \times 10^{10}$	310	0.25
$\text{ZnTPPS}^{4-}$	$1.6 \times 10^5$	$2.1 \times 10^5$	$1.0 \times 10^{11}$	300	0.39

<sup>a</sup> Determined from the absorption change. <sup>b</sup> Determined from the fluorescence change.

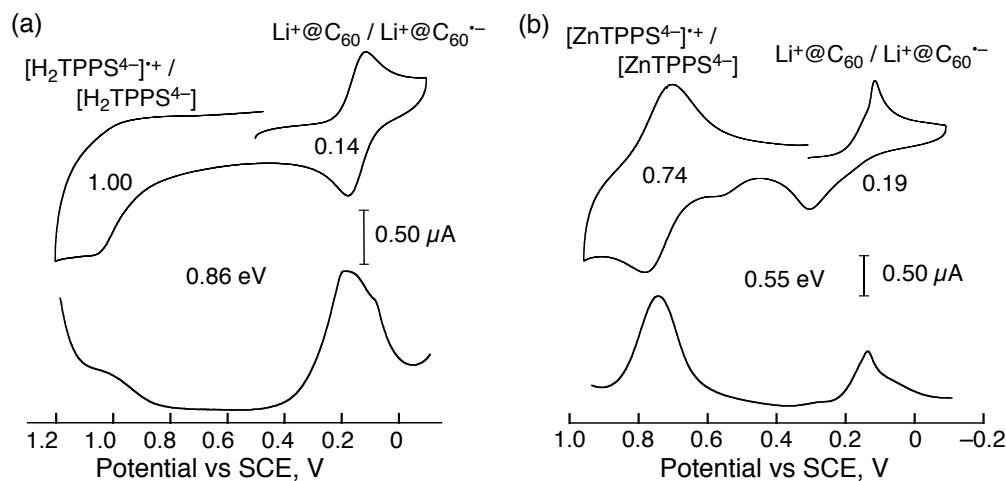


**Figure 4.** Cyclic voltammograms and differential pulse voltammograms of (a)  $\text{H}_2\text{TPPS}^{4-}/\text{Li}^+@\text{C}_{60}$  (b)  $\text{ZnTPPS}^{4-}/\text{Li}^+@\text{C}_{60}$  complexes in deaerated PhCN containing 0.10 M TBAPF<sub>6</sub>. Scan rate: 100  $\text{mV s}^{-1}$  for CV and 4  $\text{mV s}^{-1}$  for DPV.

The occurrence of the photoinduced electron or energy transfer in the supramolecular complex was confirmed by the transient absorption spectra of the  $\text{H}_2\text{TPPS}^{4-}/\text{Li}^+@\text{C}_{60}$  complex measured in PhCN using femtosecond laser flash photolysis (Figure 5). The transient absorption bands taken at 2 ps observed at 620 and 737 nm in Figure 5 is assigned to the singlet excited state of  $\text{H}_2\text{TPPS}^{4-}$ . This band decays with the rate constant ( $k_{\text{EN}}$ ) of  $9.7 \times 10^{10} \text{ s}^{-1}$  to form the singlet excited state of  $\text{Li}^+@\text{C}_{60}$  at 100 ps. The decay rate constant of  ${}^1[\text{Li}^+@\text{C}_{60}]^*$  was determined to be  $8.9 \times 10^8 \text{ s}^{-1}$ , which agrees with the rate constant of the intersystem crossing of  $\text{Li}^+@\text{C}_{60}$ . Thus, efficient energy transfer occurred from  ${}^1[\text{H}_2\text{TPPS}^{4-}]^*$  to  $\text{Li}^+@\text{C}_{60}$  rather than electron transfer. The data of a  $\text{ZnTPPS}^{4-}/\text{Li}^+@\text{C}_{60}$  complex and the reference compounds to assign the transient absorption bands are shown in Figure 5 and 6.

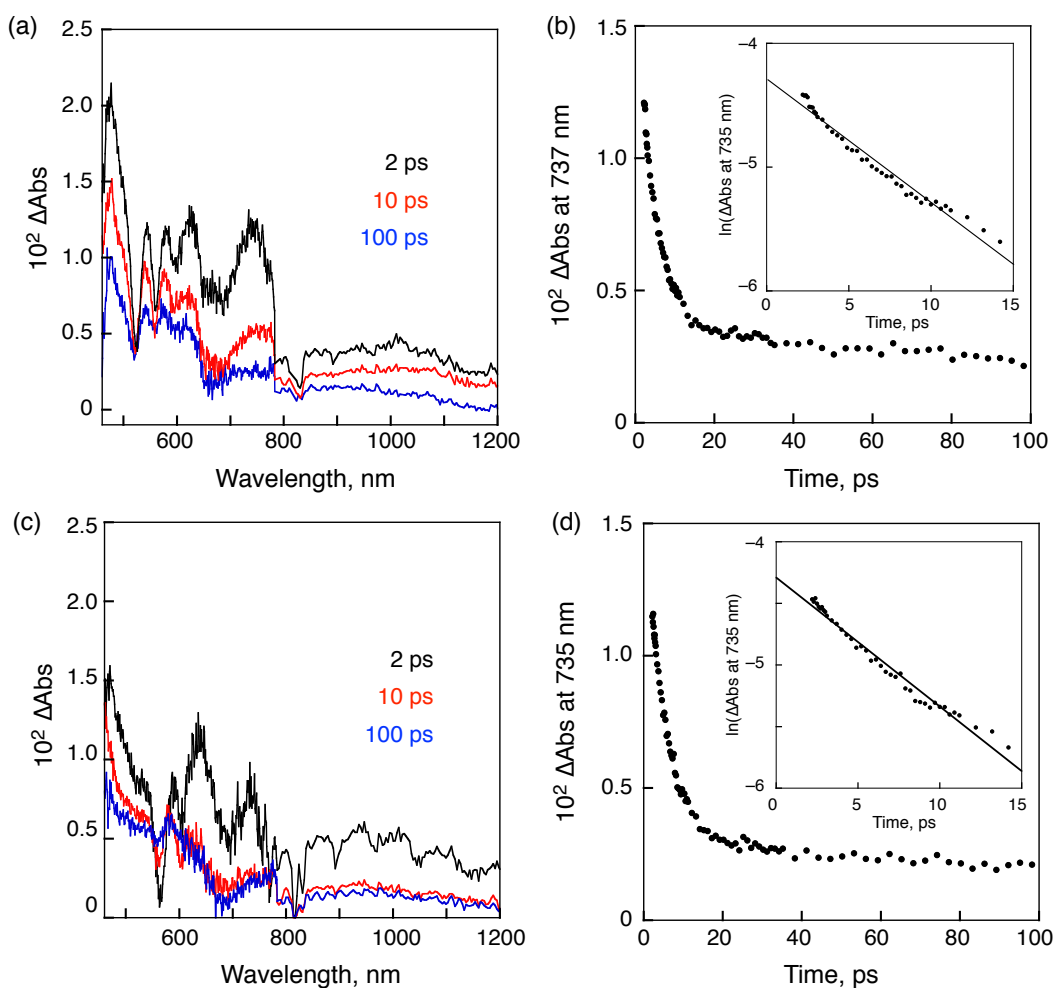


**Figure 5.** Transient absorption spectra of (a)  $\text{H}_2\text{TPPS}^{4-}$  ( $2.5 \times 10^{-5} \text{ M}$ ) and (c)  $\text{ZnTPPS}^{4-}$  ( $2.5 \times 10^{-5} \text{ M}$ ) with  $\text{Li}^+@\text{C}_{60}$  ( $5.0 \times 10^{-5} \text{ M}$ ) in deaerated PhCN at 298 K taken at 1, 10 and 100 ps after femtosecond laser excitation at 388 nm; Time profiles at (b) 737 nm and (d) 735 nm. Inset: First order plot.

The transient absorption spectra taken by nanosecond laser flash photolysis are shown in Figure 6, which agree with those of superposition of the absorption bands of  $[\text{H}_2\text{TPPS}^{4-}]^+$  correlations with the same slope irrespective of the difference in concentration of the CS state. No linear dependence was obtained in second-order analyses (Figure 7). Thus, there is no or little contribution from the bimolecular charge-recombination (CR) process of free  $[\text{H}_2\text{TPPS}^{4-}]^+$  and  $\text{Li}^+@\text{C}_{60}^{\bullet-}$  molecules. The lifetimes of the triplet CS state of the supramolecular complex is determined to be 310  $\mu\text{s}$  for  $\text{H}_2\text{TPPS}^{4-}$  and 300  $\mu\text{s}$  for  $\text{ZnTPPS}^{4-}$  at 298 K (Figure 6). This is the longest lifetime of the CS state ever reported for porphyrin/fullerene systems linked non-covalently in solution. The quantum yield of the CS state is determined to be 0.39 from the comparative method<sup>16</sup> using the absorption of the CS state ( $\text{Li}^+@\text{C}_{60}^{\bullet-}$ :  $\epsilon_{1035} = 7300 \text{ M}^{-1} \text{ cm}^{-1}$ ).<sup>12b</sup>

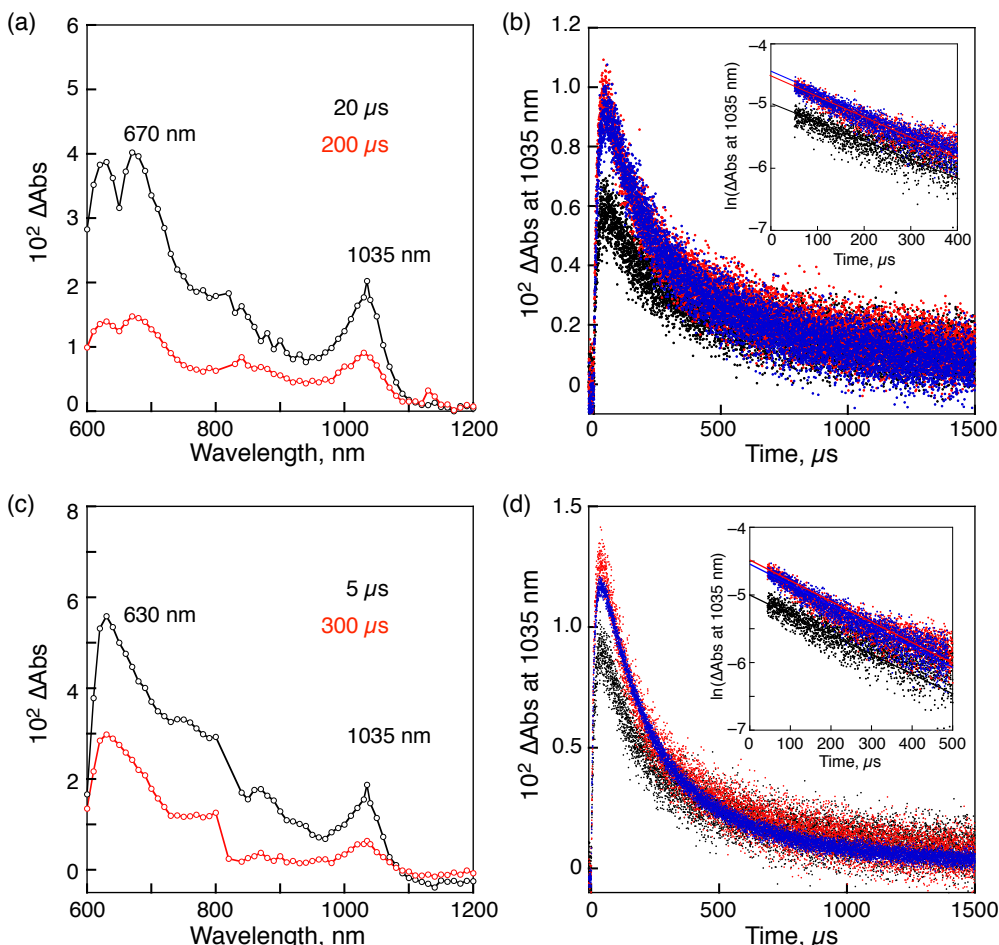


**Figure 6.** Transient absorption spectra of (a)  $\text{H}_2\text{TPPS}^{4-}$  ( $2.5 \times 10^{-5} \text{ M}$ ) and (c)  $\text{ZnTPPS}^{4-}$  ( $2.5 \times 10^{-5} \text{ M}$ ) with  $\text{Li}^+@\text{C}_{60}$  ( $5.0 \times 10^{-5} \text{ M}$ ) in deaerated PhCN at 298 K taken at 20 and 200  $\mu\text{s}$  after nanosecond laser excitation at 520 nm for  $\text{H}_2\text{TPPS}^{4-}$  and 550 nm for  $\text{ZnTPPS}^{4-}$ ; (b), (d) Decay time profiles at 1035 nm with different laser intensities (1, 3, 6 mJ/pulse).

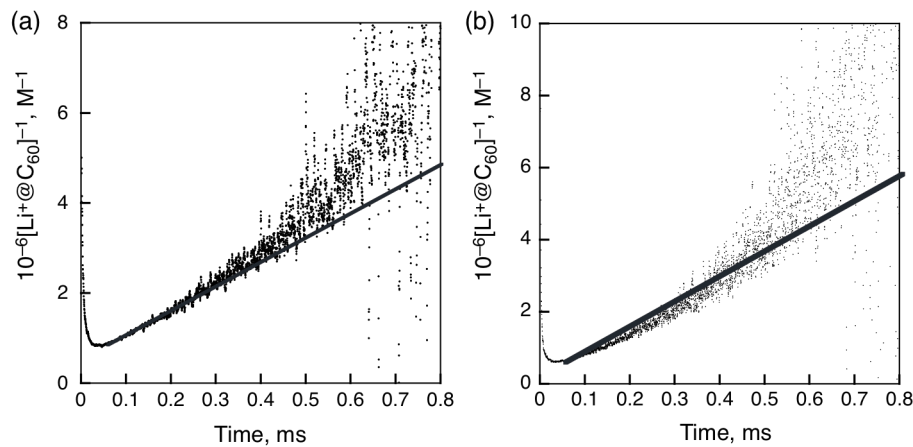


**Figure 7.** Second-order kinetic analyses for the decays of CS states of (a)  $[(\text{H}_2\text{TPPS}^{4-})/\text{Li}^+@\text{C}_{60}]$  and (b)  $[(\text{ZnTPPS}^{4-})/\text{Li}^+@\text{C}_{60}]$  with the laser intensity of 3 mJ/pulse

The temperature dependence of CR rate constant ( $k_{\text{obs}}$ ) was examined by laser flash photolysis at 25 – 70 °C. The activation enthalpies were determined to be 5.4 kcal mol<sup>-1</sup> for  $\text{H}_2\text{TPPS}^{4-}/\text{Li}^+@\text{C}_{60}$  and 3.0 kcal mol<sup>-1</sup> for  $\text{ZnTPPS}^{4-}/\text{Li}^+@\text{C}_{60}$  from the slopes of Figure 8. Such a large temperature dependence of  $k_{\text{obs}}$  indicates that there is a significant energy difference between the singlet and triplet CS states and that the CR process may occur through the thermally activated singlet CS state. The lifetime of the CS state at 77 K is estimated as long as 60 h for  $\text{H}_2\text{TPPS}^{4-}/\text{Li}^+@\text{C}_{60}$  from the linear plot in Figure 8.

Such a long-lived triplet CS state was further confirmed by the EPR measurements by photoirradiation of the  $\text{H}_2\text{TPPS}^{4-}/\text{Li}^+@\text{C}_{60}$  complex in frozen PhCN as shown in Figure 9. The spin-spin interaction in the triplet radical ion pair of the supramolecular complex is clearly

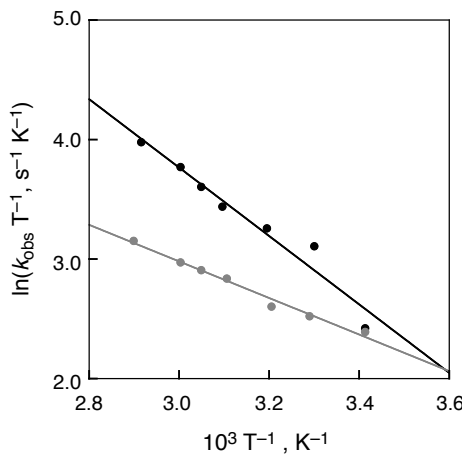


**Figure 8.** Plots of  $\ln(k_{\text{obs}} T^{-1})$  vs  $T^{-1}$  for CR of  $(\text{H}_2\text{TPPS}^{4-})^+/\text{Li}^+@\text{C}_{60}^-$  (gray) and  $(\text{ZnTPPS}^{4-})^+/\text{Li}^+@\text{C}_{60}^-$  (black) in PhCN.

shown at 77 K, where the fine structure due to the triplet CS state is clearly observed at  $g = 2$ . From the zero-field splitting values ( $D = 56$  G for  $\text{H}_2\text{TPPS}^{4-}$  and 52 G for  $\text{ZnTPPS}^{4-}$ ) the distances ( $r$ ) between two electron spins were estimated using the relation,  $D = 27800/r^3$ <sup>12b,16</sup> to be 7.9 and 8.1 Å, respectively. These  $r$  values agree with the center-to-center distance of a reported crystal structure of porphyrin/C<sub>60</sub>.

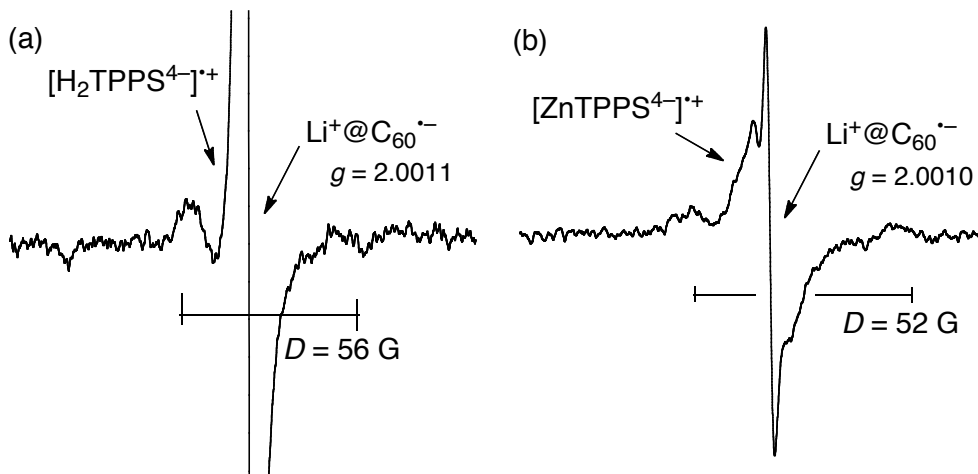


**Figure 9.** EPR spectra of (a)  $(\text{H}_2\text{TPPS}^{4-})^{\bullet+}/\text{Li}^+@\text{C}_{60}^{\bullet-}$  and (b)  $(\text{ZnTPPS}^{4-})^{\bullet+}/\text{Li}^+@\text{C}_{60}^{\bullet-}$  in PhCN generated by photoirradiation with a high-pressure Hg lamp (1000 W) at 77 K.

In summary, I have successfully shown that strong supramolecular binding occurs between anionic MTPPS<sup>4-</sup> (M = H<sub>2</sub> and Zn) and cationic Li<sup>+</sup>@C<sub>60</sub> in polar PhCN by ionic and  $\pi$ - $\pi$  interactions and that photoinduced electron transfer from MTPPS<sup>4-</sup> to the triplet excited state of Li<sup>+</sup>@C<sub>60</sub> occurs efficiently to attain the long-lived triplet CS state.

## References

- (1) Echegoyen, L.; Diederich, F.; Echegoyen, L. E. In *Fullerenes: Chemistry, Physics, and Technology*, Kadish, K. M., Ruoff, R. S., Eds.; Wiley-Interscience: New York, 2000; pp 151.
- (2) Guldi, D. M.; Fukuzumi, S. In *Fullerenes: From Synthesis to Optoelectronic Properties*; Guldi, D. M., Martin, N., Eds.; Kluwer: Dordrecht, 2003; pp 237-265.
- (3) Sgobba, V.; Rahman, G. M. A.; Guldi, D. M. In *Carbon Nanotubes in Electron Donor-Acceptor Nanocomposites, Chemistry of Carbon Nanotubes*; Basiuk, V. A., Ed.; American Scientific Publishers: California, 2006.
- (4) Fukuzumi, S.; Guldi, D. M. In *Electron Transfer in Chemistry*, Vol. 2, Balzani, V., Ed.;

Wiley-VCH: Weinheim, 2001; pp 270-337.

(5) (a) D’Souza, F.; Ito, O. *Chem. Soc. Rev.* **2012**, *41*, 86–96. (b) D’Souza, F.; Ito, O. *Chem. Commun.* **2009**, 4913–4928.

(6) (a) Fukuzumi, S.; Ohkubo, K. *J. Mater. Chem.* **2012**, *22*, 4575–4587. (b) Fukuzumi, S.; Kojima, T. *J. Mater. Chem.* **2008**, *18*, 1427–1439. (c) Fukuzumi, S. *Bull. Chem. Soc. Jpn.* **2006**, *79*, 177–195. (d) Fukuzumi, S. *Phys. Chem. Chem. Phys.* **2008**, *10*, 2283–2297.

(7) (a) Fukuzumi, S.; Saito, K.; Ohkubo, K.; Khouri, T.; Kashiwagi, Y.; Absalom, M. A.; Gadde, S.; D’Souza, F.; Araki, Y.; Ito, O. *Crossley, M. J. Chem. Commun.* **2011**, *47*, 7980–7982. (b) Fukuzumi, S.; Saito, K.; Ohkubo, K.; Troiani, V.; Qiu, H.; Gadde, S.; D’Souza, F.; Solladié, N. *Phys. Chem. Chem. Phys.* **2011**, *13*, 17019–17022.

(8) (a) D’Souza, F.; Deviprasad, G. R.; Zandler, M. E.; Hoang, V. T.; Klykov, A.; VanStipdonk, M.; Perera, A.; El-Khouly, M. E.; Fujitsuka, M.; Ito, O. *J. Phys. Chem. A* **2002**, *106*, 3243–3252. (b) El-Khouly, M. E.; Rogers, L. M.; Zandler, M. E.; Suresh, G.; Fujitsuka, M.; Ito, O.; D’Souza, F. *ChemPhysChem* **2003**, *4*, 474–481.

(9) Xiao, S.; El-Khouly, M. E.; Li, Y.; Gan, Z.; Liu, H.; Jiang, L.; Araki, Y.; Ito, O.; Zhu, D. *J. Phys. Chem. B* **2005**, *109*, 3658–3667.

(10) Grimm, B.; Schornbaum, J.; Cardona, C. M.; van Paauwe, J. D.; Boyd, P. D. W.; Guldin, D. M. *Chem. Sci.* **2011**, 1530–1537.

(11) (a) Ohkubo, K.; Fukuzumi, S. *J. Porphyrins Phthalocyanines* **2008**, *12*, 993–1004. (b) Ohkubo, K.; Fukuzumi, S. *Bull. Chem. Soc. Jpn.* **2009**, *82*, 303–315.

(12) (a) Aoyagi, S.; Nishibori, E.; Sawa, H.; Sugimoto, K.; Takata, M.; Miyata, Y.; Kitaura, R.; Shinohara, H.; Okada, H.; Sakai, T.; Ono, Y.; Kawachi, K.; Yokoo, K.; Ono, S.; Omote, K.; Kasama, Y.; Ishikawa, S.; Komuro, T.; Tobita, H. *Nature Chem.* **2010**, *2*, 678–683. (b) Fukuzumi, S.; Ohkubo, K.; Kawashima, Y.; Kim, D. S.; Park, J. S.; Jana, A.; Lynch, V. M.; Kim, D.; Sessler, J. L. *J. Am. Chem. Soc.* **2011**, *133*, 15938–15941.

(13) Kawashima, Y.; Ohkubo, K.; Fukuzumi, S. *J. Phys. Chem. A* **2012**, *116*, 8942–8948.

(14) I could not observe the formation dynamics of CS state by transient absorption measurements because the process may occur in the 10 ns–100 ns time range, which is out of the range of my laser flash systems.

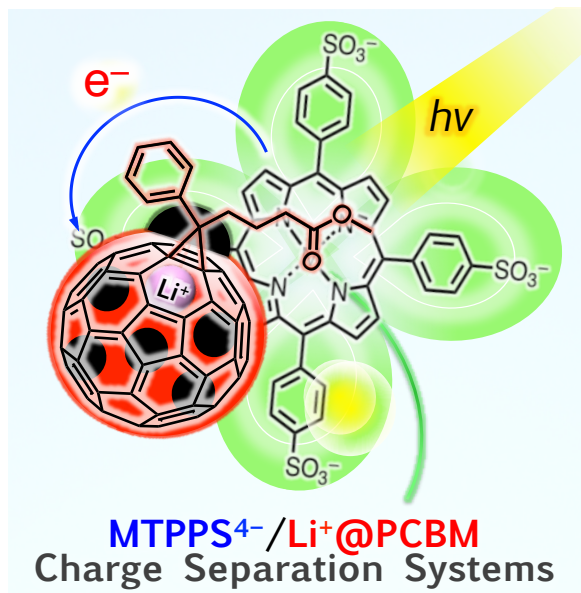
(15) Ohkubo, K.; Shao, J.; Ou, Z.; Kadish, K. M.; Li, G.; Pandey, R. K.; Fujitsuka, M.; Ito, O.; Imahori, H.; Fukuzumi, S. *Angew. Chem., Int. Ed.* **2004**, *43*, 853–856.

(16) Park, J. S.; Karnas, E.; Ohkubo, K.; Chen, P.; Kadish, K. M.; Fukuzumi, S.; Bielawski, C. W.; Hudnall, T. W.; Lynch, V. M.; Sessler, J. L. *Science* **2010**, *329*, 1324–1327.

---

## Chapter 5

Supramolecular Formation of  $\text{Li}^+@\text{PCBM}$  Fullerene with Sulfonated Porphyrins and Long-Lived Charge Separation



**Abstract:** Lithium ion-encapsulated [6,6]-phenyl-C<sub>60</sub>-butyric acid methyl ester fullerene ( $\text{Li}^+@\text{PCBM}$ ) was utilized to construct supramolecules with sulfonated *meso*-tetraphenylporphyrins ( $\text{MTPPS}^{4-}$ : M = Zn, H<sub>2</sub>) in polar benzonitrile. The association constants were determined to be  $1.8 \times 10^5 \text{ M}^{-1}$  for  $\text{ZnTPPS}^{4-}/\text{Li}^+@\text{PCBM}$  and  $6.2 \times 10^4 \text{ M}^{-1}$  for  $\text{H}_2\text{TPPS}^{4-}/\text{Li}^+@\text{PCBM}$ . From the electrochemical analyses, the energies of the charge-separated (CS) states were estimated to be 0.69 eV for  $\text{ZnTPPS}^{4-}/\text{Li}^+@\text{PCBM}$  and 1.00 eV for  $\text{H}_2\text{TPPS}^{4-}/\text{Li}^+@\text{PCBM}$ . Upon photoexcitation of the porphyrin moieties of  $\text{MTPPS}^{4-}/\text{Li}^+@\text{PCBM}$ , photoinduced electron transfer (ET) occurred to produce the CS states. The lifetimes of the CS states are 560  $\mu\text{s}$  for  $\text{ZnTPPS}^{4-}/\text{Li}^+@\text{PCBM}$  and 450  $\mu\text{s}$  for  $\text{H}_2\text{TPPS}^{4-}/\text{Li}^+@\text{PCBM}$ . The spin states of the CS states were determined to be triplet by electron paramagnetic resonance spectroscopy measurements at 4 K. The reorganization energies ( $\lambda$ ) and electronic coupling terms ( $V$ ) for back electron transfer (BET) were determined from the

temperature dependence of  $k_{\text{BET}}$  to be  $\lambda = 0.36$  eV and  $V = 8.5 \times 10^{-3}$  cm $^{-1}$  for ZnTPPS $^{4-}$ /Li $^+$ @PCBM and  $\lambda = 0.62$  eV and  $V = 7.9 \times 10^{-3}$  cm $^{-1}$  for H<sub>2</sub>TPPS $^{4-}$ /Li $^+$ @PCBM based on the Marcus theory of non-adiabatic electron transfer. Such small  $V$  values result from a small orbital interaction between MTPPS $^{4-}$  and Li $^+$ @PCBM moieties. These small  $V$  values and spin forbiddenness to afford the long-lived CS state.

## Introduction

The development of sustainable sources of energy is the most important issue of this century. Fossil fuels emit carbon dioxide (CO<sub>2</sub>) during burning, which has caused the green house effect.<sup>1,2</sup> The current energy resources will run out in the near future.<sup>3,4</sup> It is important to utilize solar energy by using solar cells to resolve these energy problems. Organic solar cells such as organic dye-sensitized solar cells<sup>5-12</sup> and organic thin film solar cells<sup>13-22</sup> have gained increased attention among the various solar cells because its production and energy costs are lower than that of inorganic solar cells such as crystalline- and amorphous silicon solar cells. The energy conversion efficiencies of the organic solar cells are around 10%, which are still lower than that of inorganic solar cells.<sup>23</sup> The energy conversion process of photovoltaic cells from the sunlight to the electricity is divided into the a few processes. Firstly, the electron donor is excited by photoirradiation to produces the excited state of electron donor, which defuses into donor-acceptor interface. Electron transfer (ET) occurred to produces electrons and holes (charge-separated (CS) state), which move to the corresponding electrodes. The formation of the long-lived CS state is desired to obtain the high energy conversion efficiency because it can efficiently supply the electrons and the holes to electrodes. Thus, various kinds of the donor-acceptor linked molecules have been reported.<sup>24-43</sup> Fullerenes have been widely used as a three-dimensional  $\pi$  electron-acceptor due to their small reorganization energy, which results from the  $\pi$ -electron system being highly delocalized over the three-dimensional curved surface together with the rigid and confined structure of the aromatic  $\pi$ -sphere.<sup>44-52</sup> Supramolecular systems have also attracted attention because they can be easily prepared without complicated and time-consuming synthesis.<sup>53-56</sup> However, the supramolecule with strong binding can not be constructed in polar solvents which stabilize the CS state of the supramolecule by solvation but destabilize the supramolecule as a whole. If nonpolar solvents are used to construct supramolecules with strong binding, photoinduced ET does not occur because the CS states are higher in energy than the triplet states of fullerene or porphyrinoids. Instead of pristine fullerene, the utilization of cationic lithium ion-encapsulated C<sub>60</sub> (Li $^+$ @C<sub>60</sub>)

---

is one way to solve this problem.<sup>57-62</sup>  $\text{Li}^+@\text{C}_{60}$  can binds with anionic porphyrinoids to form stable supramolecules in polar solvent by electrostatic interactions. The combination between sulfonated *meso*-tetraphenylporphyrins  $[(\text{Bu}_4\text{N}^+)_4\text{MTPPS}^{4-}]$ : M = Zn, H<sub>2</sub>] and  $\text{Li}^+@\text{C}_{60}$  can form stable supramolecules, which showed long lifetimes of the CS states of non-covalent monomer porphyrin-fullerene supramolecules in solution ( $\tau = 310 \mu\text{s}$ ).<sup>62a</sup>

Among the various electron acceptors, [6,6]-phenyl-C<sub>61</sub>-butyric acid methyl ester fullerene (PCBM) has been utilized to fabricate organic solar cells that exhibit high light-energy conversion efficiency.<sup>20-22</sup> Recently, lithium ion-encapsulated [6,6]-phenyl-C<sub>61</sub>-butyric acid methyl ester fullerene ( $\text{Li}^+@\text{PCBM}$ ) was synthesized; its solubility is superior to that of  $\text{Li}^+@\text{C}_{60}$ , and furthermore, its LUMO level is higher than that of  $\text{Li}^+@\text{C}_{60}$ .<sup>63</sup> However, supramolecular complexes of such derivatized  $\text{Li}^+@\text{C}_{60}$  with electron donors have yet to be reported.

I report herein the characterization of photochemical properties and electron-transfer reduction of  $\text{Li}^+@\text{PCBM}$  and the construction of supramolecular donor-acceptor CS systems of  $\text{Li}^+@\text{PCBM}$  with MTPPS<sup>4-</sup> in polar benzonitrile (PhCN) by electrostatic interactions, which afford the long-lived CS states.

## Experimental Section

**Materials.** Chemicals were purchased from commercial sources and used without further purification, unless otherwise noted. Lithium-ion-encapsulated fullerene hexafluorophosphate salt ( $\text{Li}^+@\text{C}_{60} \text{ PF}_6^-$ : 96%, Idea International Corporation) was commercially obtained from Wako Pure Chemical Industries, Ltd., Japan. Lithium-ion-encapsulated [6,6]-phenyl-C<sub>61</sub>-butyric acid methyl ester fullerene hexafluorophosphate salt ( $\text{Li}^+@\text{PCBM} \text{ PF}_6^-$ ) was synthesized by reference to published procedure.<sup>63</sup> [6,6]PCBM (99%) was obtained from SES Research Co., U.S.  $(\text{Bu}_4\text{N}^+)_4\text{MTPPS}^{4-}$  (M = Zn, H<sub>2</sub>) were synthesized by the neutralization of tetrasulfonated porphyrin (Tokyo Chemical Industry Co. Ltd.) with 4 equiv. of tetrabutylammonium hydroxide in MeOH. Decamethylferrocene ( $\text{Fc}^*$ ) was purchased from Aldrich Co. PhCN used as a solvent was distilled over phosphorus pentoxide.<sup>72</sup>

**UV–Vis–NIR Absorption and Emission Spectral Measurements.** Absorption spectra were recorded on a Hewlett-Packard 8453 diode array spectrophotometer at room temperature. Phosphorescence was measured on a Horiba FluoroMax-4 spectrofluorophotometer. 2-MeTHF solutions of  $\text{Li}^+@\text{PCBM}$ , and PCBM and, EPA (5:5:2 (v/v) = 2-propanol:diethyl ether:ethanol) solutions of  $(\text{Bu}_4\text{N}^+)_4\text{ZnTPPS}^{4-}$ , and  $(\text{Bu}_4\text{N}^+)_4\text{H}_2\text{TPPS}^{4-}$  in a quartz tube (3 mm

in diameter) were degassed by nitrogen bubbling for 10 min prior to the measurements. The sample tube was put in a quartz liquid nitrogen Dewar flask. The measurements were carried out by excitation at 300 nm for  $\text{Li}^+@\text{PCBM}$  and  $\text{PCBM}$  and 550 nm for  $(\text{Bu}_4\text{N}^+)_4\text{ZnTPPS}^{4-}$  and  $(\text{Bu}_4\text{N}^+)_4\text{H}_2\text{TPPS}^{4-}$ . Fluorescence spectra of  $\text{Li}^+@\text{PCBM}$  and  $\text{PCBM}$  were recorded on a Horiba FluoroMax-4 spectrofluorophotometer. The measurements were carried out by excitation at 300 nm in deaerated PhCN. The PhCN solutions were degassed by nitrogen bubbling for 10 min prior to the measurements.

**Laser Flash Photolysis Measurements.** Femtosecond transient absorption spectroscopy experiments were conducted using an ultrafast source: Integra-C (Quantronix Corp.), an optical parametric amplifier: TOPAS (Light Conversion Ltd.) and a commercially available optical detection system: Helios provided by Ultrafast Systems LLC. The source for the pump and probe pulses were derived from the fundamental output of Integra-C ( $\lambda = 786$  nm, 2  $\mu\text{J}/\text{pulse}$  and  $\text{fwhm} = 130$  fs) at a repetition rate of 1 kHz. 75% of the fundamental output of the laser was introduced into a second harmonic generation (SHG) unit: Apollo (Ultrafast Systems) for excitation light generation at  $\lambda = 393$  nm, while the rest of the output was used for white light generation. The laser pulse was focused on a sapphire plate of 3 mm thickness and then white light continuum covering the visible region from  $\lambda = 410$  nm to 800 nm was generated via self-phase modulation. A variable neutral density filter, an optical aperture, and a pair of polarizer were inserted in the path in order to generate stable white light continuum. Prior to generating the probe continuum, the laser pulse was fed to a delay line that provides an experimental time window of 3.2 ns with a maximum step resolution of 7 fs. In our experiments, a wavelength at  $\lambda = 393$  nm of SHG output was irradiated at the sample cell with a spot size of 1 mm diameter where it was merged with the white probe pulse in a close angle ( $< 10^\circ$ ). The probe beam after passing through the 2 mm sample cell was focused on a fiber optic cable that was connected to a CMOS spectrograph for recording the time-resolved spectra ( $\lambda = 410 - 800$  nm). Typically, 1500 excitation pulses were averaged for 3 seconds to obtain the transient spectrum at a set delay time. Kinetic traces at appropriate wavelengths were assembled from the time-resolved spectral data. All measurements were conducted at room temperature, 295 K. Nanosecond transient absorption spectral measurements were made according to the following procedure. A deaerated PhCN solutions containing  $\text{Li}^+@\text{PCBM}$ ,  $\text{PCBM}$ ,  $\text{Li}^+@\text{PCBM}$  with  $(\text{Bu}_4\text{N}^+)_4\text{ZnTPPS}^{4-}$  and  $\text{Li}^+@\text{PCBM}$  with  $(\text{Bu}_4\text{N}^+)_4\text{H}_2\text{TPPS}^{4-}$  were excited by a Panther OPO pumped Nds:YAG laser (Continuum, SLII-10, 4-6 ns fwhm) at 355 nm for  $\text{Li}^+@\text{PCBM}$  and  $\text{PCBM}$ , and 532 and 450 nm for  $\text{Li}^+@\text{PCBM}$  with  $(\text{Bu}_4\text{N}^+)_4\text{ZnTPPS}^{4-}$

---

and  $\text{Li}^+@\text{PCBM}$  with  $(\text{Bu}_4\text{N}^+)_4\text{H}_2\text{TPPS}^{4-}$ . The resulting time resolved transient absorption spectra were measured by using a continuous Xe-lamp (150 W) and a photodiode (Hamamatsu 2949) as the probe light and detector, respectively. The output from the photodiode and the photomultiplier tube was recorded using a digitizing oscilloscope (Tektronix, TDS3032, 300 MHz). The solutions were deoxygenated by  $\text{N}_2$  purging for 10 min prior to measurements. Rates of photoinduced electron-transfer reactions were monitored by the rise and decay of the absorption band due to the  $\text{Li}^+@\text{PCBM}$  radical anion. First-order rate constants were determined by a least-squares curve fit or a semilog plot.

**Electrochemical Measurements.** Cyclic voltammetry and difference pulse voltammetry measurements were performed with an ALS630B electrochemical analyzer in deaerated PhCN containing 0.1 M  $\text{Bu}_4\text{N}^+\text{PF}_6^-$  (TBAPF<sub>6</sub>) as a supporting electrolyte at 298 K. The platinum working electrode (BAS, surface i.d. 1.6 mm) was polished with BAS polishing alumina suspension and rinsed with acetone before use. The counter electrode was a platinum wire (0.5 mm dia.). The measured potentials were recorded with respect to an  $\text{Ag}/\text{AgNO}_3$  (0.01 M) reference electrode. The values of redox potentials (vs  $\text{Ag}/\text{AgNO}_3$ ) are converted into those vs SCE by addition of 0.29 V.<sup>73</sup>

**EPR Measurements.** EPR spectra were taken on a JEOL X-band spectrometer (JES-RE1XE) at 4 K for  $\text{ZnTPPS}^{4-}/\text{Li}^+@\text{PCBM}$  and  $\text{H}_2\text{TPPS}^{4-}/\text{Li}^+@\text{PCBM}$ . EPR spectra of the CS state of  $\text{ZnTPPS}^{4-}/\text{Li}^+@\text{PCBM}$  and  $\text{H}_2\text{TPPS}^{4-}/\text{Li}^+@\text{PCBM}$  in frozen PhCN were measured under photoirradiation with a high-pressure mercury lamp (USH-1005D) through a water filter focusing at the sample cell in the EPR cavity. The *g* value was calibrated using an  $\text{Mn}^{2+}$  marker. The EPR spectra were recorded under non-saturating microwave power conditions. The magnitude of modulation was chosen to optimize the resolution and the signal-to-noise (S/N) ratio of the observed spectra.

## Result and Discussion

**Electron-Transfer Reduction Properties of  $\text{Li}^+@\text{PCBM}$ .** The one-electron reduction potential of  $\text{Li}^+@\text{PCBM}$   $\text{PF}_6^-$  salt was determined by cyclic voltammetric experiments (Figure 1) in PhCN. The first one-electron reduction potential of  $\text{Li}^+@\text{PCBM}$  was determined to be +0.04 V [versus saturated calomel electrode (SCE)]. This value is shifted positively by +0.60 V relative to that of PCBM (−0.56 V) due to the encapsulation of the Li cation into the neutral PCBM cage. A negative shift by −0.10 V from that of  $\text{Li}^+@\text{C}_{60}$  (0.14 V) is caused by shrinking of the  $\pi$ -electron conjugated system on the fullerene cage.<sup>63</sup>

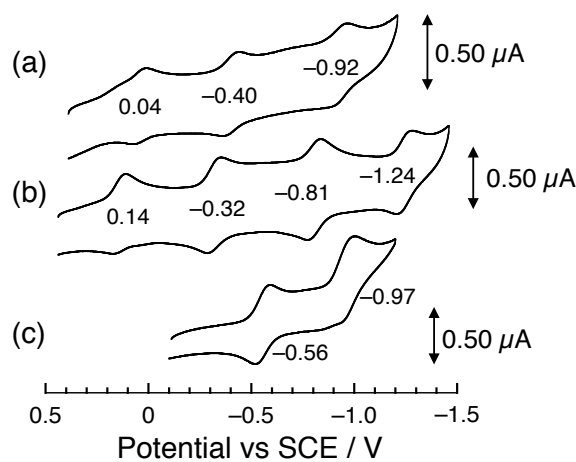


**Figure 1.** Cyclic voltammograms of (a)  $\text{Li}^+@\text{PCBM} \text{ PF}_6^-$ , (b)  $\text{Li}^+@\text{C}_60 \text{ PF}_6^-$  and (c) PCBM ( $1.0 \times 10^{-4}$  M) in deaerated PhCN containing TBAPF<sub>6</sub> (0.10 M); sweep rate: 100 mV s<sup>-1</sup>.

### Scheme 1

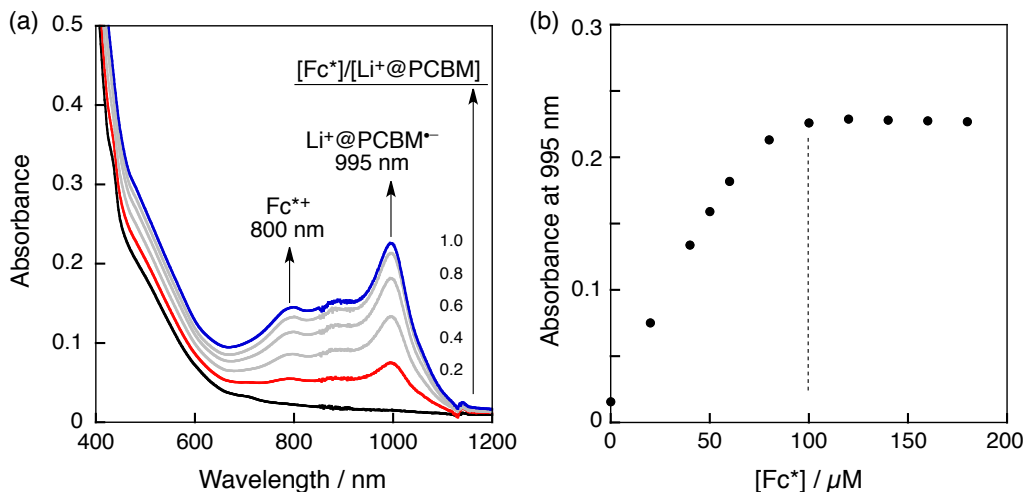
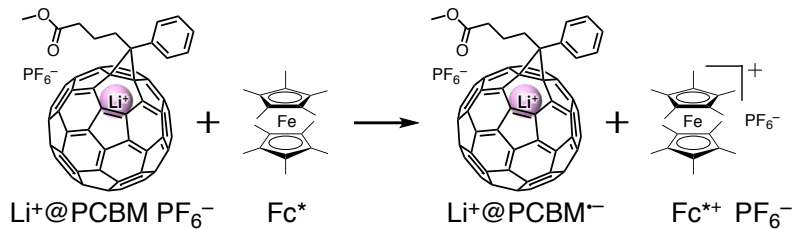


**Figure 2.** (a) UV-Vis-NIR absorption spectra of  $\text{Li}^+@\text{PCBM}^-$  produced via ET from  $\text{Fc}^*$  to  $\text{Li}^+@\text{PCBM} \text{ PF}_6^-$  ( $1.0 \times 10^{-4}$  M) in deaerated PhCN. (b) Plot of absorbance at 995 nm vs concentration of  $\text{Fc}^*$ .

UV-Vis-NIR absorption spectral titration was performed in the reaction of  $\text{Li}^+@\text{PCBM}$  and decamethylferrocene ( $\text{Fc}^*$ ) in deaerated PhCN, as shown in Figure 2a. The electron-transfer reduction of  $\text{Li}^+@\text{PCBM}$  with  $\text{Fc}^*$  ( $E_{\text{ox}} = -0.08$  V)<sup>64</sup> is energetically

favorable ( $\Delta G_{\text{et}} = -0.12$  eV) to form  $\text{Li}^+@\text{PCBM}^{\cdot-}$  and decamethylferrocenium ( $\text{Fc}^{\bullet+}$ ) (Scheme 1) as seen by the absorption bands at 995 nm and 800 nm, respectively. The absorption maximum of  $\text{Li}^+@\text{PCBM}^{\cdot-}$  ( $\lambda_{\text{max}} = 995$  nm) is blue-shifted from that of  $\text{Li}^+@\text{C}_{60}$  radical anion,  $\text{Li}^+@\text{C}_{60}^{\cdot-}$  ( $\lambda_{\text{max}} = 1035$  nm),<sup>60</sup> PCBM radical anion,  $\text{PCBM}^{\cdot-}$ , ( $\lambda_{\text{max}} = 1020$  nm)<sup>65</sup> and  $\text{C}_{60}$  radical anion,  $\text{C}_{60}^{\cdot-}$ , ( $\lambda_{\text{max}} = 1080$  nm),<sup>66,67</sup> as shown in Figure 2a. A spectral titration (Figure 2b) provided support for the stoichiometry.

Fluorescence spectrum of  $\text{Li}^+@\text{PCBM}$  was observed by photoexcitation of a deaerated PhCN solution of  $\text{Li}^+@\text{PCBM}$ . The emission maximum was observed at 710 nm (Figure 3). The singlet excitation energy ( $E_S$ ) of  $\text{Li}^+@\text{PCBM}$  was determined as 1.75 eV from the average value of absorption (710 nm; Figure 2a) and fluorescence maximum of  $\text{Li}^+@\text{PCBM}$ ; this value

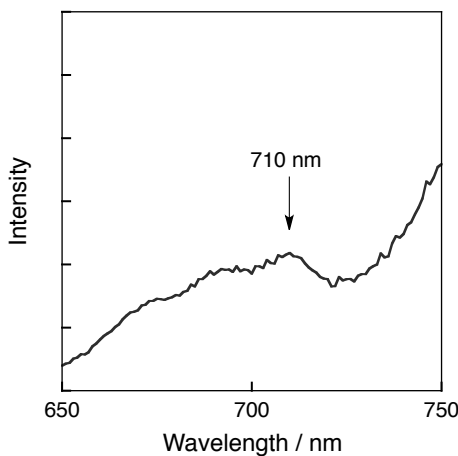


**Figure 3.** Fluorescence spectrum of  $\text{Li}^+@\text{PCBM} \text{PF}_6^-$  ( $2.5 \times 10^{-5}$  M) in deaerated PhCN observed by excitation at 300 nm.

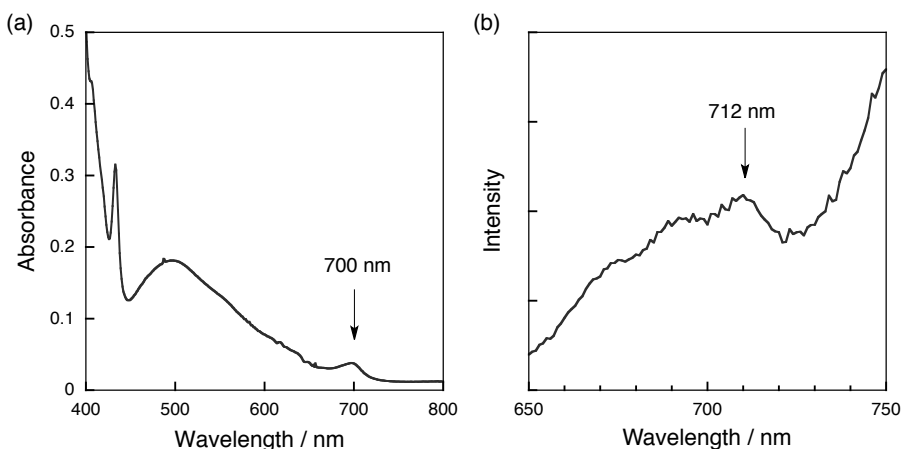


**Figure 4.** (a) UV-Vis absorption spectrum of PCBM ( $1.0 \times 10^{-4}$  M) in deaerated PhCN. (b) Fluorescence spectrum of PCBM ( $2.5 \times 10^{-5}$  M) in deaerated PhCN observed by excitation at 300 nm.

is similar to that of PCBM ( $E_S = 1.76$  eV, Figure 4) and smaller than that of  $\text{Li}^+@\text{C}_60$  ( $E_S = 1.94$  eV)<sup>61a</sup> and that of  $\text{C}_60$  ( $E_S = 1.99$  eV).<sup>67</sup> The triplet excitation energy ( $E_T$ ) of  $\text{Li}^+@\text{PCBM}$  was determined by the phosphorescence maximum (833 nm) of 2-methyltetrahydrofuran (2-MeTHF) glass at 77 K (Figure 5a) to be 1.49 eV. This value is virtually unchanged from that of PCBM ( $E_T = 1.47$  eV, Figure 5b) and smaller than that of  $\text{Li}^+@\text{C}_60$  ( $E_T = 1.53$  eV)<sup>61a</sup> and that of  $\text{C}_60$  ( $E_T = 1.57$  eV).<sup>67</sup> These differences in the values indicate that the excitation energies depend on an existence of functional groups rather than on the existence of  $\text{Li}^+$ .

Ultrafast photodynamics for intersystem crossing (ISC) from the singlet excited state of  $\text{Li}^+@\text{PCBM}$ , that is,  ${}^1[\text{Li}^+@\text{PCBM}]^*$  to the triplet excited state of  $\text{Li}^+@\text{PCBM}$  that is,  ${}^3[\text{Li}^+@\text{PCBM}]^*$  was observed by femtosecond laser flash photolysis. The transient absorption

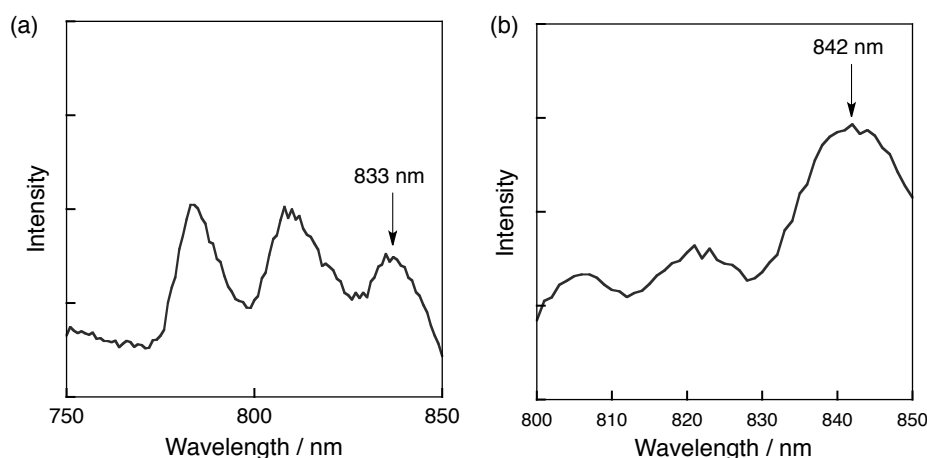


**Figure 5.** Phosphorescence spectrum of (a)  $\text{Li}^+@\text{PCBM}$  and (b) PCBM in deaerated 2-MeTHF. Excitation wavelength: 300 nm;  $T = 77$  K.

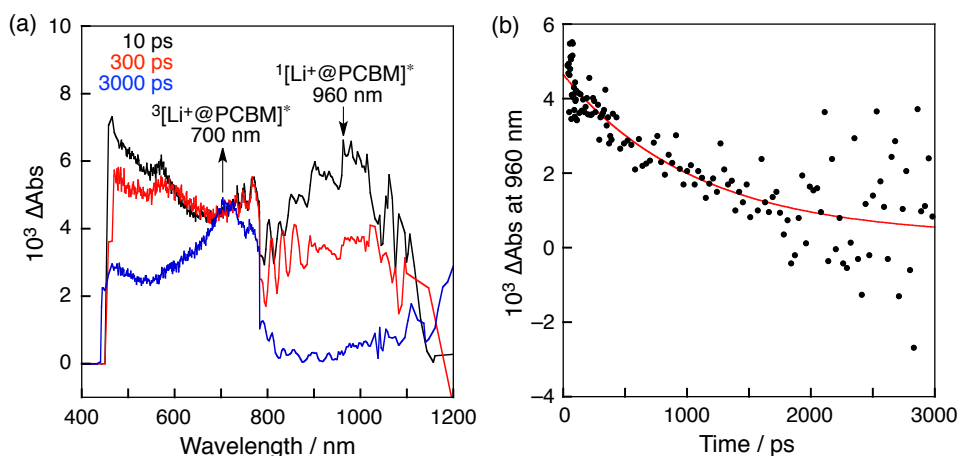


**Figure 6.** (a) Transient absorption spectra of  $\text{Li}^+@\text{PCBM} \text{PF}_6^- (1.0 \times 10^{-4} \text{ M})$  in deaerated PhCN measured at 10 ps (black), 300 ps (red) and 3000 ps (blue) after laser excitation at 393 nm. (b) Time profile at 960 nm.

band at 960 nm taken at 10 ps after photoexcitation is assigned to  ${}^1[\text{Li}^+@\text{PCBM}]^*$  (Figure 6), which is blue shifted relative to that of the singlet excited state of PCBM,  ${}^1\text{PCBM}^*$ ,  $\lambda_{\text{max}} = 980$  nm in Figure 7). The decay of absorbance due to  ${}^1[\text{Li}^+@\text{PCBM}]^*$  resulted in appearance of the new absorption band at 700 nm due to  ${}^3[\text{Li}^+@\text{PCBM}]^*$ , which is formed by intersystem crossing (Scheme 2). The rate constant of intersystem crossing ( $k_{\text{ISC}}$ ) was determined from first-order rate analysis of the decay of the absorption band at 960 nm to be  $9.4 \times 10^8 \text{ s}^{-1}$ . The value is slightly larger than that of  $\text{Li}^+@\text{C}_60$  ( $8.9 \times 10^8 \text{ s}^{-1}$ )<sup>61a</sup> and PCBM ( $8.9 \times 10^8 \text{ s}^{-1}$  in Figure 7b) in PhCN. The triplet-triplet absorption of  ${}^3[\text{Li}^+@\text{PCBM}]^*$  was also observed at 700

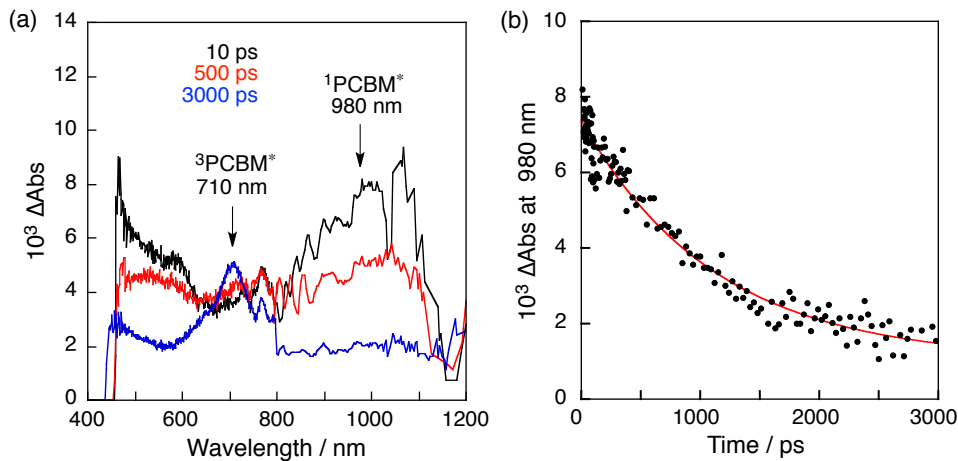


**Figure 7.** (a) Transient absorption spectra of PCBM ( $1.0 \times 10^{-4} \text{ M}$ ) in PhCN measured at 10 ps (black), 500 ps (red) and 3000 ps (blue) after laser excitation at 393 nm. (b) Decay time profile of absorbance at 980 nm.

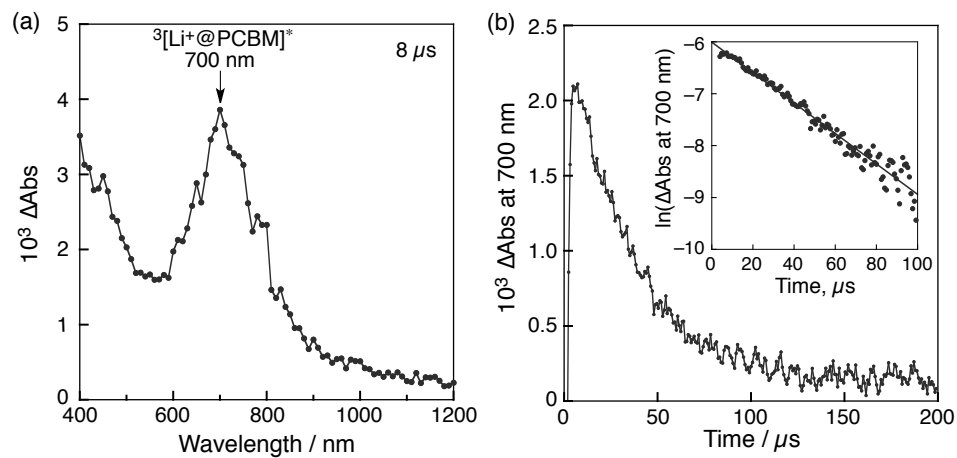


**Figure 8.** (a) Transient absorption spectrum of  $\text{Li}^+@\text{PCBM} \text{PF}_6^-$  ( $2.5 \times 10^{-5} \text{ M}$ ) in deaerated PhCN measured at  $8 \mu\text{s}$  after laser excitation at 355 nm. (b) Decay time profile of absorbance at 700 nm.

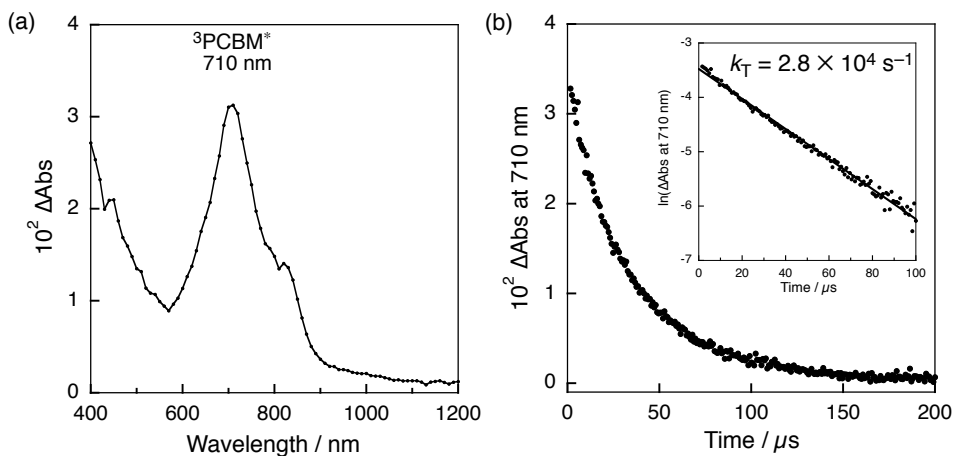


**Figure 9.** (a) Transient absorption spectra of PCBM ( $2.5 \times 10^{-5}$  M) in PhCN measured at 5 ps (blue) after laser excitation at 355 nm. (b) Decay time profile of absorbance at 710 nm.

nm by nanosecond laser flash photolysis (Figure 8). The decay rate constant of  $^3[\text{Li}^+@\text{PCBM}]^*$  was determined from the linear first-order plot and found to be  $2.9 \times 10^4 \text{ s}^{-1}$  in PhCN. The triplet lifetime is determined to be  $34 \mu\text{s}$ , which is comparable to that of PCBM ( $36 \mu\text{s}$ ; Figure 9) and shorter than that of  $\text{Li}^+@\text{C}_{60}$  ( $48 \mu\text{s}$ )<sup>61a</sup> and that of  $\text{C}_{60}$  ( $49 \mu\text{s}$ ).<sup>69,70</sup> The values are summarized in Table 1.

### Scheme 2

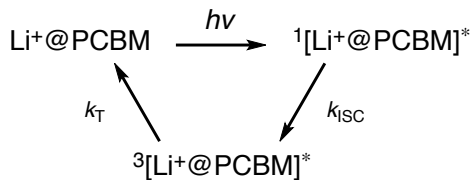


**Table 1.** One-electron reduction potentials ( $E_{\text{red1}}$ ), singlet excited energies ( $E$ ), triplet excited energies ( $E_T$ ), rate constants of intersystem crossing ( $k_{\text{ISC}}$ ) and decay of triplet excited states ( $k_T$ ) of Fullerenes

Fullerenes	$E_{\text{red1}},^a \text{ V}$	$E_S, \text{ eV}$	$E_T, \text{ eV}$	$k_{\text{ISC}}, \text{ s}^{-1}$	$k_T, \text{ s}^{-1}$
$\text{Li}^+@\text{PCBM}^b$	0.04	1.75	1.49	$9.4 \times 10^8$	$2.9 \times 10^4$
$\text{PCBM}^b$	-0.56	1.76	1.47	$8.9 \times 10^8$	$2.8 \times 10^4$
$\text{Li}^+@\text{C}_{60}$	0.14 <sup>c</sup>	1.94 <sup>d</sup>	1.53 <sup>d</sup>	$8.9 \times 10^8$ <sup>d</sup>	$2.1 \times 10^4$ <sup>d</sup>
$\text{C}_{60}$	-0.43 <sup>e</sup>	1.99 <sup>f</sup>	1.57 <sup>f</sup>	$4.1 \times 10^8$ <sup>f</sup>	$2.0 \times 10^4$ <sup>f</sup>

<sup>a</sup> V vs SCE in PhCN. <sup>b</sup> PCBM is [6,6] isomer. <sup>c</sup> Ref 60. <sup>d</sup> Ref 61a. <sup>e</sup> Ref 68. <sup>f</sup> Ref 67. <sup>g</sup> Ref 69,70.

**Supramolecules Composed of  $\text{Li}^+@\text{PCBM}$  and  $\text{ZnTPPS}^{4-}$ .** The UV–Vis absorption spectra of  $\text{ZnTPPS}^{4-}$  in PhCN at 298 K were changed upon addition of  $\text{Li}^+@\text{PCBM}$ , as shown in Figure 10a, where the Q-bands of porphyrin at 558 nm and 599 nm were red-shifted to 562 nm and 602 nm, respectively, by increasing the concentration of  $\text{Li}^+@\text{PCBM}$ . Figure 10b shows the dependence of the absorbance at 450 nm on the concentration of  $\text{Li}^+@\text{PCBM}$ . The

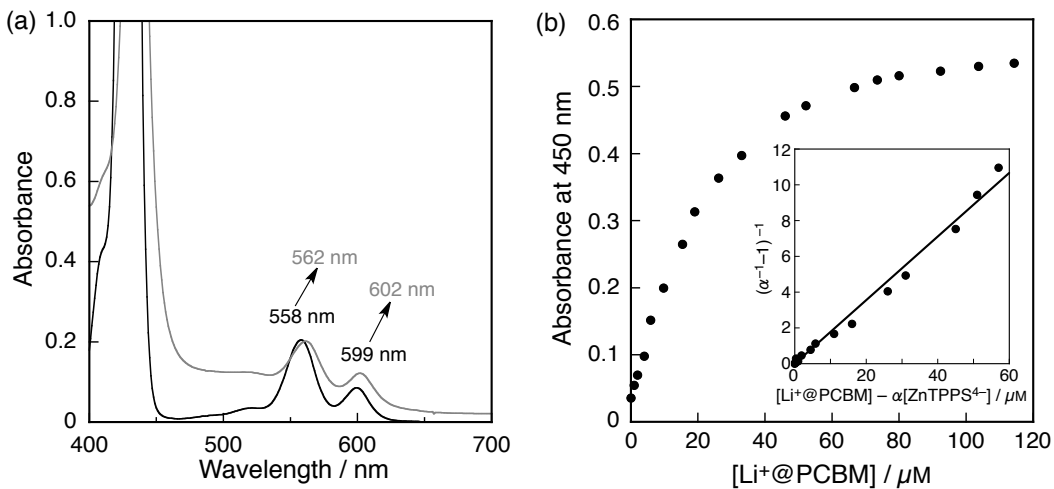
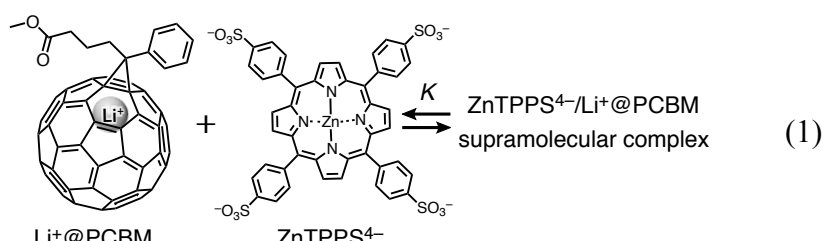


**Figure 10.** (a) UV–Vis absorption spectra of  $(\text{Bu}_4\text{N}^+)_4\text{ZnTPPS}^{4-}$  ( $2.5 \times 10^{-5}$  M) in the absence (black) and presence of  $\text{Li}^+@\text{PCBM}$   $\text{PF}_6^-$  ( $1.1 \times 10^{-4}$  M, gray) in PhCN. (b) Plot of the absorption vs  $[\text{Li}^+@\text{PCBM}]$  at 450 nm. Inset: Plot of  $(\alpha^{-1} - 1)^{-1}$  vs  $[\text{Li}^+@\text{PCBM}] - \alpha[\text{ZnTPPS}^{4-}]$ .

saturation behavior was observed with increasing concentration of  $\text{Li}^+@\text{PCBM}$ , which indicates that strong supramolecular binding occurs between  $\text{ZnTPPS}^{4-}$  and  $\text{Li}^+@\text{PCBM}$  by electrostatic interaction. According to equation (1), the change in absorbance is given by equations (2) and (3), which predict a linear correlation between  $(\alpha^{-1} - 1)^{-1}$  and  $([\text{Li}^+@\text{PCBM}] - \alpha[\text{ZnTPPS}^{4-}]_0)$ :



$$(\alpha^{-1} - 1)^{-1} = K([\text{Li}^+@\text{PCBM}] - \alpha[\text{ZnTPPS}^{4-}]_0) \quad (2)$$

$$\alpha = (A - A_0)/(A_\infty - A_0) \quad (3)$$

in which  $A_0$  and  $A$  are the absorbance of  $\text{ZnTPPS}^{4-}$  at 450 nm in the absence and presence of  $\text{Li}^+@\text{PCBM}$ , respectively, and  $[\text{ZnTPPS}^{4-}]_0$  is the initial concentration of  $\text{ZnTPPS}^{4-}$ . From a linear plot in the inset of Figure 10b, the formation constant ( $K$ ) of the  $\text{ZnTPPS}^{4-}/\text{Li}^+@\text{PCBM}$  was determined to be  $1.8 \times 10^5 \text{ M}^{-1}$  in PhCN (Figure 10b). Upon replacing  $\text{ZnTPPS}^{4-}$  by  $\text{H}_2\text{TPPS}^{4-}$ , the  $K$  value was determined to be  $6.2 \times 10^4 \text{ M}^{-1}$  as shown in (Figure 11). Formation of 1:1 supramolecules of  $\text{Li}^+@\text{PCBM}$  with  $\text{MTPPS}^{4-}$  was confirmed by Job's plots (Figure 12).

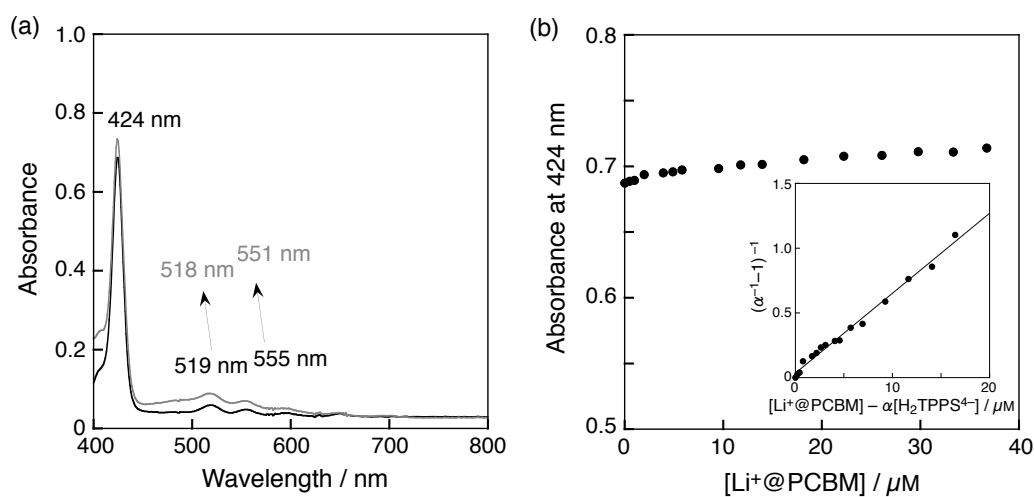


**Figure 11.** (a) UV-Vis absorption spectra of  $(\text{Bu}_4\text{N}^+)_4\text{H}_2\text{TPPS}^{4-}$  ( $2.0 \times 10^{-6} \text{ M}$ ) in the absence (black) and presence of  $\text{Li}^+@\text{PCBM}$   $\text{PF}_6^-$  ( $3.5 \times 10^{-5} \text{ M}$ , gray) in PhCN. (b) Plot of the absorption vs  $[\text{Li}^+@\text{PCBM}]$  at 424 nm. Inset: Plot of  $(\alpha^{-1} - 1)^{-1}$  vs  $[\text{Li}^+@\text{PCBM}] - \alpha[\text{H}_2\text{TPPS}^{4-}]$ .

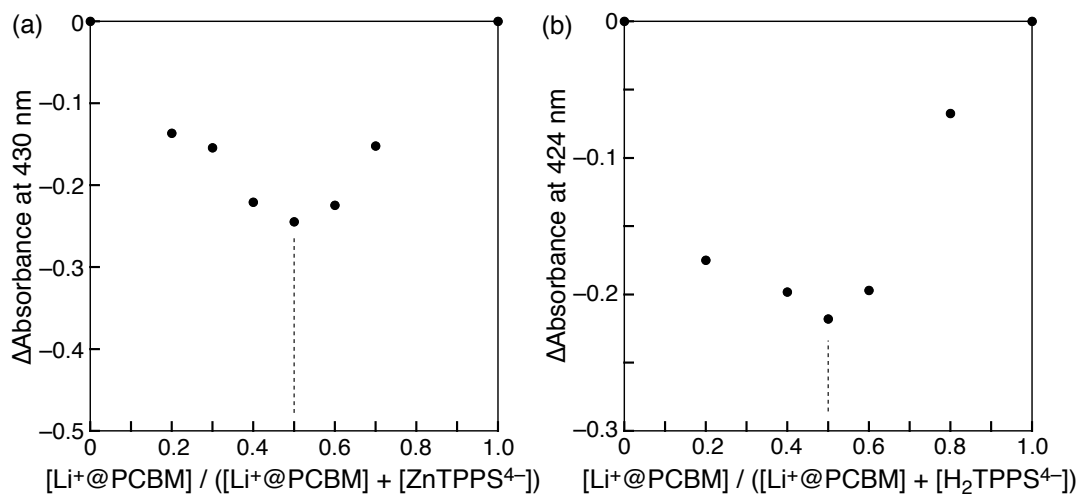


**Figure 12.** Job's plots for the formation of supramolecule between  $\text{Li}^+@\text{PCBM}$  and (a)  $\text{ZnTPPS}^{4-}$  (b)  $\text{H}_2\text{TPPS}^{4-}$  in PhCN.

**Photoinduced Charge Separation of  $\text{MTPPS}^{4-}/\text{Li}^+@\text{PCBM}$  Supramolecules.**

Photoexcitation of the Soret band of  $\text{ZnTPPS}^{4-}$  at 416 nm in deaerated PhCN results in fluorescence at  $\lambda_{\text{max}} = 609$  and 662 nm, as shown in Figure 13a. Addition of  $\text{Li}^+@\text{PCBM}$  to a PhCN solution of  $\text{ZnTPPS}^{4-}$  showed decrease in the fluorescence intensity of  $\text{ZnTPPS}^{4-}$  with increasing concentration, which exhibited saturation behavior, as shown in Figure 13b. The  $K$  value was determined to be  $1.9 \times 10^5 \text{ M}^{-1}$  from the slope of the inset in Figure 13b. Upon replacing  $\text{ZnTPPS}^{4-}$  by  $\text{H}_2\text{TPPS}^{4-}$ , similar saturation behavior was observed (Figure 14), and  $K$  value was determined to be  $7.3 \times 10^4 \text{ M}^{-1}$  from the slope of Figure 14b inset. These values

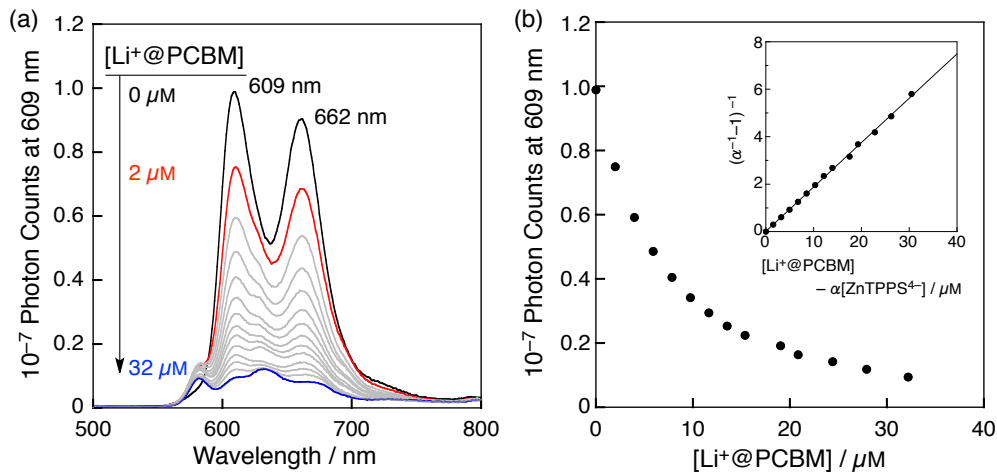


**Figure 13.** (a) Fluorescence spectra of  $(\text{Bu}_4\text{N}^+)_4\text{ZnTPPS}^{4-}$  ( $2.0 \times 10^{-6} \text{ M}$ ) in the presence of various concentrations of  $\text{Li}^+@\text{PCBM} \text{ PF}_6^-$  (0 to  $3.2 \times 10^{-5} \text{ M}$ ) in deaerated PhCN observed by excitation at 416 nm. (b) Plot of the photon counts vs  $[\text{Li}^+@\text{PCBM}]$  at 609 nm. Inset: Plot of  $(\alpha^{-1} - 1)^{-1}$  vs  $[\text{Li}^+@\text{PCBM}] - \alpha[\text{ZnTPPS}^{4-}]$ .

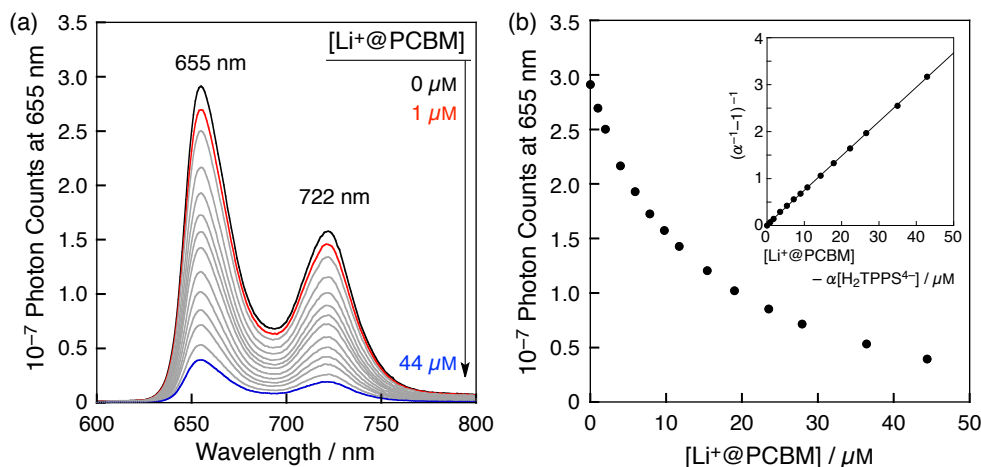


**Figure 14.** (a) Fluorescence spectra of  $(\text{Bu}_4\text{N}^+)_4\text{H}_2\text{TPPS}^{4-}$  ( $2.0 \times 10^{-6} \text{ M}$ ) in the presence of various concentration of  $\text{Li}^+@\text{PCBM} \text{ PF}_6^-$  (0 to  $4.4 \times 10^{-5} \text{ M}$ ) in deaerated PhCN observed by excitation at 420 nm. (b) Plot of the photon counts vs  $[\text{Li}^+@\text{PCBM}]$  at 655 nm. Inset: Plot of  $(\alpha^{-1} - 1)^{-1}$  vs  $[\text{Li}^+@\text{PCBM}] - \alpha[\text{H}_2\text{TPPS}^{4-}]$ .

agree with the values obtained from the absorption spectral change within  $\pm 10\%$  experimental errors (Figure 10). Thus, static quenching of the singlet excited states ( ${}^1[\text{ZnTPPS}^{4-}]^*$  and  ${}^1[\text{H}_2\text{TPPS}^{4-}]^*$ ) by  $\text{Li}^+@\text{PCBM}$  occurs in the supramolecular complexes.

The quenching process of  ${}^1[\text{ZnTPPS}^{4-}]^*$  by  $\text{Li}^+@\text{PCBM}$  in the supramolecular complex occurred through energy transfer from  ${}^1[\text{ZnTPPS}^{4-}]^*$  to  $\text{Li}^+@\text{PCBM}$ , as shown in Figure 15. The rate constant of energy transfer ( $k_{\text{EN}}$ ) from  ${}^1[\text{ZnTPPS}^{4-}]^*$  to  $\text{Li}^+@\text{PCBM}$  was determined from the absorption decay at 620 nm due to  ${}^1[\text{ZnTPPS}^{4-}]^*$  and was found to be  $2.3 \times 10^{11} \text{ s}^{-1}$ , which is faster than the rate constant of intersystem crossing of  ${}^1[\text{ZnTPPS}^{4-}]^*$  ( $7.3 \times 10^8 \text{ s}^{-1}$  in Figure 10). Similarly, the rate constant of energy transfer ( $k_{\text{EN}}$ ) from  ${}^1[\text{H}_2\text{TPPS}^{4-}]^*$  to  $\text{Li}^+@\text{PCBM}$

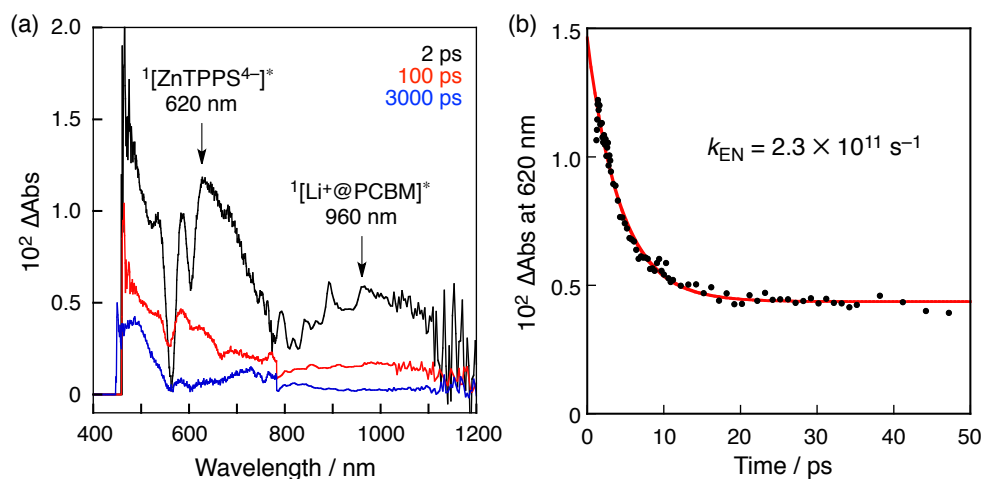


**Figure 15.** (a) Transient absorption spectra of  $(\text{Bu}_4\text{N}^+)_4\text{ZnTPPS}^{4-}$  ( $2.5 \times 10^{-5} \text{ M}$ ) and  $\text{Li}^+@\text{PCBM} \text{ PF}_6^-$  ( $5.0 \times 10^{-5} \text{ M}$ ) in PhCN measured at 2 ps (black), 100 ps (red) and 3000 ps (blue) after laser excitation at 393 nm. (b) Decay time profile of absorbance at 620 nm.

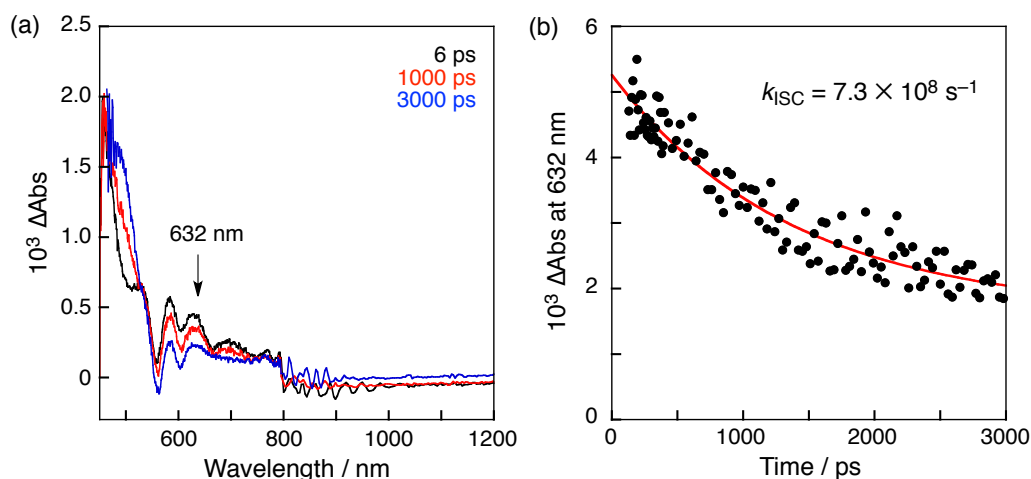


**Figure 16.** Transient absorption spectra of  $(\text{Bu}_4\text{N}^+)_4\text{ZnTPPS}^{4-}$  ( $2.5 \times 10^{-5} \text{ M}$ ) in PhCN measured at 6 ps (black), 1000 ps (red) and 3000 ps (blue) after laser excitation at 430 nm. (b) Decay time profile of absorbance at 632 nm.

was determined to be  $1.0 \times 10^{11} \text{ s}^{-1}$  (Figure 17), which is also much larger than the rate constant of intersystem crossing of  ${}^1[\text{H}_2\text{TPPS}^{4-}]^*$  ( $9.7 \times 10^8 \text{ s}^{-1}$  in Figure 18).  ${}^1[\text{Li}^+@\text{PCBM}]^*$  is converted to  ${}^3[\text{Li}^+@\text{PCBM}]^*$  with the rate constant of  $k_{\text{ISC}} = 9.4 \times 10^8 \text{ s}^{-1}$  (see above).

To estimate the energies of the CS states in the supramolecules based on the redox potentials, cyclic voltammetric and differential pulse voltammetric measurements were performed (Figure 19). The energies of the CS state were determined to be 0.69 eV for  $\text{ZnTPPS}^{4-}/\text{Li}^+@\text{PCBM}$  and 1.00 eV for  $\text{H}_2\text{TPPS}^{4-}/\text{Li}^+@\text{PCBM}$  from the potential difference between one-electron oxidation of  $\text{MTPPS}^{4-}$  (0.72 V for  $\text{ZnTPPS}^{4-}$  and 1.03 V for  $\text{H}_2\text{TPPS}^{4-}$ ) and one-electron reduction of  $\text{Li}^+@\text{PCBM}$  (0.03 V) in the corresponding supramolecules.

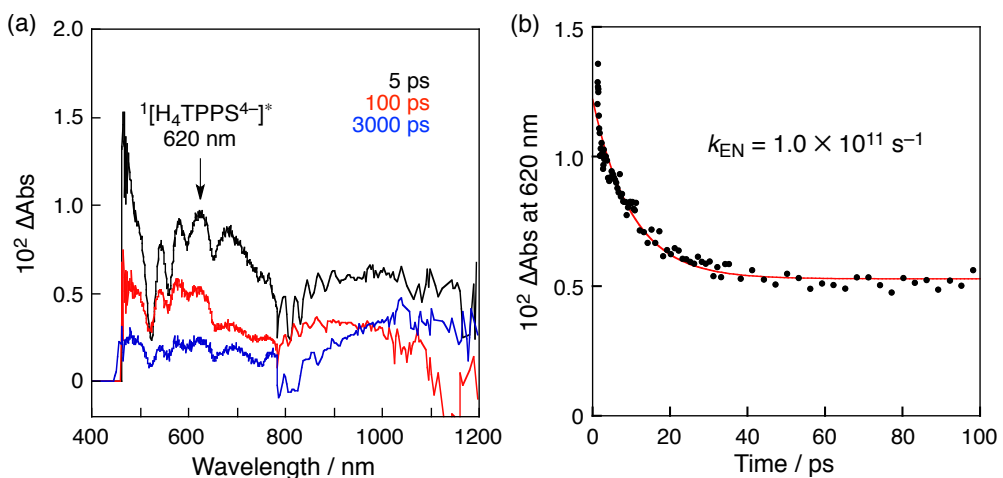


**Figure 17.** (a) Transient absorption spectra of  $(\text{Bu}_4\text{N}^+)_4\text{H}_2\text{TPPS}^{4-}$  ( $2.5 \times 10^{-5} \text{ M}$ ) and  $\text{Li}^+@\text{PCBM} \text{ PF}_6^-$  ( $5.0 \times 10^{-5} \text{ M}$ ) in deaerated PhCN measured at 5 ps (black), 100 ps (red) and 3000 ps (blue) after laser excitation at 393 nm. (b) Decay time profile of absorbance at 620 nm.

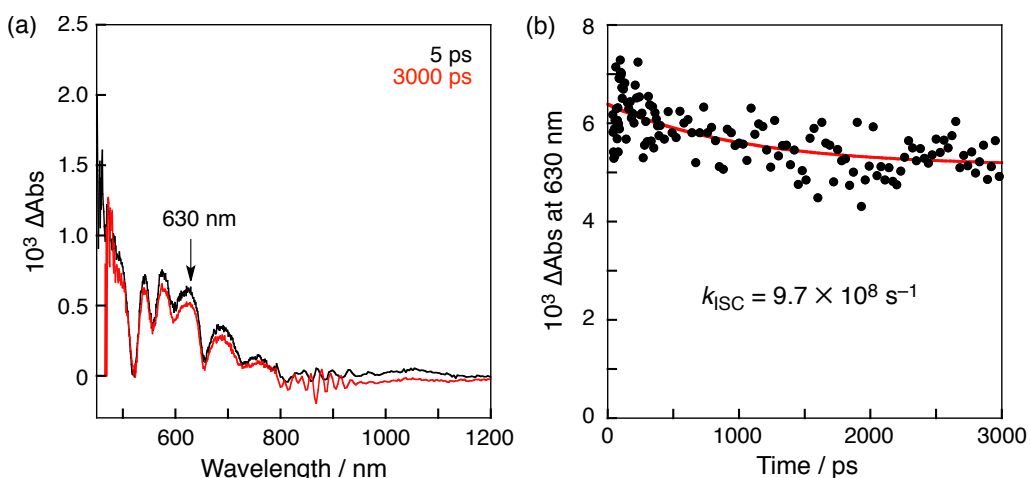


**Figure 18.** Transient absorption spectra of  $(\text{Bu}_4\text{N}^+)_4\text{H}_2\text{TPPS}^{4-}$  ( $2.5 \times 10^{-5} \text{ M}$ ) in PhCN measured at 5 ps (black) and 3000 ps (red) after laser excitation at 430 nm. (b) Decay time profile of absorbance at 630 nm.

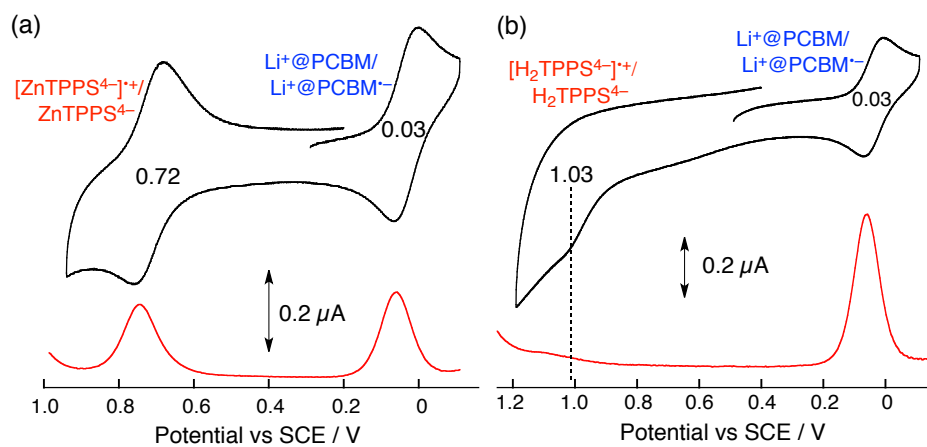


**Figure 19.** Cyclic voltammograms (CV) and differential pulse voltammograms (DPV) of  $\text{Li}^+@\text{PCBM} \text{ PF}_6^-$  (1.0  $\times$  10<sup>-4</sup> M) with (a)  $(\text{Bu}_4\text{N})_4\text{ZnTPPS}^{4-}$  (1.0  $\times$  10<sup>-4</sup> M) and (b)  $(\text{Bu}_4\text{N})_4\text{H}_2\text{TPPS}^{4-}$  (1.0  $\times$  10<sup>-4</sup> M) in deaerated PhCN containing 0.10 M TBAPF<sub>6</sub> (sweep rates: 100 mV s<sup>-1</sup> for CV and 4 mV s<sup>-1</sup> for DPV).

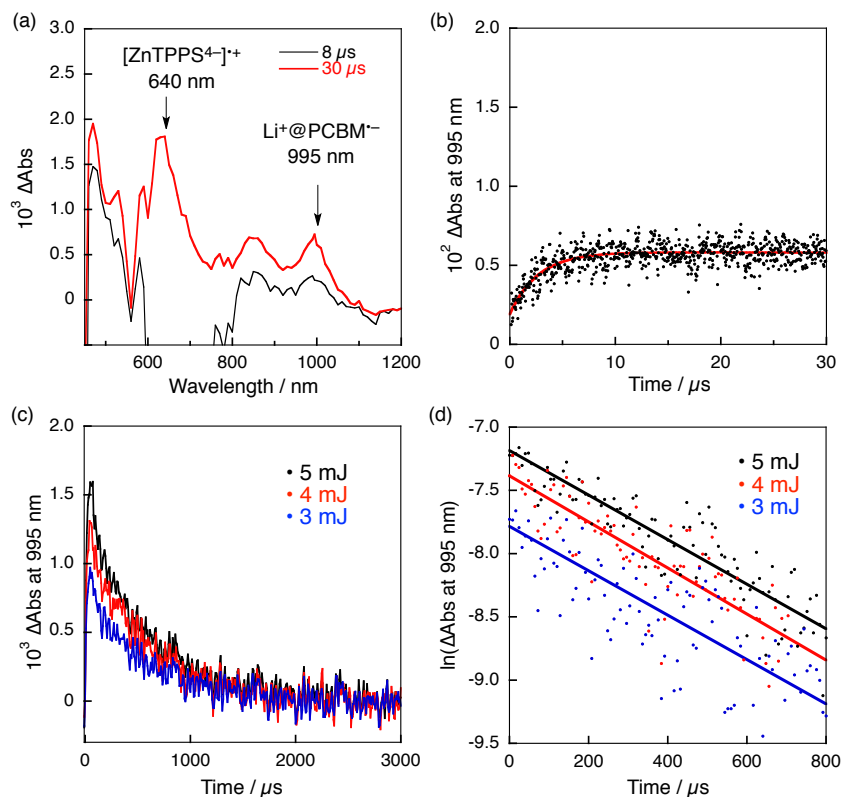


**Figure 20.** (a) Transient absorption spectra of  $(\text{Bu}_4\text{N})_4\text{ZnTPPS}^{4-}$  (2.5  $\times$  10<sup>-5</sup> M) with  $\text{Li}^+@\text{PCBM} \text{ PF}_6^-$  (5.0  $\times$  10<sup>-5</sup> M) in deaerated PhCN at 8  $\mu\text{s}$  (black) and 30  $\mu\text{s}$  (red) after nanosecond laser excitation at 450 nm. (b) Rise time profiles at 995 nm. Excitation at 532 nm. (c) Decay time profiles and (d) First-order plots at 995 nm with different laser intensities (3, 4 and 5 mJ pluse<sup>-1</sup>). Excitation at 450 nm.

The transient absorption spectra of the  $\text{ZnTPPS}^{4-}/\text{Li}^+@\text{PCBM}$  complex were measured by nanosecond laser flash photolysis, as shown in Figure 20a. The transient absorption band at 640 nm and 995 nm observed at 30  $\mu\text{s}$  are assigned to  $[\text{ZnTPPS}^{4-}]^+$  and  $\text{Li}^+@\text{PCBM}^+$ , respectively.<sup>62a</sup> The rate constant of electron transfer was determined from the rise of the absorbance at 995 nm due to  $\text{Li}^+@\text{PCBM}^+$  and was found to be  $3.7 \times 10^5 \text{ s}^{-1}$ . Similarly nanosecond laser excitation of  $\text{H}_2\text{TPPS}^{4-}/\text{Li}^+@\text{PCBM}$  also resulted in formation of the CS state (Figure 21a and 21b). The rate constant of electron transfer was also determined from the rise of the absorption band at 995 nm due to  $\text{Li}^+@\text{PCBM}^+$  to be  $6.2 \times 10^5 \text{ s}^{-1}$ . The driving forces for electron transfer from  $\text{ZnTPPS}^{4-}$  to  ${}^3[\text{Li}^+@\text{PCBM}]^*$  and from  ${}^3[\text{ZnTPPS}^{4-}]^*$  to  $\text{Li}^+@\text{PCBM}$  were determined from the triplet energies of  $\text{Li}^+@\text{PCBM}$  and  $\text{ZnTPPS}^{4-}$  (1.43 eV; Figure 22a), and the energy of the CS state to be 0.80 and 0.74 eV, respectively. The

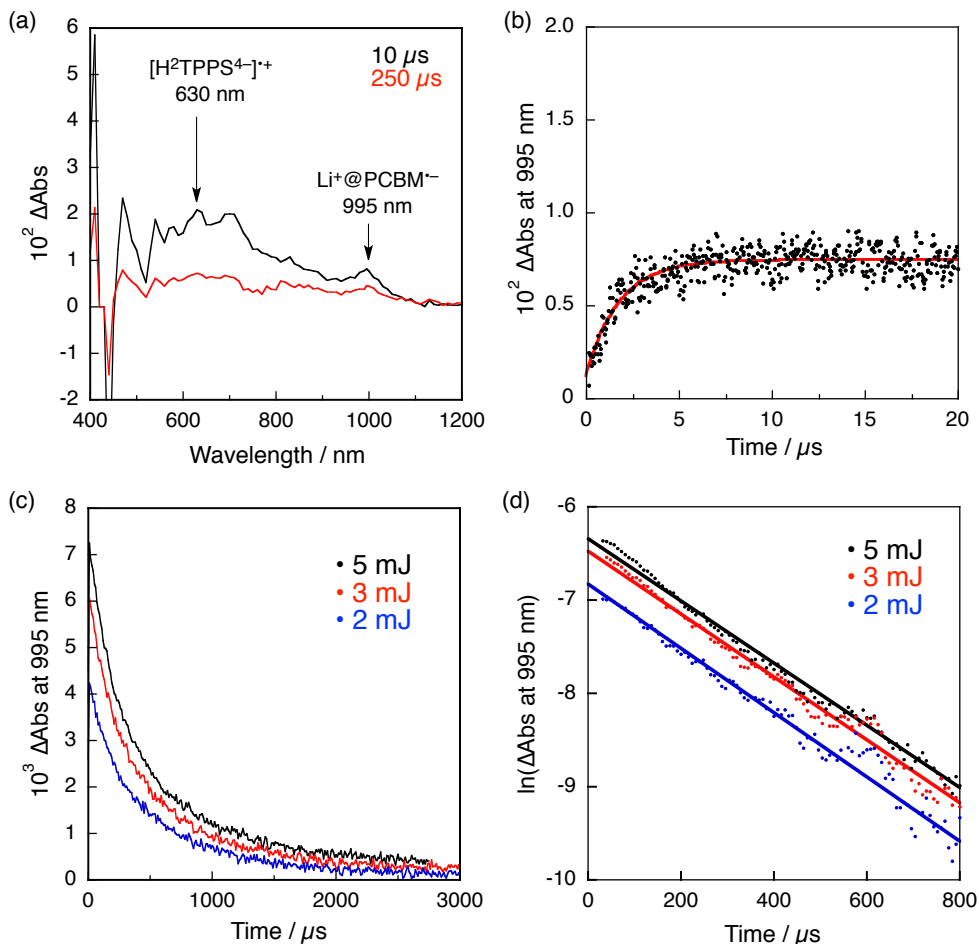


**Figure 21.** (a) Transient absorption spectra of  $(\text{Bu}_4\text{N}^+)_4\text{H}_2\text{TPPS}^{4-}$  ( $2.5 \times 10^{-5} \text{ M}$ ) with  $\text{Li}^+@\text{PCBM} \text{PF}_6^-$  ( $5.0 \times 10^{-5} \text{ M}$ ) in deaerated PhCN at 10  $\mu\text{s}$  (black) and 250  $\mu\text{s}$  (red) after nanosecond laser excitation at 532 nm. (b) Rise time profile at 995 nm. (c) Decay time profiles and (d) First-order plots at 995 nm with the various laser intensities (2, 3 and 5 mJ  $\text{pulse}^{-1}$ ).

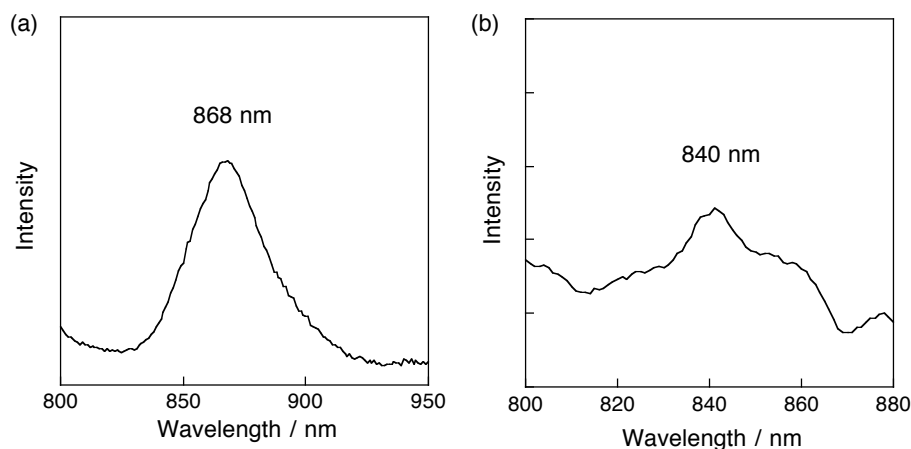


**Figure 22.** Phosphorescence spectrum of (a)  $(\text{Bu}_4\text{N}^+)_4\text{ZnTPPS}^{4-}$  (b)  $(\text{Bu}_4\text{N}^+)_4\text{H}_2\text{TPPS}^{4-}$  in deaerated EPA (5:5:2 (v/v) = 2-propanol:diethyl ether:ethanol) glass. Excitation wavelength: 550 nm;  $T = 77$  K.

driving forces for electron transfer from  $\text{H}_2\text{TPPS}^{4-}$  to  ${}^3[\text{Li}^+@\text{PCBM}]^*$  and from  ${}^3[\text{H}_2\text{TPPS}^{4-}]^*$  to  $\text{Li}^+@\text{PCBM}$  were also determined from triplet energies of  $\text{Li}^+@\text{PCBM}$  and  $\text{H}_2\text{TPPS}^{4-}$  (1.48 eV; Figure 22b), and the energy of the CS state to be 0.49 and 0.48 eV, respectively.

Figure 20c shows the decay time profiles of the absorption band at 995 nm due to  $\text{Li}^+@\text{PCBM}^-$  in PhCN. The rate constant of back electron transfer (BET) to the ground state was determined from the first-order plot, as shown in Figure 20d. The lifetime of the CS state of the  $[\text{ZnTPPS}^{4-}]^+/\text{Li}^+@\text{PCBM}^-$  was determined to be  $560\ \mu\text{s}$  [ $= (1.8 \times 10^3\ \text{s}^{-1})^{-1}$ ], which is twice as long as that of  $\text{ZnTPPS}^{4-}/\text{Li}^+@\text{C}_{60}$  system ( $300\ \mu\text{s}$ ).<sup>62a</sup> The quantum yield of the CS state was determined to be 0.42 from the comparative method<sup>43</sup> by using the absorption of the CS state and absorption coefficient of  $\text{Li}^+@\text{PCBM}^-$  at 995 nm ( $\epsilon_{995} = 2300\ \text{M}^{-1}\ \text{cm}^{-1}$ ; Figure 2). Upon replacing  $\text{ZnTPPS}^{4-}$  was replaced by  $\text{H}_2\text{TPPS}^{4-}$ , the lifetime and the quantum yield of the CS state of  $[\text{H}_2\text{TPPS}^{4-}]^+/\text{Li}^+@\text{PCBM}^-$  were determined to be  $450\ \mu\text{s}$  [ $= (2.2 \times 10^3\ \text{s}^{-1})^{-1}$ ] and 0.59, respectively (Figure 21).

These CS states were also detected by electron paramagnetic resonance (EPR) spectroscopy measurements after photoirradiation of the supramolecules in frozen PhCN, as shown in Figure 23a. The spin-spin interaction in the triplet radical ion pair of  $\text{ZnTPPS}^{4-}/\text{Li}^+@\text{PCBM}$  was clearly observed at 4 K with the fine structure due to the CS state and the triplet signal at  $g = 2.00$  and  $g = 4.31$ , respectively (Figure 23a). Thus, the spin state of the CS state can be assigned to be triplet. Similarly, the spin state of the CS state of  $\text{H}_2\text{TPPS}^{4-}/\text{Li}^+@\text{PCBM}$  was also triplet (Figure 23b). These results indicate that charge recombination processes are spin forbidden, which can afford the long-lived CS state. Moreover, from the zero-field splitting

values ( $D = 28.0$  G for  $[\text{ZnTPPS}^{4-}]^{*+}/\text{Li}^+@\text{PCBM}^{*^-}$ ,  $27.9$  G for  $[\text{H}_2\text{TPPS}^{4-}]^{*+}/\text{Li}^+@\text{PCBM}^{*^-}$ ), the distances ( $r$ ) between two electron spins were estimated to be  $10.0$  and  $9.8$  Å, using the relation  $D = 27800/r^3$ .<sup>60,62a,62d</sup> These distances are approximately  $2$  Å longer than those of MTPPS<sup>4-</sup>/Li<sup>+</sup>@C<sub>60</sub> systems ( $r = 8.1$  Å for  $[\text{ZnTPPS}^{4-}]^{*+}/\text{Li}^+@\text{C}_{60}^{*^-}$ ,  $r = 7.9$  Å for  $[\text{H}_2\text{TPPS}^{4-}]^{*+}/\text{Li}^+@\text{C}_{60}^{*^-}$ ).<sup>62a</sup>

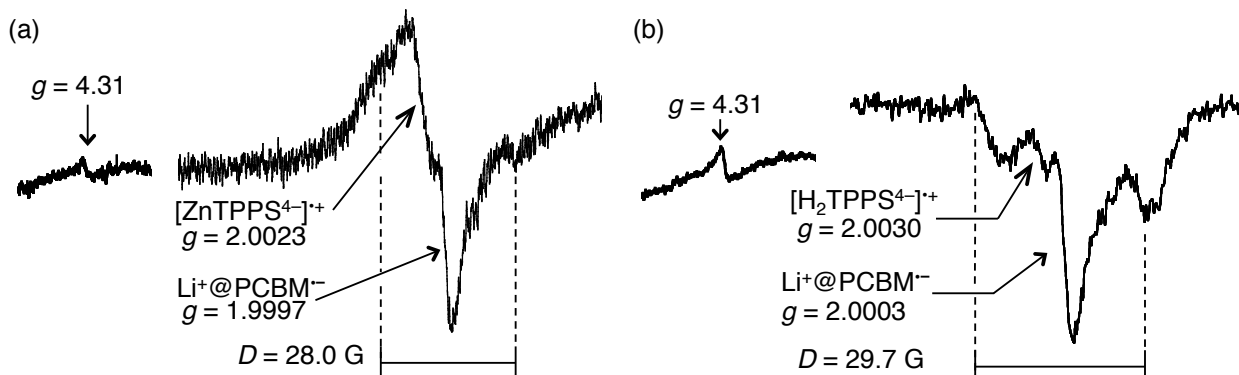


**Figure 23.** EPR spectra of the CS state (a)  $[\text{ZnTPPS}^{4-}]^{*+}/\text{Li}^+@\text{PCBM}^{*^-}$  and (b)  $[\text{H}_2\text{TPPS}^{4-}]^{*+}/\text{Li}^+@\text{PCBM}^{*^-}$  in deaerated PhCN generated by photoirradiation by using a high-pressure Hg lamp (1000 W) at 4 K focused on around  $g = 4$  (left) and  $g = 2$  (right).

The rates of BET ( $k_{\text{BET}}$ ) exhibited temperature dependence (0–90 °C), which is predicted by the Marcus equation (Equation (4)) for non-adiabatic electron transfer.<sup>71</sup> Equation (4) can be written as equation (5), which predicts a linear correlation between  $\ln(k_{\text{BET}}T^{1/2})$  and  $T^{-1}$ :

$$k_{\text{BET}} = \left( \frac{4\pi^3}{h^2 \lambda k_{\text{B}} T} \right)^{1/2} V^2 \exp\left[ -\frac{(\Delta G_{\text{BET}} + \lambda)^2}{4\lambda k_{\text{B}} T} \right] \quad (4)$$

$$\ln(k_{\text{BET}}T^{1/2}) = \ln\left( \frac{2\pi^{3/2} V^2}{h(\lambda k_{\text{B}})^{1/2}} \right) - \frac{(\Delta G_{\text{BET}} + \lambda)^2}{4\lambda k_{\text{B}} T} \quad (5)$$

in which  $k_{\text{BET}}$  is rate constant of intramolecular BET,  $\lambda$  is the reorganization energy,  $V$  is the electronic coupling term,  $-\Delta G_{\text{BET}}$  is the driving force for BET,  $h$  is the Plank's constant and  $k_{\text{B}}$  is the Boltzmann constant.

The plot of  $\ln(k_{\text{BET}}T^{1/2})$  vs  $T^{-1}$  for the intramolecular BET in the temperature range from 273 to 363 K gave the linear correlations as shown in Figure 24. According to the slope and intercept of Figure 24, the  $\lambda$  and  $V$  values were determined to be  $\lambda = 0.36$  eV and  $V = 8.5 \times 10^{-3}$  cm<sup>-1</sup> for ZnTPPS<sup>4-</sup>/Li<sup>+</sup>@PCBM and  $\lambda = 0.62$  eV and  $V = 7.9 \times 10^{-3}$  cm<sup>-1</sup> for

$\text{H}_2\text{TPPS}^{4-}/\text{Li}^+@\text{PCBM}$ . These  $V$  values are much smaller than those of another  $\text{Li}^+@\text{C}_{60}$  supramolecular systems (zinc chlorin– $\text{Li}^+@\text{C}_{60}$ :  $0.066 \text{ cm}^{-1}$ ).<sup>62d</sup> Such small  $V$  values afforded the long-lived CS states.

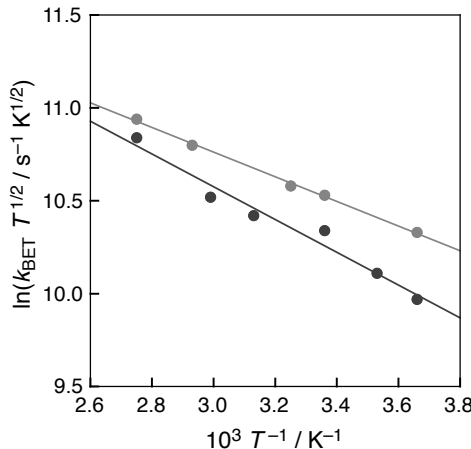
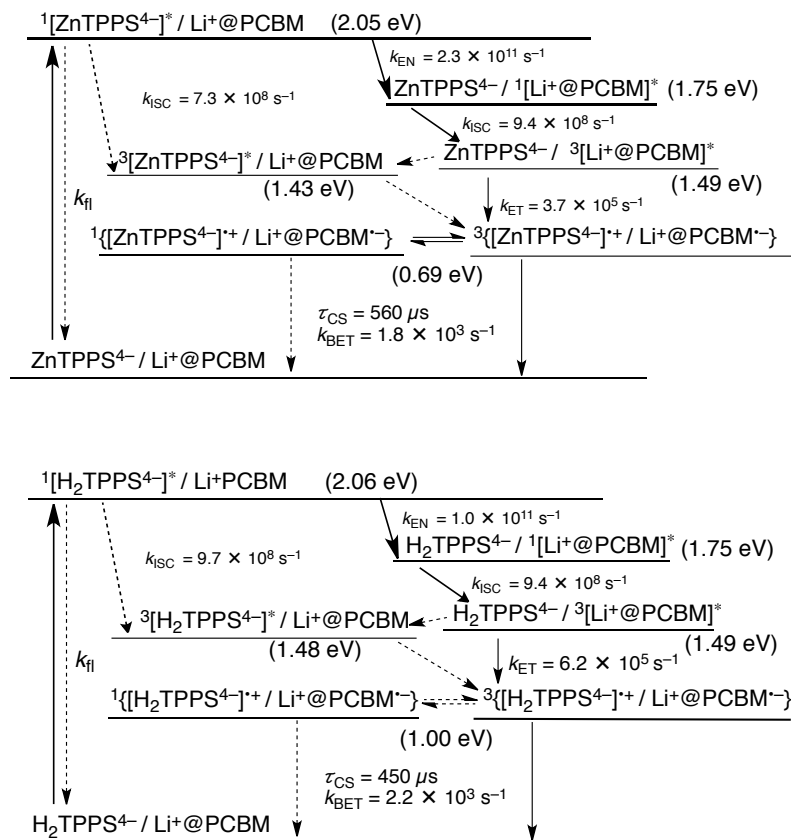


**Figure 24.** Plots of  $\ln(k_{\text{BET}} T^{1/2})$  vs  $T^{-1}$  for charge recombination of  $\{[\text{ZnTPPS}^{4-}]^+/\text{Li}^+@\text{PCBM}^{\cdot-}\}$  (black) and  $\{[\text{H}_2\text{TPPS}^{4-}]^+/\text{Li}^+@\text{PCBM}^{\cdot-}\}$  (gray) in deaerated PhCN.

On the basis of the results described above, the energy diagrams of photoinduced ET and BET of MTPPS<sup>4-</sup>/Li<sup>+</sup>@PCBM are shown in Scheme 3. The singlet excited energies of MTPPS<sup>4-</sup> were determined from the average of absorbance and fluorescence maximums (Figure 10a and 13a for ZnTPPS<sup>4-</sup> and Figure 11a and 14a for H<sub>2</sub>TPPS<sup>4-</sup>). The triplet excited energies of MTPPS<sup>4-</sup> were determined by phosphorescence maxima as 868 nm for ZnTPPS<sup>4-</sup> and 840 nm for H<sub>2</sub>TPPS<sup>4-</sup> (Figure 22). Upon photoexcitation of MTPPS<sup>4-</sup>/Li<sup>+</sup>@PCBM, <sup>1</sup>[MTPPS<sup>4-</sup>]<sup>\*</sup>/Li<sup>+</sup>@PCBM is formed, and energy transfer occurs to give MTPPS<sup>4-</sup>/<sup>1</sup>[Li<sup>+</sup>@PCBM]<sup>\*</sup>, as indicated by fluorescence and femtosecond laser flash photolysis measurements. Then intersystem crossing occurs to produce MTPPS<sup>4-</sup>/<sup>3</sup>[Li<sup>+</sup>@PCBM]<sup>\*</sup>. Electron transfer from <sup>3</sup>[Li<sup>+</sup>@PCBM]<sup>\*</sup> to MTPPS<sup>4-</sup> occurs to produce the CS state, [MTPPS<sup>4-</sup>]<sup>+</sup>/Li<sup>+</sup>@PCBM<sup>·-</sup>, through intramolecular electron transfer. No electron transfer from the singlet excited states (<sup>1</sup>[MTPPS<sup>4-</sup>]<sup>\*</sup>/Li<sup>+</sup>@PCBM and MTPPS<sup>4-</sup>/<sup>1</sup>[Li<sup>+</sup>@PCBM]<sup>\*</sup>) to produce [MTPPS<sup>4-</sup>]<sup>+</sup>/Li<sup>+</sup>@PCBM<sup>·-</sup> occurred, because the driving forces of these process are located deeply in the Marcus inverted region. No energy transfer from <sup>3</sup>[Li<sup>+</sup>@PCBM]<sup>\*</sup> to MTPPS<sup>4-</sup> were observed, because electron transfer from MTPPS<sup>4-</sup> to <sup>3</sup>[Li<sup>+</sup>@PCBM]<sup>\*</sup> occurs faster than the energy transfer due to the larger driving force of electron transfer than that of energy transfer. Intramolecular electron transfer from MTPPS<sup>4-</sup> to <sup>3</sup>[Li<sup>+</sup>@PCBM]<sup>\*</sup> occurred to

produce the triplet CS states ( ${}^3\{[\text{MTPPS}^{4-}]^+/\text{Li}^+@\text{PCBM}^-\}$ ), in which the intramolecular charge recombination occurred with remarkably long lifetimes.

**Scheme 3.** Energy Diagrams for  $\text{ZnTPPS}^{4-}/\text{Li}^+@\text{PCBM}$  and  $\text{H}_2\text{TPPS}^{4-}/\text{Li}^+@\text{PCBM}$ . Broken Arrow: Minor Pathway.



## Conclusions

In summary, I have constructed supramolecules between anionic porphyrins and  $\text{Li}^+@\text{PCBM}$ , which are strongly bound in PhCN by electrostatic interaction. Upon the laser excitation of the MTPPS<sup>4-</sup> moiety, energy transfer from  ${}^1\text{[MTPPS}^{4-}\text{]}^*$  to  $\text{Li}^+@\text{PCBM}$  occurred, followed by intersystem crossing from  ${}^1\text{[Li}^+@\text{PCBM}]\text{*}$  to  ${}^3\text{[Li}^+@\text{PCBM}]\text{*}$ , and intramolecular electron transfer from MTPPS<sup>4-</sup> to  ${}^3\text{[Li}^+@\text{PCBM}]\text{*}$  to produce the CS state with the rate constants of  $3.7 \times 10^5 \text{ s}^{-1}$  for  $\text{ZnTPPS}^{4-}/\text{Li}^+@\text{PCBM}$  and  $6.2 \times 10^5 \text{ s}^{-1}$  for  $\text{H}_2\text{TPPS}^{4-}/\text{Li}^+@\text{PCBM}$ . The lifetimes of the CS states were determined to be  $560 \mu\text{s}$  for  $\text{ZnTPPS}^{4-}/\text{Li}^+@\text{PCBM}$  and  $450 \mu\text{s}$  for  $\text{H}_2\text{TPPS}^{4-}/\text{Li}^+@\text{PCBM}$  in PhCN. This value of  $\text{ZnTPPS}^{4-}/\text{Li}^+@\text{PCBM}$  is two times longer than that of  $\text{ZnTPPS}^{4-}/\text{Li}^+@\text{C}_{60}$  system ( $300 \mu\text{s}$ )<sup>62a</sup>

by the elongation of spin-spin distance of CS state due to the bulky functional group of  $\text{Li}^+@\text{PCBM}$ . Such long CS lifetimes result from the small electronic coupling terms ( $V = 8.5 \times 10^{-3} \text{ cm}^{-1}$  for  $\text{ZnTPPS}^{4-}/\text{Li}^+@\text{PCBM}$  and  $7.9 \times 10^{-3} \text{ cm}^{-1}$  for  $\text{H}_2\text{TPPS}^{4-}/\text{Li}^+@\text{PCBM}$ ) and spin-forbidden charge-recombination processes. Thus, supramolecular complexes between anionic porphyrins and  $\text{Li}^+@\text{PCBM}$  provide excellent photoinduced ET properties for applications to organic solar cells.

## References

- (1) (a) Raval, A.; Ramanathan, V. *Nature* **1989**, *342*, 758–761. (b) Loriois, C.; Jouzel, J.; Raynaud, D.; Hansen, J.; Treut, H. Le. *Nature* **1990**, *347*, 139–145. (c) Hansen, J. E.; Lacis, A. A. *Nature* **1990**, *346*, 713–719.
- (2) Slovic, P.; Flynn, J. H.; Layman, M. *Science* **1991**, *254*, 1603–1607.
- (3) Armaroli, N.; Balzani, V. *Angew. Chem.* **2007**, *119*, 52–67; *Angew. Chem., Int. Ed.* **2007**, *46*, 52–66.
- (4) Nyambuu, U.; Semmler, W. *Econ. Model.* **2014**, *37*, 271–279.
- (5) (a) Hagfeldt, A.; Grätzel, M. *Chem. Rev.* **1995**, *95*, 49–68. (b) Grätzel, M. *Nature* **2001**, *414*, 338–344. (c) Grätzel, M. *Nature* **2003**, *421*, 586–587. (d) O'Regan, B.; Grätzel, M. *Nature* **1991**, *353*, 737–740. (e) Hagfeldt, A.; Grätzel, M. *Acc. Chem. Res.* **2000**, *33*, 269–277.
- (6) Wang, Z.-S.; Kawauchi, H.; Kashima, T.; Arakawa, H. *Coord. Chem. Rev.* **2004**, *248*, 1381–1389.
- (7) Hara, K.; Kurashige, M.; Dan-oh, Y.; Kasada, C.; Shinpo, A.; Suga, S.; Sayama, K.; Arakawa, H. *New J. Chem.* **2003**, *27*, 783–785.
- (8) Griffith, M. J.; Sunahara, K.; Wagner, P.; Wagner, K.; Wallace, G. G.; Officer, D. L.; Furube, A.; Katoh, R.; Mori, S.; Mozer, A. J. *Chem. Commun.* **2012**, *48*, 4145–4162.
- (9) (a) Huynh, W. U.; Dittmer, J. J.; Alivisatos, A. P. *Science* **2002**, *295*, 2425–2427. (b) Shah, A.; Torres, P.; Tscharner, R.; Wyrsch, N.; Keppner, H. *Science* **1999**, *285*, 692–698.
- (10) Imahori, H.; Fukuzumi, S. *Adv. Mater.* **2001**, *13*, 1197–1199.
- (11) (a) Hasobe, T. *Phys. Chem. Chem. Phys.* **2012**, *14*, 15975–15987. (b) Hasobe, T.; Sakai, H. *ECS J. Solid State Sci. Technol.* **2013**, *2*, M3015–M3022.
- (12) Fukuzumi, S.; Ohkubo, K. *Dalton Trans.* **2013**, *42*, 15846–15858.

---

(13) Tang, C. W. *Appl. Phys. Lett.* **1986**, *48*, 183–185.

(14) Sariciftci, N. S.; Smilowitz, L.; Heeger, A. J.; Wudl, F. *Science* **1992**, *258*, 1474–1746.

(15) (a) Brabec, C. J.; Cravino, A.; Zerza, G.; Sariciftci, N. S.; Kiebooms, R.; Vanderzande, D.; Hummelen, J. C. *J. Phys. Chem. B* **2001**, *105*, 1528–1536. (b) Brabec, C. J.; Sariciftci, N. S.; Hummelen, J. C. *Adv. Func. Mater.* **2001**, *11*, 15–26. (c) Troshin, P. A.; Hoppe, H.; Renz, J.; Egginger, M.; Mayorova, J. Y.; Goryachev, A. E.; Peregudov, A. S.; Lyubovskaya, R. N.; Gobsch, G.; Sariciftci, N. S.; Razumov, V. F. *Adv. Funct. Mater.* **2009**, *19*, 779–788.

(16) Hatano, J.; Obata, N.; Yamaguchi, S.; Yasuda, T.; Matsuo, Y. *J. Mater. Chem.* **2012**, *22*, 19258–19263.

(17) Matsuo, Y.; Sato, Y.; Niinomi, T.; Soga, I.; Tanaka, H.; Nakamura, E. *J. Am. Chem. Soc.* **2009**, *131*, 16048–16050.

(18) Hiramoto, M.; Fujiwara, H.; Yokoyama, M. *Appl. Phys. Lett.* **1991**, *58*, 1062–1064.

(19) Ross, R. B.; Cardona, C. M.; Guldi, D. M.; Sankaranarayanan, S. G.; Reese, M. O.; Kopidakis, N.; Peet, J.; Walker, B.; Bazan, G. C.; Van Keuren, E.; Holloway, B. C.; Drees, M. *Nature Chem.* **2009**, *8*, 208–212.

(20) Yu, G.; Gao, J.; Hummelen, J. C.; Wudl, F.; Heeger, A. J. *Science* **1995**, *270*, 1789–1791.

(21) Shaheen, S. E.; Brabec, C. J.; Sariciftci, N. S.; Padinger, F.; Fromherz, T.; Hummelen, J. C. *Appl. Phys. Lett.* **2001**, *78*, 841–943.

(22) Choi, J. H.; Son, K.-I.; Kim, T.; Kim, K.; Ohkubo, K.; Fukuzumi, S. *J. Mater. Chem.* **2010**, *20*, 475–482.

(23) Green, M. A.; Emery, K.; Hishikawa, Y.; Warta, W.; Dunlop, E. D. *Prog. Photovolt: Res. Appl.* **2014**, *22*, 1–9.

(24) Gust, D. Moore, T. A. Moore, A. L. In *Electron Transfer in Chemistry* Balzani, V., Ed.; Wiley-VCH: Weinheim, 2001; Vol. 3, pp 272–336.

(25) (a) Frey, J.; Kodis, G.; Straight, S. D.; Moore, T. A.; Moore, A. L.; Gust, D. *J. Phys. Chem. A* **2013**, *117*, 607–615. (b) Terazono, Y.; Kodis, G.; Liddell, P. A.; Garg, V.; Moore, T. A.; Moore, A. L.; Gust, D. *J. Phys. Chem. B* **2009**, *113*, 7147–7155. (c) Gust, D.; Moore, T. A.; Moore, A. L. *Acc. Chem. Res.* **1993**, *26*, 198–205. (d) Gust, D.; Moore, T. a; Moore, A. L. *Acc. Chem. Res.* **2009**, *42*, 1890–1898.

(26) (a) Ricks, A. B.; Brown, K. E.; Wenninger, M.; Karlen, S. D.; Berlin, Y. A; Co, D. T.; Wasielewski, M. R. *J. Am. Chem. Soc.* **2012**, *134*, 4581–4588. (b) Gunderson, V. L.;

Smeigh, A. L.; Kim, C. H.; Co, D. T.; Wasielewski, M. R. *J. Am. Chem. Soc.* **2012**, *134*, 4363–4372. (c) Lewis, F. D.; Letsinger, R. L.; Wasielewski, M. R. *Acc. Chem. Res.* **2001**, *34*, 159–170. (d) Wasielewski, M. R. *Acc. Chem. Res.* **2009**, *42*, 1910–1921.

(27) (a) Balzani, V. *Coord. Chem. Rev.* **2001**, *219-221*, 545–572. (b) Faiz, J. A.; Heitz, V.; Sauvage, J.-P. *Chem. Soc. Rev.* **2009**, *38*, 422–442.

(28) (a) Diederich, F.; Gómez-López, M. *Chem. Soc. Rev.* **1999**, *28*, 263–277. (b) Chambron, J.-C.; Collin, J.-P.; Dalbavie, J.-O.; Dietrich-Buchecker, C. O.; Heitz, V.; Odobel, F.; Solladié, N.; Sauvage, J.-P. *Coord. Chem. Rev.* **1998**, *178-180*, 1299–1312.

(29) (a) Fukuzumi, S. *Org. Biomol. Chem.* **2003**, *1*, 609–620. (b) Fukuzumi, S. *Phys. Chem. Chem. Phys.* **2008**, *10*, 2283–2297. (c) Fukuzumi, S. *Bull. Chem. Soc. Jpn.* **2006**, *79*, 177–195. (d) Fukuzumi, S.; Kojima, T. *J. Mater. Chem.* **2008**, *18*, 1427–1439. (e) Fukuzumi, S.; Honda, T.; Ohkubo, K.; Kojima, T. *Dalton Trans.* **2009**, 3880–3889. (f) Ohkubo, K.; Fukuzumi, S. *J. Porphyrins Phthalocyanines* **2008**, *12*, 993–1004.

(30) (a) Boyle, M. M.; Forgan, R. S.; Friedman, D. C.; Gassensmith, J. J.; Smaldone, R. A.; Stoddart, J. F.; Sauvage, J.-P. *Chem. Commun.* **2011**, *47*, 11870–11872. (b) Linke, M.; Chambron, J.-C.; Heitz, V.; Sauvage, J.-P.; Encinas, S.; Barigelletti, F.; Flamigni, L. *J. Am. Chem. Soc.* **2000**, *122*, 1834–11844. (c) Dixon, I. M.; Collin, J.-P.; Sauvage, J.-P.; Barigelletti, F.; Flamigni, L. *Angew. Chem., Int. Ed.* **2000**, *112*, 1292–1295.

(31) (a) Kamat, P. V. *J. Phys. Chem. C* **2007**, *111*, 2834–2860. (b) Subbaiyan, N. K.; Wijesinghe, C. A.; D’Souza, F. *J. Am. Chem. Soc.* **2009**, *131*, 14646–14647. (c) Imahori, H.; Umeyama, T.; Ito, S. *Acc. Chem. Res.* **2009**, *42*, 1809–1818.

(32) Imahori, H.; Tamaki, K.; Guldi, D. M.; Luo, C.; Fujitsuka, M.; Ito, O.; Sakata, Y.; Fukuzumi, S. *J. Am. Chem. Soc.* **2001**, *123*, 2607–2617.

(33) (a) Wijesinghe, C. A.; El-Khouly, M. E.; Subbaiyan, N. K.; Supur, M.; Zandler, M. E.; Ohkubo, K.; Fukuzumi, S.; D’Souza, F. *Chem.-Eur. J.* **2011**, *17*, 3147–3156. (b) Ohkubo, K.; Sintic, P. J.; Tkachenko, N. V.; Lemmetyinen, H.; E, W.; Ou, Z.; Shao, J.; Kadish, K. M.; Crossley, M. J.; Fukuzumi, S. *Chem. Phys.* **2006**, *326*, 3–14. (c) Céspedes-Guirao, F. J.; Ohkubo, K.; Fukuzumi, S.; Sastre-Santos, Á.; Fernández-Lázaro, F. J. *Org. Chem.* **2009**, *74*, 5871–5880. (d) Murakami, M.; Ohkubo, K.; Hasobe, T.; Sgobba, V.; Guldi, D. M.; Wessendorf, F.; Hirsch, A.; Fukuzumi, S. *J. Mater. Chem.* **2010**, *20*, 1457–1466. (e) Jiménez, Á. J.; Spänig, F.; Rodríguez-Morgade, M. S.; Ohkubo, K.; Fukuzumi, S.; Guldi, D. M.; Torres, T. *Org. Lett.* **2007**, *9*, 2481–2484. (f) Martín-Gomis, L.; Ohkubo, K.; Fernández-Lázaro, F.; Fukuzumi, S.; Sastre-Santos, Á.

---

*Chem. Commun.* **2010**, *46*, 3944–3946. (g) Blas-Ferrando, V. M.; Ortiz, J.; Bouissane, L.; Ohkubo, K.; Fukuzumi, S.; Fernández-Lázaro, F.; Sastre-Santos, A. *Chem. Commun.* **2012**, *48*, 6241–6243.

(34) (a) Guldi, D. M.; Sgobba, V. *Chem. Commun.* **2011**, *47*, 606–610. (b) Guldi, D. M.; Rahman, G. M. A.; Sgobba, V.; Ehli, C. *Chem. Soc. Rev.* **2006**, *35*, 471–487. (c) Bottari, G.; de la Torre, G.; Guldi, D. M.; Torres, T. *Chem. Rev.* **2010**, *110*, 6768–6816. (d) Martín, N.; Sánchez, L.; Herranz, M. A.; Illescas, B.; Guldi, D. M. *Acc. Chem. Res.* **2007**, *40*, 1015–1024.

(35) (a) Fukuzumi, S.; Kotani, H.; Ohkubo, K.; Ogo, S.; Tkachenko, N. V.; Lemmetyinen, H. *J. Am. Chem. Soc.* **2004**, *126*, 1600–1601. (b) Ohkubo, K.; Kotani, H.; Fukuzumi, S. *Chem. Commun.* **2005**, 4520–4522. (c) Fukuzumi, S.; Kotani, H.; Ohkubo, K. *Phys. Chem. Chem. Phys.* **2008**, *10*, 5159–5162. (d) Ohkubo, K.; Fukuzumi, S. *Bull. Chem. Soc. Jpn.* **2009**, *82*, 303–315.

(36) (a) Fukuzumi, S.; Ohkubo, K.; Imahori, H.; Shao, J.; Ou, Z.; Zheng, G.; Chen, Y.; Pandey, R. K.; Fujitsuka, M.; Ito, O.; Kadish, K. M. *J. Am. Chem. Soc.* **2001**, *123*, 10676–10683. (b) Ohkubo, K.; Imahori, H.; Shao, J.; Ou, Z.; Kadish, K. M.; Chen, Y.; Zheng, G.; Pandey, R. K.; Fujitsuka, M.; Ito, O.; Fukuzumi, S. *J. Phys. Chem. A* **2002**, *106*, 10991–10998.

(37) D’Souza, F.; Maligaspe, E.; Ohkubo, K.; Zandler, M. E.; Subbaiyan, N. K.; Fukuzumi, S. *J. Am. Chem. Soc.* **2009**, *131*, 8787–8797.

(38) (a) Murakami, M.; Ohkubo, K.; Fukuzumi, S. *Chem.–Eur. J.* **2010**, *16*, 7820–7832. (b) Murakami, M.; Ohkubo, K.; Nanjo, T.; Souma, K.; Suzuki, N.; Fukuzumi, S. *ChemPhysChem* **2010**, *11*, 2594–2605.

(39) Martín-Gomis, L.; Ohkubo, K.; Fernández-Lázaro, F.; Fukuzumi, S.; Sastre-Santos, Á. *J. Phys. Chem. C* **2008**, *112*, 17694–17701.

(40) Fukuzumi, S.; Imahori, H.; Okamoto, K.; Yamada, H.; Fujitsuka, M.; Ito, O.; Guldi, D. M. *J. Phys. Chem. A* **2002**, *106*, 1903–1908.

(41) (a) Kashiwagi, Y.; Ohkubo, K.; McDonald, J. A.; Blake, I. M.; Crossley, M. J.; Araki, Y.; Ito, O.; Imahori, H.; Fukuzumi, S. *Org. Lett.* **2003**, *5*, 2719–2721. (b) Lee, S.-H.; Larsen, A. G.; Ohkubo, K.; Cai, Z.-L.; Reimers, J. R.; Fukuzumi, S.; Crossley, M. J. *Chem. Sci.* **2012**, *3*, 257–269.

(42) Fukuzumi, S.; Ohkubo, K.; E, W.; Ou, Z.; Shao, J.; Kadish, K. M.; Hutchison, J. A.; Ghiggino, K. P.; Sintic, P. J.; Crossley, M. J. *J. Am. Chem. Soc.* **2003**, *125*, 14984–

14985.

(43) Ohkubo, K.; Kotani, H.; Shao, J.; Ou, Z.; Kadish, K. M.; Li, G.; Pandey, R. K.; Fujitsuka, M.; Ito, O.; Imahori, H.; Fukuzumi, S. *Angew. Chem., Int. Ed.* **2004**, *43*, 853–856.

(44) Echegoyen, L.; Diederich, F.; Echegoyen, L. E. In *Fullerenes, Chemistry, Physics, and Technology*; Kadish, K. M., Ruoff, R. S., Eds.; Wiley-Interscience: New York, 2000; pp 1–51.

(45) Guldi, D. M.; Fukuzumi, S. In *Fullerenes: From Synthesis to Optoelectronic Properties*; Guldi, D. M., Martin, N., Eds.; Kluwer: Dordrecht, 2003, pp 237–265.

(46) Sgobba, V.; Rahman, G. M. A.; Guldi, D. M. In *Carbon Nanotubes in Electron Donor-Acceptor Nanocomposites, Chemistry of Carbon Nanotubes*; Basiuk, V. A., Ed.; American Scientific Publishers: CA, 2006.

(47) Fukuzumi, S.; Guldi, D. M. In *Electron Transfer in Chemistry* Balzani, V., Ed.; Wiley-VCH: Weinheim, 2001; Vol. 2, pp 270–337.

(48) (a) Connolly, J. S.; Bolton, J. R. In *Photoinduced Electron Transfer*; Fox, M. A., Chanon, M., Eds.; Elsevier: Amsterdam, 1988; Part D, pp 303–393. (b) Wasielewski, M. R. In *Photoinduced Electron Transfer*; Fox, M. A., Chanon, M., Eds.; Elsevier: Amsterdam, 1988; Part A, pp 161–206.

(49) (a) Bixon, M.; Fajer, J.; Feher, G.; Freed, J. H.; Gamliel, D.; Hoff, A. J.; Levanon, H.; Möbius, K.; Nechushtai, R.; Norris, J. R.; Scherz, A.; Sessler, J. L.; Stehlik, D. *Isr. J. Chem.* **1992**, *32*, 369–518. (b) Kurreck, H.; Huber, M.; *Angew. Chem.* **1995**, *107*, 929–947; *Angew. Chem., Int. Ed.* **1995**, *34*, 849–866. (c) Gust, D.; Moore, T. A. In *The Porphyrin Handbook*; Kadish, K. M., Smith, K. M., Guilard, R., Eds.; Academic Press: San Diego, CA, 2000; Vol. 8, pp 153–190.

(50) (a) Elliott, K. J.; Harriman, A.; Le Pleux, L.; Pellegrin, Y.; Blart, E.; Mayer, C. R.; Odobel, F. *Phys. Chem. Chem. Phys.* **2009**, *11*, 8767–8773. (b) Benniston, A. C.; Harriman, A. *Mater. Today* **2008**, *11*, 26–34. (c) dobel, F.; Séverac, M.; Pellegrin, Y.; Blart, E.; Fosse, C.; Cannizzo, C.; Mayer, C. R.; Elliott, K. J.; Harriman, A. *Chem.–Eur. J.* **2009**, *15*, 3130–3138. (d) Fukuzumi, S.; Saito, K.; Ohkubo, K.; Troiani, V.; Qiu, H.; Gadde, S.; D’Souza, F.; Solladié, N. *Phys. Chem. Chem. Phys.* **2011**, *13*, 17019–1702.

(51) (a) Verhoeven, J. W. In *Electron Transfer-From Isolated Molecules to Biomolecules*; Jortner, J., Bixon, M., Eds.; John Wiley & Sons: New York, 1999; Part 1, pp 603–644. (b) Tokaji, S.; Yorimitsu, H.; Osuka, A. *Angew. Chem., Int. Ed.* **2012**, *51*, 12357–12361.

---

(c) Yoon, M.-C.; Lee, S.; Tokuji, S.; Yorimitsu, H.; Osuka, A.; Kim, D. *Chem. Sci.* **2013**, *4*, 1756–1746. (d) Kim, K. S.; Lim, J. M.; Osuka, A.; Kim, D. *J. Photochem. Photobiol. C* **2008**, *9*, 13–28. (e) Sun, L.; Hammarström, L.; Åkermark, B.; Styring, S. *Chem. Soc. Rev.* **2001**, *30*, 36–49.

(52) (a) Imahori, H.; Tamaki, K.; Araki, Y.; Sekiguchi, Y.; Ito, O.; Sakata, Y.; Fukuzumi, S. *J. Am. Chem. Soc.* **2002**, *124*, 5165–5174. (b) Imahori, H.; Sekiguchi, Y.; Kashiwagi, Y.; Sato, T.; Araki, Y.; Ito, O.; Yamada, H.; Fukuzumi, S. *Chem.–Eur. J.* **2004**, *10*, 3184–3196. (c) Imahori, H.; Guldi, D. M.; Tamaki, K.; Yoshida, Y.; Luo, C.; Sakata, Y.; Fukuzumi, S. *J. Am. Chem. Soc.* **2001**, *123*, 6617–6628. (d) Guldi, D. M.; Imahori, H.; Tamaki, K.; Kashiwagi, Y.; Yamada, H.; Sakata, Y.; Fukuzumi, S. *J. Phys. Chem. A* **2004**, *108*, 541–548.

(53) (a) D’Souza, F.; Ito, O. *Chem. Commun.* **2009**, 4913–4928. (b) D’Souza, F.; Sandanayaka, A. S. D.; Ito, O. *J. Phys. Chem. Lett.* **2010**, *1*, 2586–2593. (c) D’Souza, F.; Ito, O. *Coord. Chem. Rev.* **2005**, *249*, 1410–1422. (d) D’Souza, F.; Ito, O. *J. Phys. Chem. A* **2002**, *106*, 3243–3252. (e) El-Khouly, M. E.; Rogers, L. M.; Zandler, M. E.; Suresh, G.; Fujitsuka, M.; Ito, O.; D’Souza, F. *ChemPhysChem* **2003**, *4*, 474–481. (f) Flamigni, L. Johnston, M. R. Giribabu, L. *Chem.–Eur. J.* **2002**, *8*, 3938–3947.

(54) Xiao, S.; El-Khouly, M. E.; Li, Y.; Gan, Z.; Liu, H.; Jiang, L.; Araki, Y.; Ito, O.; Zhu, D. *J. Phys. Chem. B* **2005**, *109*, 3658–3667.

(55) Grimm, B.; Schornbaum, J.; Cardona, C. M.; van Paauwe, J. D.; Boyd, P. D. W.; Guldi, D. M. *Chem. Sci.* **2011**, 1530–1537.

(56) Fukuzumi, S.; Ohkubo, K.; D’Souza, F.; Sessler, J. L. *Chem. Commun.* **2012**, *48*, 9801–9815.

(57) Aoyagi, S.; Nishibori, E.; Sawa, H.; Sugimoto, K.; Takata, M.; Miyata, Y.; Kitaura, R.; Shinohara, H.; Okada, H.; Sakai, T.; Ono, Y.; Kawachi, K.; Yokoo, K.; Ono, S.; Omote, K.; Kasama, Y.; Ishikawa, S.; Komuro, T.; Tobita, H. *Nature Chem.* **2010**, *2*, 678–683.

(58) Aoyagi, S.; Nishibori, E.; Sawa, H.; Okada, H.; Tobita, H.; Kasama, Y.; Kitaura, R.; Shinohara, H. *Angew. Chem., Int. Ed.* **2012**, *51*, 3377–3381.

(59) Ueno, H.; Nakamura, Y.; Ikuma, N.; Kokubo, K.; Oshima, T. *Nano Res.* **2012**, *5*, 558–564.

(60) Fukuzumi, S.; Ohkubo, K.; Kawashima, Y.; Kim, D. S.; Park, J. S.; Jana, A.; Lynch, V. M.; Kim, D.; Sessler, J. L. *J. Am. Chem. Soc.* **2011**, *133*, 15938–15941.

(61) (a) Kawashima, Y.; Ohkubo, K.; Fukuzumi, S. *J. Phys. Chem. A* **2012**, *116*, 8942–8948.

(b) Kawashima, Y.; Ohkubo, K.; Fukuzumi, S. *J. Phys. Chem. A* **2013**, *117*, 6737–6743.

(62) (a) K. Ohkubo, Y. Kawashima, S. Fukuzumi, *Chem. Commun.* **2012**, *48*, 4314–4316. (b) T. Kamimura, K. Ohkubo, Y. Kawashima, H. Nobukuni, Y. Naruta, F. Tani, S. Fukuzumi, *Chem. Sci.* **2013**, *4*, 1451–1461. (c) K. Ohkubo, Y. Kawashima, H. Sakai, T. Hasobe, S. Fukuzumi, *Chem. Commun.* **2013**, *49*, 4474–4476. (d) Y. Kawashima, K. Ohkubo, K. Mase, S. Fukuzumi, *J. Phys. Chem. C* **2013**, *117*, 21166–21177.

(63) Matsuo, Y.; Okada, H.; Maruyama, M.; Sato, H.; Tobita, H.; Ono, Y.; Omote, K.; Kawachi, K.; Kasama, Y. *Org. Lett.* **2012**, *14*, 3784–3787.

(64) Armarego, W. L. F.; Chai, C. L. L. *Purification of Laboratory Chemicals*, 6th ed; Pergamon Press: Oxford, 2009.

(65) Mann, C. K.; Barnes, K. K. In *Electrochemical Reactions in Non-aqueous Systems*; Mercel Dekker: New York, 1970.

(66) S. Fukuzumi, H. Kotani, T. Suenobu, S. Hong, Y.-M. Lee, W. Nam, *Chem.–Eur. J.* **2010**, *16*, 354–361.

(67) Yamamoto, S.; Guo, J.; Ohkita, H.; Ito, S. *Adv. Funct. Mater.* **2008**, *18*, 2555–2562.

(68) Fukuzumi, S.; Suenobu, T.; Patz, M.; Hirasaka, T.; Itoh, S.; Fujitsuka, M.; Ito, O. *J. Am. Chem. Soc.* **1998**, *120*, 8060–8068.

(69) Guldi, D. M.; Hungerbühler, H.; Carmichael, I.; Asmus, K.-D.; Maggini, M. *J. Phys. Chem. A* **2000**, *104*, 8601–8608.

(70) Fukuzumi, S.; Suenobu, T.; Hirasaka, T.; Arakawa, R.; Kadish, K. M. *J. Am. Chem. Soc.* **1998**, *120*, 9220–9227.

(71) Mikami, K.; Matsumoto, S.; Ishida, A.; Takamuku, S.; Suenobu, T.; Fukuzumi, S. *J. Am. Chem. Soc.* **1995**, *117*, 11134–11141.

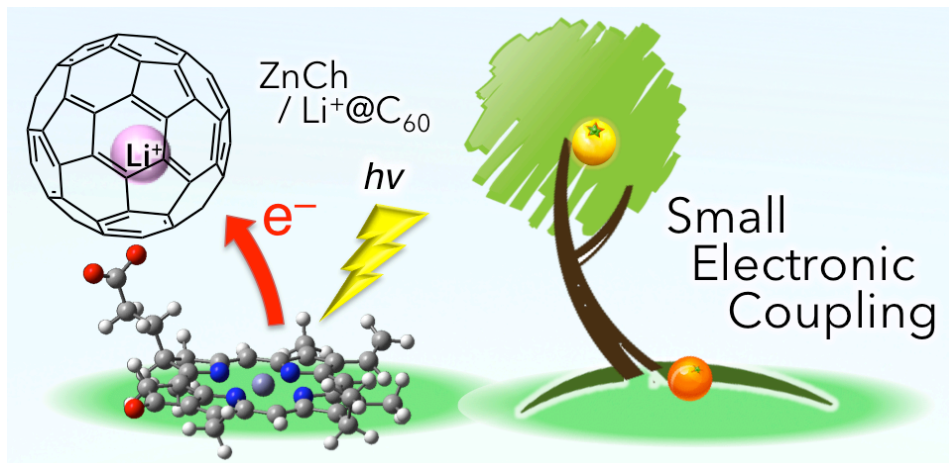
(72) (a) Arbogast, J. W.; Darmanyan, A. P.; Foote, C. S.; Diederich, F. N.; Whetten, R. L.; Rubin, Y.; Alvarez, M. M.; Anz, S. J. *J. Phys. Chem.* **1991**, *95*, 11–12. (b) Arbogast, J. W.; Foote, C. S. *J. Am. Chem. Soc.* **1991**, *113*, 8886–8889. (c) Ebbesen, T. W.; Tanigaki, K.; Kuroshima, S. *Chem. Phys. Lett.* **1991**, *181*, 501–504. (d) Kajii, Y.; Nakagawa, T.; Suzuki, S.; Achiba, Y.; Obi, K.; Shibuya, K. *Chem. Phys. Lett.* **1991**, *181*, 100–104.

(73) (a) Marcus, R. A. *Annu. Rev. Phys. Chem.* **1964**, *15*, 155–196. (b) Marcus, R. A. *Angew. Chem., Int. Ed.* **1993**, *32*, 1111–1121.

---

## Chapter 6

Electron Transfer in a Supramolecular Complex of Zinc Chlorin Carboxylate Anion with  $\text{Li}^+@\text{C}_{60}$  Affording the Long-Lived Charge-Separated State



**Abstract:** A supramolecular complex was formed between zinc chlorin carboxylate ( $\text{ZnCh}^-$ ) and lithium ion-encapsulated [60]fullerene ( $\text{Li}^+@\text{C}_{60}$ ) by an electrostatic interaction in benzonitrile (PhCN). The binding constant was determined to be  $7.7 \times 10^4 \text{ M}^{-1}$ . No fluorescence quenching of  $\text{ZnCh}^-$  was observed upon addition of  $\text{Li}^+@\text{C}_{60}$ , indicating that no electron transfer (ET) from the singlet excited state of  $\text{ZnCh}^-$  ( ${}^1[\text{ZnCh}^-]^*$ ) to  $\text{Li}^+@\text{C}_{60}$  occurred. In contrast, the transient absorption band due to triplet excited state of  $\text{ZnCh}^-$  ( ${}^3[\text{ZnCh}^-]^*$ ) was efficiently quenched by ET from  ${}^3[\text{ZnCh}^-]^*$  to  $\text{Li}^+@\text{C}_{60}$  to produce the charge-separated (CS) state,  $[\text{ZnCh}^-]^+/\text{Li}^+@\text{C}_{60}^{\cdot-}$  with the rate constant of  $k_{\text{ET}} = 5.3 \times 10^4 \text{ s}^{-1}$ . The charge-recombination dynamics was monitored by the decay of the transient absorption band at 1035 nm due to  $\text{Li}^+@\text{C}_{60}^{\cdot-}$ . The lifetime of the CS state was determined to be  $170 \mu\text{s}$ . The spin state of CS state was triplet by EPR measurements at low temperature. The reorganization energy ( $\lambda$ ) and electronic coupling term ( $V$ ) of ET and back electron transfer (BET) were

determined from the temperature dependence of  $k_{\text{ET}}$  and  $k_{\text{BET}}$  to be  $\lambda = 0.46 \pm 0.02$  eV and  $V = 0.095 \pm 0.030$  cm<sup>-1</sup> for ET and  $\lambda = 1.26 \pm 0.04$  eV and  $V = 0.066 \pm 0.010$  cm<sup>-1</sup> for BET based on the Marcus theory of non-adiabatic electron transfer. Such small  $V$  values result from the small orbital interaction between ZnCh<sup>-</sup> and Li<sup>+</sup>@C<sub>60</sub> moieties to afford the long-lived CS state.

## Introduction

In the photosynthetic reaction centers, photoinduced electron transfer from the excited chlorophyll dimer (so called "special pair") occurs to attain the final charge-separated (CS) state, which is utilized to synthesize high-energy compounds such as NADPH (nicotinamide adenine dinucleotide phosphate) and ATP (adenosine triphosphate).<sup>1,2</sup> In the field of artificial photosynthesis, there have been many reports on electron donor–acceptor linked systems to achieve long lifetimes of CS states ( $\tau_{\text{CS}}$ ).<sup>3–49</sup> In particular, fullerenes have been widely used as three-dimensional  $\pi$  electron-acceptor due to their small reorganization energy, which results from the  $\pi$ -electron system being highly delocalized over the three-dimensional curved surface together with the rigid and confined structure of the aromatic  $\pi$ -sphere.<sup>50–53</sup> The mimicry of the natural photosynthesis has prompted the design of synthetic donor–acceptor linked ensembles such as triad, tetrad and pentads.<sup>54–71</sup> For instance, a covalently linked ferrocene–zinc porphyrin–free base porphyrin–fullerene tetrad (Fc–ZnP–H<sub>2</sub>P–C<sub>60</sub>) afforded a long CS lifetime (0.38 s), which is comparable to the CS lifetime of the photosynthetic reaction center.<sup>69,70</sup> Such an extremely long-lived CS state is well explained by the Marcus equation for non-adiabatic electron-transfer reaction (eq 1),

$$\frac{1}{\tau_{\text{CS}}} = k_{\text{ET}} = \left( \frac{4\pi^3}{h^2 \lambda k_{\text{B}} T} \right)^{1/2} V^2 \exp\left[ -\frac{(\Delta G_{\text{ET}} + \lambda)^2}{4\lambda k_{\text{B}} T} \right] \quad (1)$$

where the  $k_{\text{ET}}$  is rate constant of intramolecular electron transfer,  $\lambda$  is the reorganization energy of electron transfer,  $V$  is the electronic coupling term,  $-\Delta G_{\text{ET}}$  is the driving force for electron transfer and  $k_{\text{B}}$  is the Boltzmann constant.<sup>72,73</sup> In the case of the tetrad, the  $V$  value is determined to be  $1.7 \times 10^{-4}$  cm<sup>-1</sup>, which is extremely small, because ferrocenium ion and C<sub>60</sub> radical anion of CS state (Fc<sup>+</sup>–ZnP–H<sub>2</sub>P–C<sub>60</sub><sup>·-</sup>) are spatially separated by a long edge-to-edge distance (48.9 Å). In contrast to the tetrad, zinc porphyrin–fullerene dyad (ZnP–C<sub>60</sub>) afforded a much larger  $V$  value (3.9 cm<sup>-1</sup>) and a shorter CS lifetime (0.77  $\mu$ s).<sup>70</sup> Extensive efforts have so far been devoted to modulate and predict  $V$  values.<sup>74–78</sup> In contrast to covalently linked CS

---

systems, there has been poor discussion about  $V$  values of supramolecular CS systems. A non-polar solvent is utilized to construct supramolecular CS systems with a strong binding.<sup>79–86</sup> However, CS lifetimes are normally extremely short in a non-polar solvent because the CS states are not stabilized by solvation and usually decay to produce the triplet excited states rather than the ground state, because of the higher energy of CS state than the triplet excited states.<sup>87</sup> Thus, it is preferred that to construct a supramolecular CS system by utilizing the electrostatic interaction in a polar solvent which can stabilize the CS state, which may be lower in energy than the triplet excited state of the chromophore. Although numerous supramolecular CS systems have been studied,<sup>88–94</sup> there has been no report on supramolecular CS systems that possess small  $V$  values and also afford long-lived CS state in a polar solvent.

I report herein construction of a supramolecular donor-acceptor CS system by using an electrostatic interaction, between cationic lithium ion-encapsulated fullerene ( $\text{Li}^+@\text{C}_{60}$ )<sup>95–105</sup> as electron acceptor and zinc chlorin ( $\text{ZnCh}^-$ ) as an electron donor with an anionic carboxylate group that can bind with  $\text{Li}^+@\text{C}_{60}$  by an electrostatic interaction. The redox and photophysical properties of this donor-acceptor system have been examined in detail, enabling us to analyze the driving force dependence of the rate constants of photoinduced electron transfer and back electron transfer in light of the Marcus theory of non-adiabatic electron transfer.<sup>72,73</sup> There are two merits to use  $\text{Li}^+@\text{C}_{60}$  in the supramolecular system with  $\text{ZnCh}^-$ . Firstly, a strong supramolecular complex is formed between  $\text{ZnCh}^-$  and  $\text{Li}^+@\text{C}_{60}$  by an electrostatic interaction in a polar solvent in contrast to the case of  $\text{C}_{60}$ . Secondly, the CS state is stabilized by the encapsulation of  $\text{Li}^+$  in  $\text{C}_{60}$  to afford the long-lived CS state, because  $\text{Li}^+@\text{C}_{60}$  is much more easily than pristine  $\text{C}_{60}$ .

## Experimental Section

**Materials.** Chemicals were purchased from commercial sources and used without further purification, unless otherwise noted. Lithium ion-encapsulated fullerene hexafluorophosphate salt ( $\text{Li}^+@\text{C}_{60}$   $\text{PF}_6^-$ : 96%, Idea International Corporation) was commercially obtained from Daiichi Jitsugyo Co. Ltd, Japan.  $\text{H}_2(\text{Ch})$  was obtained from *Spirulina* algae purchased from Japan Alge Corp. according to published procedures.<sup>106–110</sup> Benzonitrile (PhCN) used as a solvent was distilled over phosphorus pentoxide.<sup>111</sup> *o*-Dichlorobenzene (*o*-DCB) was purchased from Sigma-Aldrich Inc. and used as received. Acetonitrile (MeCN) was purchased from WAKO pure chemical and used as received.

**Preparation of Zinc Chlorin Carboxylate Tetra-*n*-Butylammonium Salt ( $\text{TBA}^+\text{ZnCh}^-$ ).**  $\text{ZnCh}^-$  was synthesized by following the published method.<sup>112-114</sup> A mixture of  $\text{H}_2(\text{Ch})$  (25 mg),  $\text{Zn}(\text{CH}_3\text{COO})_2 \cdot 4\text{H}_2\text{O}$  (50 mg) and  $\text{CH}_3\text{COONa}$  (50 mg) in 150 mL of  $\text{CH}_2\text{Cl}_2/\text{CH}_3\text{OH}$  [2/1 (v/v)] was refluxed under dark and nitrogen for 6 h. The reaction mixture was poured into distilled water, extracted with  $\text{CH}_2\text{Cl}_2$ , washed several times with distilled water and dried over  $\text{Na}_2\text{SO}_4$ . The product was recrystallized from  $\text{CH}_2\text{Cl}_2/\text{hexane}$  to give zinc chlorin carboxylic acid ( $\text{ZnCh}$ ) as a green solid (22 mg).  $\text{TBA}^+\text{ZnCh}^-$  was obtained by neutralization of  $\text{ZnCh}$  by adding tetra-*n*-butylammonium hydroxide (TBAOH) in  $\text{CH}_3\text{OH}$ . To give  $\text{TBA}^+\text{ZnCh}^-$  as a green solid (15 mg), solvent was removed by evaporation. MALDI-TOF-MS:  $m/z$  595.3 ( $\text{M}^+$ ). Anal. Calcd for  $\text{C}_{33}\text{H}_{31}\text{N}_4\text{O}_3\text{Zn}^-$  ( $\text{ZnCh}^-$ ):  $^1\text{H}$  NMR ( $(\text{CD}_3)_2\text{SO}$ , 300 MHz (JEOL AL-300 spectrometer),  $\text{TBA}^+\text{ZnCh}^- = 5.0 \times 10^{-3}$  M):  $\delta$  1.01 (12H, t,  $J = 13.9$  Hz,  $-\text{CH}_3$  ( $\text{TBA}^+$ )), 1.38 (8H, m,  $J = 19.8$  Hz  $-\text{CH}_2-$  ( $\text{TBA}^+$ )), 1.63 (8H, t,  $J = 19.8$  Hz  $-\text{CH}_2-$  ( $\text{TBA}^+$ )), 1.69 (3H, t,  $J = 6.8$  Hz), 1.80 (3H, d,  $J = 6.6$  Hz,  $-\text{CH}_3$ ), 2.21-2.29 (2H, m,  $-\text{CH}_2-$ ), 2.34-2.46 (2H, m,  $-\text{CH}_2-$ ), 3.21-3.30 (11H, m,  $-\text{CH}_2-$  ( $\text{TBA}^+$ ) and  $-\text{CH}_3$ )<sup>115</sup>, 3.41 (3H, s,  $-\text{CH}_3$ ), 3.72 (3H, s,  $-\text{CO}_2\text{CH}_3$ ), 3.90 (3H, s,  $-\text{CH}_3$ ), 4.07 (2H, q,  $J = 5.6$  Hz,  $-\text{CH}_2-$ ), 4.35 (1H, m,  $-\text{H}$ ), 4.63 (1H, m,  $-\text{H}$ ), 5.18 (2H, q,  $J = 21.6$  Hz,  $-\text{CH}_2-$ ), 6.25 (1H, dd,  $J = 10.2$ , 6.4 Hz,  $=\text{CH}_2$  *cis*), 6.43 (1H, dd,  $J = 17.6$ , 11.0 Hz,  $=\text{CH}_2$  *trans*), 8.01 (1H, dd,  $J = 18.6$ , 12.1 Hz,  $-\text{CH}=$ ), 8.91 (1H, s,  $-\text{H}$ ), 9.44 (1H, s,  $-\text{H}$ ), 9.82 (1H, s,  $-\text{H}$ )

**UV-Vis Absorption Spectral Measurements.** Absorption spectra were recorded on a Hewlett-Packard 8453 diode array spectrophotometer at room temperature.

**Emission Spectral Measurements.** Phosphorescence was measured on a Horiba FluoroMax-4 spectrofluorophotometer. A 2-methyltetrahydrofuran(2-MeTHF)/ethyl iodide(EtI) (9:1 v/v) solution of  $\text{TBA}^+\text{ZnCh}^-$  in a quartz tube (3 mm in diameter) was degassed by nitrogen bubbling for 10 min prior to the measurements. The sample tube was put in a quartz liquid nitrogen Dewar flask. The measurements were carried out by excitation at 550 nm for  $\text{TBA}^+\text{ZnCh}^-$ . Fluorescence spectra of  $\text{TBA}^+\text{ZnCh}^-$  were recorded on a Horiba FluoroMax-4 spectrofluorophotometer. The measurements were carried out by excitation at 445 nm for  $\text{TBA}^+\text{ZnCh}^-$  in deaerated PhCN. The PhCN solutions degassed by nitrogen bubbling for 10 min prior to the measurements. The fluorescence lifetimes ( $\tau_{\text{fl}}$ ) of the  $\text{TBA}^+\text{ZnCh}^-$  was determined in deaerated PhCN at 298 K by single photon counting using a Horiba FluoroMax-4 time-resolved spectrofluorophotometer.

**Laser Flash Photolysis Measurements.** Femtosecond transient absorption spectroscopy experiments were conducted using an ultrafast source: Integra-C (Quantronix Corp.), an

---

optical parametric amplifier: TOPAS (Light Conversion Ltd.) and a commercially available optical detection system: Helios provided by Ultrafast Systems LLC. The source for the pump and probe pulses were derived from the fundamental output of Integra-C ( $\lambda = 786$  nm, 2  $\mu\text{J}/\text{pulse}$  and  $\text{fwhm} = 130$  fs) at a repetition rate of 1 kHz. 75% of the fundamental output of the laser was introduced into a second harmonic generation (SHG) unit: Apollo (Ultrafast Systems) for excitation light generation at  $\lambda = 393$  nm, while the rest of the output was used for white light generation. The laser pulse was focused on a sapphire plate of 3 mm thickness and then white light continuum covering the visible region from  $\lambda = 410$  nm to 800 nm was generated via self-phase modulation. A variable neutral density filter, an optical aperture, and a pair of polarizer were inserted in the path in order to generate stable white light continuum. Prior to generating the probe continuum, the laser pulse was fed to a delay line that provides an experimental time window of 3.2 ns with a maximum step resolution of 7 fs. In our experiments, a wavelength at  $\lambda = 393$  nm of SHG output was irradiated at the sample cell with a spot size of 1 mm diameter where it was merged with the white probe pulse in a close angle ( $< 10^\circ$ ). The probe beam after passing through the 2 mm sample cell was focused on a fiber optic cable that was connected to a CMOS spectrograph for recording the time-resolved spectra ( $\lambda = 410 - 800$  nm). Typically, 1500 excitation pulses were averaged for 3 seconds to obtain the transient spectrum at a set delay time. Kinetic traces at appropriate wavelengths were assembled from the time-resolved spectral data. All measurements were conducted at room temperature, 295 K. Nanosecond transient absorption spectral measurements were made according to the following procedure. A deaerated PhCN solutions containing  $\text{Li}^+@\text{C}_60$  with a  $\text{TBA}^+\text{ZnCh}^-$  was excited by a Panther OPO pumped Nd:YAG laser (Continuum, SLII-10, 4-6 ns fwhm) at 450 nm. The resulting time resolved transient absorption spectra were measured by using a continuous Xe-lamp (150 W) and a photodiode (Hamamatsu 2949) as the probe light and detector, respectively. The output from the photodiode and the photomultiplier tube was recorded using a digitizing oscilloscope (Tektronix, TDS3032, 300 MHz). The solutions were deoxygenated by  $\text{N}_2$  purging for 10 min prior to measurements. Rates of photoinduced electron-transfer reactions were monitored by the rise and decay of the absorption band due to the  $\text{Li}^+@\text{C}_60$  radical anion. First-order rate constants were determined by a least-squares curve fit. All experiments were performed at 298 K.

**Electrochemical Measurements.** Cyclic voltammetry (CV) measurements were performed with an ALS630B electrochemical analyzer in deaerated PhCN containing 0.1 M  $\text{Bu}_4\text{N}^+\text{PF}_6^-$  (TBAPF<sub>6</sub>) as a supporting electrolyte at 298 K. The platinum working electrode

---

(BAS, surface i.d. 1.6 mm) was polished with BAS polishing alumina suspension and rinsed with acetone before use. The counter electrode was a platinum wire (0.5 mm dia.). The measured potentials were recorded with respect to an Ag/AgNO<sub>3</sub> (0.01 M) reference electrode. The values of redox potentials (vs Ag/AgNO<sub>3</sub>) are converted into those vs SCE by addition of 0.29 V.<sup>116</sup>

**EPR Measurements.** EPR spectra were taken on a JEOL X-band spectrometer (JES-RE1XE) at 4 K for ZnCh<sup>-</sup>/Li<sup>+</sup>@C<sub>60</sub>. EPR spectra of the CS state of ZnCh<sup>-</sup>/Li<sup>+</sup>@C<sub>60</sub> in frozen PhCN was measured under photoirradiation with a high-pressure mercury lamp (USH-1005D) through a water filter focusing at the sample cell in the EPR cavity. The *g* value was calibrated using an Mn<sup>2+</sup> marker. The EPR spectra were recorded under non-saturating microwave power conditions. The magnitude of modulation was chosen to optimize the resolution and the signal-to-noise (S/N) ratio of the observed spectra.

**Theoretical Calculations.** Density functional theory (DFT) calculations were performed on a 32CPU workstation (PQS, Quantum Cube QS8-2400C-064). Geometry optimizations were carried out using the B3LYP/6-311G(d,p) level of theory for ZnCh<sup>-</sup>/Li<sup>+</sup>@C<sub>60</sub> complex as implemented in the Gaussian 09 program Revision A.02.<sup>117-119</sup>

## Results and Discussion

**Supramolecular Complex between Li<sup>+</sup>@C<sub>60</sub> and ZnCh<sup>-</sup>.** UV-Vis absorption spectra of ZnCh<sup>-</sup> in PhCN at 298 K were changed upon addition of Li<sup>+</sup>@C<sub>60</sub> as shown in Figure 1a, where the Soret bands at 435 nm and Q-band at 665 nm were blue-shifted to 431 nm and 661 nm, respectively. Figure 1b shows the dependence of absorbance of the Soret band on concentration of Li<sup>+</sup>@C<sub>60</sub>. The saturation behavior was observed with increasing concentration of Li<sup>+</sup>@C<sub>60</sub>, indicating that the strong supramolecular binding occurs between ZnCh<sup>-</sup> and Li<sup>+</sup>@C<sub>60</sub> by electrostatic interaction. The supramolecular formation constant (*K*) was determined from the saturated curve and the linear plot shown in the inset of Figure 1b to be  $7.7 \times 10^4 \text{ M}^{-1}$ .<sup>120-122</sup> The slope is close to unity (1.06), which evidences for formation of a 1:1 supramolecular complex between ZnCh<sup>-</sup> and Li<sup>+</sup>@C<sub>60</sub> in PhCN (Scheme 1).<sup>122</sup>

To predict the structure of the ZnCh<sup>-</sup>/Li<sup>+</sup>@C<sub>60</sub> supramolecular complex, the theoretical calculations were carried out by DFT at the B3LYP/6-311G(d,p) level of theory.<sup>117-119</sup> The optimized structure is shown in Figure 2a, where Li<sup>+</sup>@C<sub>60</sub> is attached to the carboxylate group of ZnCh<sup>-</sup> by electrostatic interaction.<sup>123</sup> There may be no significant contribution of  $\pi$ - $\pi$

---

interaction between cationic  $\text{Li}^+@\text{C}_{60}$  and anionic  $\text{ZnCh}^-$  in polar PhCN. The donor-acceptor supramolecular systems with strong  $\pi$ - $\pi$  interaction have been reported with the strong quenching of the absorption band of donor upon addition of fullerene derivatives.<sup>96,124,125</sup> In contrast, the small change in absorbance upon addition  $\text{Li}^+@\text{C}_{60}$  shown in Figure 1a reveals no significant contribution of  $\pi$ - $\pi$  interaction but a strong ionic attraction between  $\text{ZnCh}^-$  and  $\text{Li}^+@\text{C}_{60}$ . When  $\text{ZnCh}^-$  was replaced by a neutral complex, zinc chlorin carboxymethyl ester ( $\text{ZnCh}_{\text{Me}}$ ), to avoid an electrostatic interaction, no supramolecular formation was observed between  $\text{ZnCh}_{\text{Me}}$  and  $\text{Li}^+@\text{C}_{60}$ , as shown in Figure 3. This indicates that a  $\text{ZnCh}^-/\text{Li}^+@\text{C}_{60}$  supramolecular complex was formed at the carboxylate moiety of  $\text{ZnCh}^-$  by electrostatic interaction.

**Scheme 1.** Formation of  $\text{ZnCh}^-/\text{Li}^+@\text{C}_{60}$  Supramolecular Complex.

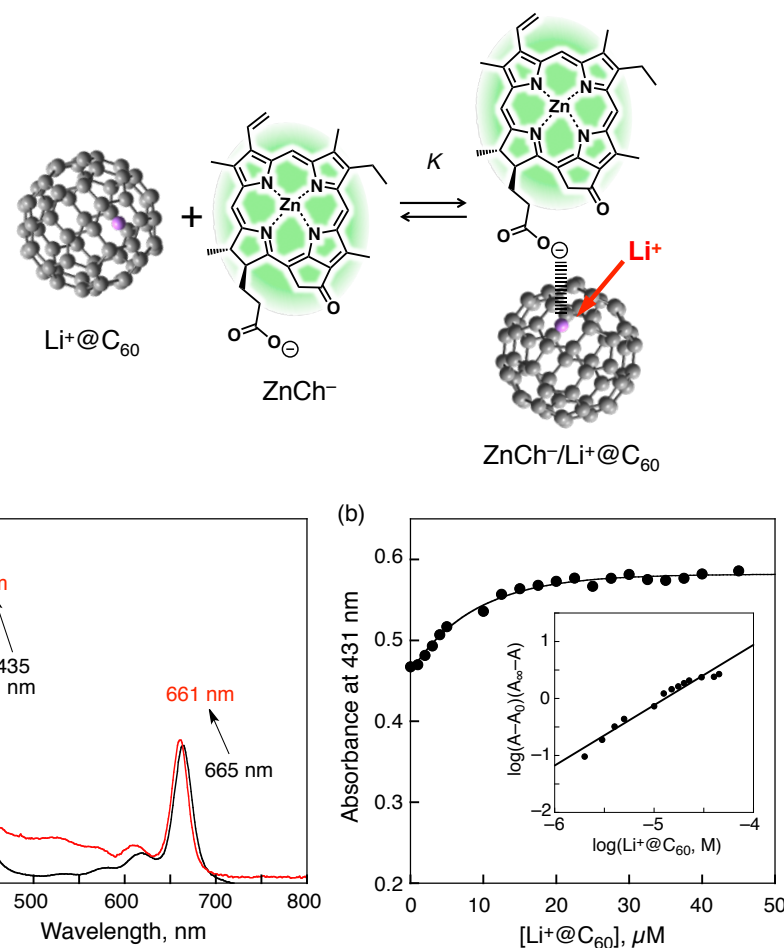


**Figure 1.** (a) UV-Vis absorption spectra of  $\text{ZnCh}^-$  ( $1.0 \times 10^{-5}$  M) in the absence (black) and presence of  $\text{Li}^+@\text{C}_{60}$  ( $4.5 \times 10^{-5}$  M, red) in PhCN. (b) Absorption profile at 431 nm. Inset: Hill plot.

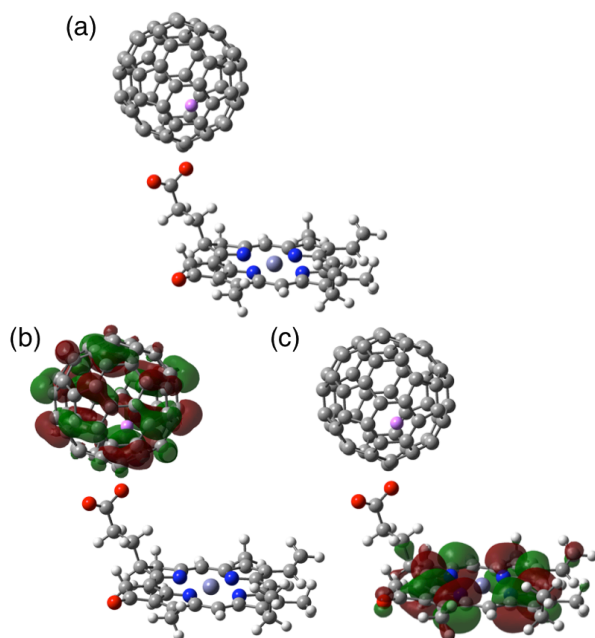


**Figure 2.** (a) Optimized structure of  $\text{ZnCh}^-/\text{Li}^+@\text{C}_{60}$  supramolecular complex. (b) LUMO and (c) HOMO calculated by a DFT method at the B3LYP/6-311G(d,p) level.

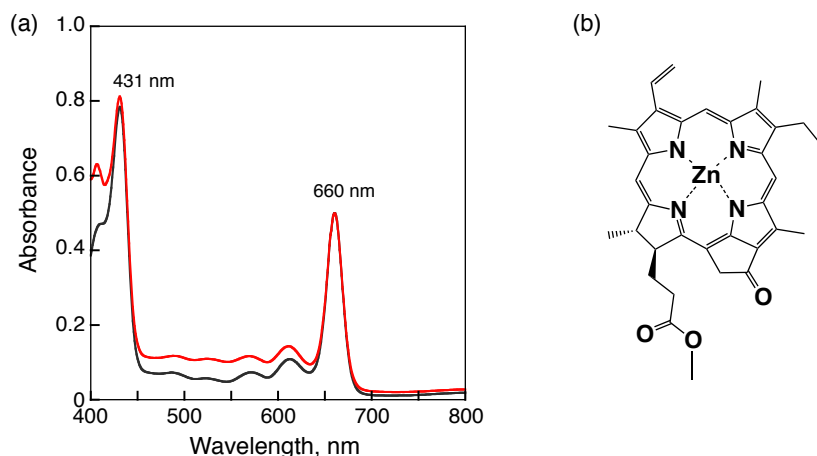
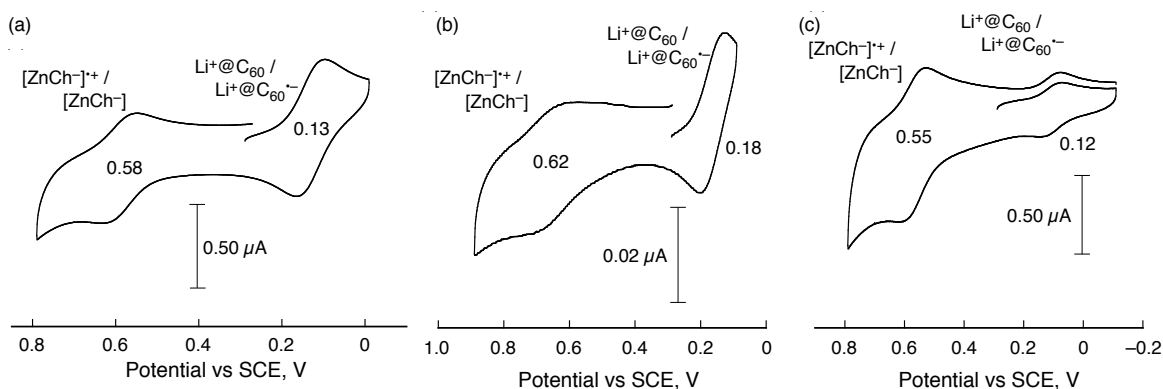


**Figure 3.** (a) UV-Vis absorption spectra of  $\text{ZnCh}_{\text{Me}}$  ( $1.0 \times 10^{-5}$  M) in the absence (black) and presence of  $\text{Li}^+@\text{C}_{60}$  ( $4.5 \times 10^{-5}$  M, red) in PhCN. (b) Chemical structure of  $\text{ZnCh}_{\text{Me}}$ .

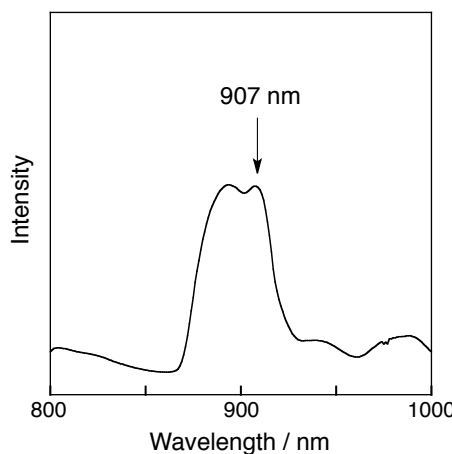
**Electrochemical Measurements of the  $\text{ZnCh}^-/\text{Li}^+@\text{C}_{60}$  Supramolecular Complex.** To estimate the energy diagram for the electron-transfer reactions in the supramolecule based on the redox potentials, cyclic voltammetric measurements were performed as shown in Figure 4a. The energy of the CS state was determined to be 0.45 eV from the potential difference between one-electron oxidation of  $\text{ZnCh}^-$  (0.58 V vs SCE) and one-electron reduction of  $\text{Li}^+@\text{C}_{60}$  (0.13 V).

When PhCN was replaced by *o*-DCB and mixed solvent of *o*-DCB and MeCN (*o*-DCB:MeCN (v/v) = 1:1), the energies of the CS state were slightly decreased to be 0.44 eV and 0.43 eV, as shown in Figure 4b and 4c, respectively. On the other hand, the energy of  $^1[\text{ZnCh}^-]^*$  (1.86 eV) was determined from the absorption and fluorescence maxima (Figure 1a and 5a). The energy of  $^3[\text{ZnCh}^-]^*$  was also determined from its the phosphorescence maximum (907 nm) at 77 K (Figure 5) to be 1.38 eV.

The excited-state energies of  $^1[\text{ZnCh}^-]^*$ ,  $^3[\text{ZnCh}^-]^*$ ,  $^1(\text{Li}^+@\text{C}_{60})^*$  (1.94 eV) and  $^3(\text{Li}^+@\text{C}_{60})^*$  (1.53 eV)<sup>97</sup> are higher than the energy of the CS state, suggesting that photoinduced electron transfer from both excited states are energetically favorable in the supramolecular complex.



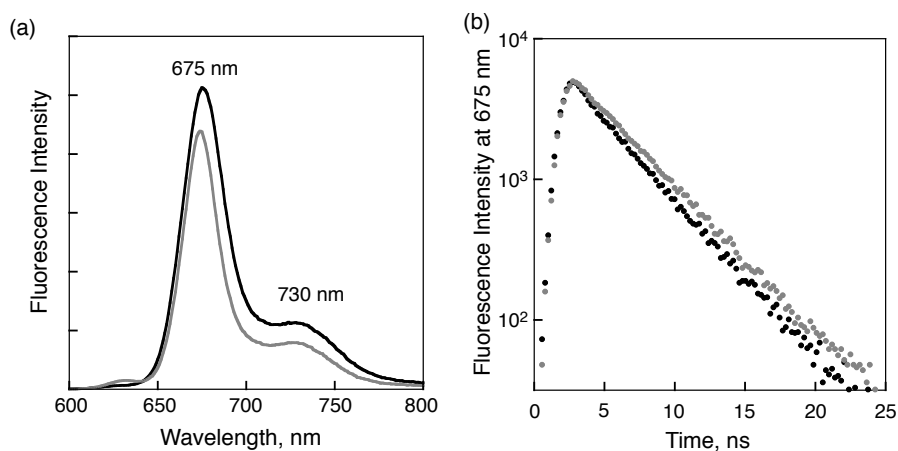
**Figure 4.** Cyclic voltammograms (CV) of (a)  $\text{ZnCh}^-$  ( $2.0 \times 10^{-4}$  M) and  $\text{Li}^+@\text{C}_{60}$  ( $2.0 \times 10^{-4}$  M) in deaerated PhCN. (b)  $\text{ZnCh}^-$  ( $1.0 \times 10^{-4}$  M) and  $\text{Li}^+@\text{C}_{60}$  ( $1.0 \times 10^{-4}$  M) in deaerated *o*-DCB and (c) *o*-DCB:MeCN (v/v) = 1:1 containing TBAPF<sub>6</sub> (0.10 M) as an electrolyte. Scan rate: 100 mV s<sup>-1</sup>.



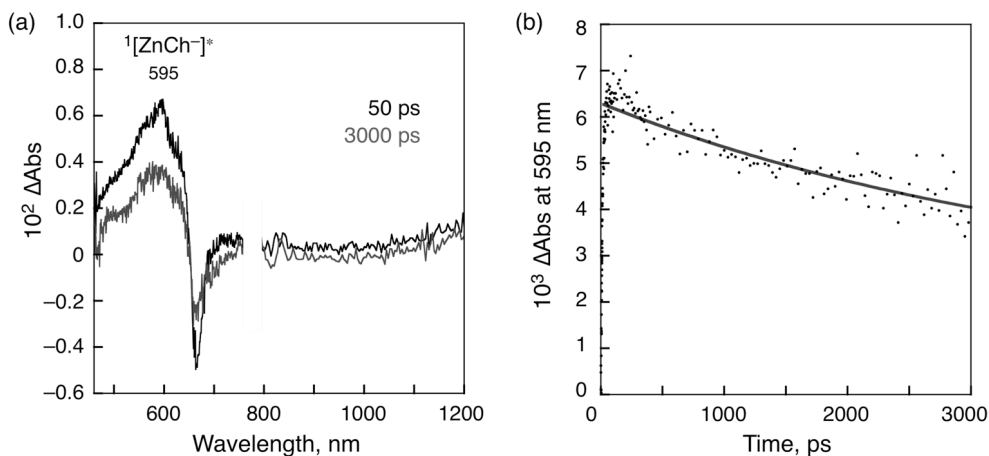
**Figure 5.** Phosphorescence spectrum of  $\text{TBA}^+\text{ZnCh}^-$  in a deaerated 2-MeTHF/EtI (9:1 v/v) transparent glass. Excitation wavelength: 550 nm;  $T = 77$  K.

### Photoinduced Charge Separation of the $\text{ZnCh}^-/\text{Li}^+@\text{C}_{60}$ Supramolecular Complex.

Photoexcitation of the Soret band of  $\text{ZnCh}^-$  at 445 nm in PhCN results in fluorescence at  $\lambda_{\text{max}} = 675$  and 730 nm, as shown in Figure 6a. Addition of  $\text{Li}^+@\text{C}_{60}$  to a PhCN solution of  $\text{ZnCh}^-$  resulted in only a slight decrease in the fluorescence intensity of  $\text{ZnCh}^-$ . The fluorescence lifetime of a PhCN solution of  $\text{ZnCh}^-$  was determined to be 3.8 ns. When  $\text{Li}^+@\text{C}_{60}$  was added to a PhCN solution of  $\text{ZnCh}^-$ , the fluorescence lifetime was virtually same (4.0 ns) as shown



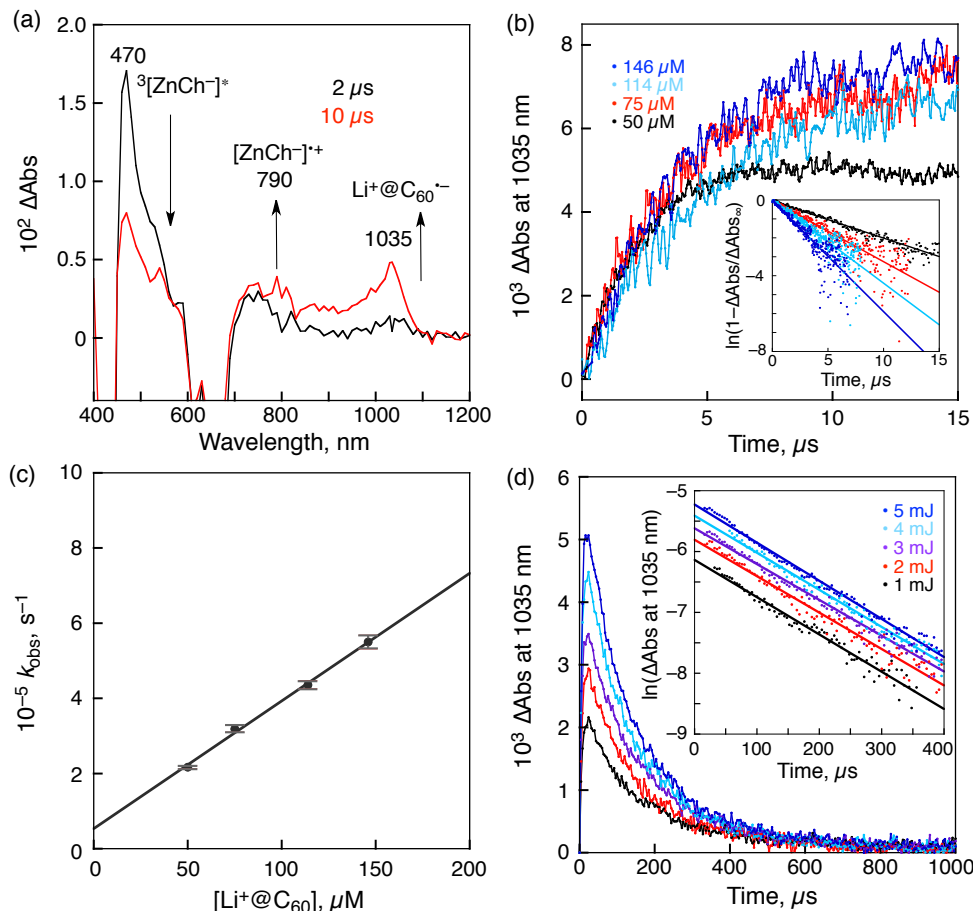
**Figure 6.** (a) Fluorescence spectra of  $\text{ZnCh}^-$  ( $1.0 \times 10^{-5}$  M, black) in the presence of  $\text{Li}^+@\text{C}_{60}$  ( $2.6 \times 10^{-5}$  M, gray line) in deaerated PhCN observed by excitation at 445 nm. (b) Fluorescence decay profiles of  ${}^1[\text{ZnCh}^-]^*$  at 675 nm in the absence (black circle) and the presence of  $\text{Li}^+@\text{C}_{60}$  ( $5.0 \times 10^{-5}$  M) (gray circle) in deaerated PhCN containing  $\text{ZnCh}^-$  ( $2.6 \times 10^{-5}$  M) observed by excitation at 450 nm.



**Figure 7.** (a) Transient absorption spectra of  $\text{ZnCh}^-$  ( $2.5 \times 10^{-5}$  M) in PhCN measured at 50 ps (black) and 3000 ps (gray) after laser excitation at 393 nm. (b) Decay of absorbance at 595 nm.

in Figure 6b. These results indicate that the intersystem crossing occurs predominantly rather than energy or electron transfer from  $^1[\text{ZnCh}^-]^*$  to  $\text{Li}^+@\text{C}_{60}$ . The transient absorption spectra of  $\text{ZnCh}^-$  were measured by femtosecond laser flash photolysis as shown in Figure 7a. The transient absorption band at 595 nm observed at 50 ps is assigned to  $^1[\text{ZnCh}^-]^*$ .<sup>49</sup> The rate constant of intersystem crossing ( $k_{\text{ISC}}$ ) was determined to be  $2.5 \times 10^8 \text{ s}^{-1}$  from the single exponential analysis of the decay of the absorbance at 595 nm due to  $^1[\text{ZnCh}^-]^*$  as shown in Figure 7b.

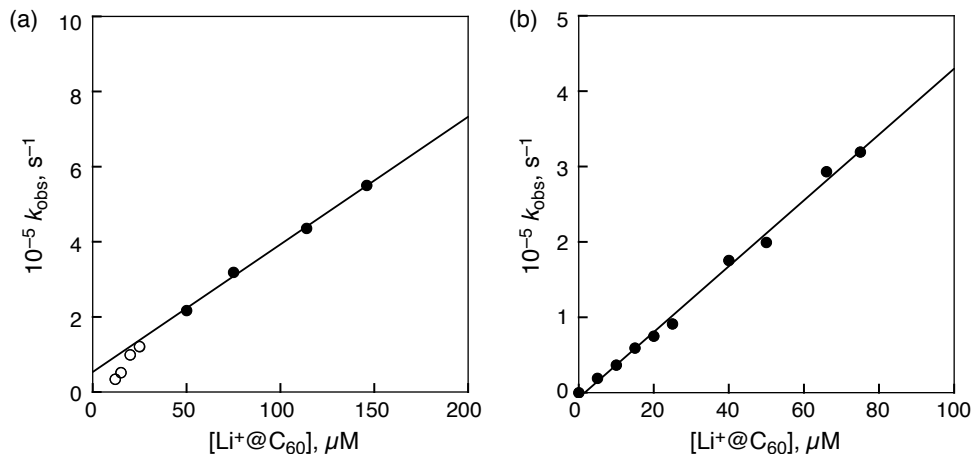
The transient absorption spectra of the  $\text{ZnCh}/\text{Li}^+@\text{C}_{60}$  complex were measured by nanosecond laser flash photolysis as shown in Figure 8a. The transient absorption band at 470 nm observed at 2  $\mu\text{s}$  is assigned to  $^3[\text{ZnCh}^-]^*$ .<sup>40</sup> Along with the decay of  $^3[\text{ZnCh}^-]^*$ , new absorption bands appeared at 790 and 1035 nm, which can be assigned to  $[\text{ZnCh}^-]^{++}$  and  $\text{Li}^+@\text{C}_{60}^{--}$ .



**Figure 8.** (a) Transient absorption spectra of  $\text{ZnCh}^-$  ( $2.5 \times 10^{-5} \text{ M}$ ) with  $\text{Li}^+@\text{C}_{60}$  ( $5.0 \times 10^{-5} \text{ M}$ ) in PhCN measured at 2.0  $\mu\text{s}$  (black) and 10  $\mu\text{s}$  (red) after laser excitation at 450 nm. (b) Time profiles of absorbance at 1035 nm with various  $\text{Li}^+@\text{C}_{60}$  concentrations ( $5.0, 7.5, 11, 15, 146 \mu\text{M}$ ) at 298 K. Inset: First-order plot. (c) Plot of the pseudo-first-order rate constant ( $k_{\text{obs}}$ ) vs concentration of  $\text{Li}^+@\text{C}_{60}$ . (d) Decay time profiles of absorbance at 1035 nm with various laser intensities (1–5 mJ/pulse). Inset: First-order plots.

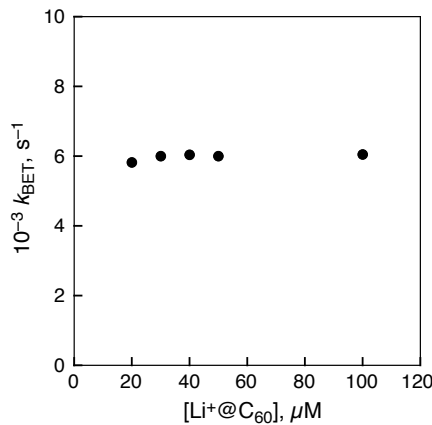
$\text{Li}^+@\text{C}_{60}^{\bullet-}$ , respectively.<sup>49,95</sup> These results clearly suggest the formation of the CS state ( $[\text{ZnCh}^-]^+$  and  $\text{Li}^+@\text{C}_{60}^{\bullet-}$ ) by photoinduced electron transfer from  ${}^3[\text{ZnCh}^-]^*$  to  $\text{Li}^+@\text{C}_{60}$ . The pseudo-first-order rate constant of the rise in absorbance at 1035 nm due to  $\text{Li}^+@\text{C}_{60}^{\bullet-}$  ( $k_{\text{obs}}$ ) increased with increasing concentration of  $\text{Li}^+@\text{C}_{60}$  as shown in Figure 8b and 8c. From the slope of the linear plot in Figure 8c, the second-order rate constant for *intermolecular* electron transfer ( $k_{\text{et}}$ ) from  ${}^3[\text{ZnCh}^-]^*$  in the supramolecular complex to  $\text{Li}^+@\text{C}_{60}$  in the supramolecular complex was determined to be  $3.4 \times 10^9 \text{ M}^{-1} \text{ s}^{-1}$ , which is close to the diffusion limiting value in PhCN ( $5.6 \times 10^9 \text{ M}^{-1} \text{ s}^{-1}$ ).<sup>97</sup> On the other hand, the rate constant of *intramolecular* electron transfer ( $k_{\text{ET}}$ ) was determined from the intercept shown in Figure 8c to be  $5.3 \times 10^4 \text{ s}^{-1}$ . At the low concentration region of  $\text{Li}^+@\text{C}_{60}$  ( $\ll 50 \mu\text{M}$ ), the  $k_{\text{obs}}$  values were smaller than expected from the linear relationship because the contribution of electron transfer from  ${}^3[\text{ZnCh}^-]^*$  to  $\text{Li}^+@\text{C}_{60}$  became dominant, judging from the formation constant ( $7.7 \times 10^4 \text{ M}^{-1}$ ) of the supramolecular complex (Figure 9a). When  $\text{ZnCh}^-$  was replaced by  $\text{ZnCh}_{\text{Me}}$ , however, only *intermolecular* photoinduced electron transfer from  ${}^3[\text{ZnCh}_{\text{Me}}]^*$  to  $\text{Li}^+@\text{C}_{60}$  was observed, no *intramolecular* electron transfer was observed between  $\text{ZnCh}_{\text{Me}}$  and  $\text{Li}^+@\text{C}_{60}$  since no intercept was observed, as shown in Figure 9b.

Figure 8d shows decay time profiles of the absorption band at 1035 nm due to the CS state  $[\text{ZnCh}^-]^+/\text{Li}^+@\text{C}_{60}^{\bullet-}$  in PhCN. The decay rate constant was determined from the first-order plot shown in the inset of Figure 8d. The lifetime of the CS state of the supramolecular



**Figure 9.** Plots of rate constant of electron transfer ( $k_{\text{obs}}$ ) vs the concentration of  $\text{Li}^+@\text{C}_{60}$  for the back electron transfer of (a)  $\text{ZnCh}^-$  ( $2.5 \times 10^{-5} \text{ M}$ ) /  $\text{Li}^+@\text{C}_{60}$  and (b)  $\text{ZnCh}_{\text{Me}}$  ( $2.5 \times 10^{-5} \text{ M}$ ) /  $\text{Li}^+@\text{C}_{60}$  systems. The open circles indicate eliminated data shown in Figure 8c in the main text because these data are impossible to be fitted by linear line for the bimolecular electron transfer due to the low concentrations of  $\text{Li}^+@\text{C}_{60}$ .

complex was determined to be  $170 \mu\text{s}$  at  $298 \text{ K}$ , as shown in Figure 8d. The quantum yield of the CS state was determined to be  $0.62$  from the comparative method<sup>49</sup> using the absorption of the CS state ( $\text{Li}^+@\text{C}_{60}^{\bullet-}$ :  $\varepsilon_{1035} = 7300 \text{ M}^{-1} \text{ cm}^{-1}$ ).<sup>95</sup> I also examined the decay of the CS state with the varying laser intensity to distinguish between bimolecular and intramolecular (unimolecular) charge recombination (CR) for the decay kinetics. The first-order plots afforded linear correlations with the same slope irrespective of the laser intensity. Moreover, no dependence of the rate constant of back electron transfer ( $k_{\text{BET}}$ ) on concentration of  $\text{Li}^+@\text{C}_{60}$  was observed as shown in Figure 10. Thus, there is virtually no contribution from the bimolecular CR process in the  $[\text{ZnCh}^-]^+/\text{Li}^+@\text{C}_{60}^{\bullet-}$  supramolecular complex.



**Figure 10** Plot of rate constant of back electron transfer ( $k_{\text{BET}}$ ) vs the concentration of  $\text{Li}^+@\text{C}_{60}$ .

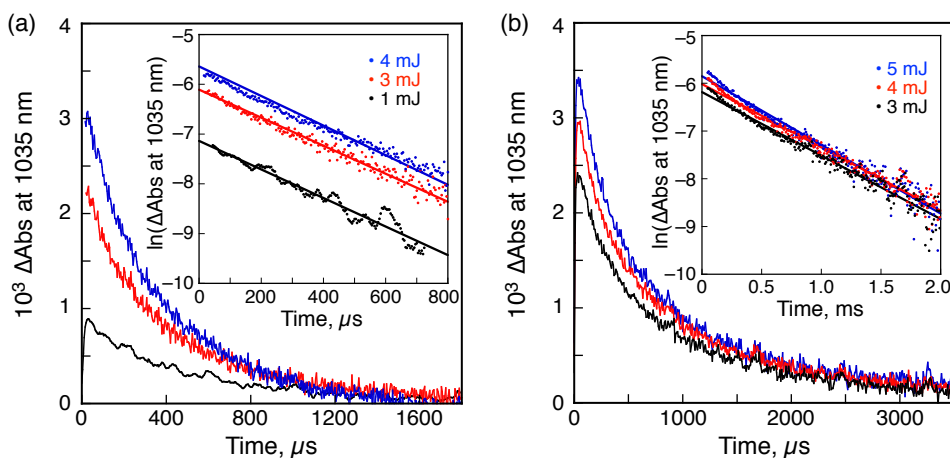


**Figure 11.** Decay time profiles of absorbance at  $1035 \text{ nm}$  observed after laser excitation at  $420 \text{ nm}$  with various laser intensities (1, 3, 4 and 5 mJ/pulse) at  $298 \text{ K}$ .  $\text{ZnCh}^- (2.5 \times 10^{-5} \text{ M})$  with  $\text{Li}^+@\text{C}_{60} (5.0 \times 10^{-5} \text{ M})$  in deaerated (a)  $o\text{-DCB}$  and (b)  $o\text{-DCB:MeCN (v/v) = 1:1}$  Inset: First-order plots.

When the solvent was replaced by *o*-DCB or by the mixed solvent (*o*-DCB:MeCN (v/v) = 1:1), the lifetimes of the CS state of the supramolecular complex increased to be 360  $\mu$ s in *o*-DCB and 630  $\mu$ s in the mixed solvent, respectively (Figure 11). In non-polar *o*-DCB, the through-solvent BET process may be slower than in polar PhCN to afford a long-lived CS state. When the mixed solvent (*o*-DCB:MeCN (v/v) = 1:1) was employed, an MeCN molecule strongly coordinates to zinc nucleus of ZnCh to prevent from  $\pi$ - $\pi$  interaction between donor radical cation and acceptor radical anion moieties at the CS state. Thus, the  $V$  values in *o*-DCB and *o*-DCB/MeCN become smaller than the value in PhCN. Such smaller  $V$  values give long-lived CS lifetimes based on the Marcus theory of electron transfer (*vide infra*).

Such a long-lived CS state was also confirmed by EPR measurements by photoirradiation of the  $\text{ZnCh}^-/\text{Li}^+@\text{C}_{60}$  complex in frozen PhCN as shown in Figure 12. The spin-spin interaction in the triplet radical ion pair of the supramolecular complex was clearly observed at 4 K with the fine structure due to the CS state and the triplet signal at  $g = 2.00$  and  $g = 4.29$ , respectively (Figure 12). Thus, the spin state of the CS state can be assigned to be triplet. From the zero-field splitting value ( $D = 25.8$  G), the distance ( $r$ ) between two electron spins was estimated to be 10.3 Å by using the relation,  $D = 27800/r^3$ .<sup>95,125</sup> This  $r$ -value agrees with the center-to-center distance between fullerene and chlorin moieties calculated for the DFT optimized structure of the  $\text{ZnCh}^-/\text{Li}^+@\text{C}_{60}$  complex (11.8 Å), as shown in Figure 2a.

The  $k_{\text{et}}$ ,  $k_{\text{ET}}$  and  $k_{\text{BET}}$  values exhibited temperature dependence as shown in Figure 13, 14 and 15. The  $k_{\text{ET}}$  values at various temperatures were determined from intercepts of the plots of

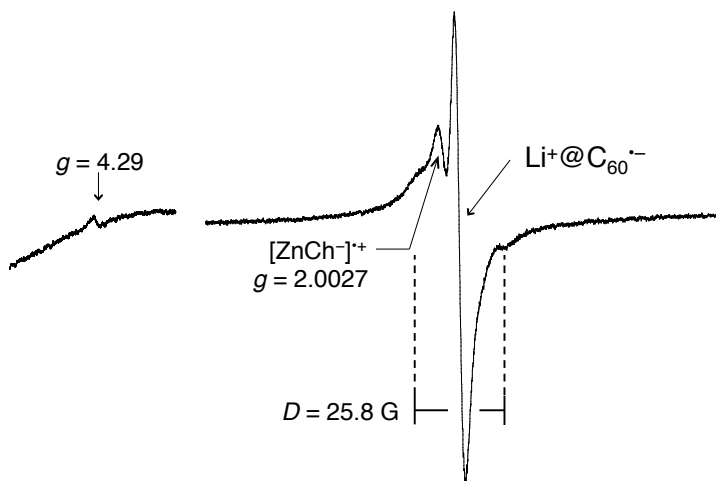


**Figure 12.** EPR spectra of the CS state ( $[\text{ZnCh}^-]^{+}/\text{Li}^+@\text{C}_{60}^{\cdot-}$ ) in PhCN generated by photoirradiation using high-pressure Hg lamp (1000 W) at 4 K focused on  $g = 4$  (left) and  $g = 2$  (right).

Figure 15a. The  $k_{\text{BET}}$  values at various temperatures were determined from the slope of the linear plot in Figure 14. Such temperature dependences of  $k_{\text{ET}}$  and  $k_{\text{BET}}$  are predicted by the Marcus equation (eq 2) for non-adiabatic electron transfer.<sup>72,73</sup> Eq 1 is rewritten as eq 2, which predicts a linear correlation between  $\ln(k_{\text{ET}}T^{1/2})$  and  $T^{-1}$ . The plot of  $\ln(k_{\text{ET}}T^{1/2})$  vs  $T^{-1}$  for the intramolecular ET and BET in the temperature range from 298 to 355 K gave linear correlations as shown in Figure 15b.

$$\ln(k_{\text{ET}}T^{1/2}) = \ln\left(\frac{2\pi^{3/2}V^2}{h(\lambda k_{\text{B}})^{1/2}}\right) - \frac{(\Delta G_{\text{ET}} + \lambda)^2}{4\lambda k_{\text{B}}T} \quad (2)$$

According to the slopes and intercept of Figure 15b, the  $\lambda$  and  $V$  values were determined to be  $\lambda = 0.46 \pm 0.02$  eV and  $V = 0.095 \pm 0.030$  cm<sup>-1</sup> for ET and  $\lambda = 1.26 \pm 0.04$  eV and  $V = 0.066 \pm 0.010$  cm<sup>-1</sup> for BET, respectively. These  $V$  values are much smaller than those reported for other charge separation systems, *e.g.*, a zinc chlorin-fullerene dyad ( $V = 6.8$  cm<sup>-1</sup>

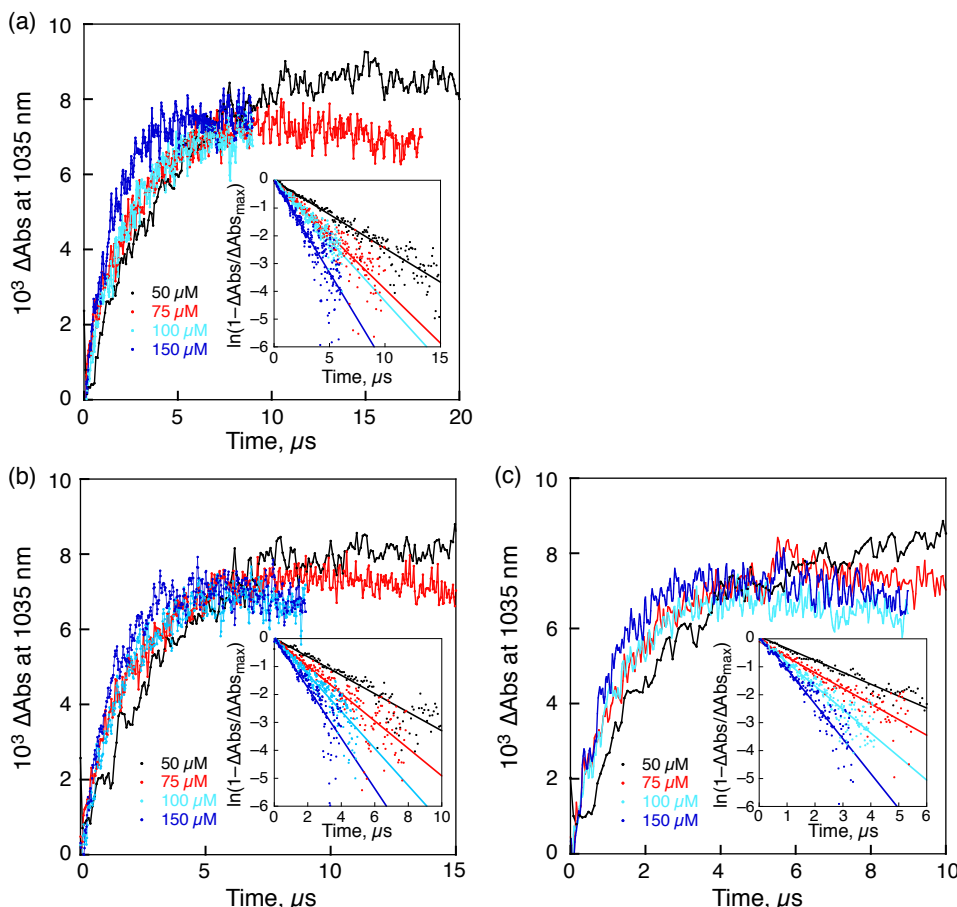


**Figure 13.** Time profiles of absorbance at 1035 nm with different  $\text{Li}^+@\text{C}_60$  concentration ( $5.0, 7.5, 10, 15 \times 10^{-5}$  M) at (a) 306 K (b) 328 K (c) 355 K in the presence of  $\text{ZnCh}^-$  ( $2.5 \times 10^{-5}$  M) observed after laser excitation at 450 nm. Inset: First-order plots.

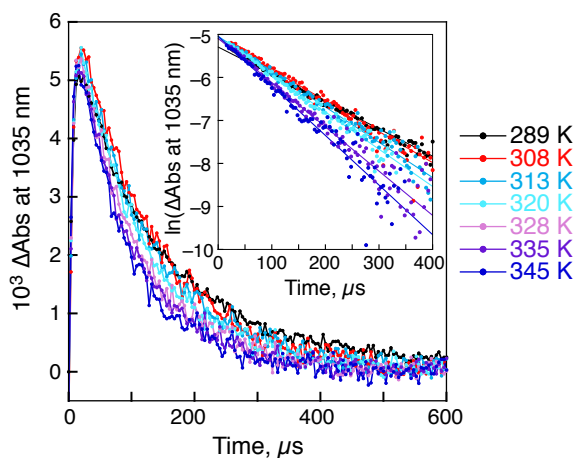


**Figure 14.** Time profiles of absorbance at 1035 nm observed after laser excitation at 450 nm at different temperatures.  $[\text{ZnCh}^-] = 2.5 \times 10^{-5} \text{ M}$ ,  $[\text{Li}^+@\text{C}_60] = 5.0 \times 10^{-5} \text{ M}$ . Inset: First-order plots.

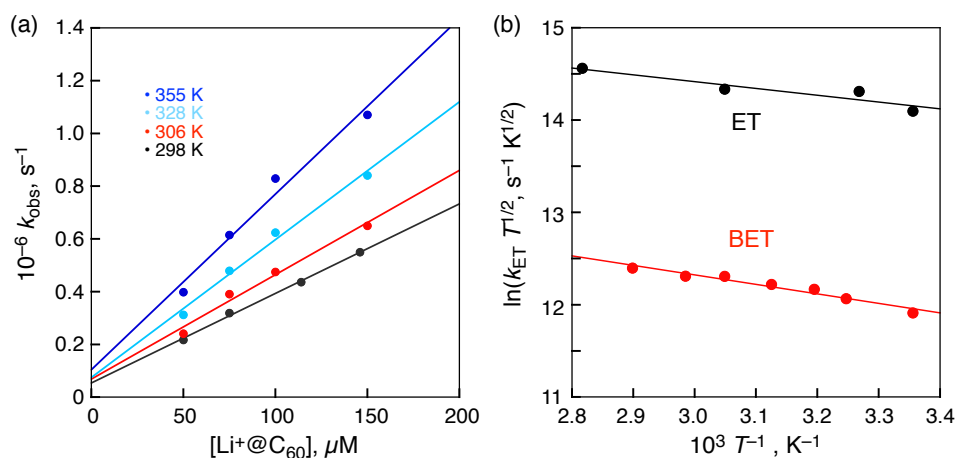


**Figure 15.** (a) Plots of the pseudo-first-order rate constant ( $k_{\text{obs}}$ ) vs concentration of  $\text{Li}^+@\text{C}_60$  at different temperatures (298, 306, 328, 355 K). (b) Plots of  $\ln(k_{\text{ET}} T^{1/2})$  vs  $T^{-1}$  for the intramolecular ET (black) and BET (red) between  $\text{ZnCh}^-$  and  $\text{Li}^+@\text{C}_60$  in PhCN determined by laser flash photolysis.

<sup>40</sup> zinc porphyrin-fullerene dyad ( $3.9 \text{ cm}^{-1}$ )<sup>26,70</sup> and  $N,N'$ -dimethylaniline-flavin dyad ( $4.5 \text{ cm}^{-1}$ ).<sup>43</sup> Such a small  $V$  value may result from the very small orbital interaction in the  $\text{ZnCh}^-/\text{Li}^+@\text{C}_60$  complex, which is consistent with the result of HOMO and LUMO of the  $\text{ZnCh}^-/\text{Li}^+@\text{C}_60$  complex (Figure 2b and 2c). Because the bimolecular ET from  ${}^3[\text{ZnCh}^-]^*$  in the complex to  $\text{Li}^+@\text{C}_60$  is diffusion limited (*vide supra*), the orbital interaction in such an intermolecular reaction may be maximized to make the ET adiabatic. In contrast, intramolecular ET and BET are highly non-adiabatic because of the fixed geometry with little

orbital interaction as shown in Figure 2.

Based on the results described above, the energy diagram of photoinduced ET and BET of  $\text{ZnCh}^-/\text{Li}^+@\text{C}_{60}$ , is shown in Scheme 2. The thermodynamic and kinetic data are summarized in Table 1. The energies of the singlet and triplet excited states were determined by UV–Vis absorption and fluorescence, and phosphorescence spectroscopy, respectively. Upon photoexcitation of  $\text{ZnCh}^-/\text{Li}^+@\text{C}_{60}$ ,  ${}^1[\text{ZnCh}^-]^*/\text{Li}^+@\text{C}_{60}$  is formed, and the intersystem crossing occurs to give  ${}^3[\text{ZnCh}^-]^*/\text{Li}^+@\text{C}_{60}$  as indicated by fluorescence and femtosecond laser flash photolysis measurements.<sup>126</sup> Electron transfer from  ${}^3[\text{ZnCh}^-]^*$  to  $\text{Li}^+@\text{C}_{60}$  occurs to produce the CS state,  $[\text{ZnCh}^-]^{+*}/\text{Li}^+@\text{C}_{60}^{*-}$  via both intermolecular and intramolecular electron transfer processes. No electron transfer in  ${}^1[\text{ZnCh}^-]^*/\text{Li}^+@\text{C}_{60}$  to afford  $[\text{ZnCh}^-]^{+*}/\text{Li}^+@\text{C}_{60}^{*-}$  occurred, because the driving force ( $-\Delta G_{\text{ET}} = 1.41$  eV) of this process is deeply in the Marcus inverted region (entry 5 in Table 1). No energy transfer from  ${}^3[\text{ZnCh}^-]^*$  to  $\text{Li}^+@\text{C}_{60}$  occurred as well, as indicated by failure to form  ${}^3[\text{Li}^+@\text{C}_{60}]^*$ . Intermolecular and intramolecular electron transfer from  ${}^3[\text{ZnCh}^-]^*$  to  $\text{Li}^+@\text{C}_{60}$  occurred to produce the CS state ( $[\text{ZnCh}^-]^{+*}/\text{Li}^+@\text{C}_{60}^{*-}$ ), in which the intramolecular charge recombination occurred in the supramolecular complex with a remarkably long lifetime.

**Scheme 2.** Energy Diagram for the  $\text{ZnCh}^-/\text{Li}^+@\text{C}_{60}$  Supramolecular Complex.

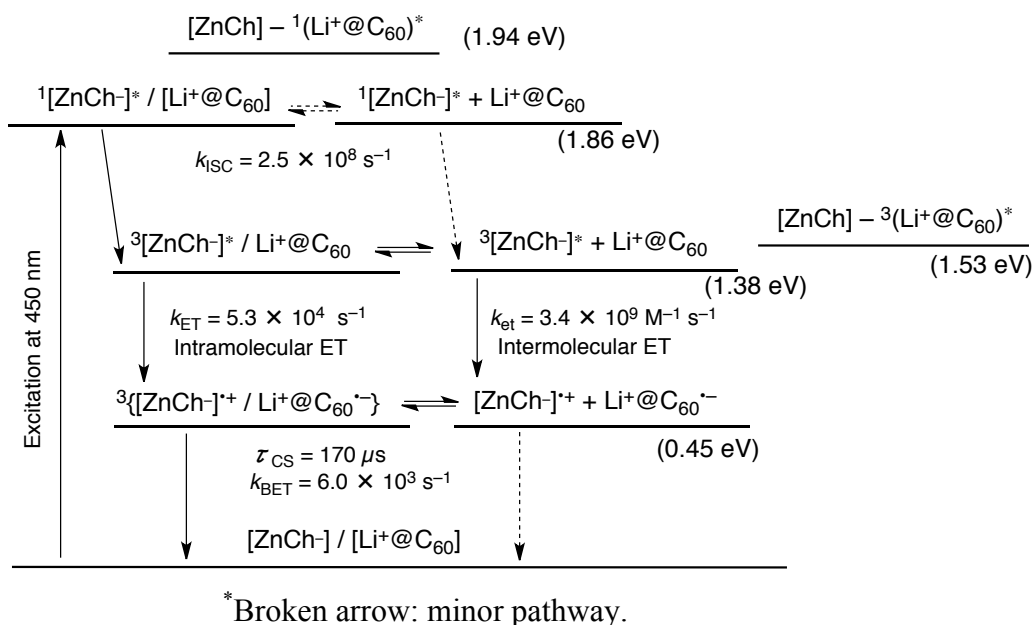


**Table 1.** Driving Forces ( $-\Delta G_{ET}$ ), Observed Rate Constants ( $k_{obs}$ ) and Calculated Rate Constants ( $k_{cal}$ ) of Electron Transfer

entry	initial state	final state	solvent	$-\Delta G_{ET}$ , eV	$k_{obs}$ , <sup>b</sup> s <sup>-1</sup>	$k_{cal}$ , <sup>c</sup> s <sup>-1</sup>
1	$^3[\text{ZnCh}^-]^*/\text{Li}^+@\text{C}_{60}$	$[\text{ZnCh}^-]^{*+}/\text{Li}^+@\text{C}_{60}^{\cdot-}$	PhCN	0.93	$5.3 \times 10^4$	—
2	$[\text{ZnCh}^-]^{*+}/\text{Li}^+@\text{C}_{60}^{\cdot-}$	$\text{ZnCh}^-/\text{Li}^+@\text{C}_{60}$	PhCN	0.45	$6.0 \times 10^3$	—
3	$[\text{ZnCh}^-]^{*+}/\text{Li}^+@\text{C}_{60}^{\cdot-}$	$\text{ZnCh}^-/\text{Li}^+@\text{C}_{60}$	<i>o</i> -DCB	0.44	$2.8 \times 10^3$	—
4	$[\text{ZnCh}^-]^{*+}/\text{Li}^+@\text{C}_{60}^{\cdot-}$	$\text{ZnCh}^-/\text{Li}^+@\text{C}_{60}$	MeCN/ <i>o</i> -DCB <sup>a</sup>	0.43	$1.5 \times 10^3$	—
5	$^1[\text{ZnCh}^-]^*/\text{Li}^+@\text{C}_{60}$	$[\text{ZnCh}^-]^{*+}/\text{Li}^+@\text{C}_{60}^{\cdot-}$	PhCN	1.41	—	$8.0 \times 10^{-2}$
6	$\text{ZnCh}^-/\text{Li}^+@\text{C}_{60}$	$[\text{ZnCh}^-]^{*+}/\text{Li}^+@\text{C}_{60}^{\cdot-}$	PhCN	1.08	—	$2.2 \times 10^3$

<sup>a</sup> *o*-DCB:MeCN (v/v) = 1:1. <sup>b</sup> Experimental error within 5%. <sup>c</sup> Calculated by eq 1 with  $\lambda = 0.48$  eV and  $V = 0.095$  cm<sup>-1</sup>.

## Conclusion

In summary, I have successfully demonstrated that strong supramolecular binding occurs between anionic  $\text{ZnCh}^-$  and cationic  $\text{Li}^+@\text{C}_{60}$  in a polar solvent by an electrostatic interaction. Upon laser excitation of  $\text{ZnCh}^-$ , intermolecular and intramolecular electron transfer from  $^3[\text{ZnCh}^-]^*$  to  $\text{Li}^+@\text{C}_{60}$  occurred to produce the CS state with rate constants of  $3.4 \times 10^9$  M<sup>-1</sup> s<sup>-1</sup> and  $5.3 \times 10^4$  s<sup>-1</sup>, respectively. The lifetimes of the resulting CS states were determined to be 170  $\mu$ s in PhCN, 360  $\mu$ s in *o*-DCB and 630  $\mu$ s in the mixed solvent (*o*-DCB:MeCN (v/v) = 1:1). Such long CS lifetimes result from the small electronic coupling term ( $V = 0.066$  cm<sup>-1</sup>) due to the spatially separated donor and acceptor moieties (Figure 2a).

## References

- (1) *The Photosynthetic Reaction Center*, Deisenhofer, J., Norris, J. R., Eds.; Academic Press: San Diego, 1993.
- (2) *Molecular Level Artificial Photosynthetic Materials*, Meyer, G. J., Ed.; Wiley: New York, 1997.

(3) Frey, J.; Kodis, G.; Straight, S. D.; Moore, T. A.; Moore, A. L.; Gust, D. *J. Phys. Chem. A* **2013**, *117*, 607–615.

(4) Gust, D.; Moore, T. A.; Moore, A. L. In *Electron Transfer in Chemistry*; Balzani, V., Ed.; Wiley: Weinheim, 2001; Vol. 3, pp 272–336.

(5) Terazono, Y.; Kodis, G.; Liddell, P. A.; Garg, V.; Moore, T. A.; Moore, A. L.; Gust, D. *J. Phys. Chem. B* **2009**, *113*, 7147–7155.

(6) Gust, D.; Moore, T. A.; Moore, A. L. *Acc. Chem. Res.* **2009**, *42*, 1890–1898.

(7) Ricks, A. B.; Brown, K. E.; Wenninger, M.; Karlen, S. D.; Berlin, Y. A.; Co, D. T.; Wasielewski, M. R. *J. Am. Chem. Soc.* **2012**, *134*, 4581–4581.

(8) Gunderson, V. L.; Smeigh, A. L.; Kim, C. H.; Co, D. T.; Wasielewski, M. R. *J. Am. Chem. Soc.* **2012**, *134*, 4363–4372.

(9) Lewis, F. D.; Letsinger, R. L.; Wasielewski, M. R. *Acc. Chem. Res.* **2001**, *34*, 159–170.

(10) Wasielewski, M. R. *Acc. Chem. Res.* **2009**, *42*, 1910–1921.

(11) Balzani, V. Recent Advances. *Coord. Chem. Rev.* **2001**, *219–221*, 545–572.

(12) Faiz, J. A.; Heitz, V.; Sauvage, J.-P. *Chem. Soc. Rev.* **2009**, *38*, 422–442.

(13) Diederich, F.; Gómez-López, M. *Chem. Soc. Rev.* **1999**, *28*, 263–277.

(14) Chambron, J.-C.; Collin, J.-P.; Dalbavie, J.-O.; Dietrich-Buchecker, C. O.; Heitz, V.; Odobel, F.; Solladié, N.; Sauvage, J.-P. *Coord. Chem. Rev.* **1998**, *178–180*, 1299–1312.

(15) Fukuzumi, S. New Perspective of Electron Transfer Chemistry. *Org. Biomol. Chem.* **2003**, *1*, 609–620.

(16) Fukuzumi, S. *Phys. Chem. Chem. Phys.* **2008**, *10*, 2283–2297.

(17) Fukuzumi, S. *Bull. Chem. Soc. Jpn.* **2006**, *79*, 177–195.

(18) Fukuzumi, S.; Kojima, T. *J. Mater. Chem.* **2008**, *18*, 1427–1439.

(19) Fukuzumi, S.; Honda, T.; Ohkubo, K.; Kojima, T. *Dalton Trans.* **2009**, 3880–3889.

(20) Boyle, M. M.; Forgan, R. S.; Friedman, D. C.; Gassensmith, J. J.; Smaldone, R. A.; Stoddart, J. F.; Sauvage, J.-P. *Chem. Commun.* **2011**, *47*, 11870–11872.

(21) Linke, M.; Chambron, J.-C.; Heitz, V.; Sauvage, J.-P.; Encinas, S.; Barigelli, F.; Flamigni, L. *J. Am. Chem. Soc.* **2000**, *122*, 11834–11844.

(22) Dixon, I. M.; Collin, J.-P.; Sauvage, J.-P.; Barigelli, F.; Flamigni, L. *Angew. Chem., Int. Ed.* **2000**, *112*, 1292–1295.

(23) Kamat, P. V. *J. Phys. Chem. C* **2007**, *111*, 2834–2860.

(24) Subbaiyan, N. K.; Wijesinghe, C. A.; D’Souza, F. *J. Am. Chem. Soc.* **2009**, *131*,

14646–14647.

(25) Imahori, H.; Umeyama, T.; Ito, S. *Acc. Chem. Res.* **2009**, *42*, 1809–1818.

(26) Imahori, H.; Tamaki, K.; Guldi, D. M.; Luo, C.; Fujitsuka, M.; Ito, O.; Sakata, Y.; Fukuzumi, S. *J. Am. Chem. Soc.* **2001**, *123*, 2607–2617.

(27) Wijesinghe, C. A.; El-Khouly, M. E.; Subbaiyan, N. K.; Supur, M.; Zandler, M. E.; Ohkubo, K.; Fukuzumi, S.; D’Souza, F. *Chem.–Eur J.* **2011**, *17*, 3147–3156.

(28) Ohkubo, K.; Sintic, P. J.; Tkachenko, N. V.; Lemmetyinen, H.; E, W.; Ou, Z.; Shao, J.; Kadish, K. M.; Crossley, M. J.; Fukuzumi, S. *Chem. Phys.* **2006**, *326*, 3–14.

(29) Céspedes-Guirao, F. J.; Ohkubo, K.; Fukuzumi, S.; Sastre-Santos, Á.; Fernández-Lázaro, F. *J. Org. Chem.* **2009**, *74*, 5871–5880.

(30) Murakami, M.; Ohkubo, K.; Hasobe, T.; Sgobba, V.; Guldi, D. M.; Wessendorf, F.; Hirsch, A.; Fukuzumi, S. *J. Mater. Chem.* **2010**, *20*, 1457–1466.

(31) Jiménez, Á. J.; Spänig, F.; Rodríguez-Morgade, M. S.; Ohkubo, K.; Fukuzumi, S.; Guldi, D. M.; Torres, T. *Org. Lett.* **2007**, *9*, 2481–2487.

(32) Martín-Gomis, L.; Ohkubo, K.; Fernández-Lázaro, F.; Fukuzumi, S.; Sastre-Santos, Á. *Chem. Commun.* **2010**, *46*, 3944–3946.

(33) Guldi, D. M.; Sgobba, V. *Chem. Commun.* **2011**, *47*, 606–610.

(34) Guldi, D. M.; Rahman, G. M. A.; Sgobba, V.; Ehli, C. *Chem. Soc. Rev.* **2006**, *35*, 471–487.

(35) Bottari, G.; de la Torre, G.; Guldi, D. M.; Torres, T. *Chem. Rev.* **2010**, *110*, 6768–6816.

(36) Martín, N.; Sánchez, L.; Herranz, M. A.; Illescas, B.; Guldi, D. M. *Acc. Chem. Res.* **2007**, *40*, 1015–1024.

(37) Fukuzumi, S.; Kotani, H.; Ohkubo, K.; Ogo, S.; Tkachenko, N. V.; Lemmetyinen, H. *J. Am. Chem. Soc.* **2004**, *126*, 1600–1601.

(38) Ohkubo, K.; Kotani, H.; Fukuzumi, S. *Chem. Commun.* **2005**, 4520–4522.

(39) Fukuzumi, S.; Kotani, H.; Ohkubo, K. *Phys. Chem. Chem. Phys.* **2008**, *10*, 5159–5162.

(40) Fukuzumi, S.; Ohkubo, K.; Imahori, H.; Shao, J.; Ou, Z.; Zheng, G.; Chen, Y.; Pandey, R. K.; Fujitsuka, M.; Ito, O.; Kadish, K. M. *J. Am. Chem. Soc.* **2001**, *123*, 10676–10683.

(41) Ohkubo, K.; Imahori, H.; Shao, J.; Ou, Z.; Kadish, K. M.; Chen, Y.; Zheng, G.; Pandey, R. K.; Fujitsuka, M.; Ito, O.; Fukuzumi, S. *J. Phys. Chem. A* **2002**, *106*, 10991–10998.

(42) D’Souza, F.; Maligaspe, E.; Ohkubo, K.; Zandler, M. E.; Subbaiyan, N. K.; Fukuzumi,

---

S. *J. Am. Chem. Soc.* **2009**, *131*, 8787–8797.

(43) Murakami, M.; Ohkubo, K.; Fukuzumi, S. *Chem.–Eur. J.* **2010**, *16*, 7820–7832.

(44) Murakami, M.; Ohkubo, K.; Nanjo, T.; Souma, K.; Suzuki, N.; Fukuzumi, S. *ChemPhysChem* **2010**, *11*, 2594–2605.

(45) Martín-Gomis, L.; Ohkubo, K.; Fernández-Lázaro, F.; Fukuzumi, S.; Sastre-Santos, Á. *J. Phys. Chem. C* **2008**, *112*, 17694–17701.

(46) Fukuzumi, S.; Imahori, H.; Okamoto, K.; Yamada, H.; Fujitsuka, M.; Ito, O.; Guldi, D. M. *J. Phys. Chem. A* **2002**, *106*, 1903–1908.

(47) Kashiwagi, Y.; Ohkubo, K.; McDonald, J. A.; Blake, I. M.; Crossley, M. J.; Araki, Y.; Ito, O.; Imahori, H.; Fukuzumi, S. *Org. Lett.* **2003**, *5*, 2719–2721.

(48) Fukuzumi, S.; Ohkubo, K.; E, W.; Ou, Z.; Shao, J.; Kadish, K. M.; Hutchison, J. A.; Ghiggino, K. P.; Sintic, P. J.; Crossley, M. J. *J. Am. Chem. Soc.* **2003**, *125*, 14984–14985.

(49) Ohkubo, K.; Kotani, H.; Shao, J.; Ou, Z.; Kadish, K. M.; Li, G.; Pandey, R. K.; Fujitsuka, M.; Ito, O.; Imahori, H.; Fukuzumi, S. *Angew. Chem., Int. Ed.* **2004**, *43*, 853–856.

(50) Echegoyen, L.; Diederich, F.; Echegoyen, L. E. In *Fullerenes, Chemistry, Physics, and Technology*; Kadish, K. M., Ruoff, R. S., Eds.; Wiley-Interscience: New York, 2000, pp 1–51.

(51) Guldi, D. M.; Fukuzumi, S. In *Fullerenes: From Synthesis to Optoelectronic Properties*, Guldi, D. M., Martin, N., Eds.; Kluwer: Dordrecht, 2003, pp 237–265.

(52) Sgobba, V.; Rahman, G. M. A.; Guldi, D. M. In *Carbon Nanotubes in Electron Donor–Acceptor Nanocomposites, Chemistry of Carbon Nanotubes*; Basiuk, V. A., Ed.; American Scientific Publishers: CA, 2006.

(53) Fukuzumi, S.; Guldi, D. M. In *Electron Transfer in Chemistry* Balzani, V., Ed.; Wiley-VCH: Weinheim, 2001; Vol 2, pp 270–337.

(54) Connolly, J. S.; Bolton, J. R. In *Photoinduced Electron Transfer*; Fox, M. A., Chanon, M., Eds.; Elsevier: Amsterdam, 1988; Part D, pp 303–393.

(55) Wasielewski, M. R. In *Photoinduced Electron Transfer*; Fox, M. A., Chanon, M., Eds.; Elsevier: Amsterdam, 1988; Part A, pp 161–206.

(56) Bixon, M.; Fajer, J.; Feher, G.; Freed, J. H.; Gamliel, D.; Hoff, A. J.; Levanon, H.; Möbius, K.; Nechushtai, R.; Norris, J. R.; Scherz, A.; Sessler, J. L.; Stehlik, D.; *Isr. J. Chem.* **1992**, *32*, 369–518.

(57) Kurreck, H.; Huber, M. *Angew. Chem., Int. Ed.* **1995**, *34*, 849–866.

(58) Gust, D.; Moore, T. A. In *The Porphyrin Handbook*; Kadish, K. M., Smith, K. M., Guilard, R., Eds.; Academic Press: San Diego, CA, 2000; Vol. 8, pp 153–190.

(59) Elliott, K. J.; Harriman, A.; Le Pleux, L.; Pellegrin, Y.; Blart, E.; Mayer, C. R.; Odobel, F. *Phys. Chem. Chem. Phys.* **2009**, *11*, 8767–8773.

(60) Benniston, A. C.; Harriman, A. *Mater. Today* **2008**, *11*, 26–34.

(61) Odobel, F.; Séverac, M.; Pellegrin, Y.; Blart, E.; Fosse, C.; Cannizzo, C.; Mayer, C. R.; Elliott, K. J.; Harriman, A. *Chem.–Eur. J.* **2009**, *15*, 3130–3138.

(62) Fukuzumi, S.; Saito, K.; Ohkubo, K.; Troiani, V.; Qiu, H.; Gadde, S.; D’Souza, F.; Solladié, N. *Phys. Chem. Chem. Phys.* **2011**, *13*, 17019–1702.

(63) Verhoeven, J. W. In *Electron Transfer-From Isolated Molecules to Biomolecules*; Jortner, J., Bixon, M., Eds.; John Wiley & Sons: New York, 1999; Part 1, pp 603–644.

(64) Tokaji, S.; Yorimitsu, H.; Osuka, A. *Angew. Chem., Int. Ed.* **2012**, *51*, 12357–12361.

(65) Yoon, M.-C.; Lee, S.; Tokaji, S.; Yorimitsu, H.; Osuka, A.; Kim, D. *Chem. Sci.* **2013**, *4*, 1756–1746.

(66) Kim, K. S.; Lim, J. M.; Osuka, A.; Kim, D. *J. Photochem. Photobiol. C* **2008**, *9*, 13–28.

(67) Sun, L.; Hammarström, L.; Åkermark, B.; Styring, S. *Chem. Soc. Rev.* **2001**, *30*, 36–49.

(68) Imahori, H.; Tamaki, K.; Araki, Y.; Sekiguchi, Y.; Ito, O.; Sakata, Y.; Fukuzumi, S. *J. Am. Chem. Soc.* **2002**, *124*, 5165–5174.

(69) Imahori, H.; Sekiguchi, Y.; Kashiwagi, Y.; Sato, T.; Araki, Y.; Ito, O.; Yamada, H.; Fukuzumi, S. *Chem.–Eur. J.* **2004**, *10*, 3184–3196.

(70) Imahori, H.; Guldi, D. M.; Tamaki, K.; Yoshida, Y.; Luo, C.; Sakata, Y.; Fukuzumi, S. *J. Am. Chem. Soc.* **2001**, *123*, 6617–6628.

(71) Guldi, D. M.; Imahori, H.; Tamaki, K.; Kashiwagi, Y.; Yamada, H.; Sakata, Y.; Fukuzumi, S. *J. Phys. Chem. A* **2004**, *108*, 541–548.

(72) Marcus, R. A. *Annu. Rev. Phys. Chem.* **1964**, *15*, 155–196.

(73) Marcus, R. A. *Angew. Chem., Int. Ed.* **1993**, *32*, 1111–1121.

(74) Sugiyama, Y.; Takahashi, S.; Ishimori, K.; Morishima, I. *J. Am. Chem. Soc.* **1997**, *119*, 9582–9583.

(75) Cave, R. J.; Newton, M. D.; Kumar, K.; Zimmt, M. B. *J. Phys. Chem.* **1995**, *99*, 17501–17504.

---

(76) Fernando, S. R. L.; Kozlov, G. V.; Ogawa, M. Y. *Inorg. Chem.* **1998**, *37*, 1900–1905.

(77) Isied, S. S.; Vassilian, A.; Wishart, J. F.; Creutz, C.; Schwarz, H. A.; Sutin, N. *J. Am. Chem. Soc.* **1988**, *110*, 635–637.

(78) Scott, J. R.; Willie, A.; McLean, M.; Stayton, P. S.; Sligar, S. G.; Durham, B.; Millett, F. *J. Am. Chem. Soc.* **1993**, *115*, 6820–6824.

(79) D’Souza, F.; Deviprasad, G. R.; Zandler, M. E.; Hoang, V. T.; Klykov, A.; VanStipdonk, M.; Perera, A.; El-Khouly, M. E.; Fujitsuka, M.; Ito, O. *J. Phys. Chem. A* **2002**, *106*, 3243–3252.

(80) D’Souza, F.; Sandanayaka, A. S. D.; Ito, O. *J. Phys. Chem. Lett.* **2010**, *1*, 2586–2593.

(81) D’Souza, F.; Ito, O. *Chem. Commun.* **2009**, 4913–4928.

(82) D’Souza, F.; Ito, O. *J. Phys. Chem. A* **2002**, *106*, 3243–3252.

(83) El-Khouly, M. E.; Rogers, L. M.; Zandler, M. E.; Suresh, G.; Fujitsuka, M.; Ito, O.; D’Souza, F. *ChemPhysChem* **2003**, *4*, 474–481.

(84) Flamigni, L. Johnston, M. R. Giribabu, L. *Chem.–Eur. J.* **2002**, *8*, 3938–3947.

(85) Xiao, S.; El-Khouly, M. E.; Li, Y.; Gan, Z.; Liu, H.; Jiang, L.; Araki, Y.; Ito, O.; Zhu, D. *J. Phys. Chem. B* **2005**, *109*, 3658–3667.

(86) Grimm, B.; Schornbaum, J.; Cardona, C. M.; van Paauwe, J. D.; Boyd, P. D. W.; Guldi, D. M. *Chem. Sci.* **2011**, 1530–1537.

(87) K. Ohkubo, S. Fukuzumi, *J. Porphyrins Phthalocyanines* **2008**, *12*, 993–1004.

(88) Fukuzumi, S.; Saito, K.; Ohkubo, K.; Khouri, T.; Kashiwagi, Y.; Absalom, M. A.; Gadde, S.; D’Souza, F.; Araki, Y.; Ito, O.; Crossley, M. J. *Chem. Commun.* **2011**, *47*, 7980–7982.

(89) D’Souza, F.; Subbaiyan, N. K.; Xie, Y.; Hill, J. P.; Ariga, K.; Ohkubo, K.; Fukuzumi, S. *J. Am. Chem. Soc.* **2009**, *131*, 16138–16146.

(90) Sessler, J. L.; Karnas, E.; Kim, S. K.; Ou, Z.; Zhang, M.; Kadish, K. M.; Ohkubo, K.; Fukuzumi, S. *J. Am. Chem. Soc.* **2008**, *130*, 15256–15257.

(91) Kojima, T.; Honda, T.; Ohkubo, K.; Shiro, M.; Kusukawa, T.; Fukuda, T.; Kobayashi, N.; Fukuzumi, S. *Angew. Chem., Int. Ed.* **2008**, *47*, 6712–6716.

(92) Fukuzumi, S.; Ohkubo, K.; D’Souza, F.; Sessler, J. L. *SChem. Commun.* **2012**, *48*, 9801–9815.

(93) Fukuzumi, S.; Ohkubo, K. *J. Mater. Chem.* **2012**, *22*, 4575–4587.

(94) Honda, T.; Nakanishi, T.; Ohkubo, K.; Kojima, T.; Fukuzumi, S. *J. Am. Chem. Soc.* **2010**, *132*, 10155–10163.

(95) Fukuzumi, S.; Ohkubo, K.; Kawashima, Y.; Kim, D. S.; Park, J. S.; Jana, A.; Lynch, V. M.; Kim, D.; Sessler, J. L. *J. Am. Chem. Soc.* **2011**, *133*, 15938–15941.

(96) Ohkubo, K.; Kawashima, Y.; Fukuzumi, S. *Chem. Commun.* **2012**, *48*, 4314–4316.

(97) Kawashima, Y.; Ohkubo, K.; Fukuzumi, S. *J. Phys. Chem. A* **2012**, *116*, 8942–8948.

(98) Kamimura, T.; Ohkubo, K.; Kawashima, Y.; Nobukuni, H.; Naruta, Y.; Tani, F.; Fukuzumi, S. *Chem. Sci.* **2013**, *4*, 1451–1461.

(99) Ohkubo, K.; Kawashima, Y.; Sakai, H.; Hasobe, T.; Fukuzumi, S. *Chem. Commun.* **2013**, *49*, 4474–4476.

(100) Kawashima, Y.; Ohkubo, K.; Fukuzumi, S. *J. Phys. Chem. A* **2013**, *117*, 6737–6743.

(101) Bill N. L.; Ishida, M.; Bähring, S.; Lim, J. M.; Lee, S.; Davis, C. M.; Lynch, V. M.; Nielsen, K. A.; Jeppesen, J. O.; Ohkubo, K.; Fukuzumi, S.; Kim, D.; Sessler, J. L. *J. Am. Chem. Soc.* **2013**, *135*, *J. Am. Chem. Soc.* **2013**, *135*, 10852–10862.

(102) Aoyagi, S.; Nishibori, E.; Sawa, H.; Sugimoto, K.; Takata, M.; Miyata, Y.; Kitaura, R.; Shinohara, H.; Okada, H.; Sakai, T.; Ono, Y.; Kawachi, K.; Yokoo, K.; Ono, S.; Omote, K.; Kasama, Y.; Ishikawa, S.; Komuro, T.; Tobita, H. *Nature Chem.* **2010**, *2*, 678–683.

(103) Aoyagi, S.; Nishibori, E.; Sawa, H.; Okada, H.; Tobita, H.; Kasama, Y.; Kitaura, R.; Shinohara, H. *Angew. Chem., Int. Ed.* **2012**, *51*, 3377–3381.

(104) Matsuo, Y.; Okada, H.; Maruyama, M.; Sato, H.; Tobita, H.; Ono, Y.; Omote, K.; Kawachi, K.; Kasama, Y. *Org. Lett.* **2012**, *14*, 3784–3787.

(105) Ueno, H.; Nakamura, Y.; Ikuma, N.; Kokubo, K.; Oshima, T. *Nano Res.* **2012**, *5*, 558–564.

(106) Wasieleski, M. R.; Svec, W. A. *J. Org. Chem.* **1980**, *45*, 1969–1974.

(107) Zheng, G.; Li, H.; Zhang, M.; L-Katz, S.; Chance, B.; Glickson, J. D. *Bioconjugate Chem.* **2002**, *13*, 392–396.

(108) Arian, D.; Cló, E.; Gothelf, K. V.; Mokhir, A. A *Chem.–Eur. J.* **2010**, *16*, 288–295.

(109) Ishigure, S.; Mitsui, T.; Ito, S.; Kondo, Y.; Kawabe, S.; Kondo, M.; Dewa, T.; Mino, H.; Itoh, S.; Nango, M. *Langmuir* **2010**, *26*, 7774–7782.

(110) Paolesse, R.; Pandey, R. K.; Forsyth, T. P.; Jaquinod, L.; Gerzevske, K. R.; Nurco, D. J.; Sengo, M. O.; Licoccia, S.; Boschi, T.; Smith, K. M. *J. Am. Chem. Soc.* **1996**, *118*, 3869–3882.

(111) Armarego, W. L. F.; Chai, C. L. L. *Purification of Laboratory Chemicals*, 6th ed; Pergamon Press: Oxford, 2009.

---

(112) Mase, K.; Ohkubo, K.; Fukuzumi, S. *J. Am. Chem. Soc.* **2013**, *135*, 2800–2808.

(113) Tamiaki, H.; Kunieda, M. *J. Org. Chem.* **2007**, *72*, 2443–2451.

(114) Huber, V.; Sengupta, S.; Würthner, F. *Chem.–Eur. J.* **2008**, *14*, 7791–7807.

(115) A peak is overlapped with that of H<sub>2</sub>O.

(116) Mann, C. K.; Barnes, K. K. In *Electrochemical Reactions in Non-aqueous Systems*; Marcel Dekker: New York, 1970.

(117) Frisch, M. J.; Trucks, G. W.; Schlegel, H. B.; Scuseria, G. E.; Robb, M. A.; Cheeseman, J. R.; Scalmani, G.; Barone, V.; Mennucci, B.; Petersson, G. A.; Nakatsuji, H.; Caricato, M.; Li, X.; Hratchian, H. P.; Izmaylov, A. F.; Bloino, J.; Zheng, G.; Sonnenberg, J. L.; Hada, M.; Ehara, M.; Toyota, K.; Fukuda, R.; Hasegawa, J.; Ishida, M.; Nakajima, T.; Honda, Y.; Kitao, O.; Nakai, H.; Vreven, T.; Montgomery, J. A., Jr.; Peralta, J. E.; Ogliaro, F.; Bearpark, M.; Heyd, J. J.; Brothers, E.; Kudin, K. N.; Staroverov, V. N.; Kobayashi, R.; Normand, J.; Raghavachari, K.; Rendell, A.; Burant, J. C.; Iyengar, S. S.; Tomasi, J.; Cossi, M.; Rega, N.; Millam, J. M.; Klene, M.; Knox, J. E.; Cross, J. B.; Bakken, V.; Adamo, C.; Jaramillo, J.; Gomperts, R.; Stratmann, R. E.; Yazyev, O.; Austin, A. J.; Cammi, R.; Pomelli, C.; Ochterski, J. W.; Martin, R. L.; Morokuma, K.; Zakrzewski, V. G.; Voth, G. A.; Salvador, P.; Dannenberg, J. J.; Dapprich, S.; Daniels, A. D.; Farkas, O.; Foresman, J. B.; Ortiz, J. V.; Cioslowski, J.; Fox, D. J. *Gaussian 09*, Revision A.02; Gaussian, Inc.: Wallingford, CT, 2009.

(118) Becke, A. D. *J. Chem. Phys.* **1993**, *98*, 5648–5652.

(119) Lee, C.; Yang, W.; Parr, R. G. *Phys. Rev. B* **1988**, *37*, 785–789.

(120) Mitra, R.; Chattopadhyay, S.; Bhattacharya, S. *Spectrochim. Acta. Part A, Molecular and biomolecular spectroscopy* **2012**, *89*, 284–293.

(121) D’Souza, F.; Chitta, R.; Gadde, S.; Islam, D.-M. S.; Schumacher, A. L.; Zandler, M. E.; Araki, Y.; Ito, O. *J. Phys. Chem. B* **2006**, *110*, 25240–25250.

(122) Kadish, K. M.; Chen, P.; Enakieva, Y. Y.; Nefedov, S. E.; Gorbunova, Y. G.; Tsivadze, A. Y.; Bessmertnykh-Lemeune, A.; Stern, C.; Guillard, R. *J. Electroanal. Chem.* **2011**, *656*, 61–71.

(123) The same optimized structure was obtained when geometry optimization was carried out by using ZnCh<sup>−</sup>/Li<sup>+</sup>@C<sub>60</sub> complex with π-π stacking as an initial structure.

(124) Hasobe, T.; Imahori, H.; Kamat, P. V.; Ahn, T. K.; Kim, S. K.; Kim, D.; Fujimoto, A.; Hirakawa, T.; Fukuzumi, S. *J. Am. Chem. Soc.* **2005**, *127*, 1216–1228.

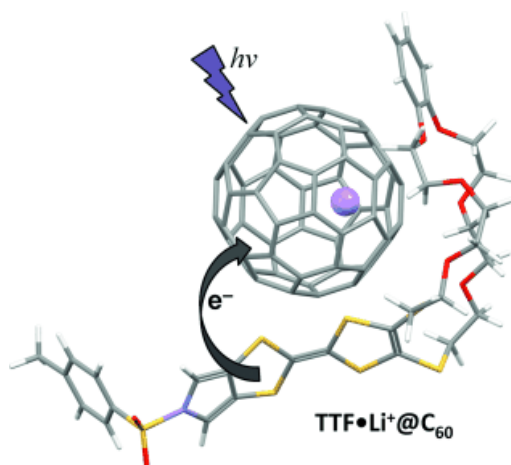
(125) Hasobe, T.; Saito, K.; Kamat, P. V.; Troiani, V.; Qiu, H.; Solladie, N.; Kim, K. S.;

Park, J. K.; Kim, D.; D'Souza, F.; Fukuzumi, S. *J. Mater. Chem.* **2007**, *17*, 4160-4170.

(126) No formation of  $\text{ZnCh}^-/\text{Li}^+@\text{C}_{60}$ <sup>\*</sup> was observed by nanosecond laser excitation at 450 nm, because the molar absorption coefficient of  $\text{ZnCh}^-$  at 450 nm ( $\varepsilon_{450} = 21000 \text{ M}^{-1} \text{ cm}^{-1}$ ) is much higher than that of  $\text{Li}^+@\text{C}_{60}$  ( $\varepsilon_{450} = 940 \text{ M}^{-1} \text{ cm}^{-1}$ ).

## Chapter 7

### Robust Inclusion Complexes of Crown Ether Fused Tetrathiafulvalenes with $\text{Li}^+@\text{C}_{60}$ to Afford Efficient Photodriven Charge Separation



**Abstract:** Inclusion complexes of benzo- and dithiabenzo- crown ether functionalized monopyrrolotetrathiafulvalene (MPTTF) molecules were formed with  $\text{Li}^+@\text{C}_{60}$  (**1**• $\text{Li}^+@\text{C}_{60}$  and **2**• $\text{Li}^+@\text{C}_{60}$ ). The strong complexation has been quantified by high binding constants that exceed  $10^6 \text{ M}^{-1}$  obtained by UV–Vis titrations in benzonitrile (PhCN) at room temperature. On the basis of DFT studies at the B3LYP/6-311G(d,p) level, the orbital interactions between the crown ether moieties and the  $\pi$  surface of the fullerene together with the endohedral  $\text{Li}^+$  have a crucial role in robust complex formation. Interestingly, complexation of  $\text{Li}^+@\text{C}_{60}$  with crown ethers accelerates the intersystem crossing upon photoexcitation of the complex, thereby yielding  ${}^3(\text{Li}^+@\text{C}_{60})^*$ , when no charge separation by means of  ${}^1(\text{Li}^+@\text{C}_{60})^*$  occurs. Photoinduced charge separation by means of  ${}^3(\text{Li}^+@\text{C}_{60})^*$  with lifetimes of 135 and 120  $\mu\text{s}$  for **1**• $\text{Li}^+@\text{C}_{60}$  and **2**• $\text{Li}^+@\text{C}_{60}$ , respectively, and quantum yields of 0.82 in PhCN have been observed by utilizing time-resolved transient absorption spectroscopy and then confirmed by electron paramagnetic resonance measurements at 4 K. The difference in crown ether structures affects the binding constant and the rates of photoinduced electron-transfer events in the corresponding complex.

## Introduction

Reorganization of tetrathiafulvalene (TTF) after donating one or two electrons has been known to require low energy because the loss of electrons results in enhanced delocalization, by which the radical cation and dication can be stabilized effectively.<sup>1</sup> Likewise, [60]fullerene (C<sub>60</sub>) has been known for its low reorganization energy and its ability to stabilize the accepted electron during an electron-transfer process on account of its extensive, spherical  $\pi$  system.<sup>2,3</sup> Consequently, TTF and C<sub>60</sub> have considerably low oxidation and reduction potentials, respectively, thus allowing charge separation in the donor–acceptor systems driven by their excited states. Based on these unique chemical and physical properties, TTF and C<sub>60</sub> have long been considered as an ideal donor–acceptor pair for organic electronics and solar-energy conversion.<sup>1–3</sup>

Photoinduced electron-transfer dynamics of the molecular and supramolecular systems of TTF and C<sub>60</sub> have been extensively investigated for potential applications. Molecular systems in which the TTF and C<sub>60</sub> moieties are covalently connected including the use of both short, rigid linkers and long, flexible spacers with various lengths.<sup>4</sup> In 2003, Martín and co-workers reported the first supramolecular dyads based on TTF and C<sub>60</sub>. In these systems, the TTF and C<sub>60</sub> moieties were held together noncovalently by means of complementary flexible linkers capable of forming hydrogen-bonding and ionic interactions in nonpolar media. However, it turned out that the photoinduced charge separation in these dyads was not efficient.<sup>5</sup> Later on supramolecular encapsulation of C<sub>60</sub> was realized by the conformational arrangement of TTF-fused calixpyrroles in the presence of chloride ion<sup>6</sup> and by the crown ether fused  $\pi$ -extended TTFs through  $\pi$ - $\pi$  and n- $\pi$  interactions.<sup>7</sup> Close proximity of the TTF units and C<sub>60</sub> in these supramolecular capsules resulted in ground-state charge-transfer transitions and the formation of short-lived charge-separated states upon photoexcitation. TTF-fused calix[4]pyrrole has also been used to capture the Li<sup>+</sup>@C<sub>60</sub> inside its cavity in the presence of an anion.<sup>8</sup> The strong reducing ability of Li<sup>+</sup>@C<sub>60</sub>, which is controlled by the encapsulated lithium ion,<sup>9</sup> led to a persistent thermal electron-transfer reaction in this supramolecular system.

In addition to their ability to strongly bind metal ions by means of electrostatic interactions, crown ethers with certain sizes are known to bind fullerene cages in suitable solvents. Inclusion complexes held together by strong n- $\pi$  interactions of various crown ethers with pristine (C<sub>60</sub> and C<sub>70</sub>)<sup>10</sup> and metalencapsulating (La@C<sub>82</sub>)<sup>11</sup> fullerenes have previously been reported. An important parameter for obtaining high binding constants for these

---

supramolecular assemblies is the desolvation of the fullerenes; in other words, the complexation with the host molecules strengthens as the solubility of the fullerenes decreases in the corresponding solvent.<sup>10a,12</sup> Although complexes of  $\text{Li}^+@\text{C}_{60}$  with negatively charged macrostructures through ionic interactions have been studied,<sup>13</sup> complexation of  $\text{Li}^+@\text{C}_{60}$  with crown ethers has yet to be examined.

Endohedral metallofullerenes (EMFs) have recently emerged as better alternatives to pristine fullerenes,<sup>14</sup> as they exhibit the rich redox features of the spherical carbon cage regulated by encapsulated metal ions. Recently,  $\text{Li}^+@\text{C}_{60}$  has been reported to have better photoelectrochemical capacity in a composite solar cell than a reference single-component system.<sup>15</sup> Nonetheless, donor–acceptor systems of TTF and  $\text{Li}^+@\text{C}_{60}$  that afford photoinduced charge separation with high efficiency are still desired for efficient solar-energy conversion.

I report herein electron donor–acceptor complexes of two crown ether functionalized monopyrrolo-TTF (MPTTF) derivatives capable of hosting  $\text{Li}^+@\text{C}_{60}$  by means of electrostatic,  $n\text{-}\pi$ , and  $\pi\text{-}\pi$  interactions. The MPTTF unit is fused to either a benzo-crown (**1**) or a dithiabenzocrown ether (**2**) moiety as shown in Figure 1. Formation of complexes between the MPTTF derivatives **1** and **2** and  $\text{Li}^+@\text{C}_{60}$  has been identified by steady-state absorption measurements and investigated theoretically by using DFT calculations. The effects of the complexation on the excited states and the photo-driven charge-separation processes of these complexes have been clarified by means of the time-resolved transient absorption measurements in polar benzonitrile (PhCN).

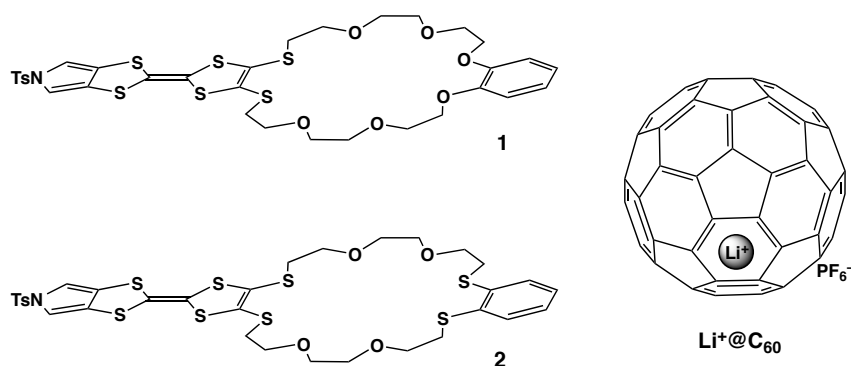


**Figure 1.** Molecular structures of the crown ether functionalized-MPTTFs, **1** and **2**, and  $\text{Li}^+@\text{C}_{60}$ .

## Experimental Section

**Materials.** The synthesis of **1** and **2** has been reported elsewhere.<sup>16</sup>  $[\text{Li}^+@\text{C}_{60}]^-\text{PF}_6^-$  (98% purity), reference TTF, and 4'-nitrobenzene[18]-crown-6 ether were obtained from commercial sources. PhCN was distilled from  $\text{P}_2\text{O}_5$  in an all-glass apparatus for purification.

**Instruments.** Steady-state absorption measurements were recorded using a Hewlett Packard 8453 diode array spectrophotometer. DFT calculations were performed using a COMPAQ DS20E computer. Geometry optimizations were carried out using the B3LYP functional and 6-311G(d,p) basis set,<sup>17</sup> as implemented in the Gaussian 03 program, revision C.02. Graphical outputs of the computational results were generated with the GaussView software program (version 3.09) developed by Semichem, Inc. Electrochemical measurements were performed using an ALS630B electrochemical analyzer in deaerated PhCN that contained 0.10 M TBAPF<sub>6</sub> as supporting electrolyte. A conventional three-electrode cell was used with a platinum working electrode (surface area of 0.3 mm<sup>2</sup>) and a platinum wire as the counter electrode. The Pt working electrode was routinely polished with ALS polishing alumina suspension (0.05 mm) and rinsed with water and acetone before use. The measured potentials were recorded with respect to a SCE. All electrochemical measurements were carried out under an atmospheric pressure of N<sub>2</sub>. Femtosecond transient absorption spectroscopy experiments were conducted using an ultrafast source: Integra-C (Quantronix Corp.), an optical parametric amplifier: TOPAS (Light Conversion Ltd.), and a commercially available optical detection system: Helios provided by Ultrafast Systems LLC. The source for the pump and probe pulses was derived from the fundamental output of Integra-C (780 nm, 2 mJ per pulse, fwhm=130 fs) at a repetition rate of 1 kHz; 75% of the fundamental output of the laser was introduced into TOPAS, which has optical frequency mixers resulting in a tunable range from 285 to 1660 nm, whereas the rest of the output was used for white-light generation. Typically, 2500 excitation pulses were averaged for 5 s to obtain the transient spectrum at a set delay time. Kinetic traces at appropriate wavelengths were assembled from the time-resolved spectral data. For nanosecond transient absorption measurements, deaerated solutions of the compounds were excited using a Panther optical parametric oscillator (OPO) equipped with an Nd:YAG laser (Continuum, SLII-10, fwhm = 4–6 ns) with a power of 8–25 mJ per pulse. The photochemical reactions were monitored by continuous exposure to a Xe lamp (150 W) as a probe light and a detector (SpectraPro 300i). The transient spectra were recorded using fresh solutions in each laser excitation. Solutions were deoxygenated by N<sub>2</sub> purging for about 15 min prior to all transient spectral measurements. All measurements were

---

conducted at room temperature. The EPR spectra were determined using a JEOL X-band spectrometer (JES-RE1XE) under photoirradiation with a high-pressure mercury lamp (USH-1005D) through a water filter by focusing the sample cell in the EPR cavity at 4 K.

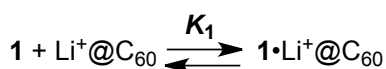
## Results and Discussion

**Complex Formation of Crown Ether Fused MPTTFs with  $\text{Li}^+@\text{C}_{60}$ .** The formation of complexes of **1** and **2** with  $\text{Li}^+@\text{C}_{60}$  (**1**• $\text{Li}^+@\text{C}_{60}$  and **2**• $\text{Li}^+@\text{C}_{60}$ ) was identified by steady-state absorption spectroscopy. By the addition of **1** to a solution of  $\text{Li}^+@\text{C}_{60}$  in PhCN, a significant rise in the absorption band at 334 nm and a finite decrease at 539 nm were observed and resulted in the formation of an isosbestic point at 503 nm in PhCN (Figure 2). The absorption features of  $\text{Li}^+@\text{C}_{60}$  show a small hypsochromic shift during the titration with compound **1**. Plotting the absorbance at 334 nm versus the molar ratio of added compound **1** to the total concentration allows the stoichiometry of the complexation to be determined (Figure 2, inset). The plot gives a break at 0.5, thus indicating that a 1:1 complex between **1** and  $\text{Li}^+@\text{C}_{60}$  is formed as illustrated in Scheme 1.<sup>10</sup> Compound **1** was also titrated with  $\text{Li}^+@\text{C}_{60}$ . During this titration, the absorption band of **1** at 326 nm markedly increased with a bathochromic shift to 332 nm. The resulting absorption features are identical to those of the former titration (Figure 3). The binding constant for the complex formed between **1** and  $\text{Li}^+@\text{C}_{60}$  ( $K_1$ ) was determined by using eq 1:<sup>8,18</sup>

$$(\alpha^{-1} - 1)^{-1} = K_1([1] - \alpha[\text{Li}^+@\text{C}_{60}]_0) \quad (1)$$

in which  $\alpha = (A - A_0)/(A_\infty - A_0)$ ;  $A$  is the absorbance of  $\text{Li}^+@\text{C}_{60}$  at 450 nm in the presence of **1**,  $A_0$  and  $A_\infty$  are the initial and the final absorbance at the same wavelength in the absence and in the presence of **1**, respectively. The linear plot in Figure 4 gives the values for  $K_1$  as  $1.9 \times 10^6 \text{ M}^{-1}$ .

Titration of  $\text{Li}^+@\text{C}_{60}$  with compound **2** resulted in similar absorption changes to those observed in the case of **1**• $\text{Li}^+@\text{C}_{60}$  (Figure 2). Correspondingly, the absorbance plot at 334 nm (Scheme 1 and Figure 2, inset) indicated a 1:1 stoichiometry between compound **2** and  $\text{Li}^+@\text{C}_{60}$  upon complexation. Using the absorbance increase at 450 nm as probe, a linear plot as shown in Figure 4, gives the formation constant of **2**• $\text{Li}^+@\text{C}_{60}$  ( $K_2$ ) as  $3.0 \times 10^5 \text{ M}^{-1}$  at room temperature.



**Scheme 1.** Complexation of MPTTFs **1** and **2** with  $\text{Li}^+@\text{C}_{60}$ .

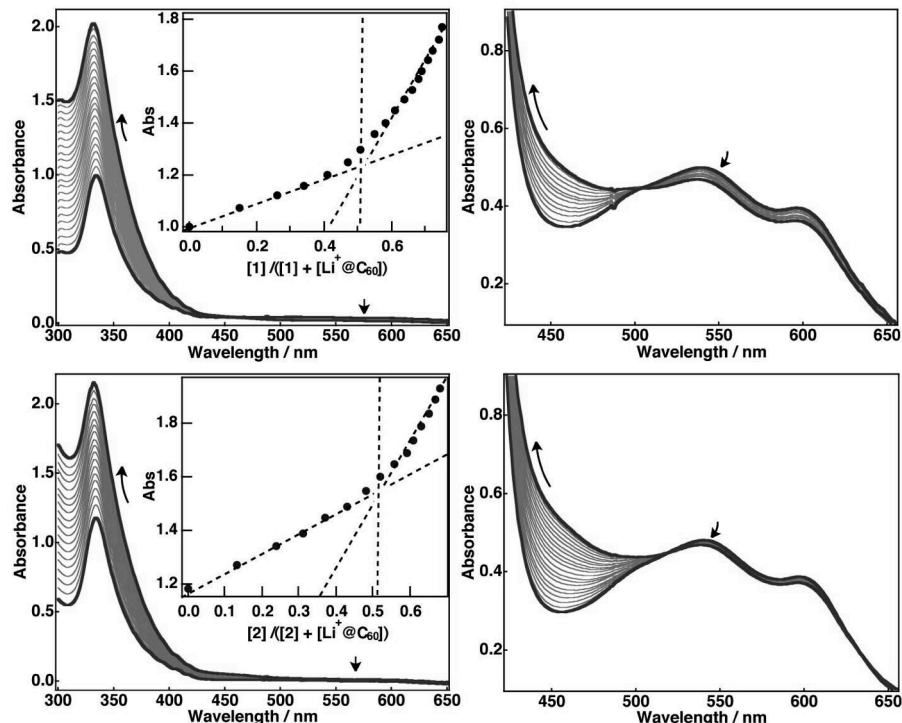


**Figure 2.** Absorption spectral changes during the titrations of  $20 \mu\text{M} \text{Li}^+@\text{C}_{60}$  with  $75 \mu\text{M}$  compound **1** (upper panel) and  $25 \mu\text{M} \text{Li}^+@\text{C}_{60}$  with  $70 \mu\text{M}$  compound **2** (lower panel) in PhCN at room temperature. Insets: Plots of absorbance at  $334 \text{ nm}$  vs  $[\mathbf{1}]/([\mathbf{1}]+[\text{Li}^+@\text{C}_{60}])$  and  $[\mathbf{2}]/([\mathbf{2}]+[\text{Li}^+@\text{C}_{60}])$ .

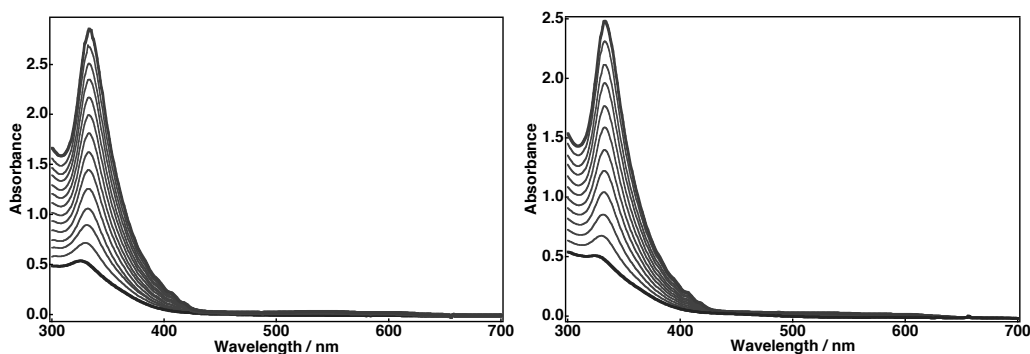


**Figure 3.** Absorption spectral changes during the titrations of  $35 \mu\text{M}$  compound **1** (left) and  $33 \mu\text{M}$  compound **2** (right) with  $\text{Li}^+@\text{C}_{60}$  ( $50 \mu\text{M}$  in total) in PhCN.

In such complexes, crown ether moieties are mainly responsible for hosting the  $C_{60}$  cage as a result of  $n-\pi$  interactions enhanced by the desolvation of the fullerenes in the corresponding solvent.<sup>10</sup> The ascending absorption features during the titrations of compound **1** and **2** with  $Li^+@C_{60}$  indicate that desolvation of the EMF cage results in strong complexation. The obtained binding constants for **1**• $Li^+@C_{60}$  and **2**• $Li^+@C_{60}$  are much higher than those of complexes of empty  $C_{60}$  with crown ethers that have similar sizes to the benzo- and dithiabenzocrown moieties present in **1** and **2**.<sup>10</sup> Electrostatic interactions between the endohedral  $Li$  ion and oxygen or sulfur atoms of crown ethers are likely to have an effect on obtaining higher association constants. In addition, interactions between the electron-rich MPTTF units in **1** and **2** and  $Li^+@C_{60}$  are feasible as observed in the complexes of fullerenes with  $\pi$ -extended TTFs attached to crown ether moieties.<sup>7</sup> To investigate the interactions of each of the components present in **1** and **2** with EMF guest,  $Li^+@C_{60}$  was separately treated

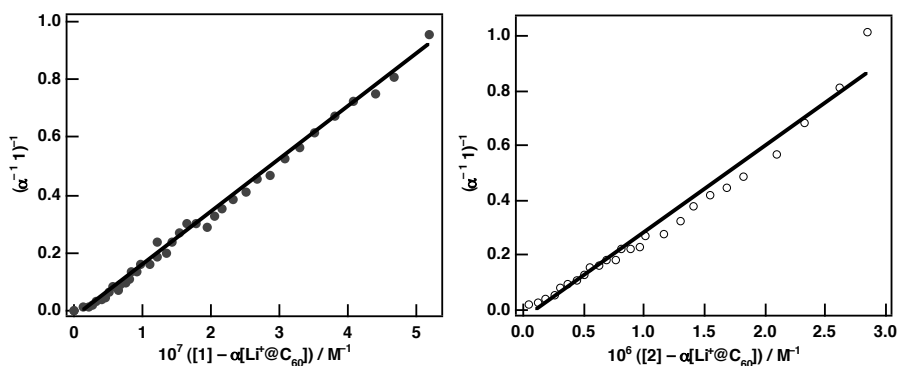


**Figure 4.** Linear plots of  $[1] - \alpha[Li^+@C_{60}]_0$  (left)  $[2] - \alpha[Li^+@C_{60}]_0$  (right) against  $(\alpha^{-1} - 1)^{-1}$  using the spectral changes at 450 nm as probe (PhCN, room temperature). The data points have been fitted by the best straight lines and the slopes of each line give the binding constants  $K_1$  for **1**• $Li^+@C_{60}$  and  $K_2$  for **2**• $Li^+@C_{60}$ , respectively, according to eq 1.

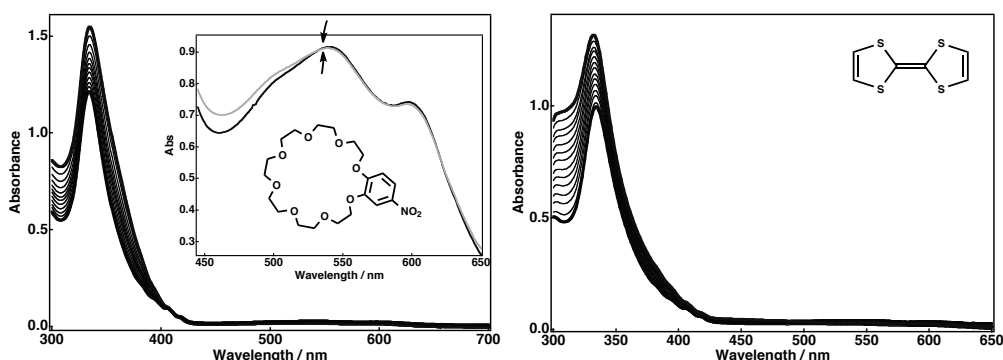


**Figure 5.** Absorption spectral changes during the titrations of  $Li^+@C_{60}$  with 4'-nitrobenzene-[18]-crown 6-ether (left) and tetrathiafulvalene (right) in PhCN.

with the reference compounds, TTF and 4'-nitrobenzene[18]crown-6 ether (Figure 5). In both cases, an increase in the absorption peak at 334 nm was observed. However, no isosbestic point could be detected, and the stoichiometry could not be established during the titrations with TTF, an observation that is most likely to be accounted for by the weak interactions between TTF and  $\text{Li}^+@\text{C}_{60}$ . In contrast, an isosbestic point was distinguished at around 530 nm when  $\text{Li}^+@\text{C}_{60}$  was titrated by the reference crown ether (Figure 5).

On account of the very close distance between donor and acceptor moieties in the inclusion complexes, the charge-transfer (CT) absorption is typically observed at longer wavelengths ( $\lambda_{\text{max}}$  750–1200 nm)<sup>6,7</sup> in their steady-state absorption spectra.<sup>19</sup> In the case of **1**• $\text{Li}^+@\text{C}_{60}$  and **2**• $\text{Li}^+@\text{C}_{60}$ , no observable CT absorption was noticed in the region from 750 to 1600 nm (Figure 6). Consequently, it can be concluded that compounds **1** and **2** seemingly host  $\text{Li}^+@\text{C}_{60}$  mainly through the interactions with the crown ethers rather than with the electron-donating MPTTF units.

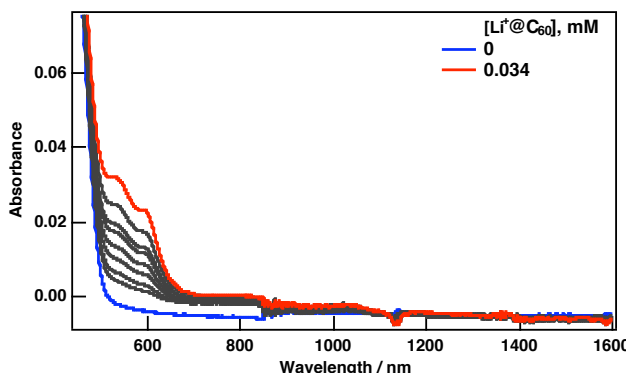


**Figure 6.** Absorption spectral changes during the titration of 0.25 mM **1** with  $\text{Li}^+@\text{C}_{60}$  in PhCN.

To gain further insight into the nature of complexation in **1**• $\text{Li}^+@\text{C}_{60}$  and **2**• $\text{Li}^+@\text{C}_{60}$ , computational studies based on density functional methods (DFT) have been performed at the B3LYP/6-311G(d,p) level of theory. The structures of corresponding complexes were optimized to a stationary point on the Born–Oppenheimer potential-energy surface. In these DFT optimized structures (Figure 7), crown ethers enfold the EMF cages, by which the complexation is realized for the most part, whereas MPTTFs curve convexly against the guest spheres. Tosyl groups are also folded towards the  $\pi$  spheres of fullerenes, which might indicate a modest effect on complexation.  $\text{Li}^+@\text{C}_{60}$  takes a position closer to the benzo-crown ether in **1**• $\text{Li}^+@\text{C}_{60}$  than dithiabenzocrown ether in **2**• $\text{Li}^+@\text{C}_{60}$ , probably on account of the larger size of the sulfur atoms. As a result of this, the distance between MPTTFs and fullerenes slightly

differs in both complexes, which causes variations in the rates of photoinduced electron-transfer reactions (see below). Top views of the complexes reveal asymmetry of the crown moieties with respect to the guest molecules.<sup>20</sup> The disposition of the endohedral Li ion

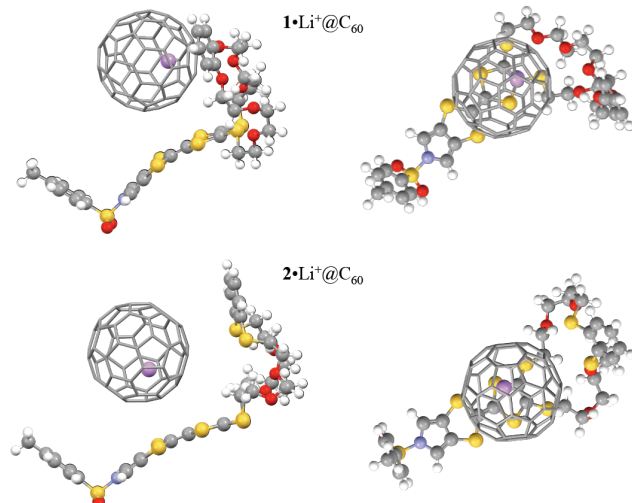


**Figure 7.** Optimized structures of  $1\bullet\text{Li}^+@\text{C}_{60}$  (upper panel) and  $2\bullet\text{Li}^+@\text{C}_{60}$  (lower panel) calculated by DFT at the B3LYP/6-311G(d,p) level of theory with side (left) and top (right) views.

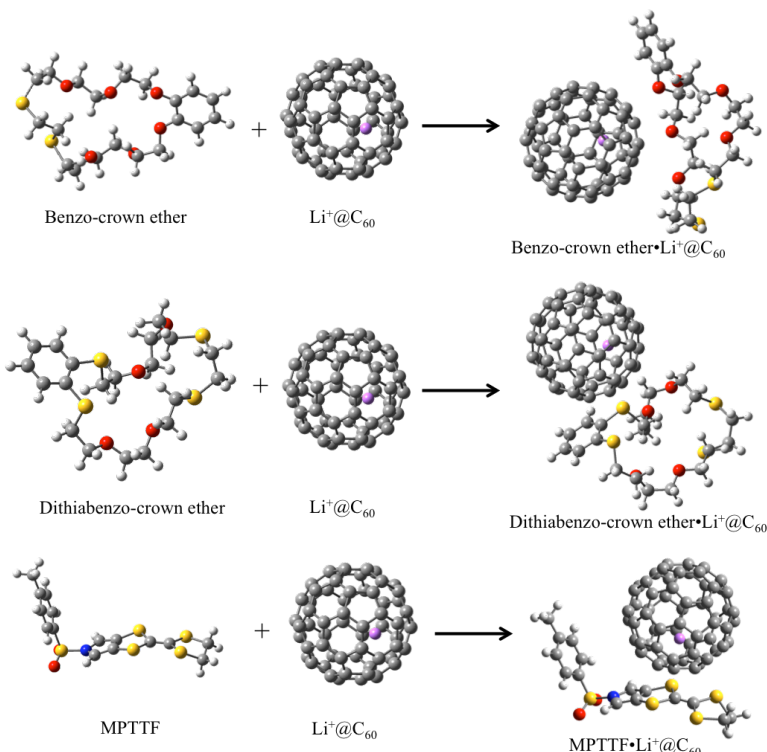


**Figure 8.** Optimized structures of indicated molecules and complexes calculated by DFT at the B3LYP/6-311G(d,p) level of theory.

with a fair proximity to the crown ethers is also noted in the optimized structures, which can result from the electrostatic interactions. DFT calculations gave values for heat of formation ( $\Delta H_f$ ) for **1**•Li<sup>+</sup>@C<sub>60</sub> and **2**•Li<sup>+</sup>@C<sub>60</sub> of  $-65.8$  and  $-44.4$  kJ mol<sup>-1</sup>, respectively. On the basis of the optimized structures, the difference in  $\Delta H_f$  values of the complexes, and in K values as well, results from the benzo and dithia groups of the crown ether moieties, which chiefly contribute to the hosting of the guest cage.

To assess the contribution of the individual components of **1** and **2** to the overall complexation, the  $\Delta H_f$  values for the complexes of benzo-crown ether, dithiabenzocrown ether, and tosyl-attached MPTTF derivative with Li<sup>+</sup>@C<sub>60</sub> were also calculated separately from their respective DFT-optimized structures (Figure 8). It transpires that the individual components virtually conserve the identical structures in the corresponding complexes as in **1**•Li<sup>+</sup>@C<sub>60</sub> and **2**•Li<sup>+</sup>@C<sub>60</sub>. The Li ion is situated close to the crown moieties and MPTTF body, which reflects an interaction with electron-rich atoms. The complexation between the benzo-crown and dithiabenzocrown ethers with Li<sup>+</sup>@C<sub>60</sub> exhibits much lower  $\Delta H_f$  values ( $-45.7$  and  $-39.8$  kJ mol<sup>-1</sup>, respectively) than that of the MPTTF with Li<sup>+</sup>@C<sub>60</sub> ( $-23.7$  kJ mol<sup>-1</sup>). These calculations clearly support the notion that stronger interactions take place between the crown ether moieties and the Li<sup>+</sup>@C<sub>60</sub> cage than between the electron-donating MPTTF unit and Li<sup>+</sup>@C<sub>60</sub>.

**Electron-Transfer Properties of Crown Ether Fused MPTTFs and Li<sup>+</sup>@C<sub>60</sub>.** The electrochemical properties of compounds **1** and **2** were examined by means of cyclic voltammetry (CV). The first one-electron oxidation potentials of **1** and **2** in PhCN at room temperature that contained 0.10 M tetrabutylammonium hexafluorophosphate (TBAPF<sub>6</sub>) were determined to be +0.63 and +0.61 V (versus saturated calomel electrode (SCE)), respectively (Figure 9). The reference TTF undergoes its first one-electron oxidation at +0.38 V under identical conditions (Figure 10). The remarkable anodic shifts are apparently due to the electron-withdrawing tosyl group appended to the monopyrrolo unit of **1** and **2**.<sup>21</sup> A difference of 20 mV in the first oxidation potentials between **1** and **2** denotes that the crown ethers are moderately involved in the oxidation process.<sup>16</sup> The second one-electron oxidation potentials show a 20 mV of anodic shift to 0.87 V for both compounds relative to reference TTF (Figure 10). Compounds **1** and **2** display the same one-electron oxidation potentials after complexation with Li<sup>+</sup>@C<sub>60</sub> (Figure 9). The first one-electron reduction of Li<sup>+</sup>@C<sub>60</sub> takes place at 0.14 V, which is also identical to the previously reported value under the same conditions.<sup>8</sup> Hence the

---

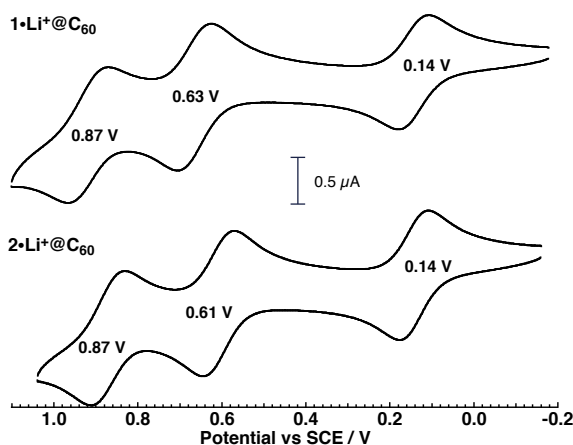


**Figure 9.** Cyclic voltammograms of **1** and **2** (0.25 mM) with  $\text{Li}^+@\text{C}_{60}$  (0.18 mM) in deaerated PhCN containing 0.10 M TBAPF<sub>6</sub> (sweep rate: 0.1 mV s<sup>-1</sup>).

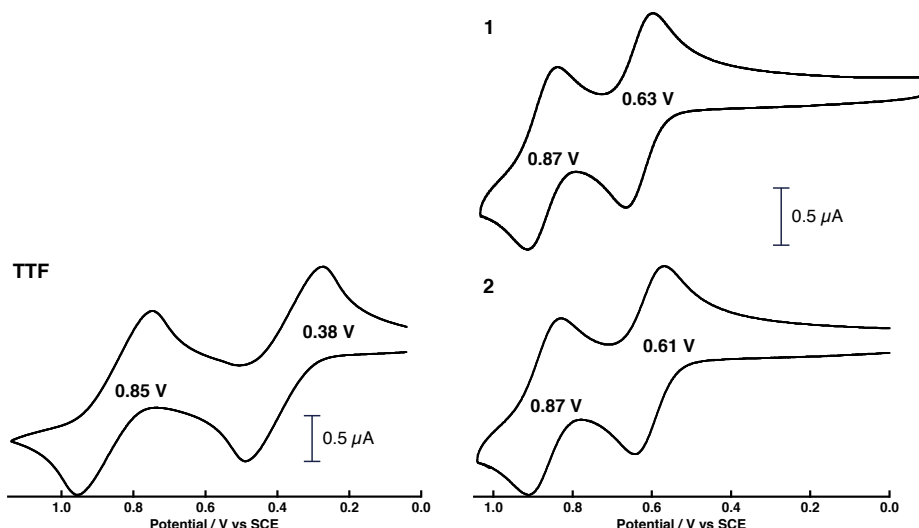


**Figure 10.** Cyclic voltammograms of **1**, **2** and reference TTF in deaerated PhCN containing 0.10 M TBAPF<sub>6</sub> (Sweep rate: 0.1 mV/s).

interactions between the host and the guest in these complexes do not have a meaningful effect on the oxidation–reduction processes. Whereas crown ethers make a major contribution to the complexation with  $\text{Li}^+@\text{C}_{60}$ , MPTTF units take part in the electron-transfer processes.

Steady-state absorption features of the oxidized species of **1** and **2** were monitored by adding the strong oxidant, nitrosonium hexafluoroantimonate (NOSbF<sub>6</sub>), in PhCN at room temperature. A radical cation of compound **1** (**1**<sup>+</sup>) appears at 434 and 797 nm (Figure 11). Further addition of an oxidizing agent results in the formation of the corresponding dication (**1**<sup>2+</sup>) as evidenced by the presence of an absorption band at 641 nm. The positions of these absorption maxima are consistent with other oxidized TTF derivatives already reported in the

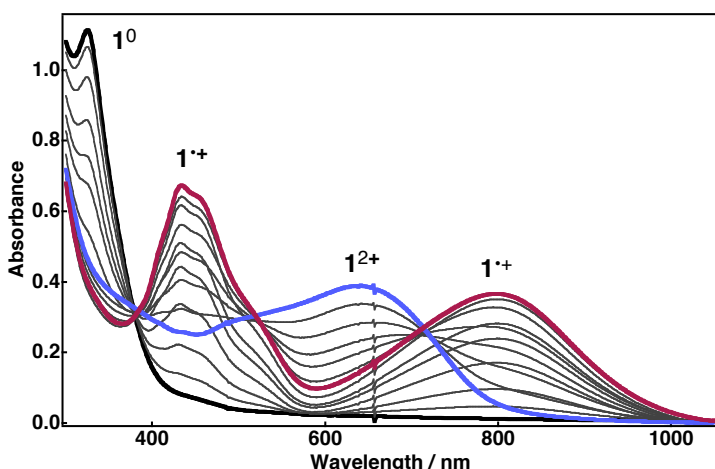


**Figure 11.** Absorption spectra of the oxidized species of compound **1**, generated by using an oxidizing agent ( $\text{NOSbF}_6$ ) in PhCN.

**Table 1.** Absorption Spectral Data of Oxidized Species of Compound **1** and **2** in PhCN with Appropriate Reference TTF Compounds

	$\lambda_{\max}$ [nm] ( $\varepsilon$ [ $\text{M}^{-1} \text{cm}^{-1}$ ])	
	Radical cation	Dication
TTF	436, <sup>a</sup> 581	—
TMT-TTF <sup>b</sup>	470, <sup>c</sup> 843 <sup>d</sup>	660 <sup>c</sup>
MPTTF <sup>e</sup>	432, 761	637
<b>1</b>	434 (12500), 797 (6100)	641 (6200)
<b>2</b>	434 (10400), 793 (6300)	669 (8700)

<sup>a</sup> Taken from Ref. 22e. <sup>b</sup> Tetramethylthiomethyltetraphiafulvalene. <sup>c</sup> Taken from Ref. 22c.

<sup>d</sup> Taken from Ref. 22d. <sup>e</sup> Taken from Ref. 22f.

literature.<sup>21</sup> Absorption spectral data for the oxidized species of compounds **1** and **2** are listed in Table 1. The monopyrrolo unit and crown ethers cause minor variations in the absorption maxima ( $\lambda_{\max}$ ) and molar absorption coefficients ( $\varepsilon$ ) of the radical cation and dication. However, the radical anion of  $\text{Li}^+@\text{C}_{60}$   $[(\text{Li}^+@\text{C}_{60})^{\bullet-}]$  was detected at 1035 nm ( $\varepsilon_{1035} = 7300 \text{ M}^{-1} \text{cm}^{-1}$ ).<sup>8,9a</sup>

The free-energy changes for photoinduced electron transfer ( $\Delta G_{\text{CS}}$ ) in **1**• $\text{Li}^+@\text{C}_{60}$  and **2**• $\text{Li}^+@\text{C}_{60}$  in PhCN have been determined according to eq 2:<sup>23</sup>

$$\Delta G_{\text{CS}} = e(E_{\text{ox}} - E_{\text{red}}) - \Delta E_{0-0} \quad (2)$$

in which  $E_{\text{ox}}$  is the first one-electron oxidation potential of compound **1** or **2**,  $E_{\text{red}}$  is the first one-electron reduction potential of  $\text{Li}^+@\text{C}_{60}$ , and  $\Delta E_{0-0}$  is the lowest excited state energy of  $\text{Li}^+@\text{C}_{60}$ . The static Coulomb energy was neglected in polar PhCN. The proposed photoinduced electron transfer from MPTTF to  $\text{Li}^+@\text{C}_{60}$  can be driven by the singlet excited states of  $\text{Li}^+@\text{C}_{60}$  [ ${}^1(\text{Li}^+@\text{C}_{60})^*$ ], the energy level of which is 1.94 eV.<sup>9a</sup> Hence the driving forces for charge separation by means of  ${}^1(\text{Li}^+@\text{C}_{60})^*$  were evaluated to be 1.45 and 1.47 eV for **1**• $\text{Li}^+@\text{C}_{60}$  and **2**• $\text{Li}^+@\text{C}_{60}$ , respectively. The energy level of the triplet excited states of  $\text{Li}^+@\text{C}_{60}$  (1.53 eV)<sup>8</sup> is sufficiently above those of the charge-separated states (0.49 and 0.47 eV for **1**• $\text{Li}^+@\text{C}_{60}$  and **2**• $\text{Li}^+@\text{C}_{60}$ , respectively).

**Photoinduced Electron-Transfer Dynamics of Crown Ether Fused MPTTFs with  $\text{Li}^+@\text{C}_{60}$  in PhCN.** Femto- and nanosecond transient absorption measurements have been performed to investigate the photoinduced processes of the complexes by excitation of  $\text{Li}^+@\text{C}_{60}$ . When excited at 330 nm, compounds **1** and **2** have weak fluorescence emission at 400 nm, which can also provide a driving force for photoinduced electron transfer (Figure 12).

However, only  $\text{Li}^+@\text{C}_{60}$  in **1**• $\text{Li}^+@\text{C}_{60}$  and **2**• $\text{Li}^+@\text{C}_{60}$  could be excited at selected wavelengths during the time-resolved transient absorption measurements. There was no transient trait to assign the singlet-excited states of **1** and **2** (Figure 13) in the femtosecond transient absorption spectra of the corresponding complexes. Femtosecond transient spectra of **1**• $\text{Li}^+@\text{C}_{60}$  and **2**• $\text{Li}^+@\text{C}_{60}$  in PhCN at room temperature show the formation of the singlet excited states of  $\text{Li}^+@\text{C}_{60}$  at 950 nm followed by the intersystem crossing that yields triplet excited states of  $\text{Li}^+@\text{C}_{60}$  at 750 nm (Figure 14).<sup>9a</sup> Time profiles at the corresponding

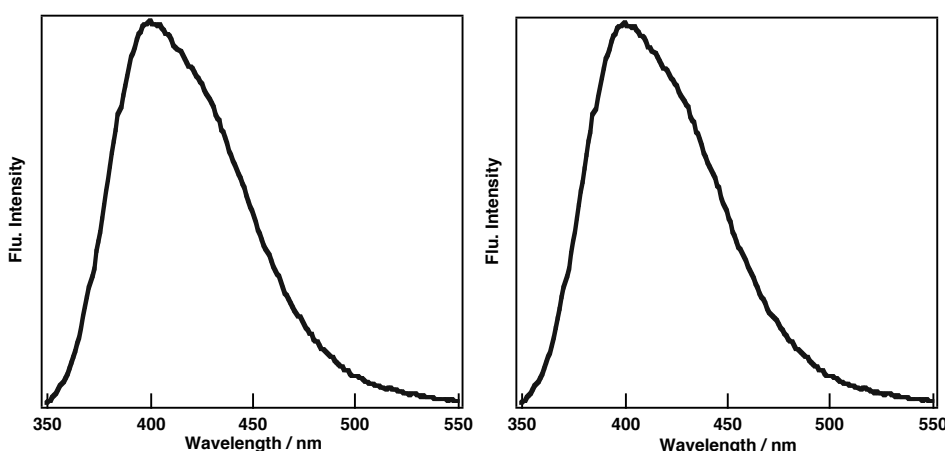


**Figure 12.** Fluorescence emission spectra of **1** (left) and **2** (right) in PhCN ( $\lambda_{\text{exc}} = 330$  nm).

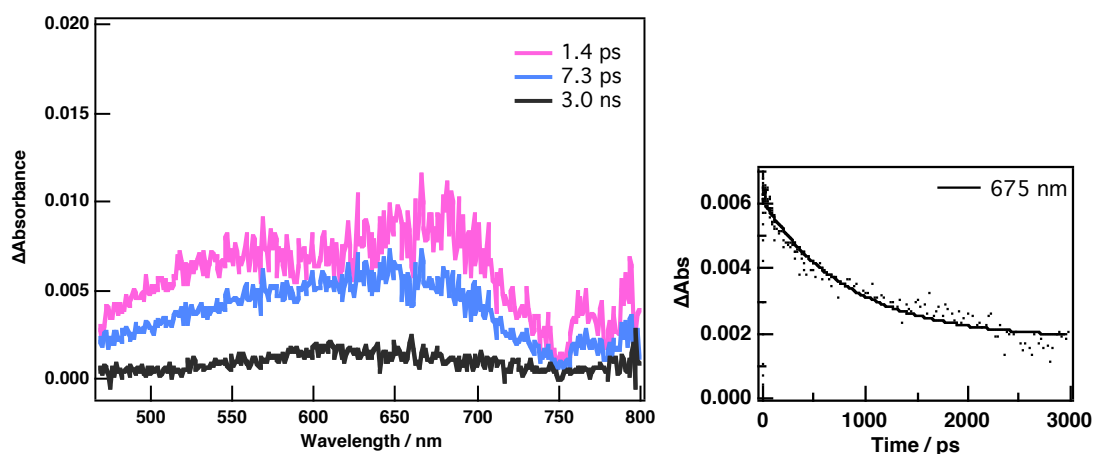


**Figure 13.** Femtosecond transient absorption spectra of **1** in PhCN at indicated time delays (left) and time profile at 675 nm (right,  $\lambda_{\text{exc}} = 390$  nm).

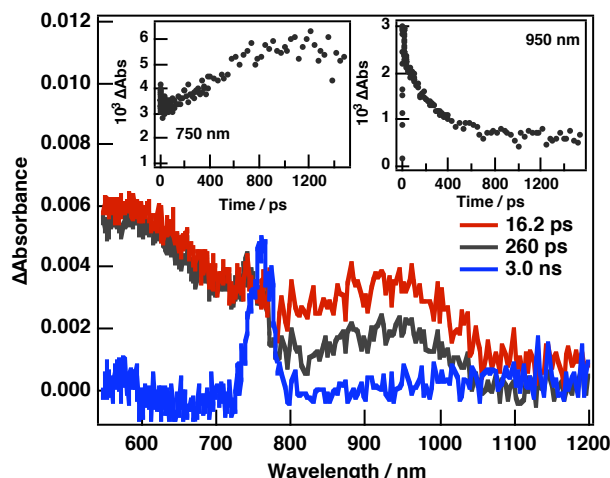


**Figure 14.** Femtosecond transient absorption spectra **1**•Li<sup>+</sup>@C<sub>60</sub> in deaerated PhCN at selected time delays at room temperature. Insets: Time profiles at indicated wavelengths ( $\lambda_{\text{exc}} = 390$  nm).

wavelengths (Figure 14 and Figure 15) reveal that the rates of intersystem crossing in these complexes are faster ( $3.4 \times 10^9$  s<sup>-1</sup> and  $2.3 \times 10^9$  s<sup>-1</sup> for **1**•Li<sup>+</sup>@C<sub>60</sub> and **2**•Li<sup>+</sup>@C<sub>60</sub>, respectively) than that of pristine Li<sup>+</sup>@C<sub>60</sub> ( $8.9 \times 10^8$  s<sup>-1</sup>).<sup>9a</sup> During the femtosecond transient absorption measurements, the formation of a radical ion pair was not detected. Li<sup>+</sup>@C<sub>60</sub> showed promoted intersystem crossing in the presence of 4'-nitrobenzene[18]crown-6 ether as well ( $1.8 \times 10^9$  s<sup>-1</sup>; Figure 16). Evidently, complexation of Li<sup>+</sup>@C<sub>60</sub> with crown ethers promotes the intersystem crossing, which suppresses the formation of the charge separation by means of <sup>1</sup>(Li<sup>+</sup>@C<sub>60</sub>)<sup>\*</sup> in **1**•Li<sup>+</sup>@C<sub>60</sub> and **2**•Li<sup>+</sup>@C<sub>60</sub>.

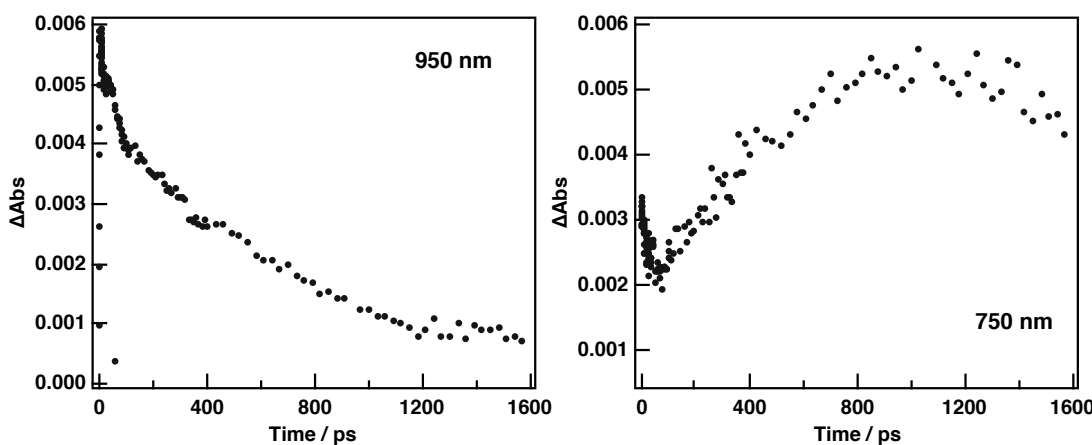


**Figure 15.** Time profiles from femtosecond transient spectra of **2**•Li<sup>+</sup>@C<sub>60</sub> in PhCN at indicated wavelengths ( $\lambda_{\text{exc}} = 390$  nm).

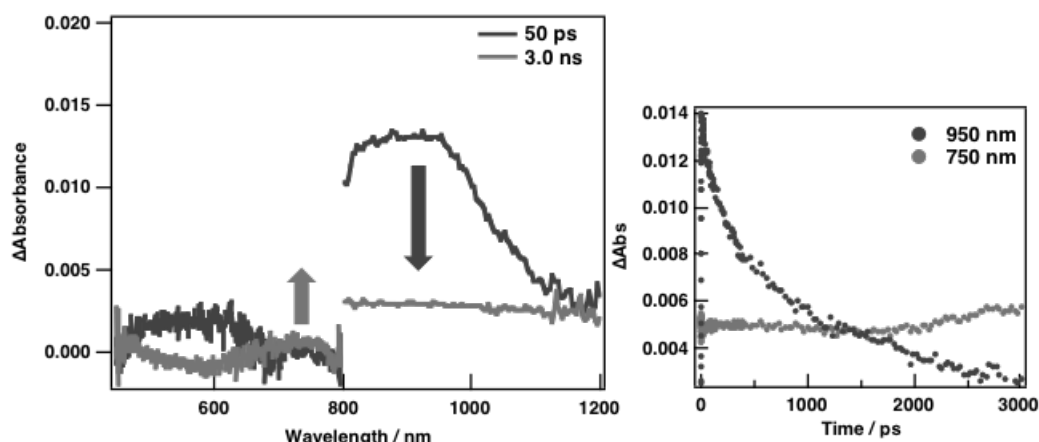


**Figure 16.** Femtosecond transient spectra of Li<sup>+</sup>@C<sub>60</sub> in the presence of 4'-nitrobenzene-[18]-crown-6 ether in PhCN at indicated time delays ( $\lambda_{\text{exc}} = 390$  nm). Inset: Time profiles at 750 and 950 nm.

Photoinduced electron transfer through  ${}^3(\text{Li}^+@\text{C}_{60})^*$  in these complexes has been monitored by the explicit formation of the radical cation of **1** and **2** at 430 nm and around 800 nm and the radical anion of Li<sup>+</sup>@C<sub>60</sub> at 1035 nm in the nanosecond transient absorption spectra following the excitation of Li<sup>+</sup>@C<sub>60</sub> at 355 nm (Figure 17). Charge separation involves intermolecular electron transfer as recognized from the time profiles at 1035 nm at different concentrations of **1** (Figure 18). The slope of the linear plot (pseudo-first-order rate constants ( $k_{\text{obs}}$ ) versus [1]) in Figure 18 gives the rate constant of intermolecular electron transfer ( $k_{\text{et}}$ ) as  $3.4 \times 10^9 \text{ M}^{-1} \text{ s}^{-1}$ , which is at the limit of the diffusion rate constant in PhCN.<sup>9a,24</sup> The rate of intramolecular electron transfer in **1**•Li<sup>+</sup>@C<sub>60</sub> ( $k_{\text{ET}}$ ) has been determined from the intercept of this plot as  $7.7 \times 10^4 \text{ s}^{-1}$ .<sup>13b</sup> Similarly, the rate constants of intermolecular ( $k_{\text{et}}$ ) and

intramolecular electron transfer ( $k_{ET}$ ) for  $\mathbf{2} \cdot \text{Li}^+@\text{C}_{60}$  have been determined as  $4.4 \times 10^9 \text{ M}^{-1} \text{ s}^{-1}$  and  $4.9 \times 10^4 \text{ s}^{-1}$ , respectively (Figure 19).

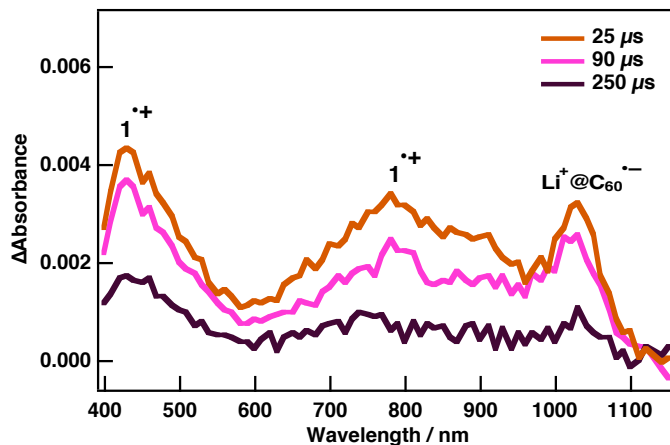


**Figure 17.** Nanosecond transient absorption spectra of 0.18 mM **1** and 0.02 mM  $\text{Li}^+@\text{C}_{60}$  in deaerated PhCN at selected time delays ( $\lambda_{\text{exc}} = 355 \text{ nm}$ ).

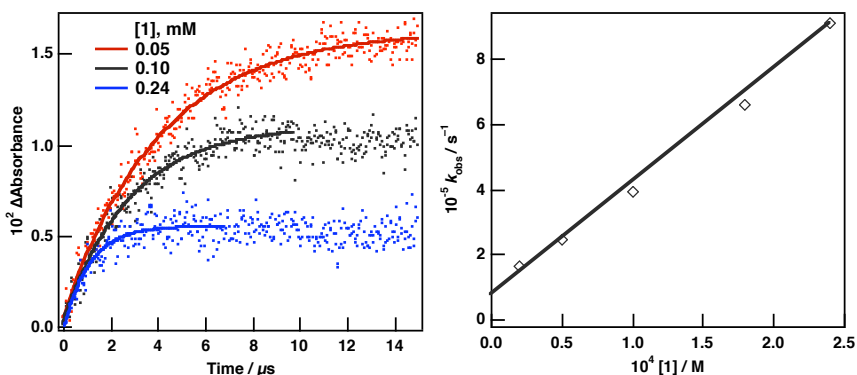


**Figure 18.** Time profiles of absorbance at 1035 nm with indicated concentrations of **1** in the presence of 0.02 mM  $\text{Li}^+@\text{C}_{60}$  in PhCN at room temperature (left) and plot of pseudo-first-order rate constants ( $k_{\text{obs}}$ ) vs concentration of **1** (right).

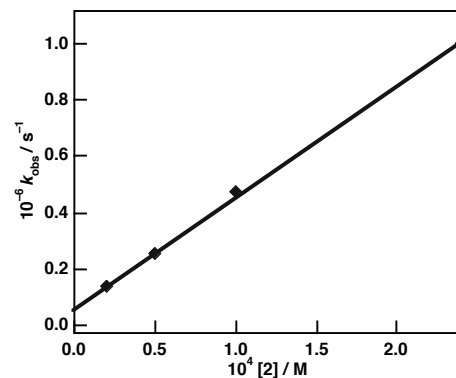


**Figure 19.** Plot of pseudo-first-order rate constants ( $k_{\text{obs}}$ ) vs concentration of **2** in the presence of 0.02 mM  $\text{Li}^+@\text{C}_{60}$ .

The first-order decays of  $\text{Li}^+@\text{C}_{60}^{\bullet-}$  at 1035 nm indicate that charge recombination is an intramolecular process for both complexes, thereby affording the lifetimes of the charge-separated states ( $\tau_{\text{CS}}$ ) of **1**• $\text{Li}^+@\text{C}_{60}$  and **2**• $\text{Li}^+@\text{C}_{60}$ : 135 and 120  $\mu\text{s}$ , respectively, in PhCN (Figure 20).<sup>24</sup> Intramolecular charge recombination was confirmed by the laser excitation at different intensities, during which the decay profiles gave the linear correlations with the same slope (Figure 21).<sup>24</sup> The change in the rate constants of **1**• $\text{Li}^+@\text{C}_{60}$  and **2**• $\text{Li}^+@\text{C}_{60}$  for charge separation ( $k_{\text{ET}}$ ) and recombination ( $k_{\text{CR}}$ ) are due to the difference in the crown ether moieties, which alter the orientation of the fullerene cage in the corresponding complexes (Figure 7). In addition, electron paramagnetic resonance (EPR) measurements at 4 K after photoexcitation of a PhCN glass that contained **1**• $\text{Li}^+@\text{C}_{60}$  and **2**• $\text{Li}^+@\text{C}_{60}$  revealed the spin state of the charge-separated state to be a triplet (Figure 22), which suggests that charge separation is realized by electron transfer from **1** and **2** to  ${}^3(\text{Li}^+@\text{C}_{60})^*$ .

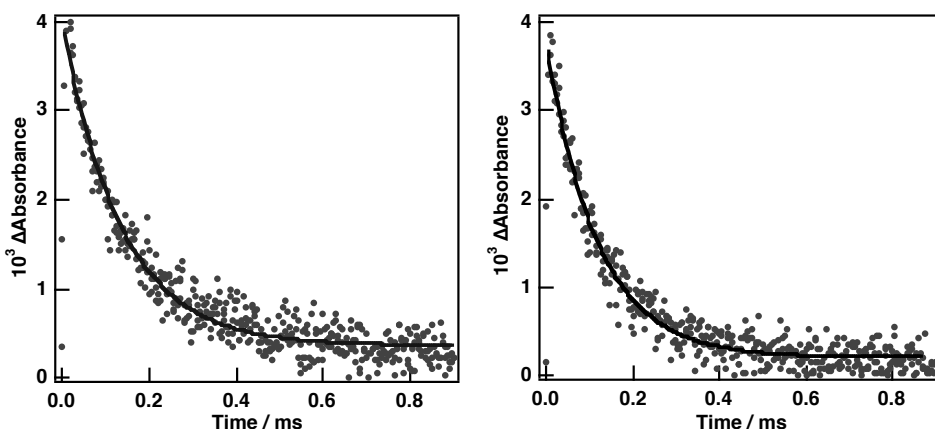


**Figure 20.** Time profiles of absorbance at 1035 nm showing the first-order decay of the radical anion of  $\text{Li}^+@\text{C}_{60}$  after the excitation of the solutions of 0.02 mM  $\text{Li}^+@\text{C}_{60}$  in the presence of 0.18 mM **1** (left) and **2** (right).

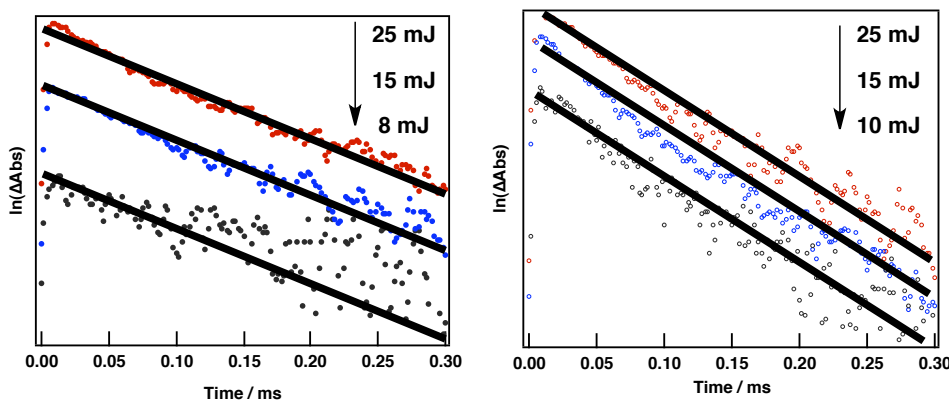


**Figure 21.** Decay time profiles of absorbance at 1035 nm at indicated laser intensities.

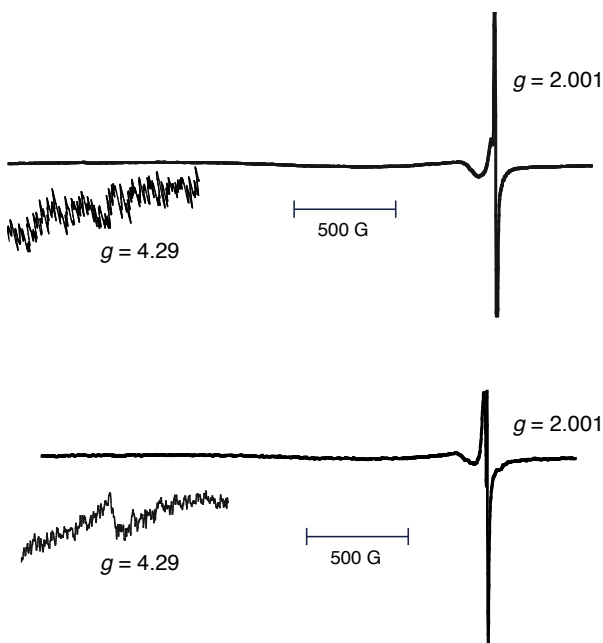


**Figure 22.** EPR spectra of **1**• $\text{Li}^+@\text{C}_{60}$  (upper) **2**• $\text{Li}^+@\text{C}_{60}$  (lower) in PhCN showing the triplet signal of  $\text{Li}^+@\text{C}_{60}$  and the radical ion pair with corresponding *g* values at 4 K observed after photoirradiation.

Charge-separation processes through  ${}^3(\text{Li}^+@\text{C}_{60})^*$  indicate that the complexation of the fullerene cage mainly takes place through the crown ethers. The reduced electronic interaction between the MPTTF core and the acceptor due to the convex structure of MPTTFs against the surface of the fullerene  $\pi$  sphere (Figures 7 and 8) has an effect on the elongation of the charge separation. Long-lived charge-separated states obtained in these complexes can be also explained by spin-restriction rules,<sup>25</sup> as  ${}^1(\text{Li}^+@\text{C}_{60})^*$  yields  ${}^3(\text{Li}^+@\text{C}_{60})^*$  by enhanced intersystem crossing.

The quantum yield of photoinduced charge separation ( $\Phi_{\text{CS}}$ ) has been estimated to be 0.82 for both complexes in PhCN by using the comparative method described previously.<sup>26</sup> Long  $t_{\text{CS}}$  values with high efficiency in these inclusion systems demonstrate a remarkable advancement among the present supramolecular systems based on TTFs and [60]fullerenes.

Photoinduced events observed in these complexes are summarized in the energy-level diagrams (Figure 23). Accelerated intersystem crossing yields  ${}^1(\text{Li}^+@\text{C}_{60})^*$  from  ${}^3(\text{Li}^+@\text{C}_{60})^*$  instead of affording charge separation with a singlet character.  ${}^3(\text{Li}^+@\text{C}_{60})^*$  provides sufficient driving force for electron transfer in both complexes owing to the lower energy level of the charge-separated states. The electron-transfer reaction rates and the corresponding electron-transfer driving forces suggest that photoinduced electron-transfer processes take place in the Marcus normal region.<sup>27</sup>

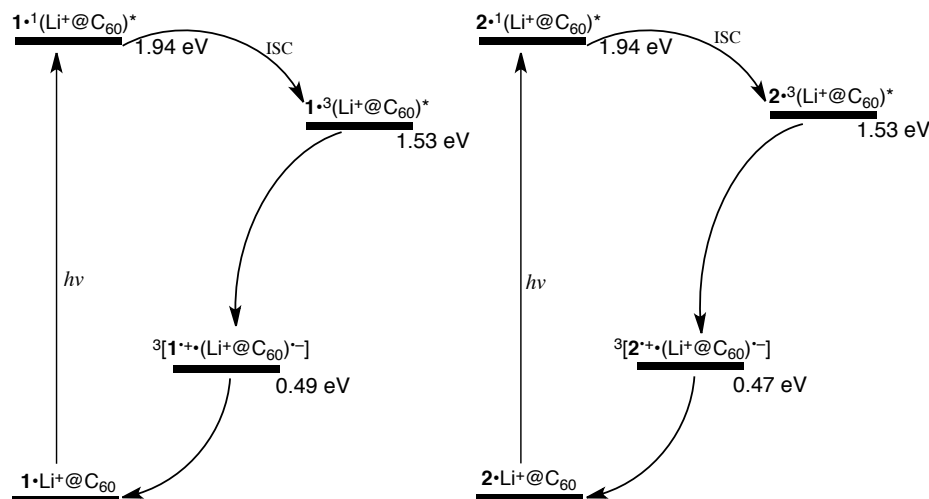


**Figure 23.** Energy level diagrams showing the photoinduced events of **1**•Li<sup>+</sup>@C<sub>60</sub> (left) and **2**•Li<sup>+</sup>@C<sub>60</sub> in PhCN.

## Conclusion

Inclusion complexes of the crown ether annexed MPTTF molecules **1** and **2** with Li<sup>+</sup>@C<sub>60</sub> and their photoinduced charge-separation processes have been thoroughly examined in a polar environment. Large binding constants revealed that very robust complexes were formed by means of electrostatic, n- $\pi$ , and  $\pi$ - $\pi$  interactions. Computational studies have been employed to understand the nature of complexation in **1**•Li<sup>+</sup>@C<sub>60</sub> and **2**•Li<sup>+</sup>@C<sub>60</sub>. Interestingly, interactions of Li<sup>+</sup>@C<sub>60</sub> with crown ether attachments of **1** and **2** facilitates the intersystem crossing that generates <sup>3</sup>(Li<sup>+</sup>@C<sub>60</sub>)<sup>\*</sup>. Formation of long-lived charge-separated states through <sup>3</sup>(Li<sup>+</sup>@C<sub>60</sub>)<sup>\*</sup> with very high efficiencies has been observed in these electron donor–acceptor complexes after the excitation of the Li<sup>+</sup>@C<sub>60</sub> by utilizing time-resolved transient absorption techniques and confirmed by EPR measurements. The present results suggest that Li<sup>+</sup>@C<sub>60</sub> can be a better alternative to the pristine fullerene in combination with TTFs for applications in organic electronics and solar energy conversion.

## References

- (1) (a) Adam, M.; Müllen, K. *Adv. Mater.* **1994**, *6*, 439–459. (b) Jørgensen, T.; Hansen, T. K.; Becher, J. *Chem. Soc. Rev.* **1994**, *23*, 41–51. (c) Bryce, M. R. *J. Mater. Chem.* **1995**, *5*, 1481–1496. (d) Garán, J. *Adv. Heterocycl. Chem.* **1995**, *62*, 249–304. (e) Schukat, G.; Fanghänel, E. *Sulfur Rep.* **1996**, *18*, 1–278. (f) Bryce, M. R. *J. Mater. Chem.* **2000**,

10, 589–598. (g) Guldi, D. M. *Chem. Commun.* **2000**, 321–327. (h) Segura, J. L.; Martín, N. *Angew. Chem.* **2001**, *113*, 1416–1455; *Angew. Chem., Int. Ed.* **2001**, *40*, 1372–1409. (i) Jeppesen, J. O.; Becher, J. *Eur. J. Org. Chem.* **2003**, *2003*, 3245–3266. (j) Jeppesen, J. O.; Nielsen, M. B.; Becher, J. *Chem. Rev.* **2004**, *104*, 5115–5132. (k) Bendikov, M.; Wudl, F.; Perepichka, D. F. *Chem. Rev.* **2004**, *104*, 4891–4946. (l) Martín, N.; Sánchez, L.; Herranz, M. A.; Illescas, B.; Guldi, D. M. *Acc. Chem. Res.* **2007**, *40*, 1015–1024.

(2) (a) Fukuzumi, S. *Org. Biomol. Chem.* **2003**, *1*, 609–620. (b) Rosokha, S. V.; Sun, D.-L.; Kochi, J. K. *J. Phys. Chem. A* **2002**, *106*, 2283–2292. (c) Fukuzumi, S.; Ohkubo, K. *J. Mater. Chem.* **2012**, *22*, 4575–4587. (d) Fukuzumi, S.; Ohkubo, K.; Suenobu, T. *Acc. Chem. Res.* **2014**, *47*, 1455–1464.

(3) Imahori, H. Guldi, D. M. Fukuzumi, S. Wuldi, F., Nagase, S., Ed.; Wiley-VCH, Verlag GmbH & Co. KGaA: Weinheim, 2010; pp 93–127.

(4) (a) Llacay, J.; Veciana, J.; Vidal-Gancedo, J.; Bourdelande, J. L.; González-Moreno, R.; Rovira, C. *J. Org. Chem.* **1998**, *63*, 5201–5210. (b) Martín, N.; Sánchez, L.; Herranz, M. A.; Guldi, D. M. *J. Phys. Chem. A* **2000**, *104*, 4648–4657. (c) Allard, E.; Cousseau, J.; Ordúna, J.; Garín, J.; Luo, H.; Araki, Y.; Ito, O. *Phys. Chem. Chem. Phys.* **2002**, *4*, 5944–5951. (d) Kreher, D.; Hudhomme, P.; Gorgues, A.; Luo, H.; Araki, Y.; Ito, O. *Phys. Chem. Chem. Phys.* **2003**, *5*, 4583–4592. (e) Chopin, S.; Gan, Z.; Cousseau, J.; Araki, Y.; Ito, O. *J. Mater. Chem.* **2005**, *15*, 2288–296. (f) Oswald, F.; Chopin, S.; de la Cruz, P.; Orduna, J.; Garín, J.; Sandanayaka, A. S. D.; Araki, Y.; Ito, O.; Delgado, J. L.; Cousseau, J.; Langa, F. *New J. Chem.* **2007**, *31*, 230–236.

(5) Segura, M.; Sánchez, L.; de Mendoza, J.; Martín, N.; Guldi, D. M. *J. Am. Chem. Soc.* **2003**, *125*, 15093–15100.

(6) (a) Nielsen, K. A.; Cho, W.-S.; Sarova, G. H.; Petersen, B. M.; Bond, A. D.; Becher, J.; Jensen, F.; Guldi, D. M.; Sessler, J. L.; Jeppesen, J. O. *Angew. Chem., Int. Ed.* **2006**, *45*, 6848–6853. (b) Nielsen, K. A.; Sarova, G. H.; Martín-Gomis, L.; Fernández-Lázaro, F.; Stein, P. C.; Sanguinet, L.; Levillain, E.; Sessler, J. L.; Guldi, D. M.; Sastre-Santos, Á.; Jeppesen, J. O. *J. Am. Chem. Soc.* **2008**, *130*, 460–462. (c) Park, J. S.; Bejger, C.; Larsen, K. R.; Nielsen, K. A.; Jana, A.; Lynch, V. M.; Jeppesen, J. O.; Kim, D.; Sessler, J. L. *Chem. Sci.* **2012**, *3*, 2685–2689.

(7) Grimm, B.; Santos, J.; Illescas, B. M.; Muñoz, A.; Guldi, D. M.; Martín, N. *J. Am. Chem. Soc.* **2010**, *132*, 17387–17389.

(8) Fukuzumi, S.; Ohkubo, K.; Kawashima, Y.; Kim, D. S.; Park, J. S.; Jana, A.; Lynch, V.

---

M.; Kim, D.; Sessler, J. L. *J. Am. Chem. Soc.* **2011**, *133*, 15938–15941.

(9) (a) Kawashima, Y.; Ohkubo, K.; Fukuzumi, S. *J. Phys. Chem. A* **2012**, *116*, 8942–8948.  
(b) Kawashima, Y.; Ohkubo, K.; Fukuzumi, S. *J. Phys. Chem. A* **2013**, *117*, 6737–6743.  
(c) Ueno, H.; Kokubo, K.; Nakamura, Y.; Ohkubo, K.; Ikuma, N.; Moriyama, H.; Fukuzumi, S.; Oshima, T. *Chem. Commun.* **2013**, *49*, 7376–7378.

(10) (a) Bhattacharya, S.; Sharma, A.; Nayak, S. K.; Chattopadhyay, S.; Mukherjee, A. K. *J. Phys. Chem. B* **2003**, *107*, 4213–4217. (b) Saha, A.; Nayak, S. K.; Chottopadhyay, S.; Mukherjee, A. K. *J. Phys. Chem. B* **2003**, *107*, 11889–11892. (c) Datta, K.; Banerjee, M.; Mukherjee, A. K. *J. Phys. Chem. B* **2004**, *108*, 16100–16106.

(11) (a) Tsuchiya, T.; Sato, K.; Kurihara, H.; Wakahara, T.; Nakahodo, T.; Maeda, Y.; Akasaka, T.; Ohkubo, K.; Fukuzumi, S.; Kato, T.; Mizorogi, N.; Kobayashi, K.; Nagase, S. *J. Am. Chem. Soc.* **2006**, *128*, 6699–6703. (b) Tsuchiya, T.; Kurihara, H.; Sato, K.; Wakahara, T.; Akasaka, T.; Shimizu, T.; Kamigata, N.; Mizorogi, N.; Nagase, S. *Chem. Commun.* **2006**, *1*, 3585–3587.

(12) Hosseini, A.; Taylor, S.; Accorsi, G.; Armaroli, N.; Reed, C. A.; Boyd, P. D. W. *J. Am. Chem. Soc.* **2006**, *128*, 15903–15913.

(13) (a) Ohkubo, K.; Kawashima, Y.; Fukuzumi, S. *Chem. Commun.* **2012**, *48*, 4314–4316.  
(b) Kawashima, Y.; Ohkubo, K. Mase, K.; Fukuzumi, S. *J. Phys. Chem. C* **2013**, *117*, 21166–21177.

(14) (a) Lu, X.; Feng, L.; Akasaka, T.; Nagase, S. *Chem. Soc. Rev.* **2012**, *41*, 7723–7760. (b) Fukuzumi, S.; Ohkubo, K.; D’Souza, F.; Sessler, J. L. *Chem. Commun.* **2012**, *48*, 9801–9815. (c) Darwish, A. D. *Annu. Rep. Prog. Chem. Sect. A: Inorg. Chem.* **2013**, *109*, 436–452. (d) Cong, H.; Yu, B.; Akasaka, T.; Lu, X. *Coord. Chem. Rev.* **2013**, *257*, 2880–2898. (e) Popov, A. A.; Yang, S.; Dunsch, L. *Chem. Rev.* **2013**, *113*, 5989–6113.

(15) Ohkubo, K.; Kawashima, Y.; Sakai, H.; Hasobe, T.; Fukuzumi, S. *Chem. Commun.* **2013**, *49*, 4474–4476.

(16) Larsen, K. R.; Johnsen, C.; Hammerich, O.; Jeppesen, J. O. *Org. Lett.* **2013**, *15*, 1452–1455.

(17) Hehre, W. J.; Radom, L.; Schleyer, P. V. R.; Pople, J. A. *Ab Initio Molecular Orbital Theory*, Wiley, New York, **1986**.

(18) Fukuzumi, S.; Kondo, Y.; Mochizuki, S.; Tanaka, T. *J. Chem. Soc. Perkin Trans. 2* **1989**, 1753–1761.

(19) For other donor–acceptor systems that show charge-transfer (CT) bands at longer

wavelengths, see: S. V. Rosokha, J. K. Kochi, Rosokha, S. V; Kochi, J. K. *Acc. Chem. Res.* **2008**, *41*, 641–653.

(20) (a) Li, L.; Clarkson, G. J. *Org. Lett.* **2007**, *9*, 497–500. (b) Noujeim, N.; Zhu, K.; Vukotic, V. N.; Loeb, S. J. *Org. Lett.* **2012**, *14*, 2484–2487.

(21) Jeppesen, J. O.; Takimiya, K.; Jensen, F.; Brimert, T.; Nielsen, K.; Thorup, N.; Becher, J. *J. Org. Chem.* **2000**, *65*, 5794–5805.

(22) (a) Torrance, J.; Scott, B.; Welber, B.; Kaufman, F.; Seiden, P. *Phys. Rev. B* **1979**, *19*, 730–741. (b) Huchet, L.; Akoudad, S.; Levillain, E.; Roncali, J.; Emge, A.; Bäuerle, P. *J. Phys. Chem. B* **1998**, *102*, 7776–7781. (c) Spanggaard, H.; Prehn, J.; Nielsen, M. B.; Levillain, E.; Allain, M.; Becher, J. *J. Am. Chem. Soc.* **2000**, *122*, 9486–9494. (d) Khodorkovsky, V.; Shapiro, L.; Krief, P.; Shames, A.; Mabon, G.; Gorgues, A.; Giffard, M. *Chem. Commun.* **2001**, 2736–2737. (e) Rosokha, S. V; Kochi, J. K. *J. Am. Chem. Soc.* **2007**, *129*, 828–838. (f) Petersen, B. M.; Jørgensen, M.; Stein, P. C.; Jeppesen, J. O. *Supramol. Chem.* **2009**, *21*, 157–163.

(23) Weller, A. *Z. Phys. Chem.* **1982**, *133*, 93–98.

(24) The time profiles of  $\mathbf{1}^+$  and  $\mathbf{2}^+$  at around 800 nm has the same formation and decay rates as of  $\text{Li}^+@\text{C}_{60}^-$  at 1035 nm

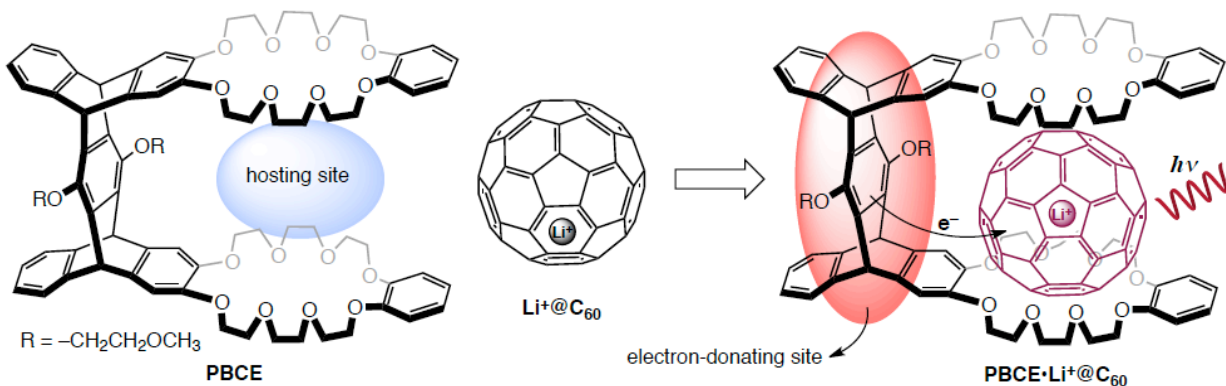
(25) (a) Konarev, D. V; Kužmin, A. V; Simonov, S. V; Khasanov, S. S.; Yudanova, E. I.; Lyubovskaya, R. N. *Dalton Trans.* **2011**, *40*, 4453–4458. (b) Konarev, D. V; Kužmin, A. V; Simonov, S. V; Khasanov, S. S.; Yudanova, E. I.; Lyubovskaya, R. N. *Dalton Trans.* **2011**, *40*, 4453–4458. (c) Suzuki, S.; Sugimura, R.; Kozaki, M.; Keyaki, K.; Nozaki, K.; Ikeda, N.; Akiyama, K.; Okada, K. *J. Am. Chem. Soc.* **2009**, *131*, 10374–10375. (d) Supur, M.; Fukuzumi, S. *Phys. Chem. Chem. Phys.* **2013**, *15*, 2539–2546. (e) Sugimura, R.; Suzuki, S.; Kozaki, M.; Keyaki, K.; Nozaki, K.; Matsushita, H.; Ikeda, N.; Okada, K. *Res. Chem. Intermed.* **2012**, *39*, 185–204.

(26) (a) Ohkubo, K.; Imahori, H.; Shao, J.; Ou, Z.; Kadish, K. M.; Chen, Y.; Zheng, G.; Pandey, R. K.; Fujitsuka, M.; Ito, O.; Fukuzumi, S. *J. Phys. Chem. A* **2002**, *106*, 10991–10998. (b) Murakami, M.; Ohkubo, K.; Fukuzumi, S. *Chem.–Eur. J.* **2010**, *16*, 7820–7832.

(27) Marcus, R. A. *Angew. Chem.* **1993**, *105*, 1161–1172; *Angew. Chem., Int. Ed.* **1993**, *32*, 1111–1121.

## Chapter 8

Long-Lived Charge Separation in a Rigid Pentiptycene  
Bis(Crown Ether)–Li<sup>+</sup>@C<sub>60</sub> Host–Guest Complex



**Abstract:** I report long-lived charge separation in a highly rigid host–guest complex of pentiptycene bis(crown ether) and Li<sup>+</sup>@C<sub>60</sub>, in which the pentiptycene framework is actively involved as an electron donor in a photoinduced electron-transfer process to the excited states of Li<sup>+</sup>@C<sub>60</sub> through a rigid distance in the complex.

### Introduction

As the essential process of solar energy conversion in photo- synthesis, charge separation with a long lifetime in the photo- synthetic reaction center (PRC) of photosystem II is realized by the arrangement of the electron donor and acceptor units through a rigid distance established by the weak interactions within the protein environment.<sup>1</sup> By the spatial alignment of redox units, fast charge recombination is prevented. Constructing a rigid distance between the electron donor and acceptor moieties, assembled via weak interactions in the supramolecular model systems, is still a challenge because in most of these systems, donor and acceptor units interact directly through weak interactions, *e.g.*  $\pi$ - $\pi$  interactions, in which no practical electron- transfer distance exists.<sup>2</sup> In the case of indirect combination of donor and acceptor through a spacer group, *e.g.* metal–ligand axial coordination, the lack of rigidity is an

obstacle for establishing a solid electron-transfer distance,<sup>3</sup> providing a slow charge recombination. There is still a demand for rigid supramolecular systems in which the electron donor and acceptor are set in fixed positions as in the natural PRC.

In this study, I proposed a new host–guest complex consisting of a rigid pentiptycene-based bis(crown ether) host (PBCE) and  $\text{Li}^+@\text{C}_{60}$  guest. PBCE hosts the fullerene cage via the cavity between two benzo-crown ether moieties (hosting site) while an electron-transfer process from the pentiptycene unit (electron-donating site), which is spatially positioned to the  $\text{Li}^+@\text{C}_{60}$ , occurs after the photoexcitation (Figure 1).

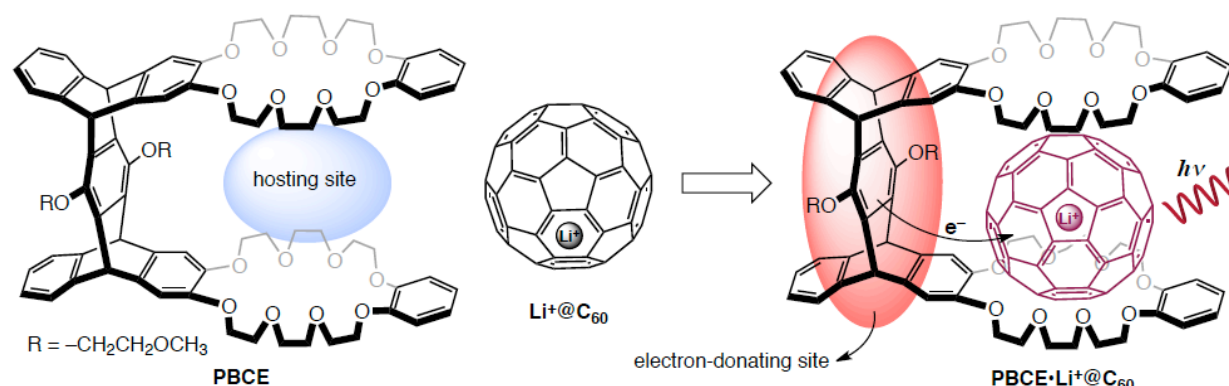


**Figure 1.** Molecular structures of the corresponding compounds and proposed host–guest complex with the description of the complexation and the electron-transfer mechanism upon the excitation of  $\text{Li}^+@\text{C}_{60}$ .

## Experimental Section

**Materials.** Synthesis of PBCE was reported elsewhere.<sup>4</sup>  $[\text{Li}^+@\text{C}_{60}]\text{PF}_6^-$  (98% purity) was obtained from commercial sources. Benzonitrile (PhCN) was distilled from  $\text{P}_2\text{O}_5$  in all-glass apparatus for purification.

**Instrumentation.** Steady-state absorption measurements were recorded on a Hewlett Packard 8453 diode array spectrophotometer. Density-functional theory (DFT) calculations were performed on a COMPAQ DS20E computer. Geometry optimizations were carried out using the B3LYP functional and 6-311G (d,p) basis set,<sup>5</sup> as implemented in the *Gaussian 03* program Rev. C.02. Graphical outputs of the computational results were generated with the *Gauss View* software program (ver. 3.09) developed by Semichem, Inc. Electrochemical measurements were performed on an ALS630B electrochemical analyzer in deaerated PhCN containing 0.10 M TBAPF<sub>6</sub> as supporting electrolyte. A conventional three-electrode cell was

used with a platinum working electrode (surface area of  $0.3\text{ mm}^2$ ) and a platinum wire as the counter electrode. The Pt working electrode was routinely polished with ALS polishing alumina suspension ( $0.05\text{ }\mu\text{m}$ ) and rinsed with water and acetone before use. The measured potentials were recorded with respect to a saturated calomel electrode (SCE). All electrochemical measurements were carried out under an atmospheric pressure of  $\text{N}_2$ . Femtosecond transient absorption spectroscopy experiments were conducted using an ultrafast source: Integra-C (Quantronix Corp.), an optical parametric amplifier: TOPAS (Light Conversion Ltd.) and a commercially available optical detection system: Helios provided by Ultrafast Systems LLC. The source for the pump and probe pulses was derived from the fundamental output of Integra-C (780 nm, 2 mJ per pulse and  $\text{fwhm} = 130\text{ fs}$ ) at a repetition rate of 1 kHz. 75% of the fundamental output of the laser was introduced into TOPAS, which has optical frequency mixers resulting in a tuneable range from 285 nm to 1660 nm, while the rest of the output was used for white light generation. Typically, 2500 excitation pulses were averaged for 5 seconds to obtain the transient spectrum at a set delay time. Kinetic traces at appropriate wavelengths were assembled from the time-resolved spectral data. For nanosecond transient absorption measurements, deaerated solutions of the compounds were excited with a Panther optical parametric oscillator (OPO) equipped with a Nd:YAG laser (Continuum, SLII-10,  $\text{fwhm} = 4\text{--}6\text{ ns}$ ) with a power of 8–25 mJ per pulse. The photochemical reactions were monitored by continuous exposure to a Xe lamp (150 W) as a probe light and a detector (SpectraPro 300i). The transient spectra were recorded using fresh solutions in each laser excitation. Solutions were deoxygenated by  $\text{N}_2$  purging for about 15 min prior to all transient spectral measurements. All measurements were conducted at room temperature. The EPR spectra were taken on a JEOL X-band spectrometer (JES-RE1XE) under photoirradiation with a high-pressure mercury lamp (USH-1005D) through a water filter focusing the sample cell in the EPR cavity at 77 K.

## Results and Discussion

Pentptycene is a good choice due to its three-dimensional rigid structure formed by a unique combination of five planar arenes with trigonal bicyclo[2.2.2]octane bridges, and it has found numerous applications in polymer and supramolecular chemistry.<sup>6</sup> The most notable use of pentptycene for the former was its integration in to the highly conjugated backbones of emissive polymers or oligomers to minimize the interchain  $\pi$ -stacking, thereby enhancing the fluorescence.<sup>7</sup> Supramolecular complexes involving pentptycene frameworks have been

---

utilized in molecular devices, such as rotors, bevel gears and so on.<sup>8</sup>

Host–guest complexes with pentiptycene scaffolds have been mostly developed after their functionalisation with crown ether moieties.<sup>9</sup> The first reported example of PBCE is where it is effectively hosting the cyclobis(paraquat-*p*-phenylene) guest through benzo-crown ethers.<sup>4</sup> After that, the trans arrangement of PBCE and pentiptycene mono(crown ether) (PMCE) were reported to form stable 2 : 1 and 1 : 1 complexes with paraquat derivatives, respectively.<sup>10</sup> Recently, benzo-crown ethers, acting as macrocycles in a PBCE-based rotaxane, were shown to oscillate simultaneously between ammonium and triazolium stations on a dumbbell molecule by acid–base stimulus.<sup>11</sup> As a result, while the pentiptycene frame conserves the rigidity of PBCE the tensile crown ethers can host molecular guests with large sizes. The electron-donating feature of pentiptycene has yet to be utilized in a photoinduced electron-transfer process in host–guest complexes of pentiptycenes.

Crown ethers with appropriate sizes have been demonstrated to associate with pristine<sup>12</sup> and metal-containing fullerenes<sup>13</sup> through n–π interactions. In a previous study,  $\text{Li}^+@\text{C}_{60}$  was reported to associate with π-electron donors bearing crown ether moieties.<sup>14</sup> Endohedral metal ions of fullerenes also assist binding with the electron-rich crown ethers.<sup>13,14</sup> While preserving the photophysical features of pristine  $\text{C}_{60}$ ,  $\text{Li}^+@\text{C}_{60}$  has a remarkably higher one-electron reduction potential.<sup>15</sup> This enables efficient photoinduced electron transfer from the pentiptycene scaffold of PBCE to the excited states of  $\text{Li}^+@\text{C}_{60}$  (Figure 1).

The complex formation was examined by UV–Vis spectroscopy. Upon the addition of PBCE to a benzonitrile (PhCN) solution of  $\text{Li}^+@\text{C}_{60}$ , a steady decrease at 334 nm was observed while the absorption at around 300 and 450 nm increased (Figure 2). Finite decreases and slight blue shifts of the absorption bands of  $\text{Li}^+@\text{C}_{60}$  were also noted at 539 and 596 nm during the titration with PBCE (Figure 3a). A plot of absorbance at 334 nm versus the molar ratio of added PBCE to the total concentration gives the stoichiometry of the complexation. The plot gives an intersection at 0.5, indicating the formation of a 1 : 1 complex ( $\text{PBCE}\cdot\text{Li}^+@\text{C}_{60}$ ) as illustrated in Figure 1. The association constant (K) for  $\text{PBCE}\cdot\text{Li}^+@\text{C}_{60}$  was determined using eq 1,<sup>14</sup>

$$(\alpha^{-1} - 1)^{-1} = K([\text{PBCE}] - \alpha[\text{Li}^+@\text{C}_{60}]_0) \quad (1)$$

where  $\alpha = (A - A_0)/(A_\infty - A_0)$ ;  $A$  is the absorbance of  $\text{Li}^+@\text{C}_{60}$  at 334 nm in the presence of PBCE,  $A_0$  and  $A_\infty$  are the initial and final absorbances at the same wavelength in the absence and in the presence of PBCE, respectively. The slope of the linear plot obtained from eq 1

---

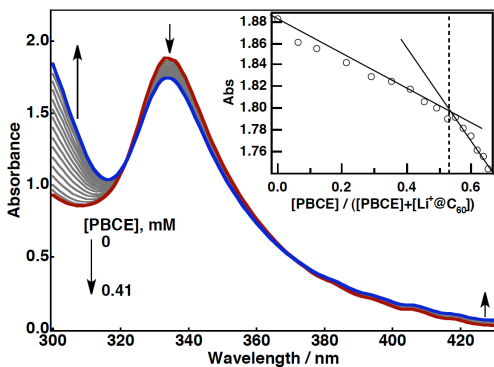


**Figure 2.** Absorption spectral changes during the titration of 0.23 mM  $\text{Li}^+@\text{C}_{60}$  with 6.3 mM PBCE in PhCN at room temperature. Inset: Plot of absorbance at 334 nm versus  $[\text{PBCE}]/([\text{PBCE}]+[\text{Li}^+@\text{C}_{60}])$  indicating the stoichiometry of the complex.

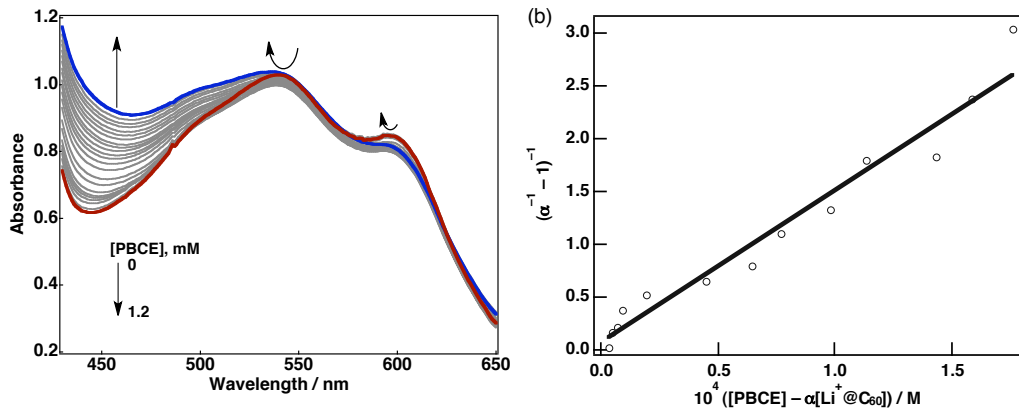


**Figure 3.** (a) Absorption spectral changes during the titration of 1.1 mM  $\text{Li}^+@\text{C}_{60}$  with 6.3 mM PBCE in PhCN at room temperature. (b) Linear plot of  $[\text{PBCE}] - \alpha[\text{Li}^+@\text{C}_{60}]$  versus  $(\alpha^{-1} - 1)^{-1}$ , where  $\alpha = (A - A_0)/(A_\infty - A_0)$ , obtained by using the spectral changes at 334 nm as probe in PhCN

(Figure 3b) affords the value for the association constant ( $K$ ) as  $1.4 \times 10^4 \text{ M}^{-1}$ .

The titration of pristine  $\text{C}_{60}$  with PBCE did not give any significant absorption change, exhibiting the indispensable effect of the Li ion inside the fullerene cage on the binding of  $\text{Li}^+@\text{C}_{60}$  to the electron-rich crown ethers (Figure 4).

The complexation between PBCE and  $\text{Li}^+@\text{C}_{60}$  was scrutinized in light of computational studies based on density functional (DFT) methods at the B3LYP/6-311G(d,p) level of theory. In the DFT-optimized structure,  $\text{Li}^+@\text{C}_{60}$  is located close to the benzo-crown ethers, by which the complexation takes place in the cavity of PBCE whereas its overall distance with the pentiptycene frame is conserved (Figure 5). In the absence of a fullerene guest, the crown ethers fold inward showing their flexibility (Figure 6).<sup>11</sup> Complexation of  $\text{Li}^+@\text{C}_{60}$  with PBCE

through one of the benzo-crown ethers outside the host cavity was also proposed. The heat of formation value for this association was calculated by DFT to be  $-54 \text{ kJ mol}^{-1}$ , whereas that of

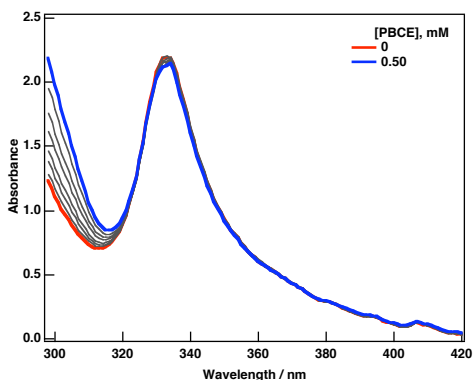


**Figure 4.** Absorption spectral changes during the titration of 0.21 mM  $\text{C}_{60}$  with 6.0 mM PBCE in PhCN at room temperature.

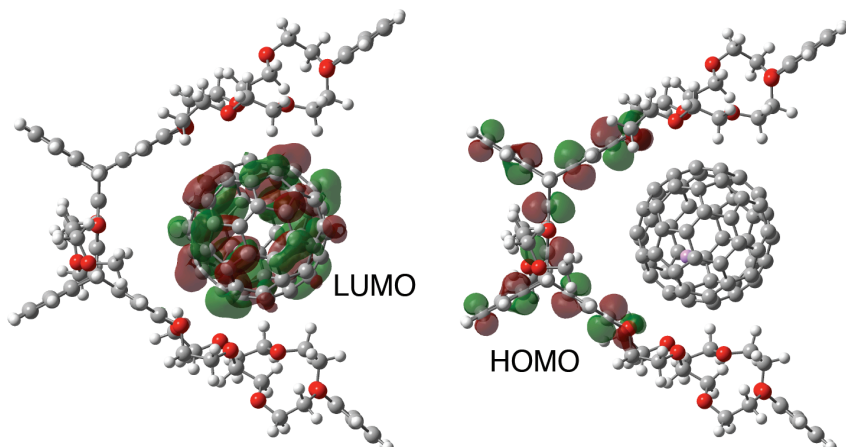


**Figure 5.** Optimized structure of  $\text{PBCE}\cdot\text{Li}^+@\text{C}_{60}$  complex showing its frontier HOMO and LUMO calculated by DFT at the B3LYP/6-311G(d,p) level of theory.

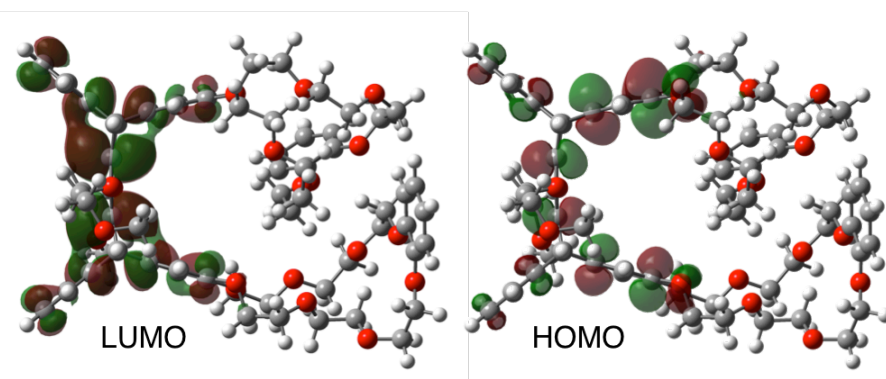


**Figure 6.** Optimized structure of PBCE showing its frontier HOMO and LUMO calculated by DFT at the B3LYP/6-311G(d,p) level of theory.

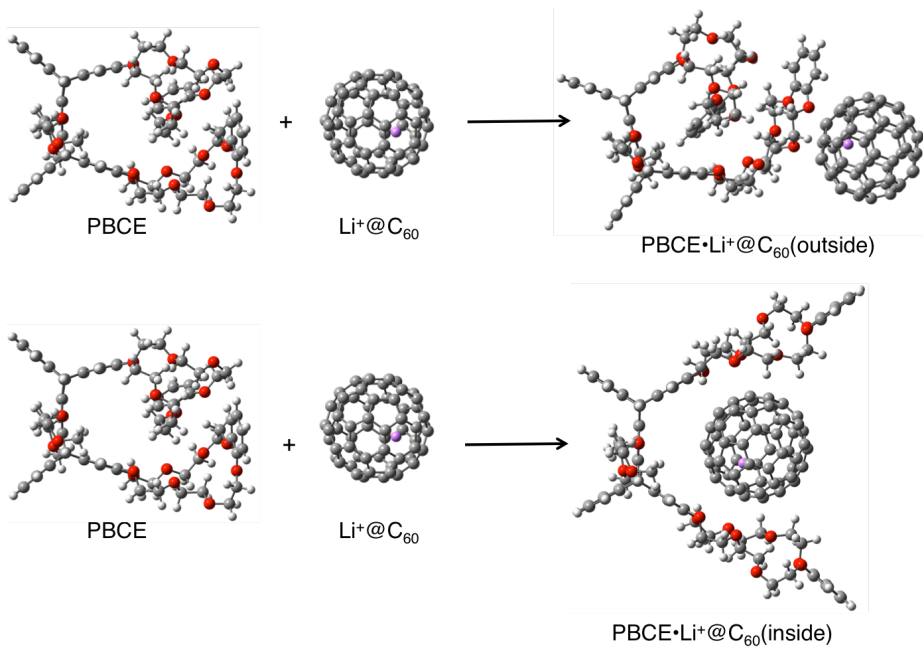


**Figure 7.** Optimized structures of indicated molecules and complexes calculated by DFT at the B3LYP/6-311G(d,p) level of theory.

complexation inside the cavity through both benzo-crown ethers was found to be  $-58 \text{ kJ mol}^{-1}$ , indicating that complexation with  $\text{Li}^+@\text{C}_{60}$  inside the cavity is more favorable (Figure 7).

While the LUMO of the complex is located on the fullerene cage, the HOMO of the complex is on the pentiptycene unit, indicating that the charge separation between pentiptycene body and  $\text{Li}^+@\text{C}_{60}$  is feasible (Figure 5). The distribution of the frontier orbitals of the complex reveals the dual character of PBCE, in which the complexation and the electron-transfer process with the guest molecule take place at different sites (*i.e.* crown ethers and pentiptycene frame).

The free-energy changes for photoinduced electron transfer in  $\text{PBCE}\cdot\text{Li}^+@\text{C}_{60}$  in PhCN was determined according to eq 2:<sup>16</sup>

$$\Delta G_{\text{CS}} = e(E_{\text{ox}} - E_{\text{red}}) - \Delta E_{0-0} \quad (2)$$

where  $e$  is the elementary charge,  $E_{\text{ox}}$  is the first one-electron oxidation potential of PBCE (+1.17 V vs SCE, Figure 8),  $E_{\text{red}}$  is the first one-electron reduction potential of  $\text{Li}^+@\text{C}_{60}$  (+0.14 V vs SCE)<sup>15a</sup> and  $\Delta E_{0-0}$  is the singlet or the triplet excited state energy of  $\text{Li}^+@\text{C}_{60}$ . The driving forces for the photoinduced electron transfer in PhCN via the singlet ( ${}^1\text{Li}^+@\text{C}_{60}^*$ , 1.94 eV)<sup>15a</sup> and the triplet excited states ( ${}^3\text{Li}^+@\text{C}_{60}^*$ , 1.53 eV)<sup>15a</sup> of  $\text{Li}^+@\text{C}_{60}$  were calculated as 0.91 and 0.50 eV, respectively. See also energy level diagram (Figure 9).

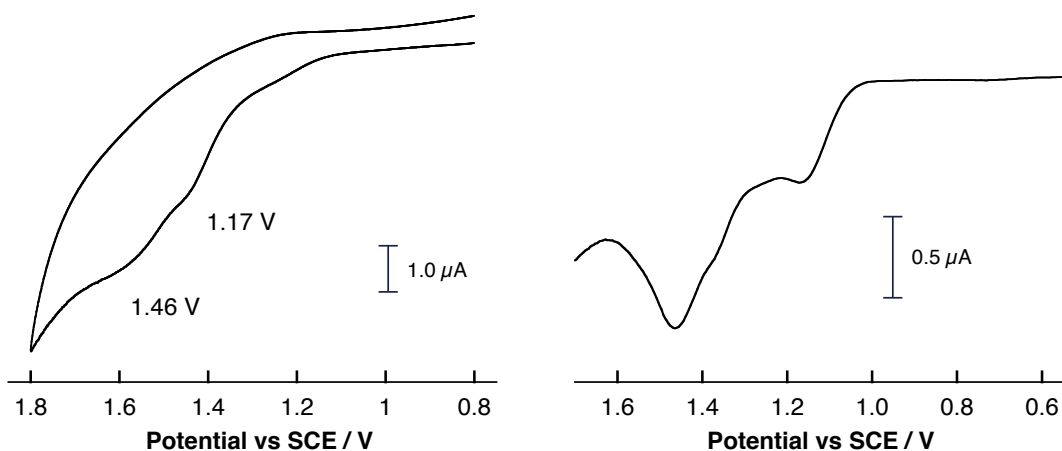


**Figure 8.** Cyclic voltammograms and differential pulse of PBCE in deaerated PhCN containing 0.10 M TBAPF<sub>6</sub> (sweep rate: 0.2 mV s<sup>-1</sup>).

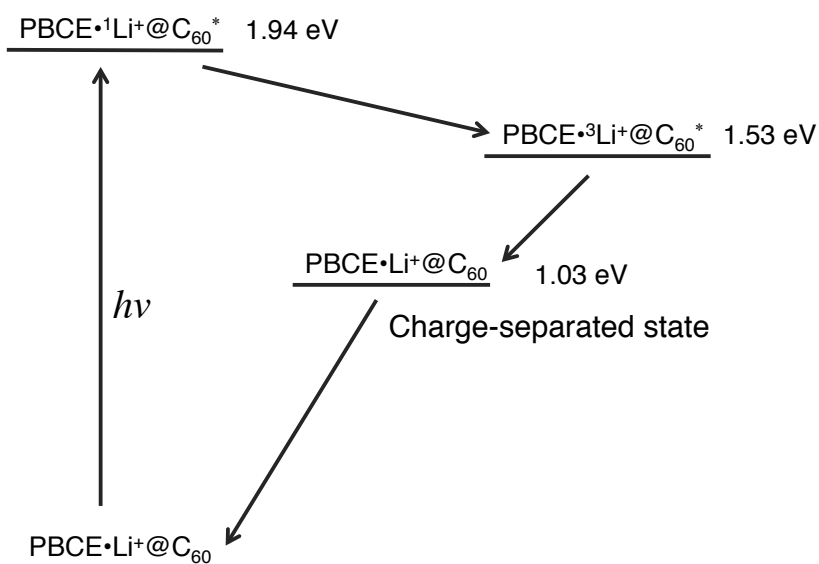


**Figure 9.** Energy level diagram of excited states of Li<sup>+</sup>@C<sub>60</sub> and charge-separated state of PBCE•Li<sup>+</sup>@C<sub>60</sub> in PhCN.

The photoinduced electron-transfer process in the PBCE•Li<sup>+</sup>@C<sub>60</sub> complex was monitored by the appearance of a transient absorption at 1035 nm due the radical anion of Li<sup>+</sup>@C<sub>60</sub> (Li<sup>+</sup>@C<sub>60</sub><sup>•-</sup>) upon photoexcitation of Li<sup>+</sup>@C<sub>60</sub> at 355 nm (Figure 10). The PBCE radical cation ( $\lambda_{\text{max}}(\text{PBCE}^{\bullet+}) = 346$  nm) was only partially observed because of the overlap with the ground state absorption of Li<sup>+</sup>@C<sub>60</sub> at around 340 nm (Figure 11 and 12). The charge-separated state has a triplet spin character because electron transfer occurs via <sup>3</sup>Li<sup>+</sup>@C<sub>60</sub><sup>\*</sup> as observed in the nanosecond transient absorption spectra (Figure 13). Complexation of Li<sup>+</sup>@C<sub>60</sub> with crown ethers promotes the inter system crossing, which

restrains the charge separation via  ${}^1\text{Li}^+@\text{C}_{60}^*$  (Figure 14) as also observed in a previous report.<sup>14</sup> Supramolecular charge separation takes place with a rate constant ( $k_{\text{CS}}$ ) of  $2.3 \times 10^6 \text{ s}^{-1}$  ( $0.43 \mu\text{s}$ ) and the lifetime of the charge-separated state ( $\tau_{\text{CS}}$ ) was estimated to be  $167 \mu\text{s}$  from the first-order decay of the transient absorbance at 1035 nm (insets, Figure 10). Considering the concentrations of PBCE (0.66 mM) and  $\text{Li}^+@\text{C}_{60}$  (0.02 mM) in Figure 10 and the  $K$  value for the association, 90% of the  $\text{Li}^+@\text{C}_{60}$  undergoes complexation with PBCE in the hosting cavity, which shields the excited state of the  $\text{Li}^+@\text{C}_{60}$  guest from the intermolecular interactions with the other complex or the free host molecules. Therefore, we estimate that the charge separation may involve only 10% of intermolecular electron-transfer process in this case.

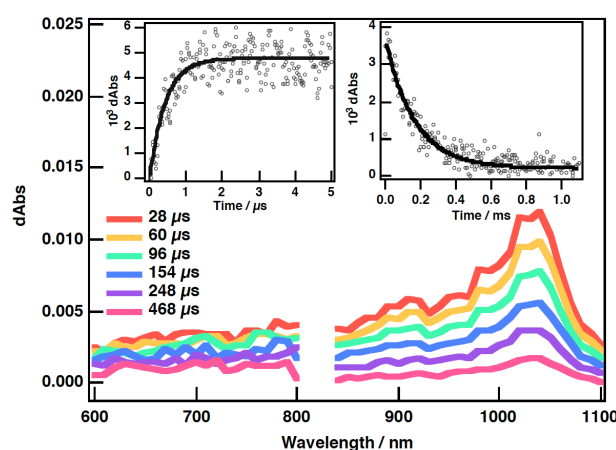


**Figure 10.** Nanosecond transient absorption spectra of PBCE and  $\text{Li}^+@\text{C}_{60}$  in deaerated PhCN at selected time delays. Inset: Time profile of the nanosecond transient spectra of 0.660 mM PBCE with 0.020 mM  $\text{Li}^+@\text{C}_{60}$  at 1035 nm ( $\lambda_{\text{exc}} = 355 \text{ nm}$ ).

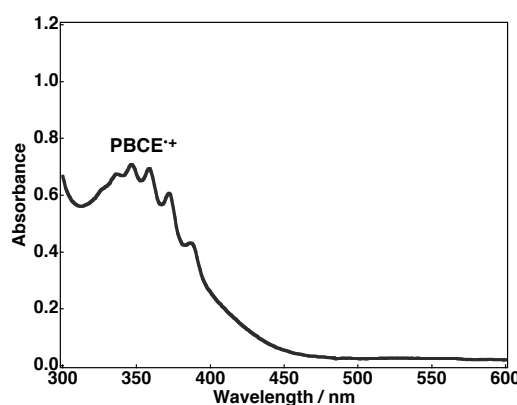


**Figure 11.** Absorption spectra of the oxidized species of PBCE, generated by using an oxidation agent ( $\text{NOSbF}_6$ ) in PhCN.

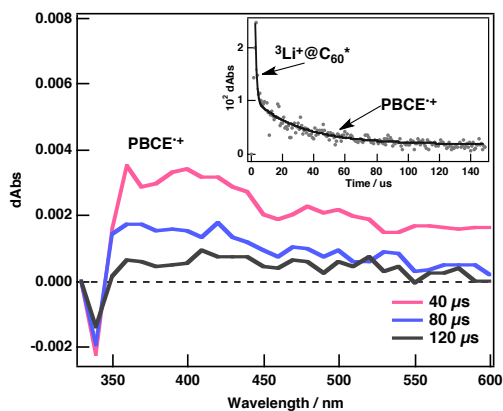


**Figure 12.** Nanosecond transient absorption spectra of PBCE and  $\text{Li}^+@\text{C}_{60}$  in deaerated PhCN at selected time delays. Inset: Time profile at 365 nm ( $\lambda_{\text{exc}} = 355$  nm).

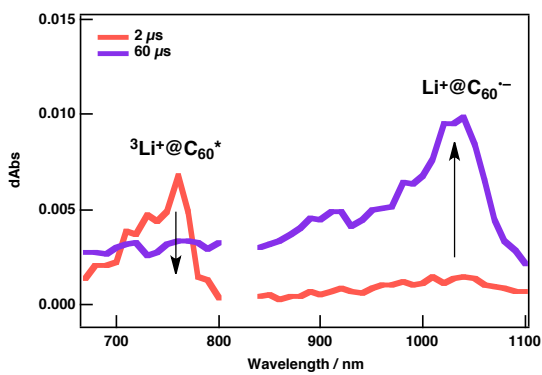


**Figure 13.** Nanosecond transient absorption spectra of PBCE and  $\text{Li}^+@\text{C}_{60}$  in deaerated PhCN at selected time delays ( $\lambda_{\text{exc}} = 355$  nm).

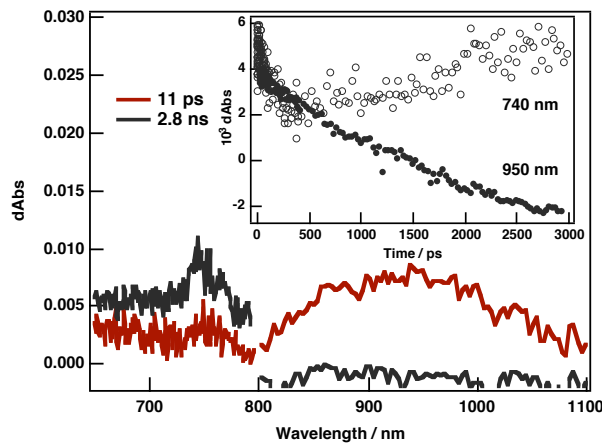


**Figure 14.** Femtosecond transient absorption spectra of PBCE and  $\text{Li}^+@\text{C}_{60}$  in deaerated PhCN at selected time delays, showing the formation of  ${}^3\text{Li}^+@\text{C}_{60}^*$  at around 740 nm via the intersystem crossing from  ${}^1\text{Li}^+@\text{C}_{60}^*$  at around 950 nm. The rate of intersystem crossing was estimated to be  $2.3 \times 10^8 \text{ s}^{-1}$ . Inset: Time profiles at indicated time delays ( $\lambda_{\text{exc}} = 390$  nm).

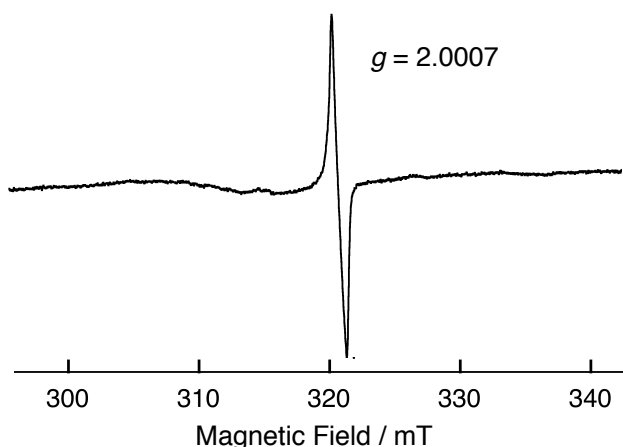


**Figure 15.** EPR spectrum of  $\text{PBCE}\bullet\text{Li}^+@\text{C}_{60}$  in PhCN showing the radical ion with corresponding  $g$  value at 77 K observed after photoirradiation.

In addition, photoinduced charge separation was confirmed by the electron paramagnetic resonance (EPR) measurements, in which the EPR spectrum of the radical ion was observed ( $g = 2.0007$ ) in PhCN glass at 77 K (Figure 15).

The quantum yield of the charge separation ( $\Phi_{\text{CS}}$ ) was determined using the comparative method. In this method,<sup>17</sup> the triplet-triplet absorption of  $\text{C}_{60}$  at 740 nm ( $\epsilon = 18800 \text{ M}^{-1} \text{ cm}^{-1}$ ,  $\Phi_{\text{triplet}} = 0.98$  in deaerated hexane) was compared with the transient traits of the generated electron transfer species, *i.e.*  $\text{Li}^+@\text{C}_{60}\bullet^-$  at 1035 nm ( $\epsilon = 7300 \text{ M}^{-1} \text{ cm}^{-1}$  in deaerated PhCN),<sup>15a</sup> in the nanosecond transient absorption spectra in the same instrumental conditions ( $\epsilon(^3\text{C}_{60}^*)$  at 740 nm)  $\Phi_{\text{triplet}} = \epsilon(\text{Li}^+@\text{C}_{60}\bullet^- \text{ at } 1035 \text{ nm})\Phi_{\text{CS}}$ ). The  $\Phi_{\text{CS}}$  was evaluated to be 0.96 for  $\text{PBCE}\bullet\text{Li}^+@\text{C}_{60}$  in PhCN.

In summary, a supramolecular host–guest complex consisting of a rigid host establishing a fixed electron-transfer distance with the electron-accepting guest through a separate hosting site was formed. Efficient photoinduced electron transfer from the electron-donating pentiptycene moiety to the  $\text{Li}^+@\text{C}_{60}$  moiety was achieved upon photoexcitation of  $\text{Li}^+@\text{C}_{60}$  in this complex to afford the long-lived charge-separated state.

## References

- (1) (a) Loll, B.; Kern, J.; Saenger, W.; Zouni, A.; Biesiadka, J. *Nature* **2005**, *438*, 1040–1044. (b) Nelson, N.; Yocom, C. F. *Annu. Rev. Plant Biol.* **2006**, *57*, 521–565.
- (2) (a) Grimm, B.; Santos, J.; Illescas, B. M.; Muñoz, A.; Guldí, D. M.; Martín, N. *J. Am. Chem. Soc.* **2010**, *132*, 17387–17389. (b) Supur, M.; Fukuzumi, S. *J. Phys. Chem. C*

2012, 116, 23274–23282.

(3) (a) Fukuzumi, S.; Honda, T.; Ohkubo, K.; Kojima, T. *Dalt. Trans.* **2009**, 3880–3889. (b) Das, S. K.; Song, B.; Mahler, A.; Nesterov, V. N.; Wilson, A. K.; Ito, O.; D’Souza, F. J. *Phys. Chem. C* **2014**, 118, 3994–4006.

(4) Cao, J.; Jiang, Y.; Zhao, J.-M.; Chen, C.-F. *Chem. Commun.* **2009**, 1987–1989.

(5) Hehre, W. J.; Radom, L.; Schleyer, P. V. R.; Pople, J. A. *Ab Initio Molecular Orbital Theory*, Wiley, New York, **1986**.

(6) (a) Yang, J.-S.; Yan, J.-L. *Chem. Commun.* **2008**, 1501–1512. (b) Chong, J. H.; MacLachlan, M. J. *Chem. Soc. Rev.* **2009**, 38, 3301–3315. (c) Jiang, Y.; Chen, C.-F. *Eur. J. Org. Chem.* **2011**, 2011, 6377–6403.

(7) (a) Yang, J.-S.; Swager, T. M. *J. Am. Chem. Soc.* **1998**, 120, 5321–5322. (b) Yang, J.-S.; Yan, J.-L.; Lin, C.-K.; Chen, C.-Y.; Xie, Z.-Y.; Chen, C.-H. *Angew. Chem., Int. Ed.* **2009**, 48, 9936–9939. (c) Lin, C.-J.; Kundu, S. K.; Lin, C.-K.; Yang, J.-S. *Chem.–Eur. J.* **2014**, 20, 14826–14833.

(8) (a) Yang, C.-H.; Prabhakar, C.; Huang, S.-L.; Lin, Y.-C.; Tan, W. S.; Misra, N. C.; Sun, W.-T.; Yang, J.-S. *Org. Lett.* **2011**, 13, 5632–5635. (b) Sun, W.-T.; Huang, S.-L.; Yao, H.-H.; Chen, I.-C.; Lin, Y.-C.; Yang, J.-S. *Org. Lett.* **2012**, 14, 4154–4157.

(9) Han, Y.; Meng, Z.; Ma, Y.-X.; Chen, C.-F. *Acc. Chem. Res.* **2014**, 47, 2026–2040.

(10) (a) Ma, Y.-X.; Han, Y.; Cao, J.; Chen, C.-F. *Org. Biomol. Chem.* **2013**, 11, 8183–8190. (b) Cao, J.; Lu, H.-Y.; Xiang, J.-F.; Chen, C.-F. *Chem. Commun.* **2010**, 46, 3586–3588. (c) Cao, J.; Lu, H.-Y.; You, X.-J.; Zheng, Q.-Y.; Chen, C.-F. *Org. Lett.* **2009**, 11, 4446–4449.

(11) Ma, Y.-X.; Meng, Z.; Chen, C. *Org. Lett.* **2014**, 16, 1860–1863.

(12) Bhattacharya, S.; Sharma, A.; Nayak, S. K.; Chattopadhyay, S.; Mukherjee, A. K. *J. Phys. Chem. B* **2003**, 107, 4213–4217.

(13) Tsuchiya, T.; Kurihara, H.; Sato, K.; Wakahara, T.; Akasaka, T.; Shimizu, T.; Kamigata, N.; Mizorogi, N.; Nagase, S. *Chem. Commun.* **2006**, 1, 3585–3587.

(14) Supur, M.; Kawashima, Y.; Larsen, K. R.; Ohkubo, K.; Jeppesen, J. O.; Fukuzumi, S. *Chem.–Eur. J.* **2014**, 20, 13976–13983.

(15) (a) Kawashima, Y.; Ohkubo, K.; Fukuzumi, S. *J. Phys. Chem. A* **2012**, 116, 8942–8948. (b) Fukuzumi, S.; Ohkubo, K.; D’Souza, F.; Sessler, J. L. *Chem. Commun.* **2012**, 48, 9801–9815.

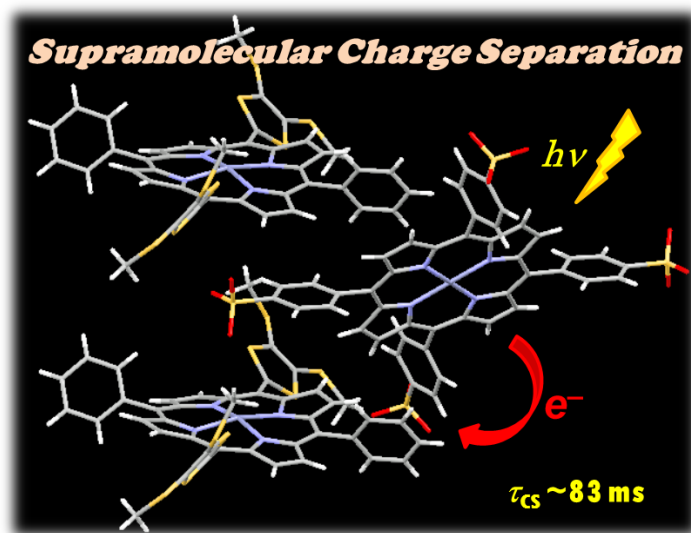
(16) Weller, A. *Z. Phys. Chem.* **1982**, 133, 93–98.

---

(17) (a) Ohkubo, K.; Kotani, H.; Shao, J.; Ou, Z.; Kadish, K. M.; Li, G.; Pandey, R. K.; Fujitsuka, M.; Ito, O.; Imahori, H.; Fukuzumi, S. *Angew. Chem., Int. Ed.* **2004**, *43*, 853–856. (b) Murakami, M.; Ohkubo, K.; Fukuzumi, S. *Chem.–Eur. J.* **2010**, *16*, 7820–7832.

## Chapter 9

Long-Lived Charge-Separated States Produced in Supramolecular Complexes between Anionic and Cationic Porphyrins



**Abstract:** A new supramolecular approach to generating a long-lived photoinduced charge separated state is described. It is predicated on the use of tetra-anionic sulfonated porphyrins (**1**-M<sup>4-</sup>; M = H<sub>2</sub> and Zn) that form 1:2 supramolecular complexes with dicationic zinc(II) porphyrinato tetrathiafulvalenes (**2**-Zn<sup>2+</sup>) via strong electrostatic interactions. The X-ray crystal structure of the complex **1**-Zn<sup>4-</sup>/(**2**-Zn<sup>2+</sup>)<sub>2</sub> reveals a slipped sandwich-type interaction wherein **1**-Zn<sup>4-</sup> is covered on both its top and bottom faces by two separate **2**-Zn<sup>2+</sup> porphyrins. Upon photoexcitation of the supramolecular ensemble, efficient photoinduced electron transfer from **1**-M<sup>4-</sup> to the triplet excited state [**2**-Zn<sup>2+</sup>]<sup>\*</sup> occurs to afford the triplet charge-separated (CS) states, as revealed by laser flash photolysis and EPR measurements. The CS state was found to decay via intramolecular back electron transfer within the supramolecular complex. This was evidenced by the observation that the CS state decay of this three-component system obeyed first-order kinetics and afforded the same long lifetimes irrespective of the initial concentrations of the CS state (e.g., 83 ms for the **1**-H<sub>2</sub><sup>4-</sup>/(**2**-Zn<sup>2+</sup>)<sub>2</sub> complex in benzonitrile at

298 K). Such an extremely long CS lifetime is thought to result from the spin-forbidden back electron transfer and the small electron coupling term, as inferred from temperature dependent studies of the CS lifetime. Decay of the CS state via intermolecular back electron transfer between two separate CS species of the type  $[1\text{-M}^{\cdot 3-}/(2\text{-Zn}^{\cdot +})(2\text{-Zn}^{2+})]$  is not observed, as revealed by the absence of second order decay kinetics. The absence of appreciable bimolecular decay processes and consequently the long-lived nature of the CS state is attributed to the central radical trianionic porphyrin ( $1\text{-M}^{\cdot 3-}$ ) being protected from close-contact interactions with other species, precluding bimolecular decay processes. This supramolecular effect is thought to be the result of the radical species,  $1\text{-M}^{\cdot 3-}$ , being sandwiched between two cationic porphyrins ( $2\text{-Zn}^{\cdot +}$  and  $2\text{-Zn}^{2+}$ ). These latter cationic entities cover the top and bottom of the anionic species thus providing both a physical and electrostatic barrier to intermolecular deactivation processes. These conclusions are supported by solution state binding studies, as well as solid state single crystal X-ray diffraction analyses.

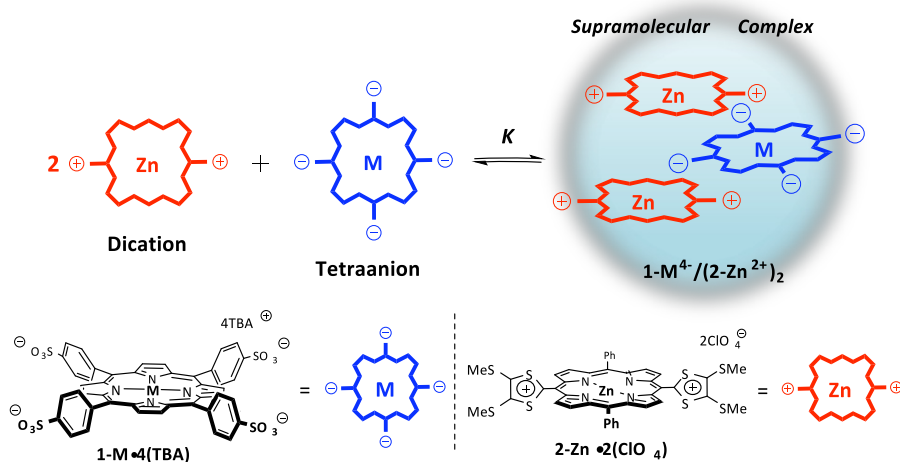
## Introduction

Extensive efforts have been devoted to developing mimics of the photosynthetic reaction center. This complex biological ensemble supports a long-lived charge-separated (CS) state that is produced via photoexcitation of a chlorophyll dimer followed by a series of subsequent electron-transfer (ET) events.<sup>1–6</sup> Several synthetic systems have previously been reported with CS lifetimes comparable to, or even longer than, that of the naturally occurring photosynthetic reaction centre.<sup>7–10</sup> Recently, supramolecular CS systems comprised of porphyrin donors and fullerene acceptors have received considerable attention. Interest in such systems reflects the fact that, in suitably designed systems, efficient photoinduced electron transfer occurs and long-lived CS states—whose decay rates parallel those observed for covalently bonded systems—are produced.<sup>11,12</sup> However, to date photoinduced CS states of electron donor-acceptor linked molecules with lifetimes longer than milliseconds have only been attained under conditions where the positions of CS molecules are fixed through use of frozen glasses or heterogeneous media.<sup>7–10,13,14</sup> In homogeneous solution, relatively fast diffusion rates dictate that bimolecular charge recombination processes predominate over what are expected to be slower intramolecular charge recombination pathways.<sup>7–10,13</sup> One approach to preventing such bimolecular charge recombination processes would be to protect the electron

donor moiety from interactions with other electron acceptor moieties (or *vice versa*). This is expected to give rise to bimolecular electron transfer processes that are highly non-adiabatic and thus significantly retarded. In the case of relatively planar systems, protection from unwanted bimolecular encounters could be achieved by covering both the top and bottom faces by large charged moieties. However, to my knowledge, supramolecular complexes that embody these design principles and which afford long-lived CS states have yet to be reported.

I detail here a supramolecular ensemble composed of one tetra-anionic porphyrin and two dicationic porphyrins. Tetraphenylporphyrin tetrasulfonates (**1-M**<sup>4-</sup>; **M** = H<sub>2</sub> and Zn) were chosen as electron donors,<sup>15</sup> whereas a dicationic porphyrinato zinc complex (**2-Zn**<sup>2+</sup>), produced by the two-electron oxidation of a  $\pi$ -extended 1,3-dithiol-2-ylidene quinoidal porphyrin (porphyrin-bridged TTF) was used as the electron acceptor.<sup>16</sup> It was found that **2-Zn**<sup>2+</sup> forms a 2:1 supramolecular complex with **1-M**<sup>4-</sup> in benzonitrile (PhCN), wherein both the top and bottom faces are covered by large charged molecules (Scheme 1). In accord with design expectations, this system gives rise to an extremely long-lived CS state upon photoirradiation. The enhanced lifetime for the CS state relative to monomeric control systems is ascribed to an absence of bimolecular decay pathways, as discussed below.

**Scheme 1.** Formation of supramolecular porphyrin complexes, **1-M**<sup>4-</sup>/**(2-Zn**<sup>2+</sup>)<sub>2</sub>; **M** = H<sub>2</sub> or Zn.



## Experimental Section

**Materials.** Reagents and chemicals of the best available grade were purchased from commercial suppliers and were used without further purification. HPLC grade solvents were used in all steady-state and time-resolved spectroscopic studies. Benzonitrile (PhCN) was distilled over phosphorus pentaoxide ( $P_2O_5$ ) immediately before use. The freebase and zinc(II) complex forms of tetra-*n*-butylammonium 5,10,15,20-*tetrakis*(phenyl-sulphonate)porphyrin (1- $H_2\bullet$ 4TBA, 1-Zn $\bullet$ 4TBA) and zinc(II) 10,20-diphenyl-5,15-*bis*(1,3-dithiol-2-yl)porphyrinato perchlorate (2-Zn $\bullet$ 2ClO<sub>4</sub>) were prepared using literature methods.<sup>12d,16</sup> The tetra-*n*-butylammonium hexafluorophosphate (TBAPF<sub>6</sub>) used for electrochemical studies was recrystallised twice from ethanol and dried *in vacuo* prior to use.

**Instruments.** <sup>1</sup>H NMR spectra were recorded on a Bruker Avance II (400 MHz for <sup>1</sup>H spectrometer. Chemical shifts ( $\delta$ -scale) are given in reference to the peak of residual non-deuterated dimethyl sulphoxide (2.50 ppm for <sup>1</sup>H). UV–Vis absorption spectra were recorded on a Hewlett Packard 8453 diode array spectrophotometer. Fluorescent spectra were recorded on a Horiba FluoroMax-4 spectrophotometer. All electrochemical measurements were performed on a CH Instruments 630B potentiostat in dry benzonitrile containing 0.1 M TBAPF<sub>6</sub> as a supporting electrolyte under N<sub>2</sub>-atmosphere, using a glassy carbon electrode (3.0 mm diameter) as a working electrode, an Ag/AgNO<sub>3</sub> electrode as a reference electrode, and a Pt wire as an auxiliary electrode. The glassy carbon electrode was polished prior to each measurement with BAS polishing alumina suspension and rinsed with deionized water and acetone before use. All potentials (vs Ag/Ag<sup>+</sup>) were converted to values vs SCE by adding 0.29 V.<sup>17</sup>

**Isothermal Titration Calorimetry (ITC).** ITC measurements were performed on a VP-ITC made by MircroCal. All measurements were performed at 298 K, and with a stir rate of 307 rpm. The calorimeter reference power was set at 25  $\mu$ cal/s. The injection volumes were 7  $\mu$ L in both cases. The titrations were continued until a minimum of 1.5 molar equivalents of **1**-M<sup>4+</sup> had been added. The data was analyzed using the Origin software provided by MircroCal.

**X-Ray Crystallography.** Crystals of **1**-Zn<sup>4-</sup>/(2-Zn<sup>2+</sup>)<sub>2</sub> were grown by layering a MeCN solution of **1**-Zn $\bullet$ 4TBA onto a THF solution of **2**-Zn $\bullet$ 2ClO<sub>4</sub> with a minimal amount of EtOH added to ensure solubility (< 5%). Over the course of three weeks, crystals of the complex grew as long dark green needles. The datum crystal was cut from a larger crystal and had

approximate dimensions:  $0.65 \times 0.19 \times 0.16$  mm. The data were collected at 153 K on a Nonius Kappa CCD diffractometer using a Bruker AXS Apex II detector and a graphite monochromator with MoK $\alpha$  radiation ( $\lambda = 0.71075$  Å). Reduced temperatures were maintained by use of an Oxford Cryosystems 600 low-temperature device. A total of 1282 frames of data were collected using  $\theta$ -scans with a scan range of 1.1° and a counting time of 44 seconds per frame. Details of crystal data, data collection, and structure refinement can be found in the supplementary information in Table S1. Data reduction were performed using SAINT V8.27B.<sup>18</sup> The structure was solved by direct methods using SIR97<sup>19</sup> and refined by full-matrix least-squares on  $F^2$  with anisotropic displacement parameters for the non-H atoms using SHELXL-97.<sup>20</sup> Structure analysis was aided by use of the programs PLATON98<sup>21</sup> and WinGX.<sup>22</sup>

Two molecules of solvent, one an ethanol molecule and one a molecule of *n*-hexane, were badly disordered. Attempts to model the disorder were unsatisfactory. The contributions to the scattering factors due to these solvent molecules were removed by use of the utility SQUEEZE<sup>23</sup> in PLATON98.

The function,  $\Sigma w(|F_o|^2 - |F_c|^2)^2$ , was minimized, where  $w = 1/[(\sigma(F_o))^2 + (0.087*P)^2 + (0.109*P)]$  and  $P = (|F_o|^2 + 2|F_c|^2)/3$ .  $R_w(F^2)$ ,  $R_w(F^2)$  refined to 0.174, with  $R(F)$  equal to 0.0666 and a goodness of fit,  $S = 1.13$ . Definitions used for calculating  $R(F)$ ,  $R_w(F^2)$  and the goodness of fit,  $S$ , are given in SI.<sup>24</sup> The data were checked for secondary extinction but no correction was necessary. Neutral atom scattering factors and values used to calculate the linear absorption coefficient are from the International Tables for X-ray Crystallography (1992).<sup>25</sup> All Figures were generated using SHELXTL/PC.<sup>26</sup>

**Laser Flash Photolysis Measurements.** Femtosecond transient absorption spectroscopy experiments were carried out in PhCN solution. The femtosecond time-resolved transient absorption (fs-TA) setup consisted of Optical Parametric Amplifiers (OPA) (Palitra, Quantronix) pumped by a Ti:sapphire regenerative amplifier system (Integra-C, Quantronix) operating at 1 kHz repetition rate and an optical detection system. The generated OPA pulses had a pulse width of ~ 100 fs and an average power of 100 mW in the 280-2700 nm spectral range. These were used as pump pulses. White light continuum (WLC) probe pulses were generated using a sapphire window (3 mm of thickness) by focusing of small portion of the fundamental 800 nm pulses, which were picked off by a quartz plate before entering into the OPA. The time delay between the pump and probe beams was carefully controlled by making the probe beam travel along a variable optical delay (ILS250, Newport). The intensities of the

---

spectrally dispersed WLC probe pulses were monitored by a High Speed spectrometer (Ultrafast Systems). To obtain the time-resolved transient absorption difference signal (DA) at a specific time, the pump pulses were chopped at 500 Hz and the absorption spectra intensities were saved alternately with or without the pump pulse. Typically, 4000 pulses were used to excite the samples and to obtain the fs-TA spectrum at a particular delay time. The polarization angle between the pump and probe beam was set at the magic angle ( $54.7^\circ$ ) using a Glan-laser polarizer with a half-wave retarder in order to prevent polarization-dependent signals. The cross-correlation full width at half maximum in pump-probe experiments was less than 200 fs and the chirp of the WLC probe pulses was measured to be 800 fs in the 400-800 nm region. To minimize chirp, all reflection optics were used in the probe beam path and a 2 mm path length of quartz cell was employed. After the fs-TA experiments, the absorption spectra of all compounds was carefully checked to detect if there were artifacts due to degradation and photo-oxidation of the samples in question. Three-dimensional data sets of  $\Delta A$  versus time and wavelength were subjected to singular value decomposition and global fitting to obtain the kinetic time constants and their associated spectra using the Surface Xplorer software (Ultrafast Systems).

Nanosecond time-resolved transient absorption measurements were carried out in PhCN solution using a laser system provided by UNISOKU Co., Ltd. Measurements of nanosecond transient absorption spectra were performed according to the following procedure: A deaerated solution was excited by a Panther optical parametric oscillator pumped by a Nd:YAG laser (Continuum, SLII-10, 4–6 ns fwhm) at  $\lambda = 430$  nm. The photodynamics were monitored by continuous exposure to a xenon lamp (150 W) as a probe light and a photomultiplier tube (Hamamatsu 2949) as a detector.

**EPR Spectroscopy.** The EPR spectra were taken on a JEOL X-band spectrometer (JES-RE1XE) with a quartz ESR tube. The EPR spectrum of the charge-separated state in frozen PhCN was measured under photoirradiation with a high-pressure mercury lamp (USHIO LIGHTING USH-1005D) through a water filter focusing at the sample cell in the EPR cavity using a liquid helium cryostat before making the spectroscopic measurements at 4 K. The *g* value was calibrated using an  $\text{Mn}^{2+}$  marker.

**Theoretical Calculations.** Hartree-Fock calculations were performed using the Gaussian 09 program<sup>27</sup> suite on a supercomputer (KISTI, IBM). The MO distribution diagram of **1-Zn<sup>4-</sup>•(2-Zn<sup>2+</sup>)<sub>2</sub>** was obtained via the HF method employing LanL2DZ basis set for all atoms.

---

## Results and Discussion

**Photocatalytic formation of the supramolecular complexes.** The synthesis and characterization of **1-M**•4TBA (M = H<sub>2</sub> and Zn) and **2-Zn**•2ClO<sub>4</sub> used in this study have been previously reported.<sup>15,16</sup> The formation of putative supramolecular assemblies of **1-H<sub>2</sub>**<sup>4-</sup>/(**2-Zn**<sup>2+</sup>)<sub>2</sub> was first examined by means of <sup>1</sup>H NMR spectral titration experiments carried out in DMSO-*d*<sub>6</sub> (Figure S1). Upon addition of **1-H<sub>2</sub>**<sup>4-</sup> to **2-Zn**<sup>2+</sup>, a broadening, and slight upfield shift in the aromatic peaks of **2-Zn**<sup>2+</sup> was observed. These changes were taken as initial evidence for the formation of supramolecular complexes in DMSO-*d*<sub>6</sub>. However, the recorded shifts were not sufficiently large to fit the data to a standard binding profile and thus deeper insights into the nature of the complexes produced could not be drawn from this data.<sup>28</sup>

Upon the addition of **1-Zn**<sup>4-</sup> to **2-Zn**<sup>2+</sup> in PhCN, changes in the absorption spectrum of **2-Zn**<sup>2+</sup> were observed (Figure 1a). Isosbestic behavior is seen, as would be expected for the intraconversion between two absorbing species. Job plot analyses are consistent with the formation of a 2:1 supramolecular ensemble involving **2-Zn**<sup>2+</sup> and **1-Zn**<sup>4-</sup> (Figure 1a). The net neutral nature of the putative ensemble leads me to suggest that its formation may be driven by electrostatic interactions. The formation constant of the supramolecular ensemble (*K*) is estimated by using a one-step binding model with a 1:2 overall stoichiometry according to eq 1:

$$K = [\mathbf{1-Zn}^{4-}/(\mathbf{2-Zn}^{2+})_2]/([\mathbf{2-Zn}^{2+}]^2[[\mathbf{1-Zn}^{4-}]] \quad (1)$$

The ratio of the complex (*α*) was determined from the absorbance change associated with the formation of the 1:2 self-associated ensemble **1-M**<sup>4-</sup>/(**2-Zn**<sup>2+</sup>)<sub>2</sub> (Figure 1b) as given by eq 2, where *A*<sub>0</sub> and *A*<sub>\*</sub> are absorbance of **2-Zn**<sup>2+</sup> and **1-M**<sup>4-</sup>/(**2-Zn**<sup>2+</sup>)<sub>2</sub>, respectively. From eqs 1 and 2, eq 3 is derived when the concentration of **2-Zn**<sup>2+</sup> is fixed and the concentration of **1-M**<sup>4-</sup> is varied.

$$\alpha = (A - A_0)/(A_* - A_0) \quad (2)$$

$$\alpha/(1 - \alpha)^2 = K[\mathbf{2-Zn}^{2+}]_0(2[\mathbf{1-Zn}^{4-}] - \alpha[\mathbf{2-Zn}^{2+}]_0) \quad (3)$$

A near-linear plot was obtained when *α*/(1 - *α*)<sup>2</sup> was plotted vs 2[**1-Zn**<sup>4-</sup>] - *α*[**2-Zn**<sup>2+</sup>]<sub>0</sub> as shown in Figure 1b. From the slope, the *K* value of **1-Zn**<sup>4-</sup>/(**2-Zn**<sup>2+</sup>)<sub>2</sub> was determined to be (5.9 ± 0.5) × 10<sup>11</sup> M<sup>-2</sup>. In the same manner, the association constant of **1-H<sub>2</sub>**<sup>4-</sup>/(**2-Zn**<sup>2+</sup>)<sub>2</sub> was determined to be (6.6 ± 0.5) × 10<sup>12</sup> M<sup>-2</sup> (Figure 2b).

---

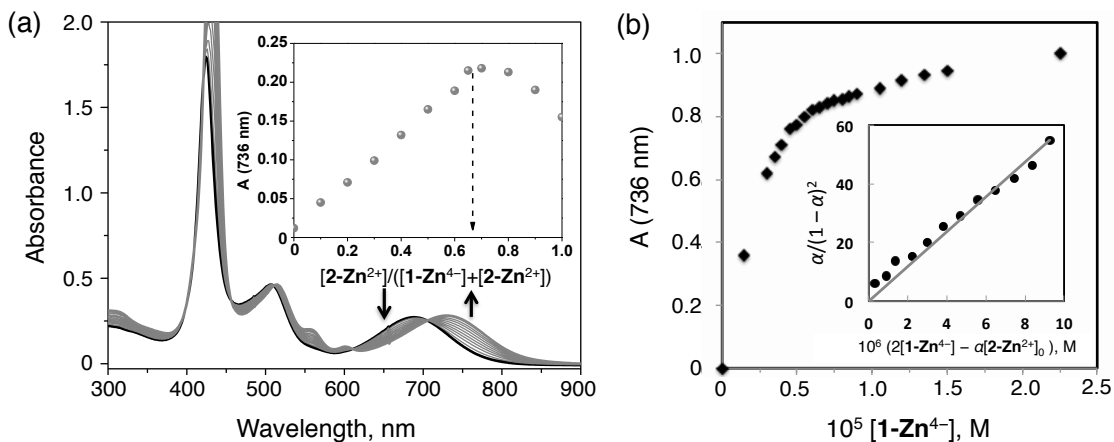


**Figure 1.** (a) Absorption spectral changes observed upon the treatment of a  $10 \mu\text{M}$  PhCN solution of **2-Zn**<sup>2+</sup> with **1-Zn**<sup>4-</sup> at 298 K. The original spectrum is the bolded black line whereas the final spectrum is highlighted in gray. The inset shows a Job's plot for the UV-Vis absorption at 732 nm constructed using various molar ratios of **2-Zn**<sup>2+</sup> and **1-Zn**<sup>4-</sup>. (b) Plot of the ratio of the extent of complex **1-Zn**<sup>4-</sup>/**(2-Zn**<sup>2+</sup>)<sub>2</sub> formed ( $\alpha$ ) vs the concentration of **1-Zn**<sup>4-</sup>. The inset shows a plot of  $\alpha / (1 - \alpha)^2$  vs  $2[1\text{-Zn}^{4-}] - \alpha[2\text{-Zn}^{2+}]_0$ ; this latter plot was used to determine the association constant,  $K$ , according to eq 3.

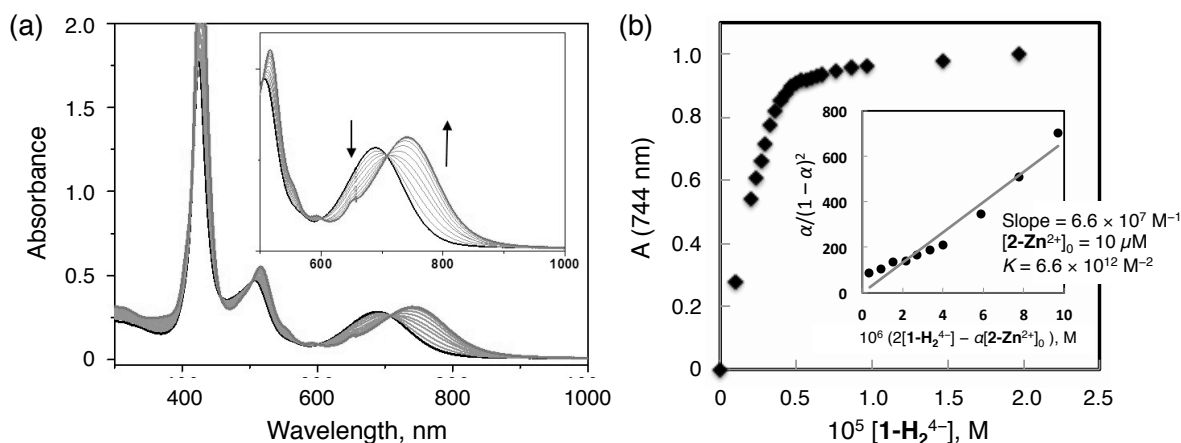


**Figure 2.** (a) UV-Vis absorption spectra of the titration **1-H<sub>2</sub>**•4TBA into  $10 \mu\text{M}$  solution of **2-Zn**•2ClO<sub>4</sub> in PhCN at 298 K. (b) The linear fitting of the data to the 2:1 binding equations, detailed above.

Upon the addition of **2-Zn**<sup>2+</sup> to **1-Zn**<sup>4-</sup> in PhCN under the conditions where the 1:2 supramolecular complex **1-Zn**<sup>4-</sup>/**(2-Zn**<sup>2+</sup>)<sub>2</sub> is expected to dominate, an attenuation of the fluorescence spectra of **1-Zn**<sup>4-</sup> was observed (Figure 3a). This finding leads me to suggest that, upon irradiation, either photoinduced electron- or energy transfer occurs from the anionic porphyrin subunit **1-Zn**<sup>4-</sup> to the **2-Zn**<sup>2+</sup> moieties in the supramolecular assemblies. In such a

case, the ratio of the complex ( $\alpha$ ) can be determined from the fluorescence intensity change due to formation of the complex  $\mathbf{1}\text{-Zn}^{4-}/(\mathbf{2}\text{-Zn}^{2+})_2$ , as per eq 4, where  $I_0$  and  $I$  are the initial fluorescence intensity of  $\mathbf{1}\text{-Zn}^{4-}$  and the fluorescence intensity in the presence of excess  $\mathbf{2}\text{-Zn}^{2+}$ , respectively. From eqs 1 and 2, eq 5 is derived when the concentration of  $\mathbf{1}\text{-Zn}^{4-}$  is fixed and the concentration of  $\mathbf{2}\text{-Zn}^{2+}$  is varied.

$$\alpha = (I_0 - I)I_0 \quad (4)$$

$$\alpha/(1 - \alpha) = K([2\text{-Zn}^{2+}] - 2\alpha[\mathbf{1}\text{-Zn}^{4-}]_0)^2 \quad (5)$$

An essentially linear plot was obtained when  $\alpha/(1 - \alpha)$  was plotted vs  $([2\text{-Zn}^{2+}] - 2\alpha[\mathbf{1}\text{-Zn}^{4-}]_0)^2$ , as shown in Figure 3b. From the slope, the  $K$  value corresponding to the formation of  $\mathbf{1}\text{-Zn}^{4-}/(\mathbf{2}\text{-Zn}^{2+})_2$  was determined to be  $(6.3 \pm 0.5) \times 10^{11} \text{ M}^{-2}$ ; this  $K$  value agrees with that determined from the absorption spectral titration (*vide infra*). Such agreement provides support for the suggestion that the fluorescence quenching of  $\mathbf{1}\text{-Zn}^{4-}$  observed upon treating with  $\mathbf{2}\text{-Zn}^{2+}$  reflects formation of the supramolecular complex  $\mathbf{1}\text{-Zn}^{4-}/(\mathbf{2}\text{-Zn}^{2+})_2$ .

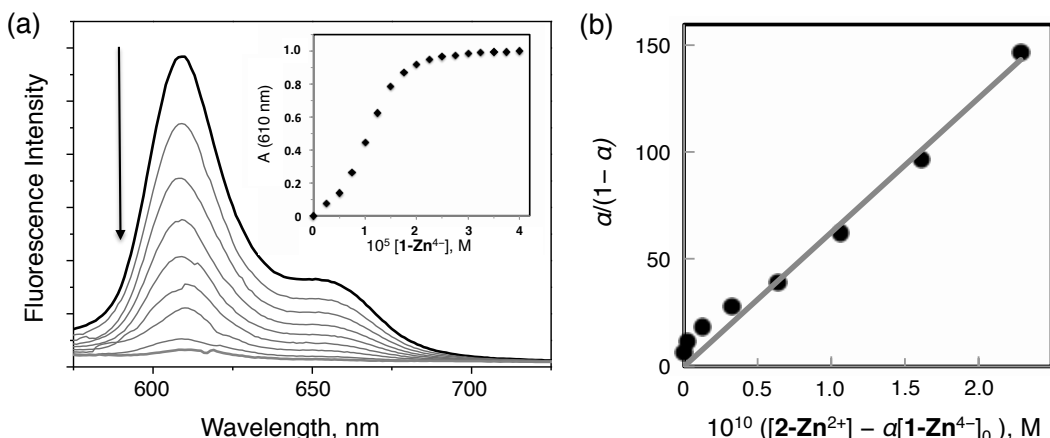


**Figure 3.** (a) Fluorescence spectral changes observed upon the treatment of a PhCN solution of  $\mathbf{1}\text{-Zn}^{4-}$  ( $10 \mu\text{M}$ ) with  $\mathbf{2}\text{-Zn}^{2+}$  at  $298 \text{ K}$ . Excitation wavelength:  $430 \text{ nm}$ . Inset shows a plot of the ratio of the complex ( $\alpha$ ) vs the concentration of  $\mathbf{2}\text{-Zn}^{2+}$ . (b) Plot of  $\alpha/(1 - \alpha)$  vs  $[2\text{-Zn}^{2+}]_0 - 2\alpha[\mathbf{1}\text{-Zn}^{4-}]_0$ , which was used to determine the association constant,  $K$ , according to eq 5.

In an effort to evaluate the thermodynamic behavior of the complexation processes between the ionic porphyrins, isothermal titration calorimetry (ITC) was performed in PhCN (Figure 4). In Figure 4, the titration of  $\mathbf{1}\text{-H}_2^{4-}$  into  $\mathbf{2}\text{-Zn}^{2+}$  is shown. An intense exothermic heat signature is observed over the first 6 injections. This thermodynamic process is ascribed to initial deaggregation of  $\mathbf{2}\text{-Zn}^{2+}$ . Therefore these points were removed from the data set for

the purpose of analyzing the binding parameters. Following the presumed initial deaggregation event, additional injections of **1-H<sub>2</sub><sup>4-</sup>** led to a sigmoidal heat signal with an *n*-value, or equivalence point, near 0.5 molar equivalents, supporting a 1:2 **1-H<sub>2</sub><sup>4-</sup>** to **2-Zn<sup>2+</sup>** binding stoichiometry. Similar curves were obtained and identical conclusions were drawn from titrations of **1-Zn<sup>4-</sup>** into **2-Zn<sup>2+</sup>** (Figure 5). The values of heat of formation ( $\Delta H$ ) of **1-Zn<sup>4-</sup>/(2-Zn<sup>2+</sup>)<sub>2</sub>** and **1-H<sub>2</sub><sup>4-</sup>/(2-Zn<sup>2+</sup>)<sub>2</sub>** were determined to be -5.5 and -5.9 kcal mol<sup>-1</sup>, respectively.

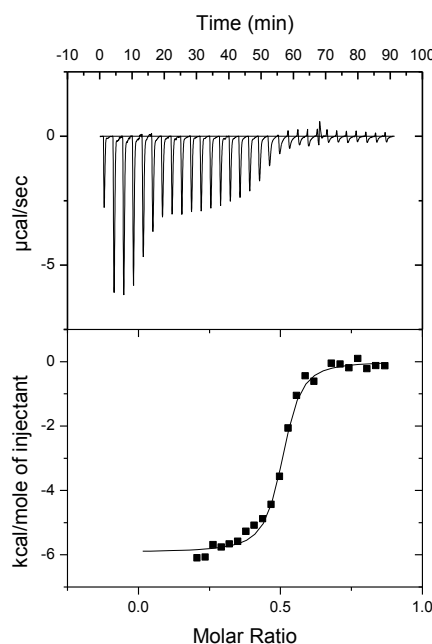


**Figure 4.** ITC titration of **1-H<sub>2</sub><sup>4-</sup>** into a PhCN solution of **2-Zn<sup>2+</sup>** at 298 K.

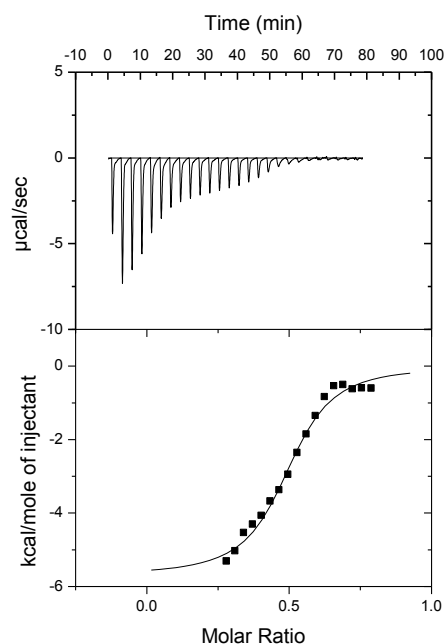


**Figure 5.** ITC titration of **1-Zn<sup>4-</sup>** into **2-Zn<sup>2+</sup>** at 298 K in PhCN.

Diffraction grade single crystals of the supramolecular complex **1-Zn<sup>4-</sup>/(2-Zn<sup>2+</sup>)<sub>2</sub>** suitable for X-ray analysis were obtained by layering an MeCN solution of **1-Zn•4TBA** onto a THF solution of **2-Zn•2ClO<sub>4</sub>** and allowing the solutions to diffuse slowly over several weeks. The resulting structure revealed a 2:1 complex in a slipped-sandwich arrangement (Figure 6).<sup>29</sup> The observed structure is consistent with the presence of electrostatic interactions between the positively charged dithio lidinium rings in **2-Zn<sup>2+</sup>** and the negative charged O-atom of the sulfonate groups in **1-Zn<sup>4-</sup>**. There is no evidence of a significant contribution to the binding from  $\pi$ - $\pi$  donor-acceptor interactions between porphyrin rings or from coordination of the sulfonate anions to the zinc-centers. The crystal lattice was characterized by an absence of external counter ions, as expected for an electronically neutral 1:2 supramolecular complex.

In order to gain insight into the electronic structure of the complex, the molecular orbital distributions (*e.g.*, HOMO and LUMO) were analyzed by single point HF/LanL2DZ calculations on the basis of the crystal structure. The electron density of the HOMO is fully localized on the **1-Zn<sup>4-</sup>** moiety, whereas the LUMO are distributed among the **2-Zn<sup>2+</sup>** groups (Figure 7). The intermolecular dipolar charge transfer character of the **1-Zn<sup>4-</sup>/(2-Zn<sup>2+</sup>)** ensemble supports the assertion that photoinduced charge transfer involves both the **1-Zn<sup>4-</sup>** donating electron density and the **2-Zn<sup>2+</sup>** acceptor moieties.

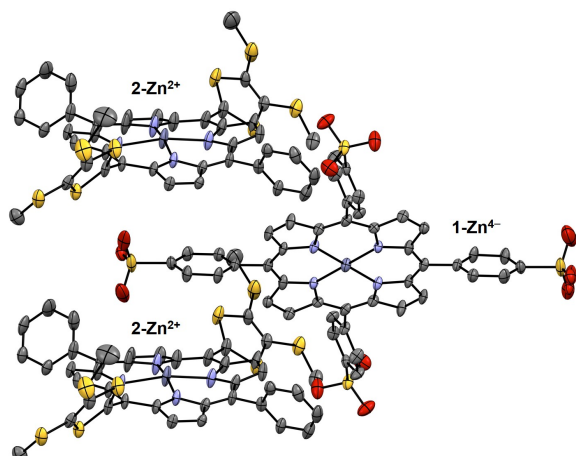


**Figure 6.** X-ray crystal structure of the supramolecular complex **1-Zn<sup>4-</sup>/(2-Zn<sup>2+</sup>)<sub>2</sub>**. Thermal ellipsoids are scaled to the 50% level. Hydrogen atoms and solvent molecules are omitted for clarity.

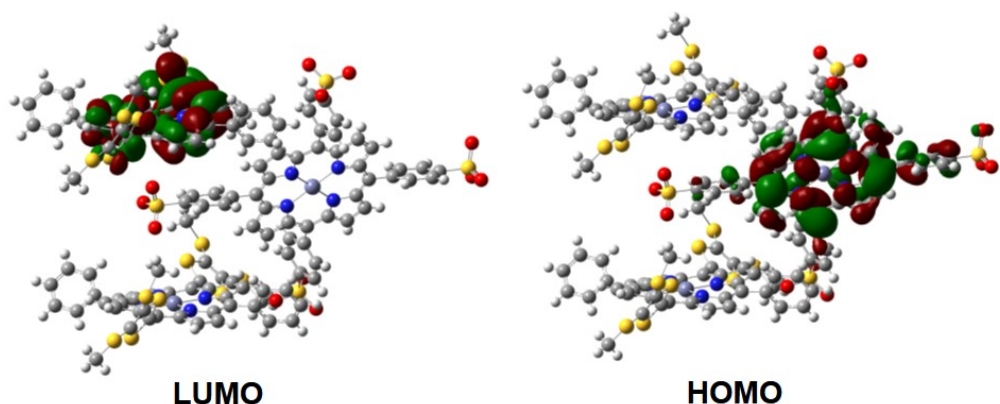


**Figure 7.** Molecular orbital distributions of the supramolecular complex of **1-Zn<sup>4-</sup>/(2-Zn<sup>2+</sup>)<sub>2</sub>** analyzed by HF/LanL2DZ calculations based on the crystal structure.

**Redox Potentials.** Electrochemical studies, carried out using cyclic and differential pulse voltammetric (CV and DPV, respectively) methods, were performed to determine the redox potentials of the supramolecular complexes (Figure 8). For **2-Zn**•2ClO<sub>4</sub> a two-electron reduction process is observed at 0.21 V vs SCE in PhCN. This value matches that previously reported for the oxidation of a neutral analogue of **2-Zn**<sup>2+</sup> in PhCN.<sup>16</sup> In the supramolecular complexes, the two-electron reduction waves of **2-Zn**<sup>2+</sup> become quasi-reversible and a slight shift in the halfwave potentials is seen (to 0.17 V vs SCE for **1-H<sub>2</sub>**<sup>4-</sup>/(**2-Zn**<sup>2+</sup>)<sub>2</sub> and 0.19 V for **1-Zn**<sup>4-</sup>/(**2-Zn**<sup>2+</sup>)<sub>2</sub>). The one-electron oxidation peaks of the sulphonated porphyrins, observed at 0.99 V and 0.69 V (vs SCE, as estimated by DPV), are also shifted in the ensemble in comparison with those of free **1-H<sub>2</sub>**<sup>4-</sup> and **1-Zn**<sup>4-</sup>, respectively. Based on these redox potentials, the thermodynamic CS energies were determined to be 0.82 eV for **1-H<sub>2</sub>**<sup>4-</sup>/(**2-Zn**<sup>2+</sup>)<sub>2</sub> and 0.50 eV for **1-Zn**<sup>4-</sup>/(**2-Zn**<sup>2+</sup>)<sub>2</sub>. The energy of the triplet and singlet excited states of **1-H<sub>2</sub>** (<sup>1</sup>[**1-H<sub>2</sub>**<sup>4-</sup>]<sup>\*</sup> (1.80 eV), <sup>3</sup>[**1-H<sub>2</sub>**<sup>4-</sup>]<sup>\*</sup> (1.48 eV) and **1-Zn** (<sup>1</sup>[**1-Zn**<sup>4-</sup>]<sup>\*</sup> (2.05 eV) and <sup>3</sup>[**1-Zn**<sup>4-</sup>]<sup>\*</sup> (1.43 eV) are all greater than the thermodynamic CS state energy of the complexes. This provides support for the suggestion that photoinduced electron transfer processes from the excited states will be exergonic in the supramolecular complexes **1-H<sub>2</sub>**<sup>4-</sup>/(**2-Zn**<sup>2+</sup>)<sub>2</sub> and **1-Zn**<sup>4-</sup>/(**2-Zn**<sup>2+</sup>)<sub>2</sub>. The energy diagram for photoinduced electron transfer in **1-M**<sup>4-</sup>/(**2-Zn**<sup>2+</sup>)<sub>2</sub> is shown in Scheme 2.

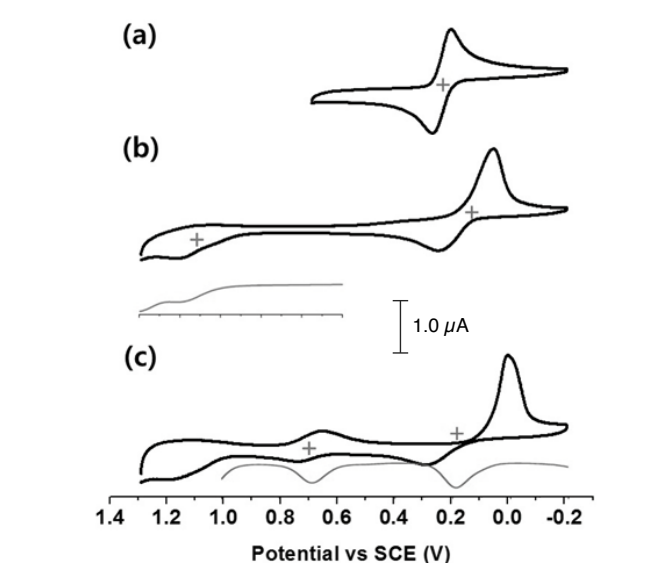
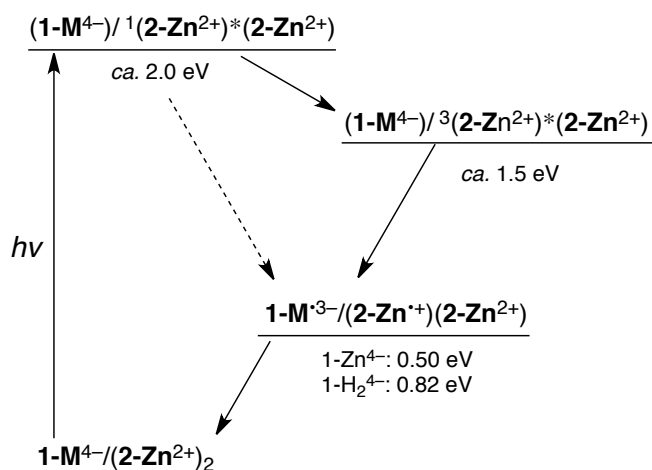


**Figure 8.** Cyclic voltammetric (CV) and differential pulse voltammetric (DPV) curves derived from electrochemical studies of (a) a 2.0 mM solution of **2-Zn**•2ClO<sub>4</sub>, (b) a mixture of a 2.0 mM solution of **2-Zn**•2ClO<sub>4</sub> and a 1.0 mM solution of and **1-H<sub>2</sub>**•4TBA (c) a mixture of a 2.0 mM solution of **2-Zn**•2ClO<sub>4</sub> and a 1.0 mM solution of **1-Zn**•4TBA. All spectra were performed in PhCN containing 0.1 M TBAPF<sub>6</sub> as a supporting electrolyte.

**Photodynamics.** The dynamics of the photoinduced excited state of  $\mathbf{1}\text{-M}^{4-}/(2\text{-Zn}^{2+})_2$  ( $\text{M} = \text{H}_2$  and  $\text{Zn}$ ) were examined by laser flash photolysis. Upon femtosecond photoexcitation of  $\mathbf{1}\text{-H}_2^{4-}/(2\text{-Zn}^{2+})_2$  at 400 nm, fast energy transfer from the  $\text{S}_2$  excited state of the  $\mathbf{1}\text{-H}_2^{4-}$  moiety to the previously characterized  $\text{S}_1$  excited state of  $\mathbf{2}\text{-Zn}^{2+}$  is observed with a rate constant of  $1.7 \times 10^{10} \text{ s}^{-1}$  (Figure 9a).<sup>30</sup> This is followed by intersystem crossing to populate the triplet excited state,  ${}^3[\mathbf{2}\text{-Zn}^{2+}]^*$ , a process that occurs with a rate constant of  $7.1 \times 10^8 \text{ s}^{-1}$ . Similar transient absorption changes were observed for the supramolecular ensemble containing  $\mathbf{1}\text{-H}_2^{4-}$  (*cf.* Figure 10). Thus, no electron transfer occurs from the singlet excited state of  $\mathbf{2}\text{-Zn}^{2+}$  to  $\mathbf{1}\text{-H}_2^{4-}$  in competition with intersystem crossing to the triplet excited state. This absence of ET holds in spite of the large driving force for electron transfer (*ca.* 1.5 and 1.2 eV for  $\mathbf{1}\text{-Zn}^{4-}/(2\text{-Zn}^{2+})_2$  and  $\mathbf{1}\text{-H}_2^{4-}/(2\text{-Zn}^{2+})_2$ , respectively). The much slower rate of electron transfer as compared to intersystem crossing may reflect the relatively small orbital interactions between the  $\mathbf{1}\text{-H}_2^{4-}$  and  $\mathbf{2}\text{-Zn}^{2+}$  moieties present in the complex. This observation is ascribed to the slipped-sandwich arrangement between the porphyrin components (Figure 6), which precludes  $\pi$ - $\pi$  interactions between the donor and acceptors that make up the complex. The transient absorption spectra obtained by nanosecond laser flash photolysis were consistent with photoinduced electron transfer from  $\mathbf{1}\text{-H}_2^{4-}$  to  $\mathbf{2}\text{-Zn}^{2+}$  (Figure 11a). For instance, a sharp absorption band at 870 nm, diagnostic of  $[\mathbf{2}\text{-Zn}^{+}]^{16}$  is seen. A faint absorption band originating from the radical trianion,  $(\mathbf{1}\text{-H}_2)^{3-}$ , around 550 nm is also observed, although the absorption from the latter species overlaps with some of the absorption features from  $\mathbf{2}\text{-Zn}^{+}$ .<sup>31</sup> Based on the time course associated with the evolution of the spectral features, electron transfer from  $\mathbf{1}\text{-H}_2^{4-}$  to  ${}^3[\mathbf{2}\text{-Zn}^{2+}]^*$  is thought to occur within 3 ns and 1  $\mu\text{s}$ .



**Scheme 2** Energy Diagram for the Supramolecular Complex  $\mathbf{1}\text{-M}^{4-}/(2\text{-Zn}^{2+})_2$

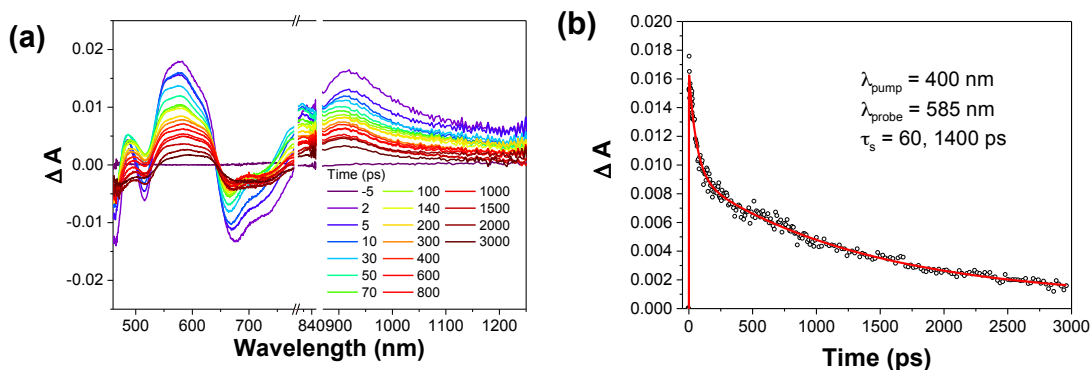


**Figure 9.** (a) Femtosecond transient absorption spectra of the supramolecular ensemble  $\mathbf{1}\text{-H}_2^{4-}/(\mathbf{2}\text{-Zn}^{2+})_2$ . The spectra were recorded *in situ* in deaerated PhCN at 298 K following laser photoexcitation at 400 nm. (b) Time profile of the spectral traces in (a) at 585 nm.

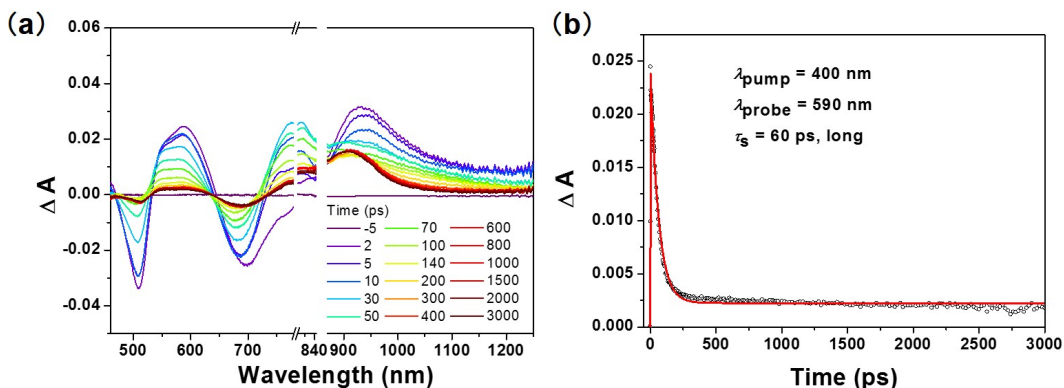


**Figure 10.** (a) Femtosecond transient absorption spectra of the  $\mathbf{1}\text{-Zn}^{4-}/(\mathbf{2}\text{-Zn}^{2+})_2$  complex generated *in situ* in deaerated PhCN at 298 K recorded after laser excitation at 400 nm. (b) Time profile of the spectral trace at 585 nm.

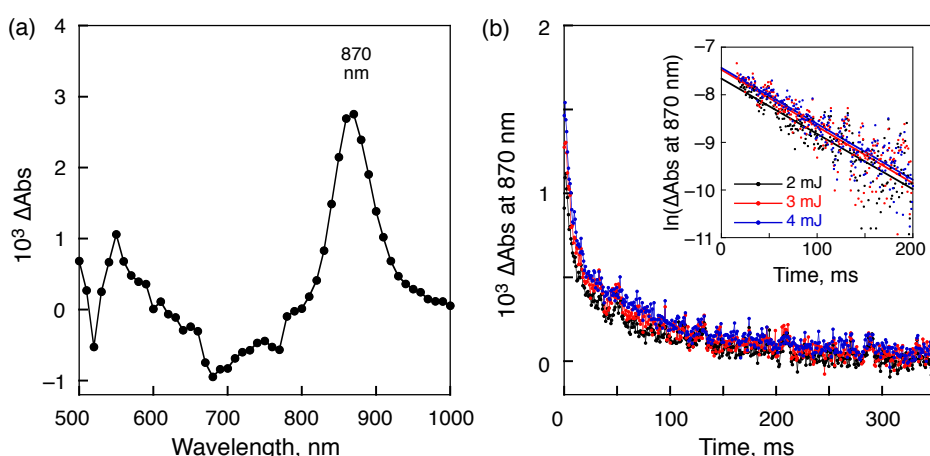


**Figure 11.** (a) Transient absorption spectra of the  $\mathbf{1}\text{-H}_2^{4-}/(\mathbf{2}\text{-Zn}^{2+})_2$  complex recorded at 1.0 ms after nanosecond laser excitation at 430 nm.  $[\mathbf{1}\text{-H}_2\bullet\text{4TBA}] = 2.0 \times 10^{-6} \text{ M}$ ,  $[\mathbf{2}\text{-Zn}\bullet\text{2ClO}_4] = 4.0 \times 10^{-6} \text{ M}$ . (b) Decay time profiles corresponding to the change in absorbance at 870 nm recorded using various laser intensities (2–4 mJ/pulse). Inset: First-order plots.

**Table 1.** Summary of CS lifetimes and rate constants for charge recombination (CR) for the supramolecular complexes

complex <sup>a</sup>	$\tau_{\text{CS}},^b$ ms	$k_{\text{CR}},^c$ s <sup>-1</sup>			$\lambda_{\text{probe}},^d$ nm
		2 mJ	3 mJ	4 mJ	
<b>1-Zn<sup>4-</sup>/(2-Zn<sup>2+</sup>)<sub>2</sub></b>	43	23	23	23	870
<b>1-H<sub>2</sub><sup>4-</sup>/(2-Zn<sup>2+</sup>)<sub>2</sub></b>	83	12	12	12	870

<sup>a</sup> Generated *in situ* in PhCN. <sup>b</sup> CS lifetime determined by ns-transient absorption spectroscopy with 4 mJ pulse<sup>-1</sup> laser power. <sup>c</sup> Rate constants of CR determined at different laser intensities. <sup>d</sup> Wavelength probed at the excited state absorption band.

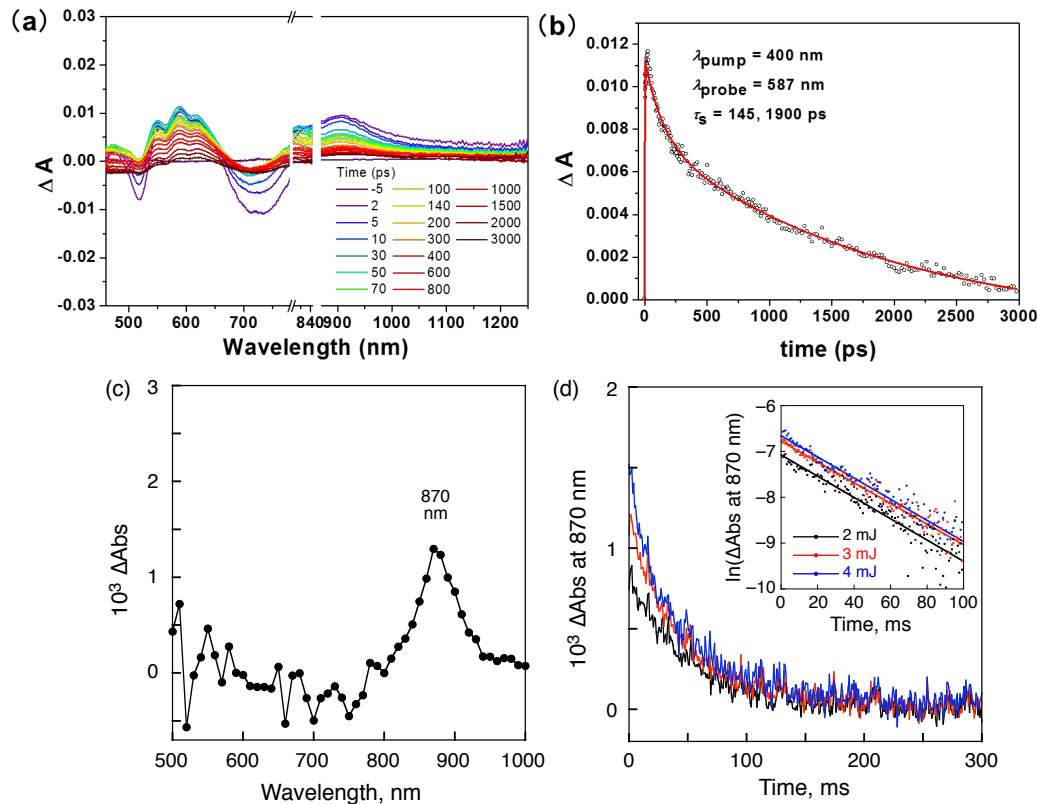


**Figure 11.** (a) Femtosecond transient absorption spectra of the **1-Zn<sup>4-</sup>/(2-Zn<sup>2+</sup>)<sub>2</sub>** complex generated *in situ* in deaerated PhCN at 298 K recorded after laser excitation at 400 nm. (b) Time profile of the spectral trace at 585 nm. (c) Nanosecond transient absorption spectrum of **1-Zn<sup>4-</sup>/(2-Zn<sup>2+</sup>)<sub>2</sub>** complex generated *in situ* in deaerated PhCN at 298 K measured at 1 ms after laser excitation at 400 nm. (d) Decay time profiles of absorbance at 870 nm; inset indicates the first-order plots with various laser power excitation (2-4 mJ).

This conclusion is based on the observation that the spectral features assigned to CS state were not evident at 3 ns, but present at 1  $\mu$ s. The transient absorption signals associated with

the CS state proved surprisingly persistent. The decay of the CS state obeys first-order kinetics and the slope of the first-order plots proved invariant to laser intensity and therefore the concentration of the photoinduced CS state. I take this as an indication that the charge recombination occurs within the supramolecular complex and there is no contribution from intermolecular charge recombination between supramolecular complexes. Such findings are consistent with our design expectations, namely that intermolecular charge recombination processes are attenuated as the result of electrostatic repulsion. Presumably, the two positively charged moieties, **2-Zn**<sup>2+</sup> and **2-Zn**<sup>+</sup>, between which the radical trianionic porphyrin **1-M**<sup>3-</sup> is sandwiched, provide a positively charged buffer layer that prevents close contacts with either another supramolecular ensemble or a free electron donor moiety (*i.e.*, **2-Zn**<sup>+</sup>). The first-order decay rate constant,  $k_{\text{CS}}$  of the CS state, **1-H<sub>2</sub>**<sup>3-</sup>/**(2-Zn**<sup>+</sup>**)(2-Zn**<sup>2+</sup>**)**, was determined to be 12 s<sup>-1</sup> (Table 1). This corresponds to a CS lifetime,  $\tau_{\text{CS}}$  of 83 ms. Similar measurements performed on the supramolecular complex **1-Zn**<sup>4-</sup>/**(2-Zn**<sup>2+</sup>**)**<sub>2</sub> also afforded millisecond long CS states (*i.e.*,  $\tau = 43$  ms) (Figure 11). No evidence of a bimolecular decay process was seen.

According to the Marcus theory of non-adiabatic electron transfer, the temperature dependence of the first-order rate constant of electron transfer ( $k_{\text{ET}}$ ) is given by eq 6,

$$\ln(k_{\text{ET}}T^{1/2}) = \ln\left(\frac{2\pi^{3/2}V^2}{h(\lambda k_B)^{1/2}}\right) - \frac{(\Delta G_{\text{ET}} + \lambda)^2}{4\lambda k_B T} \quad (6)$$

where  $T$  is the absolute temperature,  $V$  is the electronic coupling constant,  $\lambda$  is the reorganization energy,  $\Delta G_{\text{ET}}$  is the Gibbs free energy change of electron transfer,  $k_B$  is the

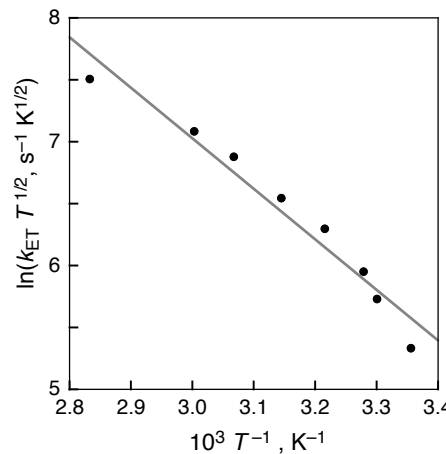


**Figure 13.** Plot of  $\ln(k_{\text{ET}} T^{1/2})$  vs  $T^{-1}$  for the charge recombination in **1-H<sub>2</sub>**<sup>3-</sup>/**(2-Zn**<sup>+</sup>**)(2-Zn**<sup>2+</sup>**)** in PhCN.

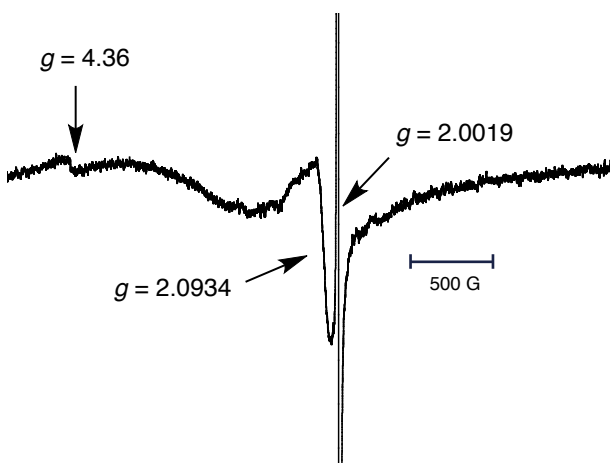


**Figure 14.** EPR spectrum of the CS state of  $\mathbf{1}\text{-H}_2^{4-}/(2\text{-Zn}^{2+})_2$  complex in PhCN generated via photoirradiation with a high-pressure Hg lamp (1000 W) at 4 K.

Boltzmann constant, and  $h$  is the Planck constant.<sup>32</sup> The temperature dependence of intramolecular back electron transfer in the CS state of the supramolecular complex  $[\mathbf{1}\text{-H}_2^{\cdot-}/(2\text{-Zn}^{\cdot+})(2\text{-Zn}^{2+})]$  was examined by nanosecond laser flash photolysis at 25–80 °C. A linear plot of  $\ln(k_{\text{ET}}T^{1/2})$  vs  $T^{-1}$  (Figure 13) in accordance with eq 6 afforded the  $\lambda$  and  $V$  values from the slope and intercept as 0.24 eV and 0.16 cm<sup>-1</sup>, respectively. The small  $V$  value results from the spin-forbidden back electron transfer of the triplet CS state and small orbital interactions between  $\mathbf{1}\text{-H}_2^{4-}$  and  $\mathbf{2}\text{-Zn}^{2+}$  moieties arising from the slipped-sandwich arrangement (Figure 6).

The CS states of the supramolecular ensembles  $\mathbf{1}\text{-M}^{4-}/(2\text{-Zn}^{2+})_2$  ( $\text{M} = \text{H}_2$  and Zn) were observed by EPR measurements at 4 K upon subjecting a PhCN glass to photoirradiation with a high pressure Hg lamp (Figure 14). EPR signals, containing broad shoulders, were observed at  $g = 2.0019$  and  $2.0934$ , respectively. This mixture of signals is as expected for a CS ensemble containing a sulphonated porphyrin radical trianion ( $g = 2.002$ )<sup>12d</sup> and a radical cation of a porphyrin-bridged TTF ( $g = 2.0036$ ).<sup>16</sup> A characteristic triplet signal was observed at  $g = 4.36$ .<sup>33</sup> Considering the MO electron distribution (Figure 7), the triplet signal leads me to suggest that a small electronic coupling between the spatially separated donor and acceptor moieties in the ensemble may be required to achieve a long-lived CS state.<sup>34</sup>

## Conclusion

In summary, I have constructed two related supramolecular donor-acceptor ensembles, namely  $\mathbf{1}\text{-H}_2^{4-}/(2\text{-Zn}^{2+})_2$  and  $\mathbf{1}\text{-Zn}^{4-}/(2\text{-Zn}^{2+})_2$ . These 1:2 complexes are formed in PhCN via

electrostatic interactions involving tetraanionic porphyrins and dication porphyrin-bridged TTF moieties. Upon photoexcitation of the supramolecular complexes, efficient photoinduced electron transfer from **1-M**<sup>4-</sup> to **2-Zn**<sup>2+</sup> occurs. The associated triplet CS states were found to be persistent on the order of milliseconds (e.g., up to 83 ms). This relatively long CS state lifetime is ascribed to the positively charged **2-Zn**<sup>2+</sup> species that flank the faces of **1-M**<sup>4-</sup> and which preclude contacts with other potential donors, such as free **2-Zn**<sup>2+</sup> or an intact three-component ensemble. The present study thus illustrates a new, supramolecular-based approach to creating long-lived CS states.

## References

- (1) (a) *The Photosynthetic Reaction Center*, ed. Deisenhofer, J.; Norris, J. R. Academic Press, San Diego, 1993. (b) *Molecular Level Artificial Photosynthetic Materials*, ed. Meyer, G. J. Wiley, New York, 1997.
- (2) (a) Frey, J.; Kodis, G.; Straight, S. D.; Moore, T. A.; Moore, A. L.; Gust, D. *J. Phys. Chem. A* **2013**, *117*, 607–615. (b) Gust, D.; Moore, T. A.; Moore, A. L. *Acc. Chem. Res.* **1993**, *26*, 198–205. (c) Gust, D.; Moore, T. A.; Moore, A. L. *Acc. Chem. Res.* **2009**, *42*, 1890–1898.
- (3) (a) Ricks, A. B.; Brown, K. E.; Wenninger, M.; Karlen, S. D.; Berlin, Y. A.; Co, D. T.; Wasielewski, M. R. *J. Am. Chem. Soc.* **2012**, *134*, 4581–4588. (b) Gunderson, V. L.; Smeigh, A. L.; Kim, C. H.; Co, D. T.; Wasielewski, M. R. *J. Am. Chem. Soc.* **2012**, *134*, 4363–4372. (c) Lewis, F. D.; Letsinger, R. L.; Wasielewski, M. R. *Acc. Chem. Res.* **2001**, *34*, 159–170. (d) Wasielewski, M. R. *Acc. Chem. Res.* **2009**, *42*, 1910–1921.
- (4) (a) Balzani, V. *Coord. Chem. Rev.* **2001**, *219–221*, 545–572. (b) (d) Faiz, J. A.; Heitz, V.; Sauvage, J.-P. *Chem. Soc. Rev.* **2009**, *38*, 422–442.
- (5) (a) Fukuzumi, S. *Org. Biomol. Chem.* **2003**, *1*, 609–620. (b) Fukuzumi, S. *Phys. Chem. Chem. Phys.* **2008**, *10*, 2283–2297. (c) Fukuzumi, S. *Bull. Chem. Soc. Jpn.* **2006**, *79*, 177–195. (d) Fukuzumi, S.; Kojima, T. *J. Mater. Chem.* **2008**, *18*, 1427–1439. (e) Fukuzumi, S.; Honda, T.; Ohkubo, K.; Kojima, T. *Dalton Trans.* **2009**, 3880–3889. (f) Ohkubo, K.; Fukuzumi, S. *J. Porphyrins Phthalocyanines* **2008**, *12*, 993–1004.
- (6) (a) Guldi, D. M.; Sgobba, V. *Chem. Commun.* **2011**, *47*, 606–610. (b) Guldi, D. M.; Rahman, G. M. A.; Sgobba, V.; Ehli, C. *Chem. Soc. Rev.* **2006**, *35*, 471–487. (c) Bottari, G.; de la Torre, G.; Guldi, D. M.; Torres, T. *Chem. Rev.* **2010**, *110*, 6768–6816. (d)

Martín, N.; Sánchez, L.; Herranz, M. A.; Illescas, B.; Guldi, D. M. *Acc. Chem. Res.* **2007**, *40*, 1015–1024.

(7) (a) Imahori, H.; Sekiguchi, Y.; Kashiwagi, Y.; Sato, T.; Araki, Y.; Ito, O.; Yamada, H.; Fukuzumi, S. *Chem.–Eur. J.* **2004**, *10*, 3184–3196. (b) Imahori, H.; Sekiguchi, Y.; Kashiwagi, Y.; Sato, T.; Araki, Y.; Ito, O.; Yamada, H.; Fukuzumi, S. *Chem.–Eur. J.* **2004**, *10*, 3184–3196. (c) Guldi, D. M.; Imahori, H.; Tamaki, K.; Kashiwagi, Y.; Yamada, H.; Sakata, Y.; Fukuzumi, S. *J. Phys. Chem. A* **2004**, *108*, 541–548.

(8) (a) Fukuzumi, S.; Kotani, H.; Ohkubo, K.; Ogo, S.; Tkachenko, N. V.; Lemmetyinen, H. *J. Am. Chem. Soc.* **2004**, *126*, 1600–1601. (b) Ohkubo, K.; Kotani, H.; Fukuzumi, S. *Chem. Commun.* **2005**, 4520–4522. (c) Fukuzumi, S.; Kotani, H.; Ohkubo, K. *Phys. Chem. Chem. Phys.* **2008**, *10*, 5159–5162.

(9) (a) Murakami, M.; Ohkubo, K.; Fukuzumi, S. *Chem.–Eur. J.* **2010**, *16*, 7820–7832. (b) Murakami, M.; Ohkubo, K.; Nanjo, T.; Souma, K.; Suzuki, N.; Fukuzumi, S. *ChemPhysChem* **2010**, *11*, 2594–2605.

(10) Fukuzumi, S.; Doi, K.; Itoh, A.; Suenobu, T.; Ohkubo, K.; Yamada, Y.; Karlin, K. D. *Proc. Natl. Acad. Sci. U. S. A.* **2012**, *109*, 15572–15577.

(11) (a) D’Souza, F.; Ito, O. *Chem. Commun.* **2009**, 4913–4928. (b) Fukuzumi, S.; Saito, K.; Ohkubo, K.; Khouri, T.; Kashiwagi, Y.; Absalom, M. A.; Gadde, S.; D’Souza, F.; Araki, Y.; Ito, O. Crossley, M. J. *Chem. Commun.* **2011**, *47*, 7980–7982. (c) Sessler, J. L.; Karnas, E.; Kim, S. K.; Ou, Z.; Zhang, M.; Kadish, K. M.; Ohkubo, K.; Fukuzumi, S. *J. Am. Chem. Soc.* **2008**, *130*, 15256–15257.

(12) (a) Fukuzumi, S.; Ohkubo, K.; D’Souza, F.; Sessler, J. L. *Chem. Commun.* **2012**, *48*, 9801–9815. (b) Fukuzumi, S.; Ohkubo, K. *J. Mater. Chem.* **2012**, *22*, 4575–4587. (c) Kamimura, T.; Ohkubo, K.; Kawashima, Y.; Nobukuni, H.; Naruta, Y.; Tani, F.; Fukuzumi, S. *Chem. Sci.* **2013**, *4*, 1451–1461. (d) Ohkubo, K.; Kawashima, Y.; Fukuzumi, S. *Chem. Commun.* **2012**, *48*, 4314–4316.

(13) Yamada, Y.; Nomura, A.; Ohkubo, K.; Suenobu, T.; Fukuzumi, S. *Chem. Commun.* **2013**, *49*, 5132–5134

(14) Mizoshita, N.; Yamanaka, K.-I.; Shimada, T.; Tani, T.; Inagaki, S. *Chem. Commun.* **2010**, *46*, 9235–9237.

(15) Li, J.; Fang, Y. *Spectrochim. Acta. Mol. Biomol. Spectrosc.* **2007**, *66*, 994–1000.

(16) Bill N. L.; Ishida, M.; Bähring, S.; Lim, J. M.; Lee, S.; Davis, C. M.; Lynch, V. M.; Nielsen, K. A.; Jeppesen, J. O.; Ohkubo, K.; Fukuzumi, S.; Kim, D.; Sessler, J. L. *J. Am.*

---

*Chem. Soc.* **2013**, *135*, 10852–10862.

(17) Mann, C. K.; Barnes, K. K. In *Electrochemical Reactions in Non-aqueous Systems*; Marcel Dekker: New York, 1970.

(18) SAINT V8.27B Bruker AXS Inc, Madison, Wisconsin, 2012.

(19) Altomare, A.; Burla, M. C.; Camalli, M.; Cascarano, G. L.; Giacovazzo, C.; Guagliardi, A.; Moliterni, A. G. G.; Polidori, G.; Spagna, R. *J. Appl. Crystallogr.* **1999**, *32*, 115–119.

(20) Sheldrick, G. M. *Acta Cryst.* **2008**, *A64*, 112–122.

(21) Spek, A. L. *PLATON, A Multipurpose Crystallographic Tool*, Utrecht University, The Netherlands, 1998.

(22) Farrugia, L. J. *J. Appl. Crystallogr.* **1999**, *32*, 837–838.

(23) Sluis, P. v. d.; Spek, A. L. *Acta Cryst.* **1990**, *A46*, 194–201.

(24)  $R_w(F^2) = \{\sum w(|F_o|^2 - |F_c|^2)^2 / \sum w(|F_o|)^4\}^{1/2}$  where w is the weight given each reflection.  $R(F) = \sum (|F_o| - |F_c|) / \sum (|F_o|)$  for reflections with  $F_o > 4(\sigma(F_o))$ .  $S = [\sum w((|F_o|^2 - |F_c|^2)^2 / (n - p))]^{1/2}$ , where n is the number of reflections and p is the number of refined parameters.

(25) *International Tables for X-ray Crystallography*; Wilson, A. J. C., Ed.; Kluwer Academic Press: Boston, 1992; Vol. C, Tables 4.2.6.8 and 6.1.1.4.

(26) Sheldrick, G. M. *SHELXTL/PC (Version 5.03)*; Siemens Analytical X-ray Instruments, Inc.: Madison; WI, 1994.

(27) *Gaussian 09*, Revision A.1, M. J. Frisch, G. W. Trucks, H. B. Schlegel, G. E. Scuseria, M. A. Robb, J. R. Cheeseman, G. Scalmani, V. Barone, B. Mennucci, G. A. Petersson, H. Nakatsuji, M. Caricato, X. Li, H. P. Hratchian, A. F. Izmaylov, J. Bloino, G. Zheng, J. L. Sonnenberg, M. Hada, M. Ehara, K. Toyota, R. Fukuda, J. Hasegawa, M. Ishida, T. Nakajima, Y. Honda, O. Kitao, H. Nakai, T. Vreven, J. A. Montgomery, Jr., J. E. Peralta, F. Ogliaro, M. Bearpark, J. J. Heyd, E. Brothers, K. N. Kudin, V. N. Staroverov, R. Kobayashi, J. Normand, K. Raghavachari, A. Rendell, J. C. Burant, S. S. Iyengar, J. Tomasi, M. Cossi, N. Rega, N. J. Millam, M. Klene, J. E. Knox, J. B. Cross, V. Bakken, C. Adamo, J. Jaramillo, R. Gomperts, R. E. Stratmann, O. Yazyev, A. J. Austin, R. Cammi, C. Pomelli, J. W. Ochterski, R. L. Martin, K. Morokuma, V. G. Zakrzewski, G. A. Voth, P. Salvador, J. J. Dannenberg, S. Dapprich, A. D. Daniels, Ö. Farkas, J. B. Foresman, J. V. Ortiz, J. Cioslowski and D. J. Fox Gaussian, Inc., Wallingford CT, 2009.

(28) Meaningful  $^1\text{H}$  NMR spectroscopic analyses in less polar solvents were precluded by the lack of requisite solubility.

(29) See the details of the X-ray experiments in SI.

- (30) The excited state dynamics of **2-Zn**<sup>2+</sup> were also analyzed by fs-TA data; see Figure 11.
- (31) The reference spectrum of radical cation species of **2-Zn** generated by thermal electron transfer with Li<sup>+</sup>-encapsulated fullerene (Li<sup>+</sup>@C<sub>60</sub>) was reported in ref 16; the  $\lambda_{\text{max}}$  is at 876 nm.

## Supporting Information for Chapter 9

**Derivation of the Equilibrium Constants Used to Determine the Binding Affinity of the Supramolecular Complexes.**

**UV-Vis Absorption Spectroscopy,  $[1\text{-Zn}^{2+}]$  is fixed:**

$$K = [1\text{-M}^{4-}/(2\text{-Zn}^{2+})_2]/([2\text{-Zn}^{2+}]^2[1\text{-M}^{4-}]) \quad (1)$$

$$\begin{aligned} [1\text{-M}^{4-}/(2\text{-Zn}^{2+})_2] &= K([2\text{-Zn}^{2+}]_0 \\ &\quad - 2[1\text{-M}^{4-}/(2\text{-Zn}^{2+})_2])^2([1\text{-M}^{4-}]_0 - [1\text{-M}^{4-}/(2\text{-Zn}^{2+})_2]) \end{aligned} \quad (2)$$

$$\alpha = 2[1\text{-M}^{4-}/(2\text{-Zn}^{2+})_2]/[2\text{-Zn}^{2+}]_0 = (A - A_0) / (A_\infty - A_0) \quad (3)$$

where  $A$ ,  $A_0$  and  $A_\infty$  represent the measured absorbance after the addition of a known aliquot of  $1\text{-M}^{4-}$ , the absorbance of  $2\text{-Zn}^{2+}$  at the start of the titration, and the absorbance of  $1\text{-M}^{4-}/(2\text{-Zn}^{2+})_2$  at the end of the titration when all of the free  $2\text{-Zn}^{2+}$  is bound to form  $1\text{-M}^{4-}/(2\text{-Zn}^{2+})_2$ , respectively.

From eqs 2 and 3, eq 4 is obtained.

$$\alpha = K[2\text{-Zn}^{2+}]_0(1 - \alpha)^2(2[1\text{-M}^{4-}]_0 - \alpha[2\text{-Zn}^{2+}]_0) \quad (4)$$

Eqn (4) is rewritten by eq 5.

$$\alpha/(1 - \alpha)^2 = K[2\text{-Zn}^{2+}]_0 (2[1\text{-M}^{4-}]_0 - \alpha[2\text{-Zn}^{2+}]_0) \quad (5)$$

Thus, a plot of  $\alpha/(1 - \alpha)^2$  vs  $2[1\text{-M}^{4-}]_0 - \alpha[2\text{-Zn}^{2+}]_0$  gives a linear correlation and from the slope  $K$  ( $\text{M}^{-2}$ ) can be determined.

**Fluorescence Spectroscopy,  $[1\text{-M}^{4-}]$  is fixed:**

$$\alpha = [1\text{-M}^{4-}/(2\text{-Zn}^{2+})_2]/[1\text{-M}^{4-}]_0 = (I_0 - I)/I_0 \quad (6)$$

From eqs 2 and 6, eq 7 is obtained.

$$\alpha/(1 - \alpha) = K ([2\text{-Zn}^{2+}]_0 - 2\alpha[1\text{-M}^{4-}]_0)^2 \quad (7)$$

## Supplemental Figures.

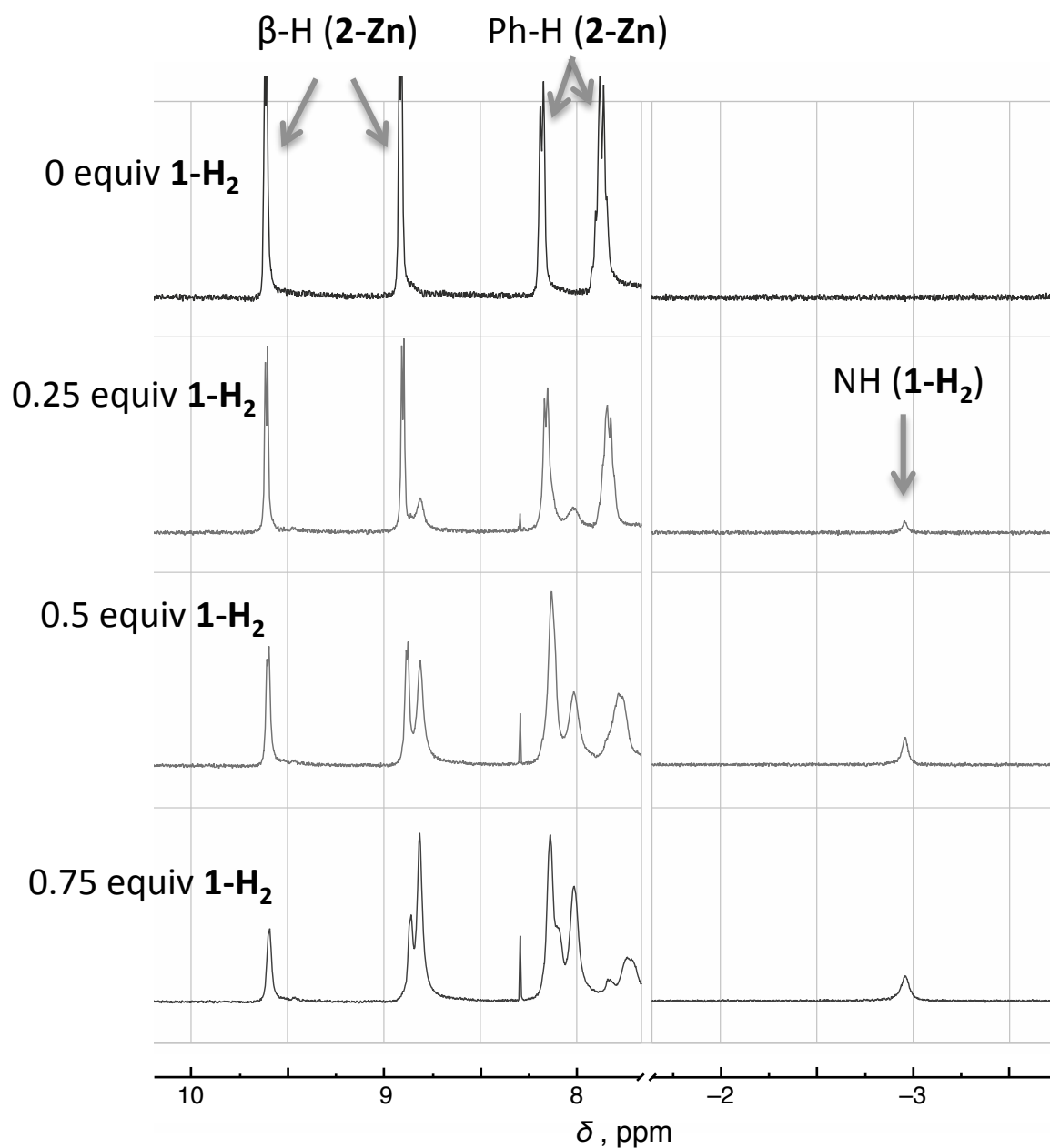


**Figure S1.** Partial  $^1\text{H}$  NMR spectra of  $\mathbf{2}\text{-Zn}\bullet\text{2ClO}_4$  (top, purple) and with increasing amounts of  $\mathbf{1}\text{-H}_2\bullet\text{4TBA}$  recorded in  $\text{DMSO-}d_6$ . In blue (second from top) there are 0.25 molar equiv, in green (third from top) there are 0.5 molar equiv and in red (bottom) there are 0.75 molar equiv of  $\mathbf{1}\text{-H}_2\bullet\text{4TBA}$ .

**Detailed X-ray experimental for  $2[(\text{C}_{42}\text{H}_{30}\text{N}_4\text{S}_8)\text{Zn}(\text{C}_2\text{H}_5\text{OH})] \cdot [(\text{C}_{44}\text{H}_{24}\text{N}_4\text{S}_4\text{O}_{12})\text{Zn}] \cdot 2(\text{C}_2\text{H}_5\text{OH}) \cdot \text{C}_6\text{H}_{14}$ :** Crystals grew as long dark green needles by layering an MeCN solution of **1-Zn•4TBA** onto a THF solution of **2-Zn•(ClO<sub>4</sub>)<sub>2</sub>** with a small amount of MeOH to solubilize the compound. The data crystal was cut from a larger crystal and had approximate dimensions;  $0.65 \times 0.19 \times 0.16$  mm. The data were collected at  $-120$  °C on a Nonius Kappa CCD diffractometer using a Bruker AXS Apex II detector and a graphite monochromator with MoK $\alpha$  radiation ( $\lambda = 0.71075$  Å). Reduced temperatures were maintained by use of an Oxford Cryosystems 600 low-temperature device. A total of 1282 frames of data were collected using  $\theta$ -scans with a scan range of  $1.1^\circ$  and a counting time of 44 seconds per frame. Details of crystal data, data collection and structure refinement are listed in Table S1. Data reduction were performed using SAINT V8.27B.<sup>S1</sup> The structure was solved by direct methods using SIR97<sup>S2</sup> and refined by full-matrix least-squares on  $F^2$  with anisotropic displacement parameters for the non-H atoms using SHELXL-97.<sup>S3</sup> Structure analysis was aided by use of the programs PLATON98<sup>S4</sup> and WinGX.<sup>S5</sup>

Two molecules of solvent, one an ethanol molecule and one a molecule of n-hexane, were badly disordered. Attempts to model the disorder were unsatisfactory. The contributions to the scattering factors due to these solvent molecules were removed by use of the utility SQUEEZE<sup>S6</sup> in PLATON98.

In addition to that described above, one of the SO<sub>3</sub> groups and a coordinated ethanol molecule were also disordered. The disorder was modeled in basically the same fashion for both. For the SO<sub>3</sub> group, the variable x was assigned to the site occupancy factors for one component of the disorder. (1-x) was assigned to the alternate component. The geometry of the two groups was restrained to be approximately equal. A common isotropic displacement parameter was refined for the six oxygen atoms while refining x. The variable x refined to a value very close to 1/2. The site occupancy factors were subsequently fixed at 1/2 for the remainder of the refinement. These oxygen atoms were refined anisotropically with their displacement parameters restrained to be approximately isotropic.

The carbon atoms of the coordinated ethanol molecule were also disordered. The refinement of the disordered resulted in a site occupancy factor of 67(2)% for atoms C1a and C2a. No hydrogen atom was calculated for the oxygen atom of this molecule in the final refinement model.

The function,  $\Sigma w(|F_o|^2 - |F_c|^2)^2$ , was minimized, where  $w = 1/[(\sigma(F_o))^2 + (0.0742*P)^2 + (0.0536*P)]$  and  $P = (|F_o|^2 + |F_c|^2)/3$ .  $R_w(F^2)$  refined to 0.174, with  $R(F)$  equal to 0.0666 and a goodness of fit,  $S$ , = 1.13. Definitions used for calculating  $R(F)$ ,  $R_w(F^2)$  and the goodness of fit,  $S$ , are given in the footnotes below. The data were checked for secondary extinction but no correction was necessary. Neutral atom scattering factors and values used to calculate the linear absorption coefficient are from the International Tables for X-ray Crystallography (1992).<sup>25</sup> All figures were generated using SHELXTL/PC.<sup>S8</sup> Tables of positional and thermal parameters, bond lengths and angles, torsion angles and figures are found in the .cif file uploaded separately.

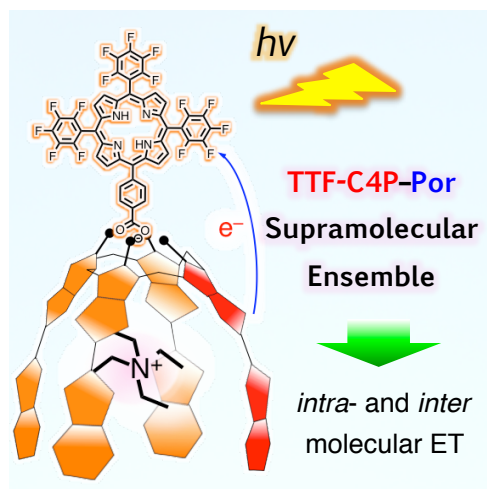
---

**Table S1.** Crystal Data and Structure Refinement for **1-Zn<sup>4-</sup>•(2-Zn<sup>2+</sup>)<sub>2</sub>**

Empirical formula	C140 H116 N12 O15 S20 Zn3	
Formula weight	3043.76	
Temperature	153(2) K	
Wavelength (MoK $\alpha$ )	0.71073 Å	
Crystal system	Triclinic	
Space group	<i>P</i> -1	
Unit cell dimensions	<i>a</i> = 10.7122(5) Å	$\alpha$ = 101.781(3)°.
	<i>b</i> = 16.4862(9) Å	$\beta$ = 102.522(3)°.
	<i>c</i> = 19.4020(10) Å	$\gamma$ = 97.189(4)°.
Volume	3222.6(3) Å <sup>3</sup>	
<i>Z</i>	1	
Density (calculated)	1.568 g cm <sup>-3</sup>	
Absorption coefficient	0.950 mm <sup>-1</sup>	
<i>F</i> (000)	1570	
Crystal size	0.65 × 0.19 × 0.16 mm	
Theta range for data collection	1.11 to 25.00°.	
Index ranges	-12 $\leftarrow$ <i>h</i> $\leftarrow$ 12, -19 $\leftarrow$ <i>k</i> $\leftarrow$ 19, 0 $\leftarrow$ <i>l</i> $\leftarrow$ 23	
Reflections collected	10792	
Independent reflections	10792 [ <i>R</i> (int) = 0.0000]	
Completeness to theta = 25.00°	95.2%	
Absorption correction	Semi-empirical from equivalents	
Max. and min. transmission	1.00 and 0.864	
Refinement method	Full-matrix least-squares on <i>F</i> <sup>2</sup>	
Data / restraints / parameters	10792 / 100 / 846	
Goodness-of-fit on <i>F</i> <sup>2</sup>	1.132	
Final <i>R</i> indices [ <i>I</i> >2σ( <i>I</i> )]	<i>R</i> <sub>1</sub> = 0.0666, <i>wR</i> <sub>2</sub> = 0.1555	
<i>R</i> indices (all data)	<i>R</i> <sub>1</sub> = 0.1322, <i>wR</i> <sub>2</sub> = 0.1738	
Largest diff. peak and hole	2.005 and -1.072 e.Å <sup>-3</sup>	
CCDC 938473.		

## Chapter 10

Photoinduced Electron Transfer  
from a Tetrathiafulvalene-Calix[4]pyrrole  
to a Porphyrin Carboxylate within a Supramolecular Ensemble



**Abstract:** A supramolecular assembly is formed upon mixing millimolar concentrations of a *tetrakis*-tetrathiafulvalene calix[4]pyrrole (TTF-C4P) and a porphyrin tetraethylammonium carboxylate salt in benzonitrile (PhCN). The TTF-C4P binds to the carboxylate moiety of the porphyrin with a 1:1 stoichiometry and a binding constant of  $6.3 \times 10^4 \text{ M}^{-1}$  in this solvent at 298 K. Laser photoexcitation of the supramolecular complex results in formation of the triplet charge-separated (CS) state composed of radical cation of the TTF-C4P and the radical anion of the porphyrin carboxylate. These processes and the resulting states were characterized by means of transient absorption and electron spin resonance (ESR) spectroscopies. The rate constants corresponding to the forward and backward intramolecular electron-transfer (ET) processes were determined to be  $2.1 \times 10^4 \text{ s}^{-1}$  and  $3.6 \times 10^2 \text{ s}^{-1}$ , respectively. The rate constants of intermolecular forward and backward electron-transfer were also determined to be  $4.4 \times 10^8$  and  $9.8 \times 10^8 \text{ M}^{-1} \text{ s}^{-1}$ , respectively. The electronic coupling constant ( $V$ ),  $1.2 \times 10^{-2} \text{ cm}^{-1}$ , and the reorganization energy ( $\lambda$ ), 0.76 eV, for back electron transfer were evaluated from the temperature dependence of the rate constants of intramolecular electron

transfer. The small  $V$  value indicates little spin-forbidden interaction between the highest occupied molecular orbital (HOMO) and the lowest unoccupied molecular orbital (LUMO) and substantiates the long-lived CS lifetime. These results were corroborated by density function theory (DFT) calculations, which provided support for the conclusion that the HOMO and LUMO, located on a TTF moiety of the TTF-C4P and the porphyrin core, respectively, have little interaction through space.

## Introduction

Over the last decade, the need for clean and renewable energy sources has resulted in considerable effort being directed toward the development of systems capable of converting light energy into chemical energy. This has led to important advances in artificial photosynthetic systems and solar cells.<sup>1,2</sup> Part of the appeal of such devices is that they are expected to generate lower levels of greenhouse gasses per unit of energy as compared with processes that rely on fossil fuels, which produce high levels of carbon dioxide and are thus implicated in global climate change.<sup>1,2</sup> Organic solar cells are able to convert solar energy into chemical energy via photon absorption that creates a potential difference in the medium and results in electron transfer (ET).<sup>3–5</sup> The steps involved in the energy conversion processes mediated by solar cells include the creation of an exciton upon photon absorption, separation and diffusion of the exciton, transport of the electron and hole to their respective electrodes, and collection of the charge.<sup>3–5</sup> To achieve efficient charge separation, the rate of back electron transfer must be slower than that of forward electron transfer.<sup>2,6,7</sup> Such dynamics are a hallmark of natural photosynthesis. However, controlling these ET rates and creating a long-lived charge-separated (CS) state is something that has proved difficult to mimic in artificial systems. Developing a simple two component system, or molecular dyad, that undergoes rapid electron transfer and results in a long lifetime could represent an important step forward in the search for organic solar cells that enable efficient solar energy conversion. While tremendous progress has been made along these lines, this is a goal that remains to be achieved in a simple and cost effective manner.<sup>2,8–11</sup> One approach that we find particularly appealing involves the use of self-assembled or noncovalent systems since, in principle, the electronics of the individual components may be tuned and the synthetic investment needed to obtain a functioning charge-separating dyad can be reduced.<sup>12–29</sup>

ET complexes involving TTF moieties and their conjugates have received considerable attention in the past few decades due to the stability of the radical cation and dication formed

upon the first and second oxidation, respectively.<sup>30</sup> The potentials of the first and second oxidations can be fine-tuned by altering the substituents on the TTF backbone.<sup>30</sup> TTF derivatives paired with suitable acceptors have been exploited in non-linear optical arrays,<sup>31</sup> environmentally responsive devices,<sup>32</sup> controlled self-assembled nanostructures,<sup>33</sup> as well as in light harvesting complexes.<sup>34</sup> Calix[4]pyrroles bearing TTF subunits were first reported in 2004 as rationally designed receptors for electron-deficient charge neutral guests,<sup>35</sup> and subsequently were used as colorimetric chemosensors for nitroaromatic explosives,<sup>36</sup> as well as in switchable ET systems that operate under thermal conditions.<sup>37-39</sup> Separate work by Sessler<sup>40,41</sup> and Jeppesen<sup>42,43</sup> resulted in the development of porphyrins with directly annulated TTF subunits. More recently, it proved possible to fuse 1,3-dithio-2-ylidene moieties across a porphyrin core, producing an  $\pi$ -extended TTF mimic whose redox properties can be modulated through anion binding.<sup>44</sup> This allowed thermal electron transfer between the TTF-fused porphyrin analogue and electron deficient species, such as  $\text{Li}^+$  encapsulated in  $\text{C}_{60}$ , to be controlled via appropriately chosen chemical inputs.<sup>44</sup>

These studies provided an incentive to investigate pairing TTF conjugates with porphyrins in systems that would undergo photoinduced ET. This would represent an advance relative to the earlier systems that relied on ground state thermodynamic effects to drive charge separation. In designing such a putative light-driven ET system, I was aware of the fact that calix[4]pyrroles bind anions through hydrogen bonding interactions in aprotic organic media. I therefore chose to use a porphyrin bearing a carboxylate group as the second component in what I expected would be a noncovalent porphyrin-tetrathiafulvalene calix[4]pyrrole electron-transfer complex. This proposed complex formation would allow for the pre-organization of the donor and acceptor species in solution before photoirradiation, with the attendant expectation that photoinduced ET would be facilitated. As detailed below, these design expectations were met. Specifically, I found that when the benzo-annulated tetra-TTF calix[4]pyrrole (**1**) is paired with the tetraethylammonium porphyrin carboxylate (**2**) a supramolecular dyad (complex **4**) is formed.

The carboxylate moiety was chosen as the anion functional group in constructing complex **4** since it is known to bind to the NH protons of the calix[4]pyrrole in a 1:1 fashion, inducing a conformational change from the 1,3-alternate to the cone conformer.<sup>45</sup> Tetraethylammonium ( $\text{TEA}^+$ ) was chosen as the counter cation to the carboxylate moiety as it is known to bind inside the bowl-shaped cavity of the cone conformer of calix[4]pyrroles.<sup>38,46,47</sup> This dual binding to the calix[4]pyrrole, involving both  $\text{TEA}^+$  and the carboxylate moiety, was expected

---

to enhance the interaction between the porphyrin and calix[4]pyrrole and increase the percentage of the supramolecular complex at any given constituent concentration. Porphyrins have been demonstrated to exhibit efficient light absorption properties and have also been found to be electron acceptors in a number of instances;<sup>48–57</sup> however, assemblies in which the final electron acceptor is a neutral, free-base porphyrin rather than a metalated or protonated porphyrin are essentially unknown.

Here, I report formation of a supramolecular complex (**4**) of the benzo-annulated TTF calix[4]pyrrole **1** as an electron donor with porphyrin **2** as an electron acceptor (Chart 1) and the detailed photodynamics as elucidated via femtosecond and nanosecond laser flash photolysis in benzonitrile (PhCN). Photoexcitation of the complex formed between these two components (ensemble **4**) in PhCN at 298 K affords the CS state, which is characterized by forward and backward *intramolecular* ET rate constants of  $2.1 \times 10^4 \text{ s}^{-1}$  and  $3.6 \times 10^2 \text{ s}^{-1}$ , respectively. To the best of my knowledge, the CS state produced as the result of photoinduced ET has the longest lifetime yet reported for any non-covalently bound dyad analyzed in solution at 298 K. Evidence for intermolecular ET is also seen. A unique feature of this system is that the free base porphyrin subunit acts as a photo-acceptor, rather than serving as source of electrons, as is typically the case for dyads based on non-metalated porphyrins.<sup>58–61</sup>

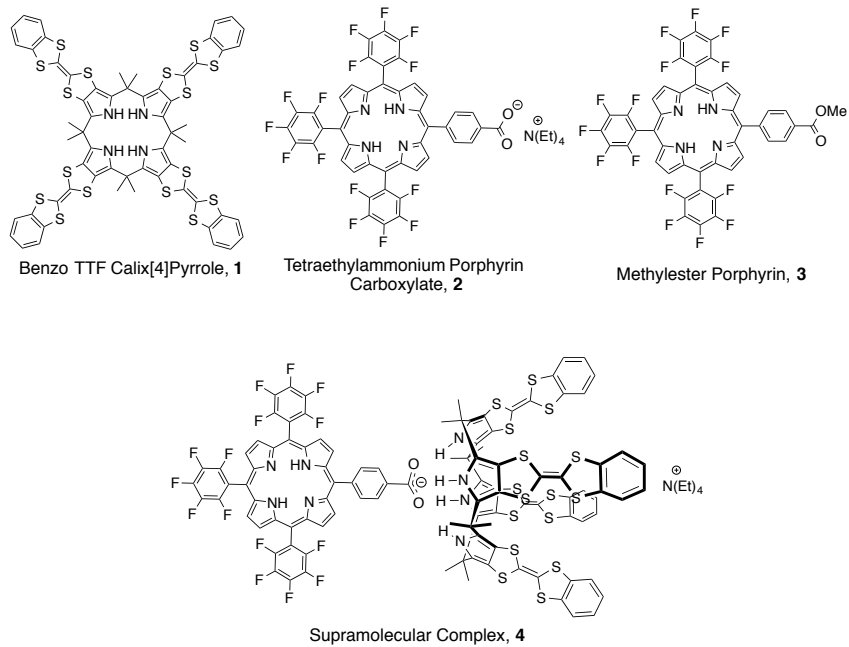


**Chart 1.** Structures of benzo-TTF-calix[4]pyrrole (**1**), tetraethylammonium porphyrin carboxylate (**2**), the methyl ester analogue (**3**), and the supramolecular ensemble produced between **1** and **2** (complex **4**).

## Experimental Section

**Materials.** General chemicals of the best grade available were purchased from commercial suppliers and were used without further purification. Unless otherwise noted, benzonitrile (PhCN) was distilled over phosphorus pentaoxide ( $P_2O_5$ ) before use. Benzo-tetrathiafulvalene calix[4]pyrrole **1** was prepared using literature methods.<sup>36</sup> Porphyrin **3**, prepared using a modification of literature procedures,<sup>62,63</sup> was saponified using sodium hydroxide in aqueous tetrahydrofuran, followed by cation exchange using tetraethylammonium hydroxide to yield the porphyrin carboxylate salt **2**.

**Instruments:**  $^1H$  NMR spectra were recorded on a Varian MR 400 MHz spectrometer in deuterated chloroform. UV–Vis absorption spectra were recorded on a Hewlett Packard 8453 diode array spectrophotometer. Fluorescent spectra were recorded on a Horiba FluoroMax-4 spectrophotometer. ITC measurements were carried out on a VP-ITC MicroCalorimeter in 99% spectroscopic grade PhCN, which was purchased from Acros Organics and used without further purification.

**Electrochemical Measurements.** Cyclic voltammetry (CV) studies were carried out using an ALS-630B electrochemical analyzer in deaerated PhCN containing 0.1 M TBAPF<sub>6</sub> as a supporting electrolyte at 298 K. A conventional three-electrode cell was used with a platinum working electrode (surface area = 0.3 mm<sup>2</sup>) and a platinum wire as the counter electrode. The Pt working electrode, purchased from BAS, was routinely polished with a polishing alumina suspension from BAS and rinsed with distilled water and acetone before use. The potentials were measured with respect to a Ag/AgNO<sub>3</sub> (10 mM) reference electrode. All electrochemical measurements were carried out under a positive argon atmosphere.

**Laser Flash Photolysis Measurements.** The femtosecond time-resolved transient absorption (TA) spectra collected in Seoul were recorded on a spectrometer that consisted of NIR optical parametric amplifier (OPA) system (Quantronix, Pallitra) pumped by a Ti:sapphire regenerative amplifier system (Quantronix, Integra-C) operating at 1 kHz repetition rate and an optical detection system. The generated OPA output signals had a pulse width of ~ 100 fs which were used as pump pulses. White light continuum (WLC) probe pulses were generated using a sapphire window (3 mm of thickness) by focusing of small portion of the fundamental 800 nm pulses. The time delay between pump and probe beams was carefully controlled by making the pump beam travel along a variable optical delay (Newport, ILS250). Intensities of the spectrally dispersed WLC probe pulses are monitored by two miniature spectrographs (Ultrafast systems, High Speed Spectrometers). To obtain the

---

time-resolved transient absorption difference signal ( $\Delta A$ ) at a specific time, the pump pulses were chopped at 500 Hz and absorption spectra intensities were saved alternately with or without pump pulse. Typically, 6000 pulses were used to excite samples so as to obtain the TA spectra at a particular delay time. The polarization angle between pump and probe beam was set at the magic angle ( $54.7^\circ$ ) in order to prevent polarization-dependent signals. Cross-correlation  $fhwm$  in pump-probe experiments was less than 200 fs and chirp of WLC probe pulses was measured to be 800 fs in the 400-1200 nm region. To minimize chirp, all reflection optics in probe beam path and 2 mm path length of quartz cell were used. After the TA experiments, the absorption spectra of all compounds were carefully checked so as to avoid artifacts arising from, *e.g.*, photo-degradation or photo-oxidation of the samples in question. HPLC grade solvents were used in all steady-state and time-resolved spectroscopic studies.

Femtosecond transient absorption spectroscopic experiments done in Osaka were carried out in PhCN using an ultrafast source consisting of an Integra-C (Quantronix Corp.), an optical parametric amplifier, TOPAS (Light Conversion Ltd.), and a commercially available optical detection system, Helios, provided by Ultrafast Systems LLC.

Nanosecond time-resolved transient absorption measurements were carried out with a laser system provided by UNISOKU Co., Ltd. Measurements of nanosecond transient absorption spectra were performed according to the following procedure: A deaerated solution was excited by a Nd:YAG laser (Continuum, SLII-10, 4–6 ns  $fhwm$ ) at  $\lambda = 532$  nm. The photodynamics were monitored by continuous exposure to a xenon lamp (150 W) as a probe light and using a photomultiplier tube (Hamamatsu 2949) as the detector. These measurements were performed in Osaka.

**ESR Spectroscopy.** ESR spectra were recorded on a JEOL X-band spectrometer (JES-RE1XE) with a quartz ESR tube. The ESR spectrum of the putative CS state in frozen PhCN was measured at 4 K using a liquid helium cryostat and 77 K using a liquid nitrogen cryostat under conditions of photoirradiation with a high-pressure mercury lamp (USHIO LIGHTING USH-1005D) focused through a water filter at the sample cell in the ESR cavity. The *g* values were calibrated using an  $Mn^{2+}$  marker.

**Theoretical Calculations.** Density functional theory (DFT) calculations were performed using the Gaussian 09 program<sup>64</sup> suite on a supercomputer (KISTI, IBM). The MO distribution diagram of complex **4**, the complex formed between calix[4]pyrrole **1** and porphyrin **2**, was obtained via the B3LYP method employing 6-31G(d) basis set for all atoms.

## Results and Discussion

**UV–Vis–NIR Absorption Spectral Measurements.** To determine the binding affinity corresponding to the interaction between **1** and **2**, UV–Vis–NIR titrations were performed. The absorption spectra of **1**, **2**, and **3** recorded in PhCN at 298 K are given in Figure 1. Changes in the absorption spectrum of **2** (50  $\mu$ M in PhCN), most notably an increase in absorbance between 700 and 400 nm, were seen upon the addition of **1** (Figure 2). These were quantified and used to determine the binding constant for the binding of the carboxylate moiety of **2** to the NH protons of **1**. It is noteworthy that no charge transfer (CT) band around 700 nm was seen upon the addition of **1** to **2**. I take this as an indication that there are no appreciable electronic interactions between the ground states of porphyrin **2** and calixpyrrole **1**.

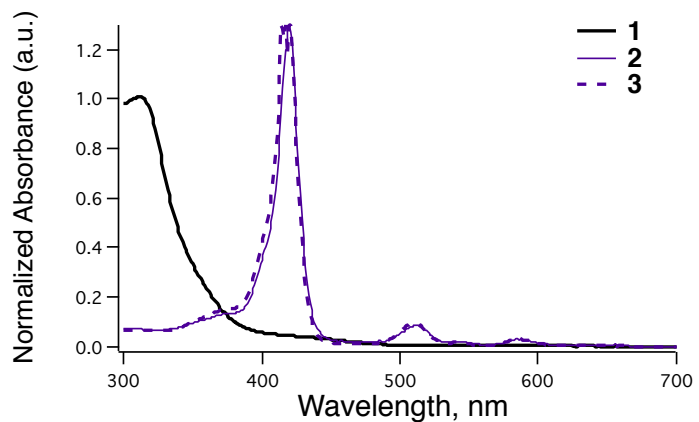


**Figure 1.** Absorption spectra for **1** (black solid), **2** (purple solid), and **3** (purple dashed) as recorded in PhCN at 298 K.

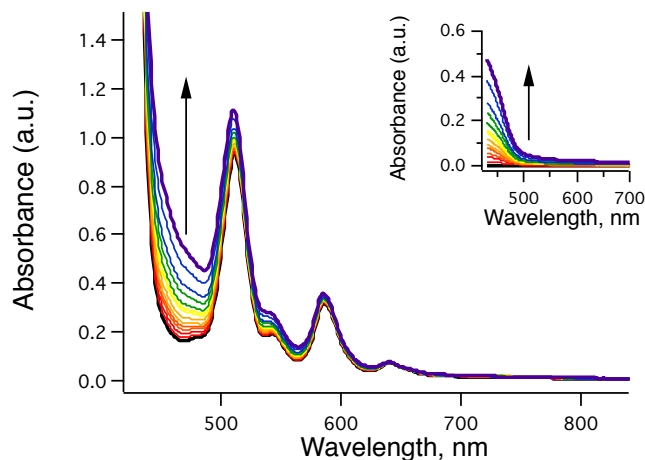


**Figure 2.** Absorbance of **2** (50  $\mu$ M) recorded upon the addition from 0 to 5 equiv of **1** at 298 K in PhCN. Inset: Changes in the absorbance spectrum of **1** as the concentration is increased from 0 to 0.25 mM in PhCN at 298 K.

A plot of the change in absorbance of **2** at 585 nm as a function of the concentration of **1** is given in Figure 3. The absorbance at 585 nm was chosen for this plot due to the minimal absorbance of **1** at this wavelength. In order to account for the residual absorbance of **1**, the absorbance of this calix[4]pyrrole at 585 nm at each indicated concentration was subtracted from the absorbance of the mixture at 585 nm containing this particular concentration of **1**. This correction allowed to monitor quantitatively the absorbance changes that are based solely on binding events.

As a control, a titration using porphyrin **3** in place of **2** was also performed. The change in absorbance of **3** seen upon the addition of **1** after correction for absorbance of **1** is also plotted in Figure 3. No saturation is seen in the titration of porphyrin **3** with **1**. In contrast, saturation behavior is seen when porphyrin **2** was titrated with **1**. This is taken as evidence that binding only occurs when the porphyrin carboxylate anion is employed in conjunction with **1**.

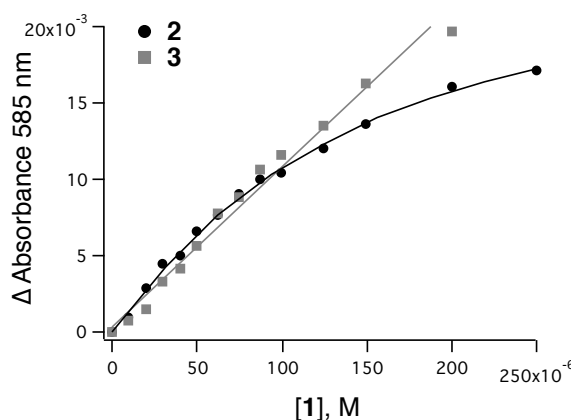


**Figure 3.** Change in absorption of **2** (black dot) and **3** (gray square) at 585 nm seen upon the addition of **1** in PhCN at 298 K. The absorption of **1** in PhCN at 298 K at each of the concentrations in question has been subtracted as noted in the text. Using equations 1 and 2 the binding constant was found to be  $1.1 \times 10^4 \text{ M}^{-1}$  in the case of **1 + 2**.

The formation constant of the complex **4** was found using the following equations:

$$(\alpha^{-1} - 1)^{-1} = K([1] - \alpha[2]_0) \quad (1)$$

$$\alpha = (A - A_0)/(A_\infty - A_0) \quad (2)$$

where  $A$  is the absorbance at a given concentration,  $A_0$  is the initial absorbance,  $A_\infty$  is the estimated absorbance under conditions of complete binding saturation, and  $K$  is the formation constant, which yielded the linear plot (Figure 4).<sup>65</sup> Using this method, the formation constant  $K$  was found to be  $1.1 \times 10^4 \text{ M}^{-1}$ . However, this value may include a large experimental error

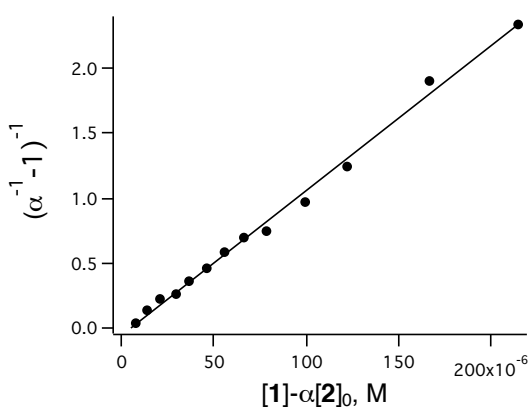


**Figure 4.** Linear plot used to determine binding constant ( $K_a$ ) corresponding to the interaction of **1** with **2**. This plot is based on the observed changes in absorption as detailed in the text. The slope ( $K_a$ ) is  $11,000 \pm 240$  with an  $R^2$  value of 0.99484. (Note:  $A_\infty$  was set to  $2.45 \times 10^{-2}$ ; see main text for definitions.)

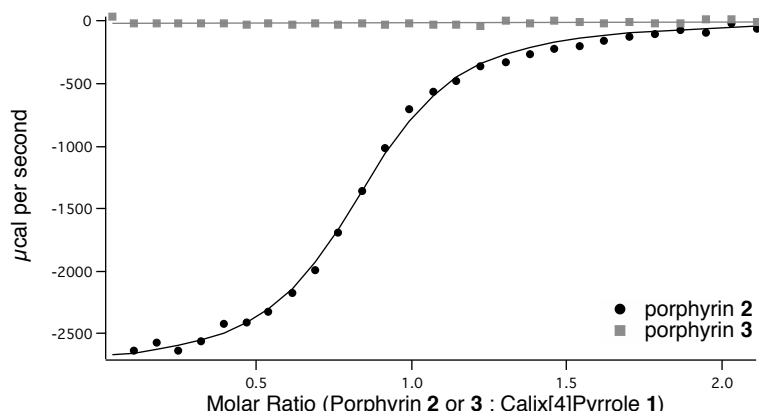


**Figure 5.** Isothermal titration calorimetry data for the addition of porphyrin **2** (5 mM, black dot) and porphyrin **3** (5 mM, gray square) into a PhCN solution of calix[4]pyrrole **1** (0.5 mM) at 298 K. Data is plotted as molar ratio vs  $\mu\text{cal}$  per second. Fitting the data for porphyrin **2** binding with **1** to a 1:1 binding profile gave a binding constant of  $(6.3 \pm 0.5) \times 10^4 \text{ M}^{-1}$  in PhCN at 298 K. For the binding of **2** to **1**, the energy values given by the fit were  $\Delta G = -6.6 \text{ kJ mol}^{-1}$ ,  $\Delta H = -2.8 \text{ kJ mol}^{-1}$ ,  $\Delta S = 13 \text{ J K}^{-1} \text{ mol}^{-1}$  in PhCN at 298 K. No evidence of binding was seen for the interaction of porphyrin **3** with **1**.

due to the overlap of the spectra of **1** and **2** even after the correction for absorbance of **1**.

Isothermal titration calorimetry (ITC) analyses were performed in PhCN to get a more accurate binding constant for the formation of complex **4** (Figure 5). The binding constant corresponding to the interaction with **1** and **2** was found to be  $6.3 \times 10^4 \text{ M}^{-1}$  with 6% error between runs. Under the same conditions, porphyrin **3** showed no binding interaction with **1** (Figure 5).  $^1\text{H}$  NMR spectra indicate binding occurs between the carboxylate moiety of **2** and the NH protons of **1** (Figure 6).

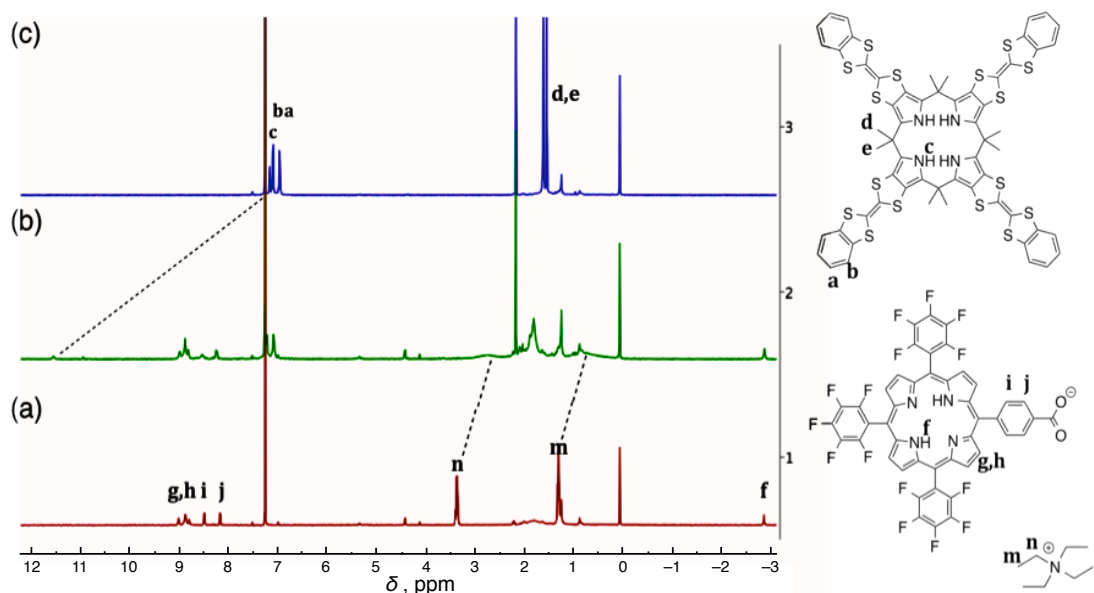


**Figure 6.**  $^1\text{H}$  NMR spectra for (a) tetraethylammonium porphyrin carboxylate **2** (2.5 mM), (b) 1:1 mixture of **1** and **2**, each at 2.5 mM, (c) calix[4]pyrrole **1** (2.5 mM). All spectra were recorded at 298 K in deuterated chloroform.

**Density Functional Theory Calculations.** Initially, I considered it important to determine whether the supramolecular complex **4** would have an electronic structure suitable for photoinduced ET. Density functional theory (DFT) studies were thus carried out in an effort to determine the location of the highest occupied molecular orbital (HOMO) and the lowest unoccupied molecular orbital (LUMO) of complex **4** (Figure 7). The HOMO is located

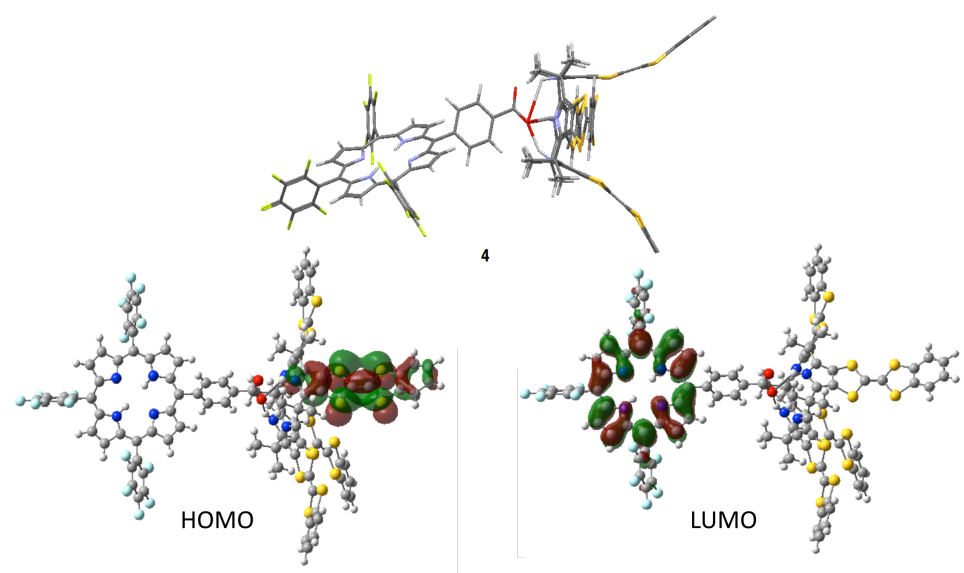


**Figure 7.** Optimized structure of complex **4** formed from **1** and **2**. HOMO and LUMO calculated using density functional theory at the B3LYP/6-31G(d) level.

on a tetrathiafulvalene moiety within calix[4]pyrrole **1**, whereas the LUMO is located on the porphyrin core of **2**. These results provide support for the proposal that photoinduced ET will take place from the electron rich TTF moiety to the electron deficient porphyrin. Conversely, because there is little to no overlap of the HOMO and the LUMO for the complex **4**, the associated electronic coupling value is expected to be low.

**Electrochemical Measurements.** Electrochemical measurements were carried out with a view to determining the redox potentials for **1**, **2**, and complex **4**. Cyclic voltammetric (CV) analyses of **2** (0.3 mM), **1** (0.5 mM), and a mixture of **1** and **2** (0.5 mM and 0.3 mM, respectively) were performed in PhCN using 0.1 M tetra-*n*-butylammonium hexafluorophosphate (TBAPF<sub>6</sub>) as the supporting electrolyte, platinum as the working electrode, platinum wire as the counter electrode, and Ag/AgNO<sub>3</sub> as the reference electrode (Figure 8). Table 1 lists the CV half wave potentials for the three solutions subject to analysis.

Using the values obtained from the CV analysis and eq 3, the energy of the CS state ( $E_{\text{CS}}$ )

$$E_{\text{CS}} = e(E_{\text{ox}} - E_{\text{red}}) \quad (3)$$

between **1** and **2** in complex **4** was found to be 1.37 eV, where  $E_{\text{ox}}$  is the first one-electron oxidation potential found by CV,  $E_{\text{red}}$  is the first one-electron reduction found by CV, and  $e$  is the elementary charge.

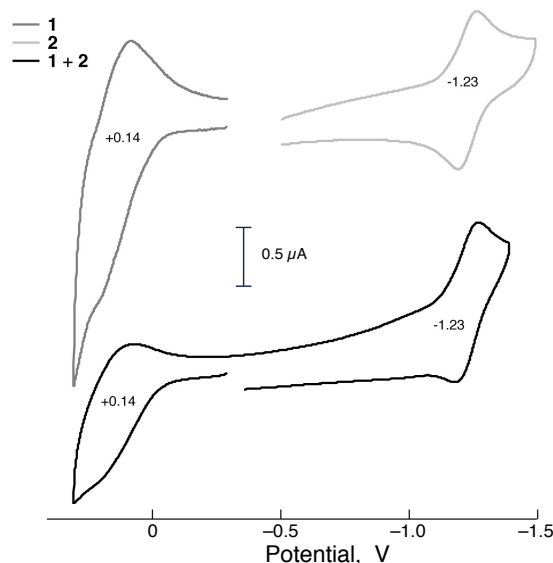


**Figure 8.** Cyclic voltammograms for **1** (0.5 mM), **2** (0.3 mM), and complex **4** as produced from **1** (0.5 mM) and **2** (0.3 mM) recorded in PhCN using 0.1 M tetra-*n*-butylammonium hexafluorophosphate as the electrolyte. The reference electrode is Ag/AgNO<sub>3</sub>, the working electrode is Pt, and the counter electrode is a Pt wire.

**Table 1.** First One-Electron Oxidation and Reduction Potentials in PhCN as Determined by CV (V vs Ag/AgNO<sub>3</sub>)

	<i>E</i> <sub>ox</sub> (V)	<i>E</i> <sub>red</sub> (V)
<b>1</b> (0.5 mM)	+0.14	—
<b>2</b> (0.3 mM)	+1.09	-1.23
<b>1</b> (0.5 mM) + <b>2</b> (0.3 mM)	+0.14	-1.23

**Fluorescence Lifetime and Phosphorescence.** To determine if ET occurs from **1** to **2** via the singlet or triplet excited state of porphyrin **2**, the fluorescence lifetime of porphyrin **2** was studied. In PhCN, the fluorescence lifetime of porphyrin **2** was found to be 13.4 ns. A mixture of **1** and **2** in PhCN was found to have the same fluorescence lifetime (Figure 9b). This is taken as evidence that energy or electron transfer occurs from the triplet excited state of **2** rather than the singlet excited state (<sup>1</sup>**2**<sup>\*</sup>); if the singlet state was involved the fluorescence lifetime of <sup>1</sup>**2**<sup>\*</sup> in the presence of **1** would be shorter than that of <sup>1</sup>**2**<sup>\*</sup> in its absence.

The absorbance maximum (640 nm, Figure 1) and fluorescence maximum (645 nm, Figure 9a) of **2** were used to determine the singlet energy level (*E*<sub>S</sub>) of the porphyrin; using eq 4, this value was determined to be 1.93 eV.

$$E_S = 1/2[(hc / \lambda_{\text{Abs}}) + (hc / \lambda_{\text{Fl}})] \quad (4)$$

In eq 4,  $\lambda_{\text{Abs}}$  is the longest wavelength of the absorbance maximum and  $\lambda_{\text{Fl}}$  is the shortest wavelength of the fluorescence maximum,  $h$  is Planck's constant, and  $c$  is the speed of light.

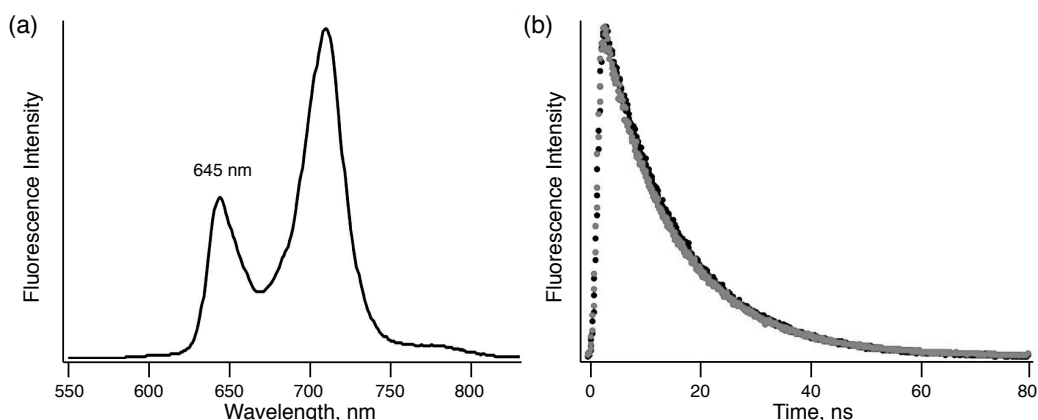


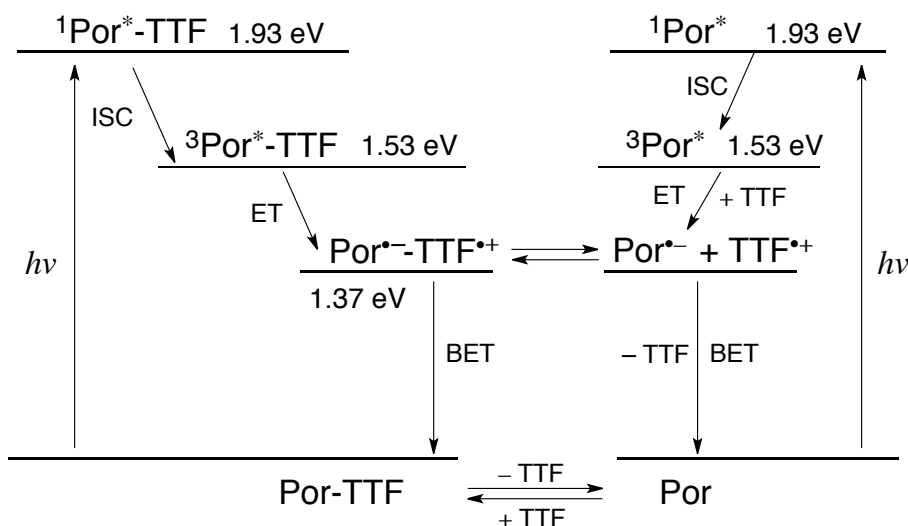
**Figure 9.** (a) Fluorescence spectrum for **2** (15 mM) in PhCN at 298 K; excitation wavelength: 510 nm. (b) Fluorescence decay profiles of the singlet-excited state of **2** (<sup>1</sup>**2**<sup>\*</sup>) observed upon excitation at 485 nm in the absence (black) and the presence of **1** (0.5 mM) (gray) in deoxygenated PhCN containing **2** (0.3 mM).

To determine the triplet excited state energy level, the phosphorescence spectrum of **2** was recorded upon excitation at 435 nm in a mixture of ethyl iodide (EtI) and 2-methyltetrahydrofuran (2-MeTHF) (~1:1) at 77 K (Figure 10). The phosphorescence was weak and required a large ratio of EtI to 2-methyl THF to increase the yield of intersystem crossing through the heavy atom effect. This weak triplet emission and underlying low phosphorescence quantum yield is, however, a well-known feature of free-base tetraphenylporphyrin derivatives.<sup>66,67</sup> The triplet energy level of **2** was found to be 1.53 eV, a reasonable value for tetraphenylporphyrins;<sup>66,67</sup> this value was obtained from the phosphorescence  $\lambda_{\text{max}}$  using the following equation,

$$E = hc/\lambda \quad (5)$$

where  $E$  is the triplet energy level,  $h$  is Planck's constant,  $c$  is the speed of light, and  $\lambda$  is the phosphorescence wavelength.

Using the energy values of the CS state (1.37 eV), singlet excited state (1.93 eV), and triplet excited state (1.53 eV) determined through eqs 3, 4, and 5, respectively, an energy diagram depicting the energetics associated with the expected electron-transfer pathway in the supramolecular complex (**4**) could be generated as shown in Scheme 1. The CS state can be also generated via *intermolecular* electron transfer from **1** to the excited state of **2** (*vide infra*).



**Scheme 1.** Energy Diagram for the Proposed Photodynamics of the Supramolecular Complex (**4**, Por-TTF) Formed between **1** (TTF) and **2** (Por), in PhCN. Photoinduced Charge Separation via *Intramolecular* Process (Left Panel) and *Intermolecular* Process (Right Panel).

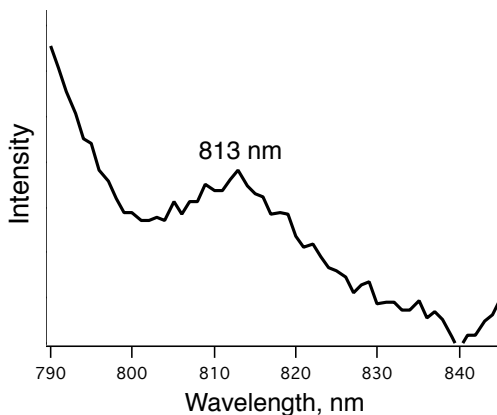


**Figure 10.** Phosphorescence spectrum of **2** recorded in a solution of 2-methyltetrahydrofuran and ethyl iodide (1:1), which was then used to form transparent glass upon cooling to  $T = 77$  K where the measurement was made via excitation at 435 nm.

**Femtosecond Laser Flash Photolysis.** Femtosecond laser flash photolysis measurements were used to record the absorption spectra of the putative ensembles. Specifically, to analyze the ET expected to occur from a TTF moiety present in **1** to the porphyrin **2** upon photoirradiation, the transient spectra of **2** were recorded. Upon irradiation at 400 nm, porphyrin **2** was promoted to the singlet-excited state  ${}^1\mathbf{2}^*$ , as reflected in an increased absorption at 620 and 670 nm in deoxygenated PhCN at 298 K (Figure 11). A single exponential analysis for the decay of  ${}^1\mathbf{2}^*$  gives the rate of intersystem crossing ( $k_{ISC}$ ), which was found to be  $3.3 \times 10^8$  s $^{-1}$  (Figure 11). When **1** (0.10 mM) was irradiated under the same conditions, absorbance features at 620 and 834 nm were seen that diminished with a decay rate of  $1.6 \times 10^9$  s $^{-1}$  for the peak at 834 nm (Figure 12).

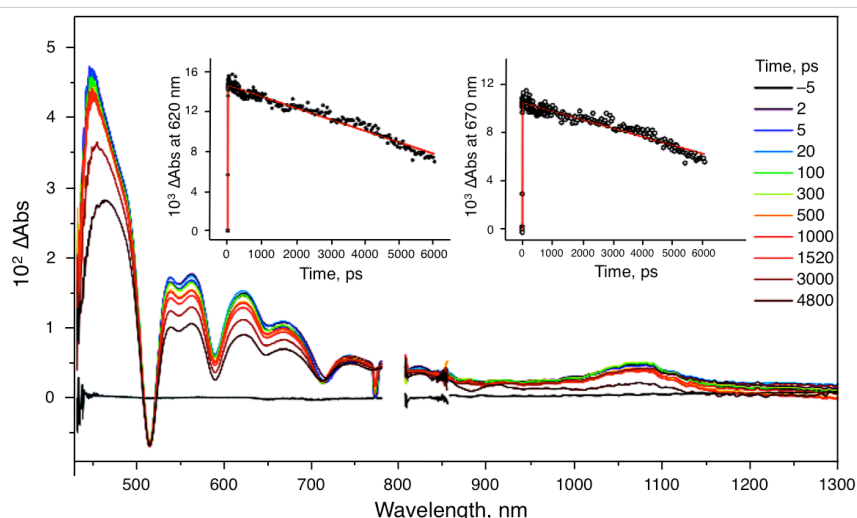


**Figure 11.** Femtosecond transient absorption spectra of  ${}^1\mathbf{2}^*$  recorded after irradiation of **2** (0.1 mM) at 400 nm in deoxygenated PhCN at 298 K.

The transient absorption spectra of a mixture of **1** (50  $\mu$ M) with **2** (50  $\mu$ M) displayed the signature absorption peaks of both species upon excitation at 400 nm (Figure 13). The decay rate of the absorption peak at 670 nm attributed to  ${}^1\mathbf{2}^*$ ,  $3.3 \times 10^8 \text{ s}^{-1}$ , proved insensitive to the presence of **1**. This is taken as an indication that adding **1** to **2** and formation of complex **4** does not increase the rate of intersystem crossings from  ${}^1\mathbf{2}^*$  to  ${}^3\mathbf{2}^*$  and that there is no reaction between **1** and the singlet excited state of **2**. The independence of the decay rate of  ${}^1\mathbf{2}^*$  with respect to **1** was also seen at larger concentrations, namely **1** (0.5 mM) and **2** (0.3 mM) as

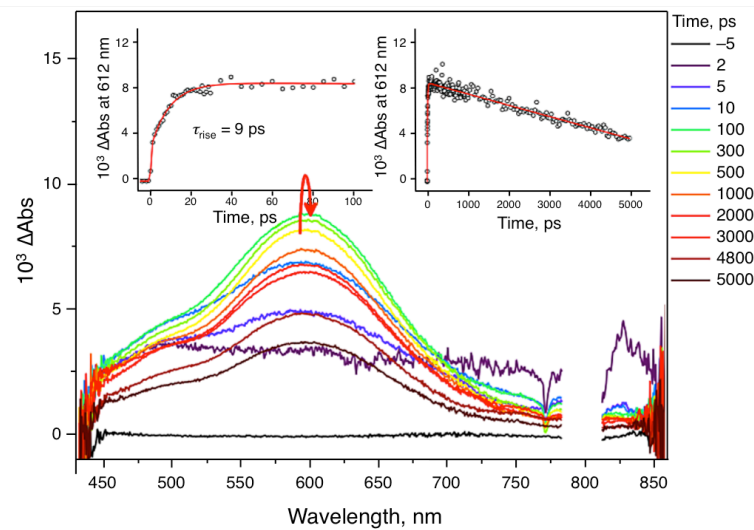


**Figure 12.** Femtosecond transient absorption features seen upon excitation of **1** (0.1 mM) at 400 nm. The changes shown after the sample is subject to laser pulse in deoxygenated PhCN at 298 K.

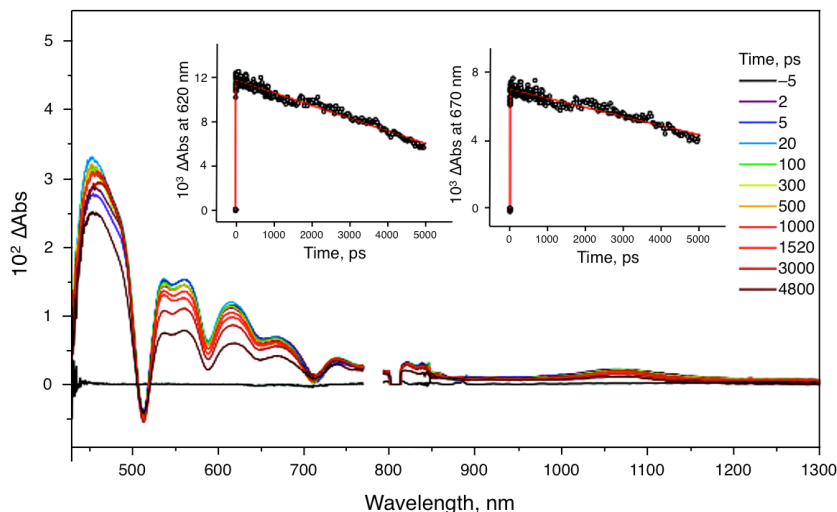


**Figure 13.** Femtosecond transient absorption spectra of a solution containing **1** (50  $\mu$ M) and **2** (50  $\mu$ M) as recorded following irradiation at 400 nm in deoxygenated PhCN at 298 K. Insets: Decay of the absorption spectral intensity seen for a mixture of **1** (50  $\mu$ M) and **2** (50  $\mu$ M) at 620 nm (left) at 670 nm (right) post excitation at 400 nm in deoxygenated PhCN at 298 K.

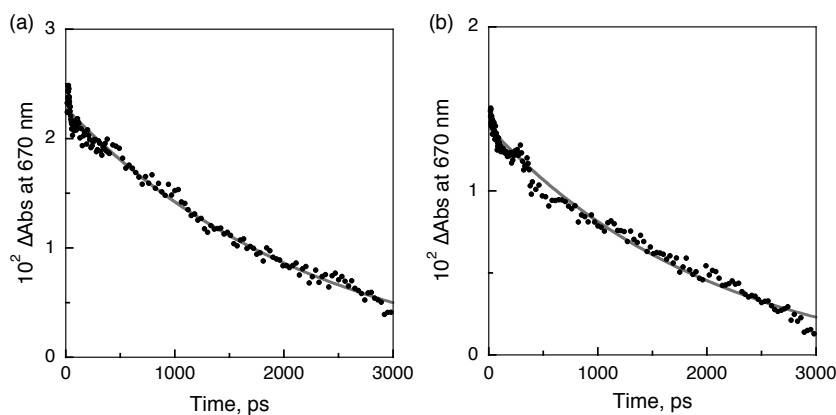


**Figure 14.** (a) Decay in the absorption intensity of  ${}^1\mathbf{2}^*$  recorded at 670 nm after excitation at 400 nm. The sample used for the analysis contained 0.3 mM of **2**. Based on curve fitting, the decay rate was found to be  $4.3 \times 10^8 \text{ s}^{-1}$  with  $R^2 = 0.992$ . (b) Decay of absorption at 670 nm attributed to  ${}^1\mathbf{2}^*$  as observed post excitation at 400 nm for a sample containing **1** (0.5 mM) and **2** (0.3 mM). Based on these data, the decay rate was calculated to be  $4.7 \times 10^8 \text{ s}^{-1}$  with an  $R^2 = 0.992$ . Both samples were done in deoxygenated benzonitrile at 298 K. These decay rates were collected in the Osaka laboratory and are relatively close to the decay rate found in the Seoul laboratory, namely  $3.3 \times 10^8 \text{ s}^{-1}$  as described in the text. The results in this figure reflect experiments carried out at higher concentrations than used in the Seoul laboratory (50  $\mu\text{M}$  for both **1** and **2**).

shown in Figure 14. These findings thus serve to reiterate the conclusion reached based on the fluorescence lifetime studies, namely that no ET occurs from the electron rich TTF moiety to singlet excited state of the porphyrin acceptor **2**. These ET processes involve primarily the triplet-excited state with little appreciable energy or electron transfer occurring in the singlet excited state (*vide infra*).

**Nanosecond Laser Flash Photolysis.** In an effort to determine if ET occurs from a TTF moiety of **1** to the porphyrin core of **2** via the triplet manifold, the nanosecond transient absorption technique was thus used. For these studies, a pure sample of porphyrin **2** (0.1 mM) was first irradiated with 532 nm light in PhCN. Under these conditions, evidence of triplet excited state formation was obtained, as reflected by a growing in of an absorption feature at 430 nm (Figure 15a). The decay rate constant for the triplet was found to be  $1.1 \times 10^4 \text{ s}^{-1}$  in deoxygenated PhCN (Figure 15b). No spectral changes were observed upon irradiation of a sample of **1** (0.1 mM in PhCN) with a 355 nm laser pulse (Figure 16).

A mixture of **1** (0.3 mM) and **2** (0.1 mM) in deoxygenated PhCN showed absorbance growth at 450 nm, 670 nm, and 850 nm upon irradiation at 532 nm (Figure 17). The absorbance band at 450 nm is attributed to the joint presence of  ${}^3\mathbf{2}^*$  and  $\mathbf{1}^+$ , two species whose

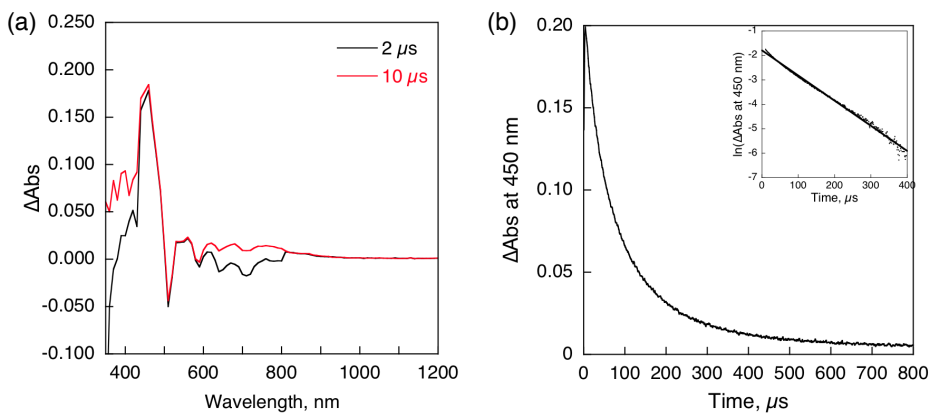


**Figure 15.** (a) Nanosecond laser flash photolysis absorption profile of  ${}^32^*$  (0.1 mM) as observed 2  $\mu$ s (black) and 10  $\mu$ s (red) after excitation at 355 nm in deoxygenated benzonitrile at 298 K. (b) Decay of absorption of  ${}^32^*$  at 450 nm post excitation at 355 nm in benzonitrile at 298 K. Based on curve fitting, the decay rate was found to be  $1.1 \times 10^4 \text{ s}^{-1}$  ( $R^2 = 0.994$ ).

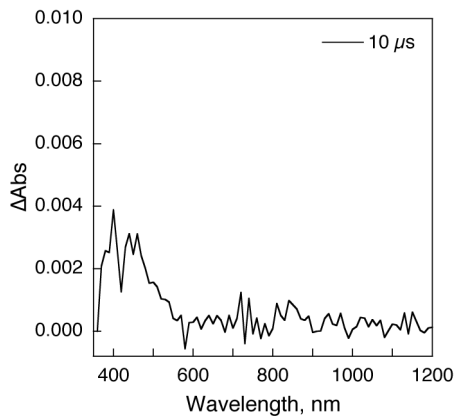


**Figure 16.** Nanosecond laser flash photolysis absorption spectrum observed upon excitation of 1 (0.3 mM) at 355 nm in deoxygenated benzonitrile at 298 K.

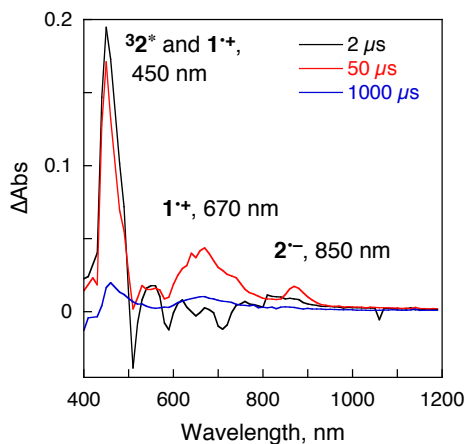


**Figure 17.** Nanosecond flash photolysis absorption spectra for a mixture of 1 (0.3 mM) and 2 (0.10 mM) upon excitation at 532 nm in deoxygenated PhCN at 298 K as recorded 2  $\mu$ s (black), 50  $\mu$ s (red), and 1000  $\mu$ s (blue) after laser pulse irradiation.

spectral features were independently characterized previously (Figures 15a and 18). The feature at 670 nm is attributed exclusively to **1**<sup>+</sup> based on the spectral changes observed when samples of **1** in PhCN are subject to direct chemical oxidation (Figure 18). Finally, the spectral feature at 850 nm is attributed to **2**<sup>−</sup>, a radical anion species previously characterized through chemical reduction of **2** (Figure 19).

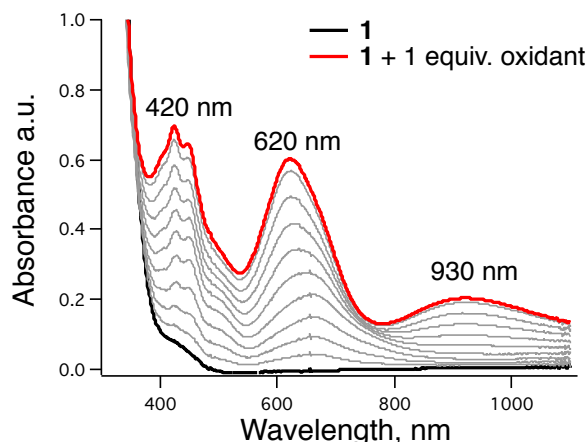


**Figure 18.** Titration of **1** (50 mM, black line) with up to 1 equivalent of the chemical oxidant “magic blue” (final spectrum shown with a red line) at 298 K in benzonitrile.

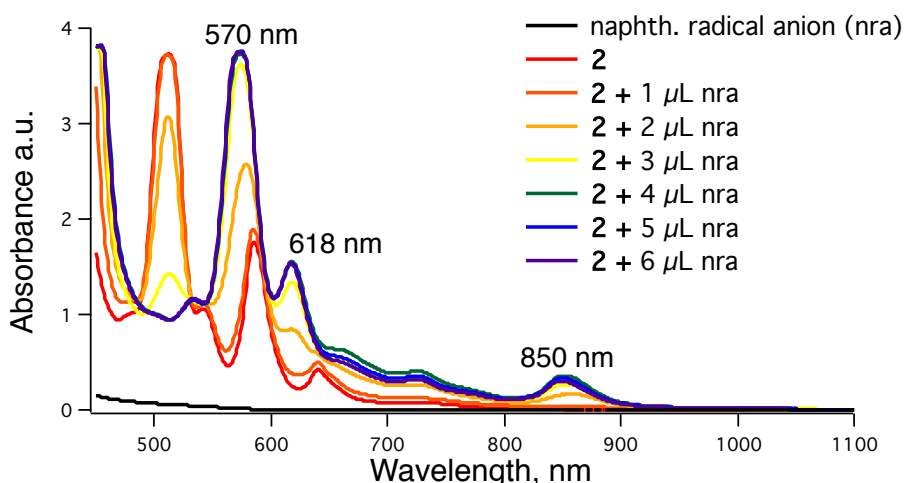


**Figure 19.** Titration of **2** (0.3 mM, benzonitrile) with the naphthalene radical anion at 298 K. Shown in this figure are the absorbance spectra of the naphthalene radical anion (black), porphyrin **2** (red), **2** with 1 mL naphthalene radical anion added (red-orange), **2** with 2 mL naphthalene radical anion (orange), **2** with 3 mL naphthalene radical anion (yellow), **2** with 4 mL naphthalene radical anion (green), **2** with 5 mL naphthalene radical anion (blue), and **2** with 6 mL naphthalene radical anion (purple).

With the concentration of **2** fixed at 0.1 mM the rate at which the absorption peak at 670 nm grew in was studied as a function of [1] in deoxygenated PhCN at 298 K (Figure 20a). Plotting the growth rate of 670 nm vs the concentration of **1** gave a linear plot as can be seen from an inspection of Figure 20b.<sup>25</sup> The second-order rate constant, corresponding to intermolecular ET, was determined from the slope of the plot in Figure 20b and was found to be  $4.4 \times 10^8 \text{ M}^{-1} \text{ s}^{-1}$ .<sup>25</sup> This rate constant is smaller than that of the diffusion limiting value expected in PhCN, namely  $5.6 \times 10^9 \text{ M}^{-1} \text{ s}^{-1}$ .<sup>69,70</sup> From the y-intercept of the line in Figure 20b the rate constant of intramolecular forward ET was determined and found to be  $2.1 \times 10^4 \text{ s}^{-1}$ .<sup>25</sup>

The decay of absorbance at 670 nm was found to fit well to a biexponential function, leading us to propose that it consists of two decay components attributed to *inter*- and *intra*-molecular back ET, respectively. The first component is characterized by a decay rate that is independent of laser intensity (Figures 21a and b), as well as the concentration of **1** (Figure 21c). Such findings are consistent with intramolecular back ET. The rate constant of this intramolecular back ET is determined to be  $3.6 \times 10^2 \text{ s}^{-1}$ , while the corresponding CS lifetime was calculated to be 2.8 ms. The second component displays second-order kinetic features and is ascribed to intermolecular back ET. For this process, the rate constant was found to be  $9.8 \times 10^8 \text{ M}^{-1} \text{ s}^{-1}$ , which is also smaller than the diffusion limited value in PhCN (Figure 22).<sup>69,70</sup>

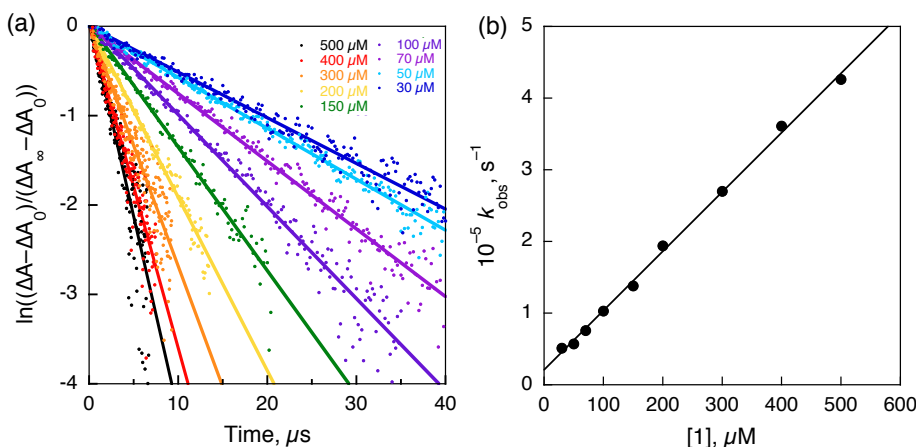


**Figure 20.** (a) Plot of the natural log of  $(\Delta A - \Delta A_0)/(\Delta A_\infty - \Delta A_0)$  vs time as recorded using a sample containing **1** at various concentrations and **2** at a fixed concentration (0.1 mM) in deoxygenated PhCN at 298 K. Concentration of **1** used in these studies: 30  $\mu\text{M}$  (dark blue), 50  $\mu\text{M}$  (light blue), 70  $\mu\text{M}$  (purple), 100  $\mu\text{M}$  (indigo), 150  $\mu\text{M}$  (green), 200  $\mu\text{M}$  (yellow), 300  $\mu\text{M}$  (orange), 400  $\mu\text{M}$  (red), and 500  $\mu\text{M}$  (black) (b) Rate constants for ET between **1** (various concentration) and **2** (0.1 mM) vs concentrations of **1** in deoxygenated PhCN at 298 K.

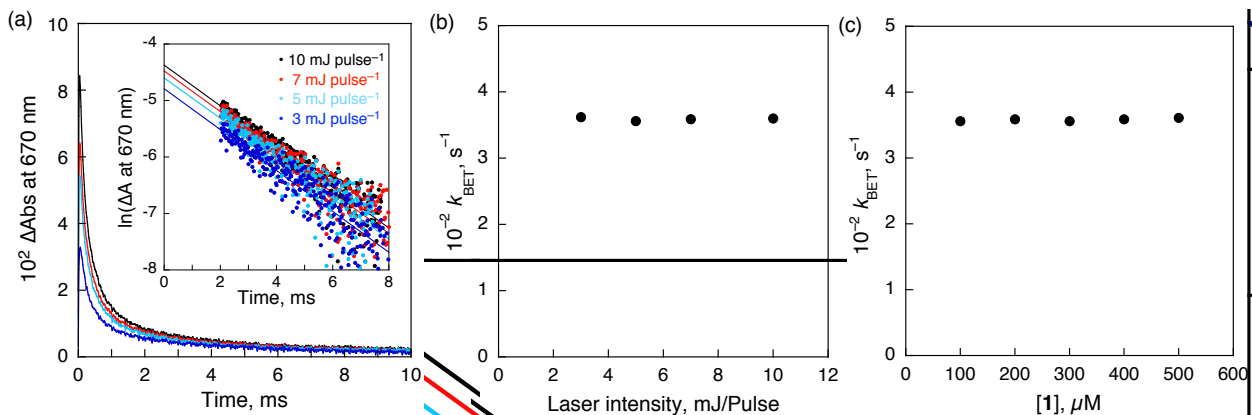


**Figure 21.** (a) Decay time profiles of absorbance at 670 nm with various laser intensities. Inset: First-order plots. Rate of *intramolecular* back electron transfer ( $k_{\text{BET}}$ ) (b) vs laser intensity for a sample containing 0.3 mM **1** and 0.1 mM **2** (left) and (c) vs  $[\mathbf{1}]$  for a sample containing 0.3 mM **2** (right) in deoxygenated benzonitrile at 298 K.

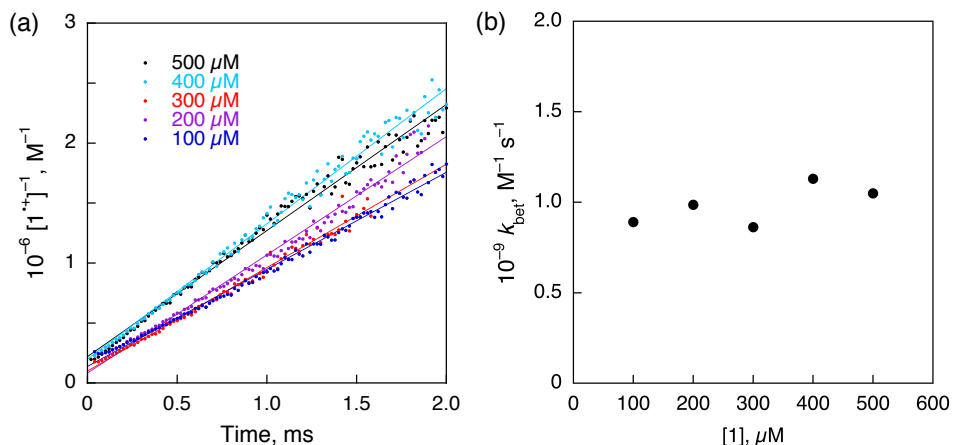


**Figure 22.** Second order decay analysis of the back electron transfer process at various concentrations of **1** as studied in the presence of 0.3 mM of **2** in deoxygenated benzonitrile at 298 K (left). Rate of back electron transfer versus concentration of **1** in a 0.3 mM solution of **2** in PhCN at 298 K. On the basis of these analyses, the intermolecular electron transfer rate was found to be  $9.8 \times 10^8 \text{ M}^{-1} \text{ s}^{-1}$  (right).

The Marcus equations, eqs 6 and 7, predict that the rate constants of intramolecular forward and backward ET will be temperature dependent for a nonadiabatic system. In eqs 6 and 7,  $k_{\text{ET}}$  is the rate constant of ET,  $T$  is the temperature,  $V$  is the electronic coupling constant,  $\lambda$  is the reorganization energy,  $\Delta G_{\text{ET}}$  is the Gibbs free energy of ET,  $k_{\text{B}}$  is the Boltzmann constant, and  $h$  is Planck's constant.<sup>6,7</sup> A Marcus plot of the temperature dependence of the rate constant of intramolecular back ET is given in Figure 23a. This plot allows for the

determination of the electronic coupling constant ( $V$ ) from the intercept and the reorganization energy ( $\lambda$ ) from the slope; these values were determined to be  $1.2 \times 10^{-2} \text{ cm}^{-1}$  and 0.76 eV, respectively. This  $V$  value is rather small, as expected given the poor calculated overlap of the HOMO and LUMO and the long distance between the components **1** and **2** that make up the self-assembled ET ensemble, as shown by DFT calculations. This small  $V$  value provides a rationale for the long lifetime of the CS state, as observed by transient absorption spectroscopy. The temperature dependency of the rate constant of intramolecular back ET was also analyzed using an Eyring plot (Figure 23b).

$$k_{\text{ET}} = \left( \frac{4\pi^3}{h^2 \lambda k_{\text{B}} T} \right)^{1/2} V^2 \exp \left[ -\frac{(\Delta G_{\text{ET}} + \lambda)^2}{4\lambda k_{\text{B}} T} \right] \quad (6)$$

$$\ln(k_{\text{ET}} T^{1/2}) = \ln \left( \frac{2\pi^{3/2} V^2}{h(\lambda k_{\text{B}})^{1/2}} \right) - \frac{(\Delta G_{\text{ET}} + \lambda)^2}{4\lambda k_{\text{B}} T} \quad (7)$$

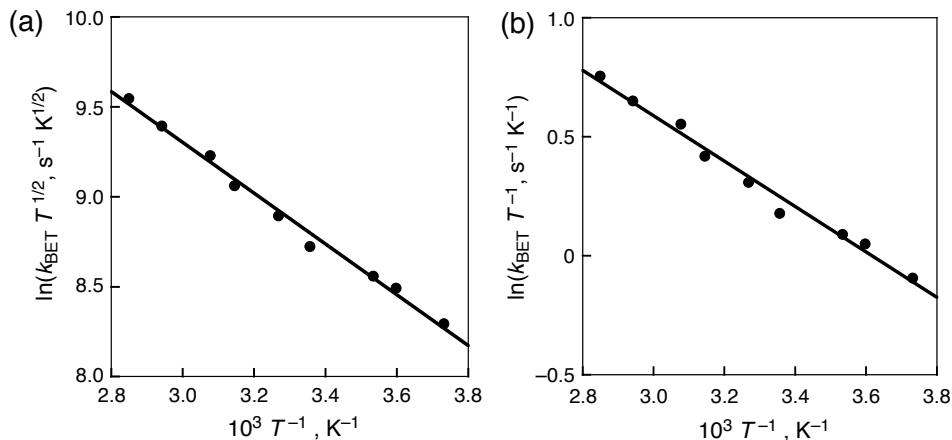


**Figure 23.** (a) Marcus plot for the changes in the rate of *intramolecular* back ET ( $k_{\text{BET}}$ ) vs temperature in PhCN. (b) Eyring plot constructed by plotting the observed changes in the rate of back electron transfer ( $k_{\text{BET}}$ ) versus temperature in benzonitrile. The concentrations of **1** and **2** were 0.3 mM and 0.1 mM, respectively.  $\Delta G^\ddagger$  was found to be 14 kcal mol<sup>-1</sup>,  $\Delta S^\ddagger$  to be -40 cal K<sup>-1</sup> mol<sup>-1</sup>, and  $\Delta H^\ddagger$  to be 1.9 kcal mol.

**ESR Studies of the Charge-Separated State Observed for the Supramolecular Complex **4**.** Typically, photoinduced ET from a neutral donor to a neutral acceptor results in the formation of radical species. It was thus expected that ET from a TTF moiety of **1** to the porphyrin **2** would result in the formation of the radical species **1**<sup>+</sup> and **2**<sup>-</sup>. To test this proposition **1** was first oxidized to the radical cation using one equivalent of the oxidant tris(4-bromophenyl)aminium hexachloridoantimonate (also known as “magic blue”); this

allowed to obtain the electron spin resonance (ESR) spectrum of  $\mathbf{1}^+$ . Separately, porphyrin  $\mathbf{2}$  was subject to reduction via treatment with the naphthalene radical anion; this produced  $\mathbf{2}^-$ , which allowed for collection of its ESR spectrum. The spectra for these radical species (*i.e.*,  $\mathbf{1}^+$  and  $\mathbf{2}^-$ ) are provided in Figure 24.

With these predicative studies complete, the ESR spectrum was taken of a sample containing both  $\mathbf{1}$  (0.5 mM) and  $\mathbf{2}$  (0.3 mM) in PhCN at 4 K under conditions of photoirradiation with a 1000 W Hg high-pressure lamp. Prior to subjecting the sample to photoirradiation no significant ESR signal is seen. However, upon photoirradiation an ESR signal at  $g = 2.005$  appeared (Figure 25). The  $g$  value for this signal is between those for the chemically induced radical anion  $\mathbf{2}^-$  ( $g = 2.0037$ ) and the chemically induced radical cation  $\mathbf{1}^+$  ( $g = 2.0067$ ).<sup>37,44</sup> Thus, the observed ESR signal in Figure 25 indicates that the intermolecular CS state composed of doublet  $\mathbf{1}^+$  and  $\mathbf{2}^-$  is dominant, because ESR measurements were performed using relatively high concentrations of  $\mathbf{1}$  and  $\mathbf{2}$  as compared with the laser flash photolysis measurements. As can be seen from an inspection of the inset to Figure 25, a signal was seen at  $g = 4.18$  that is ascribable to a triplet CS state.<sup>37,38,70–72</sup> However, the zero-field splitting pattern around  $g = 2$  due to the triplet CS state produced by the intramolecular electron transfer at low temperature was not observed clearly in Figure 25. This is ascribed to line broadening in frozen PhCN.

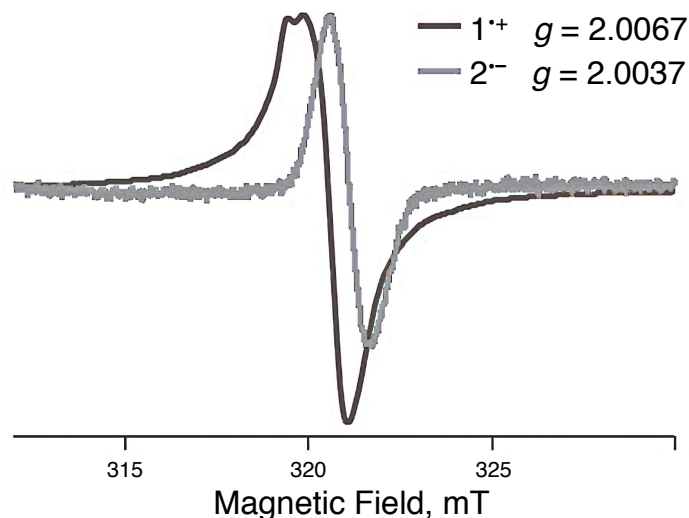


**Figure 24.** Normalized ESR spectra for chemically induced BTTF-C4P ( $\mathbf{1}^+$ ) and porphyrin carboxylate ( $\mathbf{2}^-$ ) in deaerated PhCN at 77 K.

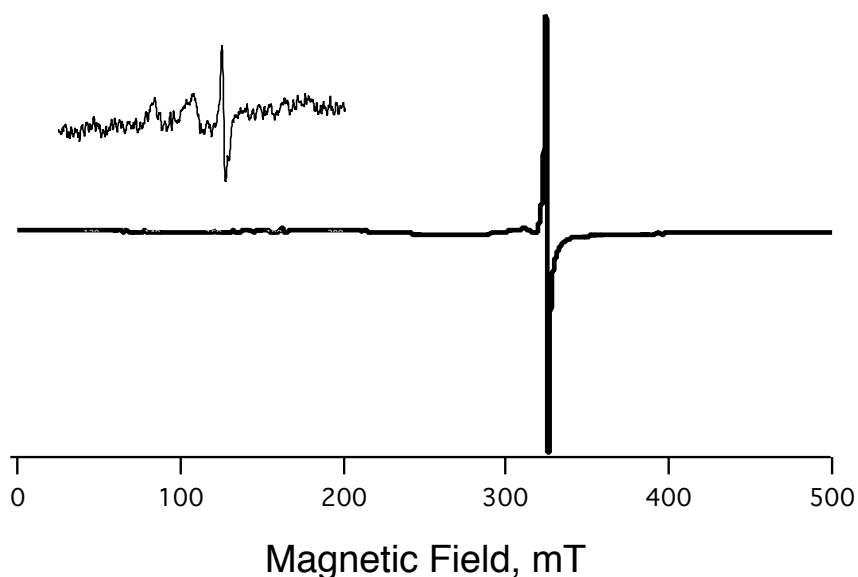


**Figure 25.** X-band ESR spectra for **1** (0.5 mM) and **2** (0.3 mM) in PhCN at 4 K under photoirradiation with a 1000 W high-pressure Hg lamp. The signal was observed at  $g = 2.005$ . Inset: Expanded region at  $g = 4$ . These results are consistent with formation of a triplet species upon these conditions.

In summary, the ET events following photoexcitation of complex **4** formed from calix[4]pyrrole **1** and the porphyrin carboxylate **2** were studied in depth. The 1:1 binding affinity corresponding to the interaction between **1** and **2** was found to be  $6.3 \times 10^4 \text{ M}^{-1}$  in PhCN at 298 K as determined from an analysis of the UV–Vis spectral changes seen upon complexation, as well as through ITC measurements. Density functional theory calculations provided support for the HOMO and LUMO being located on a TTF moiety of the calix[4]pyrrole **1** and the porphyrin core of **2**, respectively, and that ET from **1** to **2** would be possible upon photoirradiation of complex **4**. The occurrence of photoinduced ET via the triplet excited state was confirmed using laser flash photolysis measurements, which allowed the rates of both forward and backward ET to be determined. Both *inter-* and *intramolecular* ET was seen for complex **4**, with the intermolecular ET being dependent upon the concentration of species in solution. The triplet CS state produced upon photoirradiation of **2** was found to be 2.8 milliseconds, one of the longest known lifetimes for a CS generated via a photoinduced electron transfer process within a non-covalently bound complex. This ability to create a long-lived CS via the simple mixing of appropriately chosen components provides a promising springboard for the future development of readily accessible artificial photosynthetic devices.

---

## References

- (1) Lewis, N. S.; Nocera, D. G. *Proc. Natl. Acad. Sci. U.S.A.* **2006**, *103*, 15729–15735.
- (2) Fukuzumi, S. *Phys. Chem. Chem. Phys.* **2008**, *10*, 2283–2297.
- (3) Günes, S.; Neugebauer, H.; Sariciftci, N. S. *Chem. Rev.* **2007**, *107*, 1324–1338.
- (4) Nunzi, J.-M. *C. R. Physique* **2002**, *3*, 523–542.
- (5) Fukuzumi, S.; Ohkubo, K. *Dalton Trans.* **2013**, *42*, 15846–15858.
- (6) Marcus, R. A.; Sutin, N. *Biochim. Biophys. Acta.* **1985**, *811*, 265–322.
- (7) Marcus, R. A. *Angew. Chem., Int. Ed.* **1993**, *32*, 1111–1121.
- (8) Fukuzumi, S. *Pure Appl. Chem.* **2007**, *79*, 981–991.
- (9) Fukuzumi, S. Electron Transfer of  $\pi$ -Functional Systems and Applications. In *Functional Organic Materials*, Wiley-VCH: Weinheim, 2007; pp 465–510.
- (10) Ohkubo, K.; Fukuzumi, S. *Bull. Chem. Soc. Jpn.* **2009**, *82*, 303–315.
- (11) Durrant, J. R.; Haque, S. A.; Palomares, E. *Chem. Commun.* **2006**, 3279–3289.
- (12) Martín, N.; Sánchez, L.; Herranz, M. a. Á.; Illescas, B.; Guldi, D. M. *Acc. Chem. Res.* **2007**, *40*, 1015–1024.
- (13) Wasielewski, M. R. *Acc. Chem. Res.* **2009**, *42*, 1910–1921.
- (14) Fukuzumi, S.; Ohkubo, K.; D'Souza, F.; Sessler, J. L. *Chem. Commun.* **2012**, *48*, 9801–9815.
- (15) Fukuzumi, S.; Ohkubo, K. *J. Mater. Chem.* **2012**, *22*, 4575–4587.
- (16) Fukuzumi, S.; Saito, K.; Ohkubo, K.; Khoury, T.; Kashiwagi, Y.; Absalom, M. A.; Gadde, S.; D'Souza, F.; Araki, Y.; Ito, O. Crossley, M. J. *Chem. Commun.* **2011**, *47*, 7980–7982.
- (17) de la Escosura, A.; Martínez-Díaz, M. V.; Guldi, D. M.; Torres, T. *J. Am. Chem. Soc.* **2006**, *128*, 4112–4118.
- (18) Ballardini, R.; Balzani, V.; Clemente-León, M.; Credi, A.; Gandolfi, M. T.; Ishow, E.; Perkins, J.; Stoddart, J. F.; Tseng, H.-R.; Wenger, S. *J. Am. Chem. Soc.* **2002**, *124*, 12786–12795.
- (19) Wessendorf, F.; Gnochwitz, J.-F.; Sarova, G. H.; Hager, K.; Hartnagel, U.; Guldi, D. M.; Hirsch, A. *J. Am. Chem. Soc.* **2007**, *129*, 16057–16071.
- (20) D'Souza, F.; Maligaspe, E.; Ohkubo, K.; Zandler, M. E.; Subbaiyan, N. K.; Fukuzumi, S. *J. Am. Chem. Soc.* **2009**, *131*, 8787–8797.
- (21) Molina-Ontoria, A.; Fernández, G.; Wielopolski, M.; Atienza, C.; Sánchez, L.; Gouloumis, A.; Clark, T.; Martín, N.; Guldi, D. M. *J. Am. Chem. Soc.* **2009**, *131*,

12218–12229.

(22) D’Souza, F.; Amin, A. N.; El-Khouly, M. E.; Subbaiyan, N. K.; Zandler, M. E.; Fukuzumi, S. *J. Am. Chem. Soc.* **2011**, *134*, 654–664.

(23) Wessendorf, F.; Grimm, B.; Guldi, D. M.; Hirsch, A. *J. Am. Chem. Soc.* **2010**, *132*, 10786–10795.

(24) Bandi, V.; El-Khouly, M. E.; Nesterov, V. N.; Karr, P. A.; Fukuzumi, S.; D’Souza, F. *J. Phys. Chem. C* **2013**, *117*, 5638–5649.

(25) Kawashima, Y.; Ohkubo, K.; Kentaro, M.; Fukuzumi, S. *J. Phys. Chem. C* **2013**, *117*, 21166–21177.

(26) Bandi, V.; El-Khouly, M. E.; Ohkubo, K.; Nesterov, V. N.; Zandler, M. E.; Fukuzumi, S.; D’Souza, F. *J. Phys. Chem. C* **2014**, *118*, 2321–2332.

(27) Guldi, D. M.; Costa, R. D. *J. Phys. Chem. Lett.* **2013**, *4*, 1489–1501.

(28) Sessler, J. L.; Wang, B.; Harriman, A. *J. Am. Chem. Soc.* **1993**, *115*, 10418–10419.

(29) Sessler, J. L.; Jayawickramarajah, J. Functionalized Base-Pairs: Versatile Scaffolds for Self-Assembly. *Chem. Commun.* **2005**, 1939–1949.

(30) Simonsen, K. B.; Becher, J. *Synlett* **1997**, 1211–1220.

(31) Matsuo, Y.; Maruyama, M.; Gayathri, S. S.; Uchida, T.; Guldi, D. M.; Kishida, H.; Nakamura, A.; Nakamura, E. *J. Am. Chem. Soc.* **2009**, *131*, 12643–12649.

(32) Nielsen, K. A.; Sarova, G. H.; Martin-Gomis, L.; Fernandez-Lazaro, F.; Stein, P. C.; Sanguinet, L.; Levillain, E.; Sessler, J. L.; Guldi, D. M.; Sastre-Santos, Á.; Jeppesen, J. O. *J. Am. Chem. Soc.* **2008**, *130*, 460–462.

(33) Brunetti, F. G.; Romero-Nieto, C.; López-Andarias, J.; Atienza, C.; López, J. L.; Guldi, D. M.; Martín, N. *Angew. Chem., Int. Ed.* **2013**, *52*, 2180–2184.

(34) Romero-Nieto, C.; Medina, A.; Molina-Ontoria, A.; Claessens, C. G.; Echegoyen, L.; Martín, N.; Torres, T.; Guldi, D. M. *Chem. Commun.* **2012**, *48*, 4953–4955.

(35) Nielsen, K. A.; Cho, W.-S.; Jeppesen, J. O.; Lynch, V. M.; Becher, J.; Sessler, J. L. *J. Am. Chem. Soc.* **2004**, *126*, 16296–16297.

(36) Park, J. S.; Le Derf, F.; Bejger, C. M.; Lynch, V. M.; Sessler, J. L.; Nielsen, K. A.; Johnsen, C.; Jeppesen, J. O. *Chem.–Eur. J.* **2010**, *16*, 848–854.

(37) Park, J. S.; Karnas, E.; Ohkubo, K.; Chen, P.; Kadish, K. M.; Fukuzumi, S.; Bielawski, C. W.; Hudnall, T. W.; Lynch, V. M.; Sessler, J. L. *Science* **2010**, *329*, 1324–1327.

(38) Fukuzumi, S.; Ohkubo, K.; Kawashima, Y.; Kim, D. S.; Park, J. S.; Jana, A.; Lynch, V. M.; Kim, D.; Sessler, J. L. *J. Am. Chem. Soc.* **2011**, *133*, 15938–15941.

---

(39) Kim, D. S.; Lynch, V. M.; Park, J. S.; Sessler, J. L. *J. Am. Chem. Soc.* **2013**, *135*, 14889–14894.

(40) Nielsen, K. A.; Levillain, E.; Lynch, V. M.; Sessler, J. L.; Jeppesen, J. O. *Chem.–Eur. J.* **2009**, *15*, 506–516.

(41) Jana, A.; Ishida, M.; Kwak, K.; Sung, Y. M.; Kim, D. S.; Lynch, V. M.; Lee, D.; Kim, D.; Sessler, J. L. *Chem.–Eur. J.* **2013**, *19*, 338–349.

(42) Becher, J.; Brimert, T.; Jeppesen, J. O.; Pedersen, J. Z.; Zubarev, R.; Bjornholm, T.; Reitzel, N.; Jensen, T. R.; Kjaer, K.; Levillain, E. *Angew. Chem., Int. Ed.* **2001**, *40*, 2497–2500.

(43) Li, H.; Jeppesen, J. O.; Levillain, E.; Becher, J. *Chem. Commun.* **2003**, 846–847.

(44) Bill, N. L.; Ishida, M.; Bähring, S.; Lim, J. M.; Lee, S.; Davis, C. M.; Lynch, V. M.; Nielsen, K. a.; Jeppesen, J. O.; Ohkubo, K.; Fukuzumi, S.; Kim, D.; Sessler, J. L. *J. Am. Chem. Soc.* **2013**, *135*, 10852–10862.

(45) Nielsen, K. A.; Cho, W. S.; Lyskawa, J.; Levillain, E.; Lynch, V. M.; Sessler, J. L.; Jeppesen, J. O. *J. Am. Chem. Soc.* **2006**, *128*, 2444–2451.

(46) Custelcean, R.; Delmau, L. H.; Moyer, B. A.; Sessler, J. L.; Cho, W.-S.; Gross, D. E.; Bates, G. W.; Brooks, S. J.; Light, M. E.; Gale, P. A. *Angew. Chem., Int. Ed.* **2005**, *44*, 2537–2542.

(47) Sessler, J. L.; Gross, D. E.; Cho, W.-S.; Lynch, V. M.; Schmidtchen, F. P.; Bates, G. W.; Light, M. E.; Gale, P. A. *J. Am. Chem. Soc.* **2006**, *128*, 12281–12288.

(48) Kojima, T.; Honda, T.; Ohkubo, K.; Shiro, M.; Kusukawa, T.; Fukuda, T.; Kobayashi, N.; Fukuzumi, S. *Angew. Chem., Int. Ed.* **2008**, *47*, 6712–6716.

(49) Osuka, A.; Noya, G.; Taniguchi, S.; Okada, T. *Chem.–Eur. J.* **2000**, *6*, 33–46.

(50) Winters, M. U.; Pettersson, K.; Mårtensson, J.; Albinsson, B. *Chem.–Eur. J.* **2005**, *11*, 562–573.

(51) Kilså, K.; Kajanus, J.; Macpherson, A. N.; Mårtensson, J.; Albinsson, B. Bridge-Dependent Electron Transfer in Porphyrin-Based Donor-Bridge-Acceptor Systems. *J. Am. Chem. Soc.* **2001**, *123*, 3069–3080.

(52) Andersson, M.; Linke, M.; Chambron, J.-C.; Davidsson, J.; Heitz, V.; Hammarström, L.; Sauvage, J.-P. *J. Am. Chem. Soc.* **2002**, *124*, 4347–4362.

(53) Fukuzumi, S.; Ohkubo, K.; E, W.; Ou, Z.; Shao, J.; Kadish, K. M.; Hutchison, J. A.; Ghiggino, K. P.; Sintic, P. J.; Crossley, M. J. *J. Am. Chem. Soc.* **2003**, *125*, 14984–14985.

(54) Ohkubo, K.; Sintic, P. J.; Tkachenko, N. V.; Lemmetyinen, H.; E, W.; Ou, Z.; Shao, J.; Kadish, K. M.; Crossley, M. J.; Fukuzumi, S. *Chem. Phys.* **2006**, *326*, 3-14.

(55) Honda, T.; Nakanishi, T.; Ohkubo, K.; Kojima, T.; Fukuzumi, S. *J. Am. Chem. Soc.* **2010**, *132*, 10155–10163.

(56) Hutchison, J. A.; Sintic, P. J.; Brotherhood, P. R.; Scholes, C.; Blake, I. M.; Ghiggino, K. P.; Crossley, M. J. *J. Phys. Chem. C* **2009**, *113*, 11796–11804.

(57) Takai, A.; Gros, C. P.; Barbe, J.-M.; Fukuzumi, S. *Phys. Chem. Chem. Phys.* **2010**, *12*, 12160–12168.

(58) Tkachenko, N. V.; Lemmetyinen, H.; Sonoda, J.; Ohkubo, K.; Sato, T.; Imahori, H.; Fukuzumi, S. *J. Phys. Chem. A* **2003**, *107*, 8834–8844.

(59) Fungo, F.; Otero, L.; Borsarelli, C. D.; Durantini, E. N.; Silber, J. J.; Sereno, L. *J. Phys. Chem. B* **2002**, *106*, 4070–4078.

(60) Hasobe, T.; Fukuzumi, S.; Kamat, P. V. *J. Phys. Chem. B* **2006**, *110*, 25477-25484.

(61) Imahori, H.; Tamaki, K.; Guldi, D. M.; Luo, C.; Fujitsuka, M.; Ito, O.; Sakata, Y.; Fukuzumi, S. *J. Am. Chem. Soc.* **2001**, *123*, 2607–2617.

(62) Matile, S.; Berova, N.; Nakanishi, K. *J. Am. Chem. Soc.* **1995**, *117*, 7021–7022.

(63) Li, X.; Tanasova, M.; Vasileiou, C.; Borhan, B. *J. Am. Chem. Soc.* **2008**, *130*, 1885–1893.

(64) *Gaussian 09, Revision D.01*, Gaussian, Inc., Wallingford CT, 2009

(65) Ohkubo, K.; Kawashima, Y.; Fukuzumi, S. *Chem. Commun.* **2012**, *48*, 4314-4316.

(66) Gouterman, M.; Khalil, G. E. *J. Mol. Spectrosc.* **1974**, *53*, 88-100.

(67) Harriman, A. *J. Chem. Soc., Faraday Trans. I* **1980**, *76*, 1978–1985.

(68) Okura, I. *Photosensitization of Porphyrins and Phthalocyanines*. Kodansha Ltd. Gordon and Breach Science Publishers: Tokyo, 2000; p 50.

(69) Kawashima, Y.; Ohkubo, K.; Fukuzumi, S. *J. Phys. Chem. A* **2012**, *116*, 8942–8948.

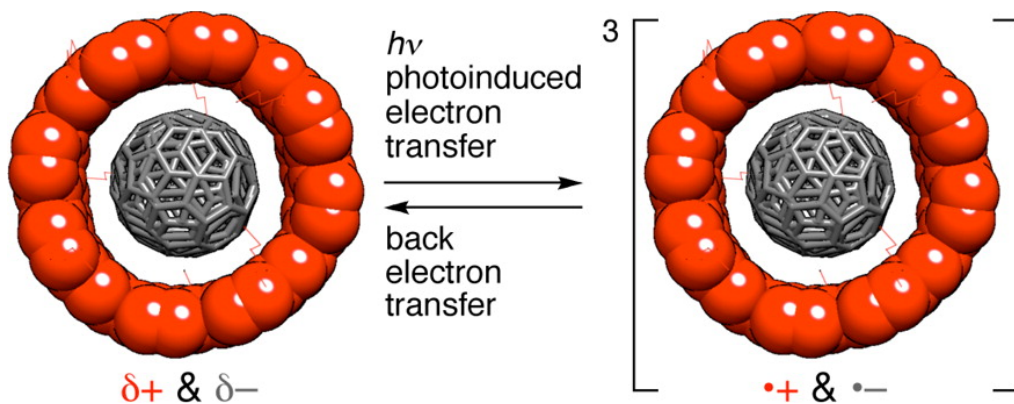
(70) Fukuzumi, S.; Ohkubo, K.; Zheng, X.; Chen, Y.; Pandey, R. K.; Zhan, R.; Kadish, K. M. *J. Phys. Chem. B* **2008**, *112*, 2738-2746.

(71) Murakami, M.; Ohkubo, K.; Nanjo, T.; Souma, K.; Suzuki, N.; Fukuzumi, S. *ChemPhysChem* **2010**, *11*, 2594-2605.

(72) Kawashima, Y.; Ohkubo, K.; Mase, K.; Fukuzumi, S. *J. Phys. Chem. C* **2013**, *117*, 21166-21177.

## Chapter 11

### Photoinduced Electron Transfer in a Dynamic Supramolecular System with Curved $\pi$ -Structures



**Abstract:** Photoinduced electron-transfer processes in a carbonaceous supramolecular combination of a tubular host and a  $C_{60}$  guest were investigated with time-resolved transient absorption spectra upon laser flash photolysis. Following the formation of triplet charge-separated species via electron transfer from the host to the guest, a rapid back electron transfer proceeded to afford triplet  $C_{60}$ .

#### Introduction

The structural chemistry of carbon nanotubes (CNT) started flourishing by the advent of synthetic tubular molecules of their segments.<sup>1-3</sup> These segmental models with molecular nature not only deepen the chemical understanding of CNT but also show unique characteristics due to their hoop-shaped structures. With our own tubular molecules, [4]cyclo-2,8-chryselenes ([4]CC), we recently demonstrated anomalous features of persistent tubular structures of  $sp^2$ -carbon networks in the field of supramolecular chemistry: the tubular structure was preorganized to accommodate fullerene guests with complementary spherical structures to afford the tightest host-guest complexes to date.<sup>4</sup> Furthermore, in the presence of such a tight association force, the nondirectional van der Waals nature allowed rapid dynamic motions for

the guest in solution or even in the solid state.<sup>4,5</sup> I also revealed the atomic-level structures of the dynamic supramolecular system, so-called molecular peapods,<sup>6,7</sup> and recognizing the presence of smoothly curved structures with rich  $\pi$ -electrons, I became greatly interested in the electronic characters. In this Letter, I wish to report my first fundamental study on the electronic characteristics of the molecular peapod. I found that electronic interactions in the tube–sphere combination at the ground state are pronounced upon photoexcitation and revealed the details of the photoinduced electron-transfer (PET) reactions at the excited state by ultrafast time-resolved transient absorption spectroscopy. This first study on the PET dynamics in the curved  $\pi$ -systems will be of fundamental importance for the understanding of peapods in general.<sup>6</sup>

## Experimental Section

**General.** Fluorescence spectra were recorded with Hitachi High-Tech F7000 spectrometer equipped with a thermostatic cell holder with stirrer. UV–Vis absorption spectra were recorded with JASCO V-670 spectrophotometer equipped with a JASCO ETC-717 temperature controller. Cyclic voltammetry and differential pulse voltammetry (DPV) were performed on a BAS ALS660C electrochemical analyzer in deaerated PhCN containing 0.1 M  $\text{Bu}_4\text{NPF}_6$  as the supporting electrolyte at ambient temperature. A conventional three-electrode cell was used with a platinum working electrode ( $d = 1.6$  mm) and a platinum wire as a counter electrode. The platinum working electrode were routinely polished with BAS polishing alumina suspension and rinsed with PhCN before use. The measured potentials were recorded with respect to an  $\text{Ag}/\text{AgNO}_3$  (0.01 M) reference electrode. All the potentials (vs  $\text{Ag}/\text{Ag}$ ) were converted to values vs SCE by adding 0.29 V. All electrochemical measurements were carried out under an  $\text{N}_2$  atmosphere. Femtosecond transient absorption spectroscopy experiments were conducted using an ultrafast source: Integra-C (Quantronix Corp.) and a commercially available optical detection system: Helios provided by Ultrafast Systems LLC. The source for the pump and probe pulses were derived from the fundamental output of Integra-C ( $\lambda = 786$  nm, 2 mJ per pulse and  $\text{fwhm} = 130$  fs) at a repetition rate of 1 kHz. 75% of the fundamental output of the laser was introduced into a second harmonic generation (SHG) unit: Apollo (Ultrafast Systems) for excitation light generation at  $\lambda = 393$  nm, while the rest of the output was used for white light generation. The laser pulse was focused on a sapphire plate of 3 mm thickness and then white light continuum covering the visible region from  $\lambda = 410$  nm to 800 nm was generated via self-phase modulation. A variable neutral density filter, an optical aperture, and a pair of polarizer were inserted in the path in order to generate stable white light continuum. Prior to generating the probe continuum,

---

the laser pulse was fed to a delay line that provides an experimental time window of 3.2 ns with a maximum step resolution of 7 fs. In my experiments, a wavelength at  $\lambda = 393$  nm of SHG output was irradiated at the sample cell with a spot size of 1 mm diameter where it was merged with the white probe pulse in a close angle ( $<10^\circ$ ). The probe beam after passing through the 2 mm sample cell was focused on a fiber optic cable that was connected to a CMOS spectrograph for recording the time-resolved spectra ( $\lambda = 410$ –800 nm). Typically, 3000 excitation pulses were averaged for 3 seconds to obtain the transient spectrum at a set delay time. Kinetic traces at appropriate wavelengths were assembled from the time-resolved spectral data. All measurements were conducted at room temperature, 295 K.

Nanosecond time-resolved transient absorption measurements were carried out using the laser system provided by UNISOKU Co., Ltd. Measurements of nanosecond transient absorption spectrum were performed according to the following procedure. A deaerated solution containing supramolecule was excited at 420 nm by a Panther OPO pumped by a Nd:YAG laser (Continuum SLII-10, 4–6 ns fwhm). The photodynamics was monitored by continuous exposure to a xenon lamp (150 W) as a probe light and a photomultiplier tube (Hamamatsu 2949) as a detector. The solution was oxygenated by nitrogen purging for 15 min prior to measurements.

A quartz EPR tube (internal diameter: 4.5 mm) containing a deaerated PhCN solution of [4]CC and C<sub>60</sub> was irradiated in the cavity of the EPR spectrometer with the focused light of a 1000-W high-pressure Hg lamp (Ushio-USH1005D) through an aqueous filter at low temperature. EPR spectra in frozen cyclohexane were measured under nonsaturating microwave power conditions using a JEOL X-band spectrometer (JES-RE1XE) with an attached variable temperature apparatus. The magnitude of modulation was chosen to optimize the resolution and the signal-to-noise (S/N) ratio of the observed spectra when the maximum slope linewidth of the EPR signals was unchanged with a larger modulation magnitude. The *g* values were calibrated with a Mn<sup>2+</sup> marker.

**Materials.** (*P*)-(12,8)-[4]cyclo-2,8-chrysenylene ((*P*)-(12,8)-[4]CC<sub>2,8</sub>) was synthesized and isolated as reported.<sup>3a</sup> Benzonitrile was distilled before use.

**Quantitative Binding Analysis.** The binding affinities of C<sub>60</sub> with the (*P*)-(12,8)-[4]CC<sub>2,8</sub> was analyzed by fluorescence quenching titration experiment. Fluorescence quenching titration method with calibration of the competitive absorbance of fullerenes was adopted in a manner reported previously.<sup>4a</sup>

**Theoretical Calculations.** The Gaussian 09 program suite was used in all calculations.<sup>8,9</sup> DFT calculations were performed by the M06-2X functional with the 6-311G(d) split valence

plus polarization basis set.<sup>10</sup> The optimized stable structure of the host-guest complex is shown in Figure 1 together with the natural bond orbital (NBO) charges of individual atoms. The net charge transferred to  $C_{60}$  was 0.09 electrons. The solvent effects of PhCN were further estimated by applying the polarizable continuum model (PCM) to the stable structure of the complex. For the PCM, the transferred charge on  $C_{60}$  was 0.06 electrons.

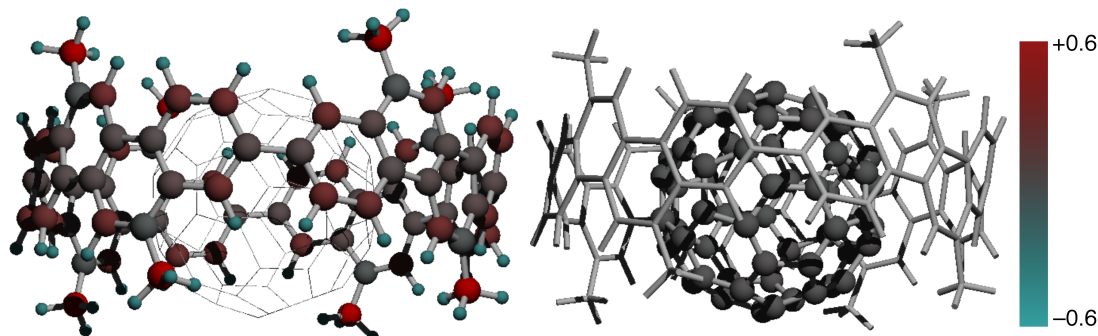


**Figure 1.** Atomic charge mapping in  $(P)$ -(12,8)-[4]CC<sub>2,8</sub>⊃C<sub>60</sub> at the ground state (M06-2X/6-311G(d)). For clarity, the charge distributions in [4]CC (left) and C<sub>60</sub> (right) are shown in separate panels. The sum of the transferred charge on C<sub>60</sub> was 0.08 electron. Note that the charge was effectively delocalized over the C<sub>60</sub> molecule to result in the very small charges on each atom.

## Result and Discussion

The first sign of photoinduced processes in the molecular peapod was noticed through titration experiments to derive the association constants.<sup>4,11</sup> Fluorescence of [4]CC was thus quenched upon encapsulation of C<sub>60</sub>. To facilitate the analysis in polar media, I now added another entry of solvents for the encapsulation and carried out the titration experiments for the formation of  $(P)$ -(12,8)-[4]CC<sub>2,8</sub>⊃C<sub>60</sub> in polar benzonitrile (PhCN) (Figure 2). As shown in Figure 3, the fluorescence of the host was effectively quenched in PhCN, and the association constant ( $K_a$ ) was determined to be  $1.0 \times 10^{10} \text{ M}^{-1}$  (25 °C;  $\log K_a = 10.0$ ). This value also confirmed the previous conclusion that the association constant of molecular peapods depends qualitatively on the solubility of C<sub>60</sub>.<sup>4</sup>

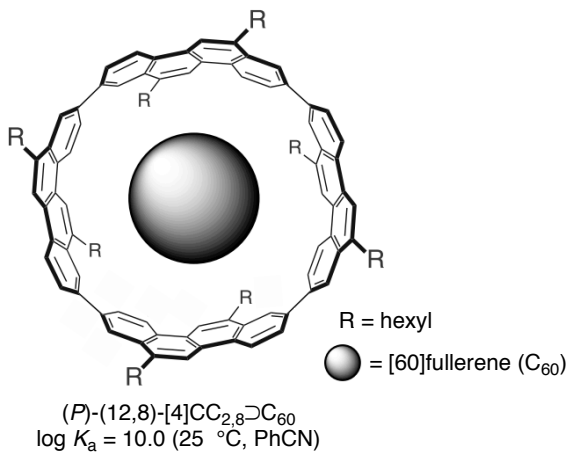


**Figure 2.** Molecular structure and association constant of  $(P)-(12,8)-[4]CC_{2,8}\supset C_{60}$ .

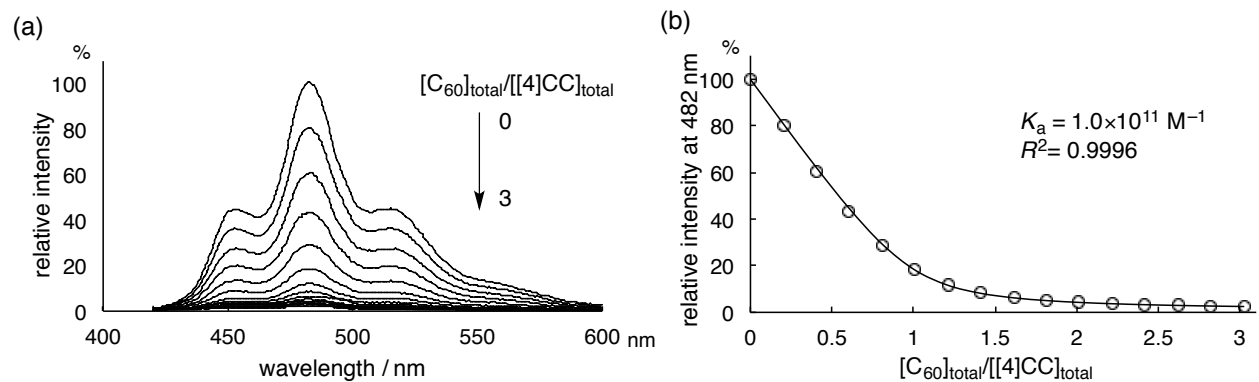


**Figure 3.** Fluorescence quenching titration experiment for  $(P)-(12,8)-[4]CC_{2,8}\supset C_{60}$  in PhCN. (a) Fluorescence spectral change of  $(P)-(12,8)-[4]CC_{2,8}$  at  $2.64 \times 10^{-9}$  M during the titration of  $C_{60}$  at  $2.66 \times 10^{-8}$  M. Excitation = 369 nm. (b) Spectral change at the fluorescence maximum. A curve from the fitting analysis is shown along with the  $\log K_a$  value and the  $R^2$  measure for the goodness-of-fit.

Fluorescence quenching by the  $C_{60}$  guest involved PET reactions, and the photodynamics in  $(P)-(12,8)-[4]CC_{2,8}\supset C_{60}$  were revealed by the time-resolved transient absorption spectra. The transient spectra recorded in deaerated PhCN upon femtosecond laser flash photolysis ( $\lambda_{\text{ex}} = 393$  nm; fwhm = 130 fs) showed absorption maxima at 480 and 1072 nm (Figure 4a). The absorption band at 1072 nm was a diagnostic signature of an electron-transfer product from the guest,  $C_{60}^{\cdot-}$ ,<sup>12</sup> and the decay time profile of this band obeyed first-order kinetics to afford the back electron-transfer rate constant ( $k_{\text{BET}}$ ) of  $6.7 \times 10^8 \text{ s}^{-1}$  and lifetime ( $\tau$ ) of the CS state to be 1500 ps. The other absorption band at 480 nm synchronously decayed at  $k = 6.5 \times 10^8 \text{ s}^{-1}$  and  $\tau = 1600$  ps.

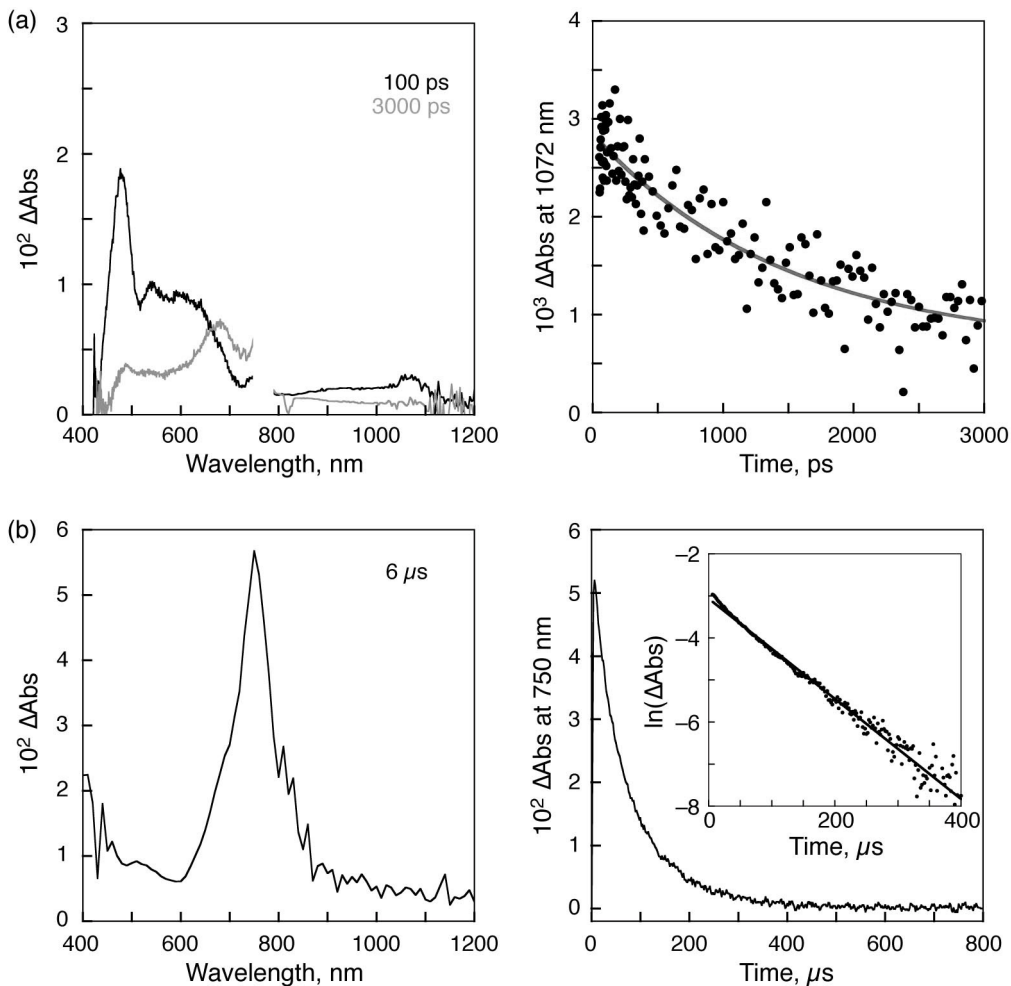


**Figure 4.** Transient absorption spectra of  $(P)$ -(12,8)-[4]CC<sub>2,8</sub>–C<sub>60</sub> in deaerated PhCN at ambient temperature. The results of kinetics analysis are embedded in the decay profiles. (a) Left: Absorption spectra with peak signals at 480 and 1072 nm taken at 100 and 3000 ps after femtosecond laser flash excitation ( $\lambda_{\text{ex}} = 393$  nm).  $[(P)$ -(12,8)-[4]CC<sub>2,8</sub>–C<sub>60</sub>] = 100  $\mu\text{M}$ . Right: Decay profile of the signal at 1072 nm affording  $k_{\text{BET}} = 6.7 \times 10^8 \text{ s}^{-1}$  and  $\tau = 1500$  ps. See Figure 5 for the synchronous decay profile of the signal at 480 nm. (b) Left: Absorption spectrum with peak signals at 750 nm taken at 6  $\mu\text{s}$  after nanosecond laser flash excitation ( $\lambda_{\text{ex}} = 420$  nm).  $[(P)$ -(12,8)-[4]CC<sub>2,8</sub>–C<sub>60</sub>] = 25  $\mu\text{M}$ . Right: Decay profile of the signal at 750 nm to give the rate of  $k_{\text{T}} = 1.2 \times 10^4 \text{ s}^{-1}$  and the lifetime of  $\tau = 80 \mu\text{s}$ . Inset: First-order plot.

(Figure 5) and was thus ascribed to the counterpart product from the donor, *i.e.*, [4]CC<sup>+</sup>. The electron paramagnetic resonance (EPR) spectrum of  $(P)$ -(12,8)-[4]CC<sub>2,8</sub>–C<sub>60</sub> after photoirradiation indeed consisted of broad signals at  $g = 2.003$  and a sharp signal at 2.0002 (Figure 6) which are assigned to [4]CC<sup>+</sup> and C<sub>60</sub><sup>–</sup>, respectively.<sup>13</sup> Another characteristic signal was also observed at  $g = 4.25$ , which showed the presence of the triplet state of the radical ion pair. Thus, a triplet charge-separated (CS) state was generated via PET.<sup>14</sup>

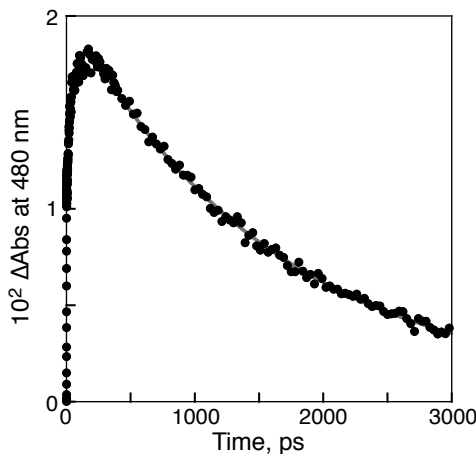


**Figure 5.** Transient absorption spectra of  $(P)$ -(12,8)-[4]CC<sub>2,8</sub>DC<sub>60</sub> in deaerated PhCN at ambient temperature. Decay profile of the signal at 480 nm affording  $k = 6.3 \times 10^8 \text{ s}^{-1}$  and  $\tau = 1600 \text{ ps}$ .

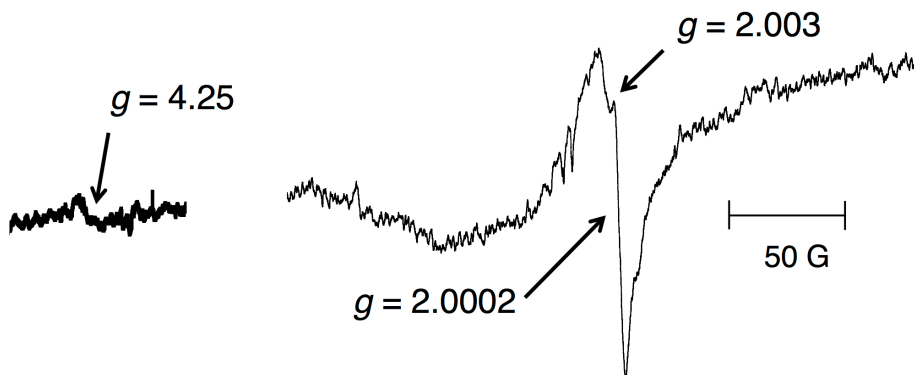


**Figure 6.** EPR spectra of a PhCN glass containing  $(P)$ -(12,8)-[4]CC<sub>2,8</sub>DC<sub>60</sub> (100  $\mu\text{M}$ ) after light irradiation using a high-pressure Hg lamp (1000 W) at low temperature.

The fate of the triplet CS state was tracked by a subsequent transient absorption spectrum upon nanosecond laser flash photolysis ( $\lambda_{\text{ex}} = 420 \text{ nm}$ ). As shown in Figure 4b, the transient absorption spectrum showed an intense band at 750 nm, which was a diagnostic signal of the triplet excited state of the guest ( ${}^3\text{C}_{60}^*$ ). The decay profile afforded a rate constant ( $k$ ) of  $1.2 \times 10^4 \text{ s}^{-1}$  and lifetime ( $\tau$ ) of  $80 \mu\text{s}$ .

The overall picture of the energetics for the photoexcitation processes has been completed by the analysis with cyclic voltammetry (CV). The voltammograms of  $(P)$ -(12,8)-[4]CC<sub>2,8</sub>DC<sub>60</sub>,  $(P)$ -(12,8)-[4]CC<sub>2,8</sub> and C<sub>60</sub> are shown in Figure 7. The CS state energy was determined from the difference of the first redox potentials in  $(P)$ -(12,8)-[4]CC<sub>2,8</sub>DC<sub>60</sub> to afford the value 1.90 eV. The energy of the singlet excited state of [4]CC host ( ${}^1[4]\text{CC}^*$ ;  $^*$  denotes the excited state) was determined from the average of the absorption and fluorescence energies ( $\lambda_{\text{max}} = 417 \text{ nm}$  and  $\lambda_{\text{fl}} = 450 \text{ nm}$ ) to be 2.87 eV.<sup>3</sup> On the other hand, the energy of the singlet excited state of C<sub>60</sub> ( ${}^1\text{C}_{60}^*$ )

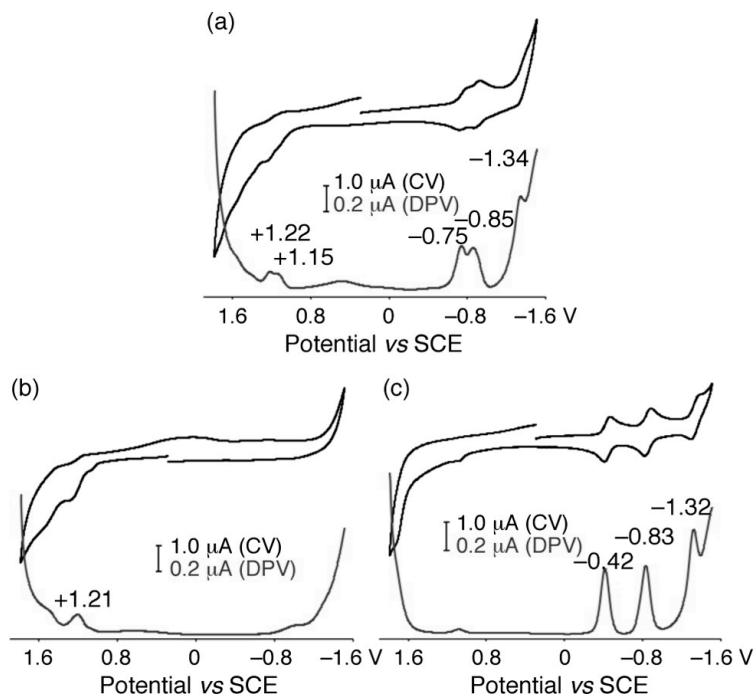


**Figure 7.** Cyclic voltammograms (CV) and differential pulse voltammograms (DPV) in deaerated PhCN at ambient temperature. Conditions: [Specimen] = 200  $\mu$ M,  $[\text{Bu}_4\text{NPF}_6]$  = 100  $\mu$ M, scan rate = 100  $\text{mV s}^{-1}$  (CV) and 4  $\text{mV s}^{-1}$  (DPV), working and counter electrodes = Pt, Reference electrode =  $\text{Ag}/\text{AgNO}_3$ . CVs and DPVs of (a) (P)-(12,8)-[4]CC<sub>2,8</sub>–C<sub>60</sub>, (b) (P)-(12,8)-[4]CC<sub>2,8</sub>, and (c) C<sub>60</sub>.

is known to be 1.99 eV.<sup>15</sup> Thus, photoinduced electron transfer to form the charge-separated state in the supramolecular complex is energetically favorable because the energy of the CS state is lower than the excited state of both of the components. The energy diagram of the photodynamic processes is summarized in Figure 8.<sup>16</sup> The photodynamic processes associated with the fluorescence quenching was thus revealed as follows: After photoexcitation of the [4]CC host, a rapid PET reaction proceeds to afford the triplet CS species at 1.90 eV. The energy of the triplet excited state of C<sub>60</sub> ( $^3\text{C}_{60}^*$ : 1.57 eV) is lower than that of the CS state (1.90 eV), facilitating the fast BET reaction of  $6.7 \times 10^8 \text{ s}^{-1}$  to afford C<sub>60</sub><sup>\*</sup> in the complex. As is the case of naked C<sub>60</sub>, the triplet C<sub>60</sub> survives with a relatively long lifetime (80  $\mu$ s) and, finally, relaxes to the ground state at the rate of  $1.2 \times 10^4 \text{ s}^{-1}$ .

Other interesting characteristics indicated by the voltammetry analysis were the effects of the complexation on the host and the guest at the ground states. Thus, the oxidation potentials of [4]CC shifted by -60 mV (from +1.21 V to +1.15 V), and the first reduction potentials of C<sub>60</sub> shifted by -330 mV (from -0.42 to -0.75 V) upon encapsulation. The negative shifts of the potentials, for both the oxidation of the host and reduction of the guest, show a ground state

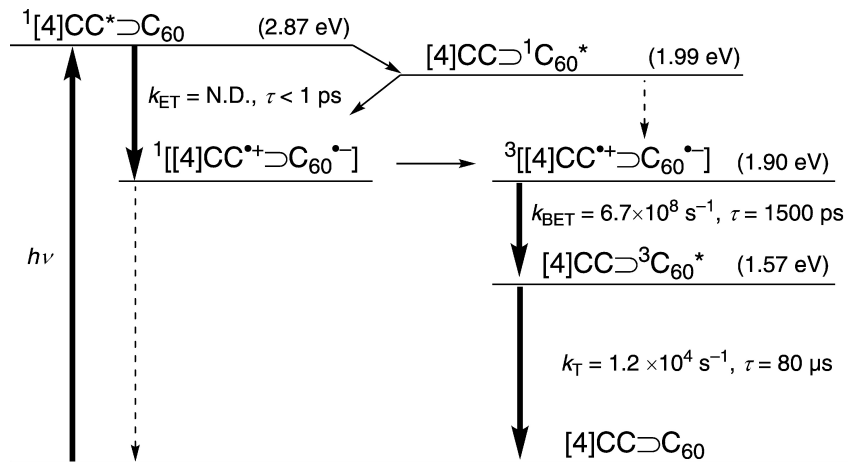


**Figure 8.** Energetics of photodynamic processes in (P)-(12,8)-[4]CC<sub>2,8</sub>–C<sub>60</sub>. The bold arrows show the pathway confirmed by the present study, and the broken arrow shows a potential minor pathway.

communication in the complex and indicate the presence of partial charge transfer from the [4]CC host and the C<sub>60</sub> guest at the ground state. The large negative shift of –330 mV in the C<sub>60</sub> guest is, in passing, among the largest values recorded in supramolecular systems of C<sub>60</sub> and is probably caused by less solvation of C<sub>60</sub><sup>•–</sup> and also by efficient electronic communications in the complex at the ground state.<sup>17,18</sup> Albeit a static view, a preliminary theoretical investigation with the DFT method on the complex indicated the presence of partial charge transfer (0.06 electrons) from the host to the guest at the ground state. The accompanying shifts in the frontier orbital levels upon complexation were +170 meV for LUMO guest and +50 meV for HOMO host, which explains the negative shifts of the redox potentials of the C<sub>60</sub> guest and the [4]CC host, respectively (Figure 9). Further theoretical studies including the dynamics behaviors are currently on going. Finally, I consider the preceding relevant results of infinite single-wall CNT (SWNT) peapods by taking into account the results obtained in this study. It has been reported that fullerene-encapsulating sites in peapods with single-wall CNTs (SWNTs) act as quantum wells in the one-dimensional system of SWNTs to modulate the band characteristics,<sup>19</sup> which may indicate that the fundamental characters of the finite systems may be, surely with great care on the applicability, extrapolated to the infinite systems. As a device application, a field-effect transistor (FET) of peapods comprising infinite SWNTs and C<sub>60</sub> was reported by Li and co-workers.<sup>20</sup> Their observation of an increased hole density in SWNT FET upon peapod formation indeed correlates well with the partial charge transfer process from the host to the guest at the ground state in this study. Interestingly, Li further observed that the threshold voltage in the peapod FET shifted back toward the negative voltage upon photoirradiation and

suggested an excess BET reaction from  $C_{60}$  to SWNT as its potential origin. Although the observation of the rapid BET reaction in our finite system may correlate well with this proposal, I may suggest that the triplet-coupled nature of the CS species from the photo- excitation could also act as a hole trap in the *p*-type FET and that such spin correlations in SWNT peapods may deserve further studies in the future.

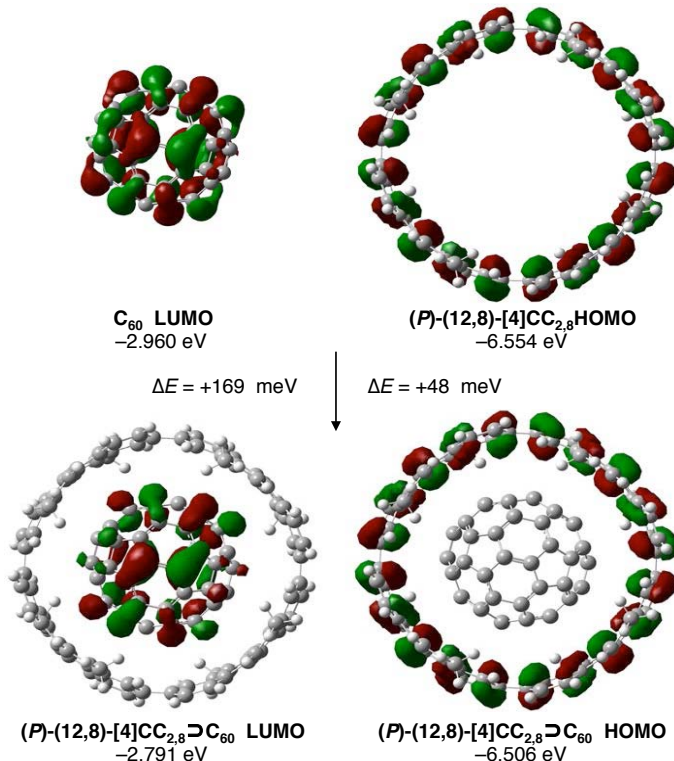


**Figure 9.** Atomic charge mapping in  $(P)-(12,8)-[4]CC_{2,8}\supset C_{60}$  at the ground state (M06-2X/6-311G(d)). For clarity, the charge distributions in  $[4]CC$  (left) and  $C_{60}$  (right) are shown in separate panels. The sum of the transferred charge on  $C_{60}$  was 0.08 electron. Note that the charge was effectively delocalized over the  $C_{60}$  molecule to result in the very small charges on each atom.

In summary, I studied the fundamental photodynamics of the molecular peapod with curved  $\pi$ -structures. Despite the dynamic structures of the peapod,<sup>4,5</sup> the PET processes were not hampered, and the photodynamics followed the energetics derived from the static molecular components. The tight and effective contacts between host and guest with highly delocalized  $\pi$ -systems may play a central role in such unique PET systems, and the detailed correlations of energetics, kinetics, and molecular dynamics will be studied in the near future. Experimental investigations for control over energetics, for instance, with other molecular peapods of both host and guest variants, are also of immediate interest.<sup>4,21</sup> The observation of triplet-coupled CS

species led us to an interesting proposal of spin correlations in SWNT peapods and may stimulate further studies along this line.

## References

- (1) Matsuno, T.; Naito, H.; Hitosugi, S.; Sato, S.; Kotani, M.; Isobe, H. *Pure Appl. Chem.* **2014**, *86*, 489–495.
- (2) (a) Jasti, R.; Bhattacharjee, J.; Neaton, J. B.; Bertozzi, C. R. *J. Am. Chem. Soc.* **2008**, *130*, 17646–17647. (b) Takaba, H.; Omachi, H.; Yamamoto, Y.; Bouffard, H.; Itami, K. *Angew. Chem., Int. Ed.* **2009**, *48*, 6112–6116. (c) Yamago, S.; Watanabe, Y.; Iwamoto, T. *Angew. Chem., Int. Ed.* **2010**, *49*, 757–759.
- (3) (a) Hitosugi, S.; Nakanishi, W.; Yamasaki, T.; Isobe, H. *Nature Commun.* **2011**, *2*, 492. Hitosugi, S.; Nakanishi, W.; Isobe, H. *Chem.-Asian J.* **2012**, *7*, 1550–1552. (b) Hitosugi, S.; Yamasaki, T.; Isobe, H. *J. Am. Chem. Soc.* **2012**, *134*, 12442–12445.
- (4) (a) Isobe, H.; Hitosugi, S.; Yamasaki, T.; Iizuka, R. *Chem. Sci.* **2013**, *4*, 1293–1297. (b) Hitosugi, S.; Iizuka, R.; Yamasaki, T.; Zhang, R.; Murata, Y.; Isobe, H. *Org. Lett.* **2013**, *15*, 3199–3201.
- (5) Sato, S.; Yamasaki, T.; Isobe, H. *Proc. Natl. Acad. Sci. U. S. A.* **2014**, *111*, 8374–8379.
- (6) (a) Smith, B. W.; Monthioux, M.; Luzzi, D. E. *Nature* **1998**, *396*, 323–324. Iijima, S. *Physica B* **2002**, *323*, 1–5. (b) Monthioux, M. *Carbon* **2002**, *40*, 1809–1823. (c) Krive, I. V.; Shekhter, R. I.; Jonson, M. *Low Temp. Phys.* **2006**, *32*, 1171–1194. (d) de Juan, A.; Pérez, E. M. *Nanoscale* **2013**, *5*, 7141–7148.
- (7) Iwamoto, T.; Watanabe, Y.; Sadahiro, T.; Haino, T.; Yamago, S. *Angew. Chem., Int. Ed.* **2011**, *50*, 8342–8344.
- (8) Gaussian 09, Revision B.01, Frisch, M. J.; Trucks, G. W.; Schlegel, H. B.; Scuseria, G. E.; Robb, M. A.; Cheeseman, J. R.; Scalmani, G.; Barone, V.; Mennucci, B.; Petersson, G. A.; Nakatsuji, H.; Caricato, M.; Li, X.; Hratchian, H. P.; Izmaylov, A. F.; Bloino, J.; Zheng, G.; Sonnenberg, J. L.; Hada, M.; Ehara, M.; Toyota, K.; Fukuda, R.; Hasegawa, J.; Ishida, M.; Nakajima, T.; Honda, Y.; Kitao, O.; Nakai, H.; Vreven, T.; Montgomery, J. A. Jr.; Peralta, J. E.; Ogliaro, F.; Bearpark, M.; Heyd, J. J.; Brothers, E.; Kudin, K. N.; Staroverov, V. N.; Kobayashi, R.; Normand, J.; Raghavachari, K.; Rendell, A.; Burant, J. C.; Iyengar, S. S.; Tomasi, J.; Cossi, M.; Rega, N.; Millam, J. M.; Klene, M.; Knox, J. E.; Cross, J. B.; Bakken, V.; Adamo, C.; Jaramillo, J.; Gomperts, R.; Stratmann, R. E.; Yazyev, O.; Austin, A. J.; Cammi, R.; Pomelli, C.; Ochterski, J. W.; Martin, R. L.; Morokuma, K.; Zakrzewski,

V. G.; Voth, G. A.; Salvador, P.; Dannenberg, J. J.; Dapprich, S.; Daniels, A. D.; Farkas, O.; Foresman, J. B.; Ortiz, J. V.; Cioslowski, J.; Fox, D. J. Gaussian, Inc., Wallingford CT, **2009**.

(9) Details including the references for the DFT method and basis set can be found online at the homepage of Gaussian, Inc.: <http://www.gaussian.com/>

(10) Zhao, Y.; Truhlar, D. G. *Theor. Chem. Acc.* **2008**, *120*, 215–241.

(11) Anslyn, E. V.; Dougherty, D. A. *Modern Physical Organic Chemistry*; University Science Books: Sausalito, CA, 2006; Chapter 16.2, pp 953–962.

(12) Arbogast, J. W.; Foote, C. S.; Kao, M. *J. Am. Chem. Soc.* **1992**, *114*, 2277–2279. Skiebe, A.; Hirsch, A.; Klos, H.; Gotschy, B. *Chem. Phys. Lett.* **1994**, *220*, 138–140. Klos, H.; Rystau, I.; Schütz, W.; Gotschy, B.; Skiebe, A.; Hirsch, A. *Chem. Phys. Lett.* **1994**, *224*, 333–337. Ito, O. *Res. Chem. Intermed.* **1997**, *23*, 389–402. Fujitsuka, M.; Luo, C.; Ito, O. *J. Phys. Chem. B* **1999**, *103*, 445–449. Isobe, H. Tanaka, T.; Nakanishi, W.; Lemiégre, L.; Nakamura, E. *J. Org. Chem.* **2005**, *70*, 4826–4832.

(13) Fukuzumi, S.; Mori, H.; Suenobu, T.; Imahori, H.; Gao, X.; Kadish, K. M. *J. Phys. Chem. A* **2000**, *104*, 10688–10694.

(14) Lee, S.-H.; Larsen, A. G.; Ohkubo, K.; Cai, Z.-L.; Reimers, J. R.; Fukuzumi, S.; Crossley, M. *J. Chem. Sci.* 2012, *3*, 257–269. Hayashi, H.; Nagakura, S.; Iwata, S. *Mol. Phys.* **1967**, *13*, 489–490.

(15) Foote, C. S. *Top. Curr. Chem.* **1994**, *169*, 348–363.

(16) Because the molar absorption coefficient of the [4]CC host is much larger than that of the guest C<sub>60</sub> at the excitation wavelengths (host:  $\varepsilon_{420} = 28100 \text{ cm}^{-1} \text{ M}^{-1}$ ,  $\varepsilon_{393} = 32700 \text{ cm}^{-1} \text{ M}^{-1}$ ; guest:  $\varepsilon_{420} = 1300 \text{ cm}^{-1} \text{ M}^{-1}$ ,  $\varepsilon_{393} = 4500 \text{ cm}^{-1} \text{ M}^{-1}$ ), I considered the photodynamics through the excitation of the host in this study.

(17) Canevet, D.; Gallego, M.; Isla, H.; de Juan, A.; Pérez, E. M.; Martín, N. *J. Am. Chem. Soc.* **2011**, *133*, 3184–3190.

(18) (a) Canevet, D.; Pérez, E. M.; Martín, N. *Angew. Chem., Int. Ed.* **2011**, *50*, 9248–9259. (b) Takai, A.; Chokounda, M.; Eggenspiller, A.; Gros, C. P.; Lachkar, M.; Barbe, J.-M.; Fukuzumi, S. *J. Am. Chem. Soc.* **2010**, *132*, 4477–4489.

(19) Lee, J.; Kim, H.; Kahng, S. J.; Kim, G.; Son, Y.-W.; Ihm, J.; Kato, H.; Wang, Z. W.; Okazaki, T.; Shinohara, H.; Kuk, Y. *Nature* **2002**, *415*, 1005–1008.

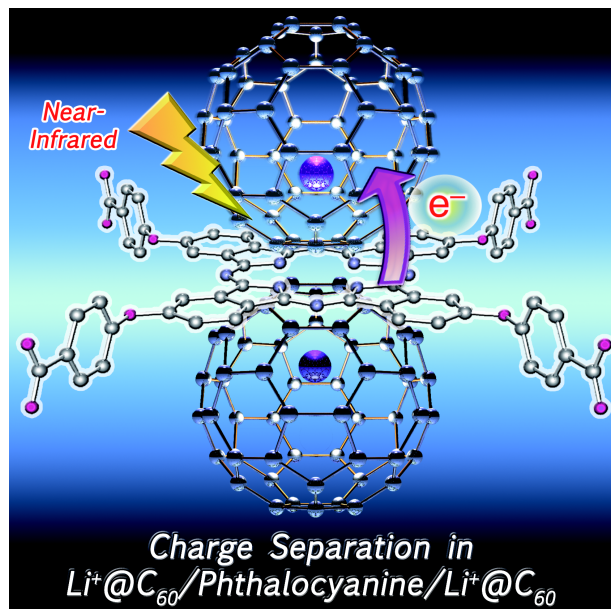
(20) Li, Y. F.; Kaneko, T.; Hatakeyama, R. *Appl. Phys. Lett.* **2008**, *92*, 183115.

(21) Matsuno, T.; Kamata, S.; Hitosugi, S.; Isobe, H. *Chem. Sci.* **2013**, *4*, 3179–3183.

---

## Chapter 12

### Near-Infrared Photoelectrochemical Conversion via Photoinduced Charge Separation in Supramolecular Complexes of Anionic Phthalocyanines with $\text{Li}^+@\text{C}_{60}$



**Abstract:** Two phthalocyanines possessing carboxylate groups ( $\text{H}_2\text{Pc}\bullet\mathbf{1}^{4-}$  and  $\text{H}_2\text{Pc}\bullet\mathbf{2}^{4-}$ ) form 1:2 supramolecular complexes with lithium cation-encapsulated  $\text{C}_{60}$  ( $\text{Li}^+@\text{C}_{60}$ ) [ $\text{H}_2\text{Pc}\bullet\mathbf{1}^{4-}/(\text{Li}^+@\text{C}_{60})_2$  and  $\text{H}_2\text{Pc}\bullet\mathbf{2}^{4-}/(\text{Li}^+@\text{C}_{60})_2$ ] in a polar mixed solvent. From the UV–Vis spectral changes, the binding constants ( $K$ ) were estimated as *ca.*  $10^{12} \text{ M}^{-2}$ . Upon the photoexcitation of constructed supramolecular complexes, photoinduced electron transfer occurred to form the charge-separated (CS) state. The lifetime of the CS state was determined to be 1.2 ms for  $\text{H}_2\text{Pc}\bullet\mathbf{2}^{4-}/(\text{Li}^+@\text{C}_{60})_2$ , which is the longest CS lifetime among the porphyrinoid/fullerene supramolecular complexes.  $\text{H}_2\text{Pc}\bullet\mathbf{1}^{4-}/(\text{Li}^+@\text{C}_{60})_2$  also afforded the long-lived CS state of 1.0 ms. The spin state of the long-lived CS states was determined to be triplet as indicated by the EPR signal at  $g = 4$ . The reorganization energy ( $\lambda$ ) and the electronic

coupling term were determined to be  $\lambda = 1.70$  eV,  $V = 0.15$  cm<sup>-1</sup> from the temperature dependence of the rate constant for the charge recombination of the CS state of H<sub>2</sub>Pc•4<sup>4-</sup>/(Li<sup>+</sup>@C<sub>60</sub>)<sub>2</sub>. The energy of the CS state (0.49 eV) is much smaller than the reorganization energy, indicating that the back electron transfer process is located in the Marcus normal region. The small electronic coupling term results from the spin-forbidden back electron transfer due to the triplet CS state. Supramolecular complexes of anionic zinc phthalocyanines with Li<sup>+</sup>@C<sub>60</sub> were also prepared and investigated. The ZnPc•4<sup>4-</sup>/Li<sup>+</sup>@C<sub>60</sub> supramolecular nanoclusters were assembled on the optically transparent electrode (OTE) of nanostructured SnO<sub>2</sub> (OTE/SnO<sub>2</sub>) to construct the dye-sensitized solar cell. The IPCE (incident photon-to-photocurrent efficiency) values of OTE/SnO<sub>2</sub>/(ZnPc•4<sup>4-</sup>/Li<sup>+</sup>@C<sub>60</sub>)<sub>n</sub> were much higher than the sum of the two IPCE values of the individual systems OTE/SnO<sub>2</sub>/(Li<sup>+</sup>@C<sub>60</sub>)<sub>n</sub> and OTE/SnO<sub>2</sub>/(ZnPc•4<sup>4-</sup>)<sub>n</sub>, covering the near infrared region.

## Introduction

Converting the solar energy into the electricity or chemical energy is the one of the most important issues to realize a sustainable society because the conventional energy resources such as fossil fuels will be used up in the near future.<sup>1-6</sup> Organic thin film solar cells<sup>7-11</sup> and dye-sensitized solar cells<sup>12-17</sup> have attracted much attention because of the cheaper cost in term of fabrication and energy than that of inorganic solar cells. In the nature, the photosynthetic reaction center produces the long-lived charge-separated CS state via photoinduced electron transfer from the excited chlorophyll dimer (special pair) to quinone derivatives to prepare high-energy compounds such as ATP (adenosine triphosphate) and NADPH (dihydronicotinamide adenine dinucleotide phosphate).<sup>18,19</sup> In the field of artificial photosynthesis, there have been many reports on electron donor–acceptor linked molecules as well as supramolecular systems to achieve the long-lived photoinduced charge-separated (CS) states.<sup>20-52</sup> In particular, supramolecular complexes composed of porphyrinoids and fullerenes have been widely studied using non-covalent interactions such as hydrogen bonds and coordination bonds, because they are suitable electron donor and acceptor for the formation of long-lived CS states.<sup>45-53</sup> The binding in such supramolecular complexes becomes stronger when nonpolar solvents such as toluene are employed.<sup>54,55</sup> However, photoinduced electron transfer is energetically disfavored in nonpolar solvents, because the energies of the CS states are often higher than the excited states of fullerenes and porphyrinoids.<sup>50</sup> In contrast to nonpolar solvents, polar solvents such as benzonitrile (PhCN) can stabilize the CS states by strong solvation to

facilitate photoinduced electron transfer but disturb formation of hydrogen bonds and coordination bonds in supramolecular complexes.<sup>48,49</sup> Non-covalent interactions, which are favored in polar solvents, are electrostatic interactions. Thus, supramolecular complexes of anionic electron donors and cationic electron acceptors can be readily formed with strong binding in polar solvents.<sup>51-52</sup> Among cationic electron acceptors, lithium cation-encapsulated C<sub>60</sub> (Li<sup>+</sup>@C<sub>60</sub>)<sup>56,57</sup> has merited special attention, because Li<sup>+</sup>@C<sub>60</sub> forms supramolecular complexes with anionic porphyrins and other electron donors with strong electrostatic interactions and Li<sup>+</sup>@C<sub>60</sub> acts a much better electron acceptor than C<sub>60</sub> due to Li<sup>+</sup> inside the C<sub>60</sub> cage.<sup>58-62</sup> The dye-sensitized solar cell composed of nanoclusters of sulfonated zinc *meso*-tetraphenylporphyrin (ZnTPPS<sup>4-</sup>) and Li<sup>+</sup>@C<sub>60</sub> exhibited a significant enhancement in the photoelectrochemical performance as compared with the reference system composed of neutral porphyrin/C<sub>60</sub> system.<sup>63,64</sup> However, such dye-sensitized solar cells composed of porphyrins as light harvesting molecules cannot utilize near infrared light, because the Q-band of porphyrins composed of two or four bands appear only in the visible region (around 550 nm). In contrast to porphyrins, phthalocyanines show the intense Q-band in the near infrared region,<sup>65-67</sup> exhibiting a superior photostability. However, there has been no report on supramolecular complexes of phthalocyanines with Li<sup>+</sup>@C<sub>60</sub> or the application to the dye-sensitized solar cell.

I report herein the formation of supramolecular complexes of four anionic phthalocyanines (Figure 1) with Li<sup>+</sup>@C<sub>60</sub>, which afford long-lived photoinduced CS states in a polar solvent. I report also the photoelectrochemical performance of dye-sensitized solar cell composed of supramolecular complexes of anionic phthalocyanines with Li<sup>+</sup>@C<sub>60</sub>.

## Experimental Section

**Tetra-*n*-butylammonium Tetra-2(3),9(10),16(17),23(24)-*p*-carboxyphenoxyphthalocyaninate, (TBA)<sub>4</sub>H<sub>2</sub>Pc•1.** 50 mg (0.05 mmol) of H<sub>2</sub>Pc•1<sup>68</sup> [see Figure S1 in Supporting Information (SI)] and 122  $\mu$ L (0.2 mmol) of tetra-*n*-butylammonium hydroxide were solved in 3 mL of a mixture solvent (MeOH/H<sub>2</sub>O (v/v) = 1:1) and stirred at room temperature under argon atmosphere for 2 h. The product was diluted in toluene and washed with H<sub>2</sub>O. The organic phase was removed with vacuum, affording 60 mg (64 %) of a green solid. <sup>1</sup>H-NMR (DMSO-*d*<sub>6</sub>)  $\delta$  0.9 (m, 48H, CH<sub>3</sub>), 1.26 (m, 32H, CH<sub>2</sub>), 1.52 (m, 32H, CH<sub>2</sub>), 3.10 (m, 32H, CH<sub>2</sub>N), 7.52 (m, 8H, ArH), 7.71 (m, 4H, HPc), 8.03 (m, 8H, ArH), 8.65 (m, 4H, HPc), 9.19 (m, 4H, HPc) (Figure S1 in SI). UV-Vis (DMSO)  $\lambda_{\text{max}}$ /nm (log  $\varepsilon$ ): 348 (4.98), 612 (4.66), 680 (5.21), 706 (5.19). FTIR (KBr)/cm<sup>-1</sup> 3411, 2962, 2875, 1599, 1556, 1476, 1382, 1233, 1559, 1115, 1093, 1012, 745 cm<sup>-1</sup>.

<sup>1</sup>H-NMR and IR spectra (KBr) of (TBA)<sub>4</sub>H<sub>2</sub>Pc•1 are shown in Figures S2 and S3 in SI.

**Tetra-*n*-butylammonium Tetra-2(3),9(10),16(17),23(24)-*p*-carboxyphenylphthalocyaninate, (TBA)<sub>4</sub>H<sub>2</sub>Pc•2.** 20 mg (0.02 mmol) of H<sub>2</sub>Pc•2 (Figure S1) and 55  $\mu$ L (0.08 mmol) of tetra-*n*-butylammonium hydroxide were solved in 2 ml of a mixture solvent (MeOH/H<sub>2</sub>O (v/v) = 1:1) and stirred at room temperature under argon atmosphere during 2 h. The product was diluted in toluene and washed with H<sub>2</sub>O. The organic phase was removed with vacuum affording 30 mg (78%) of a green solid. <sup>1</sup>H-NMR (DMSO-*d*<sub>6</sub>)  $\delta$  0.91 (m, 48H, CH<sub>3</sub>), 1.27 (m, 32H, CH<sub>2</sub>), 1.53 (m, 32H, CH<sub>2</sub>), 3.08 (m, 32H, CH<sub>2</sub>N), 8.08, 8.13 (AA'BB', 16H, ArH), 8.39 (m, 4H, HPc), 9.41 (m, 4H, HPc), 9.57 (m, 4H, HPc). UV-Vis (DMSO)  $\lambda_{\text{max}}$ /nm (log  $\varepsilon$ ): 351 (4.53), 687 (4.70). FTIR (KBr)/cm<sup>-1</sup> 3421, 2961, 2874, 1654, 1594, 1544, 1486, 1380, 1094, 1058, 791, 751 cm<sup>-1</sup>. <sup>1</sup>H-NMR and IR spectra (KBr) of (TBA)<sub>4</sub>H<sub>2</sub>Pc•2 are shown in Figures S4 and S5 in SI.

**Octa-*n*-butylammonium Octa-2,3,9,10,16,17,23,24-*p*-carboxyphenoxyphthalocyaninate, (TBA)<sub>8</sub>H<sub>2</sub>Pc•3.** 40 mg (0.03 mmol) of H<sub>2</sub>Pc•3<sup>69</sup> (Figure S1) and 134  $\mu$ L (0.2 mmol) of tetrabutylammonium hydroxide were solved in 3 mL of a mixture solvent (MeOH/H<sub>2</sub>O (v/v) = 1:1) and stirred at room temperature under argon atmosphere for 2 h. The reaction crude was diluted in toluene and washed with H<sub>2</sub>O. The organic phase was removed with vacuum, affording 80 mg (80%) of a green solid. <sup>1</sup>H-NMR (DMSO-*d*<sub>6</sub>)  $\delta$  0.88 (m, 96H, CH<sub>3</sub>), 1.23 (m, 64H, CH<sub>2</sub>), 1.48 (m, 64H, CH<sub>2</sub>), 3.06 (m, 64H, (CH<sub>2</sub>N), 7.02 (m, 16H, ArH), 7.88 (m, 16H, ArH), 8.75 (m, 8H, HPc). UV-Vis (DMSO)  $\lambda_{\text{max}}$ /nm (log  $\varepsilon$ ): 354 (5.15), 612 (4.78), 672 (5.46), 706 (5.49). FT-IR (KBr)/cm<sup>-1</sup> 3418, 2961, 2874, 1602, 1559, 1463, 1442, 1381, 1273, 1213, 1161, 1086, 1013, 880, 788, 754, 699 cm<sup>-1</sup>. <sup>1</sup>H-NMR and IR spectra (KBr) of (TBA)<sub>8</sub>H<sub>2</sub>Pc•3 are shown in Figures S6 and S7 in SI

**Tetra-*n*-butylammonium Tetra-2(3),9(10),16(17),23(24)-carboxyphthalocyaninate zinc, (TBA)<sub>4</sub>ZnPc•4.** 26 mg (0.04 mmol) of ZnPc•4<sup>70</sup> (Figure S1) and 87  $\mu$ L (0.1 mmol) of tetrabutylammonium hydroxide were solved in 3 mL of a mixture solvent (MeOH/H<sub>2</sub>O (v/v) = 1:1) and stirred at room temperature under argon atmosphere for 2 h. The product was diluted in toluene and washed with H<sub>2</sub>O. The organic phase was removed with vacuum, affording 30 mg (50%) of a green solid. <sup>1</sup>H-NMR (D<sub>2</sub>O)  $\delta$  0.87 (m, 48H, CH<sub>3</sub>), 1.26 (m, 32H, CH<sub>2</sub>), 1.55 (m, 32H, CH<sub>2</sub>), 3.08 (m, 32H, CH<sub>2</sub>N), 7.46-9.42 (m, 12H, HPc). UV-Vis (DMSO)  $\lambda_{\text{max}}$ /nm (log  $\varepsilon$ ): 339 (4.57), 603 (4.22), 672 (4.98). FT(KBr)/cm<sup>-1</sup> 3411, 2960, 2874, 1656, 1613, 1567, 1525, 1487, 1473, 1379, 882, 797, 740 cm<sup>-1</sup>. <sup>1</sup>H-NMR and IR spectra (KBr) of (TBA)<sub>4</sub>ZnPc•4 are shown in Figures S8 and S9 in SI.

**Materials.** General chemicals of the best grade available were purchased from commercial

---

suppliers and were used without further purification. Unless otherwise noted, benzonitrile (PhCN) was distilled over two times phosphorus pentaoxide ( $P_2O_5$ ), and potassium carbonate ( $K_2CO_3$ ) before use. Dimethyl sulphoxide (DMSO) was used without further purification. Lithium-ion-encapsulated fullerene hexafluorophosphate salt ( $Li^+@C_{60} PF_6^-$ , Idea International Corporation) was commercially obtained from Wako Pure Chemical Industries, Ltd., Japan.

**NMR.**  $^1H$  NMR spectra were recorded on a Varian spectrometer in deuterated dimethyl sulfoxide.

**UV–Vis Absorption Spectral Measurements.** Absorption spectra were recorded on a JASCO V-670 spectrophotometer at room temperature.

**Emission Spectral Measurements.** Phosphorescence spectra were measured on a Horiba FluoroMax-4 spectrofluorophotometer. A 2-methyltetrahydrofuran(2-MeTHF)/ethyl iodide(EtI) (9:1 v/v) solution of anionic phthalocyanines in a quartz tube (3 mm in diameter) were degassed by nitrogen bubbling for 10 min prior to the measurements. The sample tube was put in a quartz liquid nitrogen Dewar flask. The measurements were carried out by excitation at 400 nm for  $H_2Pc\bullet 1^{4-}$ , 430 nm for  $H_2Pc\bullet 2^{4-}$ , and 670 nm for  $H_2Pc\bullet 3^{8-}$  and  $ZnPc\bullet 4^{4-}$ . Fluorescence spectra of anionic phthalocyanines were recorded on a Horiba FluoroMax-4 spectrofluorophotometer. The measurements were carried out by excitation at 450 nm. in deaerated mixed solvent (DMSO and PhCN). The a mixed solvent (DMSO and PhCN) degassed by nitrogen bubbling for 10 min prior to the measurements.

**Electrochemical Measurements.** Differential pales voltammetry (DPV) studies were carried out using an ALS-630B electrochemical analyzer in deaerated PhCN or in a mixed solvent (DMSO and PhCN) containing 0.1 M TBAPF<sub>6</sub> as a supporting electrolyte at 298 K. A conventional three-electrode cell was used with a carbon working electrode (surface area = 0.3 mm<sup>2</sup>) and a platinum wire as the counter electrode. The carbon working electrode, purchased from BAS, was routinely polished with a polishing alumina suspension from BAS and rinsed with distilled water and acetonitrile before use. The potentials were measured with respect to an Ag/AgNO<sub>3</sub> (10 mM) reference electrode. All electrochemical measurements were carried out under a nitrogen atmosphere. The values of redox potentials (vs Ag/AgNO<sub>3</sub>) are converted into those vs SCE by addition of 0.29 V.

**Laser Flash Photolysis Measurements.** Nanosecond transient absorption spectral measurements were made according to the following procedure. A deaerated solutions containing  $Li^+@C_{60}$  with anionic phthalocyanines were excited by a Panther OPO pumped Nd:YAG laser (Continuum, SLII-10, 4-6 ns fwhm) at 355 nm. The resulting time resolved

transient absorption spectra were measured by using a continuous Xe-lamp (150 W) and a photodiode (Hamamatsu 2949) as the probe light and detector, respectively. The output from the photodiode and the photomultiplier tube was recorded using a digitizing oscilloscope (Tektronix, TDS3032, 300 MHz). The solutions were deoxygenated by N<sub>2</sub> purging for 10 min prior to measurements. Rates of photoinduced electron-transfer reactions were monitored by the rise and decay of the absorption band due to the Li<sup>+</sup>@C<sub>60</sub> radical anion. First-order rate constants were determined by a least-squares curve fit. All experiments were performed at 298 K.

**ESR Spectroscopy.** ESR spectra were recorded on a JEOL X-band spectrometer (JES-RE1XE) with a quartz ESR tube. The ESR spectrum of the putative CS state in frozen PhCN was measured at 4 K using a liquid helium cryostat and 4 K using a liquid nitrogen cryostat under conditions of photoirradiation with a high-pressure mercury lamp (USHIO LIGHTING USH-1005D) focused through a water filter at the sample cell in the ESR cavity. The *g* values were calibrated using an Mn<sup>2+</sup> marker.

**Photoelectrochemical Measurements.** Electrophoretic deposition was performed using a Power Pac HV (Bio-Rad). Photoelectrochemical measurements were carried out in a standard two-compartment cell consisting of a working electrode, a Pt wire gauze counter electrode. A KEITHLEY 2400 was used for recording *I-V* characteristics and photocurrent generation density under an AM 1.5 simulated light source (OTENTO-SUN II, Bunkoh Keiki Co., LTD). For the IPCE measurements, a monochromator (SM-25, Bunkoh Keiki Co., LTD) was introduced into the path of the excitation beam (150 W xenon lamp, Bunkoh Keiki Co., LTD) for the selected wavelength. The lamp intensity at each wavelength was determined using a Si photodiode (Hamamatsu Photonics S1337-1010BQ) and corrected.

**TEM Measurements.** Transmission electron micrograph (TEM) measurements were recorded on Tecnai spirit (FEI company) by applying a drop of the sample to a copper grid. TEM images were recorded on a transmission electron microscope an accelerating voltage of 120 kV for imaging.

**Dynamic light scattering (DLS) Measurements.** The particle size and distribution were measured in MeCN/PhCN (3:1 v/v) using light-scattering equipment (Zetasizer nano ZS).

## Results and Discussion

### Formation of Supramolecular Complexes of Anionic Phthalocyanines with $\text{Li}^+@\text{C}_{60}$ .

UV–Vis–NIR absorption spectrum of an anionic free base phthalocyanine derivative salt  $[(\text{TBA})_4\text{H}_2\text{Pc}\bullet\mathbf{1}; \text{Figure 1}]$  in a mixed solvent [dimethyl sulfoxide (DMSO):benzonitrile (PhCN) (v/v) = 1:1] was changed upon the addition of  $\text{Li}^+@\text{C}_{60}$  at 298 K as shown in Figure 2a, where the Q-bands at 672 and 703 nm were slightly blue-shifted to 670 and 700 nm, respectively. The absorption band at 672 nm decreased linearly with increasing concentration of  $\text{Li}^+@\text{C}_{60}$  up to 2.0 equiv of  $\text{Li}^+@\text{C}_{60}$  (Figure 2b). These results indicate that  $\text{H}_2\text{Pc}\bullet\mathbf{1}^{4-}$  forms a 1:2 supramolecular complex with  $\text{Li}^+@\text{C}_{60}$   $[\text{H}_2\text{Pc}\bullet\mathbf{1}^{4-}/(\text{Li}^+@\text{C}_{60})_2]$  in a mixed solvent (DMSO:PhCN (v/v) = 1:1). The binding constant ( $K$ ) was roughly estimated as *ca.*  $10^{12} \text{ M}^{-2}$ . Similarly,  $\text{H}_2\text{Pc}\bullet\mathbf{2}^{4-}$  (Figure 1) exhibited formation of a 1:2 supramolecular complex with  $\text{Li}^+@\text{C}_{60}$   $[\text{H}_2\text{Pc}\bullet\mathbf{2}^{4-}/(\text{Li}^+@\text{C}_{60})_2]$  (Figure 3). The binding constant ( $K$ ) was estimated as *ca.*  $10^{12} \text{ M}^{-2}$ .

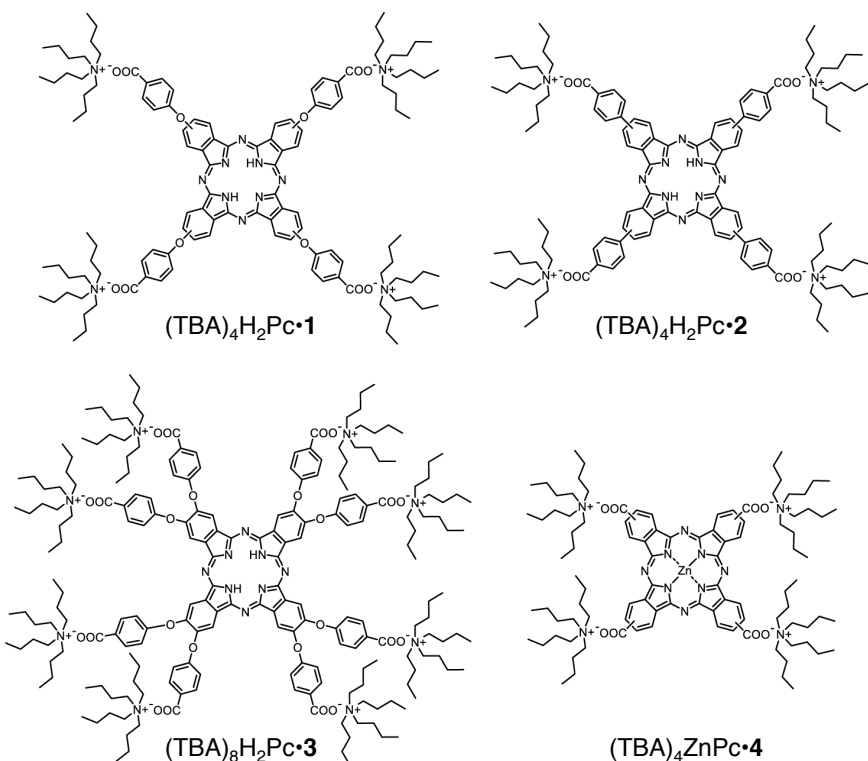


**Figure 1.** Chemical structures of  $(\text{TBA})_4\text{H}_2\text{Pc}\bullet\mathbf{1}$ ,  $(\text{TBA})_4\text{H}_2\text{Pc}\bullet\mathbf{2}$ ,  $(\text{TBA})_8\text{H}_2\text{Pc}\bullet\mathbf{3}$  and  $(\text{TBA})_4\text{ZnPc}\bullet\mathbf{4}$ .

When  $\text{H}_2\text{Pc}\bullet\mathbf{2}^{4-}$  was replaced by  $\text{H}_2\text{Pc}\bullet\mathbf{3}^{8-}$ , the absorption band at 702 nm due to the Q-band of  $\text{H}_2\text{Pc}\bullet\mathbf{3}^{8-}$  decreased with increase in concentration of  $\text{Li}^+@\text{C}_{60}$ , accompanied by a blue-shift to 700 nm (Figure 4). The 1:1 supramolecular formation of  $\text{H}_2\text{Pc}\bullet\mathbf{3}^{8-}/\text{Li}^+@\text{C}_{60}$  was confirmed from the slope (1.02) of the Hill plot (Figure 4c).<sup>59</sup> The binding constant was determined to be  $3.4 \times 10^6 \text{ M}^{-1}$  from the intercept (6.53) and the slope (Figure 4c).  $\text{ZnPc}\bullet\mathbf{4}^{4-}$  also formed a 1:1 supramolecular complex with  $\text{Li}^+@\text{C}_{60}$  with the binding constant of  $2.0 \times 10^4 \text{ M}^{-1}$  (Figure 5), which is 170 times smaller than the value of  $\text{H}_2\text{Pc}\bullet\mathbf{3}^{8-}/\text{Li}^+@\text{C}_{60}$ . The decrease in the Q-band intensity due to the  $\pi$ - $\pi$  interaction with  $\text{Li}^+@\text{C}_{60}$  was not observed in the titration of  $(\text{TBA})_4\text{ZnPc}\bullet\mathbf{4}$  by  $\text{Li}^+@\text{C}_{60}$  in a mixed solvent (DMSO:PhCN (v/v) = 2:1, Figure 5a).

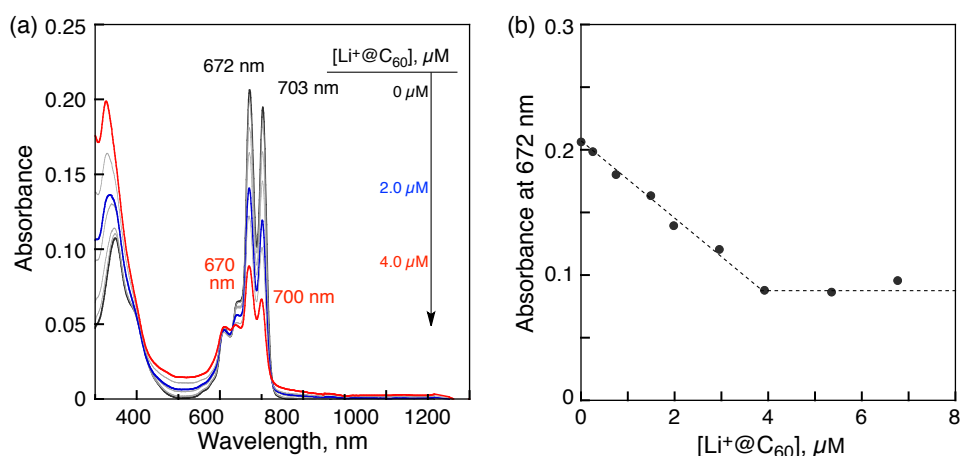


**Figure 2.** (a) Absorption spectral change of  $(\text{TBA})_4\text{H}_2\text{Pc}\bullet\mathbf{1}$  ( $2.0 \times 10^{-6} \text{ M}$ ) recorded upon the addition from 0 to *ca.* 3.5 equiv of  $\text{Li}^+@\text{C}_{60}$  at 298 K in a mixed solvent (DMSO:PhCN (v/v) = 1:1). (b) Plot of absorption changes at 672 nm.

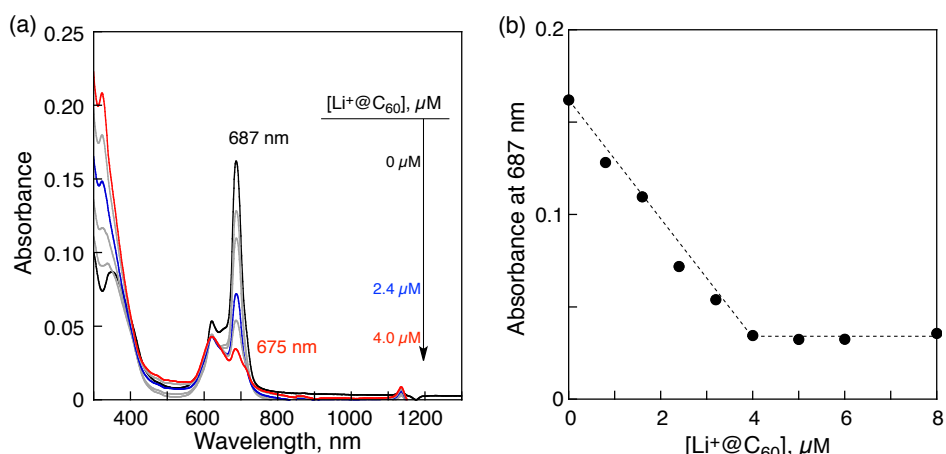


**Figure 3.** (a) Absorption spectral change of  $(\text{TBA})_4\text{H}_2\text{Pc}\bullet\mathbf{2}$  ( $2.0 \times 10^{-6} \text{ M}$ ) recorded upon the addition from 0 to 4.0 equiv of  $\text{Li}^+@\text{C}_{60}$  at 298 K in a mixed solvent (DMSO:PhCN (v/v) = 1:1). (b) Plot of absorption changes at 687 nm.

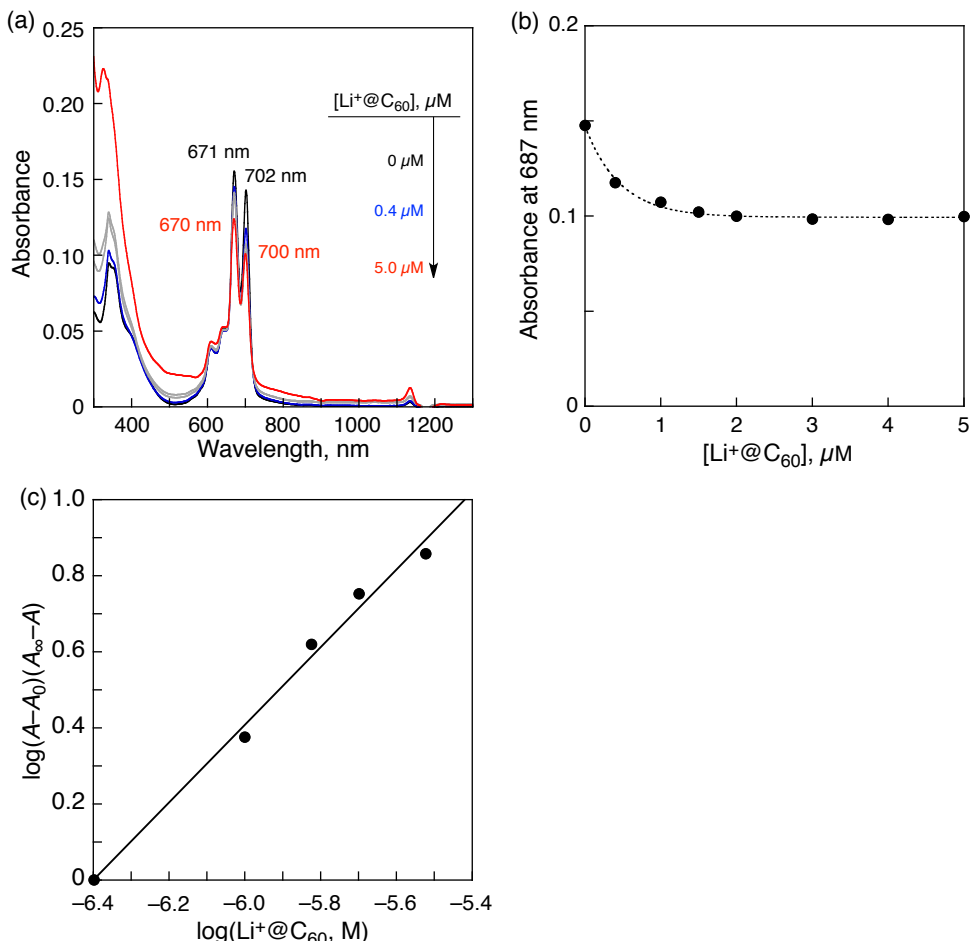


**Figure 4.** (a) Absorption spectral change of  $(TBA)_8H_2Pc\bullet 3$  ( $2.0 \times 10^{-6}$  M) recorded upon the addition from 0 to 2.5 equiv of  $Li^+@C_{60}$  at 298 K in a mixed solvent (DMSO:PhCN (v/v) = 2:1). (b) Plot of absorption changes at 687 nm and (c) Hill plot.

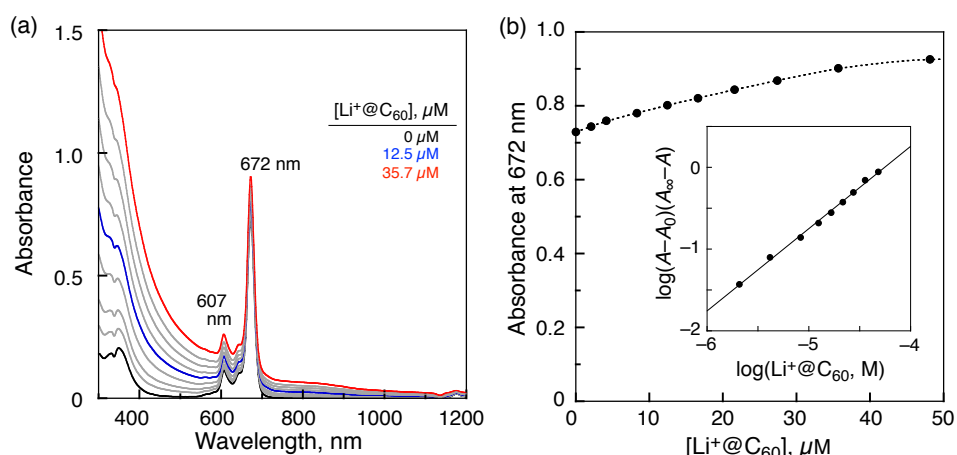


**Figure 5.** (a) Absorption spectral change of  $(TBA)_4ZnPc\bullet 4$  ( $1.0 \times 10^{-5}$  M) recorded upon the addition from 0 to 4.8 equiv of  $Zn\bullet 4^{4+}$  at 298 K in a mixed solvent (DMSO:PhCN (v/v) = 2:1). (b) Plot of absorption changes at 672 nm. Inset: Hill plot.

**Energies of Charge-Separated States.** Electrochemical measurements were performed to determine the energies of the charge-separated (CS) states. Differential pulse voltammetric (DPV) analyses of  $\text{H}_2\text{Pc}\bullet\mathbf{1}^{4-}$ ,  $\text{Li}^+@\text{C}_{60}$ , and  $\text{H}_2\text{Pc}\bullet\mathbf{1}^{4-}/(\text{Li}^+@\text{C}_{60})_2$  were performed in a mixed solvent (DMSO:PhCN (v/v) = 1:1) using 0.1 M tetra-*n*-butylammonium hexafluorophosphate (TBAPF<sub>6</sub>) as a supporting electrolyte, a carbon electrode as a working electrode, platinum wire as a counter electrode, and Ag/AgNO<sub>3</sub> as a reference electrode. The energy of the CS state of  $\text{H}_2\text{Pc}\bullet\mathbf{1}^{4-}/(\text{Li}^+@\text{C}_{60})_2$  was determined to be 0.49 eV from the difference between the one-electron oxidation potential of  $\text{H}_2\text{Pc}\bullet\mathbf{1}^{4-}$  (0.57 V vs SCE) and the one-electron reduction potential of  $\text{Li}^+@\text{C}_{60}$  (0.08 V vs SCE), as shown in Figure 6a. These values are slightly shifted from the original

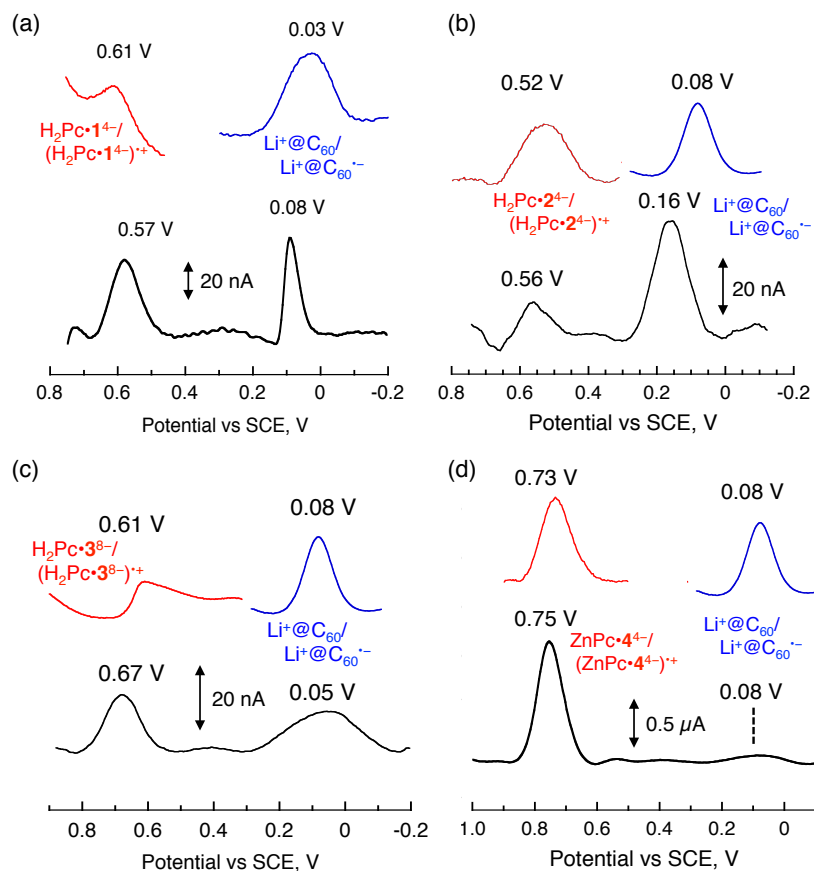


**Figure 6.** Differential pulse voltammograms of (a)  $\text{H}_2\text{Pc}\bullet\mathbf{1}^{4-}$  ( $1.0 \times 10^{-4}$  M, red),  $\text{Li}^+@\text{C}_{60}$  ( $2.5 \times 10^{-4}$  M, blue), and the supramolecular complex ( $[\text{H}_2\text{Pc}\bullet\mathbf{1}^{4-}] = 6.5 \times 10^{-5}$  M and  $[\text{Li}^+@\text{C}_{60}] = 1.3 \times 10^{-4}$  M, black) in a mixed solvent (DMSO:PhCN (v/v) = 1:1) (b)  $\text{H}_2\text{Pc}\bullet\mathbf{2}^{4-}$  ( $1.0 \times 10^{-4}$  M, red),  $\text{Li}^+@\text{C}_{60}$  ( $2.5 \times 10^{-4}$  M, blue), and supramolecule ( $[\text{H}_2\text{Pc}\bullet\mathbf{2}^{4-}] = 6.5 \times 10^{-5}$  M and  $[\text{Li}^+@\text{C}_{60}] = 1.3 \times 10^{-4}$  M, black) (c)  $\text{H}_2\text{Pc}\bullet\mathbf{3}^{8-}$  ( $1.0 \times 10^{-4}$  M, red),  $\text{Li}^+@\text{C}_{60}$  ( $2.5 \times 10^{-4}$  M, blue), and supramolecule ( $[\text{H}_2\text{Pc}\bullet\mathbf{3}^{8-}] = 6.5 \times 10^{-5}$  M and  $[\text{Li}^+@\text{C}_{60}] = 1.3 \times 10^{-4}$  M, black) (d)  $\text{ZnPc}\bullet\mathbf{4}^{4-}$  ( $6.7 \times 10^{-4}$  M, red),  $\text{Li}^+@\text{C}_{60}$  ( $2.5 \times 10^{-4}$  M, blue), and supramolecule ( $[\text{ZnPc}\bullet\mathbf{4}^{4-}] = 6.7 \times 10^{-5}$  M and  $[\text{Li}^+@\text{C}_{60}] = 1.3 \times 10^{-4}$  M, black) in a mixed solvent (DMSO:PhCN (v/v) = 1:2) with 0.1 M of TBAPF<sub>6</sub> as an electrolyte. Sweep rate: 4 mV s<sup>-1</sup>.

one-oxidation potential of  $\text{H}_2\text{Pc}\bullet\mathbf{1}^{4-}$  (0.61 V vs SCE) and the one-electron reduction potential of  $\text{Li}^+@\text{C}_{60}$  (0.03 V vs SCE) due to the charge-transfer interaction in the supramolecular complex. The energies of the other CS states were determined to be 0.40 eV for  $\text{H}_2\text{Pc}\bullet\mathbf{2}^{4-}/(\text{Li}^+@\text{C}_{60})_2$ , 0.62 eV for  $\text{H}_2\text{Pc}\bullet\mathbf{3}^{8-}/\text{Li}^+@\text{C}_{60}$ , and 0.67 eV for  $\text{ZnPc}\bullet\mathbf{4}^{4-}/\text{Li}^+@\text{C}_{60}$  (Figure 6).

The energies of the singlet-excited states of anionic phthalocyanines were determined to be 1.76 eV for  $\text{H}_2\text{Pc}\bullet\mathbf{1}^{4-}$ , 1.79 eV for  $\text{H}_2\text{Pc}\bullet\mathbf{2}^{4-}$ , 1.76 eV for  $\text{H}_2\text{Pc}\bullet\mathbf{3}^{8-}$ , and 1.82 eV for  $\text{ZnPc}\bullet\mathbf{4}^{4-}$  from the absorbance (Figure 2–5) and fluorescence maxima (Figure 7).<sup>71</sup> The energies of the triplet-excited states of anionic phthalocyanines were also determined to be 1.17 eV for  $\text{H}_2\text{Pc}\bullet\mathbf{1}^{4-}$ , 1.17 eV for  $\text{H}_2\text{Pc}\bullet\mathbf{2}^{4-}$ , 1.24 eV for  $\text{H}_2\text{Pc}\bullet\mathbf{3}^{8-}$ , and 1.24 eV for  $\text{ZnPc}\bullet\mathbf{4}^{4-}$  from the phosphorescence maxima at 77 K (Figure 8). The energies of the triplet excited states of both anionic phthalocyanines and  $\text{Li}^+@\text{C}_{60}$  (1.53 eV)<sup>72</sup> are higher than the energies of the CS states, indicating back electron transfer (BET) in the CS state to produce the triplet excited states of chromophores are energetically unfavorable.

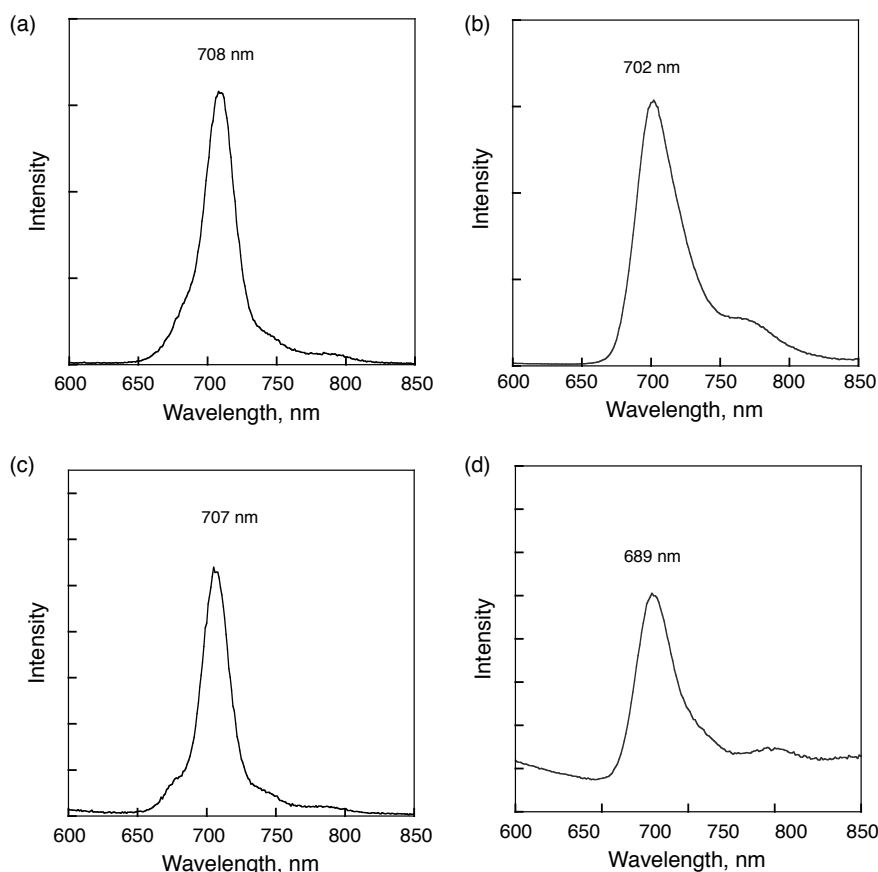


**Figure 7.** Fluorescence spectra of (a)  $(\text{TBA})_4\text{H}_2\text{Pc}\bullet\mathbf{1}$  in a mixed solvent (DMSO:PhCN (v/v) = 1:1), (b)  $(\text{TBA})_4\text{H}_2\text{Pc}\bullet\mathbf{2}$ , (c)  $(\text{TBA})_8\text{H}_2\text{Pc}\bullet\mathbf{3}$ , and (d)  $(\text{TBA})_4\text{ZnPc}\bullet\mathbf{4}$  in a mixed solvent (DMSO:PhCN (v/v) = 2:1).  $[\text{H}_2\text{Pc}\bullet\mathbf{1}^{4-}] = [\text{H}_2\text{Pc}\bullet\mathbf{2}^{4-}] = [\text{H}_2\text{Pc}\bullet\mathbf{3}^{8-}] = [\text{ZnPc}\bullet\mathbf{4}^{4-}] = 5.0 \times 10^{-6} \text{ M}$ ; Excitation: 450 nm.

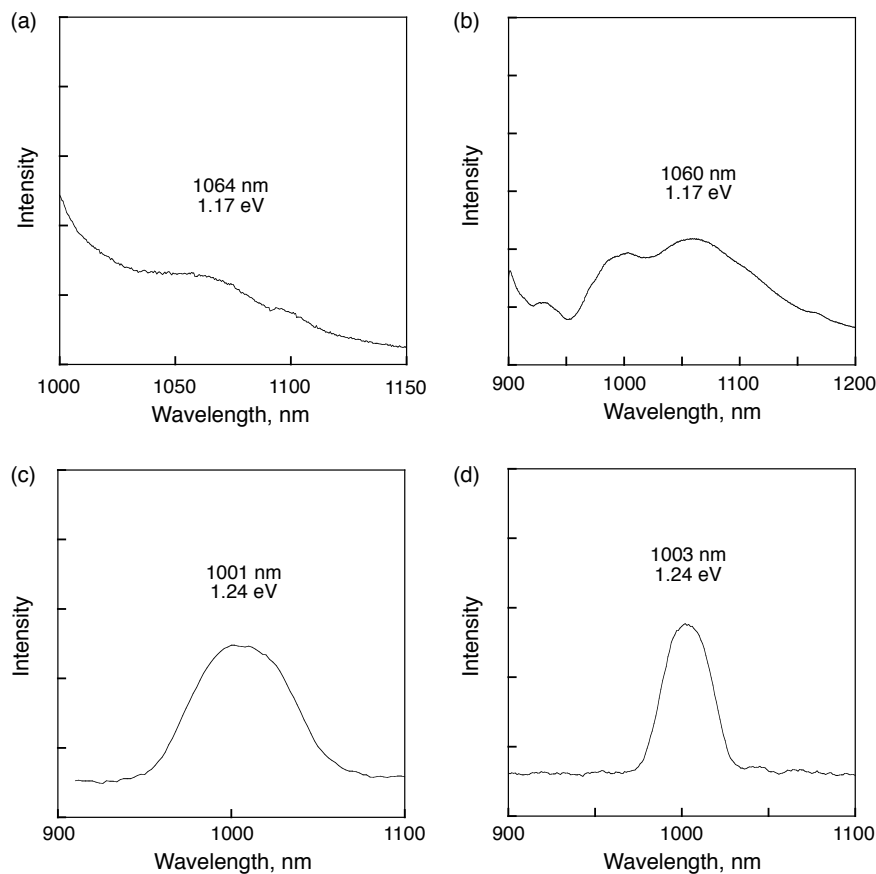


**Figure 8.** Phosphorescence spectra of (a)  $(\text{TBA})_4\text{H}_2\text{Pc}\bullet\mathbf{1}$ , (b)  $(\text{TBA})_4\text{H}_2\text{Pc}\bullet\mathbf{2}$ , (c)  $(\text{TBA})_8\text{H}_2\text{Pc}\bullet\mathbf{3}$ , and (d)  $(\text{TBA})_4\text{ZnPc}\bullet\mathbf{4}$  in a deaerated 2-MeTHF/EtI (9:1 v/v) transparent glass. Excitation wavelength: 400 nm for (a), 430 nm for (b), and 670 nm for (c) and (d);  $T = 77\text{ K}$ .

**Photoinduced Electron Transfer in Supramolecular Complexes.** The transient absorption spectrum of the  $\text{H}_2\text{Pc}\bullet\mathbf{1}^{4-}/(\text{Li}^+@\text{C}_{60})_2$  supramolecular complex taken by nanosecond laser flash photolysis is displayed in Figure 9. The formation of the radical anion of  $\text{Li}^+@\text{C}_{60}$  ( $\text{Li}^+@\text{C}_{60}^{\bullet-}$ ) at 1020 nm<sup>73</sup> was observed at 28  $\mu\text{s}$  after laser excitation. On the other hand, the radical cation of  $\text{H}_2\text{Pc}\bullet\mathbf{1}^{4-}$  [ $(\text{H}_2\text{Pc}\bullet\mathbf{1}^{4-})^{\bullet+}$ ] was not observed clearly because the absorption of  $(\text{H}_2\text{Pc}\bullet\mathbf{1}^{4-})^{\bullet+}$  is too small and broad at 900 nm to be detected. The assignment of  $(\text{H}_2\text{Pc}\bullet\mathbf{1}^{4-})^{\bullet+}$  was carried out by the electrochemical one-electron oxidation by the application of DC electric field (+0.9 V vs SCE) to  $\text{H}_2\text{Pc}\bullet\mathbf{1}^{4-}$  in a mixed solvent (DMSO:PhCN (v/v) = 1:1) containing TBAPF<sub>6</sub> (0.10 M) as an electrolyte, which are recorded by the UV–Vis–NIR absorption spectroscopy (Figure 10a). The decay rate constant of the triplet-excited state of  $\text{H}_2\text{Pc}\bullet\mathbf{1}^{4-}$  [ ${}^3(\text{H}_2\text{Pc}\bullet\mathbf{1}^{4-})^*$ ] at 500 nm ( $k_{\text{T}} = 2.2 \times 10^4\text{ s}^{-1}$ ; Figure 11) was virtually the same as the value in the presence of  $\text{Li}^+@\text{C}_{60}$  ( $k_{\text{T}} = 2.1 \times 10^4\text{ s}^{-1}$ ; Figure 9c). Thus, these results suggest that the observed absorption at 500 nm in Figure 9a is due to the free  ${}^3(\text{H}_2\text{Pc}\bullet\mathbf{1}^{4-})^*$ . Fluorescence lifetimes of  $\text{H}_2\text{Pc}\bullet\mathbf{1}^{4-}$  also remain the same in the

absence and presence of  $\text{Li}^+@\text{C}_{60}$  (Figure 12a), indicating that no electron transfer occurred from  ${}^1(\text{H}_2\text{Pc}\bullet\text{I}^{4-})^*$  or  ${}^3(\text{H}_2\text{Pc}\bullet\text{I}^{4-})^*$  to  $\text{Li}^+@\text{C}_{60}$ . The electron transfer probably occurred from  $\text{H}_2\text{Pc}\bullet\text{I}^{4-}$  to the triplet excited state of  $\text{Li}^+@\text{C}_{60}$  because the spin state of the CS state is triplet as described later.

The lifetime of the CS state was determined to be 1.0 ms (the decay rate constant =  $9.7 \times 10^2 \text{ s}^{-1}$ ) from the first-order decay of the absorption at 1020 nm due to  $\text{Li}^+@\text{C}_{60}^-$ , which is unchanged irrespective of the laser intensities, as shown in Figure 9b. This indicates that the back electron transfer is not *intermolecular* electron transfer between two molecules of the CS states but *intramolecular* electron transfer.

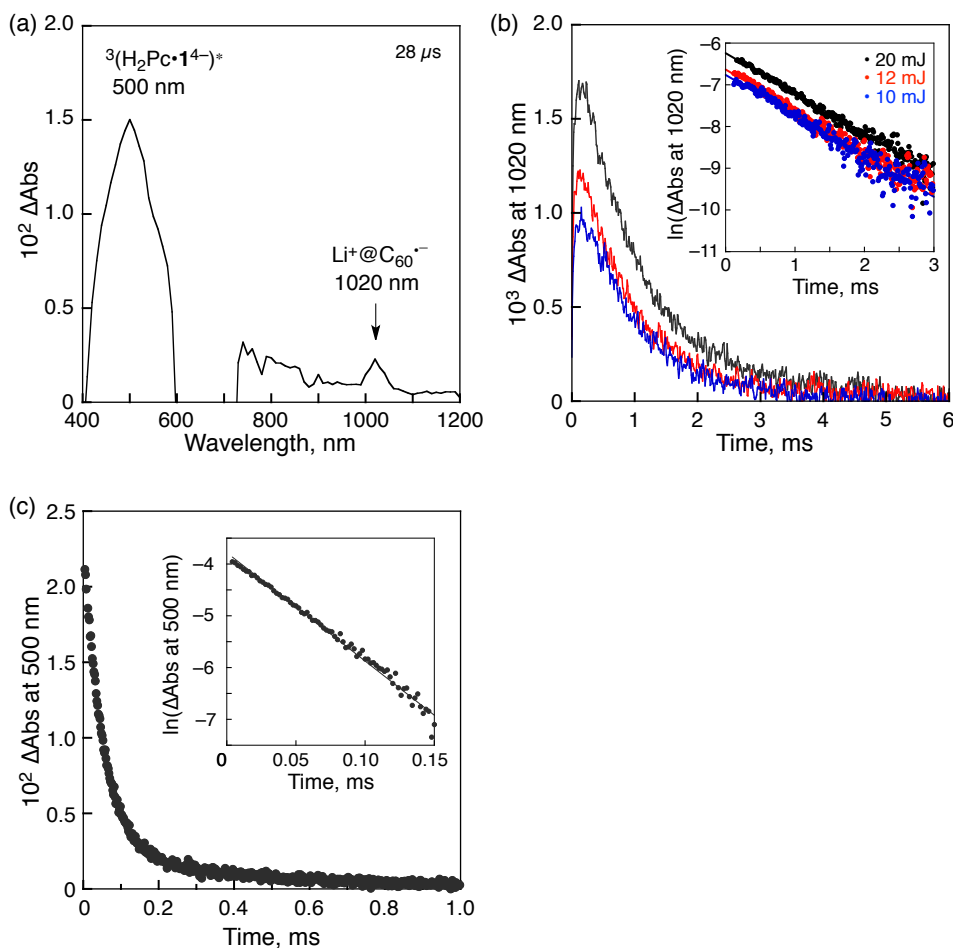


**Figure 9.** (a) Transient absorption spectra of  $\text{H}_2\text{Pc}\bullet\text{I}^{4-}$  ( $1.3 \times 10^{-5} \text{ M}$ ) with  $\text{Li}^+@\text{C}_{60}$  ( $2.5 \times 10^{-5} \text{ M}$ ) in a mixed solvent (DMSO:PhCN (v/v) = 1:1) measured at 28  $\mu\text{s}$  after laser excitation at 355 nm. (b) Decay time profiles of absorbance at 1020 nm with various laser intensities (10, 12, and 20 mJ/pulse). Inset: First-order plots. (c) Decay time profile of absorbance at 500 nm. Inset: First-order plot.

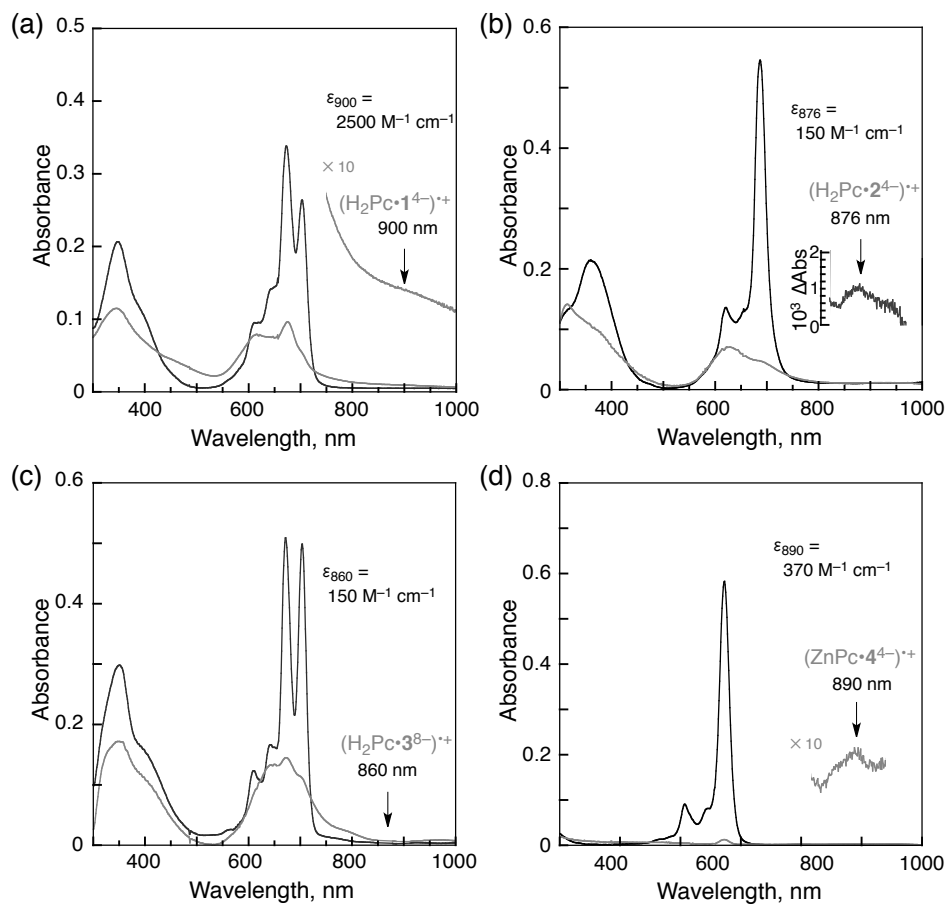


**Figure 10.** Absorption of (a)  $\text{H}_2\text{Pc}\bullet\mathbf{1}^{4-}$ , (b)  $\text{H}_2\text{Pc}\bullet\mathbf{2}^{4-}$ , (c)  $\text{H}_2\text{Pc}\bullet\mathbf{3}^{8-}$  and (d)  $\text{ZnPc}\bullet\mathbf{4}^{4-}$  radical anion generated by applying the voltage of 0.9 V vs SCE in mixed solvents containing 0.1 M of  $\text{TBAPF}_6$  as an electrolyte. Optical path length: 1 mm.  $[\text{H}_2\text{Pc}\bullet\mathbf{1}^{4-}] = [\text{H}_2\text{Pc}\bullet\mathbf{2}^{4-}] = 3.5 \times 10^{-5} \text{ M}$ ,  $[\text{H}_2\text{Pc}\bullet\mathbf{3}^{8-}] = 6.7 \times 10^{-5} \text{ M}$ ,  $[\text{ZnPc}\bullet\mathbf{4}^{4-}] = 8.0 \times 10^{-5} \text{ M}$ .

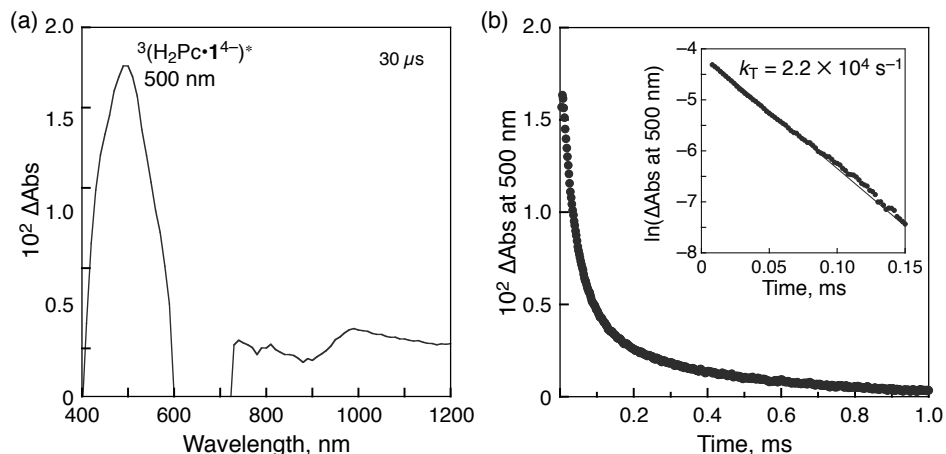


**Figure 11.** (a) Transient absorption spectrum of  $\text{H}_2\text{Pc}\bullet\mathbf{1}^{4-}$  ( $1.3 \times 10^{-5} \text{ M}$ ) in a mixed solvent (DMSO:PhCN (v/v) = 1:1) measured at  $30 \mu\text{s}$  after laser excitation at 355 nm. (d) Decay time profile of absorbance at 500 nm. Inset: First-order plots.

In the cases of  $\text{H}_2\text{Pc}\bullet\mathbf{2}^{4-}$ ,  $\text{H}_2\text{Pc}\bullet\mathbf{3}^{8-}$ , and  $\text{ZnPc}\bullet\mathbf{4}^{4-}$ , the fluorescence lifetimes also remain the same in the absence and presence of  $\text{Li}^+@\text{C}_{60}$  (Figure 12). The decay rate constant of the triplet excited state of  $\text{H}_2\text{Pc}\bullet\mathbf{3}^{8-}$  was also unchanged by the presence of  $\text{Li}^+@\text{C}_{60}$  (Figures 13 and 14), whereas the decay rate constants for the triplet excited states of  $\text{H}_2\text{Pc}\bullet\mathbf{2}^{4-}$  (Figures 15 and 16) and  $\text{ZnPc}\bullet\mathbf{4}^{4-}$  (Figures 17 and 18) were accelerated by addition of  $\text{Li}^+@\text{C}_{60}$ . These results suggest that there are the minor pathways of electron transfer from the triplet excited state of  $\text{H}_2\text{Pc}\bullet\mathbf{2}^{4-}$  or  $\text{ZnPc}\bullet\mathbf{4}^{4-}$  to the ground state of  $\text{Li}^+@\text{C}_{60}$ . The absorption spectra of  $\text{Li}^+@\text{C}_{60}\cdot^-$  due to the CS states were also detected by photoexcitation of  $\text{H}_2\text{Pc}\bullet\mathbf{2}^{4-}/(\text{Li}^+@\text{C}_{60})_2$ ,  $\text{H}_2\text{Pc}\bullet\mathbf{3}^{8-}/\text{Li}^+@\text{C}_{60}$  and  $\text{ZnPc}\bullet\mathbf{4}^{4-}/\text{Li}^+@\text{C}_{60}$  complexes as the case of the  $\text{H}_2\text{Pc}\bullet\mathbf{1}^{4-}/(\text{Li}^+@\text{C}_{60})_2$  complex. However, the

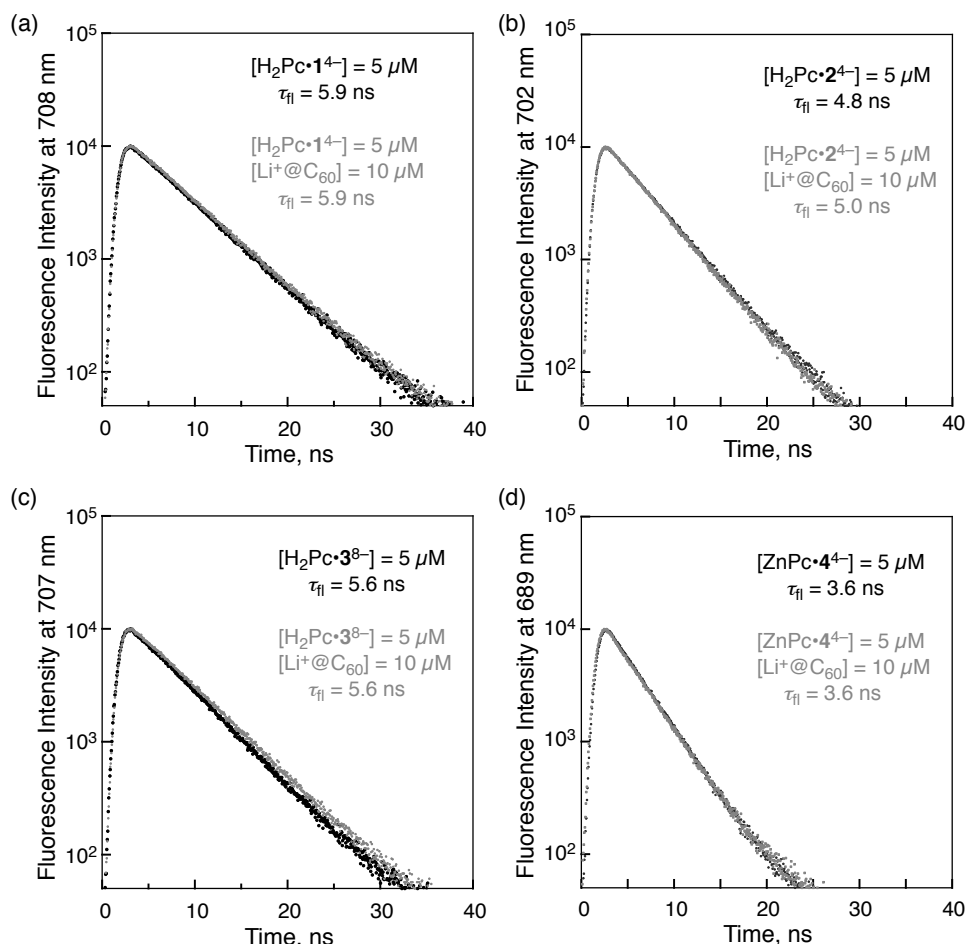


**Figure 12.** Fluorescence decay profiles of (a)  $\text{H}_2\text{Pc}\bullet\mathbf{1}^{4-}$  (black) and presence of  $\text{Li}^+@\text{C}_{60}$  (gray) in a mixed solvent (DMSO:PhCN (v/v) = 1:1), (b)  $\text{H}_2\text{Pc}\bullet\mathbf{2}^{4-}$  (black) and presence of  $\text{Li}^+@\text{C}_{60}$  (gray), (c)  $\text{H}_2\text{Pc}\bullet\mathbf{3}^{8-}$  (black) and presence of  $\text{Li}^+@\text{C}_{60}$  (gray), and (d)  $\text{ZnPc}\bullet\mathbf{4}^{4-}$  (black) and presence of  $\text{Li}^+@\text{C}_{60}$  (gray) in a mixed solvent (DMSO:PhCN (v/v) = 2:1).  $[(\text{TBA})_4\text{H}_2\text{Pc}\bullet\mathbf{1}] = [(\text{TBA})_4\text{H}_2\text{Pc}\bullet\mathbf{2}] = [(\text{TBA})_8\text{H}_2\text{Pc}\bullet\mathbf{3}] = [(\text{TBA})_4\text{ZnPc}\bullet\mathbf{4}] = 5.0 \times 10^{-6} \text{ M}$  and  $[\text{Li}^+@\text{C}_{60}] = 1.0 \times 10^{-5} \text{ M}$ ; Excitation: 450 nm.

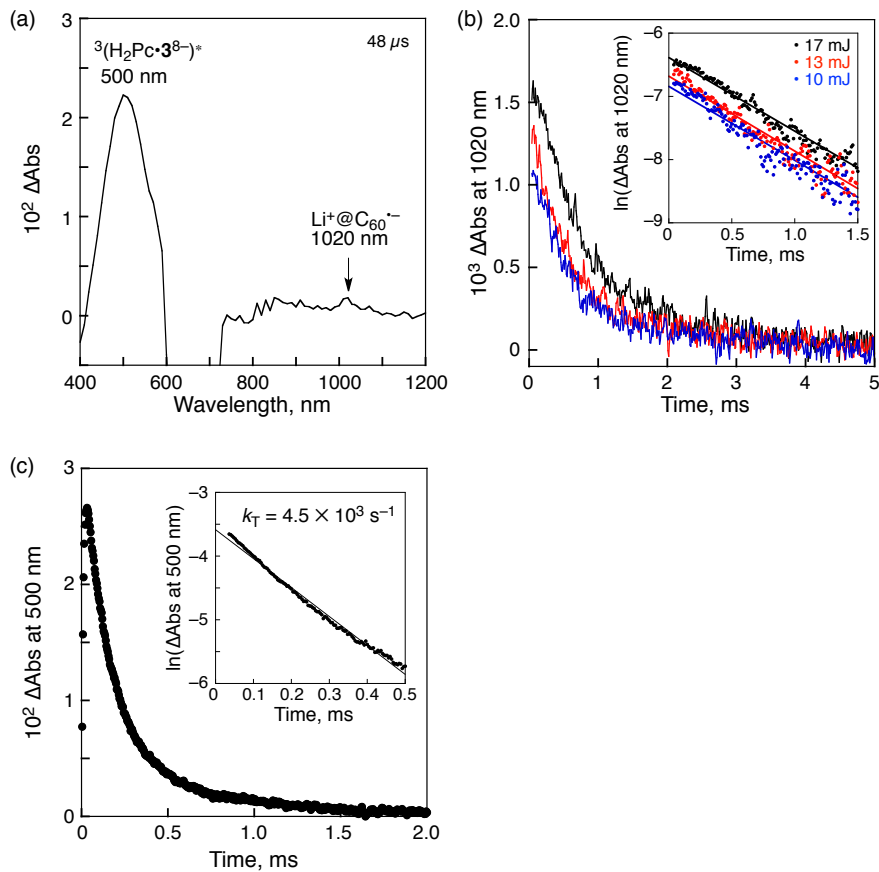


**Figure 13.** (a) Transient absorption spectrum of  $\text{H}_2\text{Pc}\bullet\text{3}^{8-}$  ( $1.3 \times 10^{-5} \text{ M}$ ) with  $\text{Li}^+\text{@C}_{60}$  ( $2.5 \times 10^{-5} \text{ M}$ ) in a mixed solvent (DMSO:PhCN (v/v) = 2:1) measured at  $48 \mu\text{s}$  after laser excitation at 355 nm. (b) Decay time profiles of absorbance at 1020 nm with various laser intensities (10, 13, and 17 mJ/pulse). Inset: First-order plots. (c) Decay time profile of absorbance at 500 nm. Inset: First-order plot.

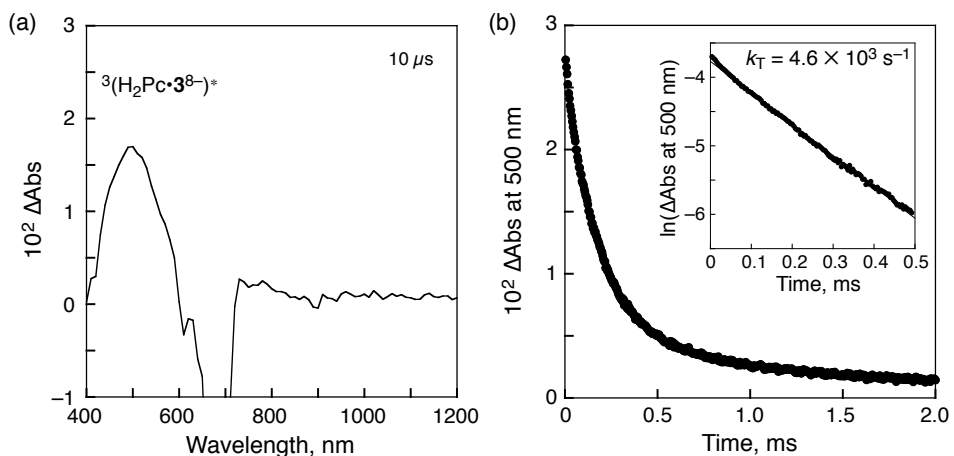


**Figure 14.** (a) Transient absorption spectrum of  $\text{H}_2\text{Pc}\bullet\text{3}^{8-}$  ( $1.3 \times 10^{-5} \text{ M}$ ) in a mixed solvent (DMSO:PhCN (v/v) = 2:1) measured at  $10 \mu\text{s}$  after laser excitation at 355 nm. (b) Decay time profile of absorbance at 500 nm. Inset: First-order plot.

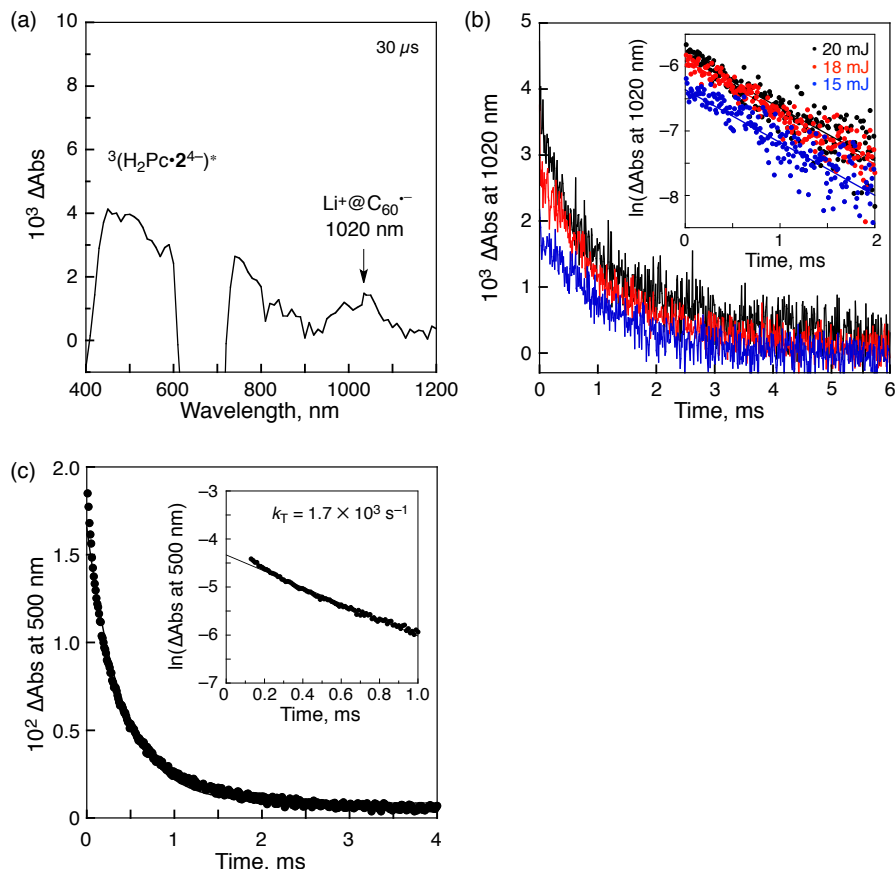


**Figure 15.** (a) Transient absorption spectrum of  $\text{H}_2\text{Pc}\cdot\text{2}^{4-}$  ( $1.3 \times 10^{-5} \text{ M}$ ) with  $\text{Li}^+\text{@C}_{60}$  ( $2.5 \times 10^{-5} \text{ M}$ ) in a mixed solvent (DMSO:PhCN (v/v) = 2:1) measured at  $30 \mu\text{s}$  after laser excitation at 355 nm. (b) Decay time profiles of absorbance at 1020 nm with various laser intensities (15, 18, and 20 mJ/pulse). Inset: First-order plots. (c) Decay time profile of absorbance at 500 nm. Inset: First-order plot.

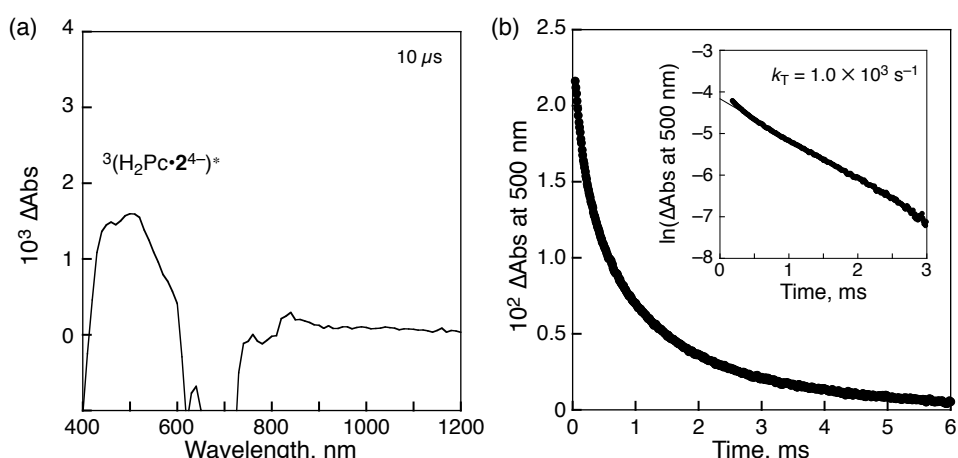


**Figure 16.** (a) Transient absorption spectrum of  $\text{H}_2\text{Pc}\cdot\text{2}^{4-}$  ( $1.3 \times 10^{-5} \text{ M}$ ) in a mixed solvent (DMSO:PhCN (v/v) = 2:1) measured at  $10 \mu\text{s}$  after laser excitation at 355 nm. (d) Decay time profile of absorbance at 500 nm. Inset: First-order plot.

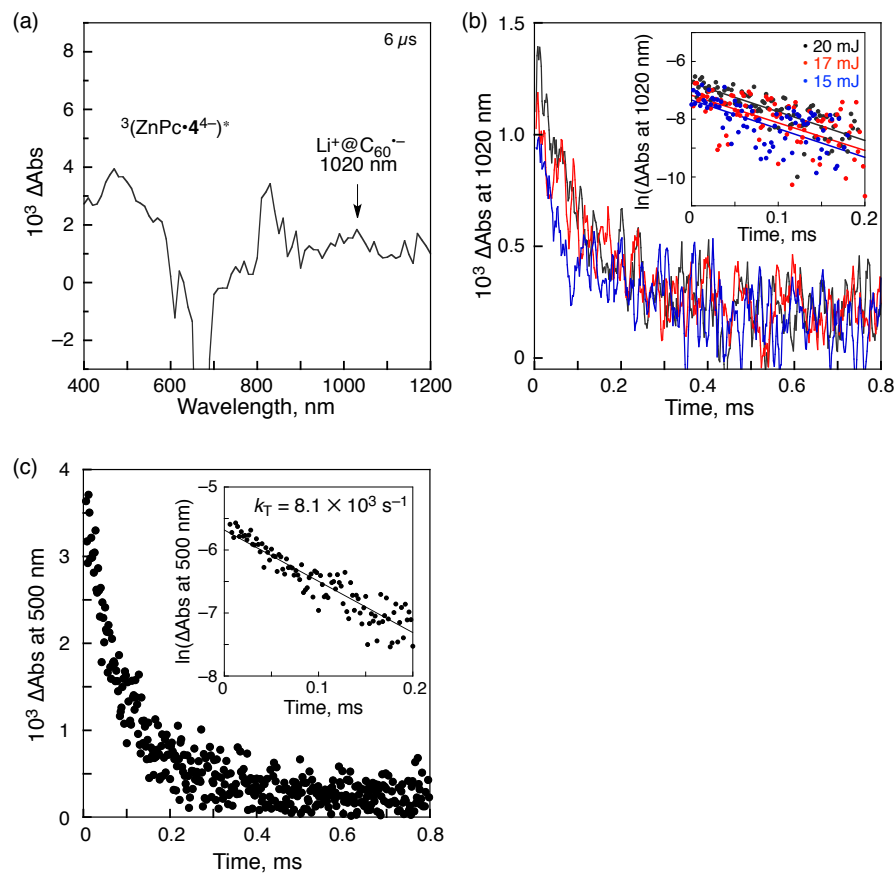


**Figure 17.** (a) Transient absorption spectrum of  $\text{ZnPc}\cdot\mathbf{4}^{4-}$  ( $1.3 \times 10^{-5} \text{ M}$ ) with  $\text{Li}^+@\text{C}_{60}$  ( $2.5 \times 10^{-5} \text{ M}$ ) in a mixed solvent (DMSO:PhCN (v/v) = 2:1) measured at  $48 \mu\text{s}$  after laser excitation at 355 nm. (b) Decay time profiles of absorbance at 1020 nm with various laser intensities (15, 17, and 20 mJ/pulse). Inset: First-order plots. (c) Decay time profile of absorbance at 500 nm. Inset: First-order plot.

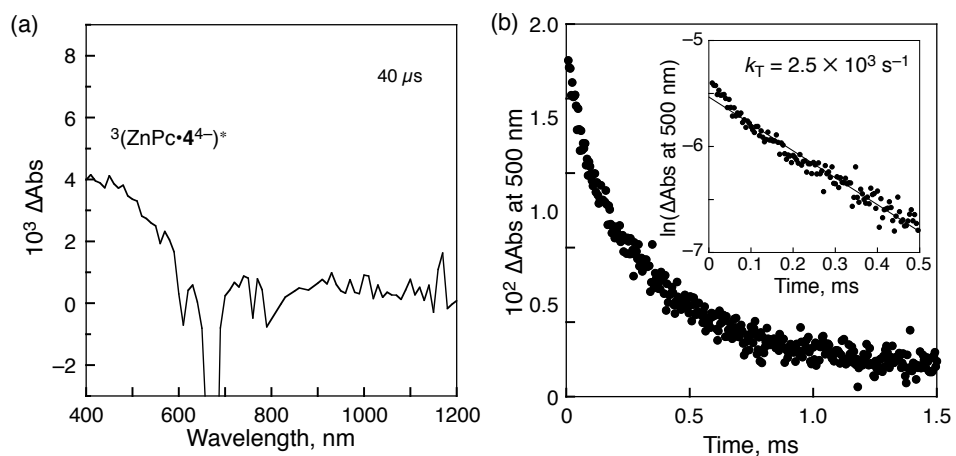


**Figure 18.** (a) Transient absorption spectra of  $\text{ZnPc}\cdot\mathbf{4}^{4-}$  ( $1.3 \times 10^{-5} \text{ M}$ ) with  $\text{Li}^+@\text{C}_{60}$  ( $2.5 \times 10^{-5} \text{ M}$ ) in a mixed solvent (DMSO:PhCN (v/v) = 2:1) measured at  $40 \mu\text{s}$  after laser excitation at 355 nm. (b) Decay time profile of absorbance at 500 nm. Inset: First-order plot.

absorption bands due to radical cation of phthalocyanines were not observed due to the small absorption coefficients to be detected (Figure 10). The lifetimes of the CS states were determined to be 1.2 ms for  $\text{H}_2\text{Pc}\bullet\mathbf{2}^{4-}/(\text{Li}^+@\text{C}_{60})_2$  and 0.83 ms for  $\text{H}_2\text{Pc}\bullet\mathbf{3}^{8-}/\text{Li}^+@\text{C}_{60}$  in a mixed solvent (DMSO:PhCN (v/v) = 2:1) at 298 K (Figures 13 and 14, respectively). The CS lifetimes are approximately 3 to 4 times longer than that of anionic porphyrin/ $\text{Li}^+@\text{C}_{60}$  (*ca.* 0.3 ms) reported previously.<sup>63</sup> The lifetime of 1.2 ms for  $\text{H}_2\text{Pc}\bullet\mathbf{2}^{4-}/(\text{Li}^+@\text{C}_{60})_2$  is the longest CS lifetime among the porphyrinoid/fullerene supramolecular complexes reported so far. In the case of  $\text{ZnPc}\bullet\mathbf{4}^{4-}/\text{Li}^+@\text{C}_{60}$ , the lifetime of the CS state was 100  $\mu\text{s}$ , which is one digit shorter than those of the other supramolecular complexes (Figure 17).

The rate constant of back electron transfer ( $k_{\text{BET}}$ ) in the CS state of  $\text{H}_2\text{Pc}\bullet\mathbf{1}^{4-}/(\text{Li}^+@\text{C}_{60})_2$  increased with increasing temperature. This temperature dependence of  $k_{\text{BET}}$  is predicted by the Marcus equation for non-adiabatic electron transfer (eq 1).<sup>74,75</sup> Eq 1 is written as eq 2, which predicts a liner correlation between  $\ln(k_{\text{BET}}T^{1/2})$  and  $T^{-1}$ .<sup>74,75</sup>

$$k_{\text{BET}} = \left( \frac{4\pi^3}{h^2 \lambda k_{\text{B}} T} \right)^{1/2} V^2 \exp\left[ -\frac{(\Delta G_{\text{BET}} + \lambda)^2}{4\lambda k_{\text{B}} T} \right] \quad (1)$$

$$\ln(k_{\text{BET}}T^{1/2}) = \ln\left( \frac{2\pi^{3/2} V^2}{h(\lambda k_{\text{B}})^{1/2}} \right) - \frac{(\Delta G_{\text{BET}} + \lambda)^2}{4\lambda k_{\text{B}} T} \quad (2)$$

in which  $k_{\text{BET}}$  is the rate constant of back electron transfer,  $\lambda$  is the reorganization energy,  $V$  is the electronic coupling term,  $-\Delta G_{\text{BET}}$  is the driving force for back electron transfer,  $h$  is the Plank's constant and  $k_{\text{B}}$  is the Boltzmann constant.<sup>74,75</sup> The plot of  $\ln(k_{\text{BET}}T^{1/2})$  vs  $T^{-1}$  for the intramolecular BET in the temperature range from 298 to 352 K gave the linear correlation, as

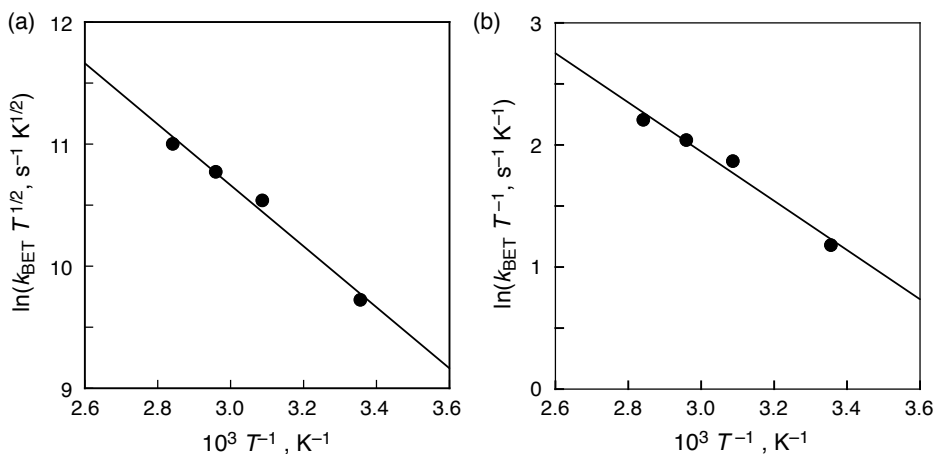


**Figure 19.** Plots of (a)  $\ln(k_{\text{BET}}T^{1/2})$  vs  $T^{-1}$  and (b)  $\ln(k_{\text{BET}}T^{-1})$  vs  $T^{-1}$  for the intramolecular BET between  $\text{H}_2\text{Pc}\bullet\mathbf{1}^{4-}$  and  $\text{Li}^+@\text{C}_{60}$  in a mixed solvent (DMSO:PhCN (v/v) = 1:1).

shown in Figure 19a. According to the slope ( $-2500$ ) and the intercept (18) in Figure 19a, the  $\lambda$  and  $V$  values were determined to be  $\lambda = 1.70$  eV and  $V = 0.15$  cm $^{-1}$ . The  $\lambda$  value is much larger than those of the previously reported supramolecular complexes composed of Li $^{+}$ @C<sub>60</sub> with electron donors, *e.g.*, anionic zinc chlorin/Li $^{+}$ @C<sub>60</sub> (1.26 eV)<sup>59</sup>, Li $^{+}$ @C<sub>60</sub>CH<sub>4</sub>-CPD<sub>Py</sub> (0.56 eV)<sup>60</sup>, and corannulene/Li $^{+}$ @C<sub>60</sub> (1.04 eV)<sup>61</sup>. The large  $\lambda$  value may result from the high polarity of the solvent due to the mixing of DMSO. The dielectric constant of a mixed solvent is estimated by the Bruggeman equation (eq 3):<sup>76</sup>

$$\left[ \frac{\varepsilon_{\text{mix}} - \varepsilon_1}{\varepsilon_2 - \varepsilon_1} \right] \left( \frac{\varepsilon_2}{\varepsilon_{\text{mix}}} \right)^{1/3} = 1 - \varphi_1 \quad (3)$$

where  $\varepsilon_1$  and  $\varepsilon_2$  are the dielectric constants for the less polar (PhCN:  $\varepsilon_1 = 25.2$ )<sup>77</sup> and more polar (DMSO:  $\varepsilon_2 = 46.6$ )<sup>78</sup> solvents, respectively,  $\varepsilon_{\text{mix}}$  is the dielectric constant of the solvent mixture, and  $\varphi_1$  is the volume fraction of the less polar solvent. The dielectric constant of a mixed solvent (DMSO:PhCN (v/v) = 1:1) was estimated as 34.9, which is higher than that of PhCN (25.2). The electronic coupling term of back electron process of H<sub>2</sub>Pc•1<sup>4-</sup>/(Li $^{+}$ @C<sub>60</sub>)<sub>2</sub> ( $V = 0.15$  cm $^{-1}$ ) is significantly smaller than that of covalently linked donor-acceptor molecules, *e.g.*, phthalocyanine–fullerene linked dyad (15 cm $^{-1}$ ),<sup>37</sup> zinc porphyrin–fullerene linked dyad (3.9 cm $^{-1}$ ),<sup>38</sup> and zinc chlorin–fullerene dyad ( $V = 6.8$  cm $^{-1}$ ).<sup>39</sup> Such a small electronic coupling term, which enables to afford a long-lived CS state, results from the spin-forbidden back electron transfer due to the triplet CS state, as described below.

On the other hand, the slope ( $-2015$ ) and intercept (8.0) of the plot of  $\ln(k_{\text{BET}} T^{-1})$  vs  $T^{-1}$  (Figure 19b) afford the activation enthalpy ( $\Delta H^{\ddagger} = 3.9$  kcal mol $^{-1}$ ) and the activation entropy ( $\Delta S^{\ddagger} = -31$  cal K $^{-1}$  mol $^{-1}$ ). Since the energy of CS state of H<sub>2</sub>Pc•1<sup>4-</sup>/(Li $^{+}$ @C<sub>60</sub>)<sub>2</sub> (0.49 eV) is much smaller than the reorganization energy (1.70 eV), the back electron transfer process is in the Marcus normal region.

**Spin State of the Charge-Separated State.** The long-lived CS states of supramolecular complexes were also observed by EPR measurements at 4 K. The spin-spin interaction of the triplet radical ion pair of the CS state of H<sub>2</sub>Pc•1<sup>4-</sup>/(Li $^{+}$ @C<sub>60</sub>)<sub>2</sub> [(H<sub>2</sub>Pc•1<sup>4-</sup>)<sup>+</sup>/(Li $^{+}$ @C<sub>60</sub>)<sup>-</sup>Li $^{+}$ @C<sub>60</sub>] was clearly observed with the fine structure around  $g = 2$  and  $g = 4$ , which are assigned to be the triplet signals as shown in Figure 20. Thus, the spin state of the CS state of H<sub>2</sub>Pc•1<sup>4-</sup>/(Li $^{+}$ @C<sub>60</sub>)<sub>2</sub> is determined to be triplet. The zero-field splitting value ( $D = 28.0$  G) gave the distance between two electron spins of 10.0 Å by using the relation,  $D = 27800/r^3$ .<sup>72</sup> Similarly, the supramolecular

complexes of  $\text{Li}^+@\text{C}_{60}$  with other phthalocyanines showed the fine structure of the CS state and the triplet signal. The distances between the two electron spins were determined to be 8.2 Å for  $\text{H}_2\text{Pc}\bullet\text{2}^{4-}$ , 7.1 Å for  $\text{H}_2\text{Pc}\bullet\text{3}^{8-}$ , and 8.2 Å for  $\text{ZnPc}\bullet\text{4}^{4-}$  (Figures 21–23).

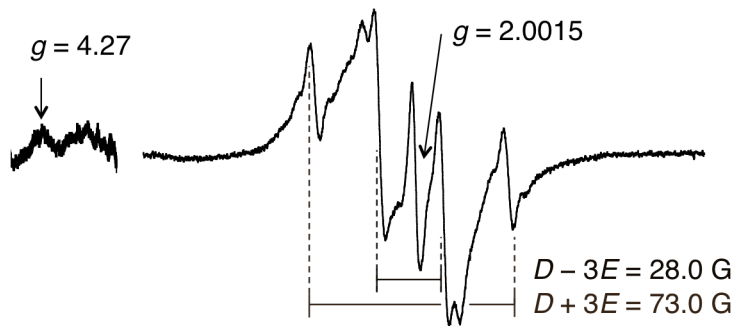


**Figure 20.** EPR spectra of the CS state  $[(\text{H}_2\text{Pc}\bullet\text{1}^{4-})^{+}/\text{Li}^+@\text{C}_{60}^{+}(\text{Li}^+@\text{C}_{60})]$  in a mixed solvent (DMSO:PhCN (v/v) = 1:1) formed by photoirradiation using a high-pressure Hg lamp (1000 W) at 4 K focused on around  $g = 4$  (left) and  $g = 2$  (right).

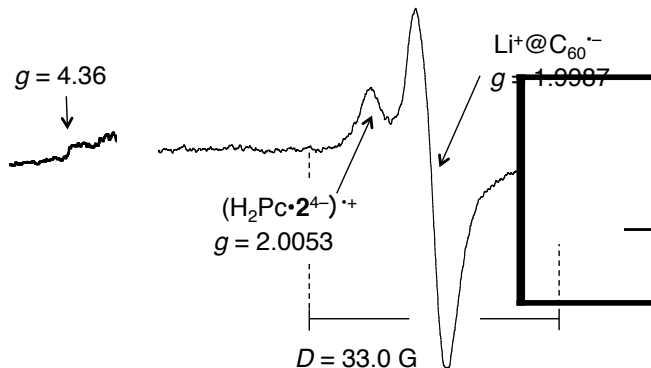


**Figure 21.** EPR spectra of the CS state  $[(\text{H}_2\text{Pc}\bullet\text{2}^{4-})^{+}/\text{Li}^+@\text{C}_{60}^{+}(\text{Li}^+@\text{C}_{60})]$  in a mixed solvent (DMSO:PhCN (v/v) = 2:1) generated by photoirradiation using a high-pressure Hg lamp (1000 W) at 4 K focused on around  $g = 4$  (left) and  $g = 2$  (right).

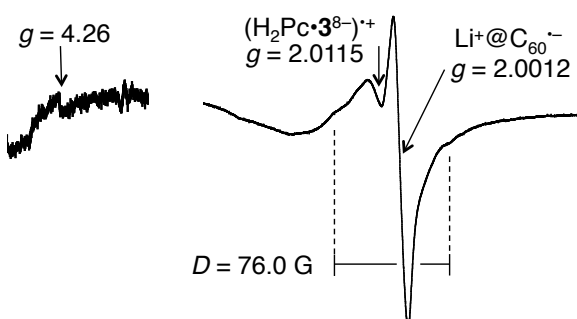


**Figure 22.** EPR spectra of the CS state  $[(\text{H}_2\text{Pc}\bullet\text{3}^{8-})^{+}/\text{Li}^+@\text{C}_{60}^{+}]$  in a mixed solvent (DMSO:PhCN (v/v) = 2:1) generated by photoirradiation using a high-pressure Hg lamp (1000 W) at 4 K focused on around  $g = 4$  (left) and  $g = 2$  (right).

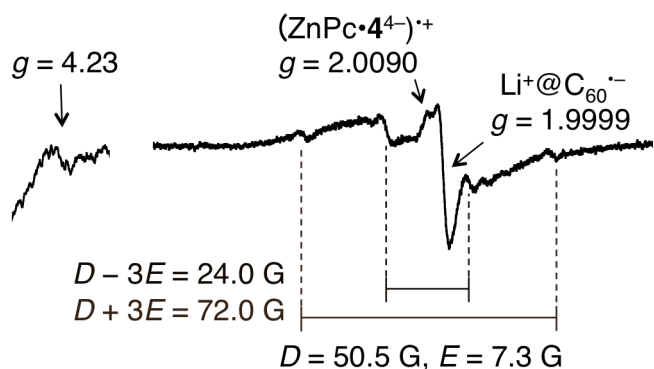


**Figure 23.** EPR spectra of the CS state  $[(\text{ZnPc}\bullet\mathbf{4}^{4-})^{++}/\text{Li}^+@\text{C}_{60}\cdot^-]$  in a mixed solvent (DMSO:PhCN (v/v) = 2:1) generated by photoirradiation using a high-pressure Hg lamp (1000 W) at 4 K focused on around  $g = 4$  (left) and  $g = 2$  (right).

**Photoelectrochemical Measurements.** The dye-sensitized solar cells composed of supramolecular nanoclusters, which are deposited on the optically transparent electrode (OTE) of nanostructured  $\text{SnO}_2$  (OTE/ $\text{SnO}_2$ ), were fabricated to examine the photoelectrochemical performance. A solution of the supramolecular complex composed of  $\text{ZnPc}\bullet\mathbf{4}^{4-}$  and  $\text{Li}^+@\text{C}_{60}$  was prepared by mixing of  $\text{ZnPc}\bullet\mathbf{4}^{4-}$  ( $2.5 \times 10^{-4}$  M) and  $\text{Li}^+@\text{C}_{60}$  ( $5.0 \times 10^{-4}$  M) in PhCN. To prepare the supramolecular nanoclusters  $[(\text{ZnPc}\bullet\mathbf{4}^{4-}/\text{Li}^+@\text{C}_{60})_n]$ , a mother PhCN solution of 1 mL was injected rapidly to an acetonitrile (MeCN) solution (3 mL). TEM image was taken to evaluate the morphology of  $(\text{ZnPc}\bullet\mathbf{4}^{4-}/\text{Li}^+@\text{C}_{60})_n$  (Figure 24a). The  $(\text{ZnPc}\bullet\mathbf{4}^{4-}/\text{Li}^+@\text{C}_{60})_n$  is composed of closely packed  $\text{ZnPc}\bullet\mathbf{4}^{4-}$  and  $\text{Li}^+@\text{C}_{60}$  composite clusters of about 100 – 200 nm size, which give a nanoporous morphology to the film. The cluster size was also evaluated as 160 nm by the dynamic light scattering (DLS) measurements (Figure 24b). The suspension of

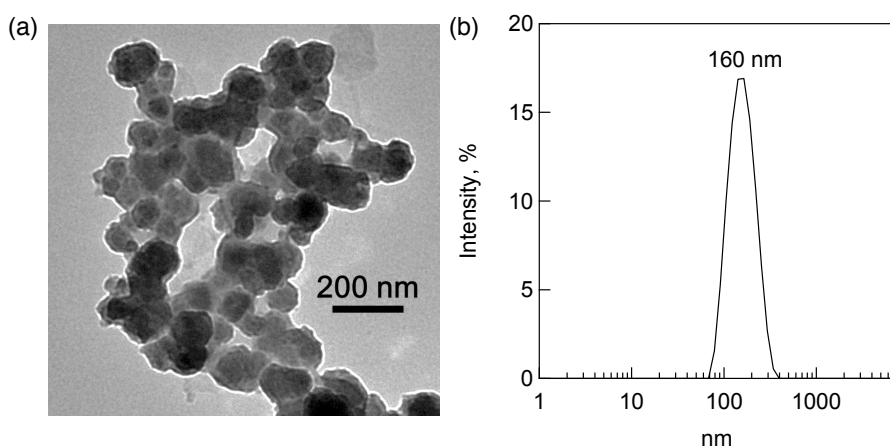


**Figure 24.** (a) TEM images of  $\text{ZnPc}\bullet\mathbf{4}^{4-}/\text{Li}^+@\text{C}_{60}$  nanoclusters. (b) Dynamic light scattering (DLS) diagram of  $(\text{ZnPc}\bullet\mathbf{4}^{4-}/\text{Li}^+@\text{C}_{60})_n$  in MeCN/PhCN (3:1 v/v).

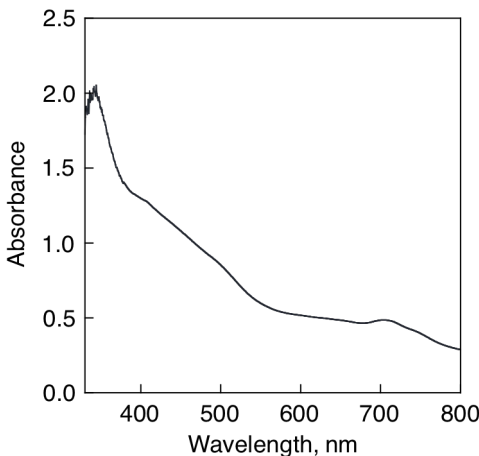


**Figure 25.** UV–Vis absorption spectrum of an OTE/SnO<sub>2</sub>/(ZnPc•4<sup>4-</sup>/Li<sup>+</sup>@C<sub>60</sub>)<sub>n</sub> electrode.

(ZnPc•4<sup>4-</sup>/Li<sup>+</sup>@C<sub>60</sub>)<sub>n</sub> was transferred into a cuvette, in which the two electrodes OTE and OTE/SnO<sub>2</sub> were placed and kept at 5 mm distance. Then, DC electric field (100 – 200 V cm<sup>-1</sup>) was applied to deposit (ZnPc•4<sup>4-</sup>/Li<sup>+</sup>@C<sub>60</sub>)<sub>n</sub> on the electrode surface when a robust thin film of OTE/SnO<sub>2</sub>/(ZnPc•4<sup>4-</sup>/Li<sup>+</sup>@C<sub>60</sub>)<sub>n</sub> was produced.

The UV–Vis absorption spectrum of an OTE/SnO<sub>2</sub>/(ZnPc•4<sup>4-</sup>/Li<sup>+</sup>@C<sub>60</sub>)<sub>n</sub> electrode is shown in Figure 25, exhibiting significant broadening as compared with that of ZnPc•4<sup>4-</sup>/Li<sup>+</sup>@C<sub>60</sub> in a mixed solvent (DMSO:PhCN (v/v) = 2:1, Figure 5a). Such a broadening behavior indicates that the molecular environment on the OTE/SnO<sub>2</sub> surface is significantly perturbed because of the aggregation of the supramolecular complex by  $\pi$ -stacking. Thus, (ZnPc•4<sup>4-</sup>/Li<sup>+</sup>@C<sub>60</sub>)<sub>n</sub> is successfully deposited on OTE/SnO<sub>2</sub>.

The IPCE (incident photon-to-photocurrent efficiency) of OTE/SnO<sub>2</sub>/(ZnPc•4<sup>4-</sup>/Li<sup>+</sup>@C<sub>60</sub>)<sub>n</sub> exhibited much higher values than the sum of the two individual IPCE values of the individual systems, OTE/SnO<sub>2</sub>/(Li<sup>+</sup>@C<sub>60</sub>)<sub>n</sub> and OTE/SnO<sub>2</sub>/(ZnPc•4<sup>4-</sup>)<sub>n</sub>. Moreover the higher electrochemical performance was observed in the near-infrared region as compared with that of anionic porphyrin/Li<sup>+</sup>@C<sub>60</sub> system.<sup>63</sup> The maximum IPCE value was determined to be 42% at 670 nm, as shown in Figure 26a. Such a high ICPE value (34%) was also observed at the Q band region at 450 nm. These high IPCE values indicate that photocurrent generation is initiated via photoinduced electron transfer in the supramolecular complex between ZnPc•4<sup>4-</sup> and Li<sup>+</sup>@C<sub>60</sub>, followed by the charge transport to the surface of OTE/SnO<sub>2</sub> electrode. Similarly, the enhancements of IPCE by using supramolecular complexes of Li<sup>+</sup>@C<sub>60</sub> with anionic free base phthalocyanines were observed (Figure 27). These values are smaller than these of (ZnPc•4<sup>4-</sup>/Li<sup>+</sup>@C<sub>60</sub>)<sub>n</sub> system (Figure 26a) probably due to the self aggregation of free base phthalocyanines.

The power conversion efficiency ( $\eta$ ) was determined by using eq 4:<sup>64</sup>

$$\eta = FF \times I_{sc} \times V_{oc}/W_{in} \quad (4)$$

in which the fill factor (FF) is defined as  $FF = [I(V)_{max}/I_{sc}]V_{oc}$  and  $V_{oc}$  is the open-circuit photovoltage and  $I_{sc}$  is the short-circuit photocurrent. OTE/SnO<sub>2</sub>/(ZnPc•4<sup>4-</sup>/Li<sup>+</sup>@C<sub>60</sub>)<sub>n</sub> has an overall  $\eta$  value of 1.1% at an input power ( $W_{in}$ ) of 20 mW cm<sup>-2</sup>, whereas  $FF = 0.44$ ,  $V_{oc} = 390$  mV and  $I_{sc} = 1.3$  mA cm<sup>-2</sup> in the OTE/SnO<sub>2</sub>/(ZnPc•4<sup>4-</sup>/Li<sup>+</sup>@C<sub>60</sub>)<sub>n</sub> (Figure 26b).

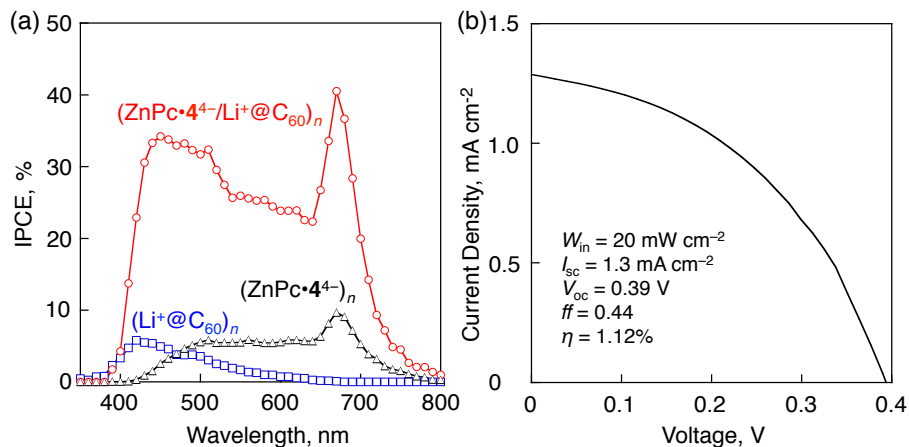


**Figure 26.** (a) Photocurrent action spectra of OTE/SnO<sub>2</sub>/(ZnPc•4<sup>4-</sup>/Li<sup>+</sup>@C<sub>60</sub>)<sub>n</sub> (red), OTE/SnO<sub>2</sub>/(Li<sup>+</sup>@C<sub>60</sub>)<sub>n</sub> (blue), and OTE/SnO<sub>2</sub>/(ZnPc•4<sup>4-</sup>)<sub>n</sub> (black). (b)  $I$ - $V$  characteristics of OTE/SnO<sub>2</sub>/(ZnTPPS<sup>4-</sup>/Li<sup>+</sup>@C<sub>60</sub>)<sub>n</sub> electrode under white light illumination (AM 1.5); input power 20 mW cm<sup>-2</sup>. Electrolyte: LiI (0.5 M) and I<sub>2</sub> (0.01 M) in MeCN.

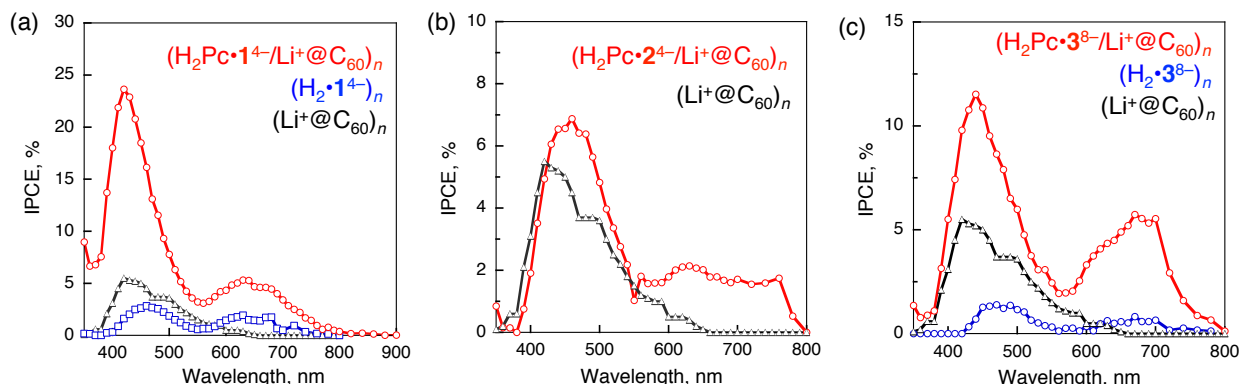


**Figure 27.** Photocurrent action spectra of (a) OTE/SnO<sub>2</sub>/(H<sub>2</sub>Pc•1<sup>4-</sup>/Li<sup>+</sup>@C<sub>60</sub>)<sub>n</sub> (red), OTE/SnO<sub>2</sub>/(H<sub>2</sub>Pc•1<sup>4-</sup>)<sub>n</sub> (blue) and OTE/SnO<sub>2</sub>/(Li<sup>+</sup>@C<sub>60</sub>)<sub>n</sub> (black). (b) OTE/SnO<sub>2</sub>/(H<sub>2</sub>Pc•2<sup>4-</sup>/Li<sup>+</sup>@C<sub>60</sub>)<sub>n</sub> (red), OTE/SnO<sub>2</sub>/(Li<sup>+</sup>@C<sub>60</sub>)<sub>n</sub> (black), and OTE/SnO<sub>2</sub>/(H<sub>2</sub>Pc•2<sup>4-</sup>)<sub>n</sub> (black). (c) OTE/SnO<sub>2</sub>/(H<sub>2</sub>Pc•3<sup>8-</sup>/Li<sup>+</sup>@C<sub>60</sub>)<sub>n</sub> (red), OTE/SnO<sub>2</sub>/(H<sub>2</sub>Pc•3<sup>8-</sup>)<sub>n</sub> (blue) and OTE/SnO<sub>2</sub>/(Li<sup>+</sup>@C<sub>60</sub>)<sub>n</sub> (black). Suspensions of supramolecular nanocluster composed of anionic phthalocyanines ( $3.1 \times 10^{-5}$  M) and Li<sup>+</sup>@C<sub>60</sub> ( $6.3 \times 10^{-5}$  M) in MeCN/PhCN (3:1 v/v) were deposited on the OTE/SnO<sub>2</sub>. Electrolyte: LiI (0.5 M) and I<sub>2</sub> (0.01 M) in MeCN.

## Conclusions

Four different phthalocyanines possessing carboxylate groups form supramolecular complexes with  $\text{Li}^+@\text{C}_{60}$  by electrostatic interaction with strong supramolecular binding in a mixed solvent (PhCN and DMSO). Upon the photoexcitation of the absorbance of phthalocyanines, photoinduced electron transfer occurred to form the CS states. The lifetime of the CS state of  $\text{H}_2\text{Pc}\bullet\text{2}^{4-}/(\text{Li}^+@\text{C}_{60})_2$  was 1.2 ms, which is the longest CS lifetime among the porphyrinoid/fullerene supramolecular complexes ever reported. Such long-lived CS states are achieved by the appropriate combination of reorganization energy, driving force, and the small electronic coupling term. The dye-sensitized solar cell composed of anionic phthalocyanines and  $\text{Li}^+@\text{C}_{60}$  supramolecular nanoclusters exhibited higher IPCE values in the near infrared region as compared with that of anionic porphyrin/ $\text{Li}^+@\text{C}_{60}$  system.<sup>63</sup> Thus, combination of anionic phthalocyanines and  $\text{Li}^+@\text{C}_{60}$  provides promising materials for efficient light energy conversion.

## References

- (1) Raval, A.; Ramanathan, V. Observational Determination of the Greenhouse Effect. *Nature* **1989**, *342*, 758–761.
- (2) Lorius, C.; Jouzel, J.; Raynaud, D.; Hansen, J.; Treut, H. Le. The Ice-Core Record: Climate Sensitivity and Future Greenhouse Warming. *Nature* **1990**, *347*, 139–145.
- (3) Hansen, J. E.; Lacis, A. A. Sun and Dust versus Greenhouse Gases: An Assessment of Their Relative Roles in Global Climate Change. *Nature* **1990**, *346*, 713–719.
- (4) Slovic, P.; Flynn, J. H.; Layman, M. *Science* **1991**, *254*, 1603–1607.
- (5) Armaroli, N.; Balzani, V. *Angew. Chem., Int. Ed.* **2007**, *46*, 52–66.
- (6) Nyambuu, U.; Semmler, W. *Econ. Model.* **2014**, *37*, 271–279.
- (7) Tang, C. W. *Appl. Phys. Lett.* **1986**, *48*, 183–185.
- (8) Sariciftci, N. S.; Smilowitz, L.; Heeger, A. J.; Wudl, F. *Science* **1992**, *258*, 1474–1746.
- (9) Lee, M. M.; Teuscher, J.; Miyasaka, T.; Murakami, T. N.; Snaith, H. J. *Science* **2012**, *338*, 643–647.
- (10) Ross, R. B.; Cardona, C. M.; Guldi, D. M.; Sankaranarayanan, S. G.; Reese, M. O.; Kopidakis, N.; Peet, J.; Walker, B.; Bazan, G. C.; Van Keuren, E.; Holloway, B. C.; Drees, M. *Nature Chem.* **2009**, *8*, 208–212..
- (11) Matsuo, Y.; Sato, Y.; Niinomi, T.; Soga, I.; Tanaka, H.; Nakamura, E. *J. Am. Chem. Soc.* **2009**, *131*, 16048–16050.

(12) Hagfeldt, A.; Grätzel, M. *Chem. Rev.* **1995**, *95*, 49–68.

(13) Grätzel, M. *Nature* **2001**, *414*, 338–344.

(14) Hasobe, T. *Phys. Chem. Chem. Phys.* **2012**, *14*, 15975–15987.

(15) Hasobe, T.; Sakai, H. *ECS J. Solid State Sci. Technol.* **2013**, *2*, M3015–M3022.

(16) Martín-Gomis, L.; Fernández-Lázaro, F.; Sastre-Santos, Á. *J. Mater. Chem. A* **2014**, *2*, 15672–15682.

(17) Wang, Z.-S.; Kawauchi, H.; Kashima, T.; Arakawa, H. *Coord. Chem. Rev.* **2004**, *248*, 1381–1389.

(18) *The Photosynthetic Reaction Center*, Deisenhofer, J., Norris, J. R., Eds.; Academic Press: San Diego, 1993.

(19) *Molecular Level Artificial Photosynthetic Materials*, Meyer, G. J., Ed.; Wiley: New York, 1997.

(20) Ricks, A. B.; Brown, K. E.; Wenninger, M.; Karlen, S. D.; Berlin, Y. A.; Co, D. T.; Wasielewski, M. R. *J. Am. Chem. Soc.* **2012**, *134*, 4581–4588.

(21) Boyle, M. M.; Forgan, R. S.; Friedman, D. C.; Gassensmith, J. J.; Smaldone, R. A.; Stoddart, J. F.; Sauvage, J.-P. *Chem. Commun.* **2011**, *47*, 11870–11872.

(22) Sukegawa, J.; Schubert, C.; Zhu, X.; Tsuji, H.; Guldi, D. M.; Nakamura, E. *Nature Chem.* **2014**, *6*, 899–905.

(23) Ohkubo, K.; Sintic, P. J.; Tkachenko, N. V.; Lemmetyinen, H.; E, W.; Ou, Z.; Shao, J.; Kadish, K. M.; Crossley, M. J.; Fukuzumi, S. *Chem. Phys.* **2006**, *326*, 3–14.

(24) Subbaiyan, N. K.; Wijesinghe, C. A.; D’Souza, F. *J. Am. Chem. Soc.* **2009**, *131*, 14646–14647.

(25) Gust, D.; Moore, T. A.; Moore, A. L. *Acc. Chem. Res.* **2009**, *42*, 1890–1898.

(26) Fukuzumi, S.; Ohkubo, K.; Suenobu, T. *Acc. Chem. Res.* **2014**, *47*, 1455–1464.

(27) Fukuzumi, S.; Ohkubo, K. *Dalton Trans.* **2013**, *42*, 15846–15858.

(28) Fukuzumi, S.; Kojima, T. *J. Mater. Chem.* **2008**, *18*, 1427–1439.

(29) Fukuzumi, S. *Org. Biomol. Chem.* **2003**, *1*, 609–620.

(30) Wielopolski, M.; Molina-Ontoria, A.; Schubert, C.; Margraf, J. T.; Krokos, E.; Kirschner, J.; Gouloumis, A.; Clark, T.; Guldi, D. M.; Martín, N. *J. Am. Chem. Soc.* **2013**, *135*, 10372–10381.

(31) Garg, V.; Kodis, G.; Chachisvilis, M.; Hambourger, M.; Moore, A. L.; Moore, T. A.; Gust, D. *J. Am. Chem. Soc.* **2011**, *133*, 2944–2954.

(32) Balzani, V. *Coord. Chem. Rev.* **2001**, *219-221*, 545–572.

---

(33) Imahori, H.; Tamaki, K.; Guldi, D. M.; Luo, C.; Fujitsuka, M.; Ito, O.; Sakata, Y.; Fukuzumi, S. *J. Am. Chem. Soc.* **2001**, *123*, 2607–2617.

(34) Gould, I. R.; Young, R. H.; Mueller, L. J.; Albrecht, A. C.; Farid, S. *J. Am. Chem. Soc.* **1994**, *116*, 3147–3148.

(35) Faiz, J. A.; Heitz, V.; Sauvage, J.-P. *Chem. Soc. Rev.* **2009**, *38*, 422–442.

(36) Lee, S.-H.; Larsen, A. G.; Ohkubo, K.; Cai, Z.-L.; Reimers, J. R.; Fukuzumi, S.; Crossley, M. J. *Chem. Sci.* **2012**, *3*, 257–269.

(37) Martín-Gomis, L.; Ohkubo, K.; Fernández-Lázaro, F.; Fukuzumi, S.; Sastre-Santos, Á. *Org. Lett.* **2007**, *9*, 3441–3444.

(38) Imahori, H.; Guldi, D. M.; Tamaki, K.; Yoshida, Y.; Luo, C.; Sakata, Y.; Fukuzumi, S. *J. Am. Chem. Soc.* **2001**, *123*, 6617–6628.

(39) Fukuzumi, S.; Ohkubo, K.; Imahori, H.; Shao, J.; Ou, Z.; Zheng, G.; Chen, Y.; Pandey, R. K.; Fujitsuka, M.; Ito, O.; Kadish, K. M. *J. Am. Chem. Soc.* **2001**, *123*, 10676–10683.

(40) Wasielewski, M. R. *Acc. Chem. Res.* **2009**, *42*, 1910–1921.

(41) D’Souza, F.; Ito, O. *Chem. Soc. Rev.* **2012**, *41*, 86–96.

(42) Natali, M.; Campagna, S.; Scandola, F. *Chem. Soc. Rev.* **2014**, *43*, 4005–4018.

(43) Blas-Ferrando, V. M.; Ortiz, J.; Ohkubo, K.; Fukuzumi, S.; Fernández-Lázaro, F.; Sastre-Santos, Á. *Chem. Sci.* **2014**, *5*, 4785–4793.

(44) Blas-Ferrando, V. M.; Ortiz, J.; Bouissane, L.; Ohkubo, K.; Fukuzumi, S.; Fernández-Lázaro, F.; Sastre-Santos, Á. *Chem. Commun.* **2012**, *48*, 6241–6243.

(45) El-Khouly, M. E.; Fukuzumi, S.; D’Souza, F. *ChemPhysChem* **2014**, *15*, 30–47.

(46) Kirner, S.; Sekita, M.; Guldi, D. M. *Adv. Mater.* **2014**, *26*, 1482–1493.

(47) Fukuzumi, S.; Ohkubo, K. Assemblies of Artificial Photosynthetic Reaction Centres. *J. Mater. Chem.* **2012**, *22*, 4575–4587.

(48) Murakami, M.; Ohkubo, K.; Hasobe, T.; Sgobba, V.; Guldi, D. M.; Wessendorf, F.; Hirsch, A.; Fukuzumi, S. *J. Mater. Chem.* **2010**, *20*, 1457–1466.

(49) Yan, Q.; Luo, Z.; Cai, K.; Ma, Y.; Zhao, D. *Chem. Soc. Rev.* **2014**, *43*, 4199–4221.

(50) Imahori, H.; El-Khouly, M. E.; Fujitsuka, M.; Ito, O.; Sakata, Y.; Fukuzumi, S. *J. Phys. Chem. A* **2001**, *105*, 325–332.

(51) Bill, N. L.; Ishida, M.; Kawashima, Y.; Ohkubo, K.; Sung, Y. M.; Lynch, V. M.; Lim, J. M.; Kim, D.; Sessler, J. L.; Fukuzumi, S. *Chem. Sci.* **2014**, *5*, 3888–3896.

(52) Davis, C. M.; Kawashima, Y.; Ohkubo, K.; Lim, J. M.; Kim, D.; Fukuzumi, S.; Sessler, J. L. *J. Phys. Chem. C* **2014**, *118*, 13503–13513.

(53) Hosseini, A.; Taylor, S.; Accorsi, G.; Armaroli, N.; Reed, C. A.; Boyd, P. D. W. *J. Am. Chem. Soc.* **2006**, *128*, 15903–15913.

(54) Haino, T.; Yanase, M.; Fukunaga, C.; Fukazawa, Y. *Tetrahedron* **2006**, *62*, 2025–2035.

(55) Chitta, R.; D’Souza, F. *J. Mater. Chem.* **2008**, *18*, 1440–1471.

(56) Aoyagi, S.; Nishibori, E.; Sawa, H.; Sugimoto, K.; Takata, M.; Miyata, Y.; Kitaura, R.; Shinohara, H.; Okada, H.; Sakai, T.; Ono, Y.; Kawachi, K.; Yokoo K.; Ono, S.; Omote, K.; Kasama, Y.; Ishikawa, S.; Komuro, T.; Tobita, H. *Nature Chem.* **2010**, *2*, 678–683.

(57) Aoyagi, S.; Sado, Y.; Nishibori, E.; Sawa, H.; Okada, H.; Tobita, H.; Kasama, Y.; Kitaura, R.; Shinohara, H. *Angew. Chem., Int. Ed.* **2012**, *51*, 3377–3381.

(58) Ohkubo, K.; Kawashima, Y.; Fukuzumi, S. *Chem. Commun.* **2012**, *48*, 4314–4316.

(59) Kawashima, Y.; Ohkubo, K.; Mase, K.; Fukuzumi, S. *J. Phys. Chem. C* **2013**, *117*, 21166–21177.

(60) Kamimura, T.; Ohkubo, K.; Kawashima, Y.; Nobukuni, H.; Naruta, Y.; Tani, F.; Fukuzumi, S. *Chem. Sci.* **2013**, *4*, 1451–1461.

(61) Yamada, M.; Ohkubo, K.; Shionoya, M.; Fukuzumi, S. *J. Am. Chem. Soc.* **2014**, *136*, 13240–13248.

(62) Supur, M.; Kawashima, Y.; Larsen, K. R.; Ohkubo, K.; Jeppesen, J. O.; Fukuzumi, S. *Chem.–Eur. J.* **2014**, *20*, 13976–13983.

(63) Ohkubo, K.; Kawashima, Y.; Sakai, H.; Hasobe, T.; Fukuzumi, S. *Chem. Commun.* **2013**, *49*, 4474–4476.

(64) Hasobe, T.; Kashiwagi, Y.; Absalom, M. A.; Sly, J.; Hosomizu, K.; Crossley, M. J.; Imahori, H.; Kamat, P. V.; Fukuzumi, S. *Adv. Mater.* **2004**, *16*, 975–979.

(65) Rio, Y.; Salomé Rodríguez-Morgade, M.; Torres, T. *Org. Biomol. Chem.* **2008**, *6*, 1877–1894.

(66) Furuyama, T.; Satoh, K.; Kushiya, T.; Kobayashi, N. *J. Am. Chem. Soc.* **2014**, *136*, 765–776.

(67) De La Torre, G.; Bottari, G.; Sekita, M.; Hausmann, A.; Guldi, D. M.; Torres, T. *Chem. Soc. Rev.* **2013**, *42*, 8049–8105.

(68) Leng, X.; Choi, C. -F.; Luo, H. -B.; Cheng, Y. -K.; Ng, D. K. P. *Org. Lett.* **2007**, *9*, 2497–2500.

(69) Woehrle, D.; Eskes, M.; Shigehara, K.; Yamada, A. *Synthesis*. **1993**, *2*, 194–196.

(70) Derkacheva, V. M.; Mikhalenko, S. A.; Solov’eva, L. I.; Alekseeva, V. I.; Marinina, L. E.; Savina, L. P.; Butenin, A. V.; Luk’yanest, E. A. *Russ. J. Gen. Chem.* **2007**, *77*, 1117–1125.

---

(71) The energies of singlet excited state were determined from the absorption maxima ( $\lambda_{\text{Abs}}$ ) and fluorescence maxima ( $\lambda_{\text{Fl}}$ ), which are  $\lambda_{\text{Abs}} = 703$  nm and  $\lambda_{\text{Fl}} = 708$  nm for  $\text{H}_2\text{Pc}\bullet\mathbf{1}^{4-}$ ,  $\lambda_{\text{Abs}} = 687$  nm and  $\lambda_{\text{Fl}} = 702$  nm for  $\text{H}_2\text{Pc}\bullet\mathbf{2}^{4-}$ ,  $\lambda_{\text{Abs}} = 702$  nm and  $\lambda_{\text{Fl}} = 707$  nm for  $\text{H}_2\text{Pc}\bullet\mathbf{3}^{8-}$ , and  $\lambda_{\text{Abs}} = 672$  nm and  $\lambda_{\text{Fl}} = 689$  nm for  $\text{ZnPc}\bullet\mathbf{4}^{4-}$ .

(72) Kawashima, Y.; Ohkubo, K.; Fukuzumi, S. *J. Phys. Chem. A* **2012**, *116*, 8942–8948.

(73) The absorption maximum of  $\text{Li}^+@\text{C}_{60}^{\bullet-}$  at 1020 nm in the mix solvent is slightly blue shifted relative to the 1035 nm in benzonitrile. See: Fukuzumi, S.; Ohkubo, K.; Kawashima, Y.; Kim, D. S.; Park, J. S.; Jana, A.; Lynch, V. M.; Kim, D.; Sessler, J. L. *J. Am. Chem. Soc.* **2011**, *133*, 15938–15941.

(74) Marcus, R. A. *Annu. Rev. Phys. Chem.* **1964**, *15*, 155–196.

(75) Marcus, R. A. *Angew. Chem., Int. Ed.* **1993**, *32*, 1111–1121.

(76) Lou, J.; Hatton, T. A.; Laibinis, P. E. *J. Phys. Chem. A* **1997**, *101*, 5262–5268.

(77) Ho, P. C.; Ramsey, J. B. *J. Chem. Eng. Data* **1986**, *31*, 430–434.

(78) Kumar, G.; Namboodiri, N.; Sharief, N. *J. Chem. Eng. Data* **1991**, *36*, 467–470.

## Supporting Information for Chapter 12

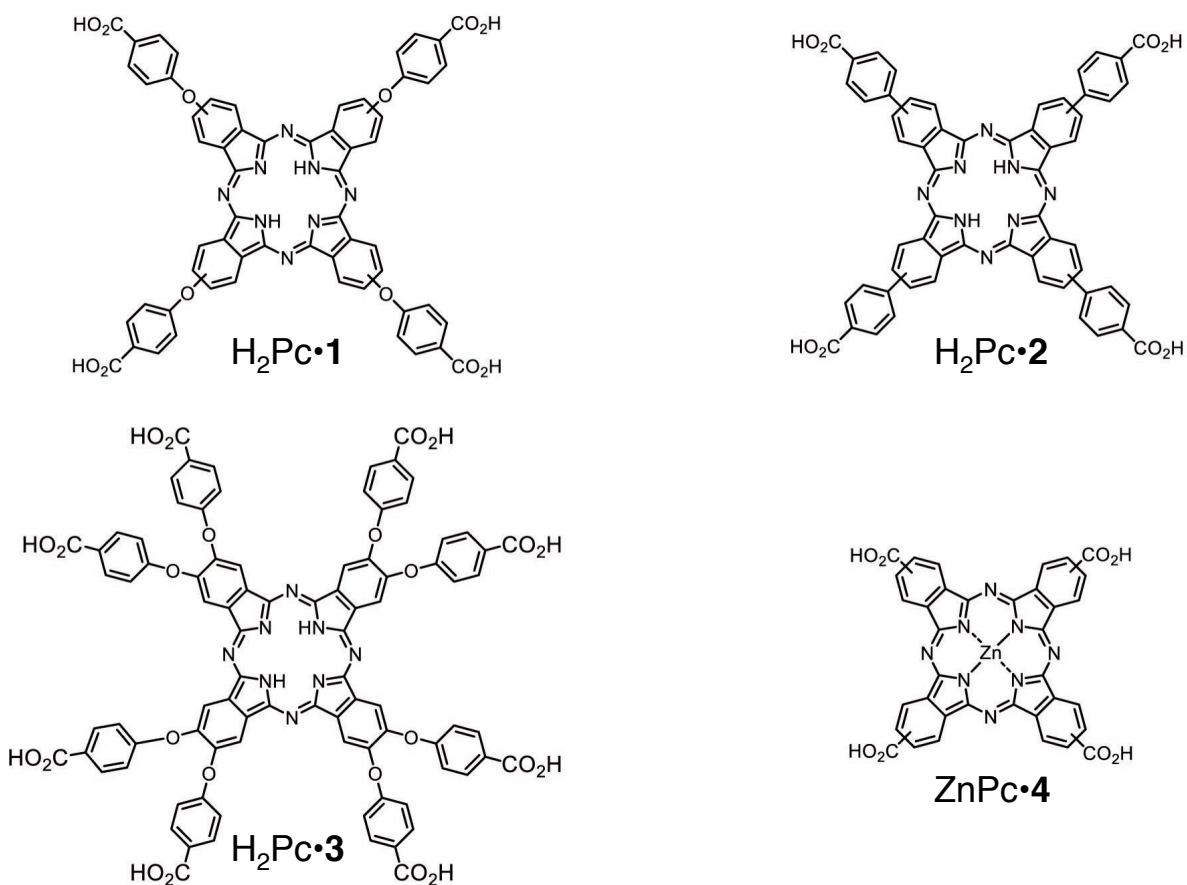


**Figure S1.** Chemical structures of H<sub>2</sub>Pc•1, H<sub>2</sub>Pc•2, H<sub>2</sub>Pc•3 and ZnPc•4.

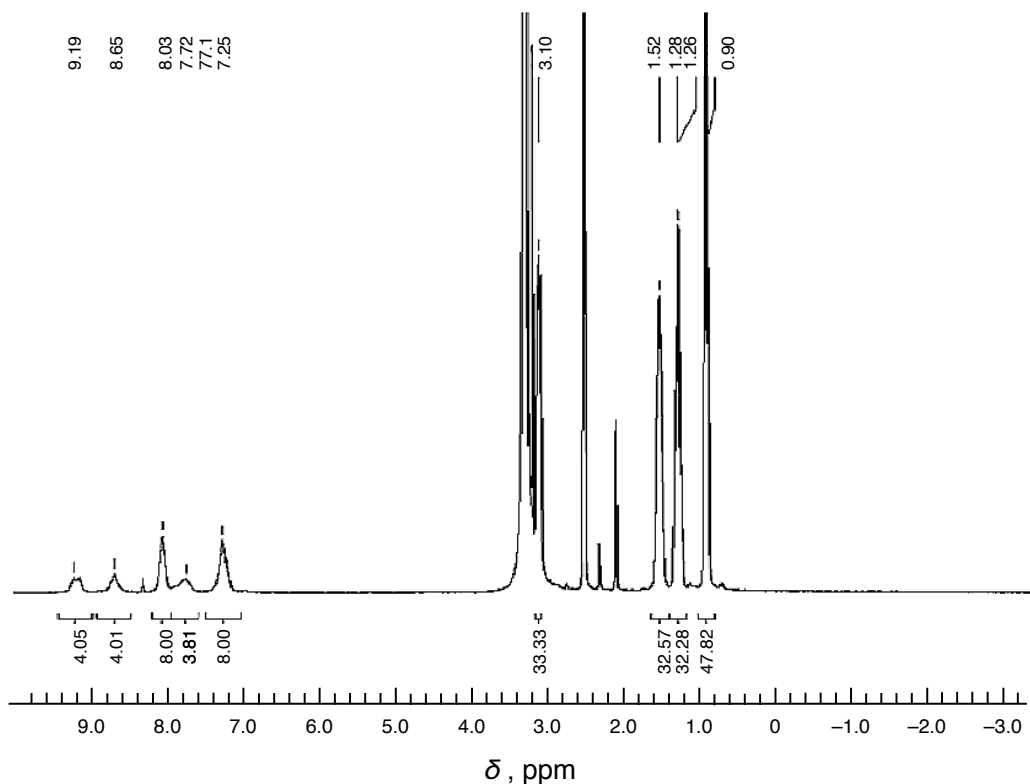


**Figure S2.**  $^1\text{H}$ -NMR ( $\text{DMSO}-d_6$ ) of  $(\text{TBA})_4\text{H}_2\text{Pc}\bullet\mathbf{1}$ . Refer to the experimental section.

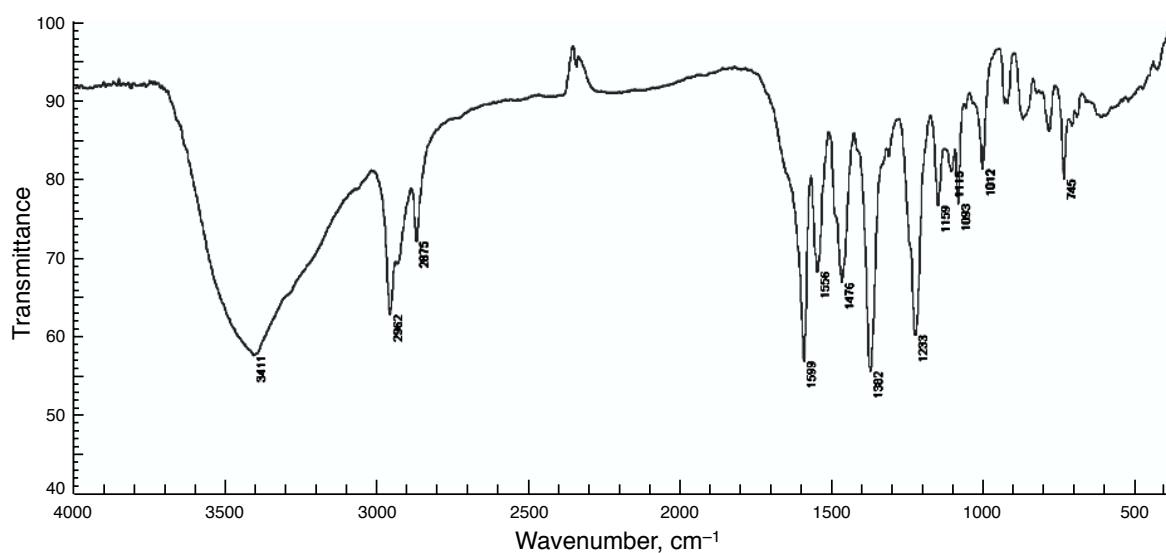


**Figure S3.** IR Spectrum (KBr) of  $(\text{TBA})_4\text{H}_2\text{Pc}\bullet\mathbf{1}$ . Refer to the experimental section.

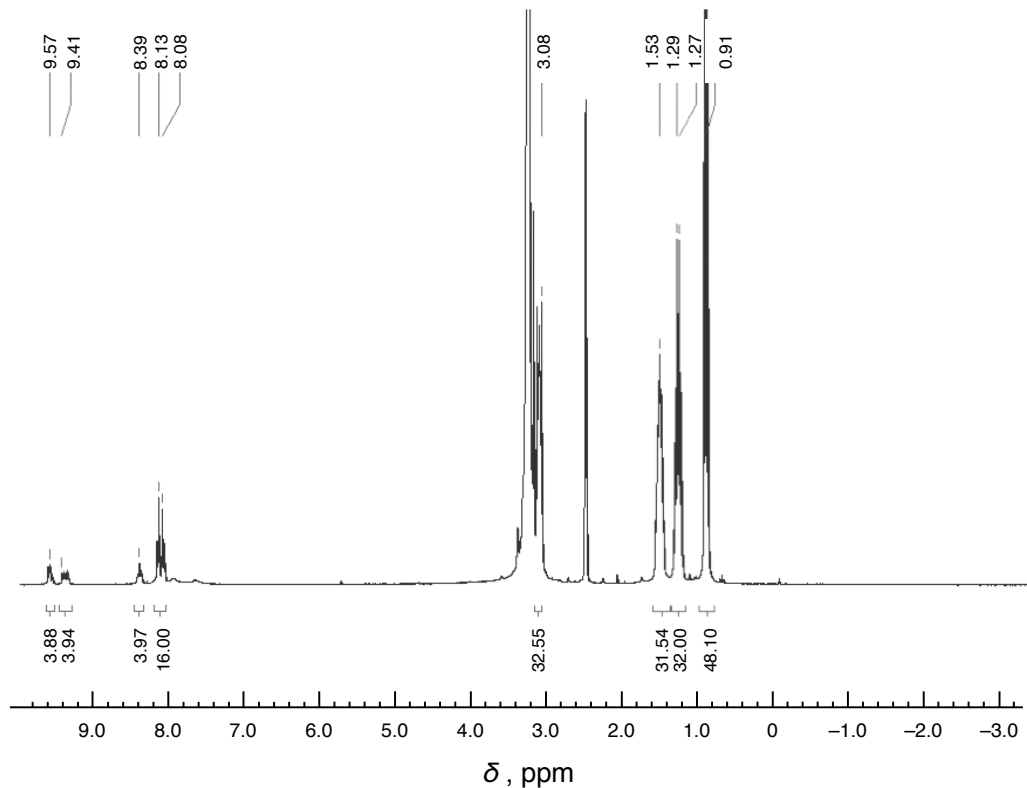


**Figure S4.**  $^1\text{H}$ -NMR (DMSO- $d_6$ ) of  $(\text{TBA})_4\text{H}_2\text{Pc}\bullet\text{2}$ . Refer to the experimental section.

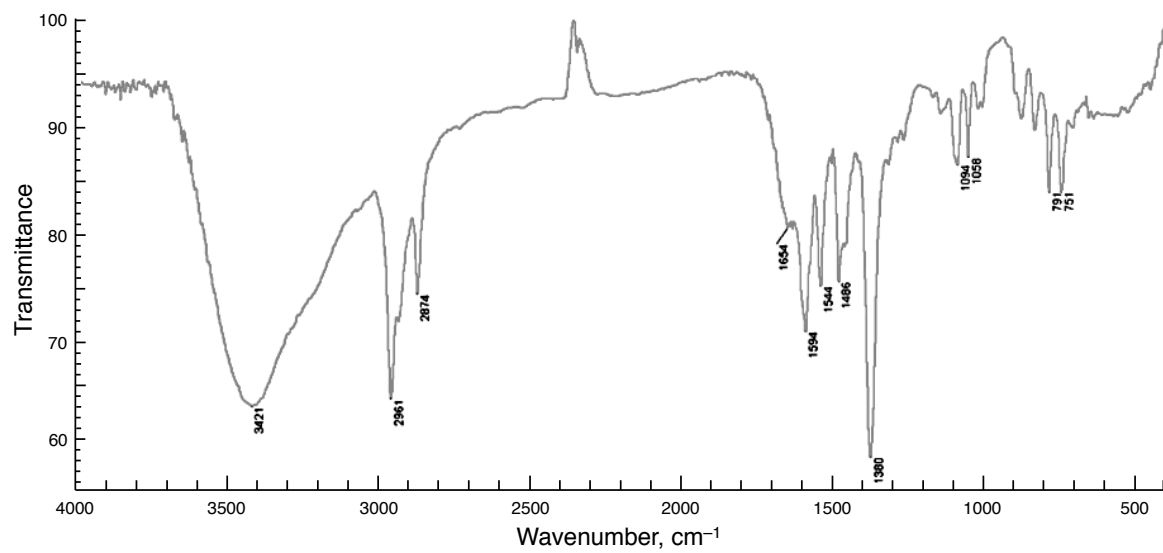


**Figure S5.** IR Spectrum (KBr) of  $(\text{TBA})_4\text{H}_2\text{Pc}\bullet\text{2}$ . Refer to the experimental section.

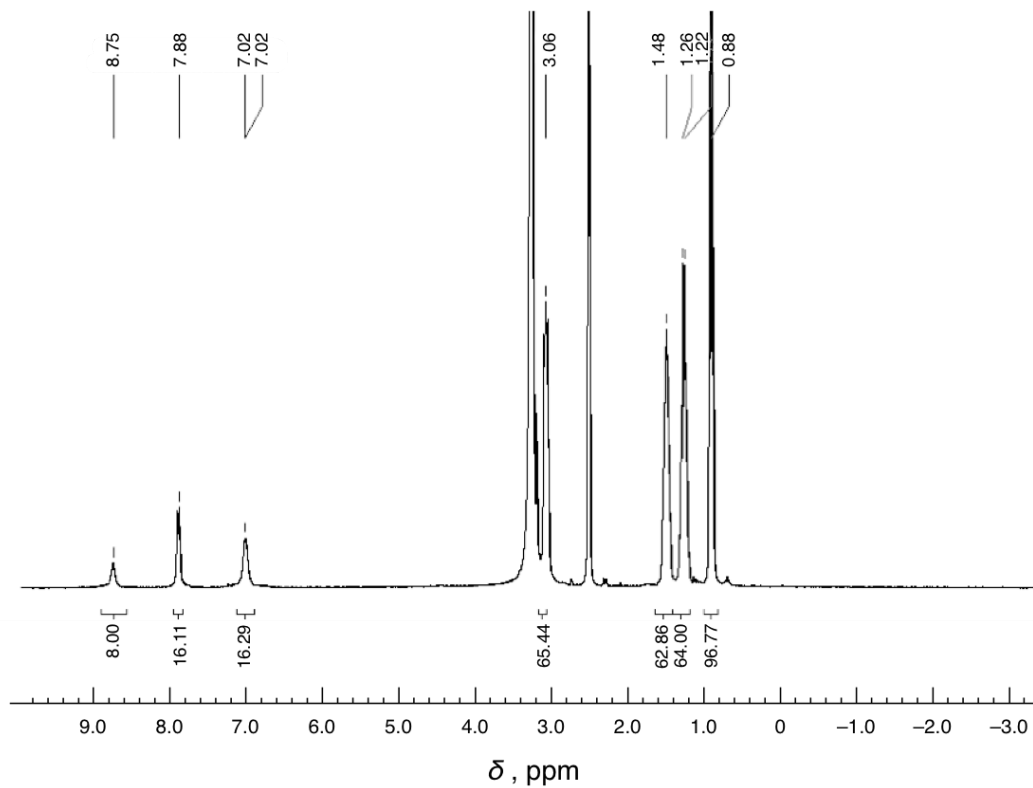


**Figure S6.**  $^1\text{H}$ -NMR (DMSO- $d_6$ ) of  $(\text{TBA})_8\text{H}_2\text{Pc}\bullet\text{3}$ . Refer to the experimental section.

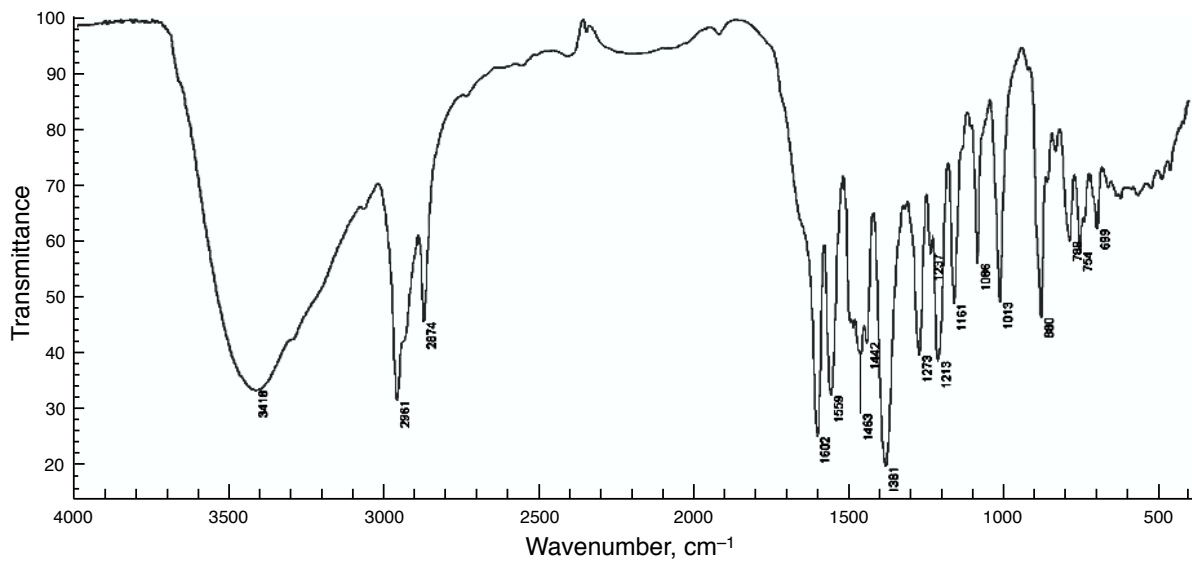


**Figure S7.** IR Spectrum (KBr) of  $(\text{TBA})_8\text{H}_2\text{Pc}\bullet\text{3}$ . Refer to the experimental section.

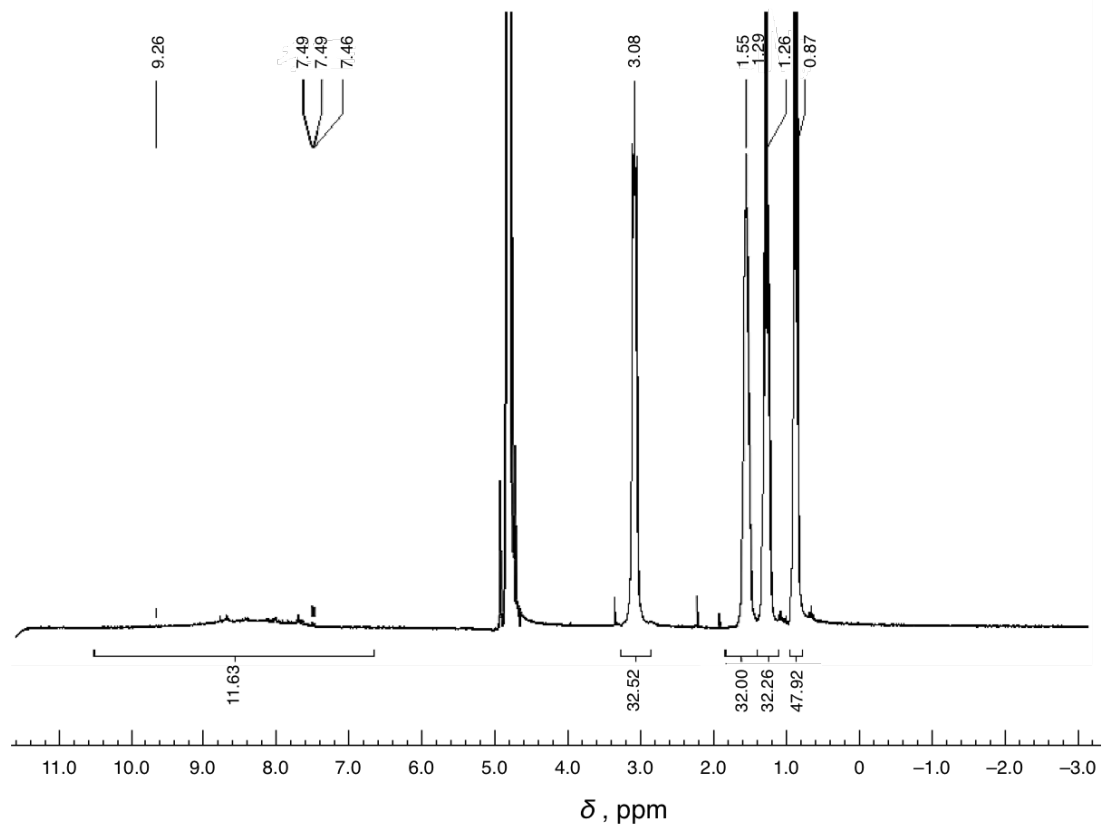


**Figure S8.**  $^1\text{H}$ -NMR (DMSO- $d_6$ ) of  $(\text{TBA})_4\text{ZnPc}\bullet\text{4}$ . Refer to the experimental section.

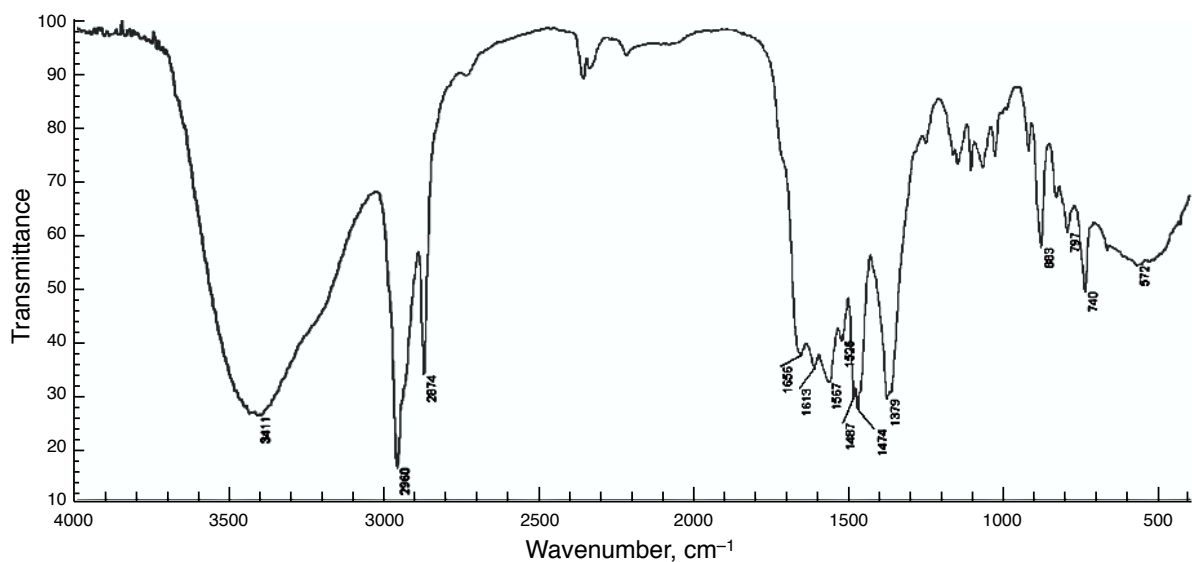
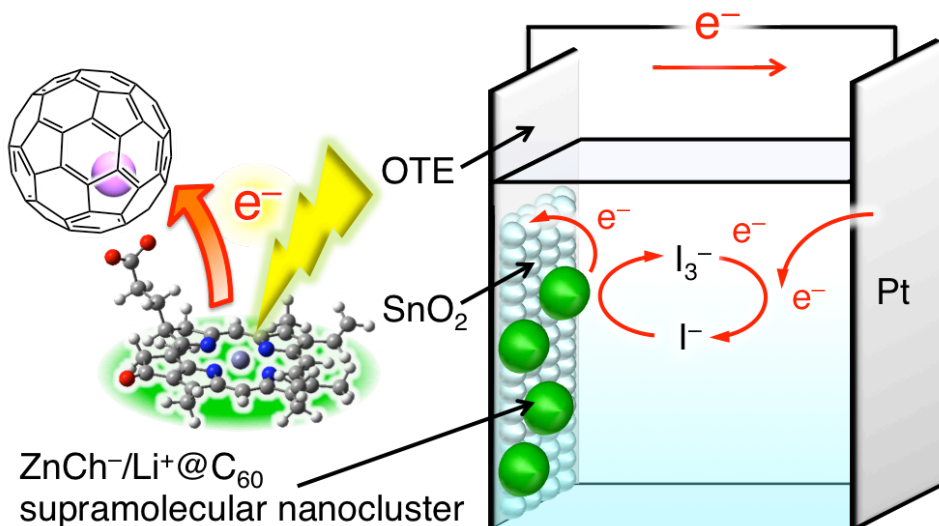


**Figure S9.** IR Spectrum (KBr) of  $(\text{TBA})_4\text{ZnPc}\bullet\text{4}$ . Refer to the experimental section.

## Chapter 13

Photoelectrochemical Properties of Supramolecular Composites of an Anionic Zinc Chlorin and  $\text{Li}^+@\text{C}_{60}$  on  $\text{SnO}_2$



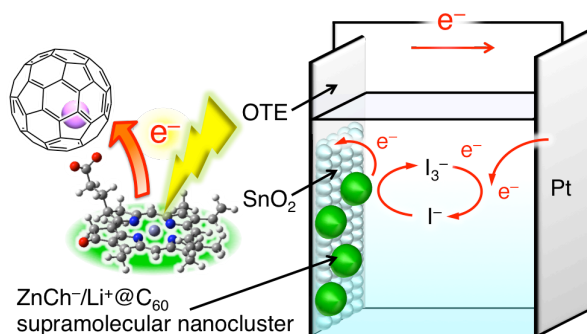
**Abstract:** An electron donor-acceptor supramolecular complex was formed between an anionic zinc chlorin carboxylate ( $\text{ZnCh}^-$ ) and lithium ion-encapsulated [60]fullerene ( $\text{Li}^+@\text{C}_{60}$ ) by an electrostatic interaction in benzonitrile (PhCN). Photoinduced electron transfer in the supramolecular complex of  $\text{ZnCh}^-/\text{Li}^+@\text{C}_{60}$  resulted in the formation of the charge-separated state via electron transfer from the triplet excited state of  $\text{ZnCh}^-$  to  $\text{Li}^+@\text{C}_{60}$ . I report herein photovoltaic cells using  $\text{ZnCh}^-/\text{Li}^+@\text{C}_{60}$  nanoclusters, which are assembled on the optically transparent electrode (OTE) of nanostructured  $\text{SnO}_2$  (OTE/ $\text{SnO}_2$ ). The photoelectrochemical behavior of the nanostructured  $\text{SnO}_2$  film of supramolecular nanoclusters of  $\text{ZnCh}^-$  and  $\text{Li}^+@\text{C}_{60}$  denoted as OTE/ $\text{SnO}_2/(\text{ZnCh}^-/\text{Li}^+@\text{C}_{60})_n$  is significantly higher than the single component films of  $\text{ZnCh}^-$  or  $\text{Li}^+@\text{C}_{60}$  clusters, denoted as OTE/ $\text{SnO}_2/(\text{ZnCh}^-)_n$  or OTE/ $\text{SnO}_2/(\text{Li}^+@\text{C}_{60})_n$ .

## Introduction

Dye-sensitized light to electrical energy conversion is initiated by photoinduced electron transfer from the excited chromophore to electrode, which results in the charge separation. The long-lived charge separation to produce hole and electron plays an important role in design of a highly efficient light-to-voltaic energy conversion system.<sup>1</sup> In nature, chlorophylls have chosen as a light-harvesting unit in natural photosynthesis. The harvested light energy is efficiently transferred to the reaction center to attain a long-lived charge-separated (CS) state and converted to chemical energy.<sup>2,3</sup> There have been a number of electron donor-acceptor (D-A) systems as artificial photosynthetic model<sup>4-13</sup> that undergo photoinduced electron-transfer reactions to afford the CS states. The use of non-covalent binding such as metal-ligand coordination, electrostatic interaction, hydrogen bonds and rotaxane formation has merited increasing attention as a simpler but more elegant way to construct electron donor-acceptor ensembles mimicking the efficient biological electron-transfer systems in which light harvesting units are combined with the charge-separation unit.<sup>14-30</sup> Porphyrin analogs that have highly delocalized  $\pi$  systems are suitable for efficient electron transfer because the uptake or release of electrons results in minimal structural and solvation changes upon electron transfer.<sup>4,9,30</sup> The number of reduced double bonds in the pyrrole rings is zero in the case of porphyrins, one in the case of chlorins. Interestingly, it has also been shown that the five-member isocyclic ring present in chlorophyll *a* can be converted into a fused six-member anhydride, an isoimide, or an imide ring.<sup>31</sup> The position of such fused ring systems extends their long-wavelength absorptions from 660 to 700 nm.<sup>31-33</sup> Therefore, it is of great interest to examine the use of chlorophyll-like molecules such as chlorins for the light harvesting unit of donor-acceptor system.<sup>34</sup> There have previously been some reports of the synthesis, photochemical and electrochemical properties of a chlorophyll-like donor (a chlorin) linked to C<sub>60</sub> (chlorin-C<sub>60</sub>) or porphyrin-C<sub>60</sub> dyads with the short spacer between the macrocycle and the [60]fullerene.<sup>34-37</sup> The combinations of chlorin and fullerene exhibited efficient photoinduced electron transfer to produce the CS state.

Lithium-ion-encapsulated fullerene (Li<sup>+</sup>@C<sub>60</sub>) is known to act as a highly efficient electron acceptor compared with pristine C<sub>60</sub>.<sup>38-43</sup> I have recently reported a donor-acceptor supramolecular system composed of anionic zinc chlorin (ZnCh<sup>-</sup>) as an electron donor and cationic Li<sup>+</sup>@C<sub>60</sub> as an electron acceptor, which are bound by an electrostatic interaction. A long-lived CS lifetime of 170  $\mu$ s was attained in PhCN at 298 K.<sup>43</sup> Elongation of wavelength to the near IR region is one of the hot topics for the rational design of the photoelectrochemical energy conversion system. However, photoelectrochemical conversion system using

$\text{ZnCh}^-/\text{Li}^+@\text{C}_{60}$  supramolecular system excited at near IR region has yet to be reported. I report herein construction of a supramolecular donor-acceptor CS system by using an electrostatic interaction, between  $\text{Li}^+@\text{C}_{60}$  as an electron acceptor and  $\text{ZnCh}^-$  as an electron donor with an anionic carboxylate group that can bind with  $\text{Li}^+@\text{C}_{60}$  by an electrostatic interaction. The supramolecular nanoclusters including  $\text{ZnCh}^-$  and  $\text{Li}^+@\text{C}_{60}$  were prepared for light to electrical energy conversion in photoelectrochemical cell. The photoelectrochemical behavior of the nanostructured  $\text{SnO}_2$  film of supramolecular nanoclusters of  $\text{Li}^+@\text{C}_{60}$  and  $\text{ZnCh}^-$  on optically transparent electrode (OTE) denoted as  $\text{OTE}/\text{SnO}_2/(\text{ZnCh}^-/\text{Li}^+@\text{C}_{60})_n$  is significantly higher than the single component films of  $\text{ZnCh}^-$  or  $\text{Li}^+@\text{C}_{60}$  clusters, denoted as  $\text{OTE}/\text{SnO}_2/(\text{ZnCh}^-)_n$  or  $\text{OTE}/\text{SnO}_2/(\text{Li}^+@\text{C}_{60})_n$  (Scheme 1).



**Scheme 1.** Photoelectrochemical Cell of  $\text{OTE}/\text{SnO}_2/\text{ZnCh}^-/\text{Li}^+@\text{C}_{60})_n$ .

## Experimental Section

**Materials.** Chemicals were purchased from commercial sources and used without further purification, unless otherwise noted. Lithium ion-encapsulated fullerene hexafluorophosphate salt ( $\text{Li}^+@\text{C}_{60} \text{ PF}_6^-$ , Idea International Corporation) was commercially obtained from Wako Pure Chemicals, Japan. Benzonitrile (PhCN) used as a solvent was distilled over phosphorus pentoxide.<sup>44</sup> Acetonitrile (MeCN) was purchased from Wako Pure Chemical and used as received.  $\text{Bu}_4\text{N}^+ \text{ZnCh}^-$  and  $\text{ZnCh}_{\text{Me}}$  were synthesized by following the published method.<sup>43,46</sup>

**UV–Vis Absorption Spectral Measurements.** Absorption spectra were recorded on a Hewlett-Packard 8453 diode array spectrophotometer at room temperature.

**Laser Flash Photolysis Measurements.** Femtosecond transient absorption spectroscopy experiments were conducted using an ultrafast source: Integra-C (Quantronix Corp.), an optical parametric amplifier: TOPAS (Light Conversion Ltd.) and a commercially available optical detection system: Helios provided by Ultrafast Systems LLC. The source for the pump and probe pulses were derived from the fundamental output of Integra-C ( $\lambda = 786 \text{ nm}$ ,  $2 \mu\text{J}/\text{pulse}$  and fwhm

$\lambda = 130$  fs) at a repetition rate of 1 kHz. 75% of the fundamental output of the laser was introduced into a second harmonic generation (SHG) unit: Apollo (Ultrafast Systems) for excitation light generation at  $\lambda = 393$  nm, while the rest of the output was used for white light generation. The laser pulse was focused on a sapphire plate of 3 mm thickness and then white light continuum covering the visible region from  $\lambda = 410$  nm to 800 nm was generated via self-phase modulation. A variable neutral density filter, an optical aperture, and a pair of polarizer were inserted in the path in order to generate stable white light continuum. Prior to generating the probe continuum, the laser pulse was fed to a delay line that provides an experimental time window of 3.2 ns with a maximum step resolution of 7 fs. In our experiments, a wavelength at  $\lambda = 393$  nm of SHG output was irradiated at the sample cell with a spot size of 1 mm diameter where it was merged with the white probe pulse in a close angle ( $< 10^\circ$ ). The probe beam after passing through the 2 mm sample cell was focused on a fiber optic cable that was connected to a CMOS spectrograph for recording the time-resolved spectra ( $\lambda = 410$  - 800 nm). Typically, 1500 excitation pulses were averaged for 3 seconds to obtain the transient spectrum at a set delay time. Kinetic traces at appropriate wavelengths were assembled from the time-resolved spectral data. All measurements were conducted at room temperature, 295 K. Nanosecond transient absorption spectral measurements were made according to the following procedure. A deaerated PhCN solutions containing  $\text{Li}^+@\text{C}_{60}$  with a  $\text{TBA}^+\text{ZnCh}^-$  was excited by a Panther OPO pumped Nd:YAG laser (Continuum, SLII-10, 4-6 ns fwhm) at 450 nm. The resulting time resolved transient absorption spectra were measured by using a continuous Xe-lamp (150 W) and a photodiode (Hamamatsu 2949) as the probe light and detector, respectively. The output from the photodiode and the photomultiplier tube was recorded using a digitizing oscilloscope (Tektronix, TDS3032, 300 MHz). The solutions were deoxygenated by  $\text{N}_2$  purging for 10 min prior to measurements. Rates of photoinduced electron-transfer reactions were monitored by the rise and decay of the absorption band due to the  $\text{Li}^+@\text{C}_{60}$  radical anion. First-order rate constants were determined by a least-squares curve fit. All experiments were performed at 298 K.

**ESR Measurements.** ESR spectra were taken on a JEOL X-band spectrometer (JES-RE1XE) at 77 K for the CS state of  $(\text{ZnCh}^-/\text{Li}^+@\text{C}_{60})_n$  in frozen MeCN/PhCN solution (3:1 v/v) was measured under photoirradiation with a high-pressure mercury lamp (USH-1005D) through a water filter focusing at the sample cell in the ESR cavity. The *g* value was calibrated using an  $\text{Mn}^{2+}$  marker. ESR spectrum was recorded under non-saturating microwave power conditions. The magnitude of modulation was chosen to optimize the resolution and the signal-to-noise (S/N) ratio of the observed spectra.

**Photoelectrochemical Measurements.** Electrophoretic deposition was performed using a Power Pac HV (Bio-Rad). Photoelectrochemical measurements were carried out in a standard two-compartment cell consisting of a working electrode, a Pt wire gauze counter electrode. A KEITHLEY 2400 was used for photocurrent generation density. For the IPCE measurements, a monochromator (SM-25, Bunkoh Keiki Co., LTD) was introduced into the path of the excitation beam (150 W xenon lamp, Bunkoh Keiki Co., LTD) for the selected wavelength. The lamp intensity at each wavelength was determined using a Si photodiode (Hamamatsu Photonics S1337-1010BQ) and corrected.

**Dynamic Light Scattering (DLS) Measurements.** The particle size and distribution were measured in MeCN/PhCN (3:1 v/v) using light-scattering equipment (Zetasizer nano ZS).

**TEM Measurements.** Transmission electron micrograph (TEM) measurements were recorded on Tecnai spirit (FEI company) by applying a drop of the sample to a copper grid. TEM images were recorded on a transmission electron microscope an accelerating voltage of 120 kV for imaging.

## Results and Discussion

UV–Vis absorption spectra of an anionic zinc chlorin tetrabutylammonium salt ( $\text{Bu}_4\text{N}^+$   $\text{ZnCh}^-$ : see the structure shown in Figure 1) in benzonitrile (PhCN) at room temperature were changed upon the addition of lithium ion-encapsulated fullerene hexafluorophosphate salt ( $\text{Li}^+@\text{C}_{60}$   $\text{PF}_6^-$ ) as shown in Figure 2a, where the Soret band at 435 nm and Q-band at 665 nm were blue-shifted to 431 nm and 661 nm, respectively<sup>43</sup>. In contrast, no UV–Vis spectral change was observed as shown in Figure 2b when  $\text{ZnCh}^-$  was replaced by a neutral zinc chlorin methyl carboxylate ester ( $\text{ZnCh}_{\text{Me}}$ ). This indicates there exists a strong electrostatic interaction between anionic  $\text{ZnCh}^-$  and cationic  $\text{Li}^+@\text{C}_{60}$ .<sup>43</sup>

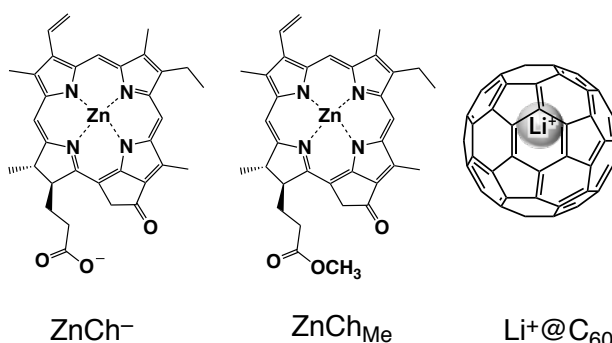


**Figure 1.** Structures of anionic zinc chlorin ( $\text{ZnCh}^-$ ), neutral zinc chlorin ( $\text{ZnCh}_{\text{Me}}$ ), and lithium ion-encapsulated fullerene used in this study.

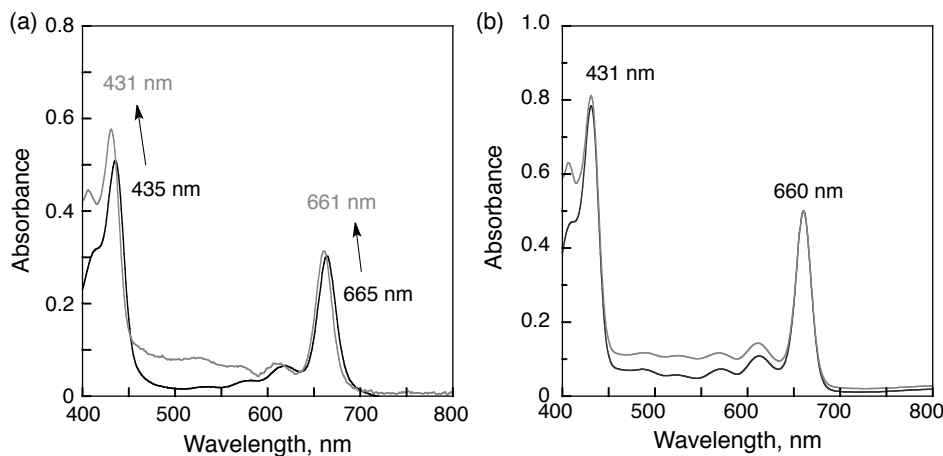


**Figure 2.** UV-Vis absorption spectra of (a)  $\text{ZnCh}^-$  ( $1.0 \times 10^{-5}$  M) and (b)  $\text{ZnCh}_{\text{Me}}$  ( $1.0 \times 10^{-5}$  M) in the absence (black) and presence of  $\text{Li}^+@\text{C}_{60}$  ( $3.2 \times 10^{-5}$  M for  $\text{ZnCh}^-$  and  $4.5 \times 10^{-5}$  M for  $\text{ZnCh}_{\text{Me}}$ , gray) in PhCN.

A mother solution of the  $\text{Li}^+@\text{C}_{60}/\text{ZnCh}^-$  supramolecule was prepared by mixing of  $\text{Li}^+@\text{C}_{60} \text{ PF}_6^-$  ( $2.5 \times 10^{-4}$  M) and  $\text{Bu}_4\text{N}^+ \text{ ZnCh}^-$  ( $2.5 \times 10^{-4}$  M) in PhCN for the preparation of nanoparticles. The solution of 1 mL was injected to an acetonitrile (MeCN) solution (3 mL) as a poor solvent for the supramolecule to produce the suspension containing the supramolecular nanoclusters  $[(\text{ZnCh}^-/\text{Li}^+@\text{C}_{60})_n]$ . The suspension including  $(\text{ZnCh}^-/\text{Li}^+@\text{C}_{60})_n$  was transferred into a cuvette, in which the two electrodes OTE and OTE/SnO<sub>2</sub> were placed and kept at  $\sim 6$  mm distance by a Teflon spacer. Then, application of DC electric field ( $\sim 100 \text{ V cm}^{-1}$ ) resulted in the deposition of  $(\text{ZnCh}^-/\text{Li}^+@\text{C}_{60})_n$  from the suspension to the electrode surface and the formation of a robust thin film of OTE/SnO<sub>2</sub>/ $(\text{ZnCh}^-/\text{Li}^+@\text{C}_{60})_n$ , as documented by discoloration of the suspension and the simultaneous coloration of the OTE/SnO<sub>2</sub> electrode. For reference purposes, thin films of only  $\text{Li}^+@\text{C}_{60}$  or  $\text{ZnCh}^-$  were analogously deposited onto the electrode surfaces to form OTE/SnO<sub>2</sub>/ $(\text{Li}^+@\text{C}_{60})_n$  or OTE/SnO<sub>2</sub>/ $(\text{ZnCh}^-)_n$ .

Steady-state UV-Vis absorption spectroscopy was used to follow the deposition of the  $\text{ZnCh}^-/\text{Li}^+@\text{C}_{60}$  supramolecular material onto the electrode surface. The UV-Vis absorption spectra of OTE/SnO<sub>2</sub>/ $(\text{ZnCh}^-/\text{Li}^+@\text{C}_{60})_n$  are shown in Figure 3, exhibiting significant broadening as compared with those in PhCN. Such broadening behavior indicates that the molecular environment on the OTE/SnO<sub>2</sub> surface is significantly perturbed because of the aggregation of the chlorin molecules or the supramolecules by  $\pi$ -stacking. Thus,  $(\text{ZnCh}^-/\text{Li}^+@\text{C}_{60})_n$  is successfully deposited on OTE/SnO<sub>2</sub>. The broad absorption band at the near IR region ( $\lambda > 750$  nm) shown in Figure 3 may be assigned to the charge-transfer band between the chlorin plane and the fullerene sphere in the 1:1 supramolecular complex as reported previously.<sup>42,45</sup>

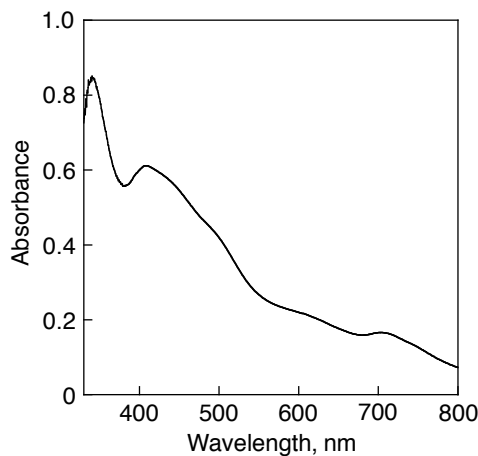


**Figure 3.** UV–Vis absorption spectrum of an OTE/SnO<sub>2</sub>/(ZnCh<sup>−</sup>/Li<sup>+</sup>@C<sub>60</sub>)<sub>n</sub> electrode.

TEM was used to evaluate the topography of (ZnCh<sup>−</sup>/Li<sup>+</sup>@C<sub>60</sub>)<sub>n</sub> as shown in Figure 4a. The (ZnCh<sup>−</sup>/Li<sup>+</sup>@C<sub>60</sub>)<sub>n</sub> are composed of closely packed ZnCh<sup>−</sup> and Li<sup>+</sup>@C<sub>60</sub> composite clusters of about 160 nm size, which renders a nanoporous morphology to the film. The cluster sizes were also evaluated by the dynamic light scattering (DLS) measurements (Figure 5). The grape bunch morphology of the cluster assembly thus provides a high surface area to the electrophoretically deposited film of Li<sup>+</sup>@C<sub>60</sub> clusters. In contrast, the TEM image of ZnCh<sup>−</sup> nanoclusters exhibited the rod shape morphology by strong  $\pi$ – $\pi$  aggregation between ZnCh<sup>−</sup> molecules (Figure 4b). As indicated earlier,<sup>47</sup> charging of chlorin and fullerene moieties in the DC electric field play an important role in the growth and deposition process. These films are quite robust and can be washed with organic solvents to remove any loosely bound ZnCh<sup>−</sup> and Li<sup>+</sup>@C<sub>60</sub> nano-assemblies.

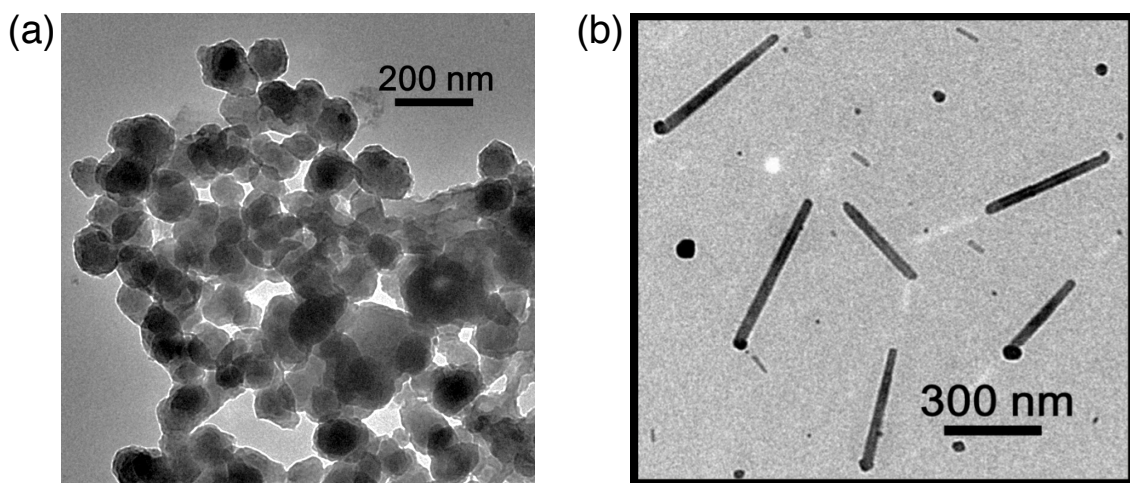


**Figure 4.** TEM images of (a) Li<sup>+</sup>@C<sub>60</sub>/ZnCh<sup>−</sup> and (b) ZnCh<sup>−</sup> nanoclusters.

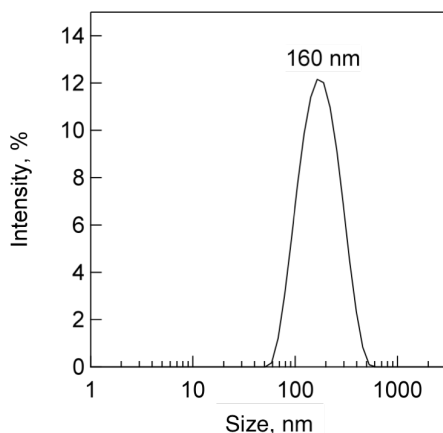


**Figure 5.** Size distribution of  $\text{Li}^+@\text{C}_{60}/\text{ZnCh}^-$  nanoclusters estimated by DLS.

Photoelectrochemical measurements were performed using a standard two-electrode system consisting of a working electrode and a Pt wire gauze electrode in air-saturated MeCN containing 0.5 M lithium iodide (LiI) and 0.01 M iodine ( $\text{I}_2$ ) (Scheme 1). In order to evaluate the response towards the photocurrent generation, a series of photocurrent action spectra were recorded. The IPCE (incident photon-to-photocurrent efficiency) values were calculated by normalizing the photocurrent values for incident light energy and intensity and using eq 1,<sup>48</sup>

$$\text{IPCE} (\%) = 100 \times 1240 \times i_{\text{sc}} / (I_{\text{inc}} \times \lambda) \quad (1)$$

where  $i_{\text{sc}}$  is the short circuit photocurrent ( $\text{A cm}^{-2}$ ),  $I_{\text{inc}}$  is the incident light intensity ( $\text{W cm}^{-2}$ ) and  $\lambda$  is the wavelength (nm). The maximum IPCE values of OTE/SnO<sub>2</sub>/ $(\text{Li}^+@\text{C}_{60})_n$  (black spectrum in Figure 6a) and OTE/SnO<sub>2</sub>/ $(\text{ZnCh}^-)_n$  (blue spectrum) are only 5% (470 nm) and 6% (420 nm), respectively. In contrast with the reference experiments, the IPCE value of OTE/SnO<sub>2</sub>/ $(\text{ZnCh}^-/\text{Li}^+@\text{C}_{60})_n$  is much higher than the sum of the two individual IPCE values of the individual systems OTE/SnO<sub>2</sub>/ $(\text{ZnCh}^-)_n$  and OTE/SnO<sub>2</sub>/ $(\text{Li}^+@\text{C}_{60})_n$  in the visible region. The maximum IPCE value attained in these experiments was 22% at 450 nm. The high ICPE value was also observed at the Q-band region to be 3% at 700 nm. The higher IPCE value of OTE/SnO<sub>2</sub>/ $(\text{ZnCh}^-/\text{Li}^+@\text{C}_{60})_n$  indicates that photocurrent generation is initiated via photoinduced electron transfer from  $\text{ZnCh}^-$  to  $\text{Li}^+@\text{C}_{60}$  in supramolecular nanoclusters, followed by the negative charge transport to the collective surface of OTE/SnO<sub>2</sub> electrode and electron transfer oxidation of LiI as an electrolyte (Scheme 1).

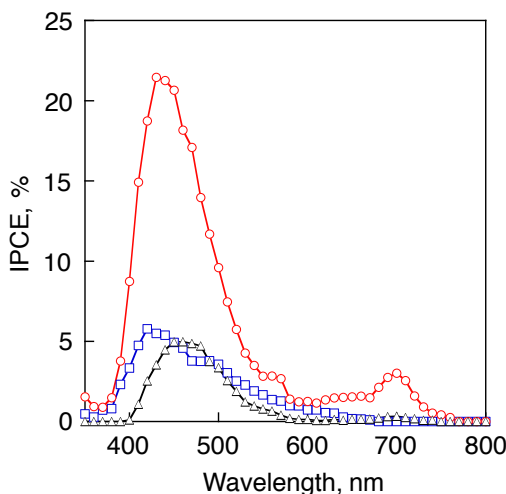


**Figure 6.** Photocurrent action spectra of (a) OTE/SnO<sub>2</sub>/(ZnCh<sup>-</sup>/Li<sup>+</sup>@C<sub>60</sub>)<sub>n</sub> (red circle), OTE/SnO<sub>2</sub>/(ZnCh<sup>-</sup>)<sub>n</sub> (blue square) and OTE/SnO<sub>2</sub>/(Li<sup>+</sup>@C<sub>60</sub>)<sub>n</sub> (black triangle). Electrolyte: 0.5 M LiI and 0.01 M I<sub>2</sub> in MeCN.

Such a significant enhancement of the IPCE value demonstrates that the strong ordering in the clusters and the efficient photoinduced charge separation in (ZnCh<sup>-</sup>/Li<sup>+</sup>@C<sub>60</sub>)<sub>n</sub> on the electrode improved the light energy conversion properties.

**Photoinduced Electron Transfer in the ZnCh<sup>-</sup>/Li<sup>+</sup>@C<sub>60</sub> Complex.** The occurrence of photoinduced electron transfer in the supramolecular complex of ZnCh<sup>-</sup>/Li<sup>+</sup>@C<sub>60</sub> in PhCN was confirmed by nanosecond transient absorption spectral spectroscopy. Time-resolved transient absorption spectra of (ZnCh<sup>-</sup>/Li<sup>+</sup>@C<sub>60</sub>)<sub>n</sub> dispersed in a deaerated MeCN/PhCN solution (3:1 v/v) are shown in Figure 7a, which clearly exhibits a broad absorption band at 1035 nm taken at 2  $\mu$ s after 532 nm laser flash excitation. This is diagnostic of formation of Li<sup>+</sup>@C<sub>60</sub><sup>•-</sup> upon laser irradiation.<sup>39-43,49</sup> Thus, photoinduced electron transfer occurs from ZnCh<sup>-</sup> to Li<sup>+</sup>@C<sub>60</sub> in the composite clusters to produce the CS state [(ZnCh<sup>-</sup>)<sup>•+</sup>/Li<sup>+</sup>@C<sub>60</sub><sup>•-</sup>]. The absorption time profile of [(ZnCh<sup>-</sup>)<sup>•+</sup>/Li<sup>+</sup>@C<sub>60</sub><sup>•-</sup>] recorded at 1035 nm is shown in Figure 7b. The first-order decay kinetics (inset of Figure 7b) corresponds to back electron transfer from Li<sup>+</sup>@C<sub>60</sub><sup>•-</sup> to (ZnCh<sup>-</sup>)<sup>•+</sup>, affording the rate constant of back electron transfer to be  $k_{\text{BET}} = 5.0 \times 10^3$  s<sup>-1</sup>. The lifetime of the CS state is 200 ms, which is long enough to inject an electron from Li<sup>+</sup>@C<sub>60</sub><sup>•-</sup> of the CS state to the SnO<sub>2</sub> electrode and electron-transfer oxidation of LiI with (ZnCh<sup>-</sup>)<sup>•+</sup> before the charge recombination of (ZnCh<sup>-</sup>)<sup>•+</sup>/Li<sup>+</sup>@C<sub>60</sub><sup>•-</sup> bound for the ground state.

When ZnCh<sup>-</sup> was replaced by neutral ZnCh<sub>Me</sub>, the transient absorption bands due to the radical ion pair in a PhCN solution was also observed by intermolecular photoinduced electron transfer from the triplet excited state of ZnCh<sub>Me</sub> to Li<sup>+</sup>@C<sub>60</sub> (Figure 8). However, the decay of

the transient absorption at 1035 nm due to  $\text{Li}^+@\text{C}_{60}^{\bullet-}$  obeyed second-order kinetics, indicating that the charge-recombination by back electron transfer occurred via a bimolecular process. In the case of  $\text{ZnCh}^-$  and empty  $\text{C}_{60}$  system, no transient absorption spectrum of radical ion pair was observed when only the triplet excited state of  $\text{C}_{60}$  and  $\text{ZnCh}^-$  was observed at 10  $\mu\text{s}$  after laser excitation as shown in Figure 9 because photoinduced electron transfer from the triplet excited state of  $\text{ZnCh}^-$  to  $\text{C}_{60}$  and from  $\text{ZnCh}^-$  to the triplet excited state of  $\text{C}_{60}$  are both unfavorable under the uncomplexed bimolecular reaction conditions.

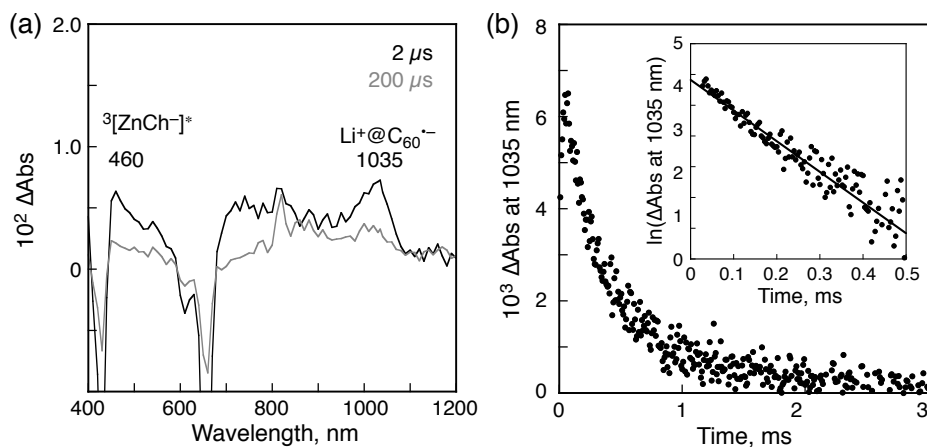


**Figure 7.** (a) Transient absorption spectra of  $(\text{ZnCh}^-/\text{Li}^+@\text{C}_{60})_n$  in deaerated MeCN/PhCN (3:1 v/v) taken at 2  $\mu\text{s}$  (black) and 200  $\mu\text{s}$  (gray) after laser excitation at 532 nm. (b) Time profile of the transient absorption at 1035 nm due to  $\text{Li}^+@\text{C}_{60}^{\bullet-}$ . Inset: first-order plot.

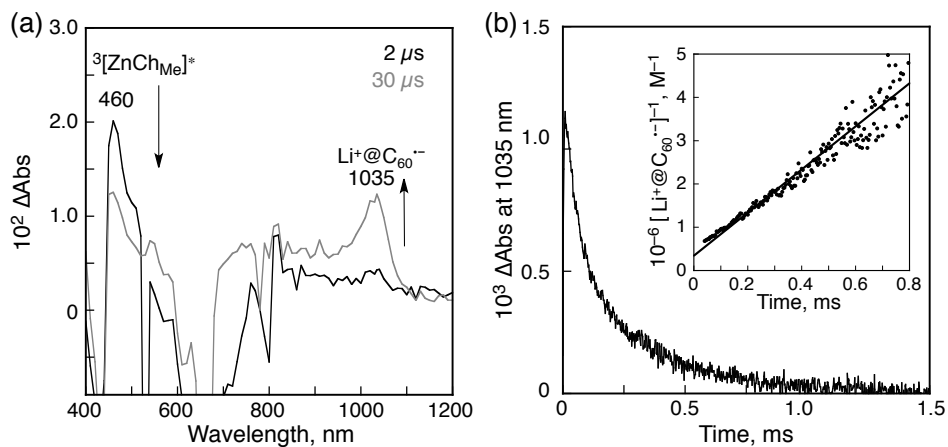


**Figure 8.** Transient absorption spectra of  $\text{ZnCh}_{\text{Me}}$  ( $2.5 \times 10^{-5}$  M) with  $\text{Li}^+@\text{C}_{60} \text{PF}_6^-$  ( $5.0 \times 10^{-5}$  M) in deaerated PhCN taken at 2  $\mu\text{s}$  (black) and 30  $\mu\text{s}$  (gray) after nanosecond laser excitation at 532 nm. (b) Time profile of absorbance at 1035 nm due to  $\text{Li}^+@\text{C}_{60}^{\bullet-}$ . Insert: second-order plot for the decay of  $\text{Li}^+@\text{C}_{60}^{\bullet-}$ .  $[\text{Li}^+@\text{C}_{60}^{\bullet-}]$  is obtained from the absorbance at 1035 nm and molar absorption coefficient ( $\epsilon$ ) value of  $7300 \text{ M}^{-1} \text{ cm}^{-1}$ .

Formation of the long-lived CS state of  $(\text{ZhCh}^-)^+/\text{Li}^+@\text{C}_{60}^-$  enabled detection of the radical ion species produced by photoinduced electron transfer in  $(\text{ZnCh}^-/\text{Li}^+@\text{C}_{60})_n$  cluster dispersed into a deaerated MeCN/PhCN (3:1 v/v) glass by ESR measurements under photoirradiation with use of a high-pressure mercury lamp (1000 W) at 77 K. The ESR spectrum is shown in Figure 10, where two characteristic ESR signals are observed and one of which is clearly attributable to  $\text{Li}^+@\text{C}_{60}^-$  at a small  $g$  value ( $g = 1.9993$ ).<sup>41,43</sup> The other due to  $(\text{ZhCh}^-)^+$  shows a broad signal at  $g = 2.003$  overlapped with the signal of  $\text{Li}^+@\text{C}_{60}^-$ . No decay of the ESR signal due to the CS state was observed at 77 K after cutting off the photoirradiation.

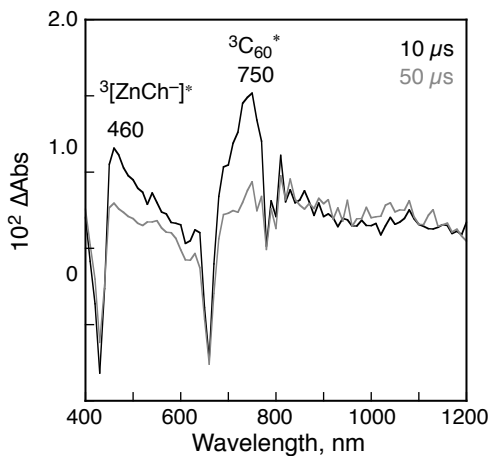


**Figure 9.** Transient absorption spectra of  $\text{ZnCh}^-$  ( $2.5 \times 10^{-5}$  M) with  $\text{C}_{60}$  ( $5.0 \times 10^{-5}$  M) in deaerated PhCN taken at  $10 \mu\text{s}$  (black) and  $50 \mu\text{s}$  (gray) after nanosecond laser excitation at  $532 \text{ nm}$ .

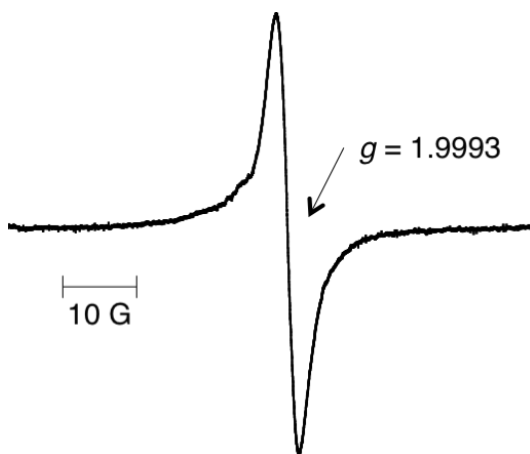


**Figure 10.** ESR spectrum of the charge-separated state of  $(\text{ZnCh}^-/\text{Li}^+@\text{C}_{60})_n$  dispersed in deaerated MeCN/PhCN (3:1 v/v) generated by Hg-lamp photoirradiation (1000 W) at 77 K

Based on the above mentioned results, the photocurrent generation is initiated by photoinduced electron transfer from  ${}^3(\text{ZnCh}^-)^*$  to  $\text{Li}^+@\text{C}_{60}$  in the cluster to produce the CS state,  $(\text{ZnCh}^-)^+/\text{Li}^+@\text{C}_{60}^{\cdot-}$ . The reduced  $\text{Li}^+@\text{C}_{60}$  ( $\text{Li}^+@\text{C}_{60}^{\cdot-}$ ) in the CS state injects electrons into the conduction band of  $\text{SnO}_2$ , whereas the oxidized species of  $\text{ZnCh}^-$  [ $(\text{ZnCh}^-)^{+}$ ] undergoes the electron-transfer reduction with the iodide in the electrolyte solution.

In conclusion, the photoinduced electron transfer from  ${}^3(\text{ZnCh}^-)^*$  to  $\text{Li}^+@\text{C}_{60}$  in the supramolecular cluster makes it possible to enhance the performance of the photoelectrochemical cell. Thus, the use of  $\text{Li}^+@\text{C}_{60}$  as an electron acceptor in the supramolecular clusters with  $\text{ZnCh}^-$  paves a new way for the design of high performance solar cell for the near IR excitation although the performance remains to be further improved.

## References

- (1) (a) Okamoto, K.; Hasobe, T.; Tkachenko, N. V.; Lemmetyinen, H.; Kamat, P. V.; Fukuzumi, S. *J. Phys. Chem. A* **2005**, *109*, 4662-4670. (b) Hattori, S.; Hasobe, T.; Ohkubo, K.; Urano, T.; Nagano, T.; Wada, Y.; Yanagida, S.; Fukuzumi, S. *J. Phys. Chem. B* **2004**, *108*, 15200–15205. (c) Hasobe, T.; Hattori, S.; Kotani, H.; Ohkubo, K.; Hosomizu, K.; Imahori, H.; Kamat, P. V.; Fukuzumi, S. *Org. Lett.* **2004**, *6*, 3103–3106.
- (2) *The Photosynthetic Reaction Center*, Deisenhofer, J., Norris, J. R., Eds.; Academic Press: San Diego, 1993.
- (3) *Anoxygenic Photosynthetic Bacteria*, Blankenship, R. E., Madigan, M. T., Bauer, C. E., Eds.; Kluwer Academic Publishing: Dordrecht, 1995.
- (4) (a) Gust, D.; Moore, T. A.; Moore, A. L. *Acc. Chem. Res.* **2001**; *34*, 40–48. (b) Gust, D.; Moore, T. A.; Moore, A. L. *Acc. Chem. Res.* **2009**, *42*, 1890–1898. (c) Gust, D.; Moore, T. A.; Moore, A. L. In *Electron Transfer in Chemistry*; Balzani, V., Ed.; Wiley: Weinheim, 2001; Vol. 3, pp 272–336. (d) Gust D.; Moore T. A.; Moore A. L. *Acc. Chem. Res.* **1993**, *26*, 198–205.
- (5) (a) D’Souza, F.; Ito, O. *Chem. Soc. Rev.* **2012**, *41*, 86–96. (b) D’Souza, F.; Ito, O. *Chem. Commun.* **2009**, 4913–4928.
- (6) McDermott, G.; Prince S. M.; Freer, A. A.; Hawthornthwaite-Lawless, A. M.; Papiz, M. Z.; Cogdell R. J.; Isaacs, N. W. *Nature* **1995**, *374*, 517–521.
- (7) (a) Wasielewski, M. R. *Acc. Chem. Res.*, **2009**, *42*, 1910–1921. (b) Wasielewski, M. R. *Chem. Rev.* **1992**, *92*, 435–461.
- (8) Jordan, K. D.; Paddon-Row, M. N. *Chem. Rev.* **1992**, *92*, 395–410.

(9) Harriman, A.; Sauvage, J. P. *Chem. Soc. Rev.* **1996**, *25*, 41–48.

(10) (a) Fukuzumi, S.; Ohkubo, K.; Suenobu, T. *Acc. Chem. Res.* **2014**, *47*, 1455–1464. (b) Fukuzumi, S.; Ohkubo, K. *Dalton Trans.* **2013**, *42*, 15846–15858. (c) Fukuzumi, S.; Ohkubo, K. *J. Mater. Chem.* **2012**, *22*, 4575–4587. (d) Fukuzumi, S.; Ohkubo, K.; D'Souza, F.; Sessler, J. L. *Chem. Commun.* **2012**, *48*, 9801–9815. (e) Fukuzumi, S.; Guldi, D. M. In *Electron Transfer in Chemistry*, Vol. 2, Balzani, V., Ed.; Wiley-VCH: Weinheim, 2001; pp 270–337. (f) Ohkubo, K.; Fukuzumi, S. *Bull. Chem. Soc. Jpn.* **2009**, *82*, 303–315. (g) Ohkubo, K.; Fukuzumi, S. *J. Porphyrins Phthalocyanines* **2008**, *12*, 993–1004.

(11) (a) Guldi D. M.; Prato M. *Acc. Chem. Res.* **2000**, *33*, 695–703. (b) Guldi D. M.; Rahman G. M. A.; Zerbetto, F.; Prato, M. *Acc. Chem. Res.* **2005**, *38*, 871–978. (c) Bottari, G.; de la Torre, G.; Guldi DM.; Torres T. *Chem. Rev.* **2010**, *110*, 6768–6816. (d) Sgobba, V.; Guldi, D. M. *Chem. Soc. Rev.* **2009**, *38*, 165–184.

(12) (a) Fukuzumi, S.; Kotani, H.; Ohkubo, K.; Ogo, S.; Tkachenko, N. V.; Lemmetyinen, H. *J. Am. Chem. Soc.* **2004**, *126*, 1600–1601. (b) Murakami, M.; Ohkubo, K.; Fukuzumi, S. *Chem.–Eur. J.* **2010**, *16*, 7820–7832. (c) D'Souza, F.; Chita, R.; Ohkubo, K.; Tasior, M.; Subbaiyan, N. K.; Zandler, M. E.; Rogacki, M.; Gryko, D. T.; Fukuzumi, S. *J. Am. Chem. Soc.* **2008**, *130*, 14263–14272.

(13) Choi, M.S.; Yamazaki, T.; Yamazaki, I.; Aida, T. *Angew. Chem., Int. Ed.* **2004**, *43*, 150–158.

(14) Sessler, J. L., Wang, B., Springs, S. L., Brown, C. T. in *Comprehensive Supramolecular Chemistry*, Atwood, J. L.; Davies J. E. D., Eds.; Pergamon, 1996.

(15) Chang C. J.; Brown J. D. K.; Chang M. C. Y.; Baker E. A.; Nocera D. G. in *Electron Transfer in Chemistry*, Vol. 3, Balzani, V., Ed.; Wiley-VCH: Weinheim, 2001; pp. 409–461.

(16) de Rege, P. J.; Williams, S. A.; Therien, M. J. *Science* **1995**, *269*, 1409–1413.

(17) Hayashi, T.; Ogoshi, H. *Chem. Soc. Rev.* **1997**, *26*, 355–364.

(18) Blanco, M. J.; Consuelo Jiménez, M.; Chambron, J. C.; Heitz, V.; Linke, M.; Sauvage, J. P. *Chem. Soc. Rev.* **1999**, *28*, 293–305.

(19) Diederich, F.; Gómez-López, M. *Chem. Rev. Soc.* **1999**, *28*, 263–277.

(20) D'Souza, F.; Deviprasad, G. R.; El-Khouly, M. E.; Fujitsuka, M.; Ito, O. *J. Am. Chem. Soc.* **2001**, *123*, 5277–5284.

(21) Piotrowiak, P. *Chem. Soc. Rev.* **1999**, *28*, 143–150.

(22) Flamigni, L.; Johnston, M.R.; Giribabu, L. *Chem.–Eur. J.* **2002**, *8*, 3938–3947.

---

(23) Li, W. S.; Kim, K. S.; Jiang, D. L.; Tanaka, H.; Kawai, T.; Kwon, J. H.; Kim, D.; Aida, T. *J. Am. Chem. Soc.* **2006**, *128*, 10527–10532.

(24) (a) D’Souza, F.; Deviprasad, G. R.; Zandler, M. E.; El-Khouly, M. E.; Fujitsuka, M.; Ito, O. *J. Phys. Chem. B* **2003**, *106*, 4952–4962. (b) D’Souza, F.; Deviprasad, G. R.; Zandler, M. E.; Hoang, V. T.; Klykov, A.; VanStipdonk, M.; Perera, A.; El-Khouly, M. E.; Fujitsuka, M.; Ito, O. *J. Phys. Chem. A* **2002**, *106*, 3243–3252.

(25) Tanaka, M.; Ohkubo, K.; Gross, C. P.; Guilard, R.; Fukuzumi, S. *J. Am. Chem. Soc.* **2006**, *128*, 14625–14633.

(26) D’Souza, F.; Maligaspe, E.; Ohkubo, K.; Zandler, M. E.; Subbaiyan, N. K.; Fukuzumi, S. *J. Am. Chem. Soc.* **2009**, *131*, 8787–8797.

(27) (a) Kojima, T.; Honda, T.; Ohkubo, K.; Shiro, M.; Kusukawa, T.; Fukuda, T.; Kobayashi, N.; Fukuzumi, S. *Angew. Chem., Int. Ed.* **2008**, *47*, 6712–6716. (b) Honda, T.; Nakanishi, T.; Ohkubo, K.; Kojima, T.; Fukuzumi, S. *J. Am. Chem. Soc.* **2010**, *132*, 10155–10163.

(28) (a) Sessler, J. L.; Karnas, E.; Kim, S. K.; Ou, Z.; Zhang, M.; Kadish, K. M.; Ohkubo, K.; Fukuzumi, S. *J. Am. Chem. Soc.* **2010**, *132*, 15256–15257. (b) Davis, C. M.; Kawashima, Y.; Ohkubo, K.; Lim, J. M.; Kim, D.; Fukuzumi, S.; Sessler, J. L. *J. Phys. Chem. C* **2014**, *118*, 13503–13513. (c) Ohkubo, K.; Mase, K.; Karnas, E.; Sessler, J. L.; Fukuzumi, S. *J. Phys. Chem. C* **2014**, *118*, 18436–18444.

(29) Walter, M. G.; Rudine, A. B.; Wamser, C. C. *J. Porphyrins Phthalocyanines* **2010**, *14*, 759–792.

(30) Kawashima, Y.; Ohkubo, K.; Fukuzumi, S. *J. Phys. Chem. A* **2013**, *117*, 6737–3743.

(31) (a) Pandey R. K.; Zheng G. In *The Porphyrin Handbook*; Kadish, K. M., Smith, K. M., Guilard, R., Eds.; Academic Press: San Diego, 2000; Vol. 6; Chap. 43. (b) Bonnett, R. *Chem. Soc. Rev.* **1995**, *24*, 19–33. (c) Pandey, R. K.; Herman, C. *Chem. Ind.* **1998**, 739–743.

(32) Scheer H.; Inhoffen H. H. in *The Porphyrins*; Dolphin D. Ed.; Academic Press: New York, 1978; Vol II, pp 45–90.

(33) (a) Hanson L. S. in *Chlorophylls*; Scheer H. Ed.; CRC Press: Boca Raton, FL, 1991; pp 993–1014. (b) Plato M, Möbius, K.; Lubitz, W. in *Chlorophylls*; Scheer H. Ed.; CRC Press: Boca Raton, FL, 1991; pp 1015–1046.

(34) (a) Fukuzumi, S.; Ohkubo, K.; Imahori, H.; Shao, J.; Ou, Z.; Zheng, G.; Chen, Y.; Pandey, R. K.; Fujitsuka, M.; Ito, O.; Kadish, K. M. *J. Am. Chem. Soc.* **2001**, *123*, 10676–10683. (b) Ohkubo, K.; Kotani, H.; Shao, J.; Ou, Z.; Kadish, K. M.; Li, G.; Pandey, R. K.;

Fujitsuka, M.; Ito, O.; Imahori, H.; Fukuzumi, S. *Angew. Chem., Int. Ed.* **2004**, *43*, 853–856. (c) Ohkubo, K.; Chen, Y.; Pandey, R. K.; Zhan, R.; Shao, J.; Kadish, K. M.; Fukuzumi, S. *J. Phys. Chem. A* **2002**, *106*, 5105–5013.

(35) Zheng, G.; Dougherty, T. J. Pandey R. K. *Chem. Commun.* **1999**, 2469–2470.

(36) (a) Helaja, J.; Tauber, A. Y.; Abel, Y.; Tkachenko, N. V.; Lemmetyinen, H.; Kilpeläinen, I.; Hynninen, P. H. *J. Chem. Soc., Perkin Trans. 1* **1999**, 2403–2408. (b) Tkachenko, N. V.; Rantala, L.; Tauber, A. Y.; Helaja, J.; Hynninen, P. H.; Lemmetyinen, H. *J. Am. Chem. Soc.* **1999**, *121*, 9378–9387. (c) Tkachenko, N. V.; Vuorimaa, E.; Kesti, T.; Alekseev, A. S.; Tauber, A. Y.; Hynninen, P. H.; Lemmetyinen H. *J. Phys. Chem. B* **2000**, *104*, 6371–6379.

(37) (a) Kutzki, O.; Walter, A.; Montforts, F-P. *Helv. Chim. Acta* **2000**, *83*, 2231–2345. (b) Montforts, F-P.; Kutzki, O. *Angew. Chem., Int. Ed.* **2000**, *39*, 599–601.

(38) Aoyagi, S.; Nishibori, E.; Sawa, H.; Sugimoto, K.; Takata, M.; Miyata, Y.; Kitaura, R.; Shinohara, H.; Okada, H.; Sakai, T.; Ono, Y.; Kawachi, K.; Yokoo K.; Ono, S.; Omote, K.; Kasama, Y.; Ishikawa, S.; Komuro, T.; Tobita, H. *Nature Chem.* **2010**, *2*, 678–683.

(39) (a) Fukuzumi, S.; Ohkubo, K.; Kawashima, Y.; Kim, D.S.; Park, J. S.; Jana, A.; Lynch, V.; Kim, D.; Sessler, J. L. *J. Am. Chem. Soc.* **2011**, *133*, 15938–15941. (b) Bill, N. L.; Ishida, M.; Bähring, S.; Lim, J. M.; Lee, S.; Davis, C. M.; Lynch, V. M.; Nielsen, K. A.; Jeppesen, J. O.; Ohkubo, K.; Fukuzumi, S.; Kim, D.; Sessler, J. L. *J. Am. Chem. Soc.* **2013**, *135*, 10852–10862.

(40) (a) Kawashima, Y.; Ohkubo, K.; Fukuzumi, S. *J. Phys. Chem. A* **2012**, *116*, 8942–8948. (b) Kawashima, Y.; Ohkubo, K.; Fukuzumi, S. *J. Phys. Chem. A* **2013**, *117*, 6737–6743.

(41) (a) Ohkubo, K.; Kawashima, Y.; Fukuzumi, S. *Chem. Commun.* **2012**, *48*, 4314–4316. (b) Kamimura, T.; Ohkubo, K.; Kawashima, Y.; Nobukuni, H.; Naruta, Y.; Tani, F.; Fukuzumi, S. *Chem. Sci.* **2013**, *4*, 1451–1461. (c) Supur, M.; Kawashima, Y.; Larsen, K.R.; Ohkubo, K.; Jeppesen, J. O.; Fukuzumi, S. *Chem.–Eur. J.* **2014**, *20*, 13976–13983. (d) Kawashima, Y.; Ohkubo, K.; Okada, H.; Matsuo, Y.; Fukuzumi, S. *ChemPhysChem* **2014**, *15*, 3782–3790. (e) Yamada, M.; Ohkubo, K.; Shionoya, M.; Fukuzumi, S. *J. Am. Chem. Soc.* **2014**, *136*, 13240–13248.

(42) Ohkubo, K.; Kawashima, Y.; Sakai, H.; Hasobe, T.; Fukuzumi, S. *Chem. Commun.* **2013**, *49*, 4474–4476.

(43) Kawashima, Y.; Ohkubo, K.; Mase, K.; Fukuzumi, S. *J. Phys. Chem. C* **2013**, *117*, 21166–21177.

---

(44) Armarego, W. L. F.; Chai, C. L. L. *Purification of Laboratory Chemicals*, 6th ed; Pergamon Press: Oxford, 2009.

(45) (a) Nobukuni, H. Tani, F.; Shimazaki, Y.; Naruta, Y.; Ohkubo, K.; Nakanishi, T.; Kojima, T.; Fukuzumi, S.; Seki, S. *J. Phys. Chem. C* **2009**, *113*, 19694–19699. (b) Tkachenko, N. V.; Lemmetyinen, H.; Sonoda, J.; Ohkubo, K.; Sato, T.; Imahori, H.; Fukuzumi, S. *J. Phys. Chem. A* **2003**, *107*, 8834–8844.

(46) (a) Mase, K.; Ohkubo, K.; Fukuzumi, S. *J. Am. Chem. Soc.* **2013**, *135*, 2800–2808. (b) Tamiaki, H.; Kunieda, M. *J. Org. Chem.* **2007**, *72*, 2443–2451. (c) Huber, V.; Sengupta, S.; Würthner, F. *Chem.—Eur. J.* **2008**, *14*, 7791–7807.

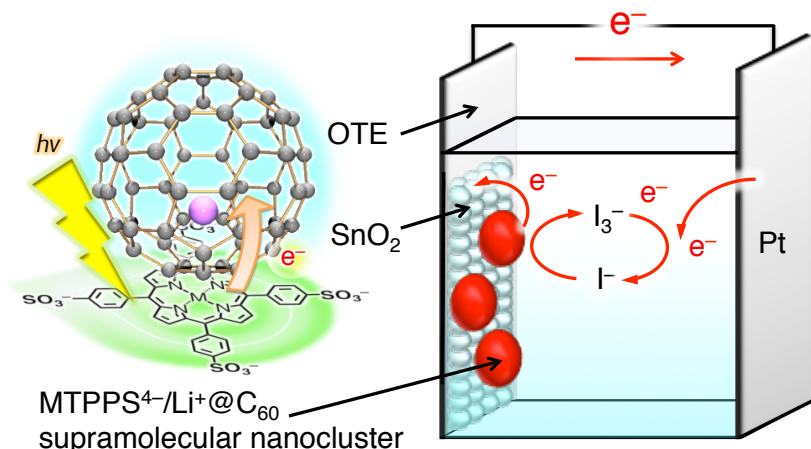
(47) Hasobe, T.; Imahori, H.; Fukuzumi, S.; Kamat, P. V. *J. Phys. Chem. B* **2003**, *107*, 12105–12112.

(48) Hasobe, T.; Kashiwagi Y.; Absalom, M. A.; Sly, J.; Hosomizu, K.; Crossley, M. J.; Imahori, H.; Kamat, P. V.; Fukuzumi, S. *Adv. Mater.* **2004**, *16*, 975–979.

(49) Ueno, H.; Kokubo, K.; Nakamura, Y.; Ohkubo, K.; Ikuma, N.; Moriyama H, Fukuzumi S.; Oshima T. *Chem. Commun.* **2013**, *49*, 7376–7378.

## Chapter 14

## Enhanced Photoelectrochemical Performance of Composite Photovoltaic Cells of $\text{Li}^+@\text{C}_{60}$ /Sulphonated Porphyrin Supramolecular Nanoclusters



**Abstract:** A photoelectrochemical solar cell composed of supramolecular nanoclusters of lithium ion-encapsulated fullerene and zinc sulphonated *meso*-tetraphenylporphyrin exhibits significant enhancement in the photoelectrochemical performance as compared with the reference system containing only each component.

### Introduction

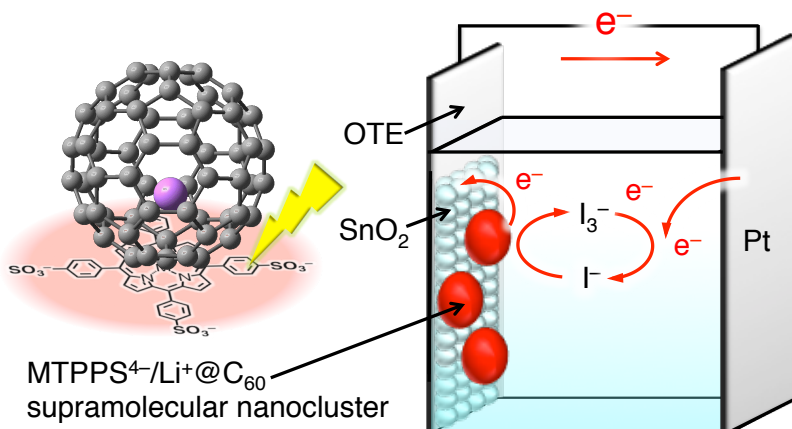
Photoelectrochemical cells (PECs) have been widely investigated as a next-generation solar cell because of their simple structure.<sup>1-3</sup> The photoinduced charge separation between the excited state of dye and the electrode plays an important role in improvement of PEC performance. In the natural photosynthetic reaction center, the efficient photoinduced electron transfer occurs to give long-lived charge separated (CS) state with high quantum yield.<sup>4</sup> Extensive efforts have so far been devoted to design and synthesize electron donor-acceptor linked molecules to achieve efficient photoinduced charge separation for applications to PECs.<sup>5,6</sup> However, the synthetic difficulty of the covalently linked donor-acceptor molecule has precluded the development of

simple photovoltaic devices using such model compounds of the photosynthetic reaction center. Among many candidates, porphyrins and fullerenes are suitable combination for construction of PECs, because porphyrins have strong visible absorption bands and fullerene exhibits efficient electron-transfer properties such as small reorganization energy due to delocalized three-dimensional  $\pi$ -system.<sup>7</sup> The supramolecular approaches for PECs are also investigated, however, there was no report of supramolecules with strong binding between neutral porphyrins and fullerenes.

I have recently designed and synthesized simple electron donor-acceptor supramolecular systems, lithium ion-encapsulated fullerene ( $\text{Li}^+@\text{C}_{60}$ ) and sulphonated *meso*-tetraphenylporphyrin ( $\text{MTPPS}^{4-}$ :  $\text{M} = \text{Zn}, \text{H}_2$ ) which have strong supramolecular binding due to the cation-anion and  $\pi$ - $\pi$  interactions ( $K = \sim 10^5 \text{ M}^{-1}$ ).<sup>8</sup> Photoexcitation of the supramolecule exhibited extremely slow charge-recombination of the CS state ( $\tau = 0.3 \text{ ms}$ ) in benzonitrile (PhCN).<sup>8</sup>  $\text{Li}^+@\text{C}_{60}$  has been reported to act as a more effective electron acceptor than pristine  $\text{C}_{60}$ .<sup>9</sup> The driving force of photoinduced electron transfer from  $\text{MTPPS}^{4-}$  to the triplet excited state of  $\text{Li}^+@\text{C}_{60}$  is highly positive ( $-\Delta G_{\text{ET}} = 0.98 \text{ eV}$  for  $\text{ZnTPPS}^{4-}$  and  $0.67 \text{ eV}$  for  $\text{H}_2\text{TPPS}^{4-}$  in polar PhCN),<sup>8</sup> which is large enough to afford the CS states even under the non-polar environment in nanoclusters.

I report herein photovoltaic cells using  $\text{Li}^+@\text{C}_{60}/\text{MTPPS}^{4-}$  nanoclusters, which are assembled on optically transparent electrode (OTE) of nanostructured  $\text{SnO}_2$  (OTE/ $\text{SnO}_2$ ). The photoelectrochemical behavior of the nanostructured  $\text{SnO}_2$  film of supramolecular nanoclusters between  $\text{Li}^+@\text{C}_{60}$  and  $\text{MTPPS}^{4-}$  denoted as OTE/ $\text{SnO}_2/(\text{MTPPS}^{4-}/\text{Li}^+@\text{C}_{60})_n$  is significantly higher than the single component films of  $\text{MTPPS}^{4-}$  or  $\text{Li}^+@\text{C}_{60}$  clusters, denoted as OTE/ $\text{SnO}_2/(\text{MTPPS}^{4-})_n$  or OTE/ $\text{SnO}_2/(\text{Li}^+@\text{C}_{60})_n$  (Scheme 1).

**Scheme 1.** Photoelectrochemical Cell of OTE/ $\text{SnO}_2/(\text{MTPPS}^{4-}/\text{Li}^+@\text{C}_{60})_n$ .



## Experimental Method

**Materials.** Chemicals were purchased from commercial sources and used without further purification, unless otherwise noted. Lithium ion-encapsulated fullerene hexafluorophosphate salt ( $\text{Li}^+@\text{C}_{60} \text{PF}_6^-$ : 96%) was obtained from Daiichi Jitsugyo Co. Ltd, Japan.  $(\text{Bu}_4\text{N}^+)_4\text{MTPPS}^{4-}$  ( $\text{M} = \text{Zn, H}_2$ ) were synthesized by the neutralization of tetrasulphonated porphyrin (Tokyo Chemical Industry Co. Ltd.) with 4 equiv. of tetrabutylammonium hydroxide in MeOH. Benzonitrile (PhCN) used as a solvent was distilled over phosphorus pentoxide. Acetonitrile (MeCN) was purchased from WAKO pure chemical and used as received.

**UV–Vis Absorption and Fluorescence Spectral Measurements.** UV–Vis absorption spectra were recorded on a Hewlett-Packard 8453 diode array spectrophotometer at room temperature. Fluorescence spectra were measured on a Horiba FluoroMax-4 spectrofluorophotometer.

**Laser Flash Photolysis Measurements.** Nanosecond time-resolved transient absorption measurements were carried out using the laser system provided by UNISOKU Co., Ltd. Measurements of nanosecond transient absorption spectrum were performed according to the following procedure. A deaerated solution containing supramolecule was excited by a Panther OPO pumped by a Nd:YAG laser (Continuum SLII-10, 4-6 ns fwhm). The photodynamics was monitored by continuous exposure to a Xenon lamp (150 W) as a probe light and a photomultiplier tube (Hamamatsu 2949) as a detector. The solution was oxygenated by nitrogen purging for 15 min prior to measurements.

**Photoelectrochemical Measurements.** Electrophoretic deposition was performed using a Power Pac HV (Bio-Rad). Photoelectrochemical measurements were carried out in a standard two-compartment cell consisting of a working electrode, a Pt wire gauze counter electrode. A KEITHLEY 2400 was used for recording  $I$ - $V$  characteristics and photocurrent generation density under an AM 1.5 simulated light source (OTENTO-SUN II, Bunkoh Keiki Co., LTD). For the IPCE measurements, a monochromator (SM-25, Bunkoh Keiki Co., LTD) was introduced into the path of the excitation beam (150 W xenon lamp, Bunkoh Keiki Co., LTD) for the selected wavelength. The lamp intensity at each wavelength was determined using a Si photodiode (Hamamatsu Photonics S1337-1010BQ) and corrected.

**TEM Measurements.** Transmission electron micrograph (TEM) measurements were recorded on Tecnai spirit (FEI company) by applying a drop of the sample to a copper grid. TEM images were recorded on a transmission electron microscope an accelerating voltage of 120 kV for imaging.

---

**Dynamic Light Scattering (DLS) Measurements.** The particle size and distribution were measured in MeCN/PhCN (3:1 v/v) using light-scattering equipment (Zetasizer nano ZS).

## Results and Discussion

A solution of  $\text{Li}^+@\text{C}_{60}/\text{MTPPS}^{4-}$  supramolecule was prepared by mixing of  $\text{Li}^+@\text{C}_{60}\text{PF}_6^-$  ( $2.5 \times 10^{-4}$  M) and  $(\text{Bu}_4\text{N}^+)_4 \text{MTPPS}^{4-}$  ( $2.5 \times 10^{-4}$  M) in PhCN. The mother PhCN solution of 1 mL was injected to an acetonitrile (MeCN) solution (3 mL) to produce the suspension containing the supramolecular nanoclusters  $[(\text{MTPPS}^{4-}/\text{Li}^+@\text{C}_{60})_n]$ . The suspension was transferred into a cuvette, in which the two electrodes OTE and OTE/SnO<sub>2</sub> were placed and kept at 5 cm distance by a Teflon spacer. Then, application of dc electric field ( $\sim 100 \text{ V cm}^{-1}$ ) resulted in the deposition of  $(\text{MTPPS}^{4-}/\text{Li}^+@\text{C}_{60})_n$  from the suspension to the electrode surface and the formation of a robust thin film of OTE/SnO<sub>2</sub>/(MTPPS<sup>4-</sup>/Li<sup>+</sup>@C<sub>60</sub>)<sub>n</sub>, as documented by discoloration of the suspension and the simultaneous coloration of the OTE/SnO<sub>2</sub> electrode. For reference purposes, a thin film of only Li<sup>+</sup>@C<sub>60</sub> or MTPPS was analogously deposited onto the electrode surface to form OTE/SnO<sub>2</sub>/(Li<sup>+</sup>@C<sub>60</sub>)<sub>n</sub> or OTE/SnO<sub>2</sub>/(MTPPS<sup>4-</sup>)<sub>n</sub>.

Steady-state UV–Vis absorption spectroscopy was used to follow the deposition of the MTPPS<sup>4-</sup>/Li<sup>+</sup>@C<sub>60</sub> supramolecular material onto the electrode surface. The UV–Vis absorption spectra of OTE/SnO<sub>2</sub>/(MTPPS<sup>4-</sup>/Li<sup>+</sup>@C<sub>60</sub>)<sub>n</sub> are shown in Figure 1, exhibiting significant broadening as compared with those in PhCN solutions of MTPPS<sup>4-</sup>. Such broadening behavior indicates that the molecular environment on the OTE/SnO<sub>2</sub> surface is significantly perturbed because of the aggregation of the porphyrin molecules or the supramolecules by  $\pi$ -stacking. Thus, MTPPS<sup>4-</sup>/Li<sup>+</sup>@C<sub>60</sub> is successfully deposited on OTE/SnO<sub>2</sub>.<sup>10</sup>

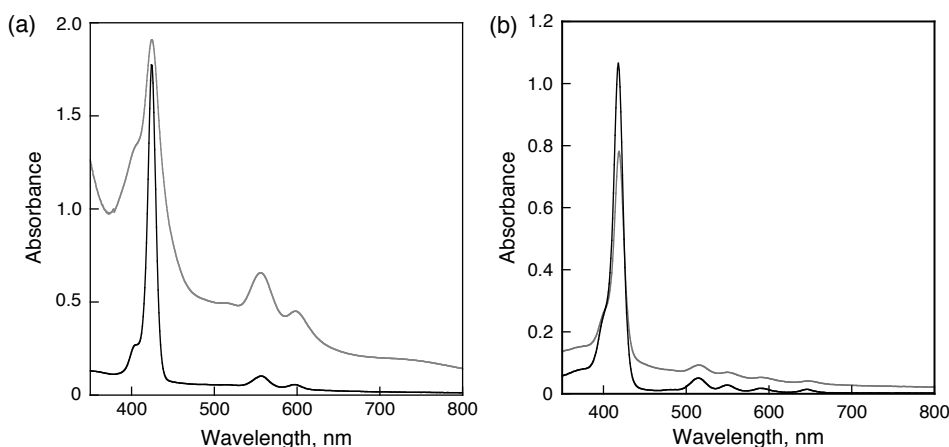


**Figure 1.** UV–Vis absorption spectra of PhCN solutions of MTPPS<sup>4-</sup> (black) and electrodes of OTE/SnO<sub>2</sub>/(MTPPS<sup>4-</sup>/Li<sup>+</sup>@C<sub>60</sub>)<sub>n</sub> (gray), M = (a) Zn and (b) H<sub>2</sub>.

TEM was used to evaluate the topography of an OTE/SnO<sub>2</sub>/(MTPPS<sup>4-</sup>/Li<sup>+</sup>@C<sub>60</sub>)<sub>n</sub> film as shown in Figure 2. The (MTPPS<sup>4-</sup>/Li<sup>+</sup>@C<sub>60</sub>)<sub>n</sub> films are composed of closely packed Li<sup>+</sup>@C<sub>60</sub> clusters of about 80 nm size, which renders a nonporous morphology to the film. The cluster sizes were also evaluated by the dynamic light scattering (DLS) measurements (Figure 3).

The grape bunch morphology of the cluster assembly thus provides a high surface area to the electrophoretically deposited film of Li<sup>+</sup>@C<sub>60</sub> clusters. As indicated earlier,<sup>11</sup> charging of fullerene moieties in the dc electric field plays an important role in the growth and deposition process. These films are quite robust and can be washed with organic solvents to remove any loosely bound Li<sup>+</sup>@C<sub>60</sub> nano-assemblies.

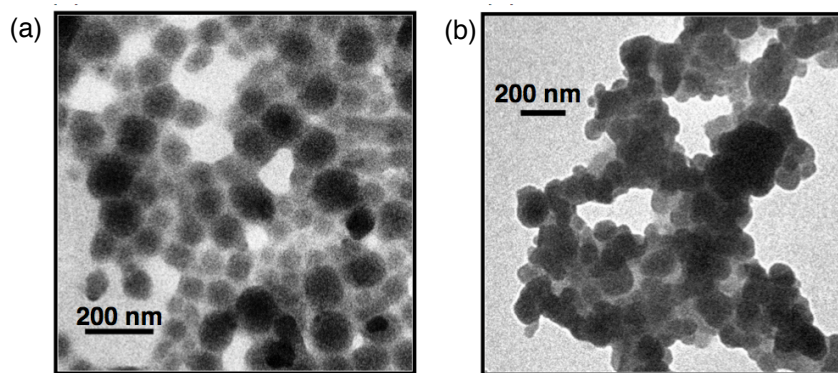


**Figure 2.** TEM images of (a) Li<sup>+</sup>@C<sub>60</sub>/ZnTPPS<sup>4-</sup> and (b) Li<sup>+</sup>@C<sub>60</sub>/H<sub>2</sub>TPPS<sup>4-</sup> nanoclusters.

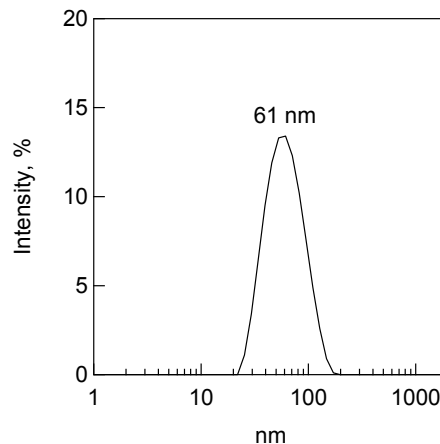


**Figure 3.** Dynamic light scattering (DLS) diagram of (ZnTPPS<sup>4-</sup>/Li<sup>+</sup>@C<sub>60</sub>)<sub>n</sub> in MeCN/PhCN (3:1 v/v).

Photoelectrochemical measurements were performed using a standard two-electrode system consisting of a working electrode and a Pt wire gauze electrode in air-saturated MeCN containing 0.5 M LiI and 0.01 M I<sub>2</sub> (Scheme 1). In order to evaluate the response towards the photocurrent generation, a series of photocurrent action spectra were recorded. The IPCE

(incident photon-to-photocurrent efficiency) values were calculated by normalizing the photocurrent values for incident light energy and intensity and using eq 1,<sup>12</sup>

$$\text{IPCE} (\%) = 100 \times 1240 \times i_{\text{sc}} / (I_{\text{inc}} \times \lambda) \quad (1)$$

where  $i_{\text{sc}}$  is the short circuit photocurrent ( $\text{A cm}^{-2}$ ),  $I_{\text{inc}}$  is the incident light intensity ( $\text{W cm}^{-2}$ ) and  $\lambda$  is the wavelength (nm). The maximum IPCE values of OTE/SnO<sub>2</sub>/(Li<sup>+</sup>@C<sub>60</sub>)<sub>n</sub> (black spectrum in Figure 4a) and OTE/SnO<sub>2</sub>/(ZnTPPS<sup>4-</sup>)<sub>n</sub> (blue spectrum) are only 5% (425 nm) and 22% (445 nm), respectively. In contrast with the reference experiments, the IPCE value of OTE/SnO<sub>2</sub>/(ZnTPPS<sup>4-</sup>/Li<sup>+</sup>@C<sub>60</sub>)<sub>n</sub> is much higher than the sum of the two individual IPCE values of the individual systems OTE/SnO<sub>2</sub>/(ZnTPPS<sup>4-</sup>)<sub>n</sub> and OTE/SnO<sub>2</sub>/(Li<sup>+</sup>@C<sub>60</sub>)<sub>n</sub> in the visible region. The maximum IPCE value attained in these experiments was 77% at 450 nm. The high IPCE value was also observed at the Q-band region to be 50% at 570 nm. Such a high IPCE value indicates that photocurrent generation is initiated via photoinduced electron transfer in supramolecules between ZnTPPS<sup>4-</sup> and Li<sup>+</sup>@C<sub>60</sub>, followed by the charge transport to the collective surface of OTE/SnO<sub>2</sub> electrode (Scheme 1). When ZnTPPS<sup>4-</sup> was replaced by H<sub>2</sub>TPPS<sup>4-</sup>, significantly low IPCE value was observed as 7% at 440 nm (Figure 4b) probably because of the self-aggregation of H<sub>2</sub>TPPS<sup>4-</sup> without binding with Li<sup>+</sup>@C<sub>60</sub>.<sup>13</sup>

I have also evaluated the power characteristics of the OTE/SnO<sub>2</sub>/(ZnTPPS<sup>4-</sup>/Li<sup>+</sup>@C<sub>60</sub>)<sub>n</sub> electrode (Figure 5). The power conversion efficiency,  $\eta$ , is calculated by using eq 2:<sup>12</sup>

$$\eta = FF \times I_{\text{sc}} \times V_{\text{oc}} / W_{\text{in}} \quad (2)$$

in which the fill factor (FF) is defined as  $FF = [I V]_{\text{max}} / I_{\text{sc}} V_{\text{oc}}$  and  $V_{\text{oc}}$  is the open-circuit

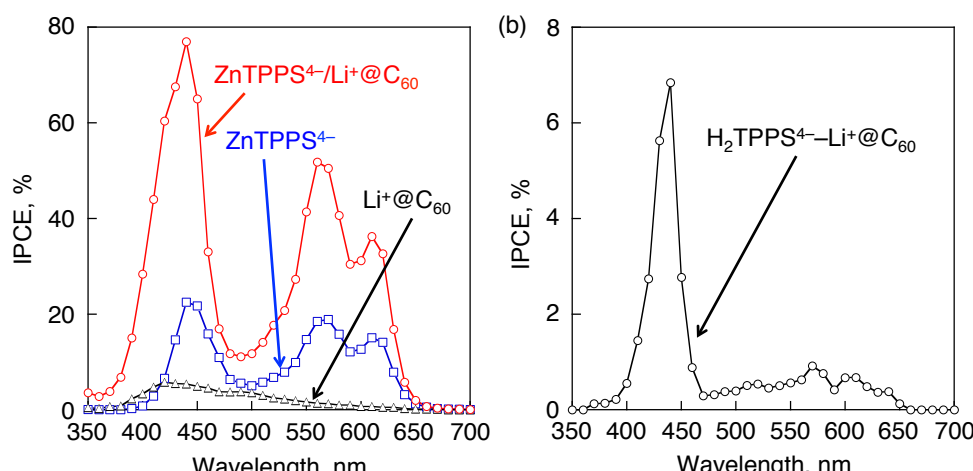


**Figure 4.** Photocurrent action spectra of (a) OTE/SnO<sub>2</sub>/(ZnTPPS<sup>4-</sup>/Li<sup>+</sup>@C<sub>60</sub>)<sub>n</sub> (red), OTE/SnO<sub>2</sub>/(MTTPPS<sup>4-</sup>)<sub>n</sub> (blue) and OTE/SnO<sub>2</sub>/(Li<sup>+</sup>@C<sub>60</sub>)<sub>n</sub> (black) and (b) OTE/SnO<sub>2</sub>/(H<sub>2</sub>TPPS<sup>4-</sup>/Li<sup>+</sup>@C<sub>60</sub>)<sub>n</sub>. Electrolyte: LiI (0.5 M) and I<sub>2</sub> (0.05 M) in MeCN.

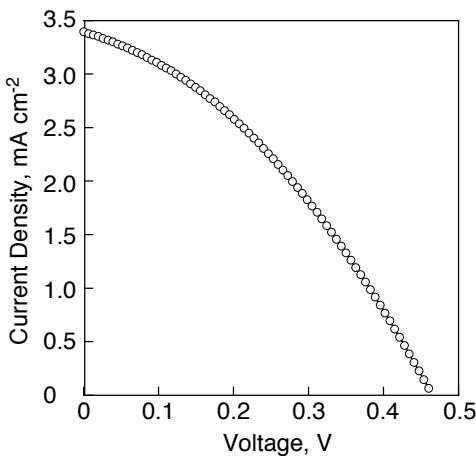


**Figure 5.**  $I$ - $V$  characteristics of OTE/SnO<sub>2</sub>/(ZnTPPS<sup>4-</sup>/Li<sup>+</sup>@C<sub>60</sub>)<sub>n</sub> electrode under white light illumination (AM 1.5); electrolyte LiI (0.5 M) and I<sub>2</sub> (0.05 M) in MeCN; input power 40 mW cm<sup>-2</sup>.

photovoltage and  $I_{sc}$  is the short-circuit photocurrent. OTE/SnO<sub>2</sub>/(ZnTPPS<sup>4-</sup>/Li<sup>+</sup>@C<sub>60</sub>)<sub>n</sub> has an overall power conversion efficiency ( $\eta$ ) of 2.1% at an input power ( $W_{in}$ ) of 28 mW cm<sup>-2</sup>, whereas  $FF = 0.37$ ,  $V_{oc} = 460$  mV and  $I_{sc} = 3.4$  mA cm<sup>-2</sup> in the OTE/SnO<sub>2</sub>/(ZnTPPS<sup>4-</sup>/Li<sup>+</sup>@C<sub>60</sub>)<sub>n</sub>. Note that the  $\eta$  value is two orders magnitude greater than that of the previously reported simple porphyrin and C<sub>60</sub> composite system (~0.03%).<sup>12</sup> Such a significant enhancement of the  $\eta$  value demonstrates that the strong ordering in the clusters and the efficient charge separation in (ZnTPPS<sup>4-</sup>/Li<sup>+</sup>@C<sub>60</sub>)<sub>n</sub> improved the light energy conversion properties.

In order to clarify the photocurrent generation mechanism, we examined formation of the CS state  $[(ZnTPPS^{4-})^{\bullet+}/Li^+@C_{60}^{\bullet-}]$  by nanosecond laser flash photolysis measurements. Time-resolved transient absorption spectra of (ZnTPPS<sup>4-</sup>/Li<sup>+</sup>@C<sub>60</sub>)<sub>n</sub> dispersed in a deaerated MeCN/PhCN solution (3:1 v/v) are shown in Figure 6a., which clearly exhibits a broad absorption band at about 1035 nm.<sup>8,9</sup> This is diagnostic of formation of Li<sup>+</sup>@C<sub>60</sub><sup>•-</sup> upon laser irradiation. Thus, photoinduced electron transfer occurs from ZnTPPS<sup>4-</sup> to Li<sup>+</sup>@C<sub>60</sub> in the composite cluster to produce the CS state  $[(ZnTPPS^{4-})^{\bullet+}/Li^+@C_{60}^{\bullet-}]$ . The absorption time profile of  $[(ZnTPPS^{4-})^{\bullet+}/Li^+@C_{60}^{\bullet-}]$  recorded at 1035 nm is shown in Figure 6b. The first-order decay kinetics (inset of Figure 6b) corresponds to back electron transfer from Li<sup>+</sup>@C<sub>60</sub><sup>•-</sup> to (ZnTPPS<sup>4-</sup>)<sup>•+</sup>, affording the rate constant of back electron transfer to be  $k_{BET} = 4.6 \times 10^3$  s<sup>-1</sup>. The lifetime of the CS state is 220  $\mu$ s, which is long enough to inject an electron from Li<sup>+</sup>@C<sub>60</sub><sup>•-</sup> of the CS state to the SnO<sub>2</sub> electrode before the charge recombination. Such a long-lived CS state was further detected by EPR under photoirradiation of a MeCN/PhCN solution (1:3 v/v) containing (ZnTPPS<sup>4-</sup>/Li<sup>+</sup>@C<sub>60</sub>)<sub>n</sub> at 77 K. The EPR signal was observed at  $g = 2.0020$ , which is (Figure 7).<sup>15</sup> When ZnTPPS<sup>4-</sup> was replaced by H<sub>2</sub>TPPS<sup>4-</sup>, the transient absorption bands due to

the CS state was significantly smaller than the case of  $\text{ZnTPPS}^{4-}$  (Figure 8). This is a reason why the IPCE value of  $\text{OTE/SnO}_2/(\text{H}_2\text{TPPS}^{4-}/\text{Li}^+@\text{C}_{60})_n$  was low as shown in Figure 4b.

Based on the above mentioned results, the photocurrent generation is initiated by photoinduced electron transfer from  $\text{ZnTPPS}^{4-}$  to  $\text{Li}^+@\text{C}_{60}$  in the cluster to produce the CS state,  $(\text{ZnTPPS}^{4-})^{+}/\text{Li}^+@\text{C}_{60}^{+}$ . The reduced  $\text{Li}^+@\text{C}_{60}$  ( $\text{Li}^+@\text{C}_{60}^{+}$ ) ( $E(\text{Li}^+@\text{C}_{60}/\text{Li}^+@\text{C}_{60}^{+}) = 0.14$  V vs SCE)<sup>8,9</sup> injects electrons into the conduction band of  $\text{SnO}_2$  (0.2 V vs SCE),<sup>11</sup> whereas the oxidized  $\text{ZnTPPS}^{4-}$  ( $E(\text{ZnTPPS}^{4-}/(\text{ZnTPPS}^{4-})^{+}) = 0.74$  V vs SCE)<sup>8</sup> undergoes the electron-transfer reduction with the iodide ( $I_3^-/I^- = 0.7$  V vs SCE)<sup>12</sup> in the electrolyte solution.

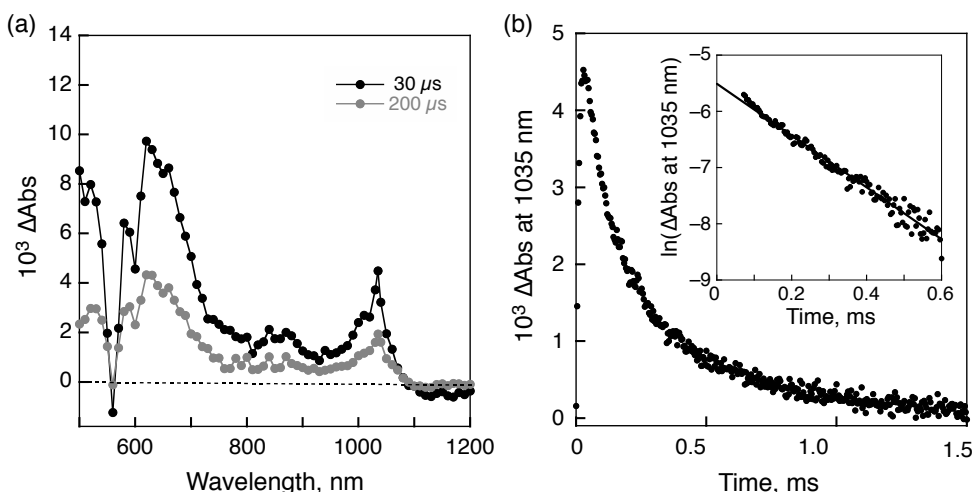


**Figure 6.** (a) Transient absorption spectra of  $(\text{ZnTPPS}^{4-}/\text{Li}^+@\text{C}_{60})_n$  in deaerated MeCN/PhCN (3:1 v/v) taken at 30  $\mu\text{s}$  (black) and 200  $\mu\text{s}$  (gray) after laser excitation at 550 nm. (b) Time profile at 1035 nm. Inset: first-order analysis.

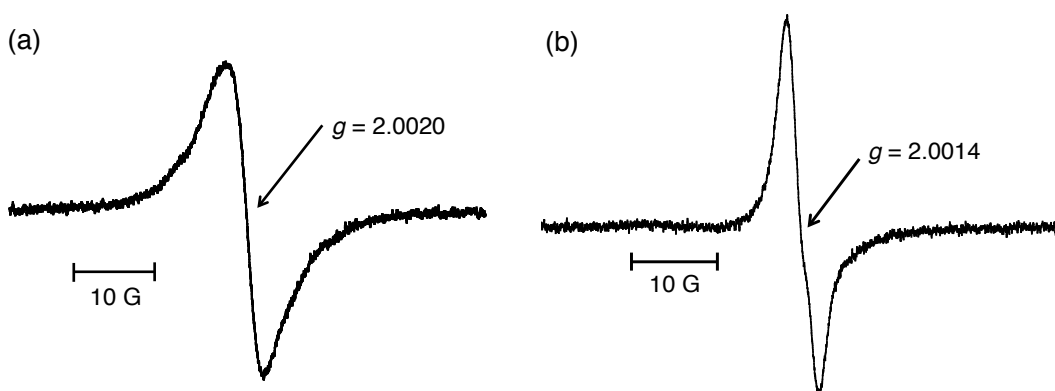


**Figure 7.** (a) EPR spectrum of the charge-separated state of  $(\text{ZnTPPS}^{4-}/\text{Li}^+@\text{C}_{60})_n$  dispersed in deaerated MeCN/PhCN (3:1 v/v) and observed after photoirradiation at 77 K. (b) EPR spectrum of  $\text{Li}^+@\text{C}_{60}^{+}$  generated by the electron-transfer reduction from dimeric 1-benzylnicotinamide to  $\text{Li}^+@\text{C}_{60}$  at 100 K.

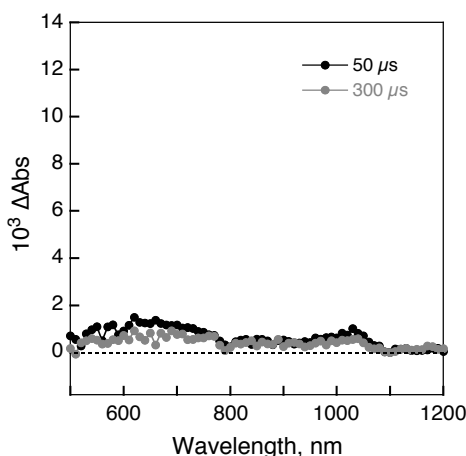


**Figure 8.** Transient absorption spectrum of  $\text{H}_2\text{TPPS}^{4-}$  ( $3.2 \times 10^{-5}$  M) with  $\text{Li}^+@\text{C}_{60}$  ( $3.2 \times 10^{-5}$  M) in deaerated MeCN/PhCN (3:1 v/v) taken at 50  $\mu\text{s}$  (black) and 300  $\mu\text{s}$  (gray) after laser excitation at 520 nm.

## Conclusions

The photoinduced electron transfer from  $\text{ZnTPPS}^{4-}$  to  $\text{Li}^+@\text{C}_{60}$  in the supramolecular cluster makes it possible to enhance the performance of the photoelectro-chemical cell. Thus, the use of  $\text{Li}^+@\text{C}_{60}$  as an electron acceptor in the supramolecular clusters with  $\text{ZnTPPS}^{4-}$  paves a new way for the design of high performance solar cell.

## References

- (1) (a) Grätzel, M. *Nature*, **2003**, *421*, 586–567. (b) M. Grätzel, *Nature*, **2001**, *414*, 338–344.  
(c) O'Regan, B.; Grätzel, M. *Nature* **1991**, *353*, 737–740.
- (2) (a) Hagfeldt, A.; Graetzel, M. *Chem. Rev.* **1995**, *95*, 49–68. (b) Hagfeldt, A.; Grätzel, M. *Acc. Chem. Res.* **2000**, *33*, 269–277.
- (3) (a) Huynh, W. U.; Dittmer, J. J.; Alivisatos, A. P. *Science* **2002**, *295*, 2425–2427. (b) Shah, A.; Torres, P.; Tscharner, R.; Wyrsch, N.; Keppner, H. *Science*, **1999**, *285*, 692–698.
- (4) *The Photosynthetic Reaction Center*, Deisenhofer, J.; Norris, J. R., Eds.; Academic Press: San Diego, 1993.
- (5) (a) Hasobe, T. *Phys. Chem. Chem. Phys.*, **2012**, *14*, 15975–15987. (b) Imahori, H.; Fukuzumi, S. *Adv. Mater.* **2001**, *13*, 1197–1199.
- (6) (a) Lahav, M.; Heleg-Shabtai, V.; Wasserman, J.; Katz, E.; Willner, I.; Dürr, H.; Hu, Y.-Z.; Bossmann, S. H. *J. Am. Chem. Soc.* **2000**, *122*, 11480–11487. (b) Eckert, J.-F.; Nicoud,

J.-F.; Nierengarten, J.-F.; Liu, S.; Echegoyen, L.; Barigelli, F.; Armaroli, N.; Ouali, L.; Krasnikov, V.; Hadzioannou, G. *J. Am. Chem. Soc.* **2000**, *122*, 7467–7479.

(7) Fukuzumi, S.; Guldi, D. M. In *Electron Transfer in Chemistry*, Vol. 2, Balzani, V., Ed.; Wiley-VCH: Weinheim, 2001; pp 270–337.

(8) Ohkubo, K.; Kawashima, Y.; Fukuzumi, S. *Chem. Commun.* **2012**, *48*, 4314–4316.

(9) (a) Fukuzumi, S.; Ohkubo, K.; Kawashima, Y.; Kim, D. S.; Park, J. S.; Jana, A.; Lynch, V. M.; Kim, D.; Sessler, J. L. *J. Am. Chem. Soc.* **2011**, *133*, 15938–15941. (b) Kawashima, Y.; Ohkubo, K.; Fukuzumi, S. *J. Phys. Chem. A* **2012**, *116*, 8942–8948.

(10) Nobukuni, H.; Tani, F.; Shimazaki, Y.; Naruta, Y.; Ohkubo, K.; Nakanishi, T.; Kojima, T.; Fukuzumi, S.; Seki, S. *J. Phys. Chem. C* **2009**, *113*, 19694–19699.

(11) Hasobe, T.; Imahori, H.; Fukuzumi, S.; Kamat, P. V. *J. Phys. Chem. B* **2003**, *107*, 12105–12112.

(12) Hasobe, T.; Kashiwagi, Y.; Absalom, M. A.; Sly, J.; Hosomizu, K.; Crossley, M. J.; Imahori, H.; Kamat, P. V.; Fukuzumi, S. *Adv. Mater.* **2004**, *16*, 975–979.

(13) Matsuzawa, H.; Kobayashi, H.; Maeda, T. *Bull. Chem. Soc. Jpn.* **2012**, *85*, 774–785.

(14) Fukuzumi, S.; Saito, K.; Ohkubo, K.; Khoury, T.; Kashiwagi, Y.; Absalom, M. a; Gadde, S.; D’Souza, F.; Araki, Y.; Ito, O.; Crossley, M. J. *J. Chem. Commun.* **2011**, *47*, 7980–7982.

(15)  $\text{Li}^+@\text{C}_{60}^{\cdot-}$  was prepared by the electron-transfer reduction from dimeric 1-benzyl-1,4-dihydronicotinamide to  $\text{Li}^+@\text{C}_{60}$ ,<sup>9a</sup> which was observed at 100 K by ESR (Figure 7b).

## Concluding Remarks

In this thesis, the author described mainly the characterization of  $\text{Li}^+@\text{C}_{60}$ , the construction supramolecular systems of  $\text{Li}^+@\text{C}_{60}$  for photoinduced charge separation and light-energy conversion.

In Chapter 1, the author constructed the supramolecular complexes of  $\text{Li}^+@\text{C}_{60}$  with two tetrathiafulvalene calix[4]pyrrole (TTF-C4P) donors and showed that the judicious addition of an anion or a cation allows to control the direction of the resulting ground state electron transfer process. The structure of electron transfer product was obtained by X-ray diffraction analysis.

In Chapter 2, the author revealed that  $\text{Li}^+@\text{C}_{60}$  has the enhanced electron acceptability and larger reorganization energy as compared to pristine  $\text{C}_{60}$  by observing photoinduced electron transfer between aromatic compounds and  $\text{Li}^+@\text{C}_{60}$ . Large reorganization energy of  $\text{Li}^+@\text{C}_{60}$  arises from localized LUMO due to the encapsulated lithium-ion (See Figure 10 in Chapter 3). In Chapter 3, the author determined the reorganization energies of photoinduced electron transfer and back electron-transfer between  $I_h$ -symmetric fullerenes in benzonitrile (PhCN) and *o*-dichlorobenzene (*o*-DCB). The observed rate constants of electron transfer fit well with the predicted driving force dependences because fullerenes are ideal molecule to examine the electron-transfer reactions involving three kinds of fullerenes in light of the Marcus theory of electron transfer. Through the studies in Chapter 1 and 2, the author obtained the physicochemical parameter of  $\text{Li}^+@\text{C}_{60}$  at the ground state and the excited state, as shown in table 1.

**Table 1.** Physicochemical Parameter of  $\text{C}_{60}$  and  $\text{Li}^+@\text{C}_{60}$  in PhCN

	$\text{C}_{60}$	$\text{Li}^+@\text{C}_{60}$
Absorption of radical anion	1080 nm <sup>1</sup>	1035 nm
One-electron reduction potential (vs SCE)	-0.43 V <sup>2</sup>	+0.14 V
Absorption of singlet excited state	920 nm <sup>3</sup>	960 nm
Absorption of triplet excited state	740 nm <sup>3</sup>	750 nm
Lifetime of singlet excited state	2.4 ns <sup>3</sup>	1.1 ns
Lifetime of triplet excited state	48 $\mu$ s <sup>4</sup>	49 $\mu$ s
Singlet excited energy	1.99 eV <sup>3</sup>	1.94 eV
Triplet excited energy	1.57 eV <sup>3</sup>	1.53 eV
Reorganization energy	0.73 eV	1.01 eV

By using excellent properties of  $\text{Li}^+@\text{C}_{60}$  the author constructed successfully the supramolecular complexes of  $\text{Li}^+@\text{C}_{60}$  with various electron donors and confirmed the formation of the CS state. The reorganization energies ( $\lambda$ ), the electronic coupling terms ( $V$ ), the lifetimes of CS states ( $\tau_{\text{CS}}$ ), the rate constants of back electron transfer ( $k_{\text{BET}}$ ), and the driving force for back electron transfer ( $-\Delta G_{\text{BET}}$ ) of the supramolecular complexes described above are summarized in Table 2. All of supramolecular complexes composed of  $\text{Li}^+@\text{C}_{60}$  or  $\text{Li}^+@\text{PCBM}$  have the long-lived CS states, and show the smaller  $V$  values as compared with covalently linked zinc chlorin-fullerene dyad ( $V = 6.8 \text{ cm}^{-1}$ ; See black line in Figure 1). Such small  $V$  values are given by spatially separated LUMO and HOMO, and spin forbidden back electron transfer process due to the triplet CS state. As mentioned in the general introduction, the overlap between HOMO and LUMO are controlled by the structure of electron donors. Judging from the  $\lambda$  values of back electron transfer processes, the charge-recombination process of  $\text{ZnTPPS}^{4-}/\text{Li}^+@\text{PCBM}$  (Entry 3 and 4 in Table 2 and Figure 1) supramolecular complexes are in the Marcus inverted region, whereas the charge-recombination processes of the  $\text{ZnCh}^-/\text{Li}^+@\text{C}_{60}$  (Entry 5) and  $\text{H}_2\text{Pc}\bullet\text{1}^{4-}/(\text{Li}^+@\text{C}_{60})_2$  (Entry 9) supramolecular complexes are in the Marcus normal region. The driving force of the charge-recombination process should be deeply in the Marcus inverted region to afford a high energy CS state with a long lifetime. Although  $\text{H}_2\text{Pc}\bullet\text{1}^{4-}/(\text{Li}^+@\text{C}_{60})_2$  supramolecular complex (Entry 9) has the largest  $\lambda$  and  $V$  values as compared with these of other supramolecular complexes in Table 2,  $\text{H}_2\text{Pc}\bullet\text{1}^{4-}/(\text{Li}^+@\text{C}_{60})_2$  supramolecular complex exhibited the longest CS lifetimes ever reported for non-covalent porphyrinoid/fullerene supramolecular

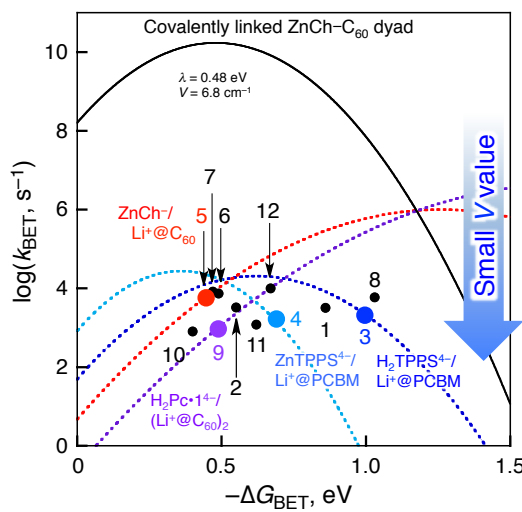


**Figure 1.** Driving force dependences of  $\log k_{\text{BET}}$ . Numbers refer to the supramolecules in Table 2. The dashed lines are drawn by the Marcus equation for nonadiabatic electron-transfer, and  $\lambda$  and  $V$  values listed in Table 2. The driving force dependence for BET of zinc chlorin-fullerene dyad drawn in black line by the Marcus equation, where the  $\lambda = 0.48 \text{ eV}$  and  $V = 6.8 \text{ cm}^{-1}$ .<sup>5</sup>

**Table 2.** Reorganization Energies ( $\lambda$ ), Electronic Coupling Terms ( $V$ ), Lifetimes of CS States ( $\tau_{\text{CS}}$ ), Rate Constants of BET ( $k_{\text{BET}}$ ) and Driving Force of BET ( $-\Delta G_{\text{BET}}$ )

entry	supramolecular complex	$\lambda$ , eV	$V$ , $\text{cm}^{-1}$	$\tau_{\text{CS}}$ , $\mu\text{s}$	$k_{\text{BET}}$ , $\text{s}^{-1}$	$-\Delta G_{\text{BET}}$ , eV
1	$\text{H}_2\text{TPPS}^{4-}/\text{Li}^+@\text{C}_{60}$	n.d.	n.d.	310	$3.2 \times 10^3$	0.86
2	$\text{ZnTPPS}^{4-}/\text{Li}^+@\text{C}_{60}$	n.d.	n.d.	300	$3.3 \times 10^3$	0.55
3	$\text{H}_2\text{TPPS}^{4-}/\text{Li}^+@\text{PCBM}$	0.62	$7.9 \times 10^{-3}$	450	$2.2 \times 10^3$	1.0
4	$\text{ZnTPPS}^{4-}/\text{Li}^+@\text{PCBM}$	0.36	$8.5 \times 10^{-3}$	560	$1.8 \times 10^3$	0.69
5	$\text{ZnCh}^-/\text{Li}^+@\text{C}_{60}$	1.26	$6.6 \times 10^{-2}$	170	$6.0 \times 10^3$	0.45
6	<b>1</b> • $\text{Li}^+@\text{C}_{60}$	n.d.	n.d.	140	$7.4 \times 10^3$	0.49
7	<b>2</b> • $\text{Li}^+@\text{C}_{60}$	n.d.	n.d.	120	$8.3 \times 10^3$	0.47
8	$\text{PBCE} \bullet \text{Li}^+@\text{C}_{60}$	n.d.	n.d.	170	$6.0 \times 10^3$	1.03
9	$\text{H}_2\text{Pc} \bullet \mathbf{1}^{4-}/(\text{Li}^+@\text{C}_{60})_2$	1.70	0.15	$1.0 \times 10^3$	$9.7 \times 10^2$	0.49
10	$\text{H}_2\text{Pc} \bullet \mathbf{2}^{4-}/(\text{Li}^+@\text{C}_{60})_2$	n.d.	n.d.	$1.2 \times 10^3$	$8.1 \times 10^2$	0.40
11	$\text{H}_2\text{Pc} \bullet \mathbf{3}^{8-}/\text{Li}^+@\text{C}_{60}$	n.d.	n.d.	830	$1.2 \times 10^3$	0.62
12	$\text{ZnPc} \bullet \mathbf{4}^{4-}/\text{Li}^+@\text{C}_{60}$	n.d.	n.d.	100	$1.0 \times 10^4$	0.67

complexes in solution, because of much larger  $\lambda$  value than  $-\Delta G_{\text{BET}}$  in the charge-recombination process of  $\text{H}_2\text{Pc} \bullet \mathbf{1}^{4-}/(\text{Li}^+@\text{C}_{60})_2$  supramolecular complex, as shown in Figure 1.

From Chapters 9 to 11, the author showed the formation of supramolecular complexes of anionic porphyrin/cationic porphyrin, anionic porphyrin/TTF-C4P, and finite single-wall CNT $\supset$  $\text{C}_{60}$  in polar solvent. Anionic porphyrin/cationic porphyrin supramolecular complex showed extremely long-lived CS state due to the quite smallest reorganization energy ( $\lambda = 0.24$  eV) as compared with the driving force for back electron transfer ( $-\Delta G_{\text{BET}} = 0.82$  eV). Such small reorganization energy is probably given by small solvation change due to the sandwiched porphyrin. This result provides guidelines for construction of supramolecular complex such as inclusion complex. Anionic porphyrin/TTF-C4P supramolecular complex exhibited the small electronic coupling term and long-lived CS state. CNT $\supset$  $\text{C}_{60}$  showed high biding constant in polar solvent. These results indicate that supramolecular donor-acceptor systems are promising approach to obtain the long-lived CS state.

The dye-sensitized solar cells of  $\text{ZnTPPS}^{4-}/\text{Li}^+@\text{C}_{60}$ ,  $\text{ZnCh}^-/\text{Li}^+@\text{C}_{60}$ , and anionic phthalocyanines/ $\text{Li}^+@\text{C}_{60}$  supramolecular nanoclusters exhibited a higher IPCE (incident photon-photocurrent efficiency) values than the sum of the individual IPCE values of individual systems of each porphyrinoids and  $\text{Li}^+@\text{C}_{60}$ , as shown in Chapters 12 to 14. Especially, the dye-sensitized solar cells of  $\text{ZnTPPS}^{4-}/\text{Li}^+@\text{C}_{60}$  supramolecular nanocluster exhibited the power conversion efficiency of 2.1%, which is significantly higher than that of reference systems

containing neutral porphyrin and fullerene (~0.03%).<sup>6</sup> In contrast to the dye-sensitized solar cell of ZnTPPS<sup>4-</sup>/Li<sup>+</sup>@C<sub>60</sub>, the power conversion efficiency of the dye-sensitized solar cell of ZnCh<sup>-</sup>/Li<sup>+</sup>@C<sub>60</sub> was too small even though ZnCh<sup>-</sup>/Li<sup>+</sup>@C<sub>60</sub> has a higher quantum yield of CS state than that of ZnTPPS<sup>4-</sup>/Li<sup>+</sup>@C<sub>60</sub> in solution ( $\Phi_{CS} = 0.62$  for ZnCh<sup>-</sup>/Li<sup>+</sup>@C<sub>60</sub> vs  $\Phi_{CS} = 0.39$  for ZnTPPS<sup>4-</sup>/Li<sup>+</sup>@C<sub>60</sub>). The lifetime of CS state of ZnCh<sup>-</sup>/Li<sup>+</sup>@C<sub>60</sub> supramolecular complex ( $\tau_{CS} = 170 \mu\text{s}$ ) is long enough to inject electrons to electrode. Thus, not only lifetimes and quantum yields of CS state but also other factors such as size and morphology of nanocluster, topography of nanocluster on electrodes should be investigated to understand the difference in the power conversion efficiency and obtain the high power conversion efficiency. Moreover, thin film solar cell of MTPPS<sup>4-</sup>/Li<sup>+</sup>@PCBM is expected to exhibit high light-conversion efficiency.

Through my study, I have provided a detailed overview of the current progress on the behavior of Li<sup>+</sup>@C<sub>60</sub> in photoinduced electron-transfer processes with different organic donors. The fabricated dye-sensitized solar cells showed higher electrochemical performance as compared with that of pristine C<sub>60</sub> and porphyrin composite system. The energy of produced CS state can be applied to not only solar cell but also other systems such as photocatalyst. The author believes that cationic Li<sup>+</sup>@C<sub>60</sub> acting as a unique cationic electron acceptor can find further interesting applications.

## References

- (1) (a) Arbogast, J. W.; Foote, C. S.; Kao, M. *J. Am. Chem. Soc.* **1992**, *114*, 2277–2279. (b) Lawson, D. R.; Feldheim, D. L.; Foss, C. A.; Dorhout, P. K.; Elliot, M.; Martin, C. R.; Parkinson, B. *J. Electrochem. Soc.* **1992**, *139*, L68–L71. (c) Fukuzumi, S.; Suenobu, T.; Patz, M.; Hirasaka, T.; Itoh, S.; Fujitsuka, M.; Ito, O. *J. Am. Chem. Soc.* **1998**, *120*, 8060–8068.
- (2) Fukuzumi, S.; Suenobu, T.; Hirasaka, T.; Arakawa, R.; Kadish, K. M. *J. Am. Chem. Soc.* **1998**, *120*, 9220–9227.
- (3) Guldi, D. M.; Hungerbühler, H.; Carmichael, I.; Asmus, K.-D.; Maggini, M. *J. Phys. Chem. A* **2000**, *104*, 8601–8608.
- (4) (a) Arbogast, J. W.; Darmayan, A. P.; Foote, C. S.; Diederich, F. N.; Whetten, R. L.; Rubin, Y.; Alvarez, M. M.; Anz, S. J. *J. Phys. Chem.* **1991**, *95*, 11–12. (b) Arbogast, J. W.; Foote, C. S. *J. Am. Chem. Soc.* **1991**, *113*, 8886–8889. (c) Ebbesen, T. W.; Tanigaki, K.; Kuroshima, S. *Chem. Phys. Lett.* **1991**, *181*, 501–504. (d) Kajii, Y.; Nakagawa, T.; Suzuki, S.; Achiba, Y.; Obi, K.; Shibuya, K. *Chem. Phys. Lett.* **1991**, *181*, 100–104. (e) Mikami,

K.; Matsumoto, S.; Ishida, A.; Takamuku, S.; Suenobu, T.; Fukuzumi, S. *J. Am. Chem. Soc.* **1995**, *117*, 11134–11141.

(5) Ohkubo, K.; Imahori, H.; Shao, J.; Ou, Z.; Kadish, K. M.; Chen, Y.; Zheng, G.; Pandey, R. K.; Fujitsuka, M.; Ito, O.; Fukuzumi, S. *J. Phys. Chem. A* **2002**, *106*, 10991–10998.

(6) Hasobe, T.; Kashiwagi, Y.; Absalom, M. A.; Sly, J.; Hosomizu, K.; Crossley, M. J.; Imahori, H.; Kamat, P. V.; Fukuzumi, S. *Adv. Mater.* **2004**, *16*, 975–979.

## List of Publication

### Original Paper

1. Ion-Controlled On-Off Switch of Electron Transfer from Tetrathiafulvalene Calix[4]pyrroles to  $\text{Li}^+@\text{C}_{60}$

Fukuzumi, S.; Ohkubo, K.; Kawashima, Y.; Kim, D. S.; Park, J. S.; Jana, A.; Lynch, V. M.; Kim, D.; Sessler, J. L.

*J. Am. Chem. Soc.* **2011**, *133*, 15938–15941. (DOI: 10.1021/ja207588c)

2. Strong Supramolecular Binding of  $\text{Li}^+@\text{C}_{60}$  with Sulfonated *meso*-Tetraphenylporphyrins and Long-Lived Photoinduced Charge Separation

Ohkubo, K.; Kawashima, Y.; Fukuzumi, S.

*Chem. Commun.* **2012**, *48*, 4314–4316. (DOI: 10.1039/C2CC31186K)

3. Enhanced Photoinduced Electron-Transfer Reduction of  $\text{Li}^+@\text{C}_{60}$  in Comparison with  $\text{C}_{60}$

Kawashima, Y.; Ohkubo, K.; Fukuzumi, S.

*J. Phys. Chem. A* **2012**, *116*, 8942–8948. (DOI: 10.1021/jp3059036)

4. Electron Transfer in a Supramolecular Complex of Zinc Chlorin Carboxylate Anion with  $\text{Li}^+@\text{C}_{60}$  Affording the Long-Lived Charge-Separated State

Kawashima, Y.; Ohkubo, K.; Mase, K.; Fukuzumi, S.

*J. Phys. Chem. C* **2013**, *117*, 21166–21177. (DOI: 10.1021/jp407976b)

5. Small Reorganization Energies of Photoinduced Electron Transfer between Spherical Fullerenes

Kawashima, Y.; Ohkubo, K.; Fukuzumi, S.

*J. Phys. Chem. A* **2013**, *117*, 6737–6743. (DOI: 10.1021/jp4047165)

6. Enhanced Photoelectrochemical Performance of Composite Photovoltaic Cells of  $\text{Li}^+@\text{C}_{60}$ -Sulphonated Porphyrin Supramolecular Nanoclusters

Ohkubo, K.; Kawashima, Y.; Sakai, H.; Hasobe, T.; Fukuzumi, S.

*Chem. Commun.* **2013**, *49*, 4474–4476. (DOI: 10.1039/c3cc41187g)

7. Photoinduced Electron Transfer from a Tetrathiafulvalene-Calix[4]pyrrole to a Porphyrin Carboxylate within a Supramolecular Ensemble  
Davis, C. M.; Kawashima, Y.; Ohkubo, K.; Lim, J. M.; Kim, D.; Fukuzumi, S.; Sessler, J. L.  
*J. Phys. Chem. C* **2014**, *118*, 13503–13513. (DOI: 10.1021/jp504087b)

8. Photoinduced Electron Transfer in a Dynamic Supramolecular System with Curved  $\pi$ -Structures  
Hitosugi, S.; Ohkubo, K.; Iizuka, R.; Kawashima, Y.; Nakamura, K.; Sato, S.; Kono, H.; Fukuzumi, S.; Isobe, H.  
*Org. Lett.* **2014**, *16*, 3352–3355. (DOI: 10.1021/ol501381x)

9. Long-Lived Charge-Separated States Produced in Supramolecular Complexes between Anionic and Cationic Porphyrins  
Bill, N. L.; Ishida, M.; Kawashima, Y.; Ohkubo, K.; Sung, Y. M.; Lynch, V. M.; Lim, J. M.; Kim, D.; Sessler, J. L.; Fukuzumi, S.  
*Chem. Sci.* **2014**, *5*, 3888–3896. (DOI: 10.1039/C4SC00803K)

10. Supramolecular Formation of  $\text{Li}^+@\text{PCBM}$  Fullerene with Sulfonated Porphyrins and Long-Lived Charge Separation  
Kawashima, Y.; Ohkubo, K.; Okada, H.; Matsuo, Y.; Fukuzumi, S.  
*ChemPhysChem* **2014**, *15*, 3782–3790. (DOI: 10.1002/cphc.201402512)

11. Robust Inclusion Complexes of Crown Ether Fused Tetrathiafulvalenes with  $\text{Li}^+@\text{C}_{60}$  to Afford Efficient Photodriven Charge Separation  
Supur, M.; Kawashima, Y.; Larsen, K. R.; Ohkubo, K.; Jeppesen, J. O.; Fukuzumi, S.  
*Chem.-Eur. J.* **2014**, *20*, 13976–13983. (DOI: 10.1002/chem.201402449)

12. Long-Lived Charge Separation in a Rigid Pentiptycene Bis(Crown Ether)- $\text{Li}^+@\text{C}_{60}$  Host-Guest Complex  
Supur, M.; Kawashima, Y.; Ma, Y.-X.; Ohkubo, K.; Chen, C.-F.; Fukuzumi, S.  
*Chem. Commun.* **2014**, *50*, 15796–15798. (DOI: 10.1039/c4cc07795d)

13. Photoelectrochemical Properties of Supramolecular Composites of an Anionic Zinc Chlorin and  $\text{Li}^+@\text{C}_{60}$  on  $\text{SnO}_2$   
Ohkubo, K.; Kawashima, Y.; Mase, Kentaro; Sakai, H.; Hasobe, T.; Fukuzumi, S.  
*J. Porphyrins Phthalocyanines* **2014**, *18*, 982–990. (DOI: 10.1142/S1088424614500825)

---

14. Near-Infrared Photoelectrochemical Conversion via Photoinduced Charge Separation in Supramolecules of Anionic Phthalocyanines with  $\text{Li}^+@\text{C}_{60}$

Kawashima, Y.; Ohkubo, K.; Blas-Ferrando, M. V.; Sakai, H.; Font-Sanchis, E.; Ortíz J.; Fernández-Lázaro, F.; Hasobe, T.; Sastre-Santos, Á; Fukuzumi, S.

*J. Phys. Chem. B* in press. (DOI: 10.1021/jp5123163)

### Supplementary

Submillisecond-Lived Photoinduced Charge Separation in Inclusion Complexes Composed of  $\text{Li}^+@\text{C}_{60}$  and Cyclic Porphyrin Dimers

Kamimura, T.; Ohkubo, K.; Kawashima, Y.; Nobukuni, H.; Naruta, Y.; Tani, F.; Fukuzumi, S. *Chem. Sci.* **2013**, *4*, 1451–1461. (DOI: 10.1039/C3SC22065F)

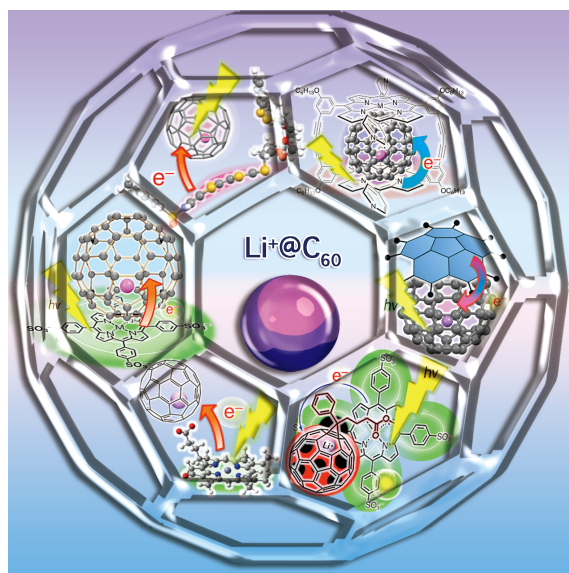
### Review

Efficient Charge Separation in  $\text{Li}^+@\text{C}_{60}$  Supramolecular Complexes with Electron Donors

Kawashima, Y.; Ohkubo, K.; Fukuzumi, S. (*Highlighted as a Featured Article*)

*Chem. Asian J.* **2015**, *10*, 44–54. (DOI: 10.1002/asia.201403075)

### Frontispiece of the Review



## Presentation at International Conference

### Invited, Oral

ECS 223rd: The 223rd Electrochemical Society Meeting in Toronto, Canada

*Photoinduced Electron Transfer From  $Sc_3@C_{80}$  to  $Li^+@C_{60}$*

Yuki Kawashima, Kei Ohkubo, Shunichi Fukuzumi

### Poster

1. 3rd International Symposium on Emergence of Highly Elaborated  $\pi$ -Space and Its Function in Tsukuba, Japan

*Ion-induced Reversible Electron Transfer between Tetrathiafulvalene Calix[4]pyrroles and  $Li^+@C_{60}$*

Yuki Kawashima, Kei Ohkubo, Dong Sub Kim, Jung Su Park, Atanu Jana, Vincent M. Lynch, Dongho Kim, Jonathan L. Sessler, Shunichi Fukuzumi

2. ICPP-7: Seventh International Conference of Porphyrins and Phthalocyanines in Jeju, Korea  
*Reversible Electron Transfer in Supramolecule of  $Li^+@C_{60}$  with Tetrathiafulvalene Calix[4]pyrroles*

Yuki Kawashima, Kei Ohkubo, Dong Sub Kim, Jung Su Park, Atanu Jana, Vincent M. Lynch, Dongho Kim, Jonathan L. Sessler, Shunichi Fukuzumi

3. ICPP-8: Eighth International Conference of Porphyrins and Phthalocyanines in Istanbul, Turkey

*Photoinduced Electron Transfer in Supramolecules of  $Li^+@C_{60}$  with Anionic Porphyrinoids*

Yuki Kawashima, Kei Ohkubo, Kentaro Mase, Shunichi Fukuzumi

## Others

### Award

1. 第22回基礎有機化学討論会 ポスター賞

「テトラチアフルバレンカリックス[4]ピロールによる  $\text{Li}@\text{C}_{60}$  のアニオン誘起電子移動還元反応」

2. 2012年光化学討論会 最優秀学生発表賞（ポスター）

「リチウムイオン内包フラーレンとアニオン性ポルフィリンの超分子における長寿命光電荷分離状態生成」

3. 日本化学会第94春季年会（2014）学生講演賞

「リチウムイオン内包 PCBM フラーレンとアニオン性ポルフィリンの超分子における長寿命光誘起電荷分離状態生成」

### Book

「フラーレン誘導体・内包技術の最前線」 "Cutting-edge Technology in Fullerene Derivatives and Endohedral Fullerenes" 松尾豊 監修

第3章5節「リチウムイオン内包フラーレンの光電子移動反応」

大久保 敬、川島 雄樹、福住 俊一、CMC 出版, 2014, pp. 126–133.

### Patent

「内包フラーレンを用いた光電変換装置」

大久保 敬、福住 俊一、川島 雄樹、羽曾部 卓、酒井 隼人

特願 2013-200603

### Invited Lecture

第四回リチウム内包フラーレン研究会

「 $\text{Li}^+@\text{C}_{60}$ /アニオン性ポルフィリノイド超分子の光誘起電子移動と光電変換特性」

## Acknowledgments

I would like to express my heartfelt gratitude to Professor Dr. Shunichi Fukuzumi and Designated Professor Dr. Kei Ohkubo for their continuous guidance, support, and encouragement throughout this study.

My appreciation also goes to Associate Professor Dr. Yusuke Yamada and Assistant Professor Dr. Tomoyoshi Suenobu for their useful suggestion and kind help throughout this study.

I deeply appreciate Professor Dr. Ángela Sastre-Santos and members of her group for their guidance on synthesis of anionic phthalocyanines, and Associate Professor Dr. Taku Hasobe and his group for guidance on fabrication of solar cells. I am also grateful to Designated Professor Dr. Yutaka Matsuo, Associate Professor Dr. Fumito Tani, Professor Dr. Jonathan L. Sessler, Assistant Professor Dr. Hayato Sakai, Professor Dr. Chuan-Feng Chen, Professor Dr. Jan O. Jeppesen, Professor Dr. Dongho Kim, Dr. Mustafa Supur, Mr. Vicente Manuel Blas-Ferrando, Mr. Takuya Kamimura, and Mr. Kentaro Mase for their valuable suggestion and collaboration.

I am grateful for having met  $\text{Li}^+@\text{C}_{60}$  to the researchers, who have carried out the preceding researches relevant to the synthesis of  $\text{Li}^+@\text{C}_{60}$ .

Special thanks to all members of the Fukuzumi group for their kind help, teaching, and friendship. Thanks are also given to all members of the laboratory of Physical Chemistry for Life Science at Department of Material and Life Science, Graduate School of Engineering, Osaka University for their help, valuable suggestions, and friendship.

I am deeply grateful to JSPS of ministry of Education, Culture, Sports, Science and Technology of Japan for their support through scholarship.

Finally, I wish to express my sincere appreciation for continuous encouragement and assistance given by my friends and family, Fujio Kawashima, Mizuko Kawashima and Naoki Kawashima.

Yuki Kawashima

*Fukuzumi Laboratory  
Department of Material and Life Science  
Division of Advanced Science and Biotechnology  
Graduate School of Engineering  
Osaka University*

January, 2015

---